Title

Methods for the synthesis and detection of perfluorinated small molecules as tools for chemical biology

Author

Miller, Margeaux A

Publication Date

2022

Peer reviewed|Thesis/dissertation

UNIVERSITY OF CALIFORNIA

Los Angeles

Methods for the synthesis and detection of perfluorinated small molecules as tools for chemical biology

A dissertation submitted in partial satisfaction of the

requirements for the degree Doctor of Philosophy

in Chemistry

by

Margeaux Anna Miller

2022

ABSTRACT OF THE DISSERTATION

Methods for the synthesis and detection of perfluorinated small molecules as tools for chemical biology

by

Margeaux Anna Miller

Doctor of Philosophy in Chemistry

University of California, Los Angeles, 2022

Professor Ellen May Sletten, Chair

The ability to study and manipulate living systems in their native environment is a major goal in the field of chemical biology. The incorporation of abiotic functionality into naturally-occurring systems has facilitated the understanding of biomolecule function *in vivo*, the development of new drugs, and the design of biomaterials. Fluorine is an abiotic element that has seen broad use in medicinal chemistry. Fluorine's high electronegativity and non-polarizability are further exaggerated in highly fluorinated molecules, like perfluorocarbons. This dissertation describes how the use of abiotic perfluorinated molecules can be used to study and manipulate biological systems. Highly perfluorinated saturated compounds form an orthogonal fluorous

phase, distinct from both water and organic solutions. This property enables the formation of perfluorocarbon nanoemulsions, which are droplets of fluorous solvent stabilized by surfactant and suspended in water. These stable nanomaterials have been used for oxygen delivery and imaging. This dissertation reports on methods for modifying and encapsulating payloads inside these fluorous droplets for therapeutic and imaging applications.

Perfluorinated aromatic compounds are also distinct from their hydrocarbon counterparts with an inverted quadrupole moment due to fluorine's electronegativity. These compounds have been used to modify peptides and proteins and enhance protein-protein interactions. Here, we designed macrocyclic hosts to bind perfluoroaromatics as an alternative approach to the bioorthogonal chemical reporter strategy.

Chapter One is a review on the role of perfluorocarbons in chemical biology. The unique properties of perfluorocarbons are explained as they relate to reactivity, self-assembly, and magnetic resonance imaging. Perfluorinated biomolecules, materials, and probes are discussed as orthogonal tools to modulate biological systems.

Chapter Two details a modular method to access branched, short-chain perfluorinated tags. These tags are biocompatible, while still providing fluorous solubility to payloads of interest. A branched, perfluorinated photosensitizer is prepared and found to be soluble in various clinically-relevant fluorous solvents. Encapsulation of this fluorous photosensitizer allowed for photodynamic therapy in cells.

Chapter Three extends the fluorous tags developed in Chapter Two to other payloads for perfluorocarbon nanoemulsions. Temporary fluorous solubility of payloads of interest is explored through the use of cleavable linkers. By linking a fluorous tag to a coumarin through a self-immolative disulfide linker, a fluorous fluorogenic probe is accessed. This probe is used to

study payload stability within fluorous nanomaterials in the presence of thiols. A similar linking strategy is used to access a fluorous prodrug of small-molecule therapeutic, Gemcitabine.

Chapter Four details the advances and limitations of the bioorthogonal chemical reporter strategy. While most improvements to bioorthogonal chemistry have been through the development of faster covalent reactions, non-covalent host-guest chemistry provides an alternative approach termed bioorthogonal complexation. Existing hosts can be repurposed for some applications of bioorthogonal complexation. Ideal guests for bioorthogonal complexation may require the design of new hosts. Abiotic perfluoroaromatics are considered as ideal guests for this approach due to their unique electronic character.

Chapter Five discusses how Whitlock's naphthalene-based cyclophane is repurposed to investigate arene-perfluoroarene interactions in host-guest systems. While this macrocycle did not bind perfluoroaromatics strongly, these studies informed the next iteration of hosts for perfluoroaromatic guests.

Chapter Six describes an expanded phenanthrene-based cyclophane, which is designed to better accommodate the width of a perfluoroaromatic guest. This host binds pentafluorophenol with millimolar binding affinity in organic solvent. Substituents on the perfluoroaryl ring are found to further increase the binding affinity by at least an order of magnitude.

Chapter Seven reports efforts toward the application of the phenanthrene-based host system in a multivalent version of bioorthogonal complexation. Various methods to modify the phenanthrene host with a conjugation handle are explored, such that phenanthrene host can be appended to a multivalent bead. Efforts to synthesize perfluoroaryl-modified mannosamine and sialic acid derivatives are described. Preliminary metabolic incorporation studies with these derivatives were performed.

The dissertation of Margeaux Anna Miller is approved.

Neil Kamal Garg

Patrick G. Harran

Kendall N. Houk

Ellen May Sletten, Committee Chair

University of California, Los Angeles

2022

This dissertation is dedicated to my teachers

TABLE OF CONTENTS

LIST OF FIGURES

Chapter 1

Chapter 2

Chapter 3

Chapter 4

Chapter 5

Chapter 6

Chapter 7

LIST OF SCHEMES

Chapter 2

Chapter 3

Chapter 5

Chapter 6

Chapter 7

LIST OF TABLES

Chapter 2

Chapter 5

Chapter 6

ACKNOWLEDGEMENTS

I would first like to express my immense gratitude to my advisor, Professor Ellen Sletten, for providing me the opportunity to join her lab and to grow as a scientist under her mentorship. She's a brilliant researcher, and I have learned an incredible amount about a broad number of topics from her insights. Thank you for your confidence in me when I failed. Thank you for challenging me to learn new techniques, take on difficult projects, and see a project through to the end. I will always appreciate your patience in allowing me (and others) to expand our skillsets, so we could have the experience of taking a project from initial chemistry experiments through to the biology. You've taught me how to condense large amounts of material with clarity to support my project and new ideas. Thank you for tolerating my indecision and many vicissitudes in both my research and career goals. Your enthusiasm and vision about the field of chemical biology continues to influence my perspective on scientific research.

I would like to thank the people who inspired me to pursue graduate school in chemistry in the first place. I am grateful to Professor Christian Rojas, who first taught me about the beauty and "awesome power of chemical synthesis" in the classroom and the lab. His genuine ability to draw connections between chemistry and the humanities were what initially drew me to organic chemistry and has continued to influence how I try to communicate science. I am also grateful to Professor Dina Merrer, who introduced me to physical organic chemistry. Both of these people exemplified what a teacher is with clarity and eloquence. Their continued support has meant so much to me.

I am grateful for the support of my qualifying exam and dissertation committee members Professors Neil Garg, Patrick Harran, Kendall Houk, and Sri Kosuri. I would like to thank Neil Garg for encouraging me to come to UCLA and allowing me to be a part of his lab for a short

time. I learned a great deal from him and his students in the time I was there that aided in my success in grad school. I admire your unwavering support of your students, and I am grateful for all the recommendation letters you have written on my behalf. Patrick Harran is an exceptional teacher, and his synthesis class was a highlight of my first year of grad school. I feel honored to have learned physical organic chemistry from Ken Houk.

Being a part of the Sletten lab in its first iteration was a great learning experience that I'll always be thankful for. The people I worked with everyday made spending long hours in lab enjoyable and has been the highlight of my time at UCLA. I'd like to thank Maly Cosco for encouraging me to join the Sletten lab before I even arrived at UCLA. Thank you for always supporting me as I figured out my path in grad school. I'd like to thank Rachael Day for answering all my biology questions and never making me feel inferior. You were a great person to commiserate with about failed experiments and things that didn't go as planned. I'll miss our spontaneous conversations and laughs. I think I would've been much less happy these past few years if I hadn't worked next to Dan Estabrook. Your eloquence and depth of knowledge inspire me, and your support has been invaluable to me. I admire Anna's confidence and ability to define her goals. I've benefitted greatly from her willingness to share her broad understanding of chemical biology. I'd like to thank Gina Lee for being a great partner on the host-guest project. I always learned a lot from our discussions on ideas for our project, your comprehensive understanding of non-covalent interactions, and your clear explanations of computation. I also appreciated your beautiful baked goods, as we share a sweet tooth. Joe Jaye's sense of humor and efficiency in lab are admirable. I appreciated sharing memes, discussing methods papers, and your willingness to help me with my crooked vacuum pump even when you were busy. I always enjoyed candy with Monica Pengshung while we talked through problems in lab and new papers.

We shared a macabre sense of humor, and if I had a difficult compound to make or purify, Monica is who I would ask for help. I admire Irene Lim's honesty and stoicism. I've enjoyed our conversations throughout the COVID evening shifts and the past year and seeing all the colorful chemistry you've done with the fluorous tags. Cesar Garcia has been a great friend to me. I'm grateful for all the conversations we have had about life, chemistry, and basketball (and the frequent rides home). I admire his imperturbable nature and work ethic. I always enjoyed tossing around far-fetched project ideas with Anthony Spearman. I love working, learning, and chatting with all these people and I've missed seeing them on a daily basis.

I'd like to thank the postdocs of the Sletten lab from whose knowledge I've benefitted. I appreciated Jon Axtell's enthusiasm, advise, and curiosity on all aspects of chemistry. His measured tone never made me feel less than or that a question was too small. I hope I have absorbed some of his wisdom. I'd like to thank Heidi van de Wouw for challenging me to have good reasons for why I do things a certain way, which ultimately made me a better scientist and teacher. Thank you for your help and advice in applying to jobs and postdocs and navigating the end of my PhD. I appreciate Shang Jia's thoughtful insights into bioconjugation and many areas of chemical biology.

I'd like to thank Erika Aguiluz Ramirez, Kaitlin Hartung, and Prairie Hammer for helping me to grow as a mentor, your contributions to my projects, and for allowing me to have input on your projects. I really enjoyed getting to work with Erika at a time in grad school that was particularly hard for me. Your work ethic and self-awareness gave me the opportunity to reflect on my own experiences, and I only wish the best for you. Working with Kait reminded me how exciting new reactions and synthetic routes can be. Your willingness to take on a challenging project is commendable, and I hope you maintain your passion for chemistry. I'd

like to thank Prairie for working with me in my last few months in the Sletten lab and being willing to take forward some of the host-guest projects. I'm excited to see where you take these projects! I'd also like to thank Kaitlin and Prairie for proofreading parts of this dissertation. It was fun to share a bay with Eric Lin and Caitlyn Fick as I wrapped up my dissertation work. Hearing about their experiences at the beginning of grad school was very nostalgic for me. I'd also like to thank Caitlyn for taking the time to carry out some of the metabolic incorporation experiments presented here.

Outside of the Sletten lab, I'm grateful for the friendships I have made at UCLA. Sarah Anthony has been a fantastic friend to me since we met as first year grad students. I cherish our late night walks home after lab, running to make it to Trader Joes from Mol Sci before it closed, and hearing your perspective over cheese and chocolate. I'm so grateful to have had you as a friend through all the difficult parts of graduate school, as well as the good parts. I'm fortunate to have had fantastic roommates in Jessica Logan and Steven Patrick. I enjoyed going home at the end of a long day in lab and getting to talk with you both about life and science and playing with your cats. I'm grateful to Edris Rivera for his willingness to help me with everything related to crystal structures and our conversations about hexafluoro-Dewar benzene, music, and food.

I'd like to thank Elias Picazo for dealing with my naivete with grace when I was a first year in the Garg lab. I've sought to emulate his patience and excitement as I mentored younger students. He was a great example to me of how to stay motivated when you run into chemistry problems. Evan Darzi, a fellow Arizonan, was always willing to answer my questions about cyclophanes and polycyclic aromatic hydrocarbons. I'm also incredibly grateful to Bryan Simmons, Lucas Morrill, and Jesus Moreno for their career advice and helpful discussions throughout grad school. I had a great time connecting with a fellow Barnard alum, Aneta Turlik,

when she began her postdoc upstairs in the Houk lab. I'm grateful for our conversations over coffee and lunch the past few years. I'd like to thank Ricky Ruiz for always putting a smile on my face.

Finally, I'd like to thank my friends and family for their unending support. Jessica Zhou, Amber Scharnow, and Asami Odate have remained incredible friends to me as we've endured grad school together but all across the country. Thank you for always taking my phone calls on my walks home. I am privileged to have family who have always embraced and encouraged my passions. My dad, Lou, has always pushed me to fulfill my potential. My mom, Carolyn, has taught me about the importance of finding humor in life and to continue to seek out knowledge beyond my comfort zone, skills that have been essential in grad school. My sister, Lacey, has always celebrated my small and large successes with the brightest enthusiasm. I'm thankful for her friendship throughout my life.

Chapter One is a version of a published review, Margeaux A. Miller, Ellen M. Sletten "Perfluorocarbons in Chemical Biology" *ChemBioChem* **2020**, *21*, 3451−3462. Miller and Sletten contributed to writing.

Chapter Two is a version of a published manuscript, Margeaux A. Miller, Ellen M. Sletten "A general approach to biocompatible branched fluorous tags for increased solubility in perfluorocarbon solvents" *Org. Lett.* **2018**, *20*, 6850−6854. Miller performed experimental work. Miller and Sletten contributed to writing.

Chapter Three is a version of a published manuscript, Margeaux A. Miller, Rachael A. Day, Daniel A. Estabrook, and Ellen M. Sletten. "A reduction-sensitive fluorous fluorogenic coumarin." *Synlett*, **2020**, *31*, 450-454. Miller, Estabrook, and Day contributed to experimental work. Miller, Estabrook, Day, and Sletten contributed to writing. Additional unpublished experimental work conducted by Miller is included.

Chapter Four is an unpublished perspective on bioorthogonal complexation written by Miller.

Chapter Five is unpublished work written by Miller. Experimental work was performed by Miller. Computational work was performed by Lee.

Chapter Six is unpublished work written by Miller. Experimental work was performed by Miller, Lee, Aguiluz Ramirez, and Hartung. Computational work was performed by Lee.

Chapter Seven is unpublished work written by Miller. Synthetic work was performed by Miller. Cell experiments were performed by Kataki-Anastasakou and Fick.

Throughout these studies, Margeaux Miller was supported by the NIH Chemistry-Biology Interface Training Program (T32 training grant, 5T32GM008496) and UCLA's Dissertation Year Fellowship.

Additional funding sources include UCLA, the American Chemical Society Petroleum Research Fund (57379-DNI4), University of California Cancer Research Coordinating Committee (CNR-18-524809), the Alfred P. Sloan Foundation (FG-2018-10855), the Hellman Fellows Fund, NIH (1DP2GM13268), and instrumentation grants provided by the NSF (MRI CHE-1048804) and NIH (1S10OD016387-01).

BIOGRAPHICAL SKETCH

EDUCATION

University of California, Los Angeles, Los Angeles, CA
MS in Chemistry 2018
GPA: 4.00/4.00

Barnard College, Columbia University, New York, NY 2012–2016
BA in Chemistry with Honors
magna cum laude, GPA: 3.85/4.00
Thesis title: "Synthesis of 2,3-oxazolidinone free reducing sugar derivatives of 2-mannosamine and 2-talosamine"

RESEARCH EXPERIENCE

Graduate Student Researcher, University of California, Los Angeles 2017–present
Advisor: Prof. Ellen M. Sletten

- Designed new host-guest complexes for non-covalent bioorthogonal chemistries
- Synthesized macrocyclic hosts for perfluorinated aromatic guests based on physical organic chemistry principles
- Developed a method to synthesize branched, short-chain perfluorinated compounds
- Synthesized fluorous photosensitizers for photodynamic therapy in cells
- Synthesized cleavable linkers and responsive payloads for encapsulating therapeutics and fluorophores in perfluorocarbon nanoemulsions
- Mentored three graduate students

Research Intern, Enable Biosciences, South San Francisco, CA Summer 2019

- Scaled-up production and purification of protein-DNA conjugates for Enable's antibody quantification platform to detect autoimmune and infectious diseases
- Explored alternative click chemistries and bioconjugation methodologies to form protein-DNA conjugates and nanoparticle-DNA conjugates and assessed degree of conjugation

Undergraduate Researcher, Barnard College 2014–2016
Advisor: Prof. Christian M. Rojas

- Synthesized 2-amino sugars via rhodium and copper metallanitrenes
- Optimized neoglycosylation reactions of 2-amino reducing sugars

FELLOWSHIPS AND AWARDS

Dissertation Year Fellowship	2021
Majeti-Alapati Dissertation Award	2021
UCLA Chemistry-Biology Interface (CBI) Trainee	2017–2020
Molecular Biology Institute Retreat Poster Prize Winner	2018
Christopher S. Foote Graduate Fellowship in Organic Chemistry	2016–2018
ACS-ORG Undergraduate Award in Organic Chemistry	2016

ACS-POLYED Award for Outstanding Achievement in Organic Chemistry	2015
Barnard College Barry M. Goldwater Scholarship Nominee	2015
Bernice G. Segal Summer Research Internship Award	2014
Barnard College Dean's List	2012–2016

PUBLICATIONS

1. **Miller, M.A.**; Sletten, E.M. "Perfluorocarbons in Chemical Biology." *ChemBioChem* **2020***, 21,* 3451–3462.
2. **Miller, M.A.***; Day, R.A.*; Estabrook, D.A.*; Sletten, E.M. "A reduction sensitive fluorous fluorogenic coumarin." *Synlett* **2020***, 31,* 450–454.
3. **Miller, M.A.**; Sletten, E.M. "A general approach to biocompatible branched fluorous tags for increased solubility in perfluorocarbon solvents." *Org. Lett.* **2018**, *20*, 6850–6854. (Highlighted in *Synfacts* **2019**, *15*, 0035.)
4. Picazo, E.; Anthony, S.M.; Giroud, M.; Simon, A.; **Miller, M.A.**; Houk, K.N.; Garg, N.K. "Arynes and cyclic alkynes as synthetic building blocks for stereodefined quarternary centers." *J. Am. Chem. Soc.* **2018**, *140*, 7605–7610.
5. Liu, S.; Odate, A.; Buscarino, I.; Chou, J.; Frommer, K.; **Miller, M.**; Scorese, A.; Buzzeo, M.; Austin, R. N. "An Advanced Spectroscopy Lab That Integrates Art, Commerce, and Science as Students Determine the Electronic Structure of the Common Pigment Carminic Acid." *J. Chem. Educ*. **2017**, *94*, 216–220.

CHAPTER ONE

Perfluorocarbons in chemical biology

Adapted from: Margeaux A. Miller, Ellen M. Sletten* "Perfluorocarbons in Chemical Biology" *ChemBioChem* **2020**, *21*, 3451−3462. DOI: 10.1002/cbic.202000297

1.1 Abstract

Perfluorocarbons, saturated carbon chains where all the hydrogen atoms are replaced with fluorine, form a separate phase from both organic and aqueous solutions. Though perfluorinated compounds are not found in living systems, they can be used to modify biomolecules to confer orthogonal behavior within natural systems, such as improved stability, engineered assembly, and cell-permeability. Perfluorinated groups also provide handles for purification, mass-spectrometry, and ^{19}F NMR studies in complex environments. Herein, we describe how the unique properties of perfluorocarbons have been employed to understand and manipulate biological systems.

1.2 Introduction

Selectivity in complex biological environments is obtained through the coordination of many non-covalent interactions. Biomolecules have evolved such that they can efficiently function without interfering with one another. Complementary protein-substrate pairs have facilitated chemically-induced protein dimerization,[1] protein-protein interactions,[2] and multicolor microscopy experiments.[3] Natural and synthetic membranes[4] form from amphiphilic lipids and define boundaries and compartments, mediating the entry and exit of ions and metabolites.[5] The exquisite specificity of DNA has resulted in an explosion of applications, including controlled cell-cell interactions,[6] biosensors,[7] and advanced nanomachines.[8]

Orthogonality has become an essential tool to allow chemical biologists to engineer selectivity in complex environments. Unique chemical handles enable natural systems to be probed and/or manipulated.[9–11] Abiotic functional groups with selective, covalent reactivity are implicated in bioorthogonal chemistries to label, purify, and study biomolecules. Rare amino acid sequences confer binding to unnatural fluorophores and probes. In this review, we highlight orthogonality imparted by a single element, fluorine, and its implications in chemical biology.

1.3 Properties of fluorine

Fluorine is rarely found in living systems,[12,13] yet has unique characteristics due to its high electronegativity, steric profile, and low polarizability. Fluorine has a van der Waals radius of 1.47 Å, which is in between the radii of the hydrogen and oxygen nuclei (Figure 1.1A). Carbon-fluorine bonds are strong (110 to 130 kcal/mol) with a bond length of 1.3 Å, longer than a C-H bond but shorter than a C-O bond (Figure 1.1B). The small size of fluorine, high metabolic stability of the C-F bond, and fluorine's ability to dramatically change the electronics of a molecule have had the most widespread impact in the pharmaceutical industry, with 20–25% of current pharmaceuticals containing at least one fluorine atom.[14,15] The applications of fluorine to medicinal chemistry have been extensively reviewed.[16–21] The same fundamental properties of fluorine that render it prime for pharmaceutical optimization give rise to the distinct properties of perfluorocarbons, which we highlight herein. One further advantageous attribute of the fluorine atom is that the nucleus is NMR active with spin 1/2 and has 100% natural abundance, rendering fluorine an ideal contrast agent for magnetic resonance imaging (MRI).[22] Unlike ^{1}H NMR, ^{19}F chemical shifts can vary drastically (>350 ppm) making ^{19}F NMR a useful tool for sensing changes in conformation and environment.[23]

The effects of fluorine are intensified as the number of fluorine atoms on a carbon chain increases. Perfluorocarbons, molecules where all C-H bonds have been replaced by C-F bonds, create a separate phase from aqueous and organic solutions, demonstrating complete orthogonality to natural compounds. The separation of perfluorocarbons into the fluorous phase is attributed to the high electronegativity of fluorine atoms precluding van der Waals interactions with neighboring molecules.[24,25] Perfluorocarbons would rather form a separate non-interacting phase than participate in induced dipole-induced dipole interactions with hydrocarbons or induced dipole-dipole interactions with water. Their low propensity for intermolecular interactions also explains the decreased boiling points of perfluorocarbons relative to their hydrocarbon counterparts (Figure 1.1C). It is important to note that the fluorous phase does not arise from enthalpically favorable fluorine-fluorine interactions, but rather the disinclination for perfluorinated molecules to interact with all other species.[26]

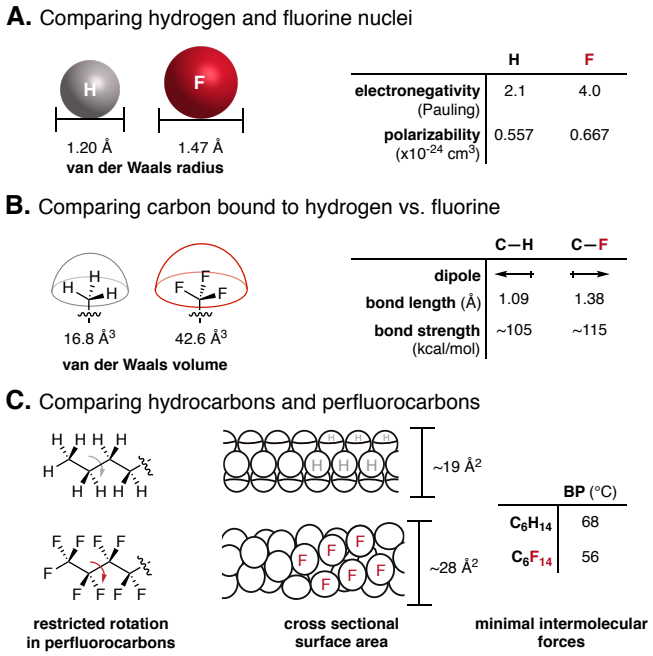

Figure 1.1 Characteristics of perfluorocarbons as they relate to the C-F bond**.** A) Comparing hydrogen and fluorine nuclei. B) Comparing the C-H and the C-F bond and the methyl and the trifluoromethyl group. C) Comparing hydrocarbons and perfluorocarbons. The larger size of

fluorine increases the rotational barrier in perfluorocarbons making them more rigid.[27–33] The larger size of fluorine also increases the overall surface area of perfluorocarbons making them more hydrophobic. The low polarizability of fluorine and C-F bonds leads to few intermolecular forces and low boiling points.[24,25,34]

When perfluorinated amphiphiles are placed in water, another intriguing effect is observed. The perfluorinated surfactants self-assemble into micelles and/or vesicles with a ΔG that is lower than analogous hydrocarbon surfactants.[35] This phenomena, referred to as the fluorous effect, originates from the larger size of fluorine as compared to hydrogen (Figure 1.1C).[36] Thus, perfluorinated amphiphiles have more high-energy water molecules associated with them than hydrocarbon amphiphiles of the same length. Upon self-assembly, more water molecules are released, resulting in an extreme version of the hydrophobic effect.

As demonstrated by the fluorous phase and the fluorous effect, the unique properties of perfluorocarbons can generally be attributed to the high electronegativity and increased size of fluorine compared to hydrogen. These simple, yet powerful attributes provide orthogonality in complex environments that allow for protein-protein stabilization, self-assembly in membranes, enhanced permeability, altered cell surfaces, and biomolecule purification and immobilization.[37,38] In this review, we primarily describe applications of perfluorocarbons in chemical biology as molecules containing CF_3 groups or longer perfluorinated chains. We note that while trifluoromethyl groups do not strictly fall under the definition of perfluorocarbons, multiple CF_3 groups on one structure can often convey similar properties to a single, longer perfluoroalkyl chain.[39–42] Other fluorinated compounds, such as those containing single fluorine atoms or sp^2 C-F bonds, also have intriguing properties which have been described elsewhere.[43–45]

1.4 Perfluorination of peptides and proteins

1.4.1 Incorporation of perfluorinated amino acids

Hydrophobicity mediates protein folding, formation of protein secondary structure, and protein-protein interactions. Perfluorocarbons are known to be even more hydrophobic than their hydrocarbon analogues (as discussed above) without significant changes in shape. As such, they provide a unique tool for designing and improving structural and functional features of many proteins. Fluorination of proteins can be achieved by unnatural amino acid (AA) incorporation or protein semi-synthesis. Tirrell, Degrado, Kumar and others have demonstrated that fluorinated amino acids can be tolerated by the natural translation machinery. Trifluorovaline **1.1**,[46,47] trifluoroleucine **1.2**,[46,48–50] trifluoroisoleucine **1.3**,[51] trifluoromethionine **1.4**,[52–54] and hexafluoroleucine **1.5**[55] can be incorporated into proteins *in vitro* with auxotrophic *E. coli* strains; though **1.1** and **1.5** require engineered hosts that overexpress the appropriate tRNA synthetase for efficient incorporation (Figure 1.2). Trifluoroethylglycine **1.6** can be incorporated with a mutated isoleucyl-tRNA synthetase.[56] Unnatural trifluoromethyl phenylalanine **1.7**[57–59] and OCF_3-phenylalanine **1.8**[60] have been incorporated site-specifically using orthogonal tRNA/aminoacyl-tRNA synthetase pairs. Alternatively, fluorinated proteins can be achieved by the incorporation of fluorinated amino acids (such as **1.9–1.15**) by solid-phase peptide synthesis (SPSS) and/or native chemical ligation (NCL).[61–69] While AAs with longer fluorinated chains ($\geq C_3F_7$) have been synthesized, their incorporation into peptides through biosynthetic methods are less common.[70–73]

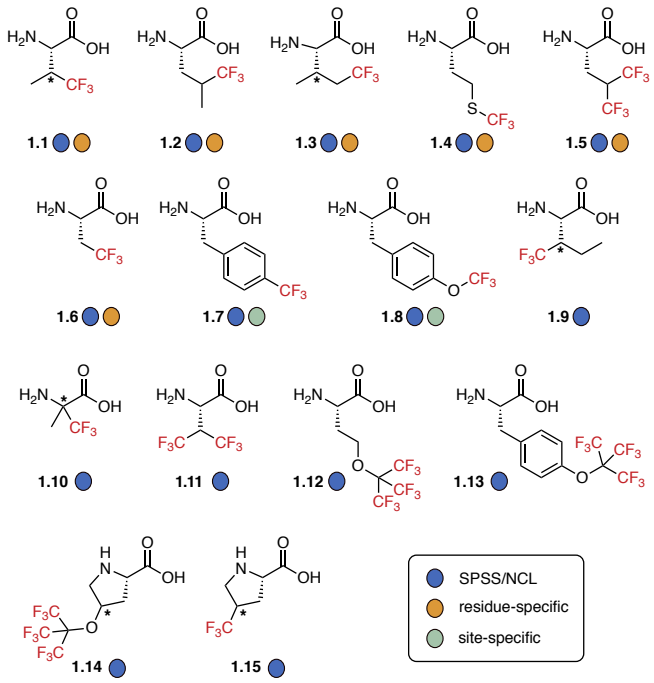

Figure 1.2 Selected examples of fluorinated amino acids and their modes of incorporation into peptides and proteins. Fluorinated residues can be incorporated using auxotrophic cell lines (orange circle) or site-specifically with amber stop codon suppression and an orthogonal aminoacyl-tRNA synthetase/tRNA pair (green circle). All the fluorinated amino acids can be incorporated via solid-phase peptide synthesis (SPSS) or native chemical ligation (NCL) (blue circle).

1.4.2 Chemical methods for perfluorination of peptides and proteins

Perfluorination of amino acids to alter protein properties and facilitate ^{19}F NMR analysis (more details in sections 1.4.3) was originally pioneered via unnatural amino acid incorporation; however, due to its success, more recent work has focused on installing fluorine atoms via chemical modification of proteins (Figure 1.3). Using classic bioconjugation reagents such as α-haloacetamides (**1.16** and **1.17**),[74–76] maleimides (**1.18**),[77] and *N*-hydroxysuccinimide-activated esters (**1.19**),[77] nucleophilic cysteine or lysine resides can be modified with trifluoromethyl groups. Fluorinated tags with different linkers (**1.19** vs **1.16**) provide distinct fluorine chemical

shifts that could be differentiated by ^{19}F NMR and be used to track proteins in a complex mixture.[77]

Perfluoroalkyl radicals provide methods to modify amino acids without the need for spacers between the fluorinated group and the amino acid. Inspired by the demonstration of trifluoromethylation with Langlois reagent **1.20** in cell lysate,[78] Davis, Gouverneur, and coworkers generated trifluoromethyl radicals under aqueous conditions and labeled aromatic amino acids and free cysteine.[79] Improved specificity could be achieved in the absence of free cysteine and at pH 6 to provide >50% conversion to CF_3-tryptophan (Figure 1.3B and C). Using fluoroalkylated iodine reagents (*i.e.* derivatives of Togni's reagent, **1.21**), tryptophan residues have also been modified with functionalized perfluoroethyl groups (Figure 1.3D).[80] With this method, minor modifications of other amino acids or other positions on the indole heterocycle are also observed. For cysteine modification, Umemoto's trifluoromethylation reagent[81] and **1.21** have been explored.[82,83] Though perfect selectivity for one amino acid has not yet been achieved, others have pursued similar strategies for trifluoromethylation of cysteine, tyrosine[84], tryptophan, and/or histidine, which have recently been reviewed.[85]

These recent advances in fluorination of intact proteins with both classic bioconjugation chemistries and reactivity specific to perfluorinated reagents have enabled ^{19}F NMR studies. Further advancements are still necessary to improve selectivity; however, once the chemistries are optimized, applications toward engineered proteins and assemblies can be pursued.

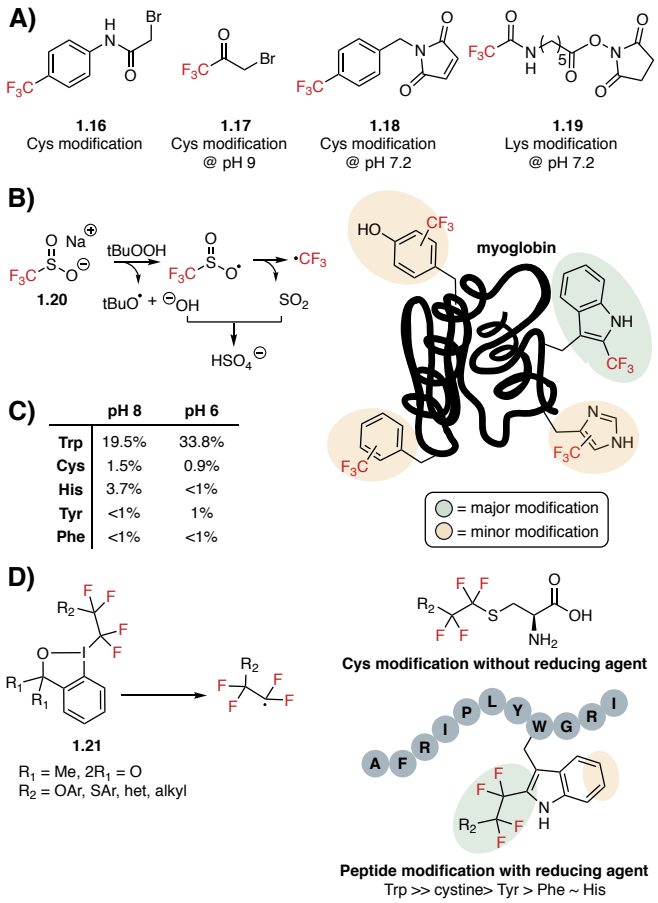

Figure 1.3 Chemical methods for perfluorination of peptides and proteins. A) Classic bioconjugation reagents used for addition of trifluoromethyl groups to cysteine and lysine residues in proteins. B) Generation of trifluoromethyl radical from Langlois reagent **1.20** under aqueous conditions leads to direct protein modification. Major trifluoromethylation occurs on tryptophan residues, though minor modification is observed on other aromatic residues and free cysteines, if present. C) Table of results from the reaction of an equimolar mixture of five amino acids and **1.20**, run to 40% conversion to determine residue specificity at different pHs.[79] D) Hypervalent iodine reagents (Togni's reagent, **1.21**) can be used to add functionalized perfluoroethyl groups to amino acids, such as cysteine. Tryptophan residues can also be perfluorinated in the presence of **1.21** and reducing agent. Modification of tryptophan under these conditions occurs primarily at the indole-C2 position with minor modifications on the other indole carbons or other aromatic residues.

1.4.3 Perfluorinated proteins studied by ^{19}F NMR

Given the absence of fluorine in biological systems and its high NMR sensitivity, incorporation of fluorinated AAs can be used to study proteins by ^{19}F NMR. The addition of

multiple, chemically equivalent fluorine atoms (*i.e.* trifluoromethyl, hexafluoroisopropyl, or perfluoro-*tert*-butyl) enhances the sensitivity of ^{19}F protein NMR experiments. Many have used the above protein fluorination methods to monitor protein dynamics and protein-membrane interactions by NMR.[74–76,86,87] Mehl, Pielak, and coworkers have used site-specific incorporation of trifluoromethyl phenylalanine (**1.7**) to study protein conformation and binding,[57] as well as detect proteins in *E. coli*.[58] While monofluorinated AAs resulted in broadened fluorine signal that was unable to be detected in large proteins, fluorine signal from **1.7** could be detected even for proteins up to 100 kDa, demonstrating the need to incorporate perfluorinated groups.

Protein fluorination can also be used to study protein-small molecule interactions with ^{19}F NMR (Figure 1.4).[88,89] Changes to protein conformation or hydration upon the introduction of a small molecule can be detected, which provides a unique assay for drug discovery. This technique, deemed protein-observed ^{19}F NMR (PrOF), is an alternative to the more commonly performed ligand-observed ^{19}F NMR methods, which rely on monitoring changes in fluorinated small-molecule fragments in the presence of a non-fluorinated protein target.[90] PrOF NMR was initially demonstrated using a monofluorinated tyrosine, but has since been extended to trifluoromethyl groups installed via protein modification as shown in Figure 1.3B.[79] By modifying lysozyme with CF_3 groups, the binding affinity of a known lysozyme inhibitor was determined by ^{19}F NMR. With a trifluoromethylated myoglobin, chemical shift changes in the presence of various ligands were also observed. The molecular information obtained in PrOF NMR makes this approach particularly advantageous for screening small-molecule fragments, which can be combined together or modified to invent selective and higher affinity inhibitors for interesting protein targets, as has been done for bromodomains.[91,92]

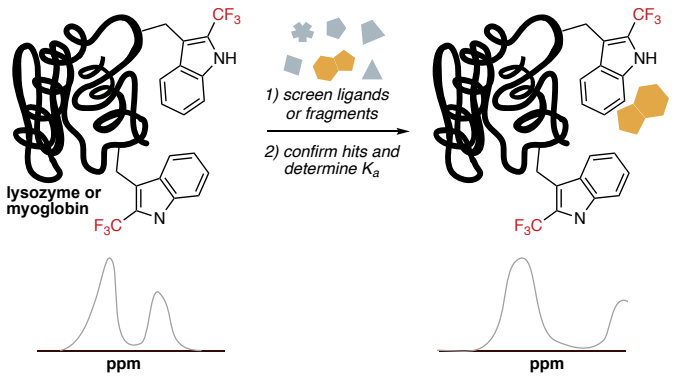

Figure 1.4 Protein-observed ^{19}F NMR (PrOF NMR). This method uses the incorporation of fluorinated amino acids to monitor protein conformational changes in the presence of small-molecule fragments for drug discovery. Proteins with trifluoromethylated tryptophan residues have been used in these types of studies.[79]

1.4.4 Perfluorination stabilizes protein-protein interactions

Beyond structural ^{19}F NMR studies, fluorination can confer stability in proteins as well as drive protein folding and arrangement. Marsh, Kumar, and Tirrell have all investigated the effects of incorporation of fluorinated amino acids on protein structure and function.[26,46,55] They have found that introduction of fluorinated amino acids minimally perturbs secondary and tertiary structure. For example, Marsh and coworkers designed a 27-residue peptide, which formed a tetrameric antiparallel 4-helix bundle (Figure 1.5). In this design, leucine or hexafluoroleucine (**1.5**) residues would point toward the center of the bundle forming the hydrophobic core. The authors found that perfluorination did not disrupt the overall structure, and that fluorination provided a stabilizing effect—increasing ΔG_{unfold} by more than 10 kcal/mol when all leucine residues were replaced by **1.5**.[93,94] The replacement of hydrophobic amino acids with their fluorinated analogues can increase protein stability to both chemical and thermal denaturation. The stabilizing effect of these replacements can be attributed to the unique ability of fluorination to increase size and hydrophobicity of a side chain, while maintaining its shape. This ability is in contrast to traditional efforts to increase side chain hydrophobicity, which

normally also alters side chain shape (*i.e.* valine to isoleucine) and thus sterically disrupts protein-protein interactions.

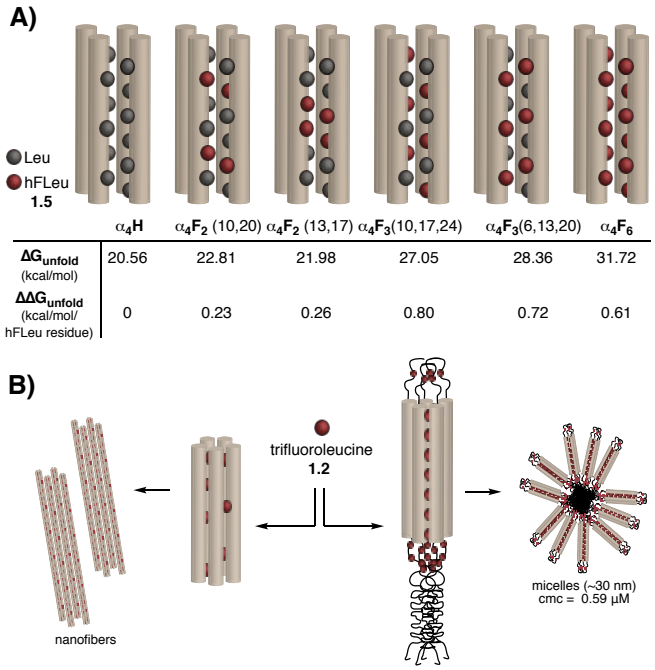

	α_4H	α_4F_2 (10,20)	α_4F_2 (13,17)	α_4F_3(10,17,24)	α_4F_3(6,13,20)	α_4F_6
ΔG_{unfold} (kcal/mol)	20.56	22.81	21.98	27.05	28.36	31.72
$\Delta\Delta G_{unfold}$ (kcal/mol/ hFLeu residue)	0	0.23	0.26	0.80	0.72	0.61

Figure 1.5 Understanding thermodynamics of fluorinated proteins and applications. A) Substituting fluorinated amino acids for their hydrocarbon counterparts can improve the stability of peptide bundles toward chemical denaturants. Both the number and placement of fluorinated hexafluoroleucine (hFLeu, **1.5**) residues can affect stability. Figure adapted and data from Marsh and coworkers.[93,94] B) Incorporation of trifluoroleucine **1.2** into different coiled-coiled proteins allows for the formation of nanostructures such as fibers and micelles. Fluorination confers stability to the fibers[95] and lowers the critical micelle concentration (cmc) of the micelles.[96]

Ultimately, enhanced stability is important in the context of the utility of proteins and enzymes. Recently, the Montclare lab has shown that different fluorinated coiled-coil proteins (containing **1.2**) can self-assemble into robust nanofibers that bind metals or a small molecule[95] or if designed appropriately, form micelles (Figure 1.5B).[96] It is thought that fluorination plays a role in the stability of these protein micelles, as the critical micelle concentration (cmc) was determined to be smaller than that of a non-fluorinated control. These nanostructures represent initial steps toward leveraging fluorination as a tool for responsive biomaterial design.[95] Protein

fluorination also provides an alternative method to stabilize enzymes against denaturation by organic solvent or high temperature for industrial applications and biocatalysis.[97]

In a therapeutic context, fluorinated proteins have been shown to retain or to have improved activity in comparison to non-fluorinated variants. Tirrell and coworkers reported that a fluorinated coiled-coil peptide maintains its ability to bind target DNA similar to its natural counterpart.[98] Marsh and coworkers have shown that fluorinated antimicrobial peptides can retain their activity as therapeutic agents, while gaining improved stability to hydrolysis.[99] While not yet as broadly used as fluorination in small-molecule drug discovery, protein fluorination is a strategy for stable nanostructures, catalysts, and therapeutics.

1.5 Enhanced membrane and cell permeability with fluorous tags

1.5.1 Perfluorination facilitates self-assembly in membranes

Given that the replacement of hydrophobic amino acids with their fluorinated counterparts can enhance the stability of proteins in solution, others have looked to how fluorination of amino acids can be used to drive the formation of protein assemblies within membranes. Perfluorocarbons are the key to designing orthogonal protein assemblies as their hydrophobicity allows for partitioning into the membrane, and their lipophobicity allows for separation from natural hydrocarbon lipids. Kumar and coworkers have shown that rationally designed fluorinated peptides can insert into vesicle bilayers[100] or micelles[101] and self-assemble to form larger defined complexes driven by the unfavorable interactions of the fluorinated side chains with natural lipids.

Adding perfluorocarbons to membranes can also be achieved through the addition of fluorinated lipids. Kumar and coworkers demonstrated that the orthogonality of fluorinated lipids

to hydrocarbon lipids allows for the formation of distinct perfluorocarbon domains in supported lipid bilayers (Figure 1.6A).[102] The affinity of perfluorocarbons for membranes can also be used to display molecules of interest on membrane surfaces to study how ligand clustering affects cell-surface interactions and alters cell adhesion.[103]

1.5.2 Fluorinated lipids and tags for cellular internalization

An extension of self-assembly and clustering of fluorinated lipids within membranes is the formation of artificial lipid rafts. Lipid rafts are rigid microdomains, generally formed via cholesterol enrichment. The formation of lipid rafts has been connected to enhancing endocytosis.[104,105] Given the tendency of fluorinated lipids to form rigid, phase-separated domains in the presence of hydrocarbon lipids (Figure 1.6A), Kumar and coworkers postulated that artificial fluorinated lipids could be used to form domains within biological membranes and enhance internalization into cells.[102,106]

Cells incubated with partially fluorinated phospholipids bearing a biotin or fluorophore head group were more readily taken up than their hydrocarbon counterparts in an energy dependent manner (Figure 1.6B). To demonstrate how this strategy could be utilized for delivering cargo into cells, partially fluorinated phospholipids with a biotin headgroup **1.22** were prepared and shown to more readily carry FITC-labeled avidin into the cytosol than the hydrocarbon analogue.[106]

Fluorinated tags have also been conjugated to oligonucleotides to facilitate their internalization into cells.[107] In some cases, it is thought that fluorination leads to self-assembly prior to internalization and that larger fluorinated oligonucleotide aggregates are preferentially

endocytosed rather than internalized by lipid-raft mediated mechanisms or passive diffusion.[108,109]

1.5.3 Fluorinated activators of cell-penetrating peptides

Perfluorinated fatty acids (ionic amphiphiles) have been employed in concert with cell-penetrating peptides (CPPs) to promote cellular internalization (Figure 1.6C). Perfluorocarbon fatty acids like **1.23**, which readily embed in cell membranes, are more basic than their hydrocarbon counterparts. Clustered perfluorinated acid **1.23** interacts with positively charged arginine residues to minimize charge repulsion and deliver fluorescently-labeled, cationic CPPs (*i.e.* **1.24**) into cells more effectively than their non-fluorinated counterparts.[110]

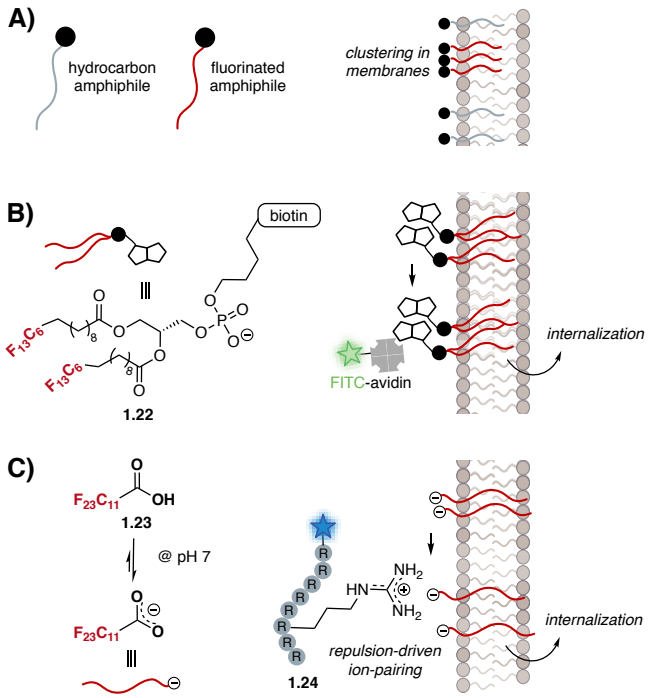

Figure 1.6 Use of fluorinated amphiphiles for cellular internalization. A) Fluorinated amphiphiles tend to aggregate together in membranes. B) Fluorinated phospholipids modified with biotin first cluster together in membranes. Addition of FITC-avidin allows for the internalization of avidin cargo into the cytosol (FITC = fluorescein isothiocyanate).[106] C) Perfluorinated carboxylic acids (like **1.23**) assemble in membranes. Due to charge repulsion, the

perfluorinated acids preferentially associate with arginine-containing, cationic peptides rather than remain aggregated together, facilitating the entry of these payloads into the cytosol.[110]

1.5.4 Transfection agents and protein delivery

The enhanced uptake of fluorinated chains has made perfluorocarbons valuable components in the design of delivery vehicles. Cationic polymers are commonly employed to encapsulate negatively charged DNA and siRNA. Two of the common issues with the use of cationic polymers and amphiphiles for gene delivery are inefficient transfection and cytotoxicity of the material due to excessive positive charge.[111] The implementation of perfluorocarbon containing polymers and lipids to encapsulate nucleic acids mitigates both of those problems due to perfluorocarbons' affinity for membranes[112] and presumably, fluorine's electronegativity altering the pKa of cationic polymers.[113,114]

In the formulation of the delivery vehicle, cationic fluorinated polymers pack tightly around nucleic acids since fluorinated chains preferentially associate with each other and not the nucleic acids. Good packing improves the stability of these materials *in vivo* and requires lower polymer to DNA charge ratios than cationic hydrocarbon polymers.[115] Highly stable materials, which are not excessively cationic, result in decreased cytotoxicity. For example, when a G5 PAMAM dendrimer is more than 50% fluorinated, efficient DNA and siRNA delivery can be achieved with minimal cytotoxicity when compared to a commercial transfection agent Lipofectamine 2000.[116]

More recently, charged fluorinated tags have also been used to encapsulate proteins for delivery to the cytosol. In 2018, Cheng and coworkers prepared a library of fluorinated and alkylated polymers from branched poly(ethyleneimine). In the presence of protein, these amphiphiles complex with proteins and assemble into uniform nanoparticles, which deliver

protein into cells more effectively than a non-fluorinated polymer control.[117] Protein cargo has also been encapsulated inside perfluorocarbon nanoemulsions using non-covalent fluorous tags that electrostatically interact with the protein surface to disperse protein inside the perfluorocarbon core of nanoemulsions. In the presence of ultrasound, perfluorocarbons can undergo a liquid-to-gas phase transition causing the emulsions to rupture and release their protein cargo.[118]

1.6 Perfluorinated artificial cell surfaces

While many have found the addition of fluorine atoms to proteins and lipids to be advantageous, perfluorination of one of the other major classes of biomolecules—carbohydrates—has been less explored. Carbohydrates on cell surfaces are well known to play important roles in cell recognition, binding events, adhesion, and viral infections. Abnormal glycosylation can be implicated in tumor progression and metathesis. Given the hydrophobic and lipophobic nature of perfluorocarbons, cell-surface fluorination could provide a means to disrupt normal interactions of carbohydrates and lectins. The Kumar laboratory has explored the effects of cell-surface fluorination and introduced unnatural perfluorinated carbohydrates by hijacking the sialic acid biosynthetic and salvage pathways, common approaches to introduce unnatural functionality into cell-surface glycans (Figure 1.7). Mannosamine derivatives can be converted to their corresponding sialic acid analogues through the sialic acid biosynthetic pathway, while unnatural sialic acids can be incorporated into cellular glycoproteins through the salvage pathway. In the latter case, there are fewer enzymatic steps that must be traversed, leading to higher levels of incorporation.

Kumar and coworkers prepared a library of fluorinated unnatural mannosamine (F-ManNAc, **1.25**) and sialic acid derivatives (F-Neu5Ac, **1.26**), which were then incubated with mammalian cell lines.[119] Fluorinated acetylated mannosamine derivatives with trifluoromethyl groups were metabolically incorporated and comprised 18% (**1.25a**) and 63% (**1.25b**) of the total membrane sialic acids respectively; however, longer fluoroalkyl groups on the mannosamine (**1.25c-e**) were not well tolerated. To incorporate longer chains, sialic acid derivative **1.26** was tested and resulted in 7% incorporation of C_2F_5 groups (**1.26d**). The metabolic incorporation of compounds **1.25** and **1.26** into the glycocalyx allowed for the display of 10^7-10^8 CF_3 groups on the cell surface. Cells modified with trifluoromethyl groups showed less adherence to fibronectin and selectins, demonstrating that fluorination can be used to modulate cell adhesion.[120,121] The orthogonality of perfluorocarbons provides a tool for engineering new adhesion interactions between cells, biomolecules of interest, and unnatural surfaces.

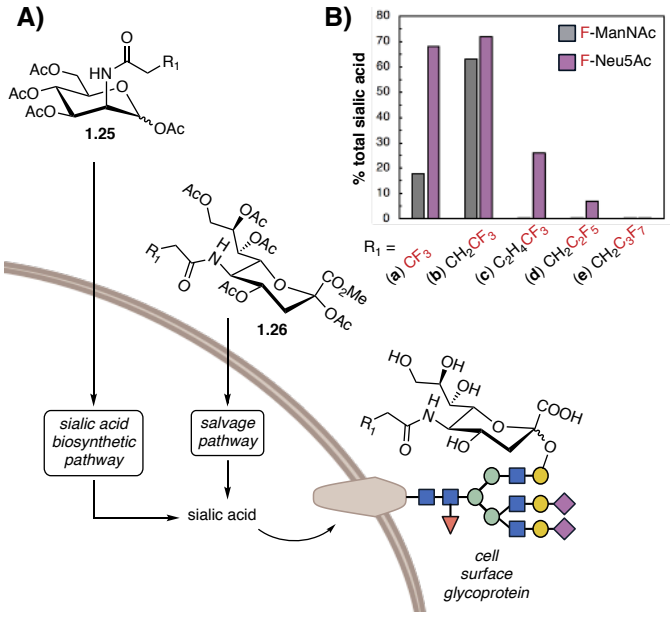

Figure 1.7 Incorporation of unnatural fluorinated carbohydrates. A) Metabolic incorporation of fluorinated monosaccharides through hijacking the sialic acid biosynthetic and salvage pathways. B) After incubation with mannosamine derivative **1.25** (F-ManNAc) or sialic acid derivative **1.26** (F-Neu5Ac), the percent of total sialic acid was obtained by acid hydrolysis of cell-surface

sialic acids, derivatizing with fluorogenic 1,2-diamino-4,5-methylene-dioxybenzene (DMB), and HPLC analysis. Data shown are for incorporation in HL60 cells.[119]

1.7 Perfluorination for purification and immobilization

The ability of perfluorocarbons to self-associate has been utilized in synthetic chemistry as a way to quickly purify products and recycle catalysts and reagents since the 1990s when fluorous biphasic catalysis was introduced by Horvath.[122] In this approach, a molecule of interest (*i.e.* an expensive metal catalyst) can be modified with a fluorinated tag or ligand such that it can be easily recovered from a reaction mixture by liquid fluorous extraction or by separation on fluorous silica gel (fluorous solid phase extraction = FSPE).[123,124] Compounds with fluorous tags interact with fluorous silica gel and can be separated from both non-fluorinated and differentially-fluorinated components of a mixture by washing with different solvent systems. This idea was quickly extended to the purification and/or enrichment of other small molecules and biomolecules, including peptides, oligonucleotides, and carbohydrates.[125] Strategies for "capping" unreacted intermediates during peptide synthesis or tagging the desired product (or an undesired reagent) with fluorous chains allows for the simple removal of the tagged component by fluorous extraction (liquid or solid-phase) or even by centrifugation.[126–128]

1.7.1 Small-molecule library synthesis

Fluorous tags can aide in drug discovery through the preparation of large compound libraries. In 2001, Curran and coworkers introduced the concept of "fluorous mixture synthesis" (Figure 1.8A).[123,129] This strategy relies on the separation of compounds by their fluorous content on fluorous silica gel. In fluorous mixture synthesis, each substrate is modified with a different fluorous tag *(i.e.* C_4F_9, C_6F_{12}, C_8F_{17}, etc. or a mixture of these tags). The fluorinated substrates

are then mixed together for a series of synthetic steps. The final compounds can be "unmixed" using FSPE and the tags can be removed in a deprotection step. The fluorous tag serves not only as a tool to separate the final products, but also as a barcode as the fluorous chain length relates to the retention time on the fluorous column and, thus, the identity of the initial substrate. Fluorous mixture synthesis has been employed to access stereoisomer libraries of macrolactones, oligoisoprenoids, and macrosphelides as well as a large number of natural product analogues.[130–133]

Fluorous tags have also been used to simplify purifications in diversity-oriented synthesis (DOS).[134] Initial substrates were modified with a fluorous tag and used in a variety of transformations. After each step, the fluorous-tagged product was separated from the reagents simply by FSPE, avoiding column chromatography over multiple steps. In comparative studies between "homogenous" DOS with fluorous tags and "heterogenous" DOS with traditional solid-supports, it was found that the fluorous-tag strategies were preferred due to the ease and speed of purification with FSPE.[135]

1.7.2 Proteomics with fluorous tags

In proteomics and molecular biology, researchers often use separation and enrichment techniques to accurately detect, identify, and quantify proteins and post-translational modifications. Traditional techniques include biotin tags for detection with avidin resins and oligohistidine peptides (His-tags) for Ni-NTA affinity chromatography. In 2005, Peters and coworkers applied a fluorous tagging strategy to proteomics (Figure 1.8B). Upon protein (or cell lysate) digest, peptides were tagged with fluorous chains. Cysteines were detected with fluorous iodoacetamides (**1.27**), amines were tagged with fluorous NHS esters (**1.28**), and *O*-

phosphorylation could be detected by β-elimination and Michael addition with a fluorous thiol (**1.29**).[136] Mixtures of tagged and untagged peptides were loaded onto a FSPE cartridge, isolated, and analyzed by mass spec. It was found that enrichment could be obtained based on differing fluorine content (*i.e.* two fluorous tags in one peptide), allowing for separation of peptides with multiple tagged residues or post-translational modifications.

Compared to biotin-based reagents, fluorous-tagged peptide fragments were easily removed from columns with fluorous-tagged silica facilitating product recovery. These fluorous tags are also inert and stable under mass spec analysis as no fragmentation is observed leading to less complicated tandem mass spec MS/MS analysis. This approach has been extended to the enrichment of peptides with other side chain functionalities and small-molecule metabolites by using perfluoroalkyl chains with different functional handles,[137] many of which are now commercially available or have additional functionality, such as photo-crosslinkers.[138,139] Fluorous tags installed through direct radical trifluoromethylation of proteins can also be used for mass spectrometry protein profiling applications.[140,141] Recently, non-covalent fluorous-tagging has been explored for isolating proteins, however this has yet to be demonstrated in a complex biological environment.[142]

1.7.3 Fluorous microarrays

Another area where fluorous tags associating with fluorinated solid supports has been leveraged is the creation of microarrays (Figure 1.8C). Generally, microarrays require covalent modification of the surface with molecules of interest. [143,144] However, Pohl and coworkers found that fluorous tagged carbohydrates could be patterned onto a fluorinated glass slide, eliminating the need for the installation of functional handles onto slides. When exposed to a

fluorescently labeled lectin, the authors observed selective binding even with repeated washes with detergent-containing buffer, demonstrating the robustness of the fluorous-derived microarray.

Since this initial report, fluorous microarrays have been used to present DNA and proteins. These works have explicitly demonstrated minimal non-specific binding on fluorous microarrays.[145,146] Fluorous-tagged DNA can be used for micropatterning in a reversible manner through five cycles of immobilization and removal.[145] Peptides can be presented for protease screening; careful design of the linker between the peptide and the fluorous tag leads to negligible enzyme inhibition.[147] Similarly, small molecules have been displayed to identify histone deacetylase inhibitors.[148]

Crude cell-lysates containing enzymes of interest can be assessed by treating fluorous-tagged enzyme substrates immobilized on a fluorous surface. Cellular material can be washed away such that only fluorous-tagged substrates and products are retained on the surface. Using nanostructure-initiator mass spectrometry (NIMS), which is a soft desorption and ionization method, a ratio between substrates and products can be measured. The non-covalent nature of fluorous microarray formation is thought to provide flexibility to the immobilized substrates, enhancing enzyme activity when compared to covalent surface attachment and also allows for ionization of the substrates.[149,150] Kiessling and coworkers have generalized the NIMS platform to less promiscuous enzymes with a clickable variant where the initial substrates are modified with an azide. Post enzymatic reaction, substrates and products are treated with perfluorinated terminal alkynes and then immobilized. With this enzyme-activity assay, P450 mutants can be screened for the oxidation of small terpenes.[151] In the future, one could envision combing fluorous tag library synthesis (section 1.7.1) with fluorous microarrays, where instead of

removing the fluorous tags from the final compounds, the compounds could be directly displayed on a microarray for target identification or enzyme activity determination by NIMS.

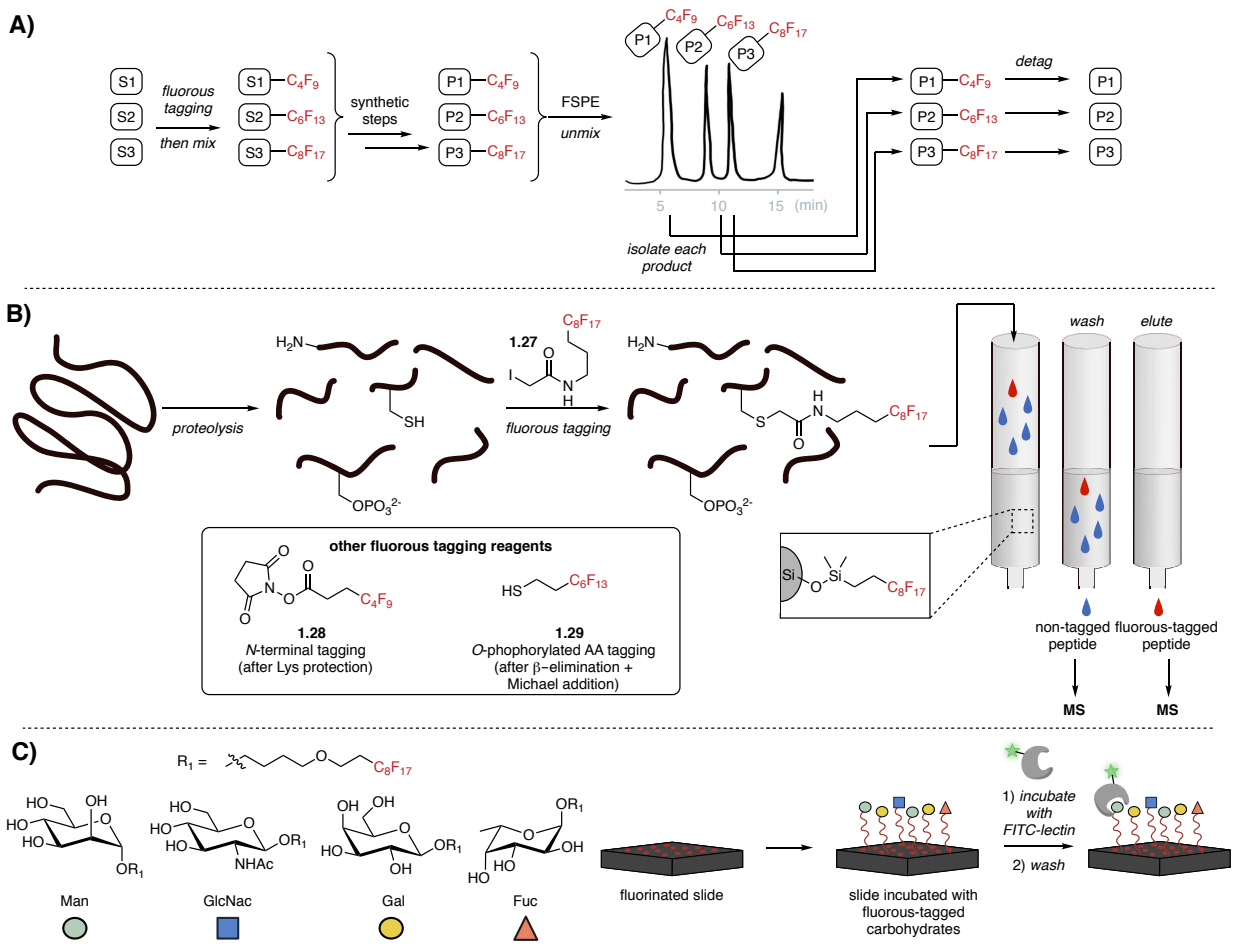

Figure 1.8 Fluorous-mediated purification, immobilization, and characterization. A) Fluorous mixture synthesis. Substrates (S) modified with fluorous tags of different chain lengths can be mixed for reaction sequences to form fluorous-tagged products (P), which can be unmixed by solid-phase fluorous extraction. B) Fluorous tagging of proteins and separation of fluorous-tagged peptide fragments by FSPE. C) Fluorous microarrays for immobilization of fluorous-tagged carbohydrates and studying carbohydrate-binding proteins.

1.8 Perfluorinated MRI tags and probes

Given the utility of perfluorocarbons for ^{19}F NMR, they are also promising molecules for magnetic resonance imaging (MRI) applications. The high sensitivity of fluorine to magnetic resonance provides opportunities for multiplexing and responsive probes. Additionally, the

absence of fluorine from biological tissue makes for little background signal. Ideally, highly symmetric perfluorocarbons (perfluoro-15-crown-5-ether **1.30**, PERFECTA **1.31**, etc.) with many chemically equivalent nuclei can be leveraged for greater signal (Figure 1.9A). [152] However, perfluoro-15-crown-ether and PERFECTA are insoluble in water, necessitating their formulation within nanomaterials, such as emulsions, for imaging applications *in cellulo* and *in vivo*. The use of fluorinated nanomaterials for medical imaging has been reviewed extensively elsewhere.[153]

Complementary to this work, we describe recent examples of small-molecule fluorinated tags, which can be used to probe cellular environments by MRI. The Pomerantz group has devised a solution to have high signal from fluorinated molecules that are still aqueous soluble. Disordered peptide **1.32** with trifluoro-acetylated lysines among multiple unmodified lysines was synthesized (Figure 1.9B).[154] In designing a highly disordered peptide without significant secondary structure, resonance degeneracy of the fluorine nuclei was achieved, providing thirty approximately equivalent fluorine atoms without significant line broadening. The placement of many lysine residues within this peptide conferred water solubility to the probe. The fluorinated oligo(lysine) peptide could then be conjugated to BSA without observing significant signal broadening that is typical for large biomolecules. Minimal signal broadening was attributed to the conformational flexibility of the fluorinated side chains appended to the peptide. This work suggests that high signal ^{19}F MRI probes can be obtained with fluorinated molecules of high structural flexibility and disorder, as an alternative to high symmetry. Ultimately for these probes to be applicable in animal models, further gain of signal could be obtained by using different fluorinated AAs with perfluoro-*tert*-butyl groups or multiple disordered peptides could be conjugated to a protein or nanomaterial.

The high sensitivity of the fluorine nuclei to its environment has also been capitalized on by the Que group. Que and coworkers have shown that fluorinated redox-sensitive metal complexes can be employed to study changes in biological environments, like enzyme activity, redox events, and the presence of reactive species or ions (Figure 1.9C).[155] A known copper PET probe was modified to alter the ligand scaffold by fluorination to access **1.33**.[156] In this system, paramagnetic d^9 Cu^{2+} shortens the spin-spin relaxation time (T_2) of nearby ^{19}F nuclei, weakening the signal of the fluorine nuclei providing an "off" state for the probe. In a hypoxic environment, Cu^{2+} is reduced to diamagnetic d^{10} Cu^{+}, resulting in a lengthening of T_2 and turning the ^{19}F signal "on". Ligand dissociation upon copper reduction also results in signal "turn on". Increasing the number of equivalent fluorine atoms in the probe improves the signal intensity (**1.33** to **1.34**). In addition, altering the distance between the copper center and the fluorine atoms with ethylene glycol linkers (**1.34**, n = 1-4), improves aqueous solubility and modulates the $Cu^{2+/}$ Cu^{+} reduction potential—improving sensitivity and selectivity for hypoxia.[157]

By choosing different paramagnetic/diamagnetic metals (*i.e.* Co^{2+} to Co^{3+}, etc.) and changing the fluorinated ligand scaffolds (**1.35**), the Que group has also been able to monitor reactive oxygen species, cysteine presence, and peroxidase activity by ^{19}F MRI.[158] Careful understanding and improved ability to design stimuli-responsive probes will enable new opportunities to bring chemical biology tools to an array of biological systems.

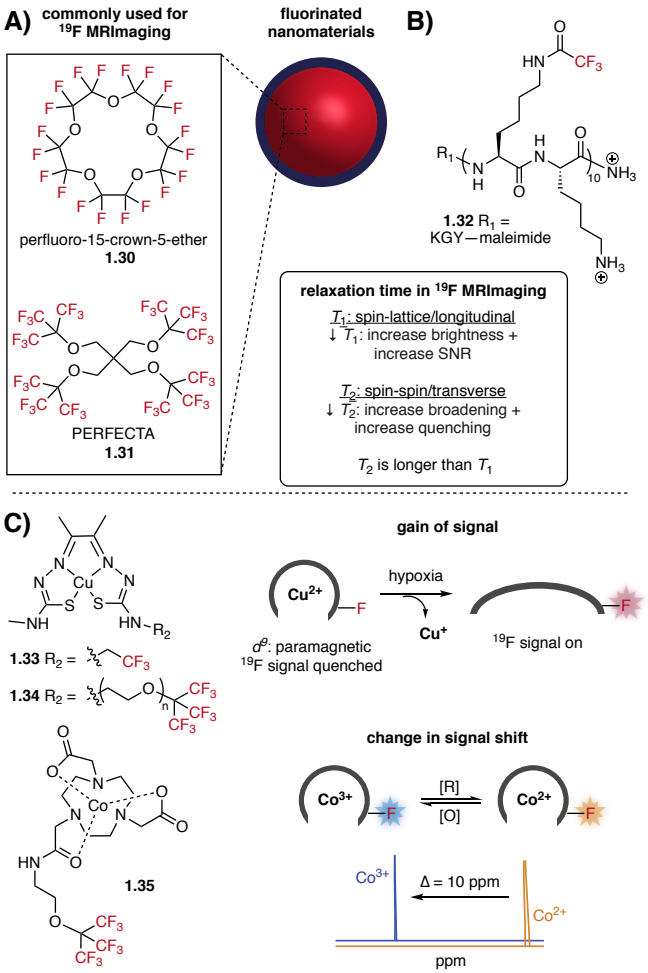

Figure 1.9 Fluorinated molecules for ^{19}F MRI**.** A) Perfluorocarbons with many chemically equivalent fluorine atoms for increased ^{19}F MRI signal when formulated as nanoemulsions. B) Disordered peptide used by Pomerantz and coworkers to achieve degenerate fluorine signal by NMR and MRI. C) Examples of metal-coordinated fluorinated probes reported by Que and coworkers.

1.9 Conclusions and Outlook

In the past decade, many have explored how abiotic, hydro- and lipophobic fluorocarbons can be integrated with naturally occurring systems. Both seemingly small (CF_3) and larger changes (C_nF_{2n+1}) can alter self-assembly, improve biomolecule stability, and facilitate cellular entry. Perfluorinated groups can interact with or be incorporated into all four classes of biomolecules. Tools to design and access fluorinated proteins have been developed, and their

structures and high stability have been extensively explored. These fundamental studies provide the basis for new applications of highly stable fluorinated proteins in the therapeutic realm. With careful engineering one could also use fluorination to design better stabilized coiled-coil protein interactions that function as improved peptide tags for protein labeling.[159,160]

Though not explicitly perfluorocarbons, linear multivicinal fluoroalkanes described by Gilmour and Carreira have been demonstrated to behave orthogonally to their all-hydrocarbon analogues.[161–164] Similarly, Janus all-*cis* perfluorocyclohexyl rings described by Glorius and O'Hagan are highly polar, resulting in interesting supramolecular assemblies.[165–167] These motifs could be further pursued for their effects on lipid membranes and in peptide and protein structure.

Direct perfluorination of biomolecules has been explored, though excellent selectivity remains difficult. Given their increased hydrophobicity, perhaps extended perfluoroalkyl radicals[168,169] could improve chemoselectivity or be harnessed for selective labeling of hydrophobic proteins and membrane-bound protein domains, which has been difficult with current radical protein-modifying techniques.[141] Fluorous tagging has been explored for proteomics and microarray formation, spanning a range of biomolecules and small molecules. New fluorous-tagging strategies are poised to be used as an orthogonal handle, alongside more traditional chemistries, for multiplexed proteomics and microarray formation.[170]

^{19}F NMR and MRI techniques have enabled researchers to study the conformational dynamics of many isolated proteins as well as identify small-molecule binders. In the future, simple and direct methods for RNA perfluorination could extend ^{19}F NMR discovery techniques to small-molecule binders of RNA.[171–173] Responsive fluorinated probes containing paramagnetic metals facilitate the study of redox changes in cellular environments by ^{19}F NMR. Continued

development of tags and probes with enhanced fluorine signal, like the perfluoro-*tert*-butyl group, could facilitate further ^{19}F NMR studies in mammalian cells and animals.[174]

Looking forward, the significant work towards incorporating perfluorinated groups into proteins, peptides, carbohydrates, and lipids should facilitate new tools for manipulating and studying biological systems in research labs and in clinical settings. Perfluorination could be a tool for subcellular localization of proteins and increase membrane affinity as palmitoylation does[175,176] or to help therapeutic biomolecules and diagnostics permeate the hydrophobic blood-brain barrier.[18,177–180] Beyond directing events *in cellulo* and *in vivo*, perfluorination could provide exciting opportunities for interfacing biological systems with unnatural hydrophobic materials as well.

1.10 References

(1) Gerry, C. J.; Schreiber, S. L. Unifying Principles of Bifunctional, Proximity-Inducing Small Molecules. *Nat. Chem. Biol.* **2020**, *16*, 369–378.

(2) Che, Y.; Gilbert, A. M.; Shanmugasundaram, V.; Noe, M. C. Inducing Protein-Protein Interactions with Molecular Glues. *Bioorg. Med. Chem. Lett.* **2018**, *28*, 2585–2592.

(3) Xue, L.; Karpenko, I. A.; Hiblot, J.; Johnsson, K. Imaging and Manipulating Proteins in Live Cells through Covalent Labeling. *Nat. Chem. Biol.* **2015**, *11*, 917–923.

(4) Mrksich, M.; Whitesides, G. M. Using Self-Assembled Monolayers to Understand the Interactions of Man-Made Surfaces with Proteins and Cells. *Annu. Rev. Biophys. Biomol. Struct.* **1996**, *25*, 55–78.

(5) Klymchenko, A. S.; Kreder, R. Fluorescent Probes for Lipid Rafts: From Model Membranes to Living Cells. *Chem. Biol.* **2014**, *21*, 97–113.

(6) Chandra, R. A.; Douglas, E. S.; Mathies, R. A.; Bertozzi, C. R.; Francis, M. B. Programmable Cell Adhesion Encoded by DNA Hybridization. *Angew. Chem. Int. Ed.* **2006**, *45*, 896–901.

(7) Drummond, T. G.; Hill, M. G.; Barton, J. K. Electrochemical DNA Sensors. *Nat. Biotechnol.* **2003**, *21*, 1192–1199.

(8) Thubagere, A. J.; Li, W.; Johnson, R. F.; Chen, Z.; Doroudi, S.; Lee, Y. L.; Izatt, G.; Wittman, S.; Srinivas, N.; Woods, D.; Winfree, E.; Qian, L. A Cargo-Sorting DNA Robot. *Science (80-.).* **2017**, *357*, eaan6558.

(9) Wong, C.-H.; Zimmerman, S. C. Orthogonality in Organic, Polymer, and Supramolecular Chemistry: From Merrifield to Click Chemistry. *Chem. Commun.* **2013**, *49*, 1679–1695.

(10) Sletten, E. M.; Bertozzi, C. R. Bioorthogonal Chemistry: Fishing for Selectivity in a Sea of Functionality. *Angew. Chem. Int. Ed.* **2009**, *48*, 6974–6998.

(11) Liu, C. C.; Jewett, M. C.; Chin, J. W.; Voigt, C. A. Toward an Orthogonal Central Dogma. *Nat. Chem. Biol.* **2018**, *14*, 103–106.

(12) Carvalho, M. F.; Oliveira, R. S. Natural Production of Fluorinated Compounds and Biotechnological Prospects of the Fluorinase Enzyme. *Crit. Rev. Biotechnol.* **2017**, *37*, 880–897.

(13) O'Hagan, D.; B. Harper, D. Fluorine-Containing Natural Products. *J. Fluor. Chem.* **1999**, *100*, 127–133.

(14) Purser, S.; Moore, P. R.; Swallow, S.; Gouverneur, V. Fluorine in Medicinal Chemistry. *Chem. Soc. Rev.* **2008**, *37*, 320–330.

(15) Wang, J.; Sánchez-Roselló, M.; Aceña, J. L.; del Pozo, C.; Sorochinsky, A. E.; Fustero, S.; Soloshonok, V. A.; Liu, H. Fluorine in Pharmaceutical Industry: Fluorine-Containing

Drugs Introduced to the Market in the Last Decade (2001–2011). *Chem. Rev.* **2014**, *114*, 2432–2506.

(16) Müller, K.; Faeh, C.; Diederich, F. Fluorine in Pharmaceuticals: Looking beyond Intuition. *Science* **2007**, *317*, 1881–1886.

(17) Gillis, E. P.; Eastman, K. J.; Hill, M. D.; Donnelly, D. J.; Meanwell, N. A. Applications of Fluorine in Medicinal Chemistry. *J. Med. Chem.* **2015**, *58*, 8315–8359.

(18) Zhou, Y.; Wang, J.; Gu, Z.; Wang, S.; Zhu, W.; Aceña, J. L.; Soloshonok, V. A.; Izawa, K.; Liu, H. Next Generation of Fluorine-Containing Pharmaceuticals, Compounds Currently in Phase II–III Clinical Trials of Major Pharmaceutical Companies: New Structural Trends and Therapeutic Areas. *Chem. Rev.* **2016**, *116*, 422–518.

(19) Meanwell, N. A. Fluorine and Fluorinated Motifs in the Design and Application of Bioisosteres for Drug Design. *J. Med. Chem.* **2018**, *61*, 5822–5880.

(20) Pan, Y. The Dark Side of Fluorine. *ACS Med. Chem. Lett.* **2019**, *10* (7), 1016–1019.

(21) Mei, H.; Han, J.; Fustero, S.; Medio-Simon, M.; Sedgwick, D. M.; Santi, C.; Ruzziconi, R.; Soloshonok, V. A. Fluorine-Containing Drugs Approved by the FDA in 2018. *Chem. Eur. J.* **2019**, *25*, 11797–11819.

(22) Ruiz-Cabello, J.; Barnett, B. P.; Bottomley, P. A.; Bulte, J. W. M. Fluorine (19F) MRS and MRI in Biomedicine. *NMR Biomed.* **2011**, *24*, 114–129.

(23) Chen, H.; Viel, S.; Ziarelli, F.; Peng, L. 19F NMR: A Valuable Tool for Studying Biological Events. *Chem. Soc. Rev.* **2013**, *42*, 7971.

(24) Riess, J. G. Understanding the Fundamentals of Perfluorocarbons and Perfluorocarbon Emulsions Relevant to In Vivo Oxygen Delivery. *Artif. Cells Blood Substit. Biotechnol.* **2005**, *33*, 47–63.

(25) Krafft, M. P.; Riess, J. G. Selected Physicochemical Aspects of Poly- and Perfluoroalkylated Substances Relevant to Performance, Environment and Sustainability-Part One. *Chemosphere* **2015**, *129*, 4–19.

(26) Marsh, E. N. G. Fluorinated Proteins: From Design and Synthesis to Structure and Stability. *Acc. Chem. Res.* **2014**, *47*, 2878–2886.

(27) Chen, S. S.; Rodgers, A. S.; Choo, J.; Wilhoit, R. C.; Zwolinski, B. J. Ideal Gas Thermodynamic Properties of Six Fluoroethanes. *J. Phys. Chem. Ref. Data* **1975**, *4*, 441.

(28) Cortés-Guzmán, F.; Cuevas, G.; Martín Pendás, Á.; Hernández-Trujillo, J. The Rotational Barrier of Ethane and Some of Its Hexasubstituted Derivatives in Terms of the Forces Acting on the Electron Distribution. *Phys. Chem. Chem. Phys.* **2015**, *17*, 19021–19029.

(29) Campos-Vallette, M.; Rey-Lafon, M. Vibrational Spectra and Rotational Isomerism in Short Chain N-Perfluoroalkanes. *J. Mol. Struct.* **1983**, *101*, 23–45.

(30) Dixon, D. A. Torsional Potential about the Central Carbon-Carbon Bond in Perfluoro-n-Butane. *J. Phys. Chem.* **2002**, *96*, 3698–3701.

(31) Röthlisberger, U.; Laasonen, K.; Klein, M. L. The Torsional Potential of Perfluoro N-Alkanes: A Density Functional Study. *J. Chem. Phys* **1996**, *104*, 3692.

(32) Eaton, D. F.; Smart, B. E. Are Fluorocarbon Chains "Stiffer" Than Hydrocarbon Chains? Dynamics of End-to-End Cyclization in a C8F16 Segment Monitored by Fluorescence. *J. Am. Chem. Soc.* **1990**, *112*, 2821–2823.

(33) Ellis, D. A.; Denkenberger, K. A.; Burrow, T. E.; Mabury, S. A. The Use of 19F NMR to Interpret the Structural Properties of Perfluorocarboxylate Acids: A Possible Correlation with Their Environmental Disposition. *J. Phys. Chem. A* **2004**, *108*, 10099–10106.

(34) Seebach, D. Organic Synthesis—Where Now? *Angew. Chem. Int. Ed.* **1990**, *29*, 1320–

1367.

(35) Sadtler, V. M.; Giulieri, F.; Krafft, M. P.; Riess, J. G. Micellization and Adsorption of Fluorinated Amphiphiles: Questioning the 1 CF2≈1.5 CH2 Rule. *Chem. Eur. J.* **1998**, *4*, 1952–1956.

(36) Buer, B. C.; Meagher, J. L.; Stuckey, J. A.; Marsh, E. N. G. Structural Basis for the Enhanced Stability of Highly Fluorinated Proteins. *Proc. Natl. Acad. Sci. U. S. A.* **2012**, *109*, 4810–4815.

(37) Yoder, N. C.; Yüksel, D.; Dafik, L.; Kumar, K. Bioorthogonal Noncovalent Chemistry: Fluorous Phases in Chemical Biology. *Curr. Opin. Chem. Biol.* **2006**, *10*, 576–583.

(38) Sicinski, K.; Montanari, V.; Kumar, K. Chemical Biology and Supramolecular Chemistry of Fluorinated Molecules. In *Frontiers of Organofluorine Chemistry*; Iwao Ojima, Ed.; World Scientific 2020, 2020; pp 561–584.

(39) Szabó, D.; Mohl, J.; Bálint, A. M.; Bodor, A.; Rábai, J. Novel Generation Ponytails in Fluorous Chemistry: Syntheses of Primary, Secondary, and Tertiary (Nonafluoro-Tert-Butyloxy)Ethyl Amines. *J. Fluor. Chem.* **2006**, *127*, 1496–1504.

(40) Zhao, X.; Ng, W. Y.; Lau, K. C.; Collis, A. E. C.; Horváth, I. T. Generation of (Nonafluoro-Tert-Butoxy)Methyl Ponytails for Enhanced Fluorous Partition of Aromatics and Heterocycles. *Phys. Chem. Chem. Phys.* **2012**, *14*, 3909–3914.

(41) Decato, S.; Bemis, T.; Madsen, E.; Mecozzi, S. Synthesis and Characterization of Perfluoro-Tert-Butyl Semifluorinated Amphiphilic Polymers and Their Potential Application in Hydrophobic Drug Delivery. *Polym. Chem.* **2014**, *5*, 6461–6471.

(42) Tirotta, I.; Mastropietro, A.; Cordiglieri, C.; Gazzera, L.; Baggi, F.; Baselli, G.; Bruzzone, M. G.; Zucca, I.; Cavallo, G.; Terraneo, G.; Baldelli Bombelli, F.; Metrangolo, P.;

Resnati, G. A Superfluorinated Molecular Probe for Highly Sensitive in Vivo 19 F-MRI. *J. Am. Chem. Soc.* **2014**, *136*, 8524–8527.

(43) Holmgren, S. K.; Taylor, K. M.; Bretscher, L. E.; Raines, R. T. Code for Collagen's Stability Deciphered. *Nature* **1998**, *392*, 666–667.

(44) Sessler, C. D.; Rahm, M.; Becker, S.; Goldberg, J. M.; Wang, F.; Lippard, S. J. CF 2 H, a Hydrogen Bond Donor. *J. Am. Chem. Soc.* **2017**, *139*, 9325–9332.

(45) Pace, C. J.; Gao, J. Exploring and Exploiting Polar−π Interactions with Fluorinated Aromatic Amino Acids. *Acc. Chem. Res.* **2013**, *46*, 907–915.

(46) Basar Bilgiçer; Alfio Fichera, A.; Kumar, K. A Coiled Coil with a Fluorous Core. *J. Am. Chem. Soc.* **2001**, *123*, 4393–4399.

(47) Wang, P.; Fichera, A.; Kumar, K.; Tirrell, D. A. Alternative Translations of a Single RNA Message: An Identity Switch of (2S,3R)-4,4,4-Trifluorovaline between Valine and Isoleucine Codons. *Angew. Chem. Int. Ed.* **2004**, *43*, 3664–3666.

(48) Tang, Y.; Ghirlanda, G.; Vaidehi, N.; Kua, J.; Mainz, D. T.; III, W. A. G.; DeGrado, W. F.; Tirrell, D. A. Stabilization of Coiled-Coil Peptide Domains by Introduction of Trifluoroleucine. *Biochemistry* **2001**, *40*, 2790–2796.

(49) Rennert, O. M.; Anker, H. S. On the Incorporation of 5',5',5'-Trifluoroleucine into Proteins of E. Coli. *Biochemistry* **1963**, *2*, 471–476.

(50) Tang, Y.; Ghirlanda, G.; Petka, W. A.; Nakajima, T.; DeGrado, W. F.; Tirrell, D. A. Fluorinated Coiled-Coil Proteins Prepared In Vivo Display Enhanced Thermal and Chemical Stability. *Angew. Chem. Int. Ed.* **2001**, *40*, 1494–1496.

(51) Wang, P.; Tang, Y.; Tirrell, D. A. Incorporation of Trifluoroisoleucine into Proteins in Vivo. *J. Am. Chem. Soc.* **2003**, *125*, 6900–6906.

(52) Leung, R. L. C.; Robinson, M. D. M.; Ajabali, A. A. A.; Karunanithy, G.; Lyons, B.; Raj, R.; Raoufmoghaddam, S.; Mohammed, S.; Claridge, T. D. W.; Baldwin, A. J.; Davis, B. G. Monitoring the Disassembly of Virus-like Particles by 19 F-NMR. *J. Am. Chem. Soc.* **2017**, *139*, 5277–5280.

(53) Duewel, H.; Daub, E.; Robinson, V.; Honek, J. F. Incorporation of Trifluoromethionine into a Phage Lysozyme: Implications and a New Marker for Use in Protein 19F NMR†. *Biochemistry* **1997**, *36*, 3404–3416.

(54) Holzberger, B.; Rubini, M.; Möller, H. M.; Marx, A. A Highly Active DNA Polymerase with a Fluorous Core. *Angew. Chem. Int. Ed.* **2010**, *49*, 1324–1327.

(55) Tang, Y.; Tirrell, D. A. Biosynthesis of a Highly Stable Coiled-Coil Protein Containing Hexafluoroleucine in an Engineered Bacterial Host. *J. Am. Chem. Soc.* **2001**, *123*, 11089–11090.

(56) Völler, J.-S.; Dulic, M.; Gerling-Driessen, U. I. M.; Biava, H.; Baumann, T.; Budisa, N.; Gruic-Sovulj, I.; Koksch, B. Discovery and Investigation of Natural Editing Function against Artificial Amino Acids in Protein Translation. *ACS Cent. Sci.* **2017**, *3*, 73–80.

(57) Jackson, J. C.; Hammill, J. T.; Mehl, R. A. Site-Specific Incorporation of a 19 F-Amino Acid into Proteins as an NMR Probe for Characterizing Protein Structure and Reactivity. *J. Am. Chem. Soc* **2007**, *129*, 1160–1166.

(58) Li, C.; Wang, G.-F.; Wang, Y.; Creager-Allen, R.; Lutz, E. A.; Scronce, H.; Slade, K. M.; Ruf, R. A. S.; Mehl, R. A.; Pielak, G. J. Protein 19 F NMR in Escherichia Coli. *J. Am. Chem. Soc.* **2010**, *132*, 321–327.

(59) Hammill, J. T.; Miyake-Stoner, S.; Hazen, J. L.; Jackson, J. C.; Mehl, R. A. Preparation of Site-Specifically Labeled Fluorinated Proteins for 19 F-NMR Structural Characterization.

Nat. Protoc. **2007**, *2*, 2601–2607.

(60) Cellitti, S. E.; Jones, D. H.; Lagpacan, L.; Hao, X.; Zhang, Q.; Hu, H.; Brittain, S. M.; Brinker, A.; Caldwell, J.; Bursulaya, B.; Spraggon, G.; Brock, A.; Ryu, Y.; Uno, T.; Schultz, P. G.; Geierstanger, B. H. In Vivo Incorporation of Unnatural Amino Acids to Probe Structure, Dynamics, and Ligand Binding in a Large Protein by Nuclear Magnetic Resonance Spectroscopy. *J. Am. Chem. Soc.* **2008**, *130*, 9268–9281.

(61) Yoder, N. C.; Kumar, K. Fluorinated Amino Acids in Protein Design and Engineering. *Chem. Soc. Rev.* **2002**, *31*, 335–341.

(62) Maisch, D.; Wadhwani, P.; Afonin, S.; Böttcher, C.; Koksch, B.; Ulrich, A. S. Chemical Labeling Strategy with (R)- and (S)-Trifluoromethylalanine for Solid State 19 F NMR Analysis of Peptaibols in Membranes. *J. Am. Chem. Soc.* **2009**, *131*, 15596–15597.

(63) Vine, W. H.; Hsieh, K.-H.; Marshall, G. R. Synthesis of Fluorine-Containing Peptides. Analogs of Angiotensin II Containing Hexafluorovaline. *J. Med. Chem.* **1981**, *24*, 1043–1047.

(64) Tressler, C. M.; Zondlo, N. J. Perfluoro- Tert -Butyl Homoserine Is a Helix-Promoting, Highly Fluorinated, NMR-Sensitive Aliphatic Amino Acid: Detection of the Estrogen Receptor·Coactivator Protein–Protein Interaction by 19 F NMR. *Biochemistry* **2017**, *56*, 1062–1074.

(65) Buer, B. C.; Levin, B. J.; Marsh, E. N. G. Perfluoro- Tert -Butyl-Homoserine as a Sensitive 19 F NMR Reporter for Peptide-Membrane Interactions in Solution. *J. Pept. Sci.* **2013**, *19*, 308–314.

(66) Tressler, C. M.; Zondlo, N. J. Synthesis of Perfluoro- Tert -Butyl Tyrosine, for Application in 19 F NMR, via a Diazonium-Coupling Reaction. *Org. Lett.* **2016**, *18*,

6240–6243.

(67) Tressler, C. M.; Zondlo, N. J. Perfluoro- Tert -Butyl Hydroxyprolines as Sensitive, Conformationally Responsive Molecular Probes: Detection of Protein Kinase Activity by 19 F NMR. *ACS Chem. Biol.* **2020**, *15*, 1096–1103.

(68) Tressler, C. M.; Zondlo, N. J. (2 S ,4 R)- and (2 S ,4 S)-Perfluoro- Tert -Butyl 4-Hydroxyproline: Two Conformationally Distinct Proline Amino Acids for Sensitive Application in 19 F NMR. *J. Org. Chem.* **2014**, *79*, 5880–5886.

(69) Kubyshkin, V.; Afonin, S.; Kara, S.; Budisa, N.; Mykhailiuk, P. K.; Ulrich, A. S. γ-(S)-Trifluoromethyl Proline: Evaluation as a Structural Substitute of Proline for Solid State 19 F-NMR Peptide Studies. *Org. Biomol. Chem.* **2015**, *13*, 3171–3181.

(70) Yajima, T.; Tonoi, T.; Nagano, H.; Tomita, Y.; Mikami, K. Direct Racemic Mixture Synthesis of Fluorinated Amino Acids by Perfluoroalkyl Radical Addition to Dehydroamino Acids Terminated by Asymmetric Protonation. *Eur. J. Org. Chem.* **2010**, *2010*, 2461–2464.

(71) Abe, H.; Amii, H.; Uneyama, K. Pd-Catalyzed Asymmetric Hydrogenation of α-Fluorinated Iminoesters in Fluorinated Alcohol: A New and Catalytic Enantioselective Synthesis of Fluoro α-Amino Acid Derivatives. *Org. Lett.* **2001**, *3*, 313–315.

(72) Larsson, U.; Carlson, R.; Leroy, J.; Hallberg, A.; Alvhäll, J.; Svenson, R.; Greune, M.; Weidlein, J.; Nasiri, A.; Okada, Y. Synthesis of Amino Acids with Modified Principal Properties. 1. Amino Acids with Fluorinated Side Chains. *Acta Chem. Scand.* **1993**, *47*, 380–390.

(73) Yajima, T.; Nagano, H. Photoinduced Diastereoselective Addition of Perfluoroalkyl Iodides to Acrylic Acid Derivatives for the Synthesis of Fluorinated Amino Acids. *Org.*

Lett. **2007**, *9*, 2513–2515.

(74) Ye, L.; Van Eps, N.; Zimmer, M.; Ernst, O. P.; Prosser, R. S. Activation of the A2A Adenosine G-Protein-Coupled Receptor by Conformational Selection. *Nature* **2016**, *533*, 265–268.

(75) Manglik, A.; Kim, T. H.; Masureel, M.; Altenbach, C.; Yang, Z.; Hilger, D.; Lerch, M. T.; Kobilka, T. S.; Thian, F. S.; Hubbell, W. L.; Prosser, R. S.; Kobilka, B. K. Structural Insights into the Dynamic Process of B2-Adrenergic Receptor Signaling. *Cell* **2015**, *161*, 1101–1111.

(76) Ye, L.; Larda, S. T.; Frank Li, Y. F.; Manglik, A.; Prosser, R. S. A Comparison of Chemical Shift Sensitivity of Trifluoromethyl Tags: Optimizing Resolution in 19F NMR Studies of Proteins. *J. Biomol. NMR* **2015**, *62*, 97–103.

(77) Edwards, J. M.; Derrick, J. P.; van der Walle, C. F.; Golovanov, A. P. 19F NMR as a Tool for Monitoring Individual Differentially Labeled Proteins in Complex Mixtures. *Mol. Pharm.* **2018**, *15*, 2785–2796.

(78) Fujiwara, Y.; Dixon, J. A.; O'Hara, F.; Funder, E. D.; Dixon, D. D.; Rodriguez, R. A.; Baxter, R. D.; Herlé, B.; Sach, N.; Collins, M. R.; Ishihara, Y.; Baran, P. S. Practical and Innate Carbon–Hydrogen Functionalization of Heterocycles. *Nature* **2012**, *492*, 95–99.

(79) Imiołek, M.; Karunanithy, G.; Ng, W.-L.; Baldwin, A. J.; Gouverneur, V.; Davis, B. G. Selective Radical Trifluoromethylation of Native Residues in Proteins. *J. Am. Chem. Soc.* **2018**, *140*, 1568–1571.

(80) Rahimidashaghoul, K.; Klimánková, I.; Hubálek, M.; Korecký, M.; Chvojka, M.; Pokorný, D.; Matoušek, V.; Fojtík, L.; Kavan, D.; Kukačka, Z.; Novák, P.; Beier, P. Reductant-Induced Free Radical Fluoroalkylation of Nitrogen Heterocycles and Innate

Aromatic Amino Acid Residues in Peptides and Proteins. *Chem. Eur. J.* **2019**, *25*, 15779–15785.

(81) Verhoog, S.; Kee, C. W.; Wang, Y.; Khotavivattana, T.; Wilson, T. C.; Kersemans, V.; Smart, S.; Tredwell, M.; Davis, B. G.; Gouverneur, V. 18 F-Trifluoromethylation of Unmodified Peptides with 5- 18 F-(Trifluoromethyl)Dibenzothiophenium Trifluoromethanesulfonate. *J. Am. Chem. Soc.* **2018**, *140*, 1572–1575.

(82) Václavík, J.; Zschoche, R.; Klimánková, I.; Matoušek, V.; Beier, P.; Hilvert, D.; Togni, A. Irreversible Cysteine-Selective Protein Labeling Employing Modular Electrophilic Tetrafluoroethylation Reagents. *Chem. Eur. J.* **2017**, *23*, 6490–6494.

(83) Matoušek, V.; Václavík, J.; Hájek, P.; Charpentier, J.; Blastik, Z. E.; Pietrasiak, E.; Budinská, A.; Togni, A.; Beier, P. Expanding the Scope of Hypervalent Iodine Reagents for Perfluoroalkylation: From Trifluoromethyl to Functionalized Perfluoroethyl. *Chem. Eur. J.* **2016**, *22*, 417–424.

(84) Ichiishi, N.; Caldwell, J. P.; Lin, M.; Zhong, W.; Zhu, X.; Streckfuss, E.; Kim, H.-Y.; Parish, C. A.; Krska, S. W. Protecting Group Free Radical C–H Trifluoromethylation of Peptides. *Chem. Sci.* **2018**, *9*, 4168–4175.

(85) Guerrero, I.; Correa, A. Site-Selective Trifluoromethylation Reactions of Oligopeptides. *Asian J. Org. Chem.* **2020**, *9*, 898–909.

(86) Di Pietrantonio, C.; Pandey, A.; Gould, J.; Hasabnis, A.; Prosser, R. S. Understanding Protein Function Through an Ensemble Description: Characterization of Functional States by 19F NMR. *Methods Enzymol.* **2019**, *615*, 103–130.

(87) Marsh, E. N. G.; Suzuki, Y. Using 19 F NMR to Probe Biological Interactions of Proteins and Peptides. *ACS Chem. Biol.* **2014**, *9*, 1242–1250.

(88) Keith, M.; Arntson, E.; Pomerantz, W. C. K. Protein-Observed Fluorine NMR: A Bioorthogonal Approach for Small Molecule Discovery. *J. Med. Chem.* **2016**, *59*, 5158–5171.

(89) Divakaran, A.; Kirberger, S. E.; Pomerantz, W. C. K. SAR by (Protein-Observed) 19 F NMR. *Acc. Chem. Res.* **2019**, *52*, 3407–3418.

(90) Dalvit, C.; Vulpetti, A. Ligand-Based Fluorine NMR Screening: Principles and Applications in Drug Discovery Projects. *J. Med. Chem.* **2019**, *62*, 2218–2244.

(91) Urick, A. K.; Hawk, L. M. L.; Cassel, M. K.; Mishra, N. K.; Liu, S.; Adhikari, N.; Zhang, W.; dos Santos, C. O.; Hall, J. L.; Pomerantz, W. C. K. Dual Screening of BPTF and Brd4 Using Protein-Observed Fluorine NMR Uncovers New Bromodomain Probe Molecules. *ACS Chem. Biol.* **2015**, *10*, 2246–2256.

(92) Carlson, A. S.; Cui, H.; Divakaran, A.; Johnson, J. A.; Brunner, R. M.; Pomerantz, W. C. K.; Topczewski, J. J. Systematically Mitigating the P38α Activity of Triazole-Based BET Inhibitors. *ACS Med. Chem. Lett.* **2019**, *10*, 1296–1301.

(93) Buer, B. C.; Marsh, E. N. G. Fluorine: A New Element in Protein Design. *Protein Sci.* **2012**, *21*, 453–462.

(94) Buer, B. C.; Levin, B. J.; Marsh, E. N. G. Influence of Fluorination on the Thermodynamics of Protein Folding. *J. Am. Chem. Soc.* **2012**, *134*, 13027–13034.

(95) More, H. T.; Zhang, K. S.; Srivastava, N.; Frezzo, J. A.; Montclare, J. K. Influence of Fluorination on Protein-Engineered Coiled-Coil Fibers. *Biomacromolecules* **2015**, *16*, 1210–1217.

(96) Hill, L. K.; Frezzo, J. A.; Katyal, P.; Hoang, D. M.; Ben Youss Gironda, Z.; Xu, C.; Xie, X.; Delgado-Fukushima, E.; Wadghiri, Y. Z.; Montclare, J. K. Protein-Engineered

Nanoscale Micelles for Dynamic 19 F Magnetic Resonance and Therapeutic Drug Delivery. *ACS Nano* **2019**, *13*, 2969–2985.

(97) Biava, H.; Budisa, N. Evolution of Fluorinated Enzymes: An Emerging Trend for Biocatalyst Stabilization. *Eng. Life Sci.* **2014**, *14*, 340–351.

(98) Son, S.; Tanrikulu, I. C.; Tirrell, D. A. Stabilization of Bzip Peptides through Incorporation of Fluorinated Aliphatic Residues. *ChemBioChem* **2006**, *7*, 1251–1257.

(99) Gottler, L. M.; Lee, H.-Y.; Shelburne, C. E.; Ramamoorthy, A.; Marsh, E. N. G. Using Fluorous Amino Acids to Modulate the Biological Activity of an Antimicrobial Peptide. *ChemBioChem* **2008**, *9*, 370–373.

(100) Naarmann, N.; Bilgiçer, B.; Meng, H.; Kumar, K.; Steinem, C. Fluorinated Interfaces Drive Self-Association of Transmembrane α Helices in Lipid Bilayers. *Angew. Chem. Int. Ed.* **2006**, *45*, 2588–2591.

(101) Bilgiçer, B.; Kumar, K. De Novo Design of Defined Helical Bundles in Membrane Environments. *Proc. Natl. Acad. Sci. U.S.A* **2004**, *101*, 15324–15329.

(102) Yoder, N. C.; Kalsani, V.; Schuy, S.; Vogel, R.; Janshoff, A.; Kumar, K. Nanoscale Patterning in Mixed Fluorocarbon-Hydrocarbon Phospholipid Bilayers. *J. Am. Chem. Soc.* **2007**, *129*, 9037–9043.

(103) Schumacher, G.; Bakowsky, U.; Gege, C.; Schmidt, R. R.; Rothe, U.; Bendas, G. Lessons Learned from Clustering of Fluorinated Glycolipids on Selectin Ligand Function in Cell Rolling. *Biochemistry* **2006**, *45*, 2894–2903.

(104) Partlow, K. C.; Lanza, G. M.; Wickline, S. A. Exploiting Lipid Raft Transport with Membrane Targeted Nanoparticles: A Strategy for Cytosolic Drug Delivery. *Biomaterials* **2008**, *29*, 3367–3375.

(105) Nabi, I. R.; Le, P. U. Caveolae/Raft-Dependent Endocytosis. *J. Cell Biol.* **2003**, *161*, 673–677.

(106) Dafik, L.; Kalsani, V.; Leung, A. K. L.; Kumar, K. Fluorinated Lipid Constructs Permit Facile Passage of Molecular Cargo into Living Cells. *J. Am. Chem. Soc.* **2009**, *131*, 12091–12093.

(107) Dolain, C.; Patwa, A.; Godeau, G.; Barthélémy, P.; Dolain, C.; Patwa, A.; Godeau, G.; Barthélémy, P. Nucleic Acid Based Fluorinated Derivatives: New Tools for Biomedical Applications. *Appl. Sci.* **2012**, *2*, 245–259.

(108) Godeau, G.; Arnion, H.; Brun, C.; Staedel, C.; Barthélémy, P. Fluorocarbon Oligonucleotide Conjugates for Nucleic Acids Delivery. *Med. Chem. Commun.* **2010**, *1*, 76–78.

(109) Ellipilli, S.; Murthy, R. V.; Ganesh, K. N. Perfluoroalkylchain Conjugation as a New Tactic for Enhancing Cell Permeability of Peptide Nucleic Acids (PNAs) via Reducing the Nanoparticle Size. *Chem. Commun.* **2016**, *52*, 521–524.

(110) Chuard, N.; Fujisawa, K.; Morelli, P.; Saarbach, J.; Winssinger, N.; Metrangolo, P.; Resnati, G.; Sakai, N.; Matile, S. Activation of Cell-Penetrating Peptides with Ionpair−π Interactions and Fluorophiles. *J. Am. Chem. Soc.* **2016**, *138*, 11264–11271.

(111) Lv, H.; Zhang, S.; Wang, B.; Cui, S.; Yan, J. Toxicity of Cationic Lipids and Cationic Polymers in Gene Delivery. *J. Control. Release* **2006**, *114*, 100–109.

(112) Zeng, H.; Johnson, M. E.; Oldenhuis, N. J.; Tiambeng, T. N.; Guan, Z. Structure-Based Design of Dendritic Peptide Bolaamphiphiles for SiRNA Delivery. *ACS Cent. Sci.* **2015**, *1*, 303–312.

(113) Fuller, R. W.; Molloy, B. B. The Effect of Aliphatic Fluorine on Amine Drugs. In

Biochemistry Involving Carbon-Fluorine Bonds; 1976; pp 77–98.

(114) Fjelbye, K.; Marigo, M.; Clausen, R. P.; Jørgensen, E. B.; Christoffersen, C. T.; Juhl, K. Elucidation of Fluorine's Impact on PKa and in Vitro Pgp-Mediated Efflux for a Series of PDE9 Inhibitors. *Med. Chem. Commun.* **2018**, *9*, 893–896.

(115) Wang, M.; Liu, H.; Li, L.; Cheng, Y. A Fluorinated Dendrimer Achieves Excellent Gene Transfection Efficacy at Extremely Low Nitrogen to Phosphorus Ratios. *Nat. Commun.* **2014**, *5*, 3053.

(116) Wang, M.; Cheng, Y. Structure-Activity Relationships of Fluorinated Dendrimers in DNA and SiRNA Delivery. *Acta Biomater.* **2016**, *46*, 204–210.

(117) Zhang, Z.; Shen, W.; Ling, J.; Yan, Y.; Hu, J.; Cheng, Y. The Fluorination Effect of Fluoroamphiphiles in Cytosolic Protein Delivery. *Nat. Commun.* **2018**, *9*, 1377.

(118) Sloand, J. N.; Nguyen, T. T.; Zinck, S. A.; Cook, E. C.; Zimudzi, T. J.; Showalter, S. A.; Glick, A. B.; Simon, J. C.; Medina, S. H. Ultrasound-Guided Cytosolic Protein Delivery via Transient Fluorous Masks. *ACS Nano* **2020**, *14*, 4061–4073.

(119) Dafik, L.; D'Alarcao, M.; Kumar, K. Fluorination of Mammalian Cell Surfaces via the Sialic Acid Biosynthetic Pathway. *Bioorg. Med. Chem. Lett.* **2008**, *18*, 5945–5947.

(120) Oetke, C.; Brossmer, R.; Mantey, L. R.; Hinderlich, S.; Isecke, R.; Reutter, W.; Keppler, O. T.; Pawlita, M. Versatile Biosynthetic Engineering of Sialic Acid in Living Cells Using Synthetic Sialic Acid Analogues. *J. Biol. Chem.* **2002**, *277*, 6688–6695.

(121) Dafik, L.; D'Alarcao, M.; Kumar, K. Modulation of Cellular Adhesion by Glycoengineering. *J. Med. Chem.* **2010**, *53*, 4277–4284.

(122) Horvath, I. T.; Rabai, J. Facile Catalyst Separation Without Water: Fluorous Biphase Hydroformylation of Olefins. *Science* **1994**, *266*, 72–75.

(123) Luo, Z.; Zhang, Q.; Oderaotoshi, Y.; Curran, D. P. Fluorous Mixture Synthesis: A Fluorous-Tagging Strategy for the Synthesis and Separation of Mixtures of Organic Compounds. *Science* **2001**, *291*, 1766–1769.

(124) Curran, D. P.; Luo, Z. Fluorous Synthesis with Fewer Fluorines (Light Fluorous Synthesis): Separation of Tagged from Untagged Products by Solid-Phase Extraction with Fluorous Reverse-Phase Silica Gel. *J. Am. Chem. Soc.* **1999**, *121*, 9069–9072.

(125) Zhang, W. Fluorous Tagging Strategy for Solution-Phase Synthesis of Small Molecules, Peptides and Oligosaccharides. *Curr. Opin. Drug Discov. Devel.* **2019**, *7*, 784–797.

(126) Montanari, V.; Kumar, K. Just Add Water: A New Fluorous Capping Reagent for Facile Purification of Peptides Synthesized on the Solid Phase. *J. Am. Chem. Soc.* **2004**, *126*, 9528–9529.

(127) Montanari, V.; Kumar, K. Enabling Routine Fluorous Capping in Solid Phase Peptide Synthesis. *J. Fluor. Chem.* **2006**, *127*, 565–570.

(128) Montanari, V.; Kumar, K. A Fluorous Capping Strategy for Fmoc-Based Automated and Manual Solid-Phase Peptide Synthesis. *Eur. J. Org. Chem.* **2006**, 874–877.

(129) Zhang, W.; Curran, D. P. Synthetic Applications of Fluorous Solid-Phase Extraction (F-SPE). *Tetrahedron* **2006**, *62*, 11837–11865.

(130) Moretti, J. D.; Wang, X.; Curran, D. P. Minimal Fluorous Tagging Strategy That Enables the Synthesis of the Complete Stereoisomer Library of SCH725674 Macrolactones. *J. Am. Chem. Soc.* **2012**, *134*, 7963–7970.

(131) Yeh, E. A.-H.; Kumli, E.; Damodaran, K.; Curran, D. P. Bare-Minimum Fluorous Mixture Synthesis of a Stereoisomer Library of 4,8,12-Trimethylnonadecanols and Predictions of NMR Spectra of Saturated Oligoisoprenoid Stereoisomers. *J. Am. Chem. Soc.* **2013**, *135*,

1577–1584.

(132) Curran, D. P.; Sinha, M. K.; Zhang, K.; Sabatini, J. J.; Cho, D.-H. Binary Fluorous Tagging Enables the Synthesis and Separation of a 16-Stereoisomer Library of Macrosphelides. *Nat. Chem.* **2012**, *4*, 124–129.

(133) Zhang, W.; Luo, Z.; Christine Hiu-Tung Chen; Curran, D. P. Solution-Phase Preparation of a 560-Compound Library of Individual Pure Mappicine Analogues by Fluorous Mixture Synthesis. *J . Am. Chem. Soc.* **2002**, *124*, 10443–10450.

(134) Morton, D.; Leach, S.; Cordier, C.; Warriner, S.; Nelson, A. Synthesis of Natural-Product-Like Molecules with Over Eighty Distinct Scaffolds. *Angew. Chemie Int. Ed.* **2009**, *48*, 104–109.

(135) Sanz-Cervera, J. F.; Blasco, R.; Piera, J.; Cynamon, M.; Ibáñez, I.; Murguía, M.; Fustero, S. Solution versus Fluorous versus Solid-Phase Synthesis of 2,5-Disubstituted 1,3-Azoles. Preliminary Antibacterial Activity Studies. *J. Org. Chem.* **2009**, *74*, 8988–8996.

(136) Brittain, S. M.; Ficarro, S. B.; Brock, A.; Peters, E. C. Enrichment and Analysis of Peptide Subsets Using Fluorous Affinity Tags and Mass Spectrometry. *Nat. Biotechnol.* **2005**, *23*, 463–468.

(137) Go, E. P.; Uritboonthai, W.; Apon, J. V; Trauger, S. A.; Nordstrom, A.; O'maille, G.; Brittain, S. M.; Peters, E. C.; Siuzdak, G. Selective Metabolite and Peptide Capture/Mass Detection Using Fluorous Affinity Tags. *J. Proteome Res.* **2007**, *6*, 1492–1499.

(138) Kumar, A. B.; Anderson, J. M.; Manetsch, R. Design, Synthesis and Photoactivation Studies of Fluorous Photolabels. *Org. Biomol. Chem.* **2011**, *9*, 6284–6292.

(139) Song, Z.; Zhang, Q. Fluorous Aryldiazirine Photoaffinity Labeling Reagents. *Org. Lett.* **2009**, *11*, 4882–4885.

(140) Cheng, M.; Guo, C.; Gross, M. L. The Application of Fluorine-Containing Reagents in Structural Proteomics. *Angew. Chem. Int. Ed.* **2020**, *59*, 5880 –5889.

(141) Cheng, M.; Zhang, B.; Cui, W.; Gross, M. L. Laser-Initiated Radical Trifluoromethylation of Peptides and Proteins: Application to Mass-Spectrometry-Based Protein Footprinting. *Angew. Chem. Int. Ed.* **2017**, *56*, 14007–14010.

(142) Bassanini, I.; Galli, C.; Ferrandi, E. E.; Vallone, F.; Andolfo, A.; Romeo, S. Perfluorinated Probes for Noncovalent Protein Recognition and Isolation. *Bioconjug. Chem.* **2020**, *31*, 513–519.

(143) Kwang-Seuk Ko; Firoz A. Jaipuri, A.; Pohl, N. L. Fluorous-Based Carbohydrate Microarrays. *J. Am. Chem. Soc.* **2005**, *127*, 13162–13163.

(144) Pohl, N. L. Fluorous Tags Catching on Microarrays. *Angew. Chem. Int. Ed.* **2008**, 3868–3870.

(145) Flynn, G. E.; Withers, J. M.; Macias, G.; Sperling, J. R.; Henry, S. L.; Cooper, J. M.; Burley, G. A.; Clark, A. W. Reversible DNA Micro-Patterning Using the Fluorous Effect. *Chem. Commun.* **2017**, *53*, 3094–3097.

(146) Li, B.-Y.; Juang, D. S.; Adak, A. K.; Hwang, K.-C.; Lin, C.-C. Fabrication of a Protein Microarray by Fluorous-Fluorous Interactions. *Sci. Rep.* **2017**, *7*, 7053.

(147) Collet, B. Y. M.; Nagashima, T.; Yu, M. S.; Pohl, N. L. B. Fluorous-Based Peptide Microarrays for Protease Screening. *J. Fluor. Chem.* **2009**, *130*, 1042–1048.

(148) Vegas, A. J.; Bradner, J. E.; Tang, W.; McPherson, O. M.; Greenberg, E. F.; Koehler, A. N.; Schreiber, S. L. Fluorous-Based Small-Molecule Microarrays for the Discovery of Histone Deacetylase Inhibitors. *Angew. Chem. Int. Ed.* **2007**, *46*, 7960–7964.

(149) Northen, T. R.; Lee, J.-C.; Hoang, L.; Raymond, J.; Hwang, D.-R.; Yannone, S. M.;

Wong, C.-H.; Siuzdak, G. A Nanostructure-Initiator Mass Spectrometry-Based Enzyme Activity Assay. *Proc. Natl. Acad. Sci. U. S. A.* **2008**, *105*, 3678–3683.

(150) de Rond, T.; Peralta-Yahya, P.; Cheng, X.; Northen, T. R.; Keasling, J. D. Versatile Synthesis of Probes for High-Throughput Enzyme Activity Screening. *Anal. Bioanal. Chem.* **2013**, *405*, 4969–4973.

(151) de Rond, T.; Gao, J.; Zargar, A.; de Raad, M.; Cunha, J.; Northen, T. R.; Keasling, J. D. A High-Throughput Mass Spectrometric Enzyme Activity Assay Enabling the Discovery of Cytochrome P450 Biocatalysts. *Angew. Chem. Int. Ed.* **2019**, *58*, 10114–10119.

(152) Schmieder, A. H.; Caruthers, S. D.; Keupp, J.; Wickline, S. A.; Lanza, G. M. Recent Advances in 19 Fluorine Magnetic Resonance Imaging with Perfluorocarbon Emulsions. *Engineering* **2015**, *1*, 475–489.

(153) Tirotta, I.; Dichiarante, V.; Pigliacelli, C.; Cavallo, G.; Terraneo, G.; Bombelli, F. B.; Metrangolo, P.; Resnati, G. 19 F Magnetic Resonance Imaging (MRI): From Design of Materials to Clinical Applications. *Chem. Rev.* **2015**, *115*, 1106–1129.

(154) Kirberger, S. E.; Maltseva, S. D.; Manulik, J. C.; Einstein, S. A.; Weegman, B. P.; Garwood, M.; Pomerantz, W. C. K. Synthesis of Intrinsically Disordered Fluorinated Peptides for Modular Design of High-Signal 19F MRI Agents. *Angew. Chem. Int. Ed.* **2017**, *56*, 6440–6444.

(155) Xie, D.; Yu, M.; Kadakia, R. T.; Que, E. L. 19F Magnetic Resonance Activity-Based Sensing Using Paramagnetic Metals. *Acc. Chem. Res.* **2020**, *53*, 2–10.

(156) Xie, D.; King, T. L.; Banerjee, A.; Kohli, V.; Que, E. L. Exploiting Copper Redox for 19 F Magnetic Resonance-Based Detection of Cellular Hypoxia. *J. Am. Chem. Soc.* **2016**, *138*, 2937–2940.

(157) Xie, D.; Kim, S.; Kohli, V.; Banerjee, A.; Yu, M.; Enriquez, J. S.; Luci, J. J.; Que, E. L. Hypoxia-Responsive 19 F MRI Probes with Improved Redox Properties and Biocompatibility. *Inorg. Chem.* **2017**, *56*, 6429–6437.

(158) Yu, M.; Bouley, B. S.; Xie, D.; Enriquez, J. S.; Que, E. L. 19F PARASHIFT Probes for Magnetic Resonance Detection of H 2 O 2 and Peroxidase Activity. *J. Am. Chem. Soc.* **2018**, *140*, 10546–10552.

(159) Zane, H. K.; Doh, J. K.; Enns, C. A.; Beatty, K. E. Versatile Interacting Peptide (VIP) Tags for Labeling Proteins with Bright Chemical Reporters. *ChemBioChem* **2017**, *18*, 470–474.

(160) Doh, J. K.; White, J. D.; Zane, H. K.; Chang, Y. H.; López, C. S.; Enns, C. A.; Beatty, K. E. VIPER Is a Genetically Encoded Peptide Tag for Fluorescence and Electron Microscopy. *Proc. Natl. Acad. Sci. U. S. A.* **2018**, *115*, 12961–12966.

(161) Bentler, P.; Erdeljac, N.; Bussmann, K.; Ahlqvist, M.; Knerr, L.; Bergander, K.; Daniliuc, C. G.; Gilmour, R. Stereocontrolled Synthesis of Tetrafluoropentanols: Multivicinal Fluorinated Alkane Units for Drug Discovery. *Org. Lett.* **2019**, *21* (19), 7741–7745.

(162) Bentler, P.; Bergander, K.; Daniliuc, C. G.; Mück-Lichtenfeld, C.; Jumde, R. P.; Hirsch, A. K. H.; Gilmour, R. Inverting Small Molecule–Protein Recognition by the Fluorine Gauche Effect: Selectivity Regulated by Multiple H→F Bioisosterism. *Angew. Chemie - Int. Ed.* **2019**, *58*, 10990–10994.

(163) Fischer, S.; Huwyler, N.; Wolfrum, S.; Carreira, E. M. Synthesis and Biological Evaluation of Bromo- and Fluorodanicalipin A. *Angew. Chemie* **2016**, *55*, 2555–2558.

(164) Huchet, Q. A.; Kuhn, B.; Wagner, B.; Kratochwil, N. A.; Fischer, H.; Kansy, M.; Zimmerli, D.; Carreira, E. M.; Müller, K. Fluorination Patterning: A Study of Structural

Motifs That Impact Physicochemical Properties of Relevance to Drug Discovery. *J. Med. Chem.* **2015**, *58* (22), 9041–9060.

(165) Wiesenfeldt, M. P.; Nairoukh, Z.; Li, W.; Glorius, F. Hydrogenation of Fluoroarenes: Direct Access to All-Cis-(Multi)Fluorinated Cycloalkanes. *Science (80-.).* **2017**, *357* (6354).

(166) Clark, J. L.; Neyyappadath, R. M.; Yu, C.; Slawin, A. M. Z.; Cordes, D. B.; O'Hagan, D. Janus All-Cis 2,3,4,5,6-Pentafluorocyclohexyl Building Blocks Applied to Medicinal Chemistry and Bioactives Discovery Chemistry. *Chem. – A Eur. J.* **2021**, *27* (64), 16000–16005.

(167) Clark, J. L.; Taylor, A.; Geddis, A.; Neyyappadath, R. M.; Piscelli, B. A.; Yu, C.; Cordes, D. B.; Slawin, A. M. Z.; Cormanich, R. A.; Guldin, S.; O'Hagan, D. Supramolecular Packing of Alkyl Substituted Janus Face All-Cis 2,3,4,5,6-Pentafluorocyclohexyl Motifs. *Chem. Sci.* **2021**, *12* (28), 9712–9719.

(168) Dolbier Jr., W. R. Structure, Reactivity, and Chemistry of Fluoroalkyl Radicals. *Chem. Rev.* **1996**, *96*, 1557–1584.

(169) Shtarev, A. B.; Tian, F.; Dolbier Jr., W. R.; Smart, B. E. Absolute Rates of Intermolecular Carbon−Hydrogen Abstraction Reactions by Fluorinated Radicals. *J. Am. Chem. Soc.* **1999**, *121*, 7335–7341.

(170) Pappireddi, N.; Martin, L.; Wühr, M. A Review on Quantitative Multiplexed Proteomics. *ChemBioChem* **2019**, *20*, 1210–1224.

(171) Scott, L. G.; Hennig, M. 19F-Site-Specific-Labeled Nucleotides for Nucleic Acid Structural Analysis by NMR. *Methods Enzymol.* **2016**, *566*, 59–87.

(172) Kreutz, C.; Kählig, H.; Konrat, R.; Micura, R. A General Approach for the Identification

of Site-Specific RNA Binders by 19F NMR Spectroscopy: Proof of Concept. *Angew. Chem. Int. Ed.* **2006**, *45*, 3450–3453.

(173) Kiviniemi, A.; Virta, P. Characterization of RNA Invasion by 19F NMR Spectroscopy. *J. Am. Chem. Soc.* **2010**, *132*, 8560–8562.

(174) Veronesi, M.; Giacomina, F.; Romeo, E.; Castellani, B.; Ottonello, G.; Lambruschini, C.; Garau, G.; Scarpelli, R.; Bandiera, T.; Piomelli, D.; Dalvit, C. Fluorine Nuclear Magnetic Resonance-Based Assay in Living Mammalian Cells. *Anal. Biochem.* **2016**, *495*, 52–59.

(175) Blaskovic, S.; Blanc, M.; van der Goot, F. G. What Does S-Palmitoylation Do to Membrane Proteins? *FEBS J.* **2013**, *280*, 2766–2774.

(176) Gao, H.; Sun, W.; Song, Z.; Yu, Y.; Wang, L.; Chen, X.; Zhang, Q. A Method to Generate and Analyze Modified Myristoylated Proteins. *ChemBioChem* **2017**, *18*, 324–330.

(177) Gomes, B.; Loureiro, J.; Coelho, M.; Carmo Pereira, M. The Potential Effect of Fluorinated Compounds in the Treatment of Alzheimer's Disease. *Curr. Pharm. Des.* **2015**, *21*, 5725–5735.

(178) Shah, P.; Andrew, &; Westwell, D. D. The Role of Fluorine in Medicinal Chemistry. *J. Enzyme Inhib. Med. Chem.* **2007**, *22*, 527–540.

(179) Sun, S.; Adejare, A. Fluorinated Molecules as Drugs and Imaging Agents in the CNS. *Curr. Top. Med. Chem.* **2006**, *6*, 1457–1464.

(180) Dabur, M.; Loureiro, J. A.; Pereira, M. C. Fluorinated Molecules and Nanotechnology: Future 'Avengers' against the Alzheimer's Disease? *Int. J. Mol. Sci.* **2020**, *21*, 2989.

CHAPTER TWO

A general approach to biocompatible branched fluorous tags for increased solubility in perfluorocarbon solvents

Adapted from: Margeaux A. Miller, Ellen M. Sletten* "A general approach to biocompatible branched fluorous tags for increased solubility in perfluorocarbon solvents" *Org. Lett.* **2018**, *20*, 6850−6854. DOI: 10.1021/acs.orglett.8b02976

2.1 Abstract

A modular, cost-effective route to a library of branched fluorous tags with two short, biocompatible, fluorinated chains (C_6F_{13}) is reported. These branched fluorous tags provide high fluorous content without the use of long-chain linear perfluorocarbons (*e.g.* perfluorooctanoic acid), which have rising health concerns due to their bioaccumulation. By attaching these tags to a porphyrin, it is demonstrated that high solubility can be achieved in fluorous solvents that are readily cleared from mammals. This work enhances the biocompatibility of perfluorocarbon nanoemulsions for photodynamic therapy.

2.2 Introduction

Perfluorocarbons, molecules where all the hydrogen atoms are replaced with fluorine atoms, are an unnatural class of compounds with distinct characteristics due to the size and electronegativity of fluorine.[1] The inert nature and non-polarizability of perfluorinated materials have been widely realized through the success of poly(tetrafluoroethylene) as a non-stick coating.[2,3] The high gas content of perfluorocarbons, coupled with their low boiling points and metabolic stability, were exploited for oxygen delivery using perfluorocarbon nanoemulsions in the 1980s.[4] The synthetic chemistry community was introduced to the orthogonality of perfluorocarbons in 1994 as a means to efficiently recycle catalysts.[5] This work coined the term "fluorous" and initiated the field of fluorous phase chemistry where perfluorinated tags were

appended to organic compounds to facilitate purification by fluorous extraction. The use of fluorous tags has since been extended to biological applications to streamline proteomics,[6] display bioactive molecules on microarrays,[7–9] improve transport into cells,[10,11] and encapsulate chromophores inside perfluorocarbon nanoemulsions.[12,13]

Given the broad applications of perfluorinated compounds, the molecular requirements for obtaining fluorous phase solubility have been extensively explored. Strategies to solubilize compounds in perfluorocarbon include increasing the weight percent fluorine (wt% F, ideally to above 60%) through the addition of fluorous tags.[14] Initially, C_8F_{17} tags were determined to have the appropriate balance of synthetic ease and fluorous character.[15] However, concerns regarding the environmental persistence of long-chain perfluorinated compounds (C7 or greater, *e.g.* perfluorooctanoic acid) prevent the use of C_8F_{17} chains as fluorous solubilizing groups.[16,17] For the full potential of the fluorous phase to be realized, methods to render molecules soluble in perfluorocarbon with C_6F_{13} fluorous tags or shorter are necessary.

Branched tags are a promising approach to employ short fluorous segments, yet still obtain high wt% F. Furthermore, branched alkyl chains have been shown to improve the solubility of planar aromatic compounds in organic solution,[18,19] indicating that branched tags may impart superior fluorous solubility at lower wt% F.

Previously reported strategies to access branched C_6F_{13} tags include malonate alkylation,[20,21] Grignard addition,[22,23] and sequential iodo-ene/elimination reactions[24,25] (Figure 2.1A). Perfluorinated *tert*-butyl groups have also been investigated as biocompatible fluorous tags through the addition of perfluoro-*tert*-butoxide.[26,27] Collectively, these approaches have validated the use of short fluorous segments to impart solubility in perfluorocarbons; yet, there remains no tag that can easily be appended to compounds with a variety of different chemistries.

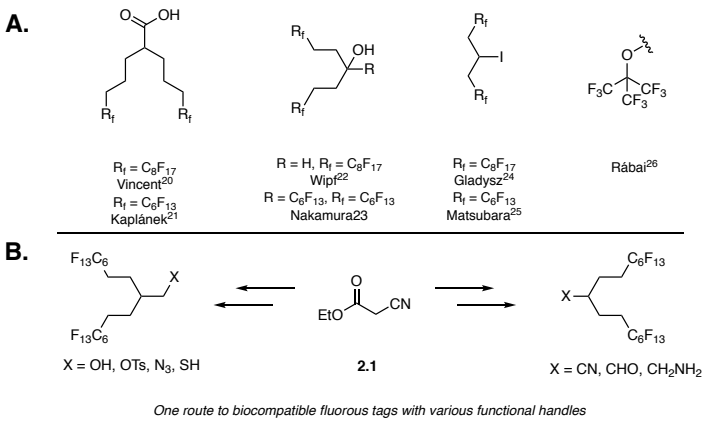

Figure 2.1 Approaches to branched fluorous tags. (A) Existing approaches. (B) Our approach from ethyl cyanoacetate **2.1** leading to multiple functional handles in minimal steps.

To showcase the general utility of these tags, we prepared a highly fluorous-soluble porphyrin. We compared the porphyrin containing branched C_6F_{13} chains to one containing linear C_8F_{17} chains. Leveraging the absorbance and emission of porphyrins, we determined that the branched fluorous tags resulted in an increased fluorous partition coefficient, solubility in an array of perfluorocarbons, and superior retention in droplets of fluorous solvent *(e.g.* perfluorocarbon nanoemulsions). Efficient encapsulation of porphyrins in perfluorocarbon nanoemulsions is of particular interest for applications in photomedicine. The combination of enhanced solubility imparted by branched fluorous tags and the removal of persistent fluorinated chains increases the biocompatibility of perfluorocarbon (PFC) nanoemulsions for photodynamic therapy.

2.3 Discussion and results

In efforts to develop a general strategy for the preparation of biocompatible branched fluorous tags, we looked to employ readily available starting materials that could be converted to multiple functional handles in a few, simple steps. We envisioned that alkylation chemistry would be the most efficient to install two fluorous chains in one pot. We targeted (perfluorohexyl)ethyl iodide **2.2** as the fluorous starting material due to its low cost and high

wt% F. Previously, malonate esters have been employed for direct addition of two fluorous chains via alkylation; however, (perfluoroalkyl)propyl iodides were necessary (Figure 2.1A). Our attempts to doubly alkylate malonate esters with (perfluorohexyl)ethyl iodide resulted in monoaddition at mild temperatures and elimination at elevated temperatures (Table 2.1). Looking to increase the reactivity of the nucleophile, we found that ethyl cyanoacetate **2.1** could be successfully dialkylated with **2.2** to provide **2.3** in 90% yield, with less than 1% of fluoride elimination observed (Scheme 2.1A).[31]

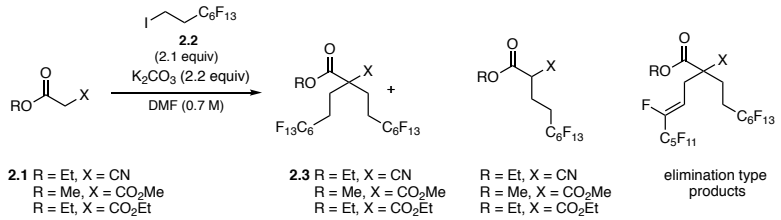

R	X	time (h)	temp	di-alkylation	mono-alkylation	elimination
Et	CN	24	rt	97%	<2%	<1%
Et	CN	48	rt	97%	<2%	<1%
Me	CO_2Me	72	rt	26%	74%	--
Et	CO_2Et	72	rt	30-40%[a]	60-70%[a]	--

Table 2.1 Dialkylation and monoalkylation of different nucleophiles: ethyl cyanoacetate **2.1**, dimethylmalonate, and diethylmalonate. Percent conversion to alkylated products and elimination side products were determined by crude NMR using 1,3,5-trimethoxybenzene as an external standard for ^{1}H NMR. [a] Determined by ^{19}F NMR.

The ethyl cyanoacetate provided increased reactivity as well as two separate functional groups that could be transformed into branched fluorous tags with different functional handles (Scheme 2.1B). In one step from **2.3**, we could access nitrile tag **2.4** through Krapcho decarboxylation. The nitrile could be reduced to the primary amine **2.5** or aldehyde **2.6**, demonstrating the immediate modularity of this approach. Concurrently, a sequential saponification and decyanation provided branched carboxylic acid tag **2.7** in 89% yield. The acid can be readily reduced to the corresponding alcohol **2.8**. From primary alcohol **2.8**, we

prepared tosylate **2.9**, which can be displaced with azide or thioacetate to give **2.10** and **2.11**, respectively. Tags **2.4**, **2.6**, **2.10**, and **2.11** represent popular chemical handles for click chemistries,[32,33] facilitating the simple installation of fluorous content.

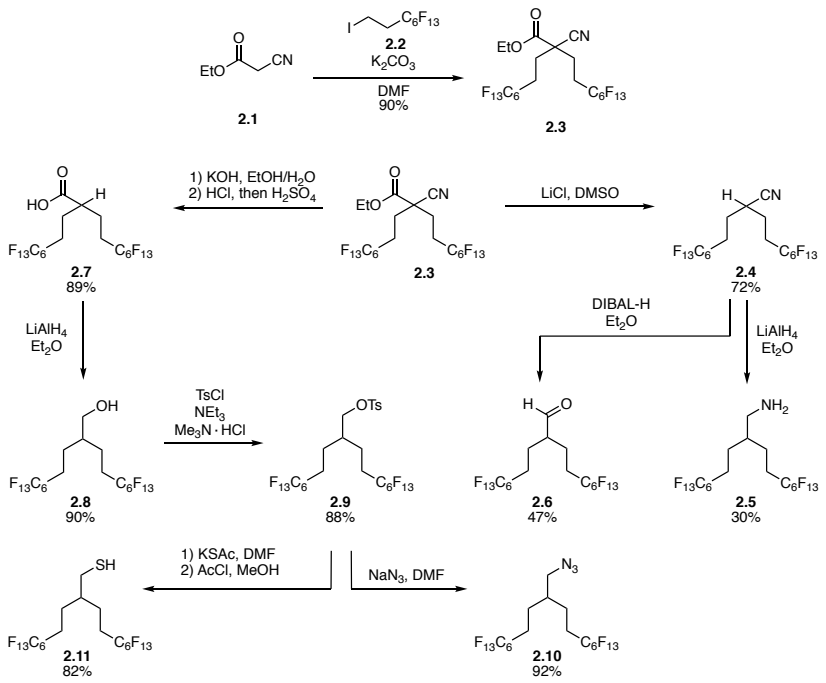

Scheme 2.1 Synthesis of fluorous tags. **(**A) Synthesis of modular building block **2.3**. (B) Synthesis of a library of branched fluorous tags from **2.3**.

To evaluate the ability of the branched fluorous tags to solubilize organic compounds in perfluorocarbon solvents, we performed a nucleophilic aromatic substitution reaction with **2.11** and 5,10,15,20-tetrakis(pentafluorophenyl)porphyrin **2.12** to yield **2.13** with 51 wt% F.[34] We compared **2.13** to previously reported **2.14**,[35] which contained linear C_8F_{17} tags and 46 wt% F (Figure 2.2B). We determined the fluorous partition coefficient (P)[14,36] of **2.13** and **2.14** by subjecting each to a 1:1 mixture of perfluoro(methylcyclohexane) (C_7F_{14}):toluene (PhMe) and quantifying the amount in each layer by UV-Vis spectroscopy.[37] Branched fluorous porphyrin **2.13** had a P = 24 (96:4 in C_7F_{14}:PhMe) whereas porphyrin **2.14** has a P = 1.7 (63:37 in

C_7F_{14}:PhMe). This striking difference suggests that branching and increased wt% F are acting synergistically to enhance fluorous solubility. Another avenue to assay the fluorous character of the tagged molecules is to evaluate their tendency to remain in the core of PFC nanoemulsions (Figure 2.2C) as the aqueous suspension of droplets is continually partitioned against 1-octanol.[12] Previously, we have shown that **2.14** displays some leaching into the 1-octanol.[13] When we performed the identical assay with **2.13**, we found that 50% less porphyrin escaped the droplets (Figure 2.2D), corroborating the partition coefficient results and demonstrating the efficacy of the branched fluorous tags.

The ability for branched fluorous porphyrin **2.13** to remain inside perfluorocarbon nanoemulsions in the presence of aqueous and lipophilic media is of particular interest for applications in photodynamic therapy. Photodynamic therapy is a clinically approved treatment for skin, esophageal, and lung cancers.[38–40] This procedure requires three components: a photosensitizer, molecular oxygen, and light. We recently reported that enhanced photodynamic therapy could be achieved when perfluorocarbon nanoemulsions containing **2.14,** acting as a photosensitizer, were irradiated with light.[13] These nanoemulsions were composed of a mixture of 7:3 perfluorodecalin **2.15**:perfluorotripropylamine **2.16**, analogous to the previously FDA-approved formulation for oxygen delivery. Thus, with this system we are able to deliver both oxygen and photosensitizer simultaneously.

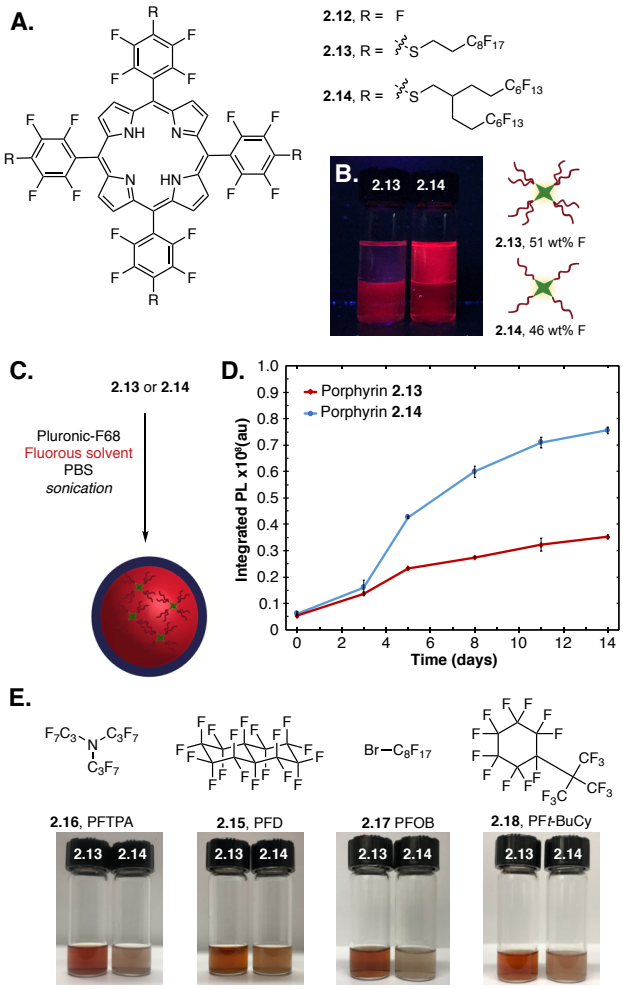

Figure 2.2 Synthesis and evaluation of branched fluorous porphyrin. (A) Branched **2.13** and linear **2.14** fluorous porphyrins prepared from **2.12**. (B) Fluorous partition coefficient in toluene (upper phase) and perfluoro(methylcyclohexane) (lower phase). (C) Preparation of PFC nanoemulsions containing branched **2.13** and linear **2.14** fluorous porphyrin. Both porphyrins were dissolved in separate 7:3 mixtures of PFD **2.15**:PFTPA **2.16** (10 vol%) and combined with Pluronic F-68 (2.8 wt%) in phosphate buffered saline. Sonication (35% amp, 90 s, 0 °C) of the mixture provided PFC nanoemulsions. (D) Leaching of porphyrin **2.13** (red, diamond) or **2.14** (blue, circle) from the fluorous interior of PFC nanoemulsions into 1-octanol over time. Error bars represent the standard deviation of 3 replicates. (E) Structures of fluorous solvents previously employed as the core of PFC nanoemulsions and solubility of porphyrins **2.13** and **2.14** in each solvent.

Despite the advantageous dual delivery, concerns regarding clearance of both the C_8F_{17} chains[16] and perfluorotripropylamine (PFTPA, **2.16**)[41,42] limit the translation of these materials to higher organisms. Looking to overcome both these limitations, we evaluated the solubility of **2.13**

compared to **2.14** in the readily cleared solvents of perfluorodecalin (PFD, **2.15**), perfluorooctyl bromide (PFOB, **2.17**), and perfluoro(*tert*-butylcyclohexane) (PF*t*-BuCy, **2.18**).[43] We found that **2.13** was more soluble than **2.14** in all cases (Figure 2.2E), facilitating the preparation of emulsions for photodynamic therapy from these solvents.

Finally, we performed photodynamic therapy with more biocompatible perfluorocarbon nanoemulsions (Figure 2.6A). We prepared droplets of PFD **2.15**, PFOB **2.17**, PF*t*-BuCy **2.18**, and 7:3 PFD **2.15**:PFTPA **2.16** (20 wt% fluorous solvent) containing **2.13** stabilized by Pluronic F-68 (2.8 wt%) in phosphate buffered saline (PBS) (Scheme 2.2). As a control, we also prepared droplets without **2.13** (Figure 2.3 and 2.4) and droplets containing **2.14** for efficiency comparison (Figure 2.5). All emulsions were 160–190 nm in size with polydispersities of 0.06-0.07 (Figure 2.3).

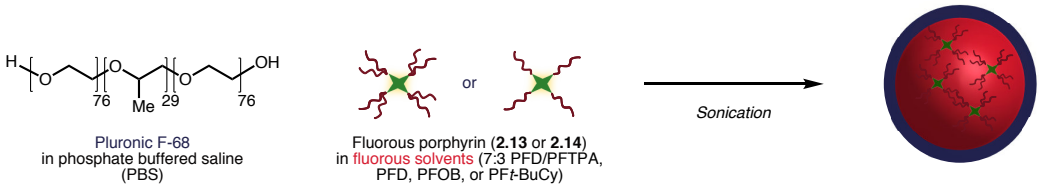

Scheme 2.2 Perfluorocarbon nanoemulsion formation using Pluronic F-68 as a surfactant.

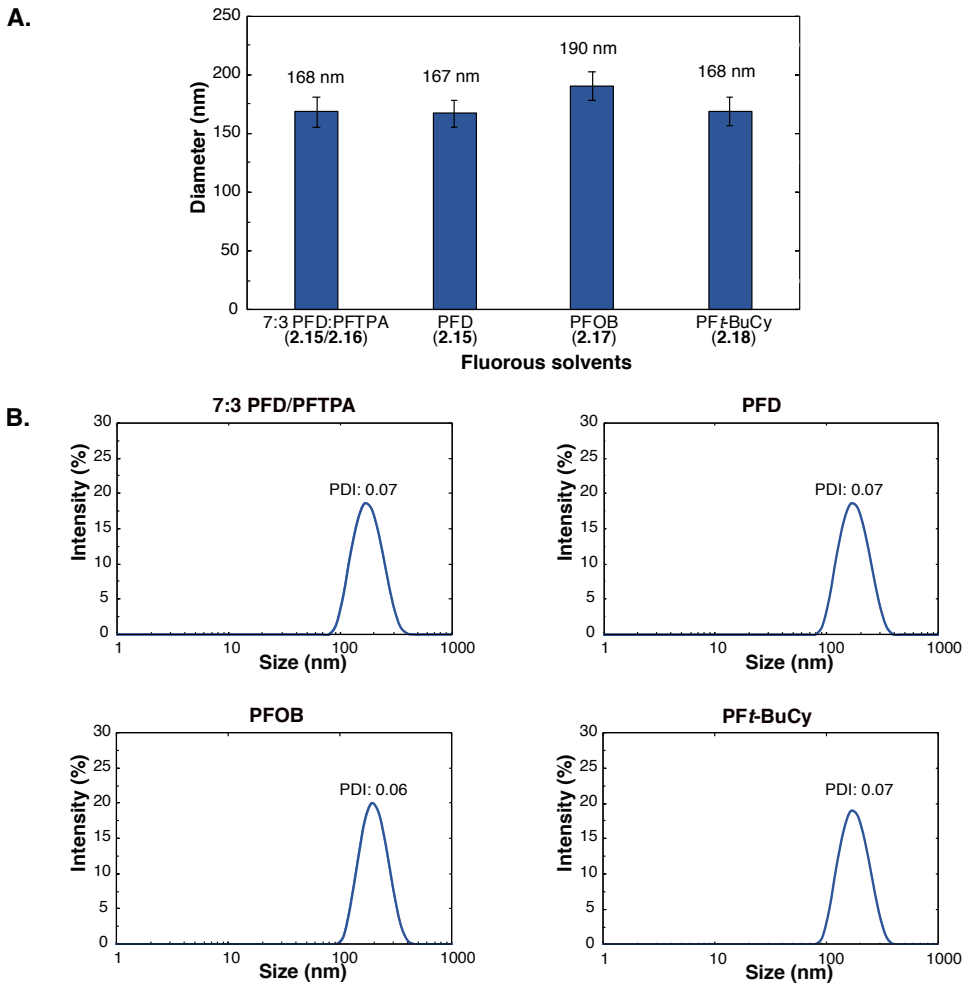

Figure 2.3 Characterization of PFC nanoemulsions without photosensitizer. (A) Initial size distribution of PFC nanoemulsions composed of different fluorous solvents. Emulsions were prepared by sonicating a solution of 2.8 wt% Pluronic F-68 in phosphate buffered saline (PBS) with 10 vol% fluorous solvent (7:3 PFD **2.15**:PFTPA **2.16**, PFD **2.15**, PFOB **2.17**, or PF*t*-BuCy **2.18**). (B) Dynamic light scattering data for the PFC nanoemulsions stabilized by Pluronic F-68. Data is an average of three replicate measurements.

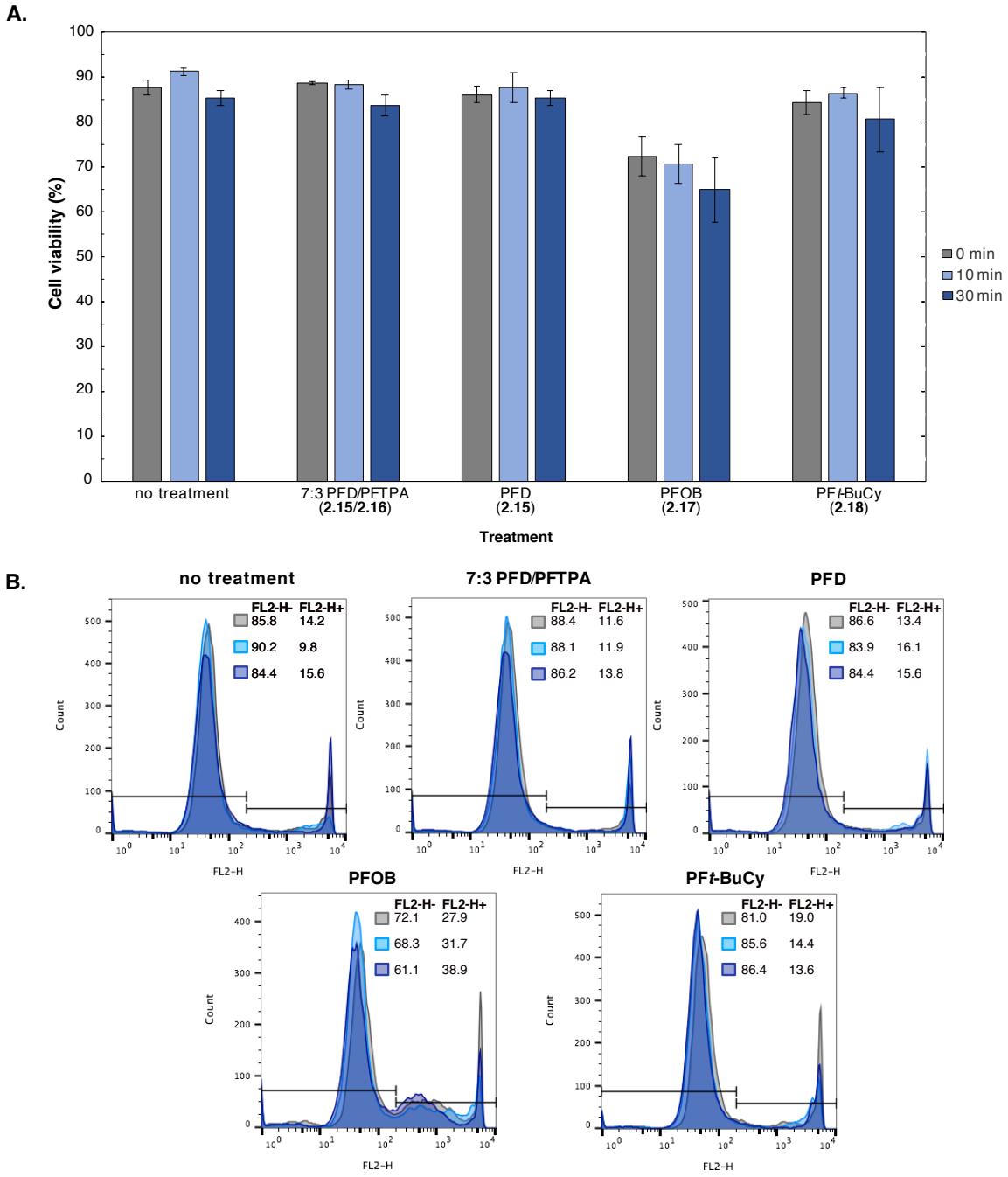

Figure 2.4 Photodynamic therapy with empty perfluorocarbon nanoemulsions composed of different fluorous solvents without photosensitizer. Light treatment (420 nm LED, 8.5 mW/cm^2) is indicated as follows: grey = 0 min, light blue = 10 min, dark blue = 30 min. (A) Cell viability with emulsions composed of different fluorous solvents (7:3 PFD **2.15**: PFTPA **2.16**, PFD **2.15**, PFOB **2.17**, PF*t*-BuCy **2.18**) and no photosensitizer. Error bars represent the standard deviation of 3 replicate samples. (B) Histograms for A375 cell viability flow cytometry data.

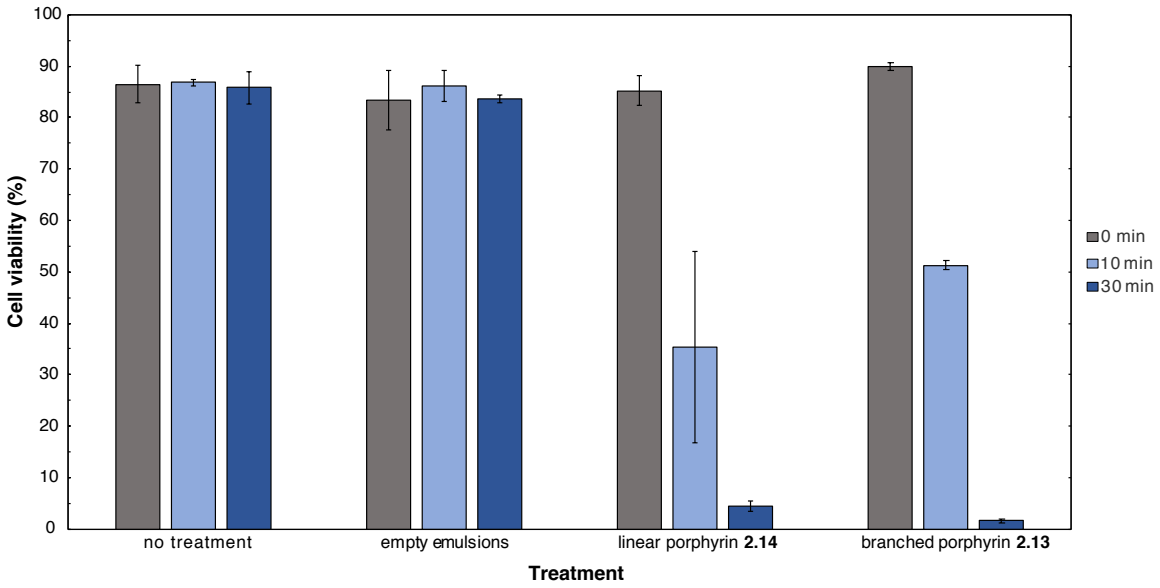

Figure 2.5 Cell viability comparison of photodynamic therapy efficiency of linear porphyrin **2.14** and branched porphyrin **2.13**. For comparison, emulsions composed of 7:3 PFD **2.15**: PFTPA **2.16** were employed as linear porphyrin **2.14** was not readily soluble in the other fluorous solvents. We found that linear porphyrin **2.14** and branched porphyrin **2.13** were similarly effective at inducing cell death when irradiated, suggesting that the branched tags do not affect the ability of porphyrin **2.13** to sensitize oxygen. Light treatment (420 nm LED, 8.5 mW/cm^2) is indicated as follows: grey = 0 min, light blue = 10 min, dark blue = 30 min. Error bars represent the standard deviation of 2 replicate samples.

We incubated each of the emulsions with A375 melanoma cells for 3 hours, at which point, excess emulsions were washed away and the cells underwent light treatment for 0, 10, or 30 min. The degree of cell death was quantified by immediate treatment with propidium iodide and analysis by flow cytometry. We found that all emulsions containing branched porphyrin **2.13** displayed no dark toxicity and equivalent levels of cell death, greatly expanding the fluorous solvents that can be employed for photodynamic therapy with perfluorocarbon nanoemulsions (Figure 2.6B and 2.7). Ultimately, we envision that optimized versions of these nanomaterials can be systemically administered and accumulate at disease sites for light mediated therapies.

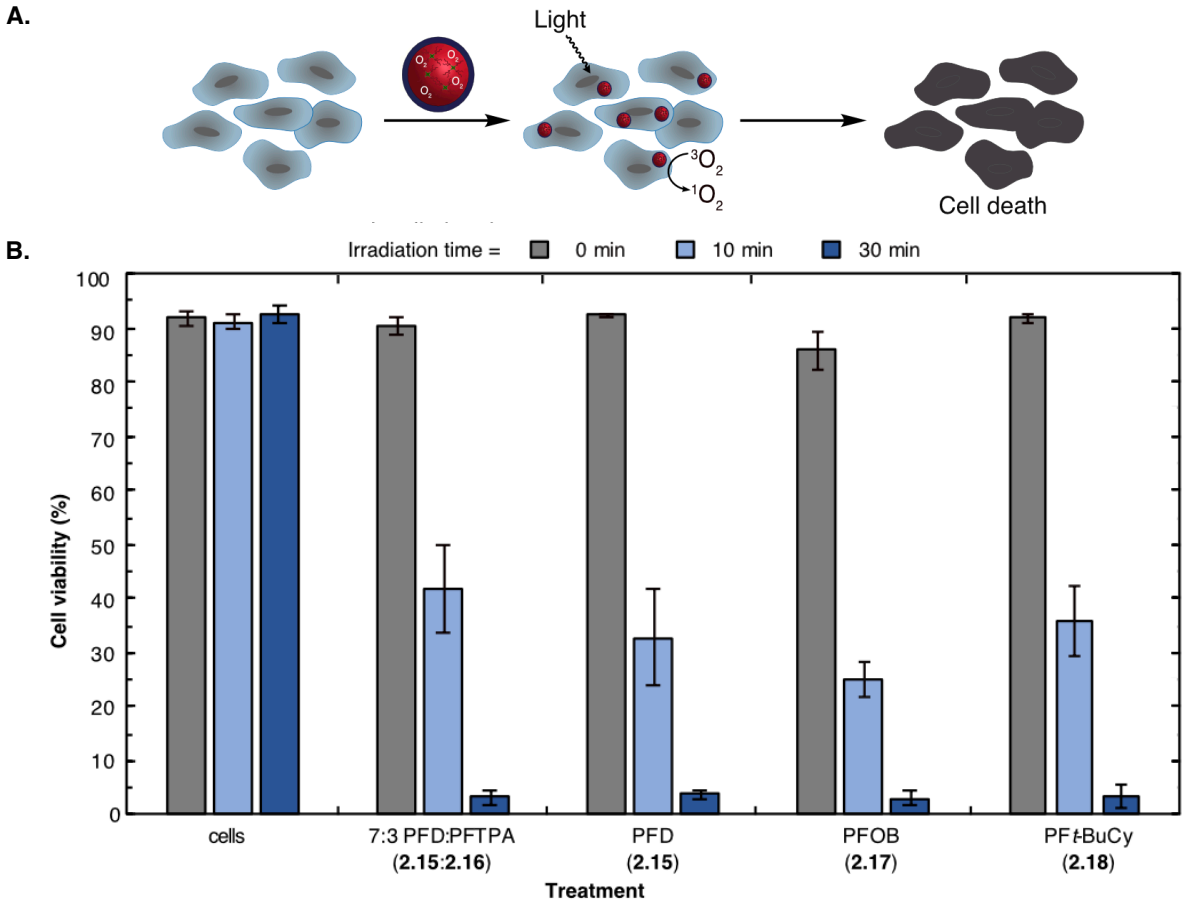

Figure 2.6 (A) Photodynamic therapy with perfluorocarbon nanoemulsions containing **2.13** (0.5 mM). Cells were incubated with PFC emulsions containing **2.13**, washed via centrifugation, and irradiated (420 nm, 8.5 mW/cm^2) for 0 min (grey), 10 min (light blue), or 30 min (dark blue). (B) Flow cytometry analysis after light treatment. After incubation, washing, and light treatment, cells were stained with propidium iodide and analyzed by flow cytometry to determine the degree of cell death. Dead cells were characterized as exhibiting fluorescence >10^2 (Figure 2.7). Error bars represent the standard deviation of 3 replicate samples.

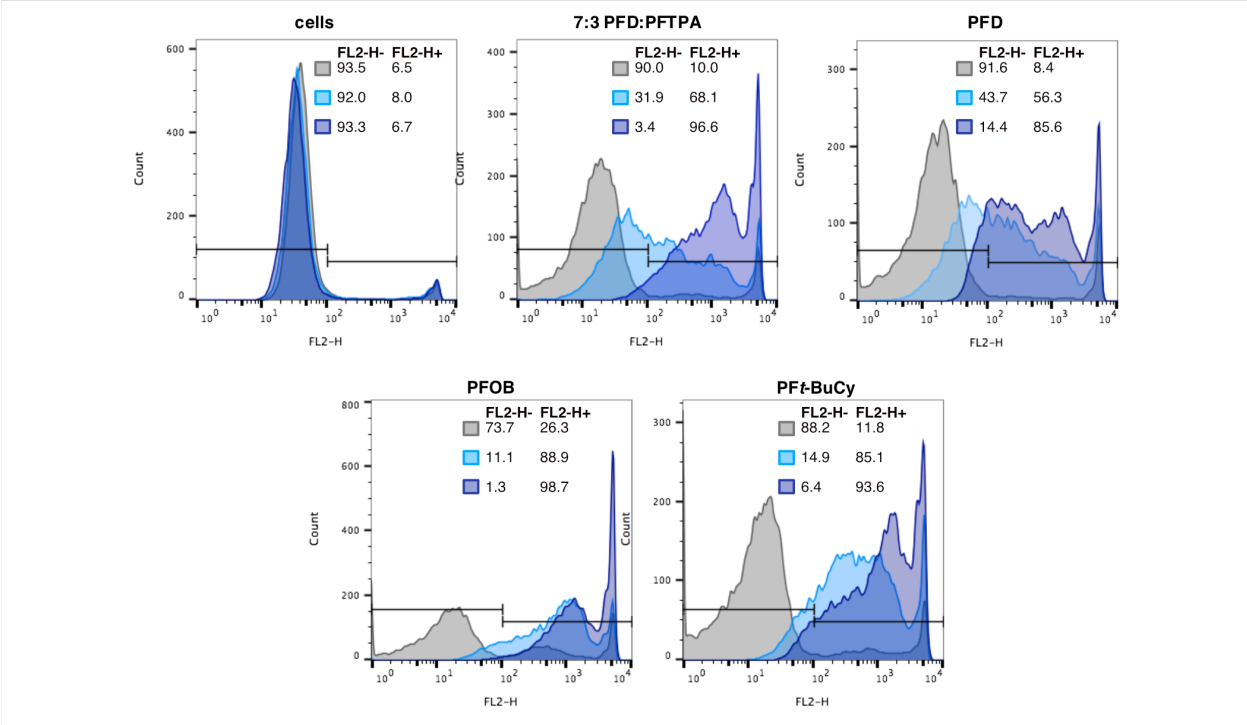

Figure 2.7 Histograms for flow cytometry data in Figure 2.6B. Light treatment (420 nm LED, 8.5 mW/cm^2) is indicated as follows: grey = 0 min, light blue = 10 min, dark blue = 30 min.

2.4 Conclusion

In summary, we have developed a route to a library of biocompatible branched fluorous tags with two C_6F_{13} chains. These tags are derived from ethyl cyanoacetate **2.1** and (perfluorohexyl)ethyl iodide **2.2** to provide modular building block **2.3** with two functional handles and high fluorous content. We converted **2.3** to eight branched fluorous tags with distinct functionalities, including azides, aldehydes, and thiols for standard click chemistries. We employed the thiol tag for nucleophilic aromatic substitution to prepare fluorous porphyrin **2.13**. We demonstrate that **2.13** is more soluble in fluorous solvent than its linear counterpart **2.14**, facilitating the incorporation of **2.13** into stable perfluorocarbon nanoemulsions. The high solubility of **2.13** in readily cleared, volatile fluorous solvents allowed for photodynamic therapy to be carried out with PFC nanoemulsions composed of clinically relevant fluorous solvents.

Looking forward, the simple, modular synthesis of branched fluorous tags from readily available starting materials will provide the community with biocompatible methods to impart fluorous content to molecules and materials, allowing the unique properties of perfluorocarbons to continue to be exploited.

2.5 Experimental procedures

Chemical reagents were purchased from Sigma-Aldrich, Alfa Aesar, Fisher Scientific, Acros Organics, Synquest, or TCI and used without purification unless noted otherwise. Anhydrous DMSO was obtained from a Sure-Seal™ bottle (Aldrich). Anhydrous and deoxygenated solvents DCM, MeOH, THF, and DMF were dispensed from a Grubb's-type Phoenix Solvent Drying System. Anhydrous, but oxygenated Et_2O was prepared by drying over 4 Å molecular sieves for at least 3 days. Thin layer chromatography was performed using Silica Gel 60 F_{254} (EMD Millipore) plates. Flash chromatography was executed with technical grade silica gel with 60 Å pores and 40–63 μm mesh particle size (Sorbtech Technologies). Solvent was removed under reduced pressure with a Büchi Rotovapor with a Welch self-cleaning dry vacuum pump and further dried with a Welch DuoSeal pump. Bath sonication was performed using a Branson 3800 ultrasonic cleaner. Emulsions were prepared using a QSonica (Q125) sonicator. Masses for analytical measurements were taken on a Sartorius MSE6.6S-000-DM Cubis Micro Balance. Size and surface charge were measured with Malvern Zetasizer Nano instrument. All ^{1}H, ^{13}C, and ^{19}F NMR spectra are reported in ppm and relative to residual solvent signals (^{1}H and ^{13}C). Spectra were obtained on Bruker AV-300, AV-400, DRX-500, or AV-500 instruments and processed with MestReNova software. Mass spectra (electron impact (EI), electrospray ionization (ESI), and matrix assisted laser desorption ionization (MALDI)) were

collected on either an Agilent 7890B-7250 Quadrupole Time-of-Flight GC/MS, Thermo Scientific Q Exactive™ Plus Hybrid Quadrupole-Orbitrap™ with Dionex UltiMate 3000 RSLCnano System, or Bruker Ultraflex MALDI TOF-TOF.

2.5.1 General photophysics procedures

Absorbance spectra were collected on a JASCO V-770 UV-Visible/NIR spectrophotometer with a 4000 nm/min scan rate after blanking with the appropriate solvent. Photoluminescence spectra were obtained on a Horiba Instruments PTI QuantaMaster Series fluorometer. Quartz cuvettes (1 cm) were used for absorbance and photoluminescence measurements unless otherwise noted. All irradiation was performed with THORLabs M420L3 (420 nm) LED with SM1P25-A lens. Power was supplied with a KORAD KD3005D Digital-control DC Power Supply: 0-30V, 0-5A. Samples were placed 18 cm from the lens and kept in the center of the light. Power densities were measured with a FieldMate Laser Power Meter + Iris.

2.5.2 General nanoemulsion formation procedures

Emulsions were prepared by predissolving **2.13** or **2.14** (for amounts see individual figure procedures) in fluorous solvent (10 vol%, 20 μL) in an S33 Eppendorf tube. Pluronic F-68 was predissolved in PBS pH 7.4 (28 mg/mL), and this solution (200 μL, 2.8 wt%) was added to the fluorous solvent. The mixture was sonicated at 35% amplitude for 90 seconds at 0 °C on a QSonica (Q125) sonicator. Sonication was performed by lowering the probe directly at the liquid-liquid interface of the two immiscible solvents, resulting in emulsions of sizes shown in Figure 2.3 without filtration.

2.5.3 General cell culture procedures

A375 cells were purchased from ATCC. A375 cells were cultured in Dulbecco's Modified Eagle Media (Life Technologies, cat# 11995073) supplemented with 10% fetal bovine serum (Corning, lot# 35016109) and 1% penicillin-streptomycin (Life Technologies, cat# 15070063). Cells were washed with PBS, or PBS supplemented with 1% fetal bovine serum (FACS buffer). Cells were incubated at 37 ˚C, 5% CO_2, during treatments and throughout culturing, in HERACell 150i CO_2 incubators. Cells were pelleted through use of Sorvall ST 40R centrifuge. All cell work was performed in 1300 Series A2 biosafety cabinets.

For cell viability experiments: following incubation, cells were washed three times by centrifugation (526xg, 3 min, 4 ˚C). Propidium iodide solution (1 μL of 0.25 mg/mL in DI H_2O) was added to each well. Cells were transferred to FACS tubes with a final volume of 300 μL FACS buffer (PBS + 1% FBS). Cells were incubated on ice for 15 minutes prior to flow cytometry measurement. Propidium iodide fluorescence was measured on FL2 channel. Data was analyzed by splitting the population at 10^2 as a live/dead line. Flow cytometry was performed on a BDBiosciences FACSCalibur equipped with 488 nm and 635 nm lasers.

Abbreviations: DCM = dichloromethane; DMF = dimethylformamide; DMSO = dimethylsulfoxide; EtOH = ethanol; EtOAc = ethyl acetate; Et_2O = diethyl ether; FACS = phosphate buffered saline supplemented with 1% fetal bovine serum; MeOH = methanol; PBS = phosphate buffered saline; PFD = perfluorodecalin; PFTPA = perfluorotripropylamine; PFOB = perfluorooctylbromide; PF*t*-BuCy = perfluoro(*tert*-butylcyclohexane); TEA = triethylamine.

2.5.4 Synthetic experimental procedures

2,2-bis((perfluorohexyl)ethyl) ethyl cyanoacetate (2.3). To perfluorohexyl ethyl iodide (0.65 mL, 2.6 mmol, 2.1 equiv), was added ethyl cyanoacetate (135 μL, 1.27 mmol, 1.0 equiv), freshly powdered and flame dried K_2CO_3 (388 mg, 2.80 mmol, 2.2 equiv), and anhydrous DMF (1.8 mL, 0.70 M). The vial was sealed under nitrogen and stirred at rt. Note: if the reactants begin to solidify, the mixture can be warmed to 30 °C without formation of significant byproducts. After 72 h, the reaction mixture was evaporated to dryness. The resulting solids were dissolved in acetone and absorbed onto SiO_2. The crude product was purified by column chromatography (silica gel, 98% → 95% → 90% pentane/Et_2O) to afford **2.3** as a white solid (922 mg, 1.14 mmol, 90%). R_f = 0.8 in 20% EtOAc/hexanes. ^{1}H NMR (400 MHz, $CDCl_3$): δ 4.36 (q, J = 7.1 Hz, 2H), 2.49 – 2.08 (m, 8H), 1.36 (t, J = 7.1 Hz, 3H). ^{13}C NMR (101 MHz, $CDCl_3$): δ 167.0, 117.1, 64.1, 47.7, 28.3, 27.6 (t, J_{CF} = 22.1 Hz), 14.1. ^{19}F NMR (376 MHz, $CDCl_3$): δ -80.7 (t, J = 9.8 Hz, 6F), -114.2 (m, 4F), -122.0 (m, 4F), -122.7 (m, 4F), -123.2 (m, 4F), -126.1 (m, 4F). HRMS (ESI) calcd. for $C_{21}H_{13}F_{26}NO_2Cl^-$ $[M + Cl]^-$: 840.0225; found 840.0221.

2,2-bis((perfluorohexyl)ethyl)ethylnitrile (2.4). To **2.3** (307 mg, 0.382 mmol, 1.0 equiv), was added lithium chloride (56 mg, 1.3 mmol, 3.5 equiv), DMSO (3.0 mL, 0.13 M), and H_2O (1.0 mL). The reaction mixture was heated to 160 °C and stirred for 12 h. The reaction mixture was allowed to cool to room temperature, and product crashes out of solution. The crude product was rinsed with water, dissolved in EtOAc, and evaporated to dryness. The crude product was dissolved in EtOAc, absorbed onto SiO_2, and purified by column chromatography (silica gel, 97% → 95% hexanes/EtOAc) to afford **2.4** as a white solid (201 mg, 0.274 mmol, 72%). R_f = 0.3 in 10% DCM/hexanes. ^{1}H NMR (500 MHz, $CDCl_3$): δ 2.78 (sep, J = 5.0 Hz, 1H), 2.52 – 2.18

(m, 4H), 2.07 – 1.91 (m, 4H). ^{13}C NMR (126 MHz, $CDCl_3$): δ 119.8–108.0 (m, CF_n peaks), 119.3 (CN), 30.8, 28.7 (t, J_{CF} = 22.6 Hz), 23.6. ^{19}F NMR (376 MHz, $CDCl_3$): δ -80.8 (t, J = 9.9 Hz, 6F), -112.7 – -115.9 (m, 4F), -121.8 (bs, 4F), -122.8 (bs, 4F), -123.3 (bs, 4F), -126.1 (bs, 4F). HRMS (EI) calcd. for $C_{18}H_8F_{25}N^+$ $[M – HF]^+$: 713.0252; found 713.0256.

2,2-bis(3,3,4,4,5,5,6,6,7,7,8,8,8-tridecafluorooctyl)ethylamine (2.5). To nitrile **2.4** (96 mg, 0.13 mmol, 1.0 equiv) was added dry Et_2O (5.5 mL, 0.02 M) under nitrogen. Nitrile **2.4** was stirred until it was fully dissolved, and then cooled to 0 °C. Lithium aluminum hydride (1.0 M in THF, 0.26 mmol, 2.0 equiv) was added. After 1 h, the reaction was let warm to room temperature and stirred for 5 h. The reaction was quenched by dropwise addition of H_2O with stirring, and then extracted with EtOAc, dried ($MgSO_4$), filtered, and evaporated to dryness. The crude mixture was evaporated onto SiO_2 from EtOAc and purified by column chromatography (silica gel, 100% DCM→1% MeOH/DCM→ 5% MeOH/DCM (all with 1% TEA)) to provide the product **2.5** as a yellow oil (29 mg, 0.04 mmol, 30%). R_f = 0.5 in 10% MeOH/DCM. ^{1}H NMR (500 MHz, MeOD-d_4): δ 2.65 (d, J = 5.5 Hz, 2H), 2.28 – 2.15 (m, 4H), 1.79 – 1.48 (m, 5H). ^{13}C NMR (126 MHz, MeOD-d_4): δ 122.2 – 109.8 (CF_n), 44.6, 40.3, 29.02 (t, J_{CF} = 22.1 Hz), 22.42. ^{19}F NMR (282 MHz, MeOD-d4): δ -83.9 – -84.1 (m, 6F), -116.7 – -117.4 (m, 4F), -124.5 (bs, 4F), -125.4 (bs, 4F), -126.0 (bs, 4F), -127.9 – -130.4 (m, 4F). HRMS (ESI) calcd. for $C_{18}H_{14}F_{26}N^+$ $[M + H]^+$: 738.0706; found 738.0684.

2,2-bis(3,3,4,4,5,5,6,6,7,7,8,8,8-tridecafluorooctyl)-1-ethanal (2.6). To nitrile **2.4** (30 mg, 0.04 mmol, 1.0 equiv) dissolved in dry Et_2O (2.0 mL, 0.02 M) at -78 °C, DIBAL-H (1.0 M in Hexanes, 0.09 mmol, 2.3 equiv) was added dropwise. After 2 h, additional DIBAL-H (45 μL, 1.2

equiv) was added, and the reaction was stirred for 2 h more at -78 °C. EtOAc (2 mL) was added slowly, then a saturated aq Rochelle salt solution (2 mL) was added, and the mixture was stirred at room temperature until there were two clear layers (~ 1 h). The aqueous layer was extracted with additional EtOAc (2 x 3 mL). The combined organic layers were dried ($MgSO_4$), filtered, and concentrated. The crude mixture was dissolved in EtOAc (2 mL) and stirred with 1 M HCl (2 mL) to hydrolyze any remaining imine. The organic layer was separated, evaporated onto SiO_2, and purified by column chromatography (silica gel, 3% DCM/hexanes→ 5% DCM/hexanes → 10% DCM/hexanes). This procedure yielded the aldehyde **2.6** as a white solid (14 mg, 0.02 mmol, 47% yield). R_f = 0.5 in 20% DCM/hexanes. ^{1}H NMR (500 MHz, $CDCl_3$): δ 9.68 (d, J = 1.6 Hz, 1H), 2.56 – 2.42 (m, 1H), 2.24 – 1.99 (m, 6H), 1.86 – 1.73 (m, 2H). ^{13}C NMR (126 MHz, $CDCl_3$): δ 201.6, 49.6, 28.2 (t, J_{CF} = 22.4 Hz), 19.2. ^{19}F NMR (376 MHz, $CDCl_3$) δ -80.8 (t, J = 10.0 Hz, 6F), -114.6 (bs, 4F), -121.9 (bs, 4F), -122.8 (bs, 4F), -123.4 (bs, 4F), -126.0 – -126.3 (m, 4F). HRMS (ESI) calcd. for $C_{18}H_9F_{26}O^-$ $(M – H)^-$: 735.0244; found 735.0239.

2,2-bis((perfluorohexyl)ethyl)-1-carboxylic acid (2.7). To ethyl cyanoacetate **2.3** (1.39 g, 1.73 mmol, 1.00 equiv.) and powdered KOH (297 mg, 5.29 mmol, 3.1 equiv), absolute ethanol (21 mL, 0.08 M) and H_2O (21 mL, 0.08 M) were added. The reaction was heated to 80 °C. After 3 h, 1 M HCl (~20 mL) was added, and the mixture was extracted with Et_2O (3 x 60 mL). The organics were washed with brine, dried ($MgSO_4$), and evaporated to dryness to yield branched fluorous cyanoacid as a white solid (1.26 g, 1.61 mmol, 93% crude yield). Branched fluorous cyanoacid (938 mg, 1.20 mmol) suspended in conc. HCl (27 mL, 0.04 M) was stirred and heated to 100 °C for 2 h, then cooled to 0 °C, and conc. H_2SO_4 (27 mL, 0.04 M) was added slowly. The

reaction mixture was heated to 160 °C. Note: reaction is connected to a base trap before venting into a fume hood. After 14 h, the reaction was stopped, diluted with H_2O, and extracted with Et_2O (4 x 50 mL). The organics were dried ($MgSO_4$), filtered, and concentrated to yield **2.7** as an off-white solid (832 mg, 1.11 mmol, 92%). From **2.3**, the two step yield is 89%. R_f = 0.05 in 30% Et_2O/pentane (streaks). ^{1}H NMR (500 MHz, MeOD-d_4): δ 2.55 (sep, J = 5.0 Hz, 1H), 2.32 – 2.17 (m, 4H), 1.99 – 1.79 (m, 4H). ^{13}C NMR (101 MHz, MeOD-d_4): δ 177.2, 44.5, 29.6 (t, J_{CF} = 22.6 Hz), 23.7. ^{19}F NMR (376 MHz, MeOD-d_4): δ -82.5 (tt, J = 10.2, 2.7 Hz, 6F), -114.9 – -116.4 (m, 4F), -123.0 (bs, 4F), -123.9 (bs, 4F), -124.6 (bs, 4F), -127.3 – -127.4 (m, 4F). HRMS (ESI) calcd. for $C_{18}H_9F_{26}O_2^-$ $[M – H]^-$: 751.0193; found 751.0183.

2,2-bis((perfluorohexyl)ethyl)-1-ethanol (2.8). To lithium aluminum hydride (1.0 M in THF, 3.6 mmol, 2.4 equiv) in Et_2O (15 mL), was added branched fluorous carboxylic acid **2.7** (1.11 g, 1.47 mmol, 1.00 equiv) in Et_2O (15 mL) slowly under nitrogen. After 3.5 h, the reaction was quenched by slow addition of H_2O and saturated $NaHCO_3$, and then extracted with Et_2O (4 x 20 mL). The organics were dried ($MgSO_4$), filtered, and concentrated. Crude reaction mixture was absorbed onto SiO_2 and purified by flash column chromatography (silica gel, 15% Et_2O/pentane) to provide the product **2.8** as a colorless oil (981 mg, 1.33 mmol, 90%). R_f = 0.4 in 30% Et_2O/pentane. ^{1}H NMR (500 MHz, $CDCl_3$): δ 3.64 (apparent t, J = 4.3 Hz, 2H), 2.29 – 1.99 (m, 4H), 1.78 – 1.62 (m, 5H), 1.44 (t, J = 4.6 Hz, 1H). ^{13}C NMR (126 MHz, $CDCl_3$): δ 120.8 – 106.3 (CF_n), 64.4, 39.1, 28.6 (t, J_{CF} = 22.4 Hz), 21.6. ^{19}F NMR (376 MHz, $CDCl_3$): δ -80.9 (tt, J = 10.0, 5.2 Hz, 6F), -114.6 – -114.7 (m, 4F), -122.0 (bs, 4F), -122.9 (bs, 4F), -123.5 (bs, 4F), -126.2 – -126.3 (m, 4F). HRMS (ESI) calcd. for $C_{18}H_{12}F_{26}OCl^-$ $[M + Cl]^-$: 773.0167; found 773. 0165.

2,2-bis((perfluorohexyl)ethyl)-1-ethyl tosylate (2.9). Tosylate **2.9** was synthesized using a

procedure adapted from Yoshida, et. al.[44] To alcohol **2.8** (453 mg, 0.614 mmol, 1.00 equiv), was added DCM (3 mL, 0.2 M), triethylamine (0.21 mL, 1.53 mmol, 2.49 equiv), and trimethylamine hydrochloride (60 mg, 0.61 mmol, 1.0 equiv). The reaction mixture was stirred vigorously, cooled to 0 °C, and tosyl chloride (175 mg, 0.921 mmol, 1.50 equiv) was added in DCM (1.9 mL). The reaction was let warm to room temperature and stirred for 12 h. The organics were washed with H_2O (2x) and brine (2x), dried ($MgSO_4$), filtered, and evaporated to dryness. The crude product was evaporated onto silica from DCM and purified by column chromatography (silica gel, 50% toluene/hexanes) to afford **2.9** as a white solid (481 mg, 0.539 mmol, 88%). R_f = 0.2 in 10% EtOAc/hexanes. ^{1}H NMR (500 MHz, $CDCl_3$): δ 7.79 (d, J = 8.0 Hz, 2H), 7.37 (d, J = 8.0 Hz, 2H), 3.98 (d, J = 4.5 Hz, 2H), 2.45 (s, 3H), 2.04 – 1.95 (m, 4H), 1.83 – 1.76 (m, 1H), 1.66 – 1.62 (m, 4H). ^{13}C NMR (101 MHz, $CDCl_3$): δ 145.5, 132.5, 130.2, 128.0, 70.3, 36.7, 28.1 (t, J_{CF} = 22.4 Hz), 21.7, 21.5. ^{19}F NMR (376 MHz, $CDCl_3$) δ -80.8 (t, J = 10.0 Hz, 6F), -114.5 – -114.6 (m, 4F), -121.9 (bs, 4F), -122.8 (bs, 4F), -123.4 (bs, 4F), -126.0 – -126.2 (m, 4F). HRMS (EI) calcd. for $C_{25}H_{18}F_{26}O_3S^+$ $[M]^+$: 892.0561; found 892.0560.

2,2-bis((perfluorohexyl)ethyl)-1-ethyl azide (2.10). To tosylate **2.9** (60 mg, 0.07 mmol, 1.0 equiv.) was added sodium azide (11 mg, 0.17 mmol, 2.5 equiv) and DMF (3 mL, 0.02 M). The mixture was heated to 80 °C. After 12 h, the reaction mixture was evaporated to dryness. The crude product was taken up in DCM and filtered, to provide the product **2.10** as a colorless oil (47 mg, 0.060 mmol, 92%). R_f = 0.6 in 10% EtOAc/hexanes. ^{1}H NMR (500 MHz, $CDCl_3$): δ 3.38 (d, J = 4.2 Hz, 2H), 2.19 – 2.05 (m, 4H), 1.74 – 1.64 (m, 5H). ^{13}C NMR (101 MHz, $CDCl_3$): δ 54.1, 37.1, 28.3 (t, J_{CF} = 22.6 Hz), 22.3.^{19}F NMR (282 MHz, $CDCl_3$): δ -80.7 – -80.8 (m, 6F), -114.4 – -114.6 (m, 4F), -121.9 (bs, 4F), -122.9 (bs, 4F), -123.4 (bs, 4F), -126.1 – -126.2 (m, 4F).

HRMS (EI) calcd. for $C_{18}H_{11}F_{26}N^+$ $[M – N_2]^+$: 735.0471; found 735.0491.

2,2-bis((perfluorohexyl)ethyl)-1-ethanethiol (2.11). To tosylate **2.9** (169 mg, 0.190 mmol, 1.00 equiv), was added DMF (5.6 mL, 0.03 M) and potassium thioacetate (38 mg, 0.33 mmol, 1.7 equiv). The reaction was heated to 80 °C and stirred for 4 h. The reaction mixture was evaporated to dryness, taken up in DCM, filtered, and concentrated to yield an off-white solid (135 mg, 0.169 mmol, 90% crude yield). Branched fluorous thioacetate **(**122 mg, 0.150 mmol) was dissolved in MeOH (1.0 mL, 0.2 M) and under nitrogen, acetyl chloride (80 μL, 1.0 mmol, 7.5 equiv) was added dropwise. The reaction mixture was stirred at 65 °C for 5.5 h, and then evaporated to dryness. The crude product was absorbed onto silica and purified by column chromatography (silica gel, 1% Et_2O/pentane → 5% Et_2O/pentane) to afford the product **2.11** as a colorless oil (105 mg, 0.139 mmol, 91%). The two step yield from **2.9** is 82%. R_f = 0.6 in 10% EtOAc/hexanes. ^{1}H NMR (500 MHz, $CDCl_3$): δ 2.60 (dd, J = 8.2, 4.7 Hz, 2H), 2.17 – 1.99 (m, 4H), 1.82 – 1.65 (m, 5H), 1.26 (t, J = 8.2 Hz, 1H). ^{13}C NMR (101 MHz, $CDCl_3$): δ 39.0, 28.3 (t, J_{CF} = 22.3 Hz), 27.5, 22.7. ^{19}F NMR (376 MHz, $CDCl_3$): δ -80.8 (t, J = 10.0 Hz, 6F), -114.4 – -114.5 (m, 4F), -121.9 (bs, 4F), -122.9 (bs, 4F), -123.4 (bs, 4F), -126.1 – -126.2 (m, 4F). HRMS (EI) calcd. for $C_{18}H_{12}F_{26}S^+$ $[M]^+$: 754.0245; found 754.0262.

5,10,15,20-tetrakis(4-(2,2-bis(perfluorohexylethyl)ethyl-thio)-2,3,5,6-tetrafluorophenyl)porpyrin (2.13). Procedure was adapted from Tüxen, et. al.[45] Branched thiol **11** (104 mg, 0.138 mmol, 10.0 equiv) was dissolved in DMF (2.0 mL), EtOAc (0.5 mL), and diethylamine (41 μL, 0.40 mmol, 28.5 equiv). To this mixture, 5,10,15,20-tetrakis(pentafluorophenyl)porphyrin **2.12** (13.4 mg, 0.0140 mmol, 1.0 equiv) dissolved in DMF

(1.4 mL) was added. The reaction mixture was stirred for 17 h at room temperature, at which point the product had precipitated from solution. The mixture was filtered, and the precipitate was dissolved in chloroform. The crude product was evaporated onto silica from acetone and purified by column chromatography (silica gel, 3% → 4% → 5% → 10% acetone/pentane) to afford the product **2.13** as a dark purple solid (46 mg, 0.12 mmol, 85%). R_f = 0.4 in 20% in acetone/hexanes. ^{1}H NMR (500 MHz, $CDCl_3$): δ 8.87 (s, 8H), 3.29 (d, J = 4.7 Hz, 8H), 2.27 – 2.17 (m, 16H), 2.07 – 1.89 (m, 20H), -2.89 (s, 2H). ^{19}F NMR (282 MHz, $CDCl_3$): δ -80.9 (t, J = 9.8 Hz, 24F), -114.2 – -114.4 (m, 16F), -121.8 (bs, 16F), -122.9 (bs, 16F), -123.3 (bs, 16F), -126.1 – -126.3 (m, 16F), -134.0 (dd, J = 24.9, 12.3 Hz, 8F), -136.5 (dd, J = 24.8, 12.2 Hz, 8F). HRMS (MALDI): calcd for $C_{116}H_{54}F_{120}N_4S_4^+$ $(M + H)^+$: 3911.1388; found 3911.2753. Absorbance (7:3 PFD **2.15**:PFTPA **2.16**): 408, 502, 584 nm. Emission (7:3 PFD **2.15**:PFTPA **2.16**, Ex 410 nm): 651, 709 nm.

2.5.5 Figure experimental procedures

Figure 2.2B. Porphyrins **2.13** and **2.14** were added to individual dram vials from stock solutions (1.0 mg/mL) in acetone, solvent was removed, and porphyrins were dried on high vacuum (<100 mTorr). Fluorous porphryins **2.13** (0.02 mg, 0.07 mmol) and **2.14** (0.03 mg, 0.07 mmol) were dissolved in perfluoromethylcyclohexane (1.5 mL) and then sonicated for 1 min. Toluene (1.5 mL) was added. The dram vials containing each porphyrin were allowed to roll freely on a KJ-201BD Orbital shaker for 22 h. Aliquots (200 μL) from each layer (toluene and perfluoromethylcyclohexane) were dried on high vacuum to remove residual solvent. Samples were diluted in DMF (5.0 mL). Absorbance values were obtained on a JASCO V-770 UV-Visible/NIR spectrophotometer with a 2000 nm/min scan rate. The fluorous partition coefficient

was determined by taking the ratio of the absorbance in perfluoromethylcyclohexane and toluene. Photographs were taken under long-wave UV light (UVGL-25, 365 nm).

Figure 2.2D. Emulsions were prepared as described in general nanoemulsion formation procedure with **2.13** (0.14 mg, 0.04 μmol) or **2.14** (0.13 mg, 0.04 μmol) in 7:3 PFD/PFTPA (10 vol%, 20 μL). The emulsions (200 μL) were diluted to 5 mL in PBS. A portion of these solutions (1 mL) was taken and placed in the presence of 1-octanol (0.5 mL) in an Eppendorf tube. The biphasic samples were then rocked for 2 weeks. The Eppendorf tubes containing the samples were allowed to roll freely on a KJ-201BD Orbital shaker at 20 rpm. The fluorescence of the 1-octanol layer was monitored over time to determine the amount of **2.13** and **2.14** that diffused out of the emulsions. Emission values were obtained by taking an aliquot (200 μL) of the 1-octanol in a 0.3 mL quartz cuvette and measuring the fluorescence on a Horiba Instruments PTI QuantaMaster Series fluorometer with the following settings: slits 5 nm, step size 1 nm, integration time 0.1 s (Ex 410 nm, collection 450-800 nm). The 1-octanol was returned to the sample after the measurement.

Figure 2.2E. Porphyrins **2.13** and **2.14** (0.36 mmol) were dissolved in the indicated fluorous solvents (1 mL) through inversion or minimal sonication (<10 min, bath sonicator). Photographs were taken under visible light.

Figure 2.3. Empty emulsions were prepared as described in the general nanoemulsion formation procedure by sonicating fluorous solvent (10 vol%, 20 uL, 7:3 PFD **2.15**:PFTPA **2.16**, PFD **2.15**, PFOB **2.17**, or PF*t*-BuCy **2.18**) with Pluronic F-68 predissolved in PBS pH 7.4 (28 mg/mL, 2.8

wt%, 200 μL). Emulsions were diluted in MilliQ H_2O (20 μL emulsions in 2 mL MilliQ H_2O, Ω = -18 mV) in a plastic cuvette. The size was monitored by dynamic light scattering (Malvern Zetasizer Nano) and data is representative of three replicate measurements. Error bars represent the standard deviation of the product of the $Z_{average}$ and the polydispersity index of three measurements.

Figure 2.4. Cell viability with empty perfluorocarbon nanoemulsions was determined using the same procedure described for Figure 2.6B.

Figure 2.5. Cell viability comparison with **2.14** (7 nmol) and **2.13** (7 nmol) in perfluorocarbon nanoemulsions composed of 7:3 PFD **2.15**:PFTPA **2.16** was determined using the same procedure described for Figure 2.6B. Less porphyrin was used due to the lower solubility of **2.14** in 7:3 PFD:PFTPA.

Figure 2.6B/2.7. Emulsions with fluorous solvents (7:3 PFD **2.15** :PFTPA **2.16**, PFD **2.15**, PFOB **2.17**, or PF*t*-BuCy **2.18)** were prepared as described in the general nanoemulsion formation procedure with porphyrin **2.13** (0.04 mg, 0.01 μmol). A375 cells were placed in a 96-well plate (200,000 cells per 150 μL/well). The emulsions were diluted in FACS buffer (200 μL emulsions in 1 mL, PBS buffer + 1% FBS). Cells suspended in 150 μL media were treated with 50 μL of the diluted emulsions. Cells were incubated in the presence of emulsions (37 ˚C, 5% CO_2, 3 h). Cells were washed by centrifugation (3x, 526xg, 3 min) and resuspended in FACS buffer (PBS with 1% FBS) to a final volume of 200 μL. Cells were irradiated (30 min or 10 min, 420 nm LED, 8.5 mW/cm^2). After irradiation, the cells were diluted to 300 μL with FACS buffer

and incubated (0 ˚C, 15 min) with propidium iodide (1 μL, 0.25 mg/ml solution). Cell death was analyzed by FL2 channel on FACSCalibur. 15,000 cells were collected per sample.

2.5.6 NMR spectra

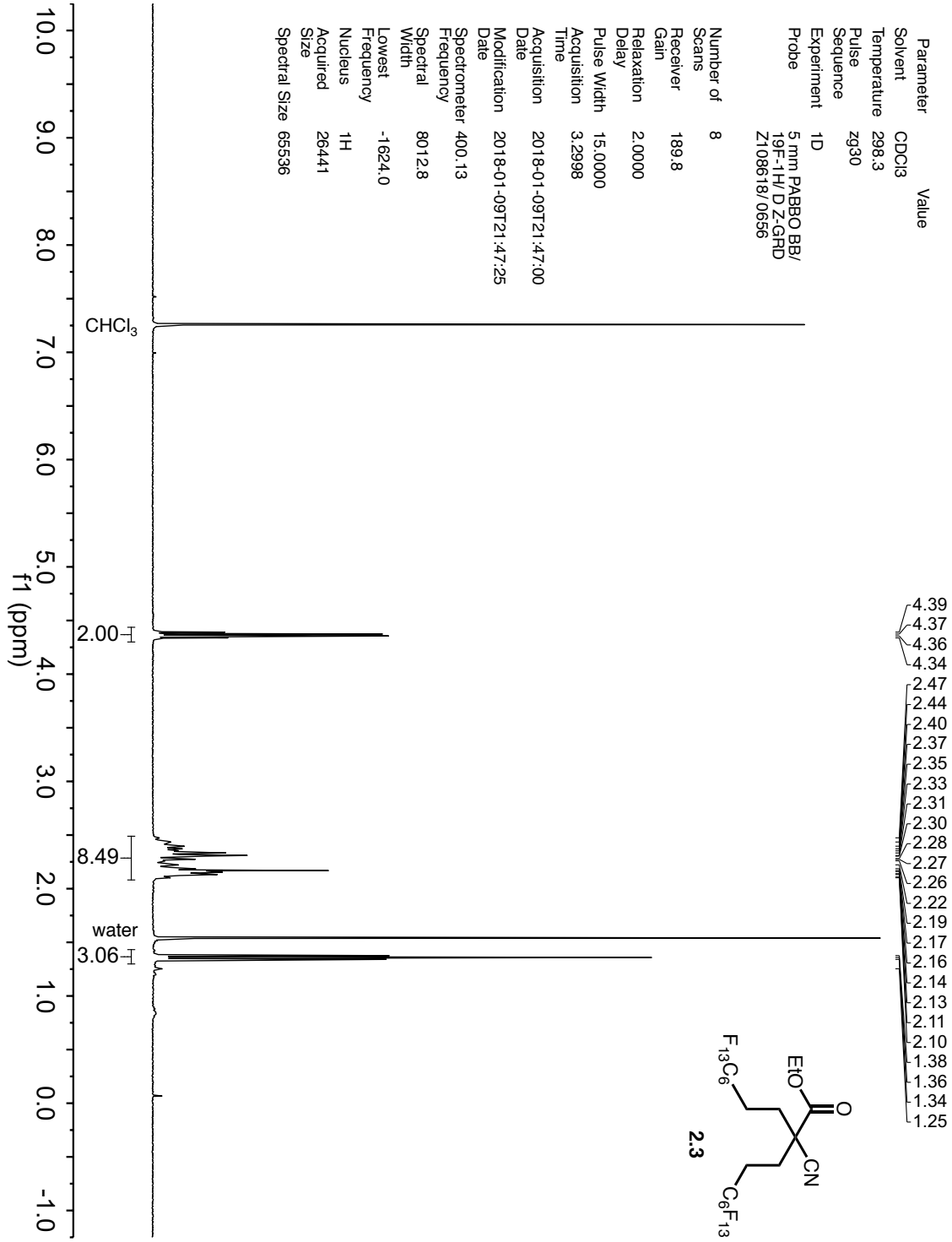

Parameter	Value
Solvent	CDCl3
Temperature	298.8
Pulse Sequence	zgpg30
Experiment	1D
Probe	5 mm PABBO BB/ 19F-1H/ D Z-GRD Z108618/ 0656
Number of Scans	500
Receiver Gain	189.8
Relaxation Delay	2.0000
Pulse Width	10.0000
Acquisition Time	1.2976
Acquisition Date	2018-02-22T13:13:00
Modification Date	2018-02-22T13:13:25
Spectrometer Frequency	100.61
Spectral Width	25252.5
Lowest Frequency	-1041.7
Nucleus	13C
Acquired Size	32768
Spectral Size	65536

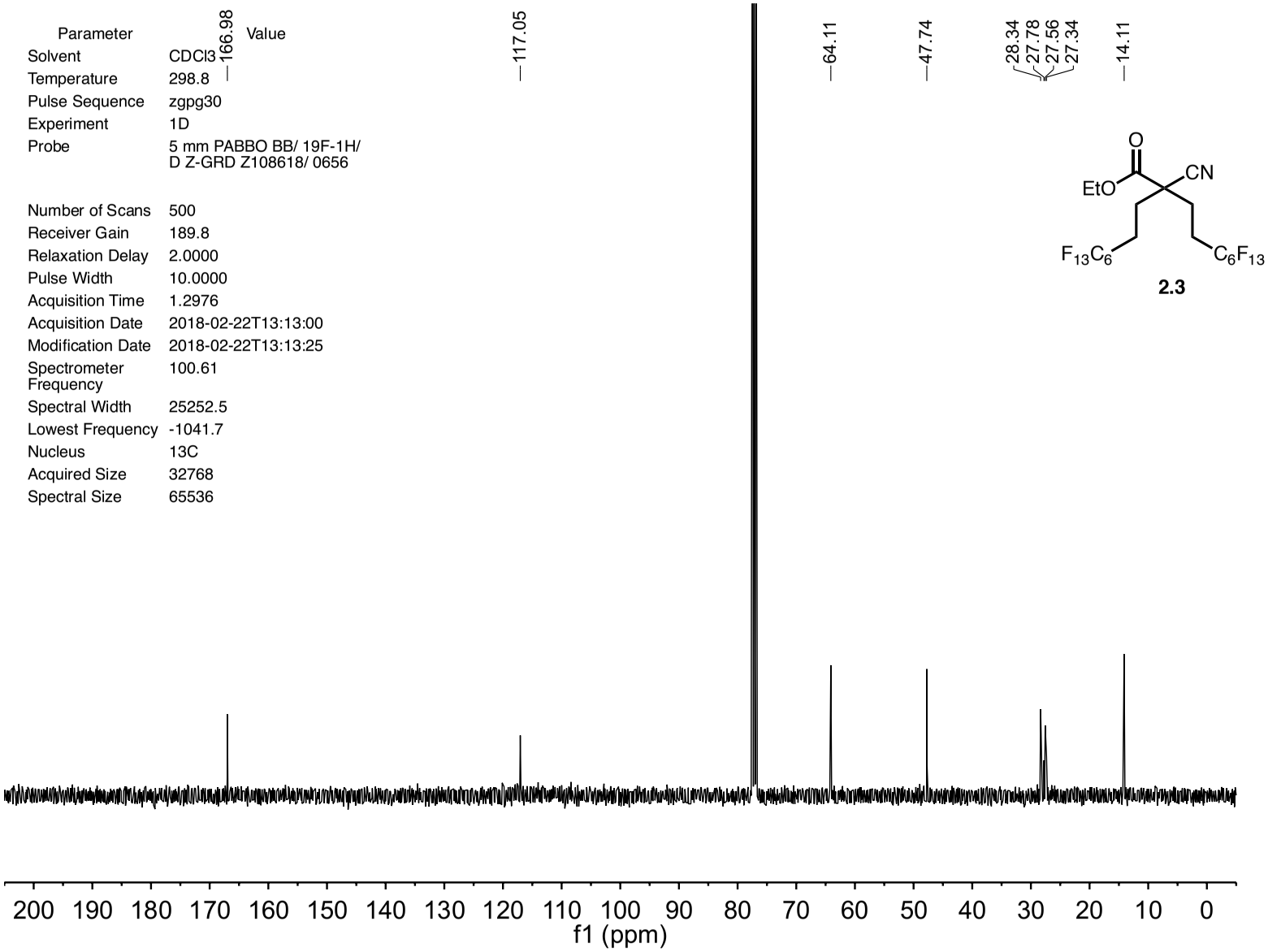

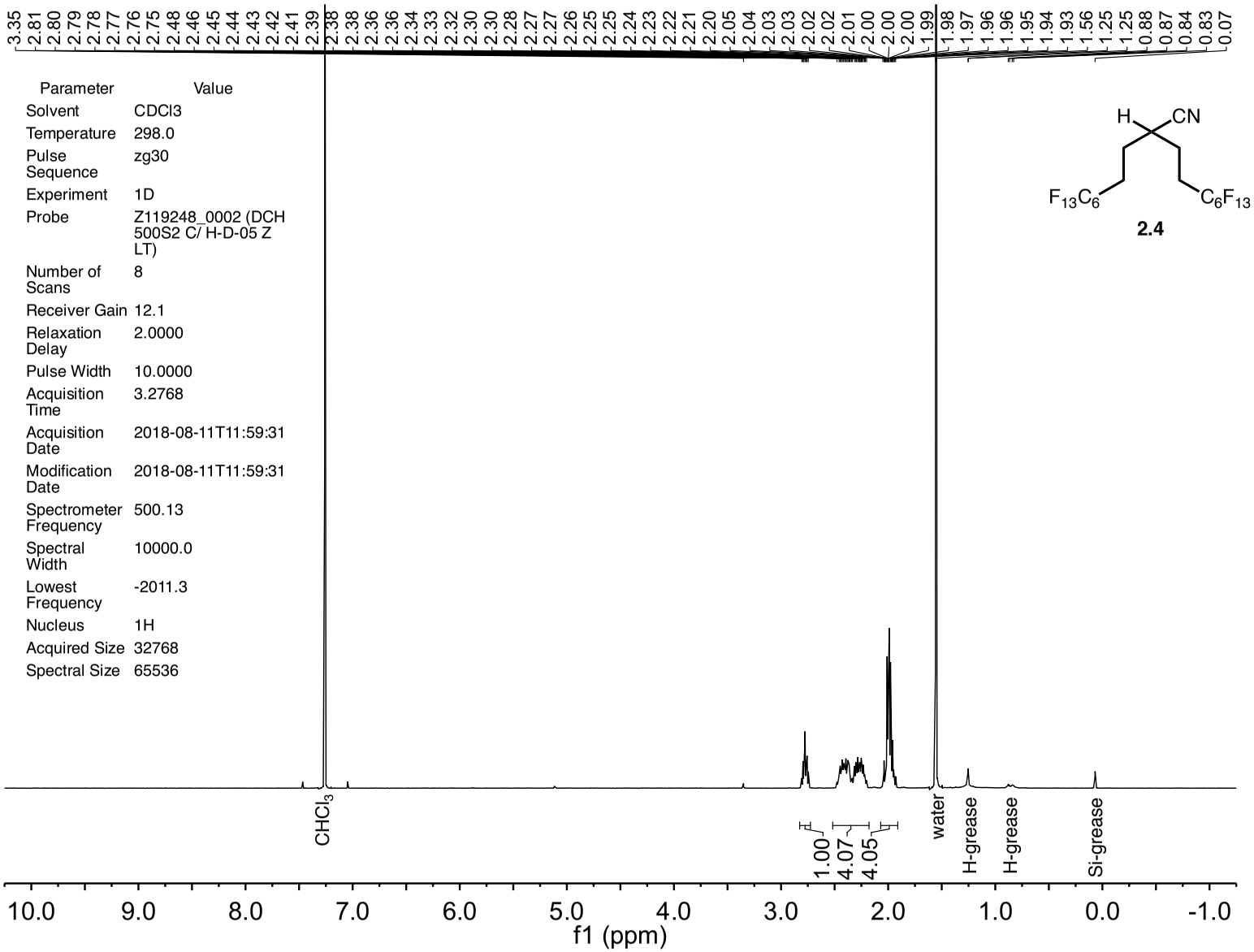

Parameter	Value
Solvent	CDCl3
Temperature	298.0
Pulse Sequence	zg30
Experiment	1D
Probe	Z119248_0002 (DCH 500S2 C/ H-D-05 Z LT)
Number of Scans	8
Receiver Gain	12.1
Relaxation Delay	2.0000
Pulse Width	10.0000
Acquisition Time	3.2768
Acquisition Date	2018-08-11T11:59:31
Modification Date	2018-08-11T11:59:31
Spectrometer Frequency	500.13
Spectral Width	10000.0
Lowest Frequency	-2011.3
Nucleus	1H
Acquired Size	32768
Spectral Size	65536

Parameter	Value
Solvent	CDCl3
Temperature	298.0
Pulse Sequence	zgpg30
Experiment	1D
Probe	Z119248_0002 (DCH 500S2 C/ H-D-05 Z LT)
Number of Scans	256
Receiver Gain	204.5
Relaxation Delay	2.0000
Pulse Width	9.6300
Acquisition Time	1.0486
Acquisition Date	2018-07-31T20:34:58
Modification Date	2018-07-31T20:34:59
Spectrometer Frequency	125.76
Spectral Width	31250.0
Lowest Frequency	-1163.1
Nucleus	13C
Acquired Size	32768
Spectral Size	131072

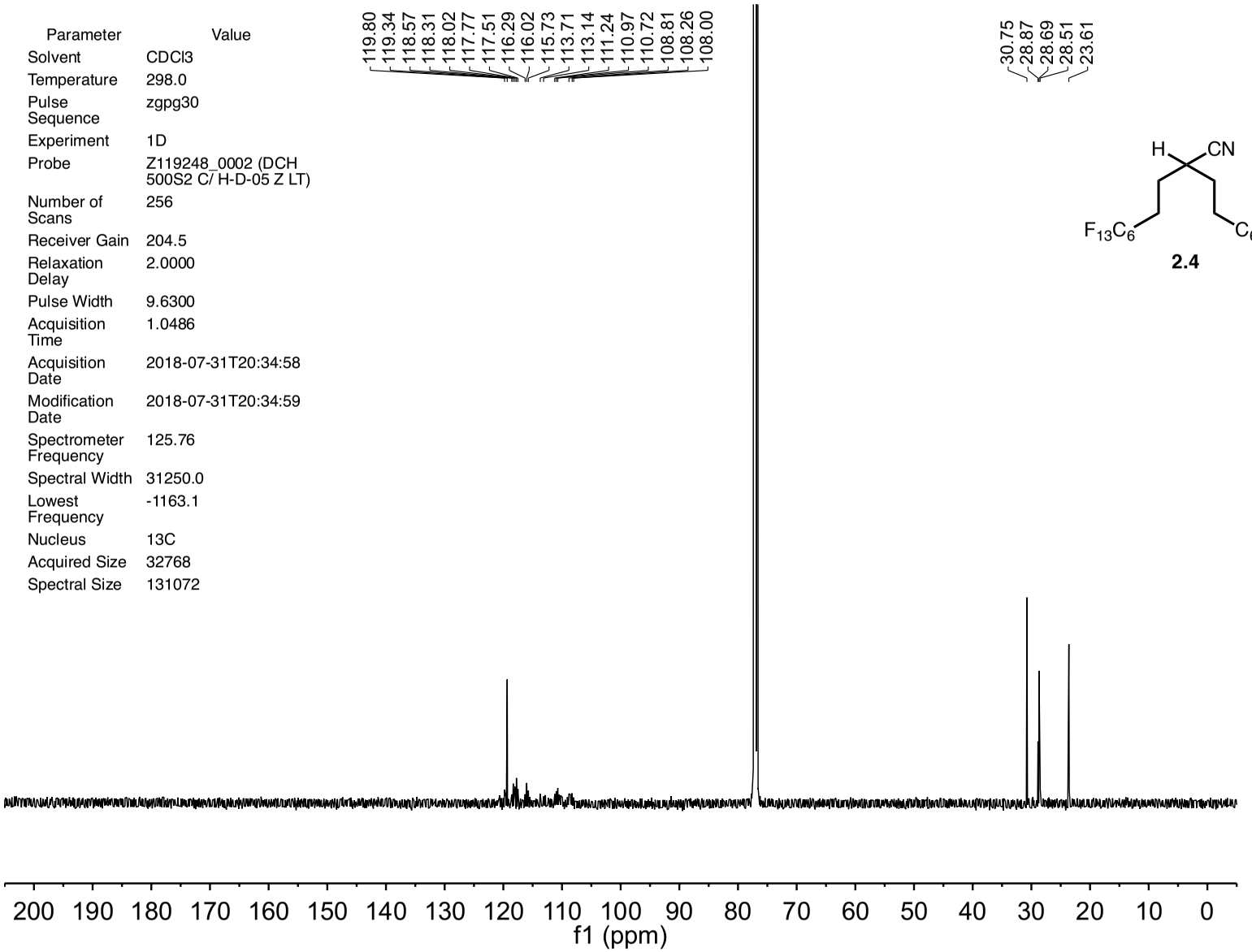

Parameter	Value
Solvent	MeOD
Temperature	298.0
Pulse Sequence	zg30
Experiment	1D
Probe	Z119248_0002 (DCH 500S2 C/ H-D-05 Z LT)
Number of Scans	16
Receiver Gain	12.1
Relaxation Delay	2.0000
Pulse Width	10.0000
Acquisition Time	3.2768
Acquisition Date	2018-09-16T12:47:36
Modification Date	2018-09-16T12:47:36
Spectrometer Frequency	500.13
Spectral Width	10000.0
Lowest Frequency	-2008.8
Nucleus	1H
Acquired Size	32768
Spectral Size	65536

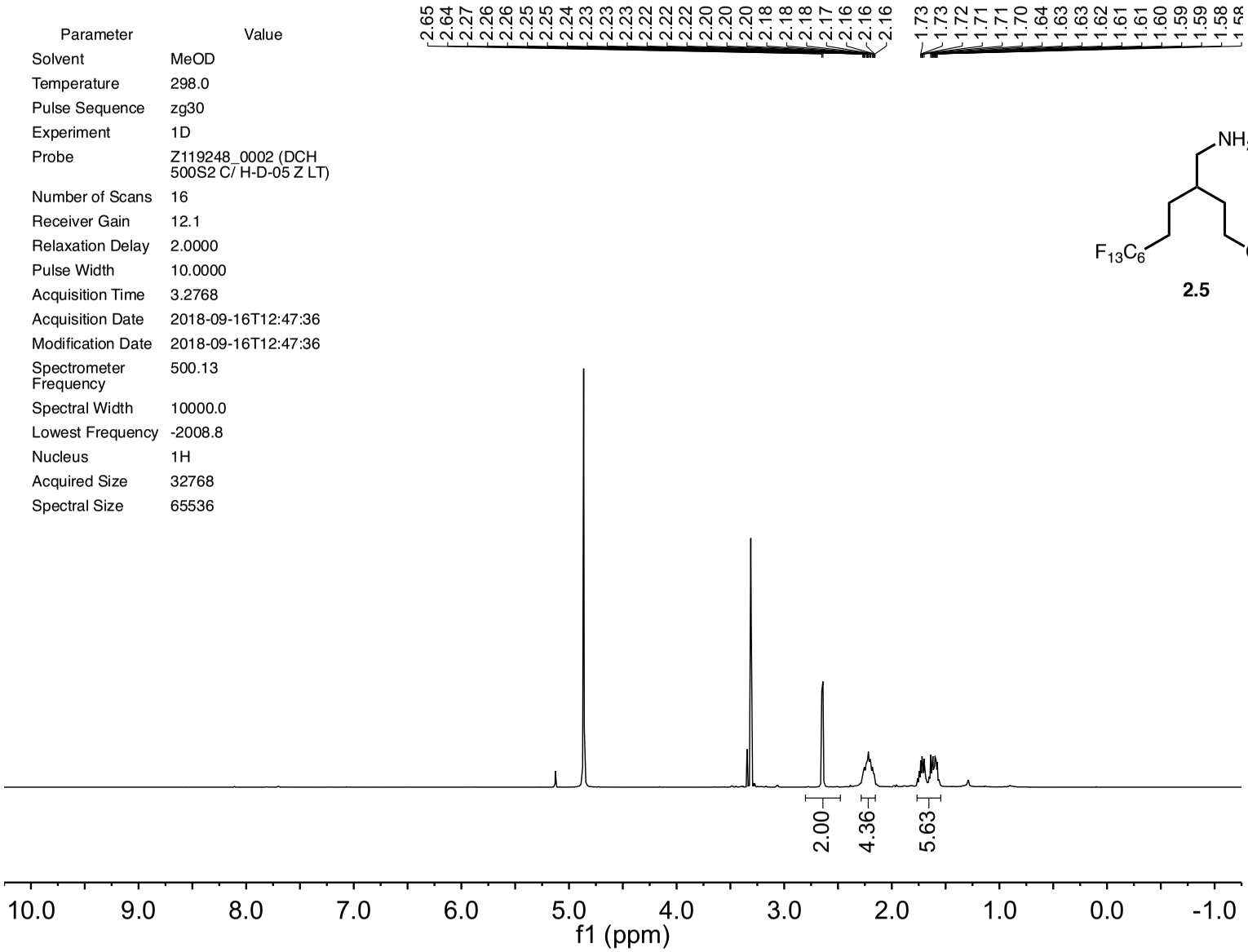

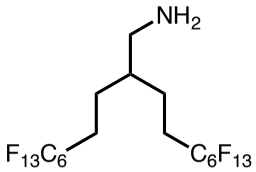

2.5

Parameter	Value
Solvent	CDCl3
Temperature	0.0
Pulse Sequence	zgfhigqn.2
Experiment	1D
Probe	5 mm PABBO BB/ 19F-1H/ D Z-GRD Z108618/ 0656
Number of Scans	16
Receiver Gain	189.8
Relaxation Delay	1.0000
Pulse Width	14.5000
Acquisition Time	1.7476
Acquisition Date	2018-07-30T12:04:00
Modification Date	2018-07-30T12:04:43
Spectrometer Frequency	376.50
Spectral Width	75000.0
Lowest Frequency	-75149.8
Nucleus	19F
Acquired Size	131072
Spectral Size	262144

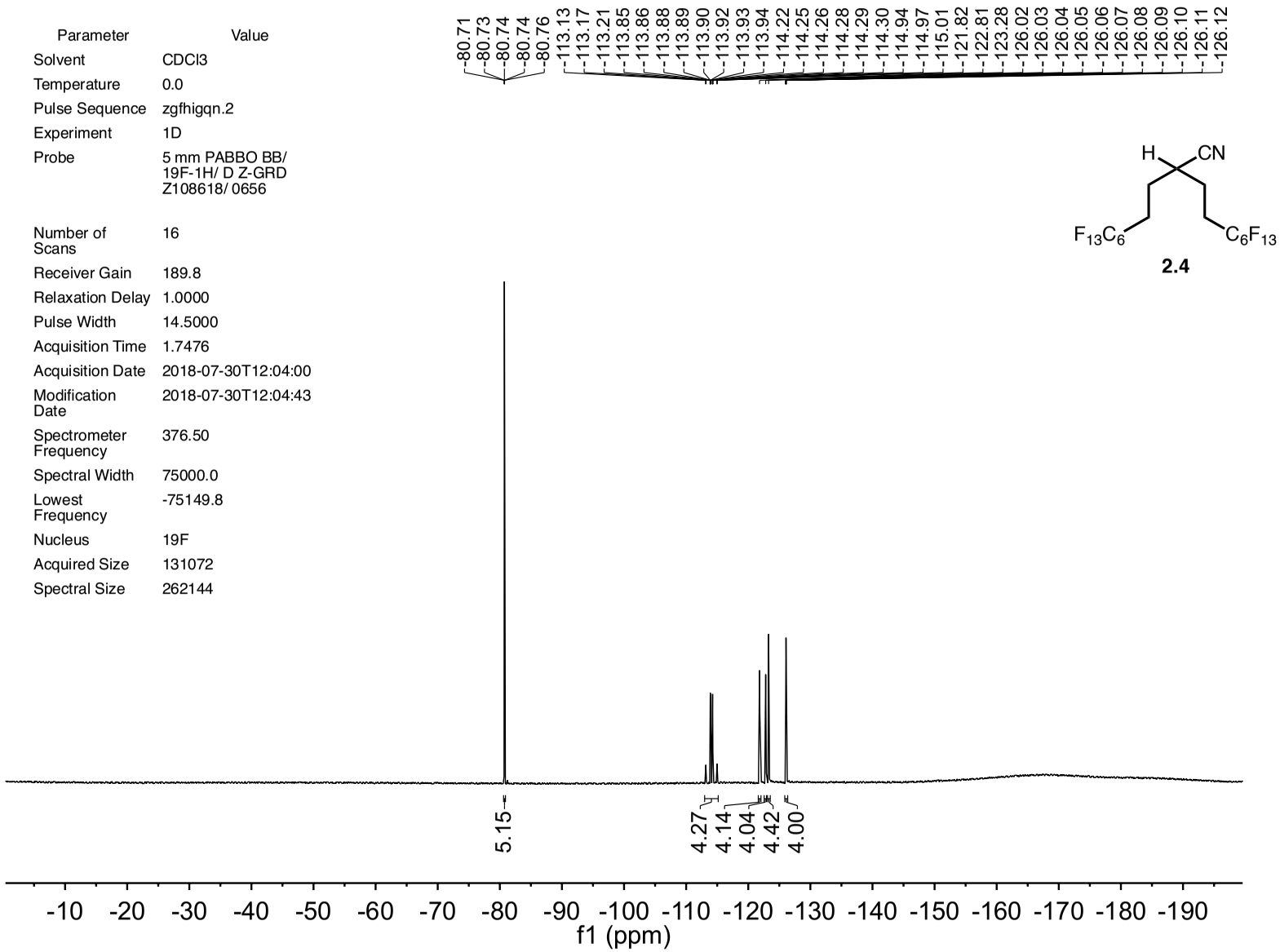

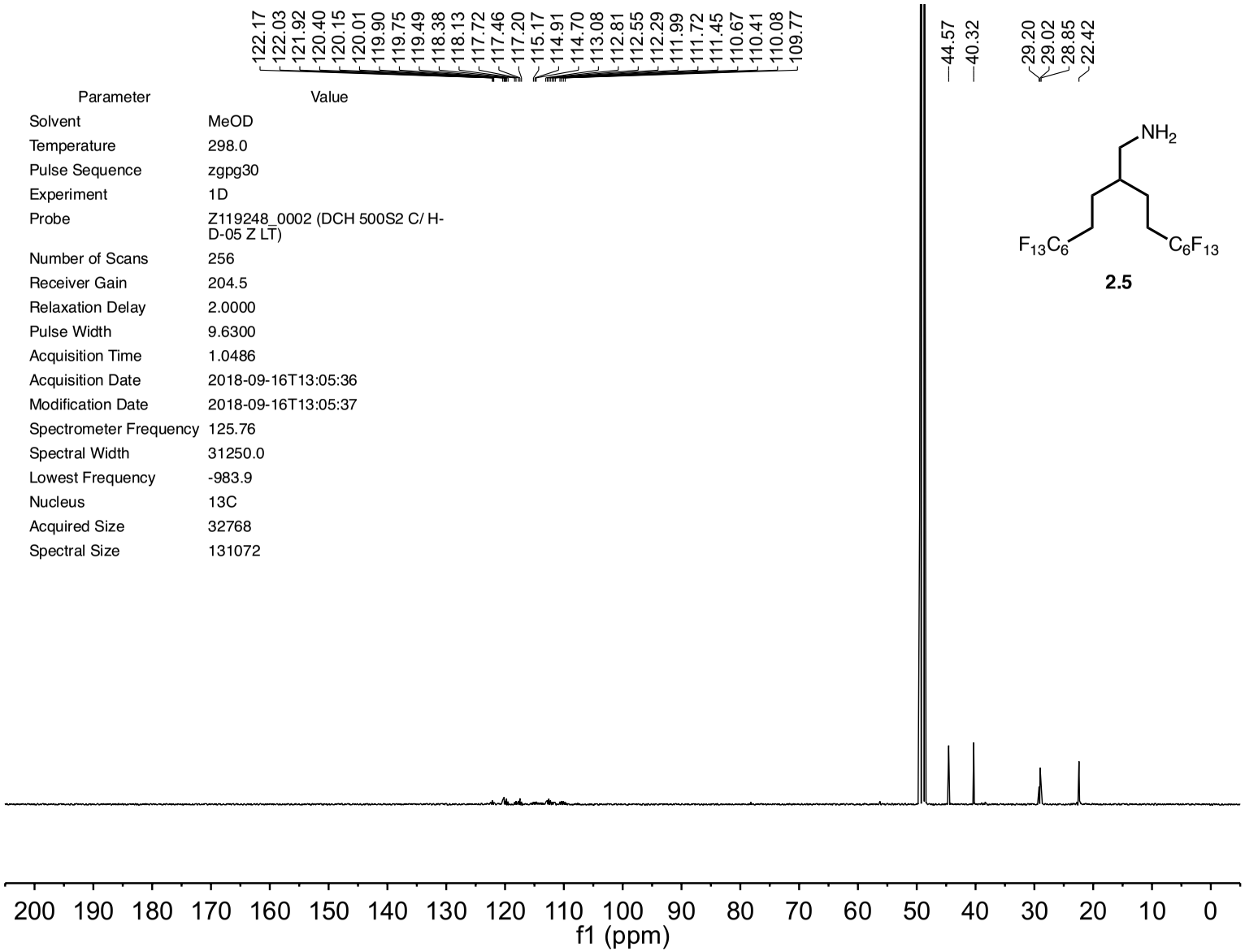

Parameter	Value
Solvent	MeOD
Temperature	298.0
Pulse Sequence	zgpg30
Experiment	1D
Probe	Z119248_0002 (DCH 500S2 C/ H-D-05 Z LT)
Number of Scans	256
Receiver Gain	204.5
Relaxation Delay	2.0000
Pulse Width	9.6300
Acquisition Time	1.0486
Acquisition Date	2018-09-16T13:05:36
Modification Date	2018-09-16T13:05:37
Spectrometer Frequency	125.76
Spectral Width	31250.0
Lowest Frequency	-983.9
Nucleus	13C
Acquired Size	32768
Spectral Size	131072

Parameter	Value
Solvent	MeOD
Temperature	298.0
Pulse Sequence	zg30
Experiment	1D
Probe	Z119248_0002 (DCH 500S2 C/ H-D-05 Z LT)
Number of Scans	16
Receiver Gain	12.1
Relaxation Delay	2.0000
Pulse Width	10.0000
Acquisition Time	3.2768
Acquisition Date	2018-09-16T12:47:36
Modification Date	2018-09-16T12:47:36
Spectrometer Frequency	500.13
Spectral Width	10000.0
Lowest Frequency	-2008.8
Nucleus	1H
Acquired Size	32768
Spectral Size	65536

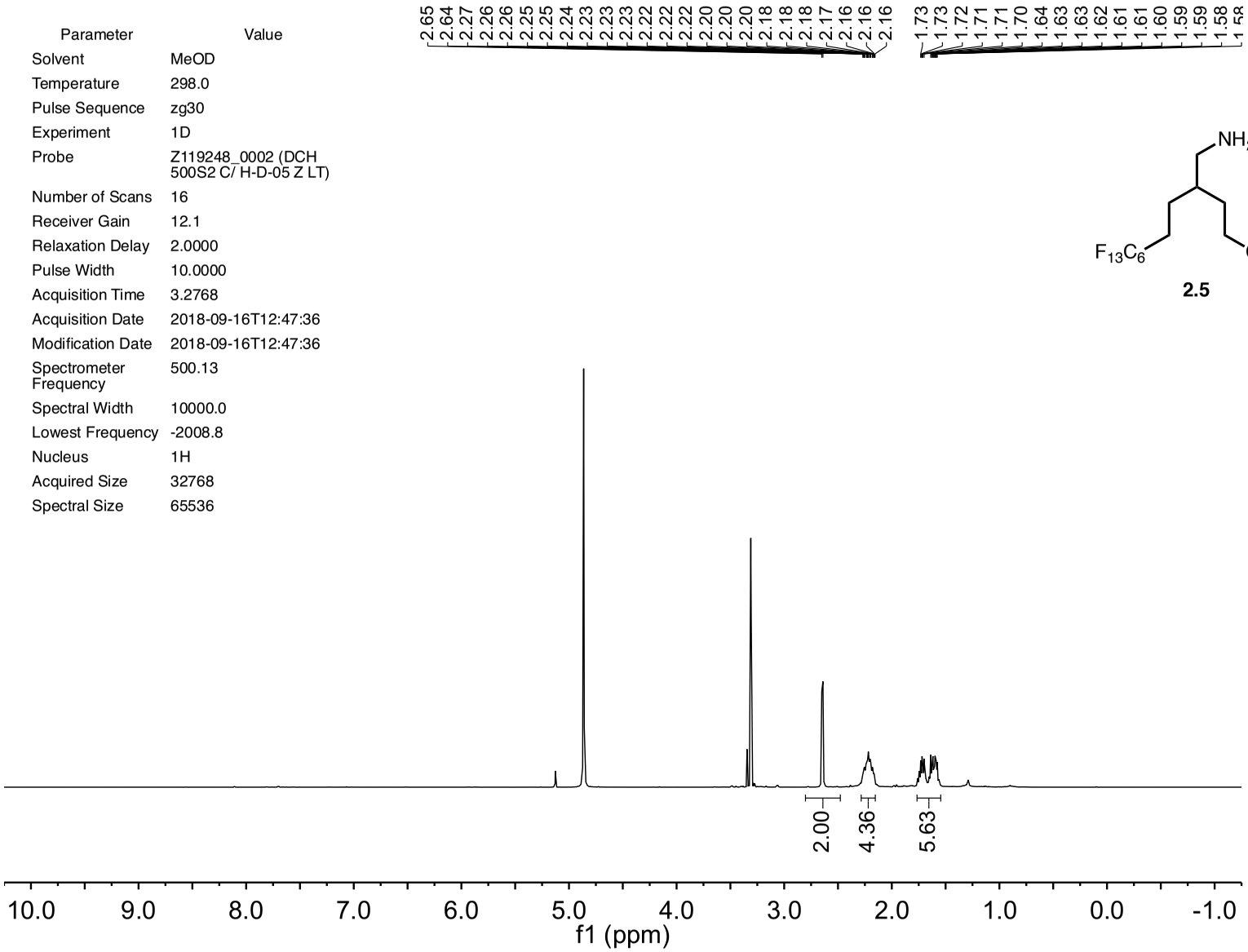

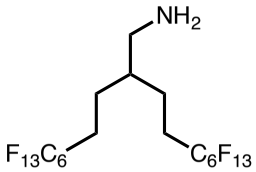

2.5

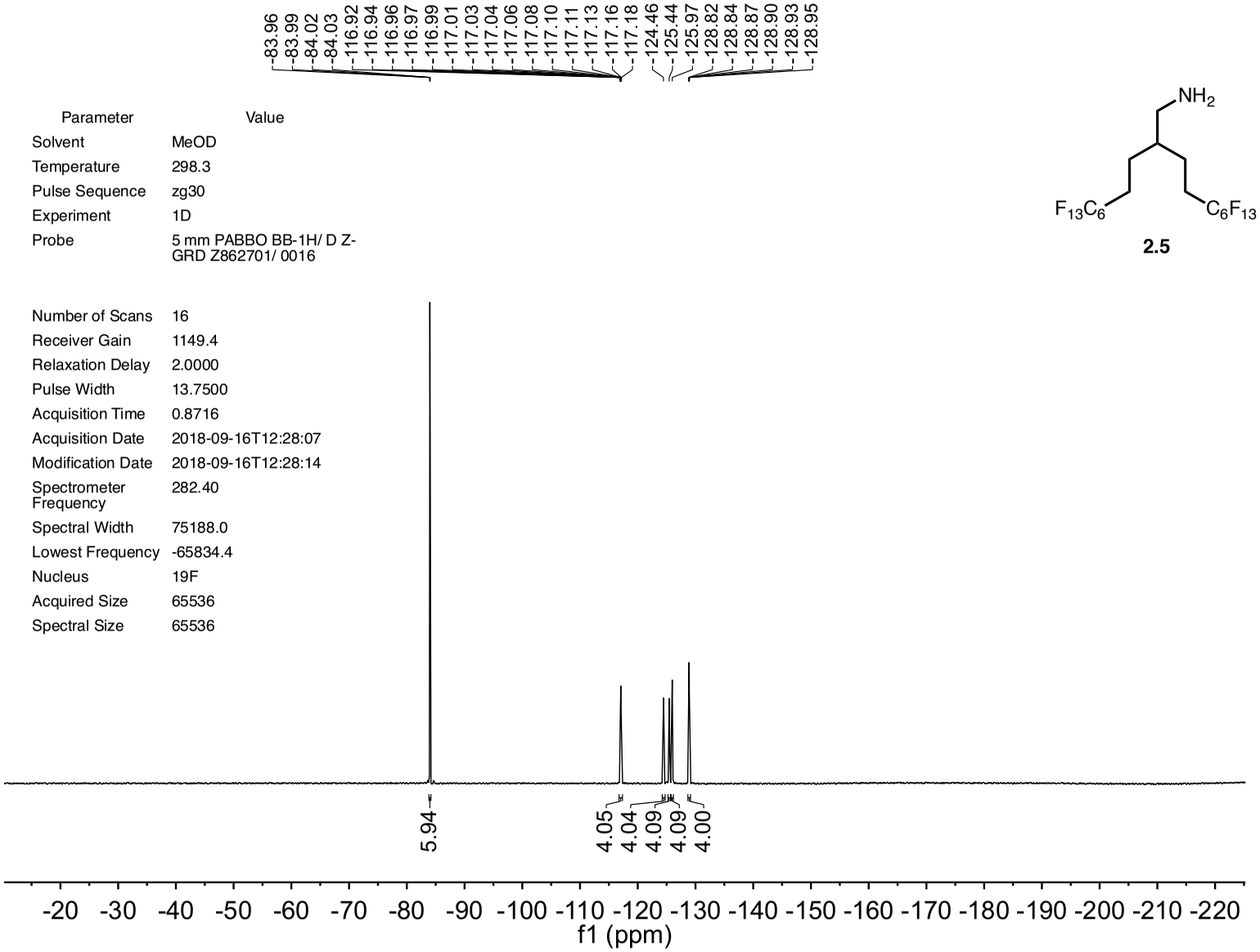

Parameter	Value
Solvent	MeOD
Temperature	298.3
Pulse Sequence	zg30
Experiment	1D
Probe	5 mm PABBO BB-1H/ D Z-GRD Z862701/ 0016
Number of Scans	16
Receiver Gain	1149.4
Relaxation Delay	2.0000
Pulse Width	13.7500
Acquisition Time	0.8716
Acquisition Date	2018-09-16T12:28:07
Modification Date	2018-09-16T12:28:14
Spectrometer Frequency	282.40
Spectral Width	75188.0
Lowest Frequency	-65834.4
Nucleus	19F
Acquired Size	65536
Spectral Size	65536

2.5

Parameter	Value
Solvent	CDCl3
Temperature	298.0
Pulse Sequence	zgpg30
Experiment	1D
Probe	Z119248_0002 (DCH 500S2 C/ H-D-05 Z LT)
Number of Scans	800
Receiver Gain	204.5
Relaxation Delay	2.0000
Pulse Width	10.5000
Acquisition Time	1.0486
Acquisition Date	2018-09-13T20:43:25
Modification Date	2018-09-13T20:43:26
Spectrometer Frequency	125.76
Spectral Width	31250.0
Lowest Frequency	-1163.1
Nucleus	13C
Acquired Size	32768
Spectral Size	131072

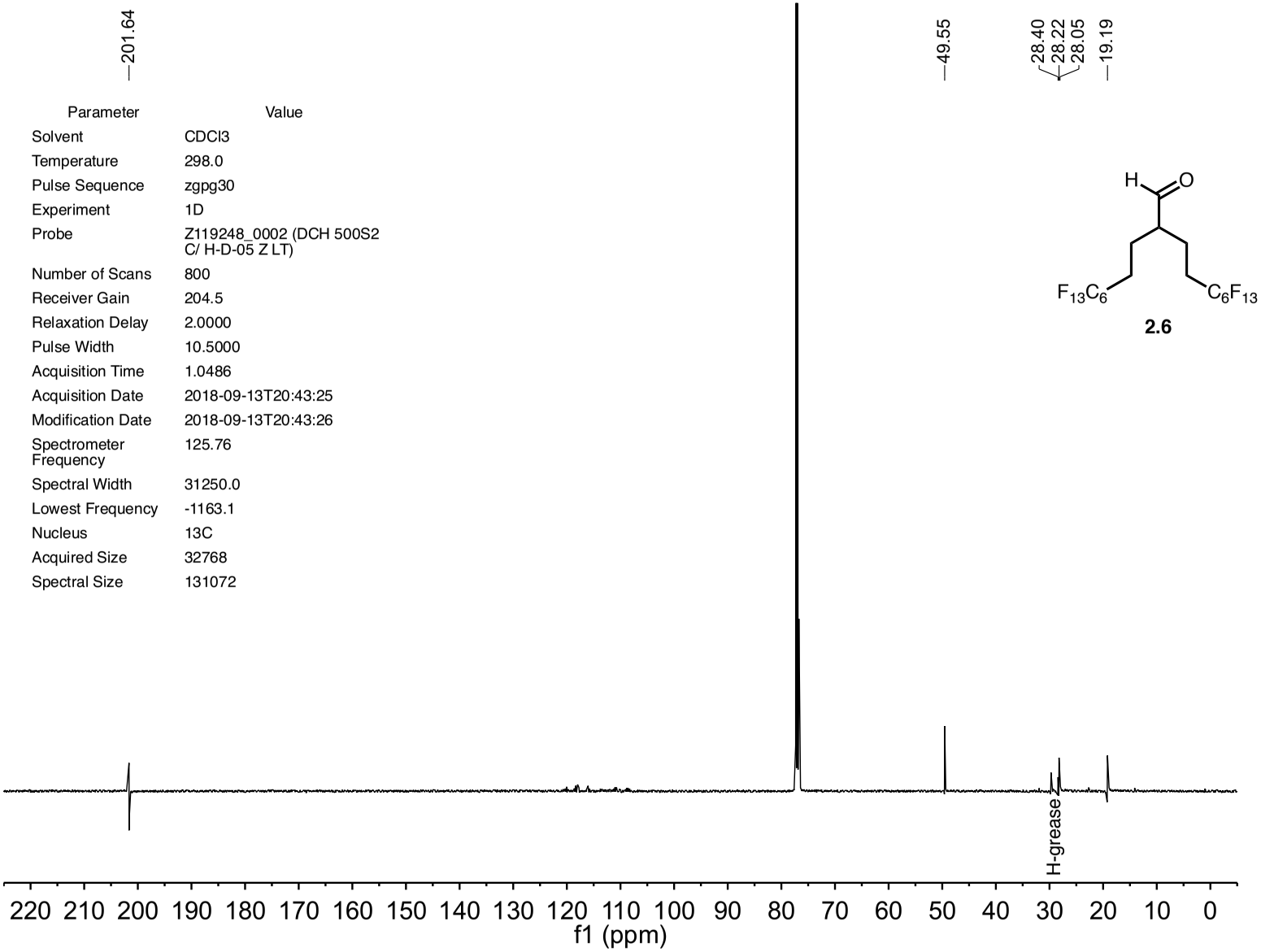

2.6

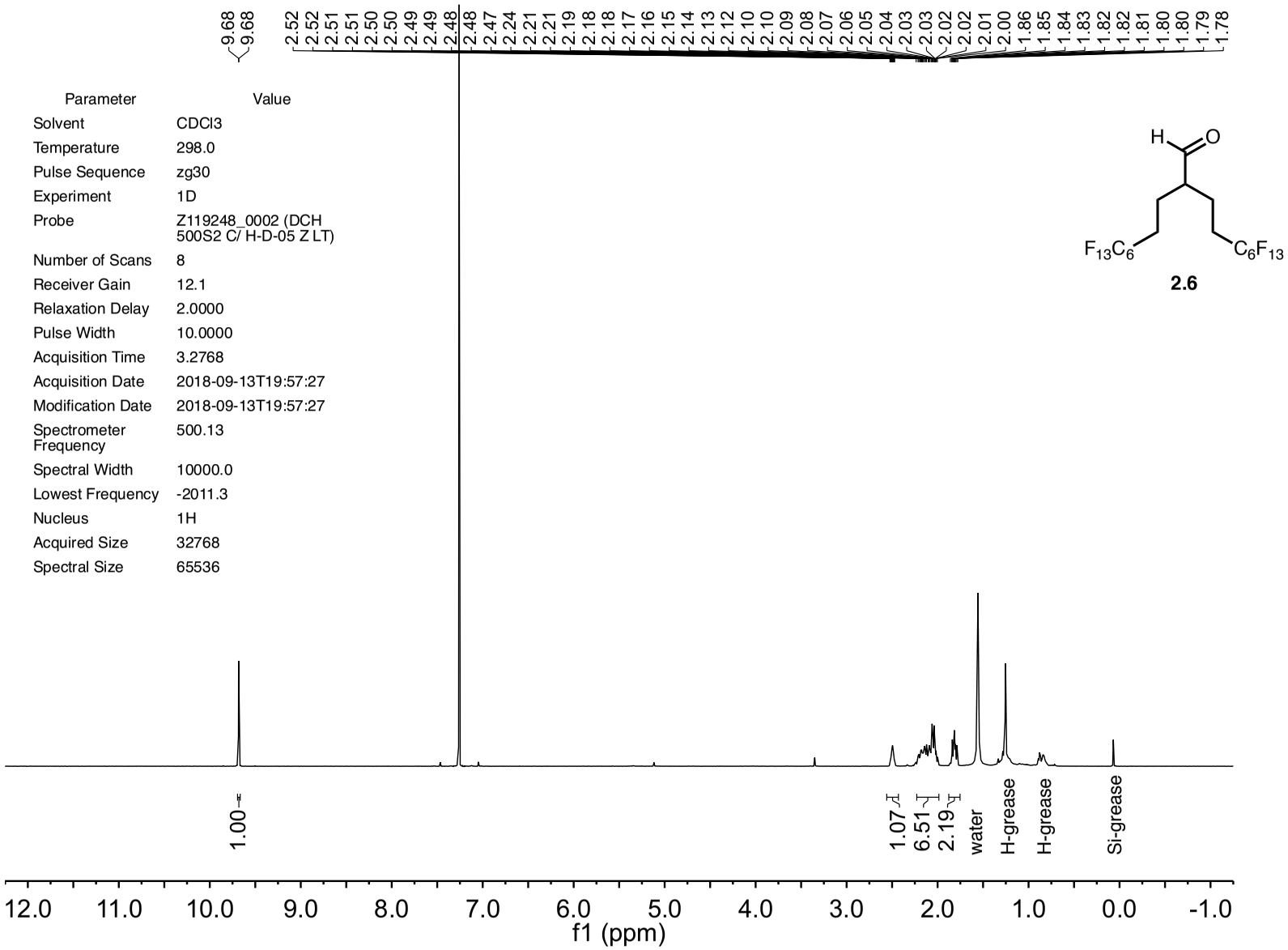

Parameter	Value
Solvent	CDCl3
Temperature	298.0
Pulse Sequence	zg30
Experiment	1D
Probe	Z119248_0002 (DCH 500S2 C/ H-D-05 Z LT)
Number of Scans	8
Receiver Gain	12.1
Relaxation Delay	2.0000
Pulse Width	10.0000
Acquisition Time	3.2768
Acquisition Date	2018-09-13T19:57:27
Modification Date	2018-09-13T19:57:27
Spectrometer Frequency	500.13
Spectral Width	10000.0
Lowest Frequency	-2011.3
Nucleus	1H
Acquired Size	32768
Spectral Size	65536

2.6

Parameter	Value
Solvent	CDCl3
Temperature	298.3
Pulse Sequence	zgfhigqn.2
Experiment	1D
Probe	5 mm PABBO BB/ 19F-1H/ D Z-GRD Z108618/ 0656
Number of Scans	16
Receiver Gain	189.8
Relaxation Delay	1.0000
Pulse Width	14.5000
Acquisition Time	1.7476
Acquisition Date	2018-09-14T01:46:00
Modification Date	2018-09-14T01:46:14
Spectrometer Frequency	376.50
Spectral Width	75000.0
Lowest Frequency	-75149.8
Nucleus	19F
Acquired Size	131072
Spectral Size	262144

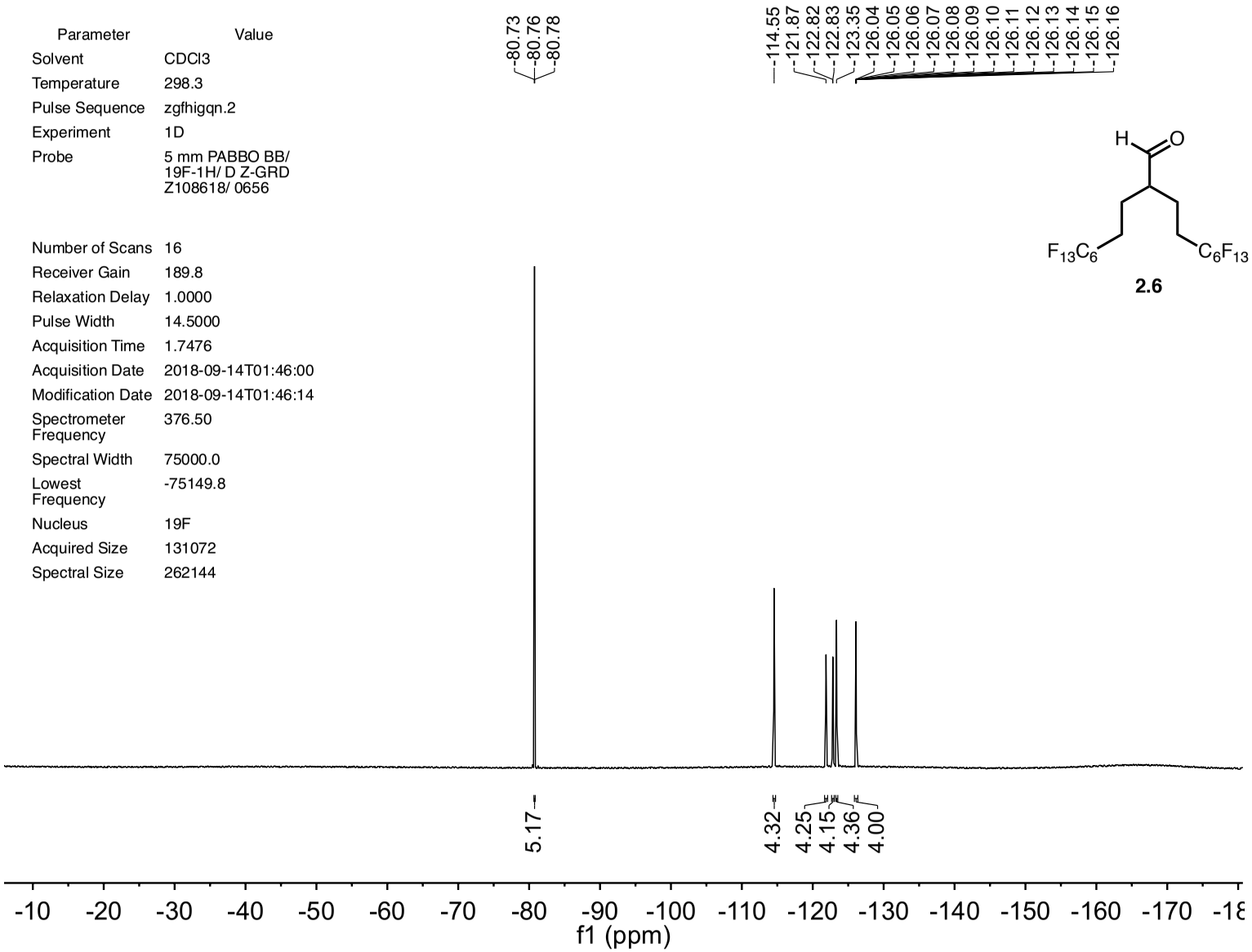

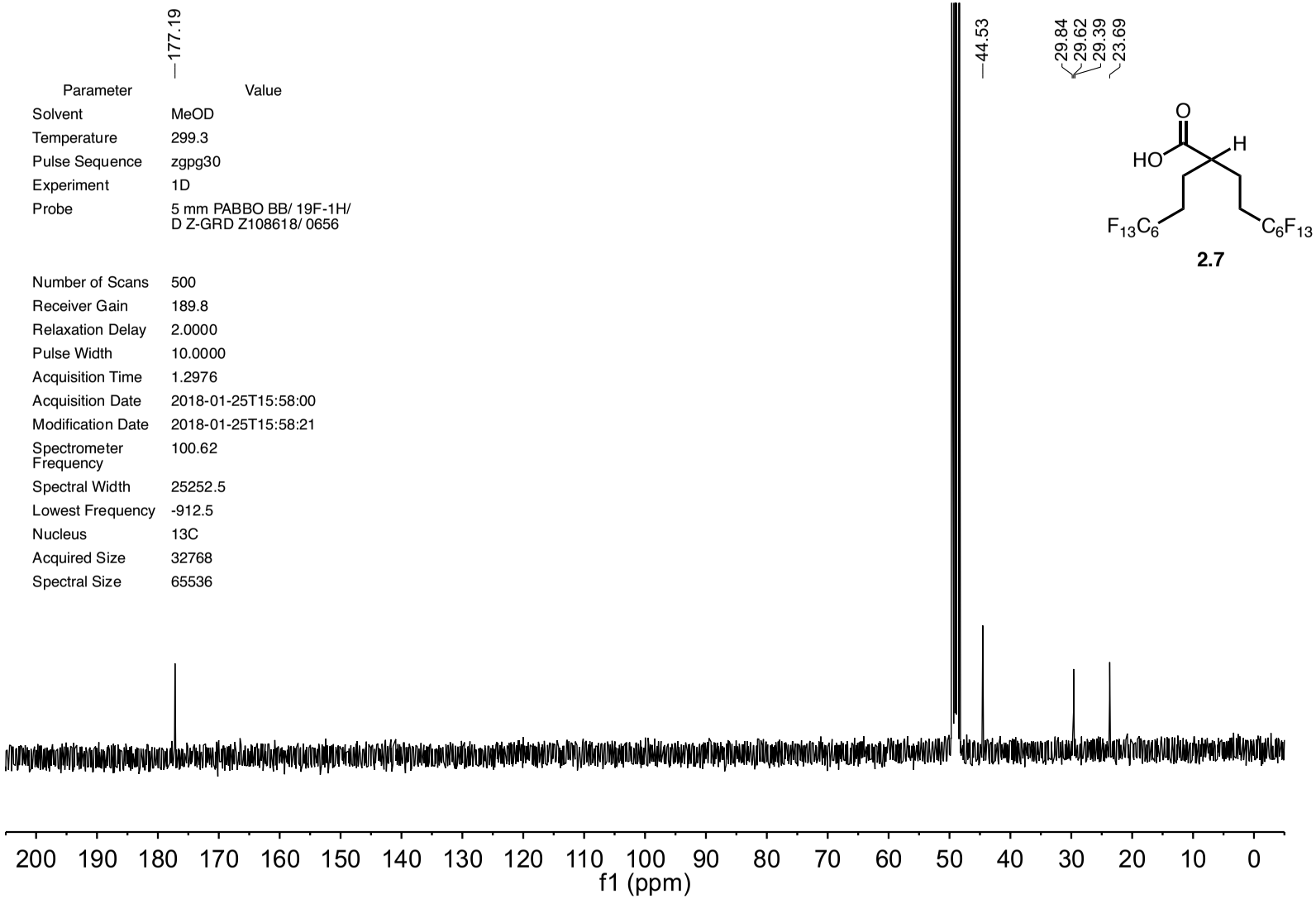

Parameter	Value
Solvent	MeOD
Temperature	299.3
Pulse Sequence	zgpg30
Experiment	1D
Probe	5 mm PABBO BB/ 19F-1H/ D Z-GRD Z108618/ 0656
Number of Scans	500
Receiver Gain	189.8
Relaxation Delay	2.0000
Pulse Width	10.0000
Acquisition Time	1.2976
Acquisition Date	2018-01-25T15:58:00
Modification Date	2018-01-25T15:58:21
Spectrometer Frequency	100.62
Spectral Width	25252.5
Lowest Frequency	-912.5
Nucleus	13C
Acquired Size	32768
Spectral Size	65536

Parameter	Value
Solvent	MeOD
Temperature	298.0
Pulse Sequence	zg30
Experiment	1D
Probe	Z119248_0002 (DCH 500S2 C/ H-D-05 Z LT)
Number of Scans	8
Receiver Gain	19.1
Relaxation Delay	2.0000
Pulse Width	10.0000
Acquisition Time	3.2768
Acquisition Date	2018-01-25T13:41:38
Modification Date	2018-01-25T13:41:38
Spectrometer Frequency	500.13
Spectral Width	10000.0
Lowest Frequency	-2008.7
Nucleus	1H
Acquired Size	32768
Spectral Size	65536

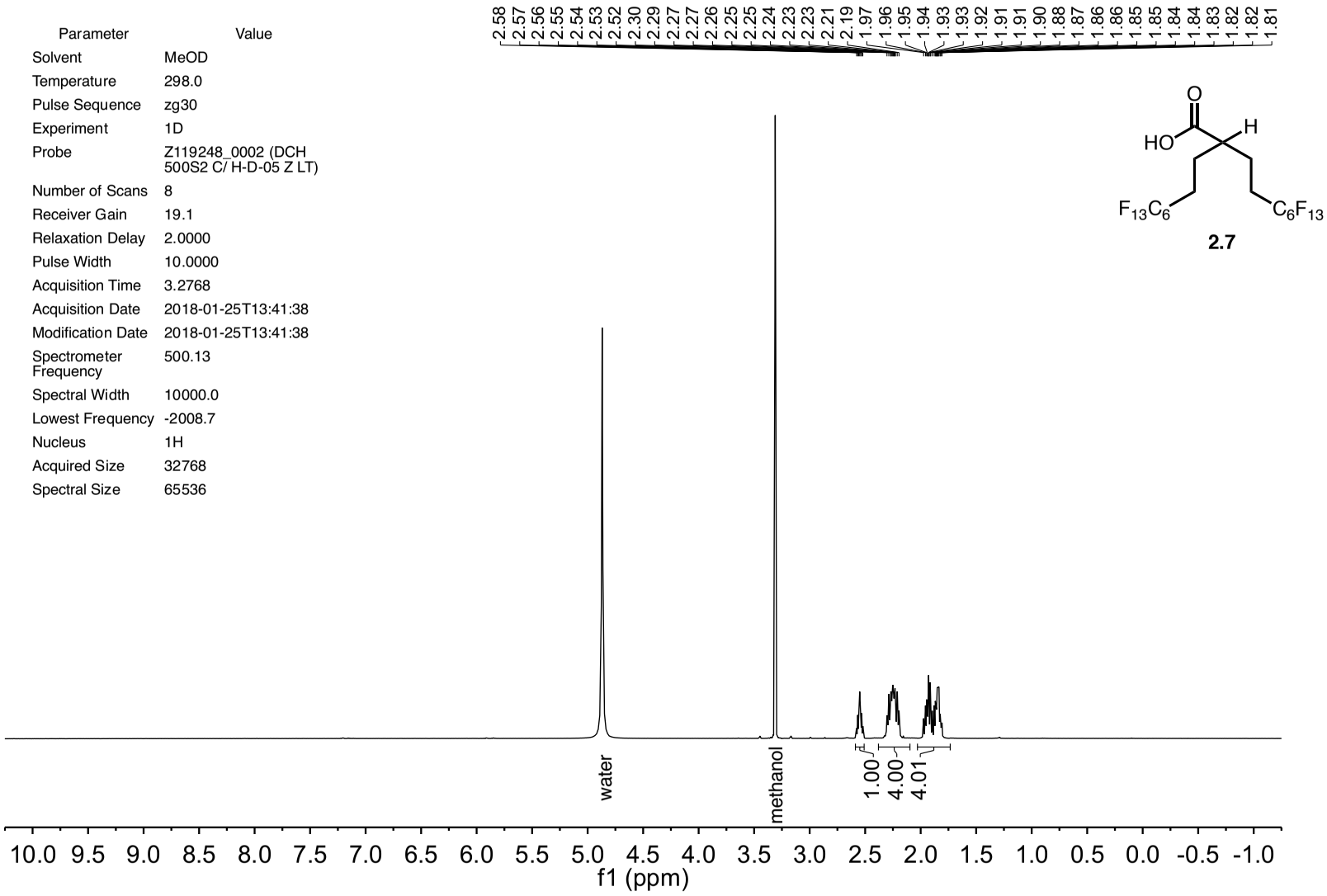

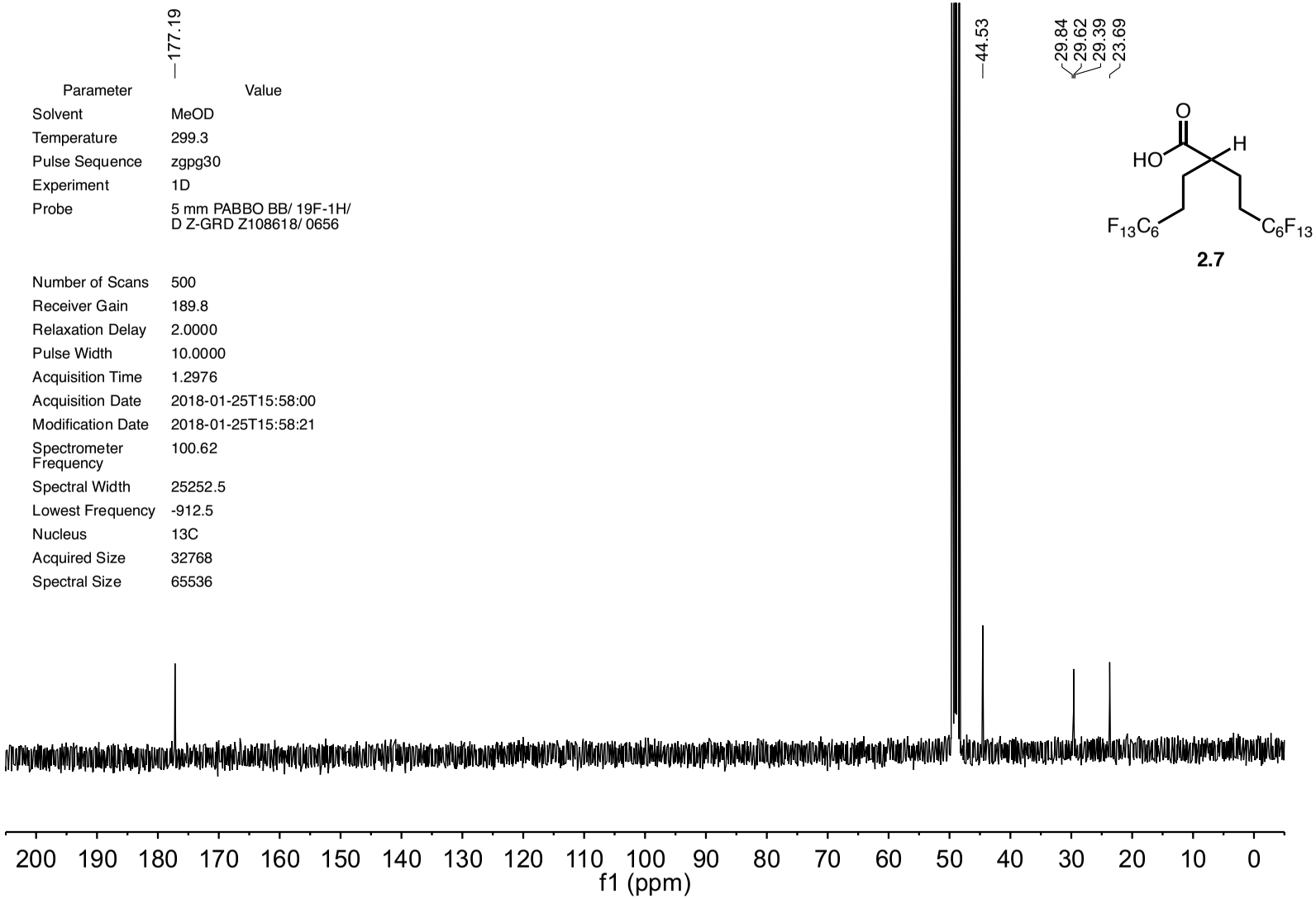

Parameter	Value
Solvent	MeOD
Temperature	299.3
Pulse Sequence	zgpg30
Experiment	1D
Probe	5 mm PABBO BB/ 19F-1H/ D Z-GRD Z108618/ 0656
Number of Scans	500
Receiver Gain	189.8
Relaxation Delay	2.0000
Pulse Width	10.0000
Acquisition Time	1.2976
Acquisition Date	2018-01-25T15:58:00
Modification Date	2018-01-25T15:58:21
Spectrometer Frequency	100.62
Spectral Width	25252.5
Lowest Frequency	-912.5
Nucleus	13C
Acquired Size	32768
Spectral Size	65536

Parameter	Value
Solvent	MeOD
Temperature	298.2
Pulse Sequence	zgfhigqn.2
Experiment	1D
Probe	5 mm PABBO BB/ 19F-1H/ D Z-GRD Z108618/ 0656
Number of Scans	8
Receiver Gain	189.8
Relaxation Delay	1.0000
Pulse Width	14.5000
Acquisition Time	1.7476
Acquisition Date	2018-01-25T19:13:00
Modification Date	2018-01-25T19:13:34
Spectrometer Frequency	376.46
Spectral Width	75000.0
Lowest Frequency	-75149.8
Nucleus	19F
Acquired Size	131072
Spectral Size	262144

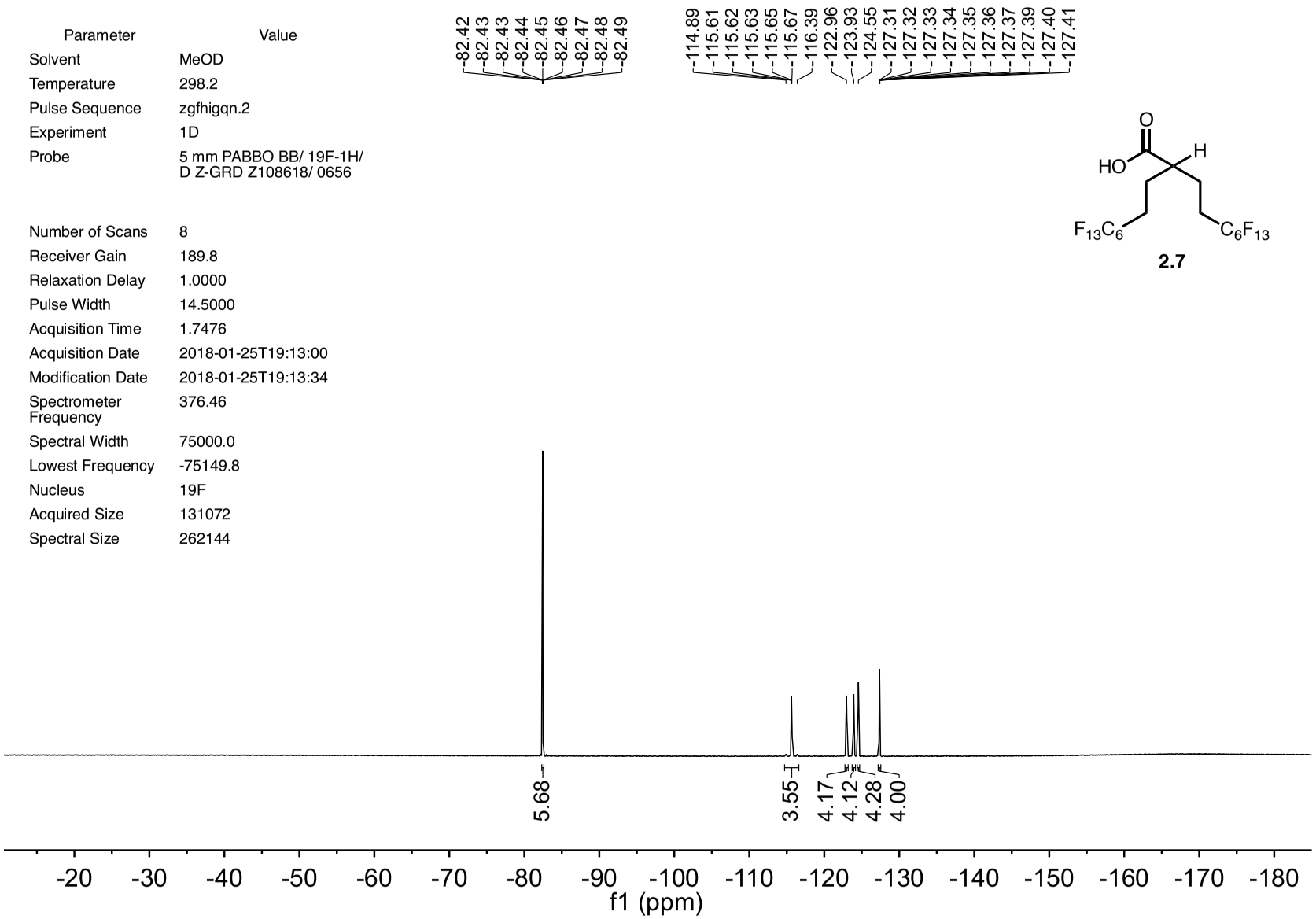

Parameter	Value
Solvent	CDCl3
Temperature	298.4
Pulse Sequence	zg30
Experiment	1D
Probe	5 mm PABBO BB/ 19F-1H/ D Z-GRD Z108618/ 0656
Number of Scans	8
Receiver Gain	155.8
Relaxation Delay	2.0000
Pulse Width	15.0000
Acquisition Time	3.2998
Acquisition Date	2018-02-02T14:20:00
Modification Date	2018-02-02T14:20:47
Spectrometer Frequency	400.13
Spectral Width	8012.8
Lowest Frequency	-1623.3
Nucleus	1H
Acquired Size	26441
Spectral Size	65536

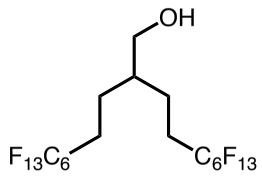

2.8

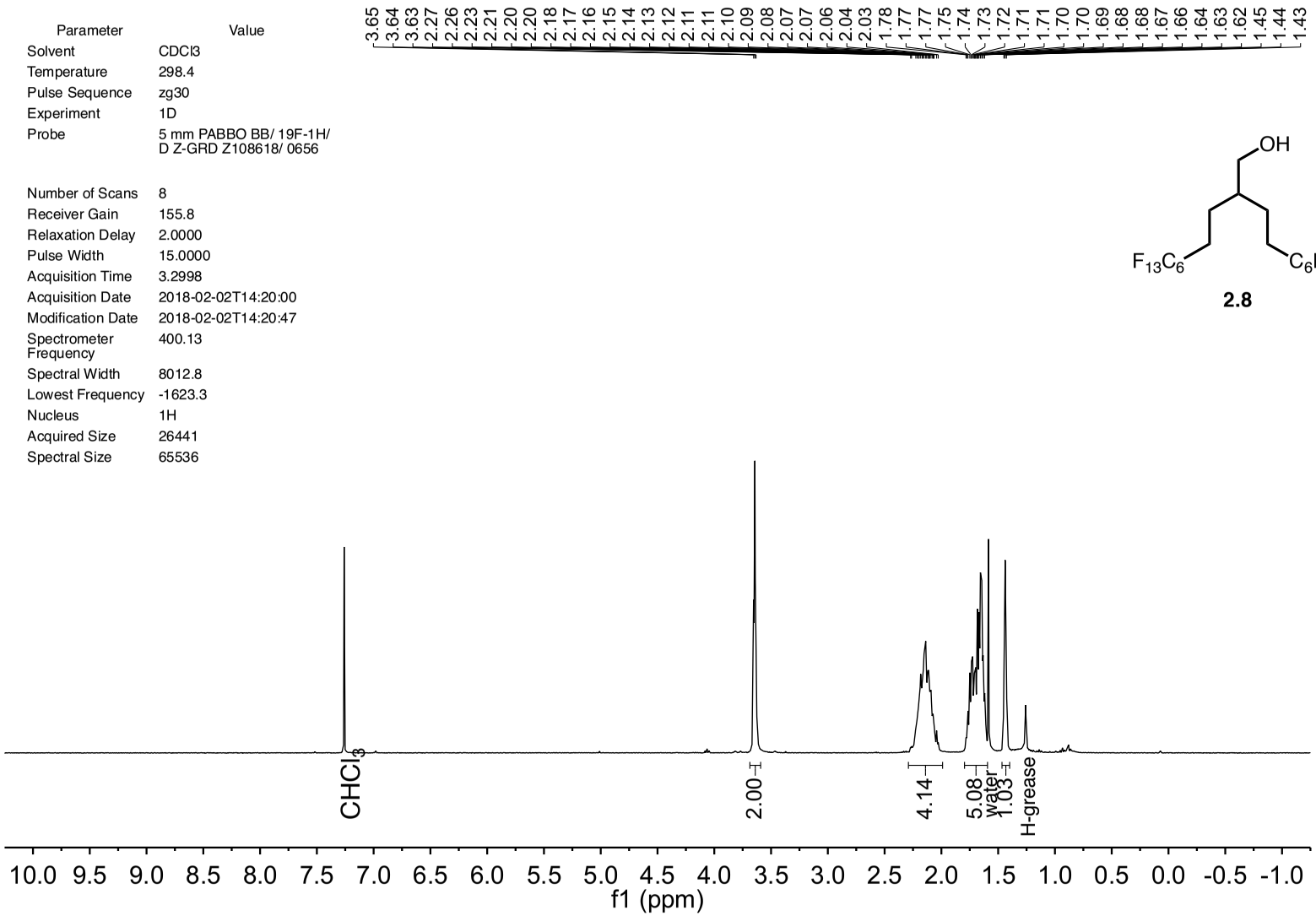

Parameter	Value
Solvent	CDCl3
Temperature	298.5
Pulse Sequence	zgfhigqn.2
Experiment	1D
Probe	5 mm PABBO BB/ 19F-1H/ D Z-GRD Z108618/ 0656
Number of Scans	8
Receiver Gain	189.8
Relaxation Delay	1.0000
Pulse Width	14.5000
Acquisition Time	1.7476
Acquisition Date	2018-02-02T14:24:00
Modification Date	2018-02-02T14:24:12
Spectrometer Frequency	376.50
Spectral Width	75000.0
Lowest Frequency	-75149.8
Nucleus	19F

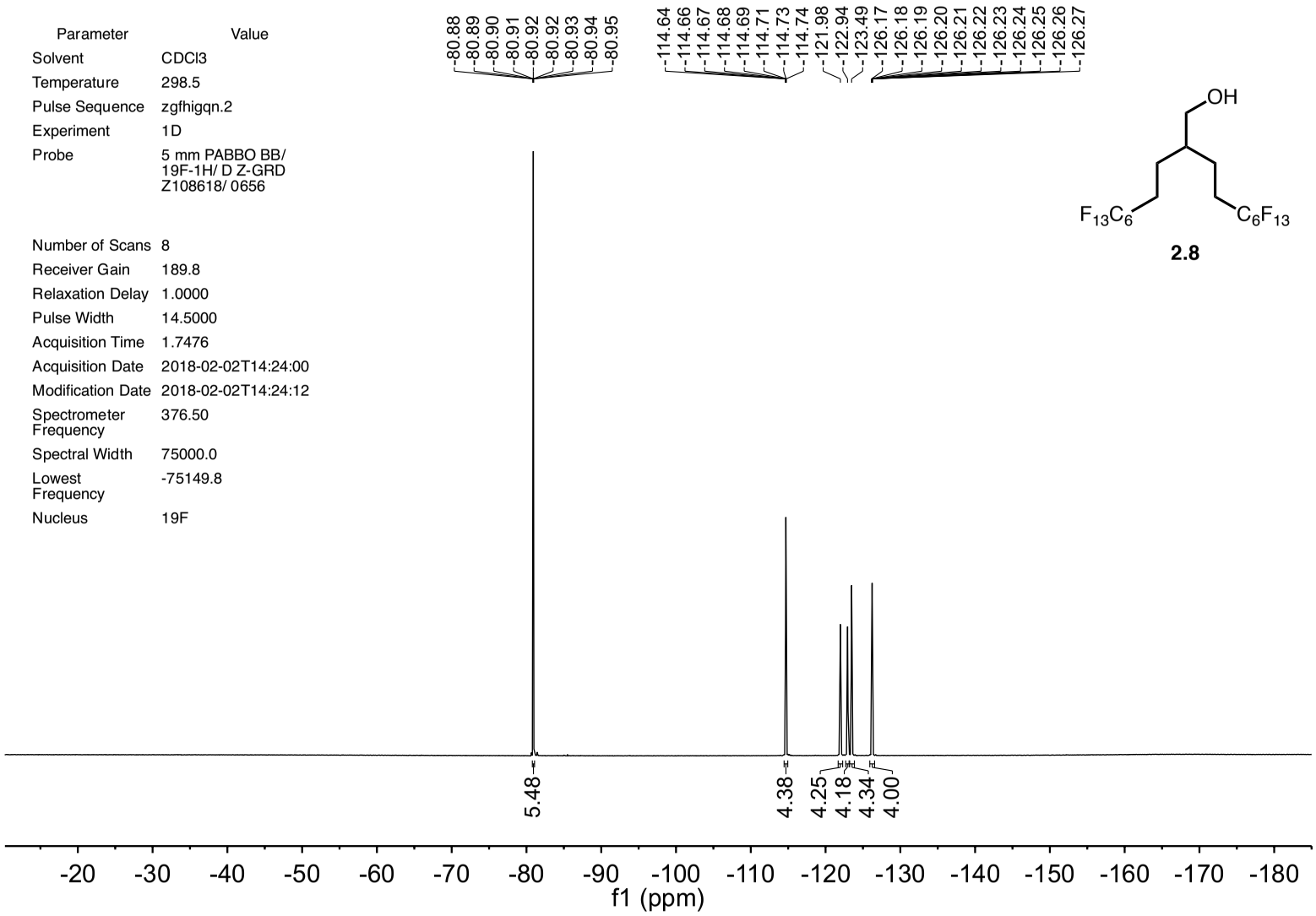

2.8

Parameter	Value
Solvent	CDCl3
Temperature	298.0
Pulse Sequence	zgpg30
Experiment	1D
Probe	Z119248_0002 (DCH 500S2 C/ H-D-05 Z LT)
Number of Scans	65
Receiver Gain	204.5
Relaxation Delay	2.0000
Pulse Width	9.6300
Acquisition Time	1.0486
Acquisition Date	2018-02-03T12:38:21
Modification Date	2018-02-03T12:38:22
Spectrometer Frequency	125.76
Spectral Width	31250.0
Lowest Frequency	-1141.0
Nucleus	13C
Acquired Size	32768
Spectral Size	131072

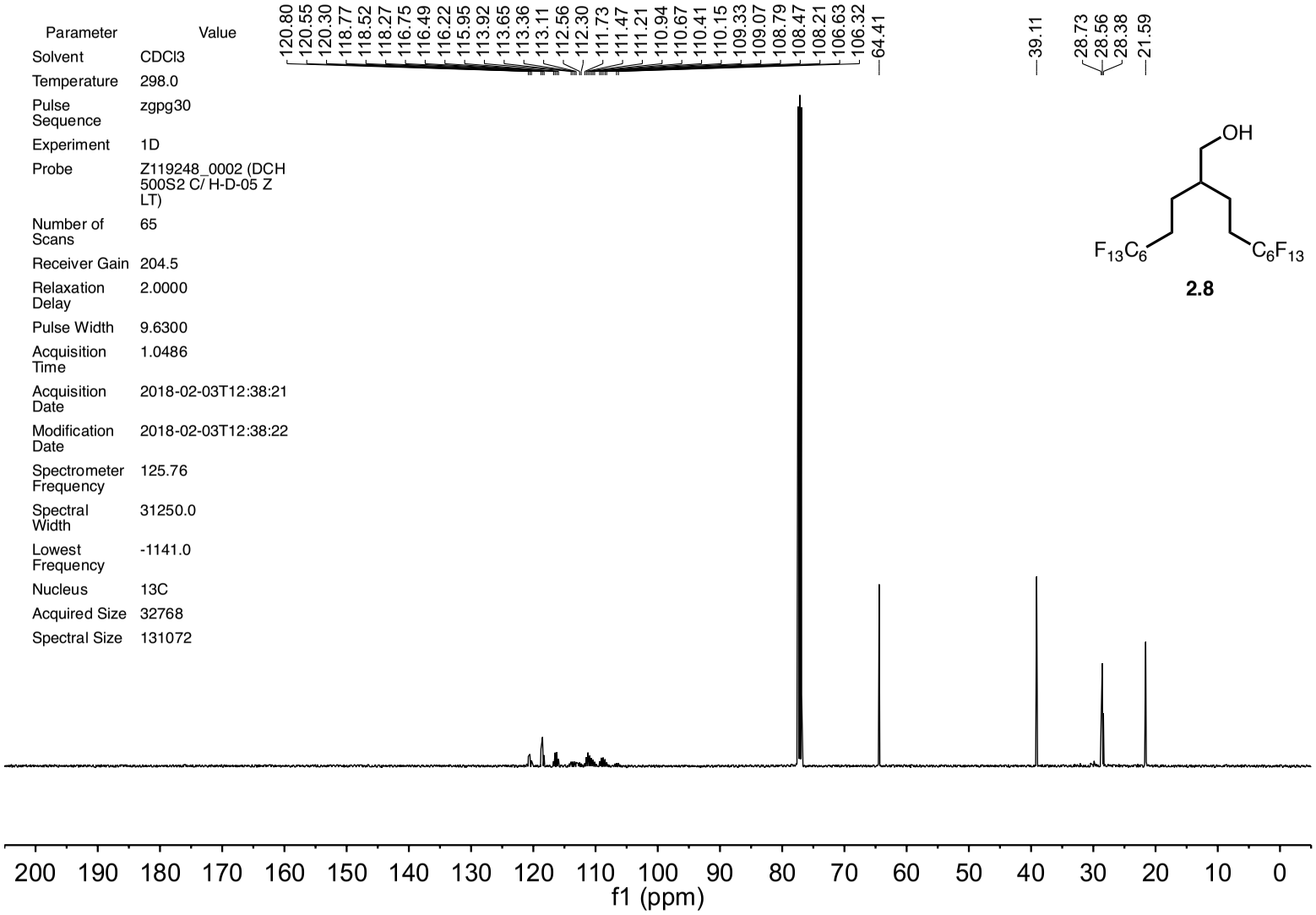

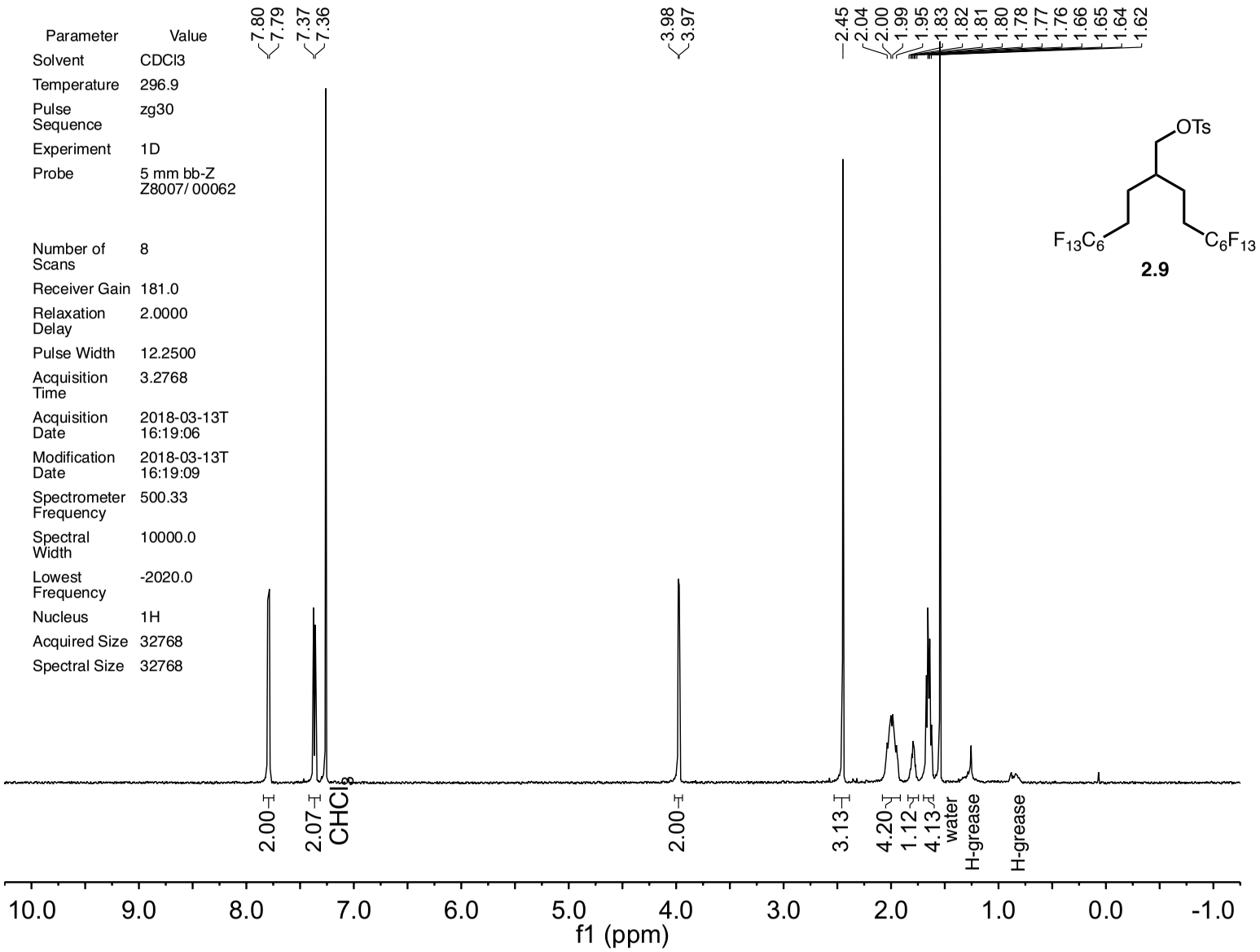
Parameter Value
Solvent CDCl3
Temperature 296.9
Pulse Sequence zg30
Experiment 1D
Probe 5 mm bb-Z Z8007/ 00062
Number of Scans 8
Receiver Gain 181.0
Relaxation Delay 2.0000
Pulse Width 12.2500
Acquisition Time 3.2768
Acquisition Date 2018-03-13T 16:19:06
Modification Date 2018-03-13T 16:19:09
Spectrometer Frequency 500.33
Spectral Width 10000.0
Lowest Frequency -2020.0
Nucleus 1H
Acquired Size 32768
Spectral Size 32768
7.80
7.79
7.37
7.36
3.98
3.97
2.45
2.04
2.00
1.99
1.95
1.83
1.82
1.81
1.80
1.78
1.77
1.76
1.66
1.65
1.64
1.62
OTs
F13C6
C6F13
2.9
2.00
2.07
CHCl3
2.00
3.13
4.20
1.12
4.13
water
H-grease
H-grease
10.0
9.0
8.0
7.0
6.0
5.0
4.0
3.0
2.0
1.0
0.0
-1.0
f1 (ppm)

Parameter	Value
Solvent	CDCl3
Temperature	298.4
Pulse Sequence	zgfhigqn.2
Experiment	1D
Probe	5 mm PABBO BB/ 19F-1H/ D Z-GRD Z108618/ 0656
Number of Scans	8
Receiver Gain	189.8
Relaxation Delay	1.0000
Pulse Width	14.5000
Acquisition Time	1.7476
Acquisition Date	2018-03-13T18:00:00
Modification Date	2018-03-13T18:00:40
Spectrometer Frequency	376.50
Spectral Width	75000.0
Lowest Frequency	-75149.8
Nucleus	19F
Acquired Size	131072
Spectral Size	262144

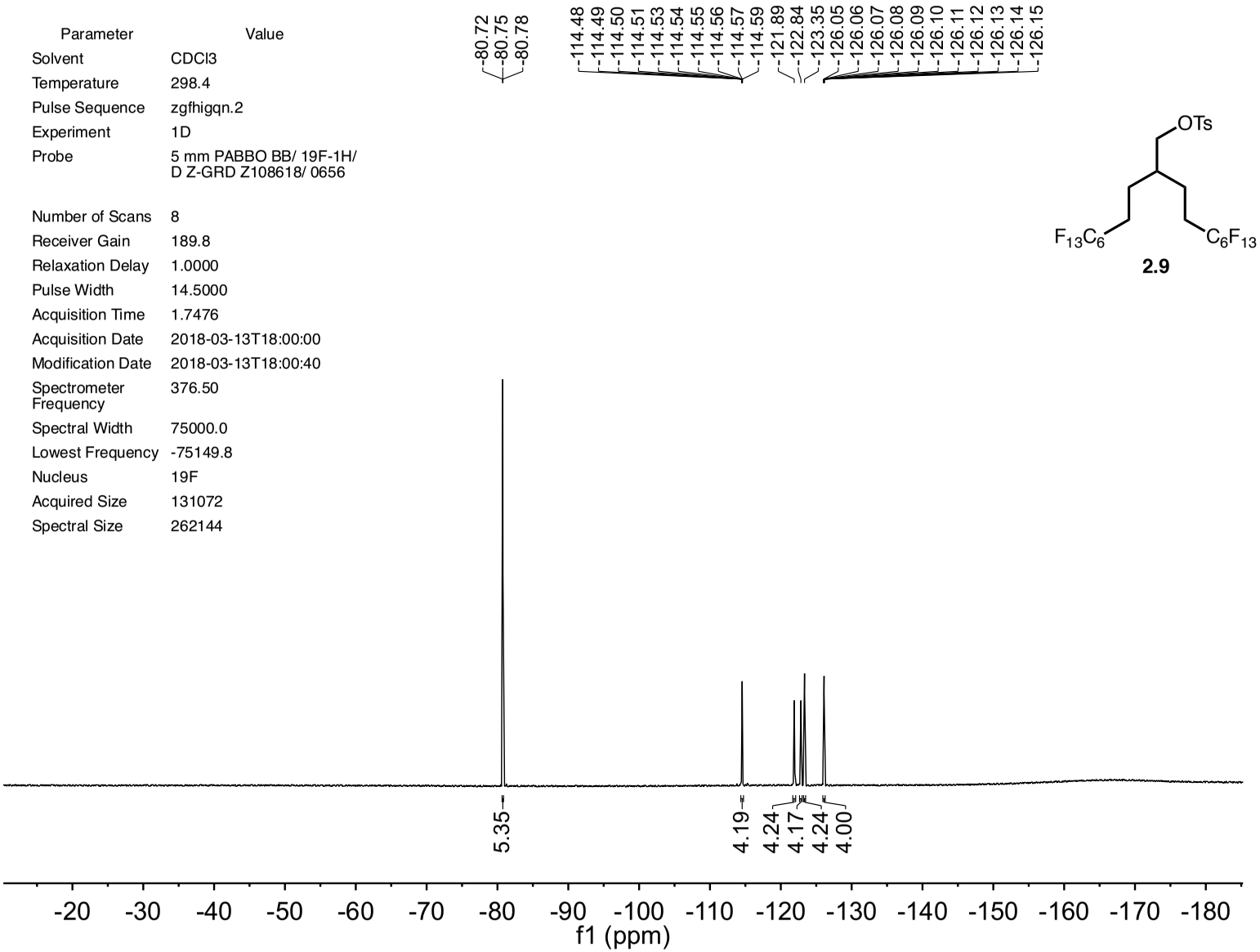

Parameter	Value
Solvent	CDCl3
Temperature	299.3
Pulse Sequence	zgpg30
Experiment	1D
Probe	5 mm PABBO BB/ 19F-1H/ D Z-GRD Z108618/ 0656
Number of Scans	512
Receiver Gain	189.8
Relaxation Delay	2.0000
Pulse Width	10.0000
Acquisition Time	1.2976
Acquisition Date	2018-09-12T00:30:00
Modification Date	2018-09-12T00:30:42
Spectrometer Frequency	100.61
Spectral Width	25252.5
Lowest Frequency	-1042.0
Nucleus	13C
Acquired Size	32768
Spectral Size	65536

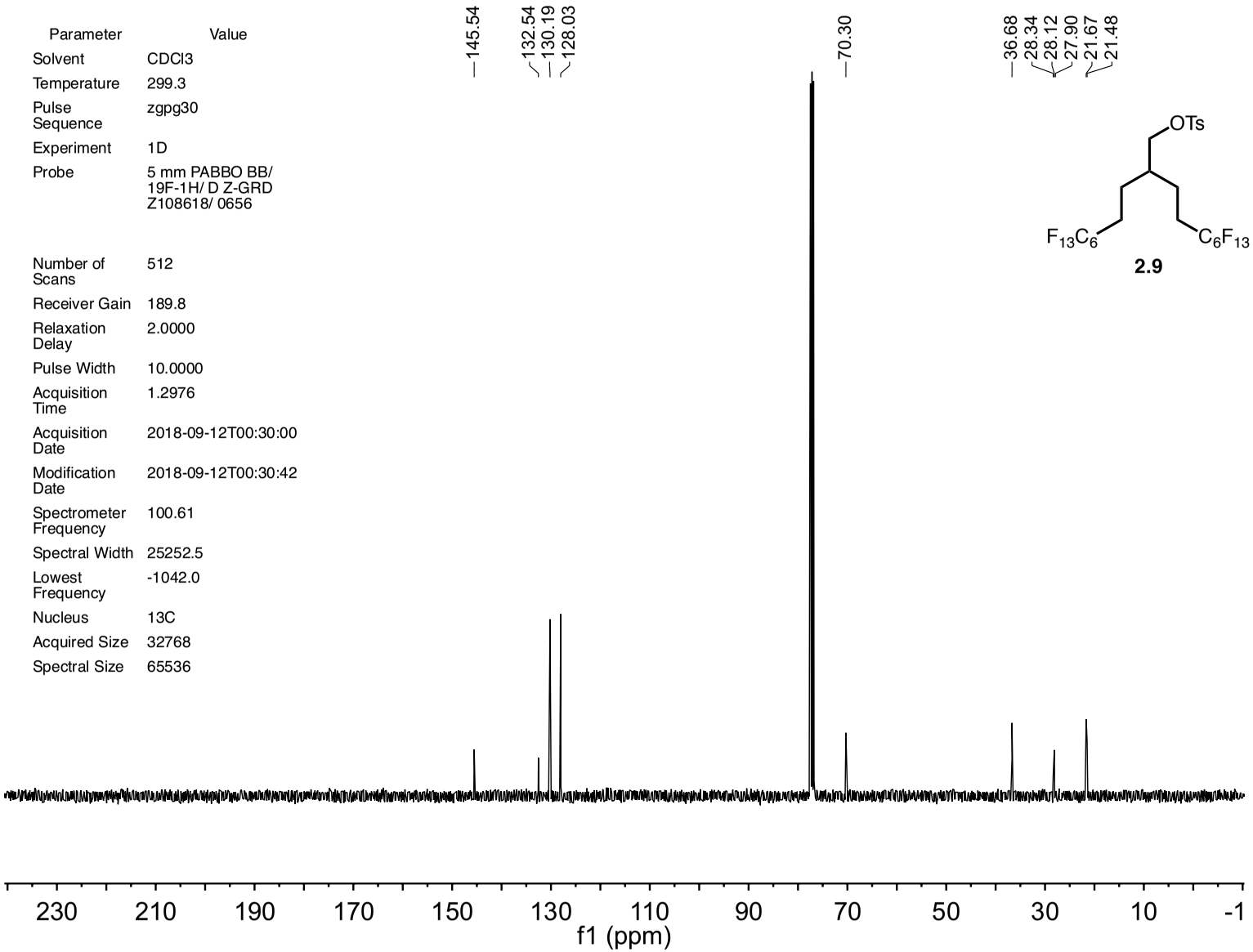

Parameter	Value
Solvent	CDCl3
Temperature	298.0
Pulse Sequence	zg30
Experiment	1D
Probe	Z119248_0002 (DCH 500S2 C/ H-D-05 Z LT)
Number of Scans	2
Receiver Gain	12.1
Relaxation Delay	2.0000
Pulse Width	10.0000
Acquisition Time	3.2768
Acquisition Date	2018-06-15T15: 37:58
Modification Date	2018-06-15T15: 37:59
Spectrometer Frequency	500.13
Spectral Width	10000.0
Lowest Frequency	-2011.4
Nucleus	1H
Acquired Size	32768
Spectral Size	65536

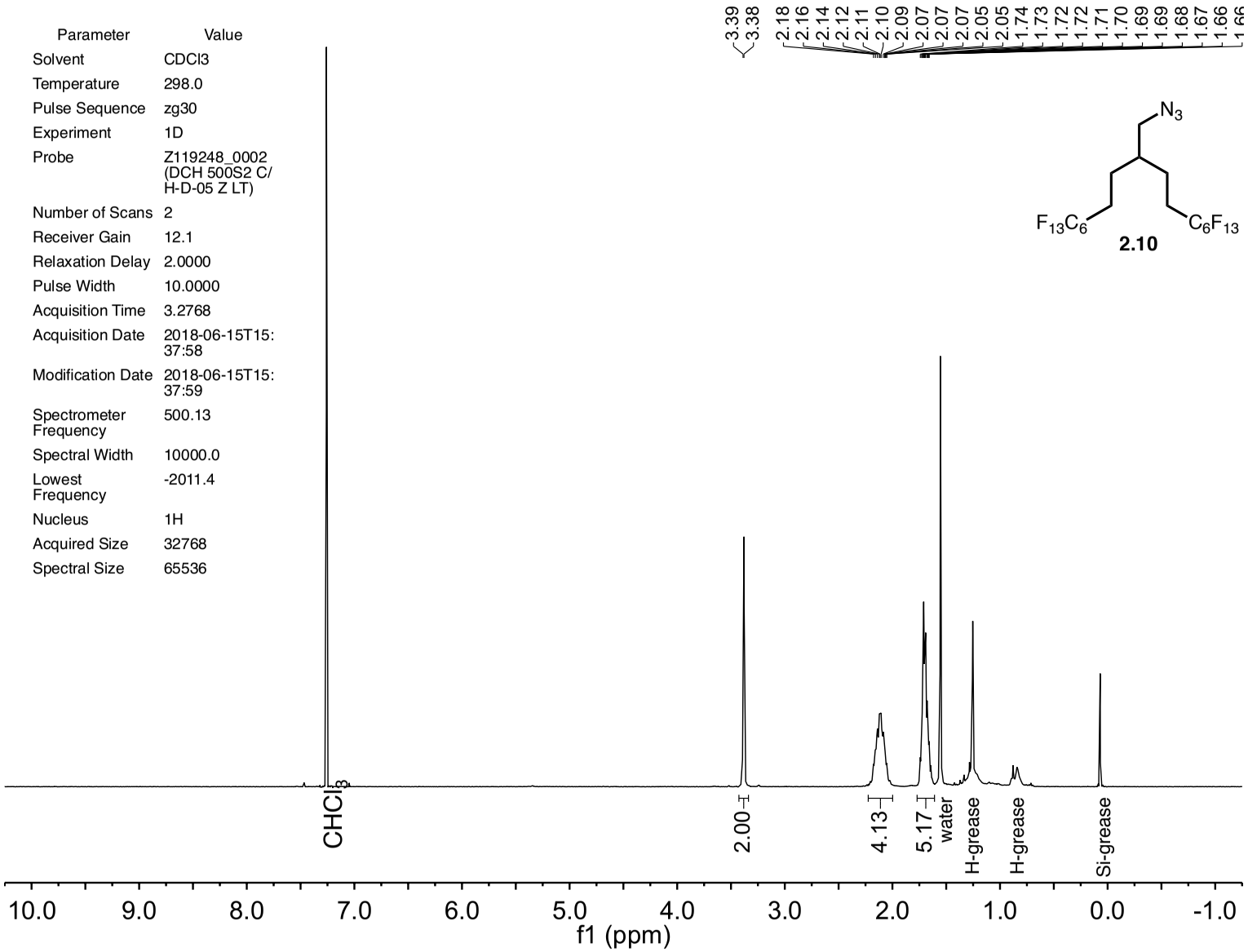

Parameter	Value
Solvent	CDCl3
Temperature	299.3
Pulse Sequence	zgpg30
Experiment	1D
Probe	5 mm PABBO BB/ 19F-1H/ D Z-GRD Z108618/ 0656
Number of Scans	500
Receiver Gain	189.8
Relaxation Delay	2.0000
Pulse Width	10.0000
Acquisition Time	1.2976
Acquisition Date	2018-07-03T21:10:00
Modification Date	2018-07-03T21:10:17
Spectrometer Frequency	100.61
Spectral Width	25252.5
Lowest Frequency	-1041.7
Nucleus	13C
Acquired Size	32768
Spectral Size	65536

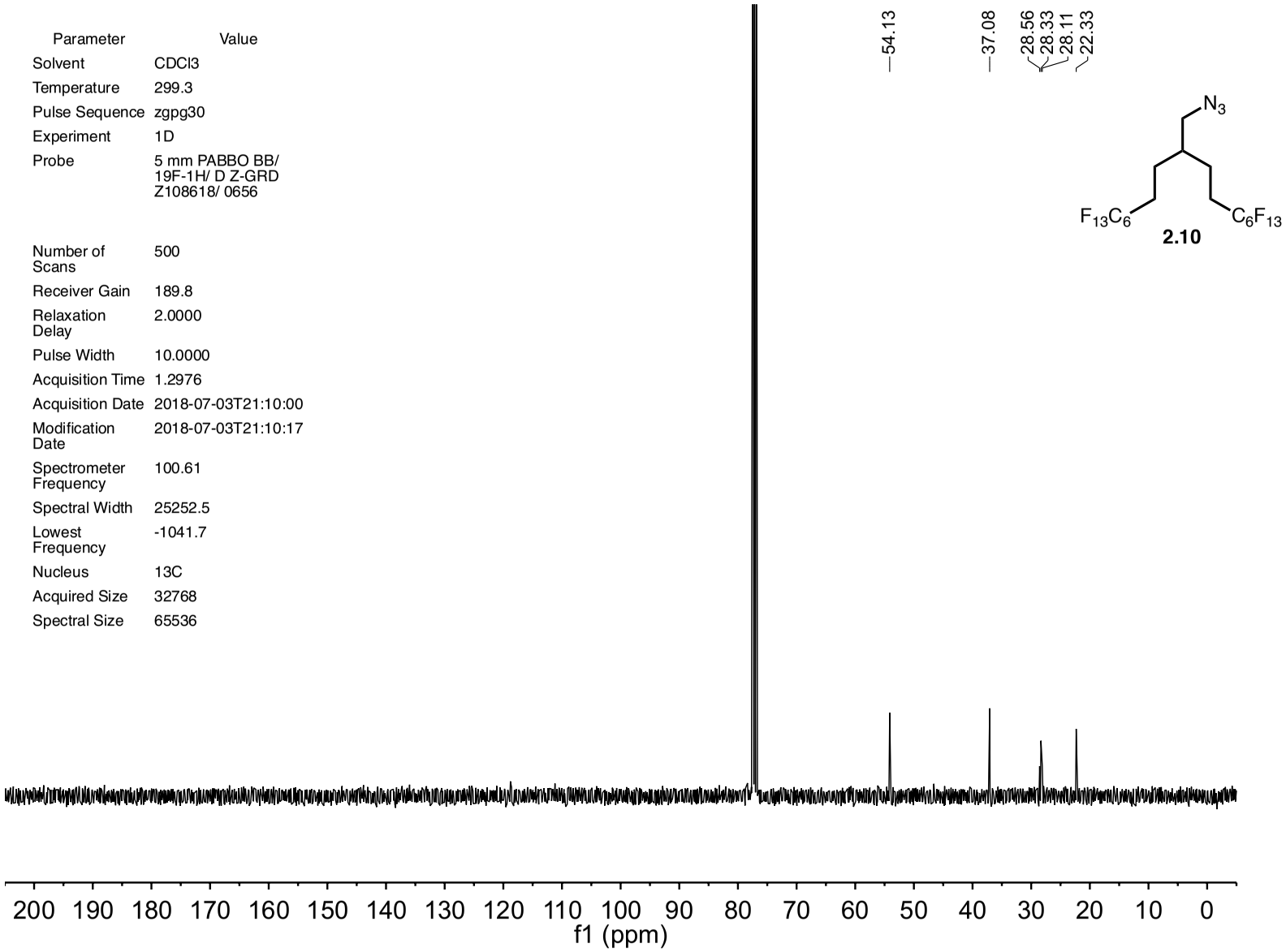

Parameter	Value
Solvent	CDCl3
Temperature	298.7
Pulse Sequence	zg30
Experiment	1D
Probe	5 mm PABBO BB-1H/ D Z-GRD Z862701/ 0016
Number of Scans	8
Receiver Gain	1024.0
Relaxation Delay	2.0000
Pulse Width	13.7500
Acquisition Time	0.8716
Acquisition Date	2018-06-15T14:50:25
Modification Date	2018-06-15T14:50:32
Spectrometer Frequency	282.40
Spectral Width	75188.0
Lowest Frequency	-65834.4
Nucleus	19F
Acquired Size	65536
Spectral Size	65536

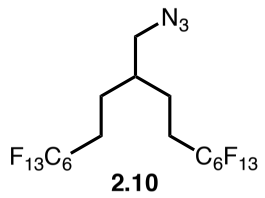

2.10

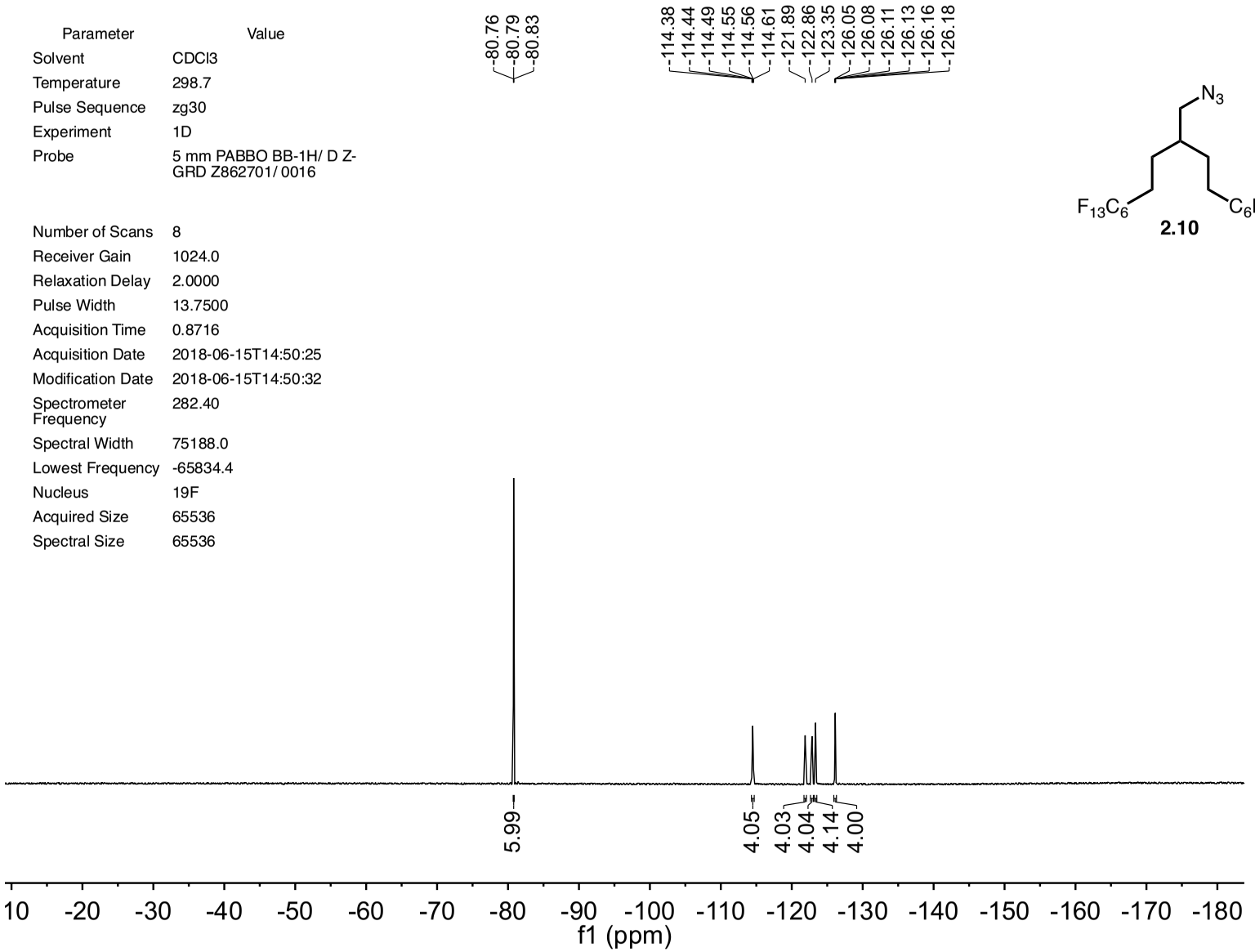

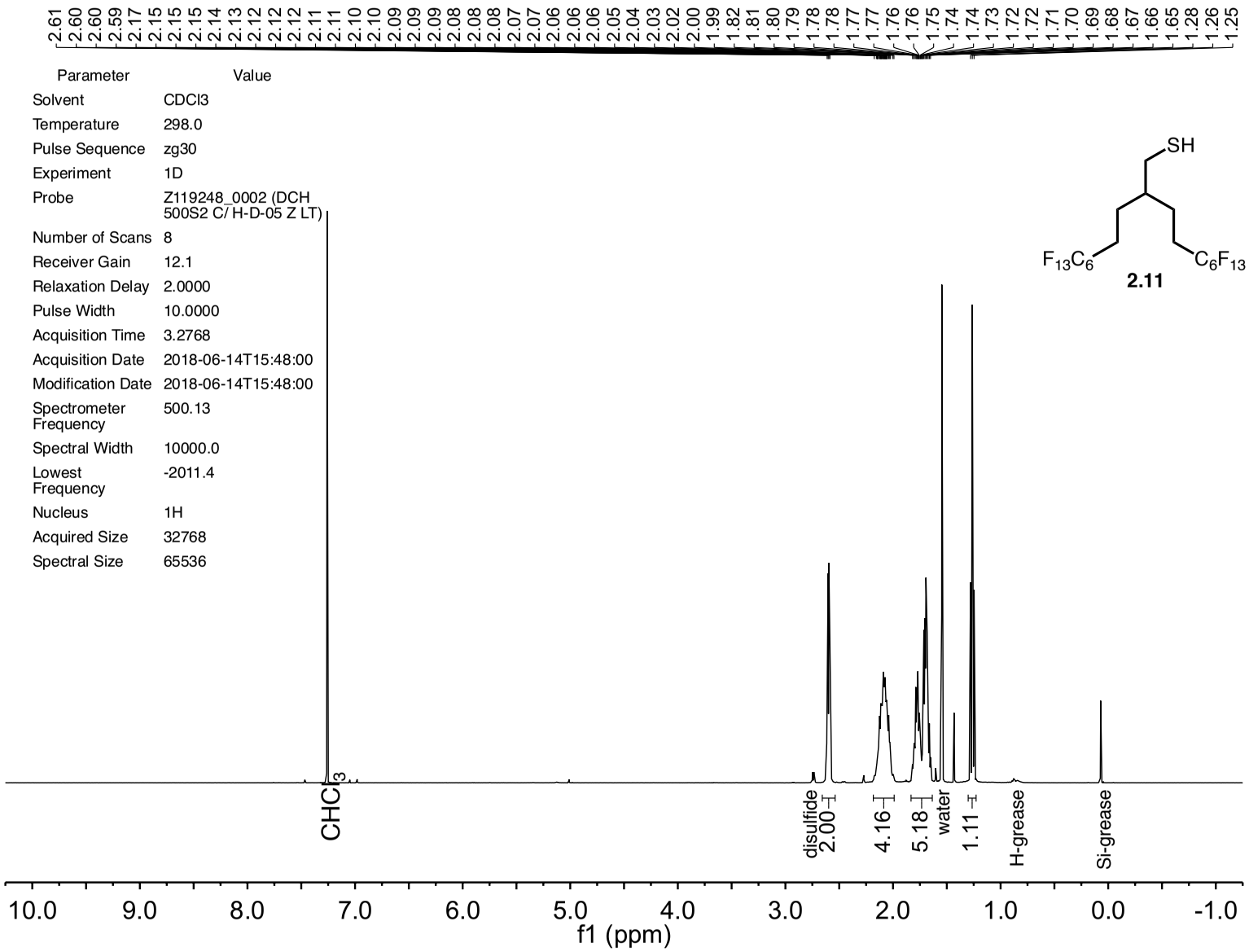
2.61 2.60 2.60 2.59 2.17 2.15 2.15 2.15 2.14 2.13 2.12 2.12 2.12 2.11 2.11 2.10 2.10 2.09 2.09 2.09 2.08 2.08 2.08 2.07 2.07 2.06 2.06 2.06 2.05 2.04 2.03 2.02 2.00 1.99 1.82 1.81 1.80 1.79 1.78 1.78 1.77 1.77 1.76 1.76 1.75 1.74 1.74 1.73 1.72 1.72 1.71 1.70 1.69 1.68 1.67 1.66 1.65 1.28 1.26 1.25
Parameter Value
Solvent CDCl3
Temperature 298.0
Pulse Sequence zg30
Experiment 1D
Probe Z119248_0002 (DCH 500S2 C/ H-D-05 Z LT)
Number of Scans 8
Receiver Gain 12.1
Relaxation Delay 2.0000
Pulse Width 10.0000
Acquisition Time 3.2768
Acquisition Date 2018-06-14T15:48:00
Modification Date 2018-06-14T15:48:00
Spectrometer Frequency 500.13
Spectral Width 10000.0
Lowest Frequency -2011.4
Nucleus 1H
Acquired Size 32768
Spectral Size 65536
SH
F13C6
C6F13
2.11
CHCl3
disulfide
2.00
4.16
5.18
water
1.11
H-grease
Si-grease
10.0 9.0 8.0 7.0 6.0 5.0 4.0 3.0 2.0 1.0 0.0 -1.0
f1 (ppm)

Parameter	Value
Solvent	CDCl3
Temperature	299.3
Pulse Sequence	zgpg30
Experiment	1D
Probe	5 mm PABBO BB/ 19F-1H/ D Z-GRD Z108618/ 0656
Number of Scans	256
Receiver Gain	189.8
Relaxation Delay	2.0000
Pulse Width	10.0000
Acquisition Time	1.2976
Acquisition Date	2018-06-14T16:06:00
Modification Date	2018-06-14T16:06:16
Spectrometer Frequency	100.61
Spectral Width	25252.5
Lowest Frequency	-1040.6
Nucleus	13C
Acquired Size	32768
Spectral Size	65536

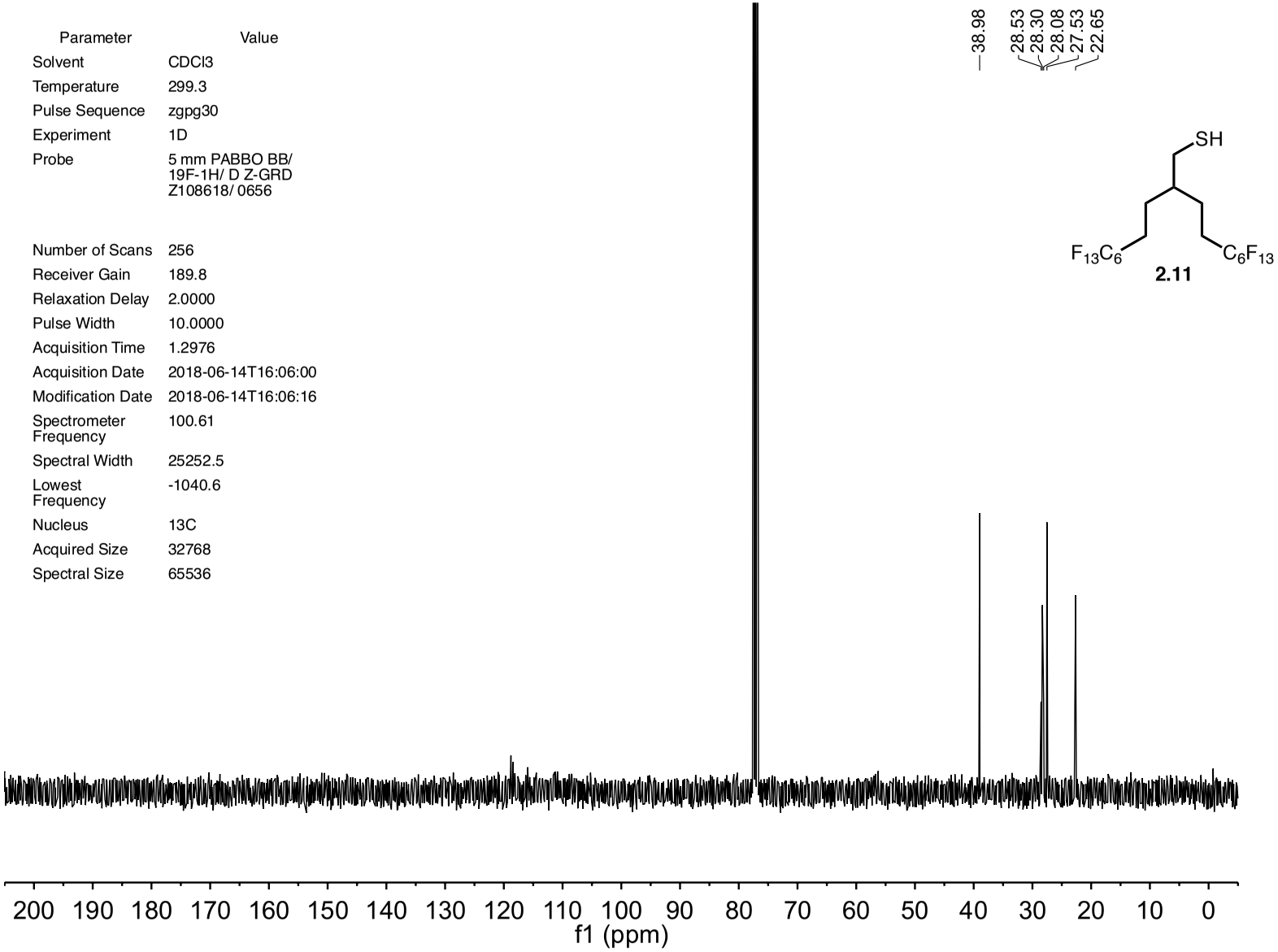

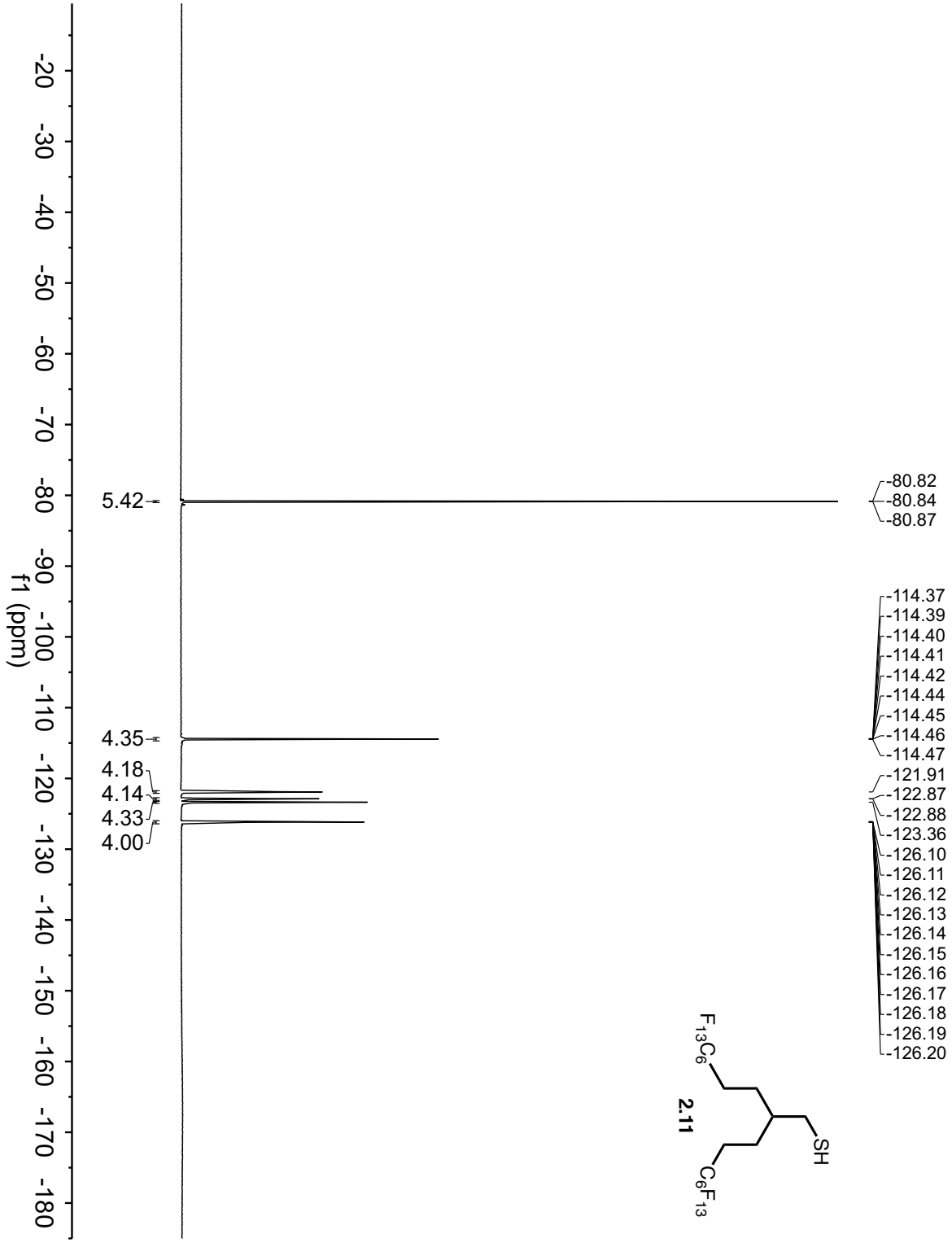
-80.82
-80.84
-80.87
-114.37
-114.39
-114.40
-114.41
-114.42
-114.44
-114.45
-114.46
-114.47
-121.91
-122.87
-122.88
-123.36
-126.10
-126.11
-126.12
-126.13
-126.14
-126.15
-126.16
-126.17
-126.18
-126.19
-126.20
5.42
4.35
4.18
4.14
4.33
4.00
f1 (ppm)
-20
-30
-40
-50
-60
-70
-80
-90
-100
-110
-120
-130
-140
-150
-160
-170
-180
$F_{13}C_6$
SH
C_6F_{13}
2.11

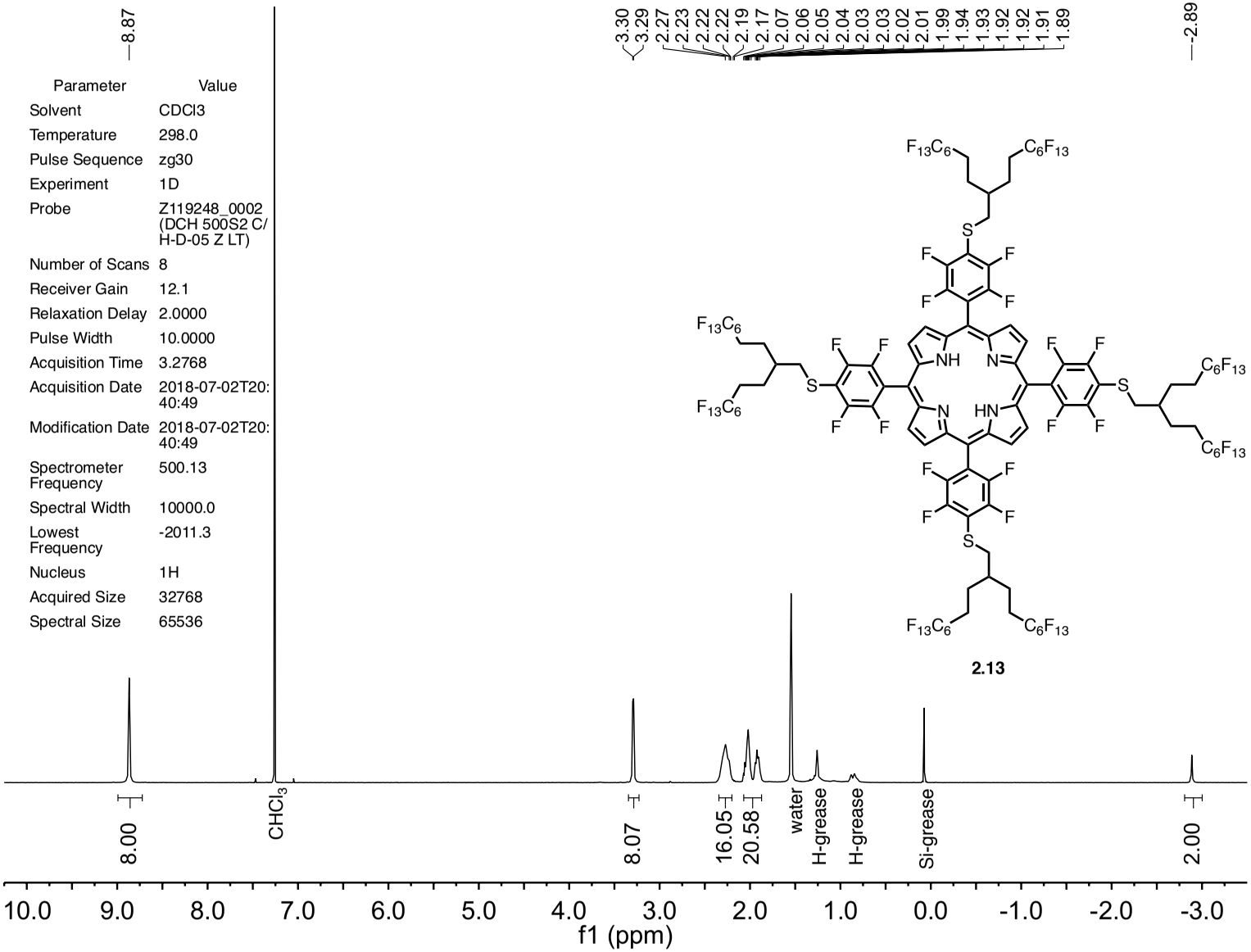
8.87
3.30
3.29
2.27
2.23
2.22
2.22
2.19
2.17
2.07
2.06
2.05
2.04
2.03
2.03
2.02
2.01
1.99
1.94
1.93
1.92
1.92
1.91
1.89
-2.89
Parameter Value
Solvent CDCl3
Temperature 298.0
Pulse Sequence zg30
Experiment 1D
Probe Z119248_0002 (DCH 500S2 C/H-D-05 Z LT)
Number of Scans 8
Receiver Gain 12.1
Relaxation Delay 2.0000
Pulse Width 10.0000
Acquisition Time 3.2768
Acquisition Date 2018-07-02T20:40:49
Modification Date 2018-07-02T20:40:49
Spectrometer Frequency 500.13
Spectral Width 10000.0
Lowest Frequency -2011.3
Nucleus 1H
Acquired Size 32768
Spectral Size 65536
2.13
8.00
CHCl3
8.07
16.05
20.58
water
H-grease
H-grease
Si-grease
2.00
10.0 9.0 8.0 7.0 6.0 5.0 4.0 3.0 2.0 1.0 0.0 -1.0 -2.0 -3.0
f1 (ppm)

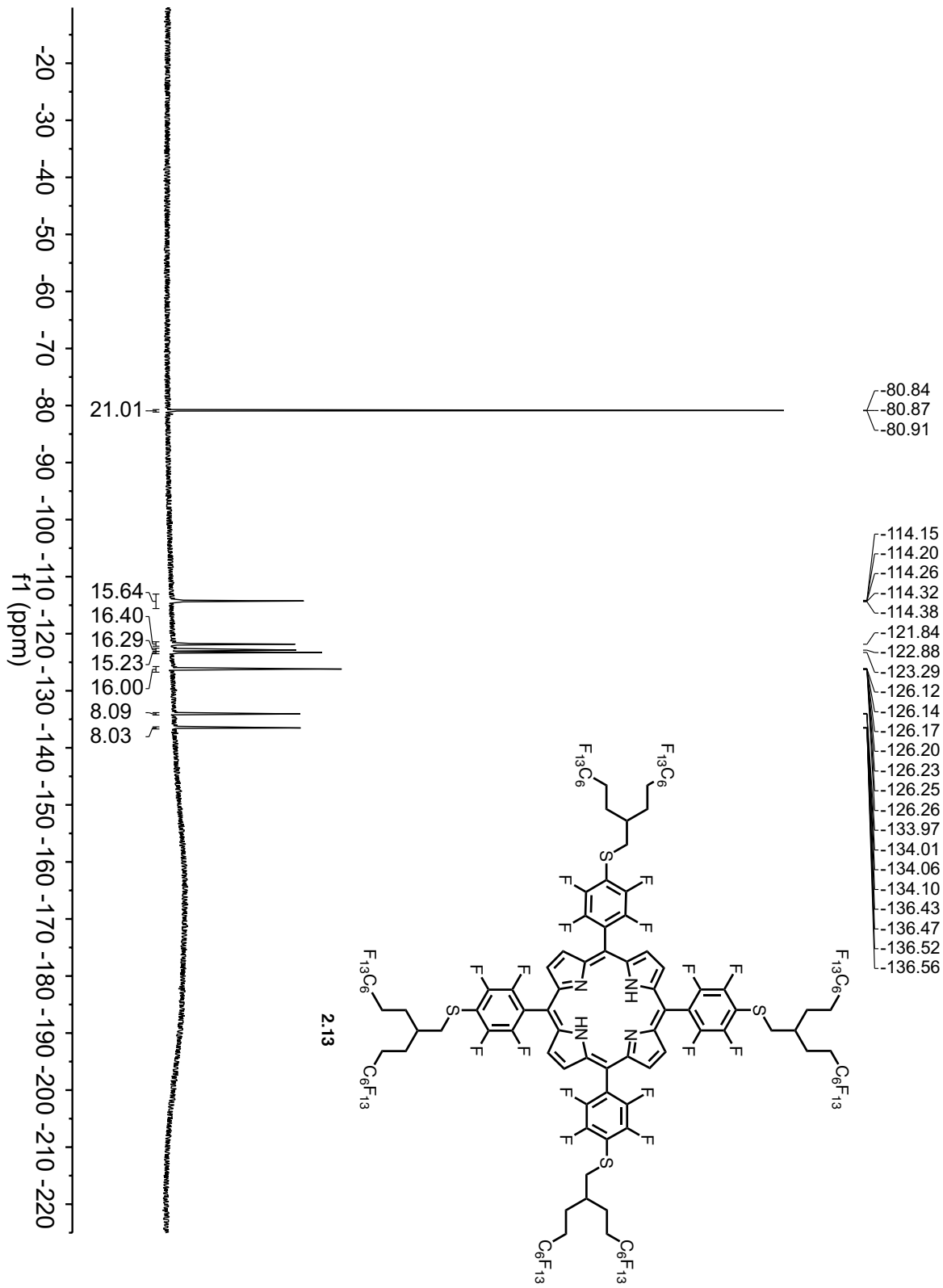
-80.84
-80.87
-80.91
-114.15
-114.20
-114.26
-114.32
-114.38
-121.84
-122.88
-123.29
-126.12
-126.14
-126.17
-126.20
-126.23
-126.25
-126.26
-133.97
-134.01
-134.06
-134.10
-136.43
-136.47
-136.52
-136.56
21.01
15.64
16.40
16.29
15.23
16.00
8.09
8.03
-20 -30 -40 -50 -60 -70 -80 -90 -100 -110 -120 -130 -140 -150 -160 -170 -180 -190 -200 -210 -220
f1 (ppm)
2.13

2.6 References

(1) Gladysz, J. A.; Curran, D. P.; Horváth, I. T. *Handbook of Fluorous Chemistry*; Wiley-VHC: Weinheim, 2004.

(2) Vincent, J. M. Recent Advances of Fluorous Chemistry in Material Sciences. *Chem. Commun.* **2012**, *48*, 11382–11391.

(3) Ameduri, B.; Boutevin, B. *Well-Architectured Fluoropolymers: Synthesis, Properties and Applications*; Elsevier: Oxford, 2004.

(4) Riess, J. G. Understanding the Fundamentals of Perfluorocarbons and Perfluorocarbon Emulsions Relevant to in Vivo Oxygen Delivery. *Artif. Cells. Blood Substit. Immobil. Biotechnol.* **2005**, *33*, 47–63.

(5) Horvath, I. T.; Rabai, J. Facile Catalyst Separation Without Water: Fluorous Biphase Hydroformylation of Olefins. *Science* **1994**, *266*, 72–75.

(6) Brittain, S. M.; Ficarro, S. B.; Brock, A.; Peters, E. C. Enrichment and Analysis of Peptide Subsets Using Fluorous Affinity Tags and Mass Spectrometry. *Nat. Biotechnol.* **2005**, *23*, 463–468.

(7) Ko, K.S.; Jaipuri, F.A.; Pohl, N. L. Fluorous-Based Carbohydrate Microarrays. *J. Am. Chem. Soc.* **2005**, *127*, 13162–13163.

(8) Vegas, A. J.; Bradner, J. E.; Tang, W.; McPherson, O. M.; Greenberg, E. F.; Koehler, A. N.; Schreiber, S. L. Fluorous-Based Small-Molecule Microarrays for the Discovery of Histone Deacetylase Inhibitors. *Angew. Chem.* **2007**, *46*, 7960–7964.

(9) Flynn, G. E.; Withers, J. M.; Macias, G.; Sperling, J. R.; Henry, S. L.; Cooper, J. M.; Burley, G. A.; Clark, A. W. Reversible DNA Micro-Patterning Using the Fluorous Effect. *Chem. Commun.* **2017**, *53*, 3094–3097.

(10) Dafik, L.; Kalsani, V.; Leung, A. K. L.; Kumar, K. Fluorinated Lipid Constructs Permit Facile Passage of Molecular Cargo into Living Cells. *J. Am. Chem. Soc.* **2009**, *131*, 12091–12093.

(11) Zamora, C. Y.; Dafik, L.; Kumar, K. Chemical Biology Using Fluorinated Building Blocks. In *Supramolecular Chemistry: From Molecules to Nanomaterials*; John Wiley & Sons: Chichester, 2012.

(12) Sletten, E. M.; Swager, T. M. Fluorofluorophores: Fluorescent Fluorous Chemical Tools Spanning the Visible Spectrum. *J. Am. Chem. Soc.* **2014**, *136*, 13574–13577.

(13) Day, R. A.; Estabrook, D. A.; Logan, J. K.; Sletten, E. M. Fluorous Photosensitizers Enhance Photodynamic Therapy with Perfluorocarbon Nanoemulsions. *Chem. Commun.* **2017**, *53*, 13043–13046.

(14) Kiss, L. E.; Kovesdi, I.; Rabai, J. An Improved Design of Fluorophilic Molecules: Prediction of the Ln P Fluorous Partition Coefficient, Fluorophilicity, Using 3D QSAR Descriptors and Neural Networks. *J. Fluorine Chem.* **2001**, *108*, 95–109.

(15) Rocaboy, C.; Hampel, F.; Gladysz, J. A. Syntheses and Reactivities of Disubstituted and Trisubstituted Fluorous Pyridines with High Fluorous Phase Affinities: Solid State, Liquid Crystal, and Ionic Liquid-Phase Properties. *J. Org. Chem.* **2002**, *67*, 6863–6870.

(16) Krafft, M. P.; Riess, J. G. Per- and Polyfluorinated Substances (PFASs): Environmental Challenges. *Curr. Opin. Colloid Interface Sci.* **2015**, *20*, 192–212.

(17) Krafft, M. P.; Riess, J. G. Selected Physicochemical Aspects of Poly- and Perfluoroalkylated Substances Relevant to Performance, Environment and Sustainability-Part One. *Chemosphere* **2015**, *129*, 4–19.

(18) Langhals, H.; Ismael, R.; Yu, O. Persistent Fluorescence of Perylene Dyes by Steric

Inhibition of Aggregation. *Tetrahedron* **2000**, *56*, 5435–5441.

(19) Thamyongkit, P.; Speckbacher, M.; Diers, J. R.; Kee, H. L.; Kirmaier, C.; Holten, D.; Bocian, D. F.; Lindsey, J. S. Swallowtail Porphyrins: Synthesis, Characterization and Incorporation into Porphyrin Dyads. *J. Org. Chem.* **2004**, *69*, 3700–3710.

(20) Loiseau, J.; Fouquet, E.; Fish, R. H.; Vincent, J. M.; Verlhac, J. B. A New Carboxylic Acid with Branched Ponytails for the Solubilization of Mn(II) and Co(II) Ions in Perfluorocarbons. *J. Fluorine Chem.* **2001**, *108*, 195–197.

(21) Kaplanek, R.; Briza, T.; Havlik, M.; Dolensky, B.; Kejik, Z.; Martasek, P.; Kral, V. Branched Polyfluorinated Triflate—An Easily Available Polyfluoroalkylating Agent. *J. Fluorine Chem.* **2006**, *127*, 386.

(22) Wipf, P.; Reeves, J. T. Synthesis and Applications of a Highly Fluorous Alkoxy Ethyl Ether Protective Group. *Tetrahedron Lett.* **1999**, *40*, 5139–5142.

(23) Nakamura, Y.; Takeuchi, S.; Okumura, K.; Ohgo, Y. Enantioselective Addition of Diethylzinc to Aldehydes Catalyzed by Fluorous β-Aminoalcohols. *Tetrahedron* **2001**, *57*, 5565–5571.

(24) Wende, M.; Seidel, F.; Gladysz, J. A. Synthesis and Properties of Fluorous Arenes and Triaryl Phosphorus Compounds with Branched Fluoroalkyl Moieties ("Split Pony Tails"). *J. Fluorine Chem.* **2003**, *124*, 45–54.

(25) Matsubara, S.; Mitani, M.; Utimoto, K. A Facile Preparation of 1-Perflouroalkylalkenes and Alkynes. Palladium Catalyzed Reaction of Perfluoroalkyl Iodides with Organotin Compounds. *Tetrahedron Lett.* **1987**, *28*, 5857–5860.

(26) Szabo, D.; Mohl, J.; Balint, A. M.; Bodor, A.; Rabai, J. Novel Generation Ponytails in Fluorous Chemistry: Syntheses of Primary, Secondary, and Tertiary (Nonafluoro-*tert*-

butyloxy)Ethyl Amines. *J. Fluorine Chem.* **2006**, *127*, 1496–1504.

(27) Zhao, X.; Ng, W. Y.; Lau, K. C.; Collis, A. E. C.; Horvath, I. T. Generation of (Nonafluoro-*tert*-butoxy)Methyl Ponytails for Enhanced Fluorous Partition of Aromatics and Heterocycles. *Phys. Chem. Chem. Phys.* **2012**, *14*, 3909–3914.

(28) Oakwood Chemicals, Accessed 9-03-18, 75g/$100.

(29) Manchester Organics, Accessed 9-07-18, 25 g/$900.

(30) In our hands, conversion of (perfluorohexyl)propyl alcohol to the corresponding iodide provided low yields and inefficient conversion.

(31) We found one report of the alkylation of cyanoacetate with (perfluorohexyl)ethyl iodide in the patent literature: Read, R. Fluorous Acetylation, Int. Patent Appl. PCT/AU03/00218, 2003.

(32) Kolb, H. C.; Finn, M. G.; Sharpless, K. B. Click Chemistry: Diverse Chemical Function from a Few Good Reactions. *Angew. Chem.* **2001**, *40*, 2004–2021.

(33) Hoyle, C. E.; Lowe, A. B.; Bowman, C. N. Thiol-Click Chemistry: A Multifaceted Toolbox for Small Molecule and Polymer Synthesis. *Chem. Soc. Rev.* **2010**, *39*, 1355–1387.

(34) Highly fluorous porphyrins have been synthesized, but their fluorous partition coefficients have not been determined. Tuxen, J.; Eibenberger, S.; Gerlich, S.; Arndt, M.; Mayor, M. Highly Fluorous Porphyrins as Model Compounds for Molecule Interferometry. *Eur. J. Org. Chem.* **2011**, 4823–4833.

(35) Gerlich, S.; Eibenberger, S.; Tomandl, M.; Nimmrichter, S.; Hornberger, K.; Fagan, P. J.; Tuxen, J.; Mayor, M.; Arndt, M. Quantum Interference of Large Organic Molecules. *Nat. Commun.* **2011**, *2*, 263.

(36) Horvath, I. T. Fluorous Biphase Chemistry. *Acc. Chem. Res.* **1998**, *31*, 641–650.

(37) Fluorous partition coefficients can be obtained by UV-Vis spectroscopy. El Bakkari, M.; McClenaghan, N.; Vincent, J. M. The Pyridyl-Tag Strategy Applied to the Hydrocarbon/Perfluorocarbon Phase-Switching of a Porphyrin and a Fullerene. *J. Am. Chem. Soc.* **2002**, *124*, 12942–12943.

(38) Lovell, J. F.; Liu, T. W. B.; Chen, J.; Zheng, G. Activatable Photosensitizers for Imaging and Therapy. *Chem. Rev.* **2010**, *110*, 2839–2857.

(39) Protti, S.; Albini, A.; Viswanathan, R.; Greer, A. Targeting Photochemical Scalpels or Lancets in the Photodynamic Therapy Field - The Photochemist's Role. *Photochem. Photobiol.* **2017**, *93*, 1139–1153.

(40) van Straten, D.; Mashayekhi, V.; de Bruijn, H. S.; Oliveira, S.; Robinson, D.J.; van Straten, D.; Mashayekhi, V.; de Bruijn, H. S.; Oliveira, S.; Robinson, D. J. Oncologic Photodynamic Therapy: Basic Principles, Current Clinical Status and Future Directions. *Cancers* **2017**, *9*, 19–73.

(41) Flaim, S. F. Pharmacokinetics and Side Effects of Perfluorocarbon-Based Blood Substitutes. *Artif. Cells Blood Substit. Biotechnol.* **1994**, *22*, 1043–1054.

(42) Lowe, K. C. Perfluorochemical Respiratory Gas Carriers: Applications in Medicine and Biotechnology. *Sci. Prog.* **1997**, *80*, 169–193.

(43) Castro, C. I.; Briceno, J. C. Perfluorocarbon-Based Oxygen Carriers: Review of Products and Trials. *Artif. Organs* **2010**, *34*, 622–634.

(44) Yoshida, Y.; Sakakura, Y.; Aso, N.; Okada, S.; Tanabe, Y. Practical and efficient methods for sulfonylation of alcohols using Ts(Ms)Cl/Et_3N and catalytic $Me_3H{\cdot}HCl$ as combined base: Promising alternative to traditional pyridine. *Tetrahedron* **1999**, *55*, 2183-2192.

(45) Tüxen, J.; Eibenberger, S.; Gerlich, S.; Arndt, M.; Mayor, M. Highly Fluorous Porphyrins as Model Compounds for Molecule Interferometry. *Eur. J. Org. Chem.* **2011**, 4823-4833.

CHAPTER THREE

Cleavable fluorous tags for temporary solubility in fluorous solvent and stimuli-responsive release from perfluorocarbon emulsions

Adapted from: Miller, M.A.[±]; Day, R.D.[±]; Estabrook, D.A.[±]; Sletten, E.M.* "A reduction-sensitive fluorous fluorogenic coumarin." *Synlett* **2020**, *31*, 450–454. and unpublished work.

3.1 Abstract

The ability to synthesize branched fluorous tags allowed us to encapsulate payloads of interest inside perfluorocarbon (PFC) nanoemulsions. Encapsulation of payloads is useful for applications where the cargo remains inside the nanoparticle, such as in photodynamic therapy or imaging. However, we would ultimately like to have control over whether the payload remains inside the nanoemulsions and how it would be released. We imaged that branched fluorous tags could be combined with self-immolative linkers to result in payloads that could be used as probes for PFC nanoemulsions. A branched, fluorous-soluble fluorogenic coumarin is reported as a reduction-sensitive probe to study the interior and exterior environment of perfluorocarbon nanoemulsions and micelles. We describe additional perfluorinated coumarins that were synthesized. We imagined this cleavable linker strategy could be extended to drug delivery of a small-molecule from the nanoemulsions. We extend this reduction-sensitive fluorous linker strategy by synthesizing a fluorous prodrug of small-molecule therapeutic, Gemcitabine. While this work was not viable for applications *in cellulo*, we discuss future directions that could be pursued for payloads made fluorous-soluble through cleavable linkers.

3.2 Introduction

We previously demonstrated that covalent modification of fluorophores with branched perfluorinated tags allows for encapsulation of these payloads inside perfluorocarbon

nanoemulsions (Figure 3.1A). This approach works well for imaging experiments and applications where the payload can remain localized inside the nanoemulsion (i.e. photodynamic therapy). The lifetime of the fluorous-tagged molecule inside the emulsions can be correlated to the length of the fluorous chains or number of fluorous tags (see leaching study in Chapter 2, Figure 2.2). However, more controlled strategies that rely on specific stimuli rather than simple leaching are desirable, particularly for drug-delivery applications, where the payload needs to be released from the nanoemulsions at a specific location (Figure 3.1B and C).

Cleavable linkers are useful for the controlled release of payloads of interest.[1] We imagined that a payload could be modified with a fluorous tag through a cleavable linker rather than a permanent covalent bond to access temporarily fluorous-soluble payloads, which could be encapsulated inside perfluorocarbon (PFC) nanoemulsions. In the presence of a stimuli, the cleavable linker could be broken apart to return the payload to its nonfluorous-soluble state. We imaged that this strategy would allow us to gain information about how the interior core of the emulsions experiences its exterior environment. Additionally, the stimuli-responsive fluorous-soluble payloads could be coupled with a stimuli-responsive polymer surfactant for controlled release from PFC nanoemulsions.

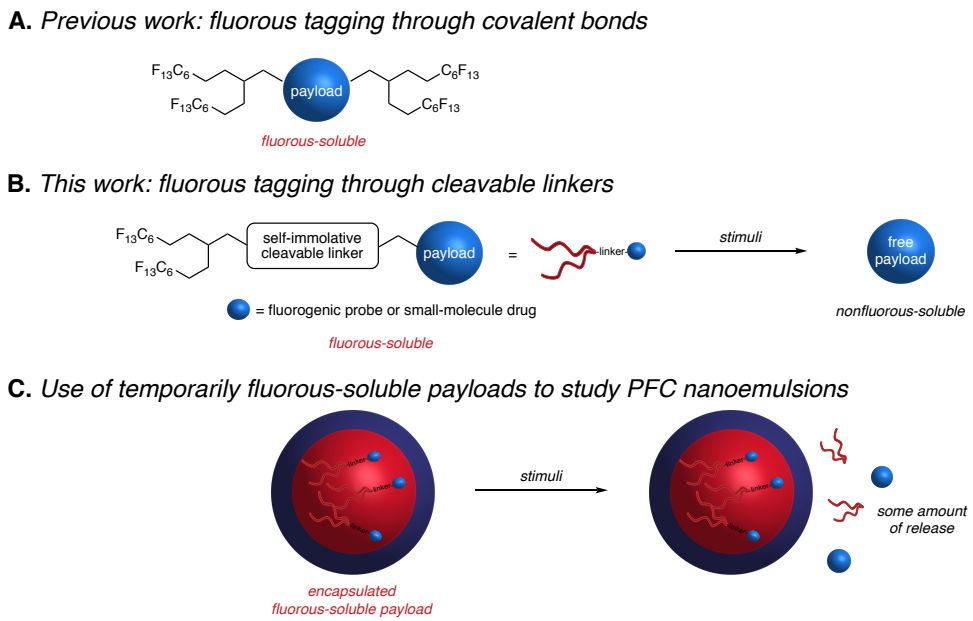

Figure 3.1 General approach to temporarily fluorous-soluble payloads. (A) Previous work using covalent bonds to solubilize payloads in fluorous solvent. B) Use of cleavable linkers to append branched fluorous tags to payloads of interest. This approach can be generalized such that the probe is sensitive to different stimuli. (C) Encapsulation of temporarily fluorous-soluble payloads into PFC nanoemulsions allows for study of how the emulsion experiences its environment. In the future, greater release of the payload could be observed with a degradable emulsion.

We intended first to develop a stimuli-responsive fluorous probe compound and then extend that design to a fluorous prodrug. To gain quantitative information about the interior and exterior environment of the PFC nanoemulsions, we chose to start with a fluorogenic fluorous probe like **3.2** (Figure 3.2C). Fluorogenic probes allow one to use fluorescence-based assays to study chemical changes, reactions, or an altered environment (i.e. solvent polarity) (Figure 3.2A).[2–4] Some examples of fluorous-soluble chromophores that are sensitive to their environment have been described in the literature. For example, 9-(α-perfluoroheptyl-β,β-dicyanovinyl)julolidine **3.1** displays solvatochromic behavior with a bathochromic shift in λ_{abs} in more polar solvents (Figure 3.2A and B).[5] A fluorous-soluble copper carboxylate complex has been used in tandem with an organic porphyrin for histamine sensing[6] and a BINOL-derivative

modified with fluorous groups has been used for enantioselectivity measurements.[7] Though a probe that would fit our needs did not exist in the literature, these works provided precedent for the general plan of a fluorogenic probe we had in mind.

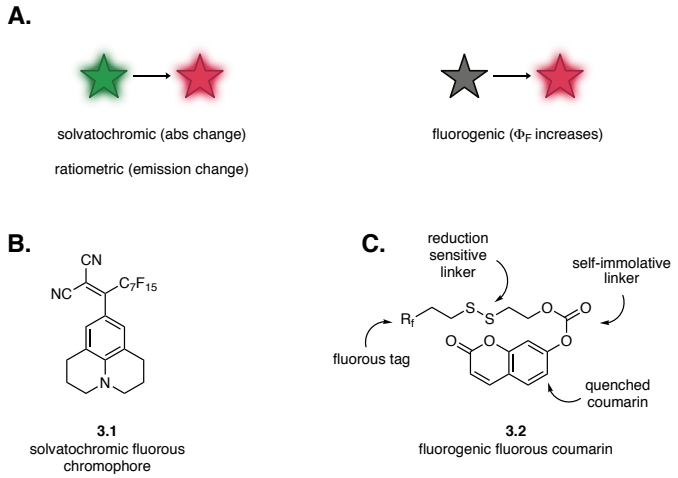

Figure 3.2 Chromophores sensitive to their environment. (A) Schematic of chromophores sensitive to their environment. (B) Solvatochromic fluorous fluorophore **3.1** from ref. 5. (C) Fluorogenic fluorous coumarin **3.2** described in this work.

Once we had plans for an initial fluorous fluorogenic probe, we considered small-molecule therapeutic that could be our initial target for a fluorous prodrug. We became interested in the FDA-approved chemotherapeutic, Gemcitabine. Gemcitabine is rapidly deactivated in serum,[8,9] making it an ideal compound for prodrug strategies[10,11] and carrier facilitated delivery.[12] Gemcitabine is relatively small with multiple handles for functionalizing with fluorous tags. Gemcitabine also has two fluorine atoms at the C2' position, which we imagined could aide in ^{19}F NMR identification of the prodrug and free drug if needed.

3.3 Discussion and results

Starting with the probe design, we imagined 7-hydroxycoumarin could be a model payload, as coumarins have been previously solubilized in fluorous solvent.[13–17] It is known that

the fluorescent properties of coumarins can be modulated by substituents at the 7-position,[4,18–20] more specifically that coumarin fluorescence is quenched when the 7-hydroxyl group is protected. With this approach, we could use fluorescence-based assays to evaluate the stability of the payload and its release from PFC nanoemulsions. We chose to use a disulfide as the initial cleavable linker as disulfides can be readily cleaved by glutathione or other thiols in the highly reducing environment of the cytosol (5-10 mM concentration of GSH in cytosol vs 10 μM concentration of GSH extracellularly).[21–23]

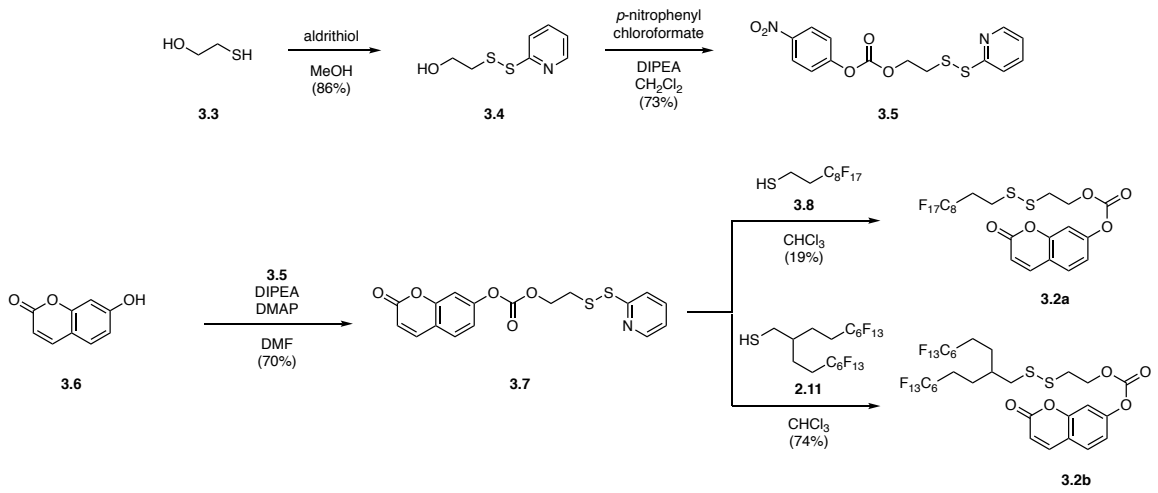

Scheme 3.1 Synthesis of heterobifunctional linker **3.5** and fluorous-tagged coumarins **3.2a**/**b**.

Specifically variations of **3.2** became our target structure which linked 7-hydroxycoumarin to a fluorous tag through a self-immolative disulfide linker that has been described on similar payloads (Figure 3.1C).[24–26] To begin, aldrithiol was reacted with β-mercaptoethanol **3.3** to access **3.4** (Scheme 3.1). The free alcohol was converted to heterobifunctional linker **3.5** in the presence of *p*-nitrophenylchloroformate. The activated carbonate **3.5** and 7-hydroxycoumarin **3.6** were coupled to provide the esterified coumarin with an activated disulfide **3.7**. Finally, disulfide exchange was carried out in chloroform with fluorous thiols. The disulfide exchange is thermodynamically favorable and proceeds readily as

it leads to the formation of 2-thiopyridone. While we initially used a linear fluorous thiol **3.8** (43 wt%F), we found this linear fluorous coumarin **3.2a** to be non-fluorous soluble. We then moved on to disulfide exchange with the branched fluorous thiol **2.11**, which provided moderately fluorous-soluble coumarin **3.2b** at 48 wt%F.

It was found that **3.2b** was stable in non-thiol containing solution over time. We have reported that in a biphasic fluorous water solution in the presence of various reducing agents (β-mercaptoethanol, DTT, TCEP, and GSH), the disulfide of **3.2b** is reduced and free coumarin **3.6** is released (Scheme 3.2).[27] Branched fluorous fluorogenic coumarin **3.2b** can also encapsulated in and slowly released from perfluorocarbon nanoemulsions or polymeric micelles over 48 hours in the presence of reducing agent.

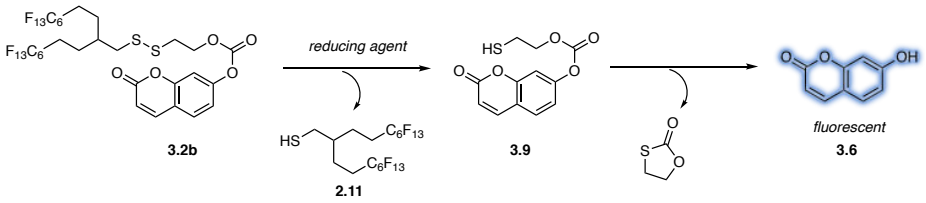

Scheme 3.2 Cleavage of disulfide bond in **3.2b** in the presence of reducing agent to release a free thiol **2.11** and then undergoes self-immolation to give fluorescent 7-hydroxycoumarin **3.6**.

Preliminary attempts were made to redshift this fluorogenic probe such that it could be visualized on microscopes in our laboratory for use *in cellulo*. We chose a coumarin with a CF_3 group at the 4-position, which is known to redshift coumarin emission by approximately 50 nm (λ_{em} = 454nm for 7-hydroxycoumarin **3.6** to 499nm for 7-hydroxy-4-trifluoromethylcoumarin).[28] We also incorporated an additional alcohol that could be modified with a fluorous tag to make doubly-fluorous fluorogenic coumarin **3.14** (53 wt%F) more soluble than **3.2b** (48 wt% F) in more fluorous solvents.

Towards second generation fluorous fluorogenic coumarin **3.14**, **3.12** was prepared by a $Sc(OTf)_3$ mediated Pechmann condensation of ethyl 4,4,4-trifluoroacetoacetate **3.10** and phloroglucinol **3.11** in low yield, due to the formation of other fluorescent species (Scheme 3.3). Ester formation at the more sterically hindered phenol at the 5-position of coumarin **3.12** was difficult under standard conditions described in Scheme 3.1. Esterification reactions with triphosgene were minimally successful to yield **3.13** in poor yield. Disulfide exchange of **3.13** with branched fluorous thiol **2.11** resulted in small amounts of the desired product **3.14**. Ultimately, we did not pursue the use of **3.14** further due to poor yields throughout the synthesis.

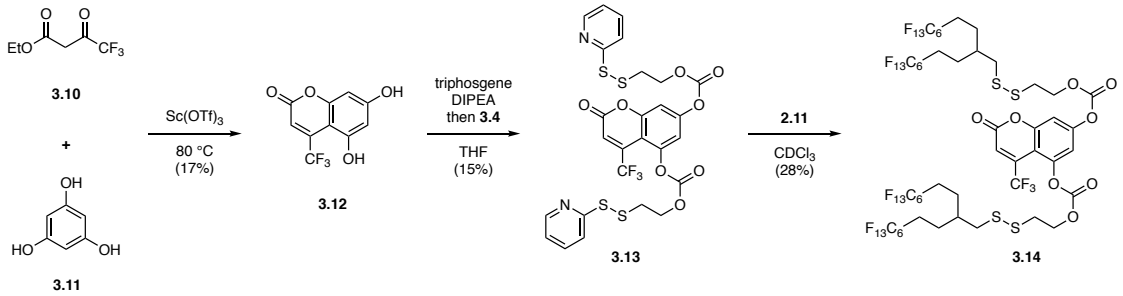

Scheme 3.3 Synthesis of second generation red-shifted branched fluorous fluorogenic coumarin **3.14**.

With some understanding of payloads with fluorous tags attached through cleavable linkers, we extended this strategy to a small-molecule therapeutic, Gemcitabine **3.15**. Gemcitabine is has previously been used as a prodrug.[10,11] Gemcitabine has two free alcohols and one free amine, providing multiple handles for functionalization with fluorous tags. Using Gemcitabine as a model, we could explore how many fluorous tags were necessary for rendering a highly polar small-molecule fluorous soluble. Using similar chemistry as shown above for fluorogenic fluorous coumarins, we synthesized three different variants of Gemcitabine with activated disulfides (Gem-(S-S-pyr)$_{1\text{-}3}$ **3.16**–**3.18** (Scheme 3.4). Initially, we synthesized two Gemcitabine variants with linear fluorous chains **3.19a** and **3.20a**. Once the chemistry had been

established, we began to use the branched fluorous thiol **2.11** for disulfide exchange reactions. We found that only when Gemcitabine was modified with three branched fluorous chains was Gemcitabine made fully fluorous soluble in PFOB. Attempts to release free Gemcitabine **3.15** from **3.21b** in the presence of BME or glutathione were made by Dan Estabrook and Rachael Day. However, these assays were complicated by the large difference in solubility between free Gemcitabine and the fluorous variant **3.21b**. Additionally, the high molecular weight of **3.21b** (and partially reduced intermediates **3.20b** and **3.19a**) made it difficult to observe reduction events by LCMS.

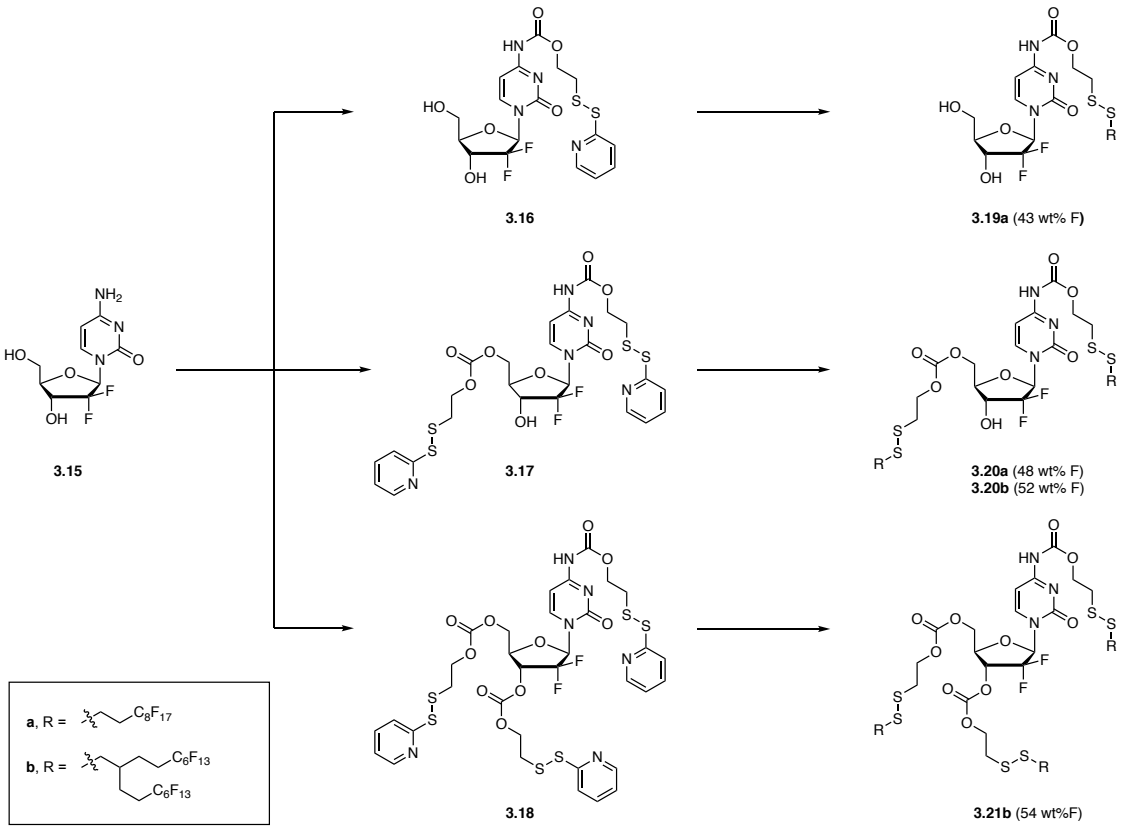

Scheme 3.4 Synthesis of fluorous-tagged Gemcitabine prodrugs.

3.4 Conclusion

In summary, we synthesized a fluorogenic fluorous-soluble fluorophore **3.2b** that was sensitive to reducing agents. This probe was used in experiments to assess to what extent the interior of a fluorous nanomaterial experiences its external environment. We attempted to extend this strategy for the release of a small-molecule therapeutic from PFC nanoemulsions. A fluorous-soluble Gemcitabine prodrug was synthesized. However, it was difficult to assess reduction of **3.21b** in solution and when encapsulated inside PFC nanoemulsions. Future work will decouple the stimuli required for payload release from the stimuli required for nanoemulsion degradation, such that optimization of the material degradation can be decoupled from payload release. Alternative stimuli, such as acid-cleavable linkers to release payloads, will take advantage of the inherent pH of the endosome, as non-targeted PFC nanoemulsions are internalized through endocytosis.[29–31]

3.5 Experimental Procedures

Chemical reagents were purchased from Sigma-Aldrich, Alfa Aesar, Fisher Scientific, Acros Organics, Synquest, or TCI and used without purification unless noted otherwise. Anhydrous dimethyl sulfoxide (DMSO) was obtained from a Sure-Seal™ bottle (Aldrich). Anhydrous and deoxygenated solvents dichloromethane (DCM), dimethylformamide (DMF), acetonitrile (MeCN), methanol (MeOH), and tetrahydrofuran (THF) were dispensed from a Grubb's-type Phoenix Solvent Drying System. Thin layer chromatography was performed using Silica Gel 60 F_{254} (EMD Millipore) plates. Flash chromatography was executed with technical grade silica gel with 60 Å pores and 40–63 μm mesh particle size (Sorbtech Technologies). Solvent was removed under reduced pressure with a Büchi Rotovapor with a Welch self-cleaning

dry vacuum pump and further dried with a Welch DuoSeal pump. Bath sonication was performed using a Branson 3800 ultrasonic cleaner. NMR spectra were recorded on Bruker AV-500 (^{1}H and ^{13}C) and AV-400 (^{19}F) instruments and processed with MestReNova software. NMR peaks are calibrated using residual undeuterated solvent ($CHCl_3$ at 7.26 ppm ^{1}H NMR, 77.16 ppm ^{13}C NMR). Masses for analytical measurements were taken on a Sartorius MSE6.6S-000-DM Cubis Micro Balance. HRMS (electrospray ionization (ESI)) were collected on a Thermo Scientific Q Exactive™ Plus Hybrid Quadrupole-Orbitrap™ with Dionex UltiMate 3000 RSLCnano System and LRMS (electrospray ionization (ESI)) were collected on an Agilent 1260 Infinity II HPLC-tandem MS system.

3.5.1 Synthetic experimental procedures

4-nitrophenyl 2-(pyridin-2-yldisulfanyl)ethylcarbonate (3.5) was prepared following a literature procedure.[26] ^{1}H NMR (500 MHz, $CDCl_3$): δ 8.55 – 8.45 (m, 1H), 8.35 – 8.21 (m, 2H), 7.73 – 7.58 (m, 2H), 7.44 – 7.32 (m, 2H), 7.12 (ddd, J = 6.7, 4.8, 1.8 Hz, 1H), 4.56 (t, J = 6.4 Hz, 2H), 3.16 (t, J = 6.4 Hz, 2H).

2-oxo-2*H*-chromen-7-yl (2-(pyridin-2-yldisulfaneyl)ethyl) carbonate (3.7). To activated disulfide **3.5** (600 mg, 1.64 mmol, 1.00 equiv) was added 7-hydroxy coumarin **3.6** (318 mg, 1.97 mmol, 1.20 equiv), DMF (31 mL, 0.05 M), and DMAP (23 mg, 0.20 mmol, 0.12 equiv). To the solution was added DIPEA (340 uL, 1.97 mmol, 1.20 equiv). The solution was stirred for 21 h at room temperature and then concentrated. The crude material was purified by column chromatography (silica gel, 35%→50% EtOAc/hexanes). Extensive drying provided the product **3.7** as a white amorphous solid (427 mg, 1.14 mmol, 70% yield). R_f = 0.17 in 40% EtOAc/hexanes. ^{1}H NMR (500 MHz, $CDCl_3$): δ 8.49 (ddd, J = 4.8, 1.8, 1.0 Hz, 1H), 7.71 – 7.62

(m, 3H), 7.50 (d, J = 8.5 Hz, 1H), 7.21 (d, J = 2.2 Hz, 1H), 7.16 – 7.08 (m, 2H), 6.41 (d, J = 9.6 Hz, 1H), 4.55 (t, J = 6.4 Hz, 2H), 3.16 (t, J = 6.4 Hz, 2H). ^{13}C NMR (101 MHz, $CDCl_3$): δ 160.3, 159.3, 154.8, 153.3, 152.6, 150.0, 142.8, 137.2, 128.8, 121.2, 120.3, 117.8, 117.0, 116.5, 110.0, 66.7, 36.9. HRMS (ESI) calcd. for $C_{17}H_{14}NO_5S_2^+$ $(M + H)^+$: 376.0313; found 376.0307.

Linear fluorous fluorogenic coumarin (3.2a). Activated disulfide coumarin **3.7** (13.3 mg, 0.0354 mmol, 1.00 equiv) was added to a dram vial and dissolved in DMF (0.6 mL, 0.06 M). Linear perfluorooctylethyl thiol **3.8** (10.1 mL, 0.0354 mmol, 1.00 equiv) was added to the reaction. After 17 h, the reaction was diluted with DCM and water was added. The organic layer was separated, dried (Na_2SO_4), and concentrated. Crude material was purified by column chromatography (silica gel, 100% DCM→2%MeOH/DCM) to provide mostly pure product. This material was further purified by column chromatography (silica gel, 30% Et_2O/pentane) to give product **3.2a** (5.2 mg, 0.0070 mmol, 19% yield). R_f = 0.18 in 25% EtOAc/hexanes. ^{1}H NMR (500 MHz, $CDCl_3$): δ 7.70 (d, J = 9.5 Hz, 1H), 7.50 (d, J = 8.5 Hz, 1H), 7.23 (d, J = 2.3 Hz, 1H), 7.15 (dd, J = 8.5, 2.3 Hz, 1H), 6.42 (d, J = 9.5 Hz, 1H), 4.55 (t, J = 6.5 Hz, 2H), 3.05 (t, J = 6.5 Hz, 2H), 2.96 – 2.88 (m, 2H), 2.55 (tt, J = 17.7, 8.1 Hz, 2H). ^{19}F NMR (376 MHz, $CDCl_3$): δ -80.7 (m, 3F), -113.6 (t, 2F), -121.6 (bs, 2F), -121.8 (bs, 4F), -122.7 (bs, 2F), -123.2 (bs, 2F), -126.1 (m, 2F).

Branched fluorous fluorogenic coumarin (3.2b). To branched fluorous thiol **2.11** (120 mg, 0.158 mmol, 1.10 equiv) was added **3.7** (54 mg, 0.14 mmol, 1.0 equiv) and chloroform (2.9 mL, 0.050 M). The solution became pale yellow within five minutes, and became more yellow over time. The reaction was stirred at room temperature for 18 h. The crude product was evaporated

onto SiO_2 from chloroform and purified by column chromatography (silica gel, 20%→ 40%→ 60% EtOAc/hexanes) to afford the product as a white solid (107 mg, 0.105 mmol, 75% yield). (The average yield across three reactions was 74%). R_f = 0.66 in 40% EtOAc/hexanes. ^{1}H NMR (500 MHz, $CDCl_3$): δ 7.69 (dd, J = 9.6, 0.6 Hz, 1H), 7.50 (d, J = 8.5 Hz, 1H), 7.22 (d, J = 2.3 Hz, 1H), 7.14 (dd, J = 8.5, 2.3 Hz, 1H), 6.42 (d, J = 9.6 Hz, 1H), 4.55 (t, J = 6.5 Hz, 2H), 3.04 (t, J = 6.5 Hz, 2H), 2.79 (d, J = 6.1 Hz, 2H), 2.19 – 2.05 (m, 4H), 1.90 (h, J = 6.3 Hz, 1H), 1.84 – 1.67 (m, 4H). ^{13}C NMR (126 MHz, $CDCl_3$): δ 160.3, 154.8, 153.3, 152.8, 142.8, 128.8, 117.7, 117.1, 116.5, 110.0, 66.8, 43.2, 36.8, 36.7, 28.2 (t, J_{CF} = 22.6 Hz), 23.0 (t, J_{CF} = 31.4 Hz). ^{19}F NMR (282 MHz, $CDCl_3$): δ -80.6 – -80.9 (m), -114.2 – -114.5 (bs, 4F), -121.9 (bs, 4F), -122.8 (bs, 4F), -123.3 (bs, 4F), -125.9 – -126.3 (m, 4F). HRMS (ESI) calcd for $C_{30}H_{20}F_{26}O_5S_2$ $(M + H)^+$: 1019.0415; found 1019.0405.

5,7-dihydroxy-4-(trifluoromethyl)coumarin (3.12). 3.12 was prepared following a procedure modified from the literature.[32] To a dram vial was added $Sc(OTf)_3$ (98 mg, 0.20 mmol, 0.10 equiv), phloroglucinol **3.11** (324 mg, 2.00 mmol, 1.00 equiv), and β-ketoester **3.10** (440 mg, 2.40 mmol, 1.20 equiv). The vial was sealed and heated to 80 °C for 3 h. The crude reaction mixture was suspended in water, but could not be filtered. All crude material was then dissolved in acetone and absorbed onto SiO_2. The crude product was purified by column chromatography (silica gel, 15% EtOAc/hexanes) to yield the product **3.12** (82 mg, 0.33 mmol, 17% yield), as well as other unidentified fluorescent species. R_f = 0.45 in 50% EtOAc/hexanes. ^{1}H NMR (500 MHz, DMSO-d_6): δ 10.92 (s, 1H), 10.67 (s, 1H), 6.53 (s, 1H), 6.32 (d, J = 2.4 Hz, 1H), 6.29 (d, J = 2.3 Hz, 1H). MS (ESI) m/z 359.0 $[M+TFA–H]^–$.

5,7-di-((2-(pyridin-2-yldisulfaneyl)ethyl)carbonate)-4-trifluoromethylcoumarin (3.13). To a flame-dried dram vial was added 5,7-dihydroxy-4-trifluoromethylcoumarin **3.12** (20 mg, 0.081 mmol, 1.0 equiv). Triphosgene (72 mg, 0.24 mmol, 3.0 equiv) was added. The dram vial was sealed, purged with N_2, and attached to a 1 M NaOH base trap. Dry THF (0.50 mL, 0.15 M) was added, and DIPEA (43 mL, 0.24 mmol, 3.0 equiv) was added dropwise. The reaction was heated to 50 °C for 1 h and then cooled to RT. Alcohol **3.4** in THF (0.5 mL) was added to the reaction. The reaction was stirred overnight and then concentrated under a stream of air. EtOAc and brine were added, and the organic layer was separated. The aqueous layer was washed with DCM, and the DCM layer was combined with the other organic layers. The organics were dried (Na_2SO_4), filtered, and concentrated. The crude material was absorbed onto SiO_2 and purified by column chromatography (silica gel, 15%→20%→40%EtOAc/hexanes→100%EtOAc) to yield ~20 mg of mostly pure product. This material was further purified on a pipette column (silica gel, 7% acetone/toluene) to yield the desired product **3.13** (8.4 mg, 0.012 mmol, 15% yield). R_f = 0.8 in 30% acetone/toluene. ^{1}H NMR (500 MHz, Acetone-d_6): δ 8.46 (ddt, J = 3.7, 2.8, 1.4 Hz, 2H), 7.86 – 7.75 (m, 4H), 7.40 (d, J = 2.4 Hz, 1H), 7.36 (d, J = 2.4 Hz, 1H), 7.25 – 7.19 (m, 2H), 7.03 (d, J = 1.0 Hz, 1H), 4.59 (dt, J = 6.8, 6.2 Hz, 4H), 3.26 (td, J = 6.3, 3.6 Hz, 4H). MS (ESI) *m/z* 673.0 $[M+H]^+$.

Di-branched fluorous-tagged trifluoromethyl coumarin (3.14). To a flame-dried dram vial was added **3.13** (6.4 mg, 0.0095, 1.0 equiv). Branched fluorous thiol **2.11** (21.5 mg, 0.0285 mmol, 3.00 equiv) was added in $CDCl_3$ (0.2 mL, 0.05 M). The reaction was sealed under N_2. After 12 h, the reaction was concentrated and purified by preparatory TLC (silica gel plate, 10% acetone/toluene) to yield 15 mg of partially pure product. That material was absorbed onto SiO_2 and purified on a

pipette column (silica gel, 20% Et_2O/pentane→50% Et_2O/pentane) to yield **3.14** (5.3 mg, 0.0027 mmol, 28% yield). R_f = 0.18 in 20% Et_2O/pentane. ^{1}H NMR (500 MHz, Acetone-d_6): δ 7.40 (d, J = 2.4 Hz, 1H), 7.35 (d, J = 2.4 Hz, 1H), 7.03 (d, J = 1.1 Hz, 1H), 4.58 (td, J = 6.4, 1.5 Hz, 4H), 3.14 (dt, J = 7.7, 6.4 Hz, 4H), 3.01 (d, J = 6.3 Hz, 4H), 2.36 (dt, J = 19.7, 10.8 Hz, 8H), 2.13 – 2.08 (m, 2H), 1.85 (m, 8H). ^{19}F NMR (282 MHz, $CDCl_3$): δ -64.1 (s, 3F), -80.8 (tt, J = 9.8, 2.6 Hz, 12F), -114.4 (ddt, J = 18.2, 9.0, 4.8 Hz, 8F), -121.9 (s, 8F), -122.9 (s, 8F), -123.3 (s, 8F), -126.1 (s, 8F).

Mono-(2-(pyridin-2-yldisulfaneyl)ethyl)carbamate-Gemcitabine (3.16). 4-nitrophenyl 2-(pyridin-2-yldisulfanyl)ethylcarbonate **3.5** (94 mg, 0.26 mmol, 1.0 equiv) was dissolved in DMF (5 mL, 0.05 M). Gemcitabine **3.15** (83.3 mg, 0.325 mmol, 1.27 equiv) and DMAP (2.5 mg, 0.020 mmol, 0.080 equiv) were added, followed by DIPEA (50 µL, 0.33 mmol, 1.1 equiv). The reaction was stirred under N_2 for 19 h and concentrated to dryness. The crude was purified by column chromatography (silica gel, 6% →8%→9%→10%→15%→20% MeOH/DCM) to yield **3.16** as a white solid (57 mg, 0.12 mmol, 47% yield) and doubly modified product **3.17** (41 mg, 0.059 mmol, 23% yield) as a colorless oil. **3.16** R_f = 0.5 in 10% MeOH/DCM. ^{1}H NMR (500 MHz, Methanol-d_4): δ 8.41 (ddd, J = 4.9, 1.8, 1.0 Hz, 1H), 7.89 – 7.75 (m, 3H), 7.24 (ddd, J = 7.2, 4.9, 1.4 Hz, 1H), 6.30 (t, J = 8.8 Hz, 1H), 5.93 (d, J = 7.6 Hz, 1H), 5.28 (dt, J = 12.9, 6.9 Hz, 1H), 4.50 – 4.40 (m, 2H), 4.18 (dt, J = 6.7, 3.1 Hz, 1H), 3.86 (ddd, J = 69.3, 12.8, 3.1 Hz, 2H), 3.14 (t, J = 6.1 Hz, 2H). ^{19}F NMR (376 MHz, Methanol-d_4): δ -115.9 (d, J = 244.4 Hz, 1F), -119.0 (d, J = 247.9 Hz, 1F). **Di-(2-(pyridin-2-yldisulfaneyl)ethyl)carbamate-Gemcitabine (3.17).** R_f = 0.19 in 10% MeOH/DCM. ^{1}H NMR (400 MHz, $CDCl_3$): δ 8.50 – 8.42 (m, 2H), 7.75 (s, 1H), 7.70 – 7.56 (m, 4H), 7.35 (d, J = 7.5 Hz, 1H), 7.16 – 7.04 (m, 2H), 6.33 (s, 1H), 6.09 (s,

1H), 5.87 (d, J = 7.6 Hz, 1H), 5.19 (s, 1H), 4.55 – 4.36 (m, 6H), 4.29 (ddd, J = 6.4, 4.3, 3.3 Hz, 1H), 3.08 (td, J = 6.5, 5.4 Hz, 4H). ^{19}F NMR (376 MHz, $CDCl_3$): δ -115.3 (d, J = 246.4 Hz, 1F), -119.3 (bs, 1F). MS (ESI) *m/z* 690.2 $[M+ H]^+$.

Tri-(2-(pyridin-2-yldisulfaneyl)ethyl)carbamate-Gemcitabine (3.18) To a flame-dried dram vial was added Gemcitabine **3.15** (18.6 mg, 0.071 mmol, 1.00 equiv), K_2CO_3 (38 mg, 0.27 mmol, 3.9 equiv), and DMF (0.55 mL, 0.13 M). Activated carbonate **3.5** (100 mg, 0.280 mmol, 4.00 equiv) was added in DMF (0.55 mL, 0.13 M). The solution immediately turned yellow. After 2 days, the reaction was concentrated and purified by column chromatography (silica gel, 70%→80%→90%EtOAc/hexanes→100%EtOAc→4%MeOH/EtOAc→6%MeOH/EtOAc→10% MeOH/EtOAc) to yield **3.18** (5.7 mg, 0.0063 mmol, 9% yield). R_f = 0.31 in 80% EtOAc/hexanes. ^{1}H NMR (400 MHz, $CDCl_3$): δ 8.48 (s, 3H), 7.73 (s, 1H), 7.69 – 7.61 (m, 6H), 7.16 – 7.06 (m, 3H), 6.42 (s, 1H), 5.19 (s, 1H), 4.56 – 4.32 (m, 10H), 3.09 (td, J = 6.5, 1.5 Hz, 6H). ^{19}F NMR (376 MHz, $CDCl_3$): δ -115.4 (d, J = 247.1 Hz, 1F), -118.5 (bs, 1F). MS (ESI) *m/z* 904.2 $[M+ H]^+$.

Mono-linear fluorous-tagged Gemcitabine (3.19a). To a flame-dried dram vial, was added activated disulfide **3.16** (9.1 mg, 0.019 mmol, 1.0 equiv) and $CDCl_3$. Perfluoroocytl ethyl thiol **3.8** (9.1 mg, 0.019 mmol, 1.0 equiv) was added. The reaction mixture was heated to 40 °C under N_2. After 4 h, the reaction mixture was evaporated to dryness. The crude reaction mixture was purified by flash column chromatography (silica gel, 5% → 10% MeOH/DCM) to provide **3.19a** as a white solid (7.5 mg, 0.009 mmol, 47%). R_f= 0.3 in 10% MeOH/DCM. ^{1}H NMR (400 MHz, Methanol-d_4): δ 7.79 (dd, J = 7.6, 1.3 Hz, 1H), 6.29 (t, J = 8.8 Hz, 1H), 5.93 (d, J = 7.6 Hz, 1H),

5.31 (dd, J = 12.6, 6.5 Hz, 1H), 4.48 (td, J = 6.3, 2.0 Hz, 2H), 4.18 (dt, J = 6.7, 3.1 Hz, 1H), 3.87 (ddd, J = 56.5, 12.8, 3.1 Hz, 2H), 3.05 (t, J = 6.3 Hz, 2H), 3.01 – 2.93 (m, 2H), 2.62 (tt, J = 18.0, 8.0 Hz, 2H). ^{19}F NMR (376 MHz, Methanol-d_4): δ -82.4 (t, J = 10.2 Hz, 3F), -114.7 (dt, J = 17.0, 8.7 Hz, 2F), -115.9 (d, J = 244.6 Hz, 1F), -118.6 (s, 1F), -122.6 (d, J = 16.6 Hz, 2F), -122.8 (s, 4F), -123.7 (s, 2F), -124.3 (s, 2F), -127.0 – -127.5 (m, 2F).

Di-linear fluorous-tagged Gemcitabine (3.20a). To a flame-dried dram vial, was added activated bis-disulfide **3.17** (16.1 mg, 0.023 mmol, 1.00 equiv) and $CDCl_3$. Perfluoroocytl ethyl thiol **3.8** (56 mg, 0.12 mmol, 5.0 equiv) was added. The reaction mixture was heated to 40 °C under nitrogen. After 24 h, the reaction mixture was evaporated to dryness. The crude reaction mixture was washed with MeCN (3 x 1 mL) and then washed perfluorohexanes (2 x 1 mL). The remaining white solid was placed on high vacuum to afford the dry product (11.1 mg, 39%). R_f = 0.7 in 5% MeOH/EtOAc. ^{1}H NMR (500 MHz, $CDCl_3$/HFIP-d_2): δ 7.61 (dd, J = 7.7, 1.8 Hz, 1H), 6.27 (dd, J = 10.4, 6.5 Hz, 1H), 5.96 (d, J = 7.6 Hz, 1H), 5.14 (ddd, J = 13.2, 6.3, 3.3 Hz, 1H), 4.60 – 4.45 (m, 6H), 3.01 (td, J = 6.3, 1.3 Hz, 4H), 2.98 – 2.89 (m, 4H), 2.57 (tt, J = 17.4, 7.9 Hz, 4H). ^{19}F NMR (376 MHz, $CDCl_3$): δ -81.8 (s, 6F), -114.5 (s, 4F), -115.6 (d, J = 249.3 Hz, 1F), -120.0 (d, J = 245.6 Hz, 1F), -122.2 (s, 4F), -122.5 (s, 8F), -123.3 (s, 4F), -124.0 (s, 4F), -126.9 (s, 4F).

Di-branched fluorous-tagged Gemcitabine (3.20b). To a vial containing **3.17** (14 mg, 0.020 mmol, 1.0 equiv) was added branched fluorous thiol **2.11** (58 mg, 0.077 mmol, 3.9 equiv) and $CDCl_3$ (0.6 mL, 0.03 M). The vial was sealed under N_2 and heated to 40 °C. After 24 h, the reaction was concentrated and purified by column chromatography (silica gel, 50%→60% EtOAc/hexanes→100% EtOAc) to provide **3.20b** (25.7 mg, 0.130 mmol, 65% yield). R_f = 0.61

in 100% EtOAc ($KMnO_4$). ^{1}H NMR (500 MHz, $CDCl_3$): δ 7.43 (d, J = 7.5 Hz, 1H), 6.38 (s, 1H), 5.89 (d, J = 7.2 Hz, 1H), 5.18 (d, J = 9.8 Hz, 1H), 4.54 – 4.39 (m, 6H), 4.37 – 4.30 (m, 1H), 2.96 (td, J = 6.6, 1.5 Hz, 4H), 2.76 (d, J = 6.1 Hz, 4H), 2.18 – 2.04 (m, 8H), 1.88 (h, J = 6.4 Hz, 2H), 1.84 – 1.65 (m, 8H). ^{19}F NMR (376 MHz, $CDCl_3$): δ -80.8 (t, J = 10.0 Hz, 12F), -114.4 (t, J = 13.8 Hz, 8F), -115.8 (d, J = 247.4 Hz, 1F), -121.9 (s, 8F), -122.9 (s, 8F), -123.3 (s, 8F), -126.2 (td, J = 15.2, 6.6 Hz, 8F).

Tri-branched fluorous-tagged Gemcitabine (3.21b). To a vial containing **3.18** (17.3 mg, 0.019 mmol, 1.00 equiv) was added branched fluorous thiol **2.11** (61.4 mg, 0.0817, 4.30 equiv) in $CDCl_3$ (0.58 mL, 0.033M). The solution becomes immediately yellow, is sealed under N_2, and heated to 40 °C. After 21 h, the reaction mixture was loaded directly onto a column (silica gel, 10%→20%→30%→40%→50%→70% EtOAc/hexanes) to provide **3.21b** (15.1 mg, 0.00530 mmol, 28% yield). R_f = 0.24 in 40% EtOAc/hexanes. ^{1}H NMR (500 MHz, $CDCl_3$): δ 7.73 (d, J = 7.7 Hz, 1H), 7.30 (d, J = 7.6 Hz, 1H), 6.41 (s, 1H), 5.25 – 5.16 (m, 1H), 4.57 – 4.41 (m, 8H), 4.38 (dt, J = 5.8, 3.8 Hz, 1H), 2.96 (td, J = 6.6, 2.2 Hz, 7H), 2.76 (dd, J = 6.1, 3.0 Hz, 6H), 2.21 – 2.01 (m, 15H), 1.89 (hept, J = 6.4 Hz, 3H), 1.84 – 1.64 (m, 11H). ^{19}F NMR (282 MHz, $CDCl_3$): δ -80.8 (s, 18F), -114.4 (s, 12F), -115.8 (d, J = 245.4 Hz, 1F), -121.9 (s, 12F), -122.9 (s, 12F), -123.3 (s, 12F), -126.2 (s, 12F).

3.5.2 NMR spectra

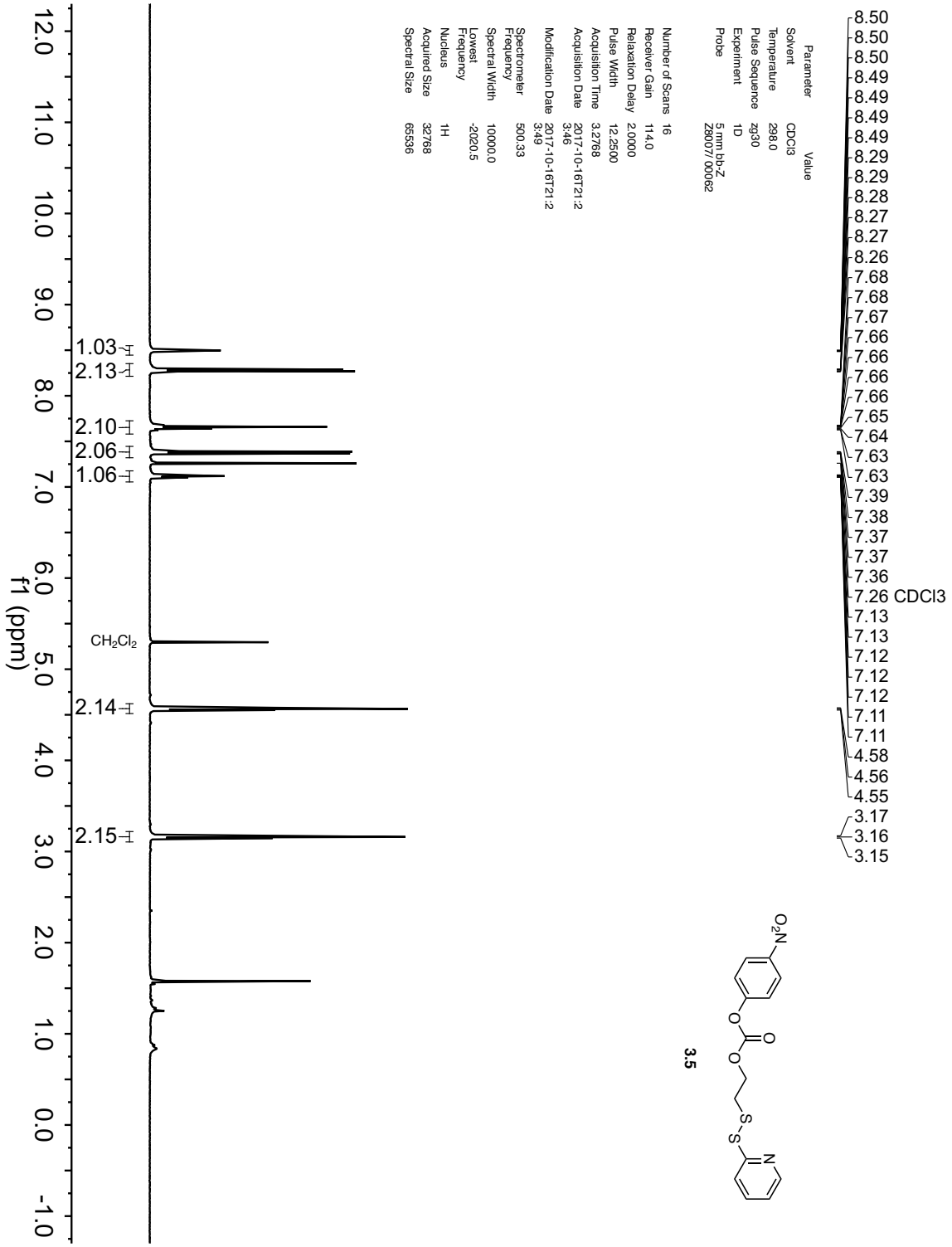

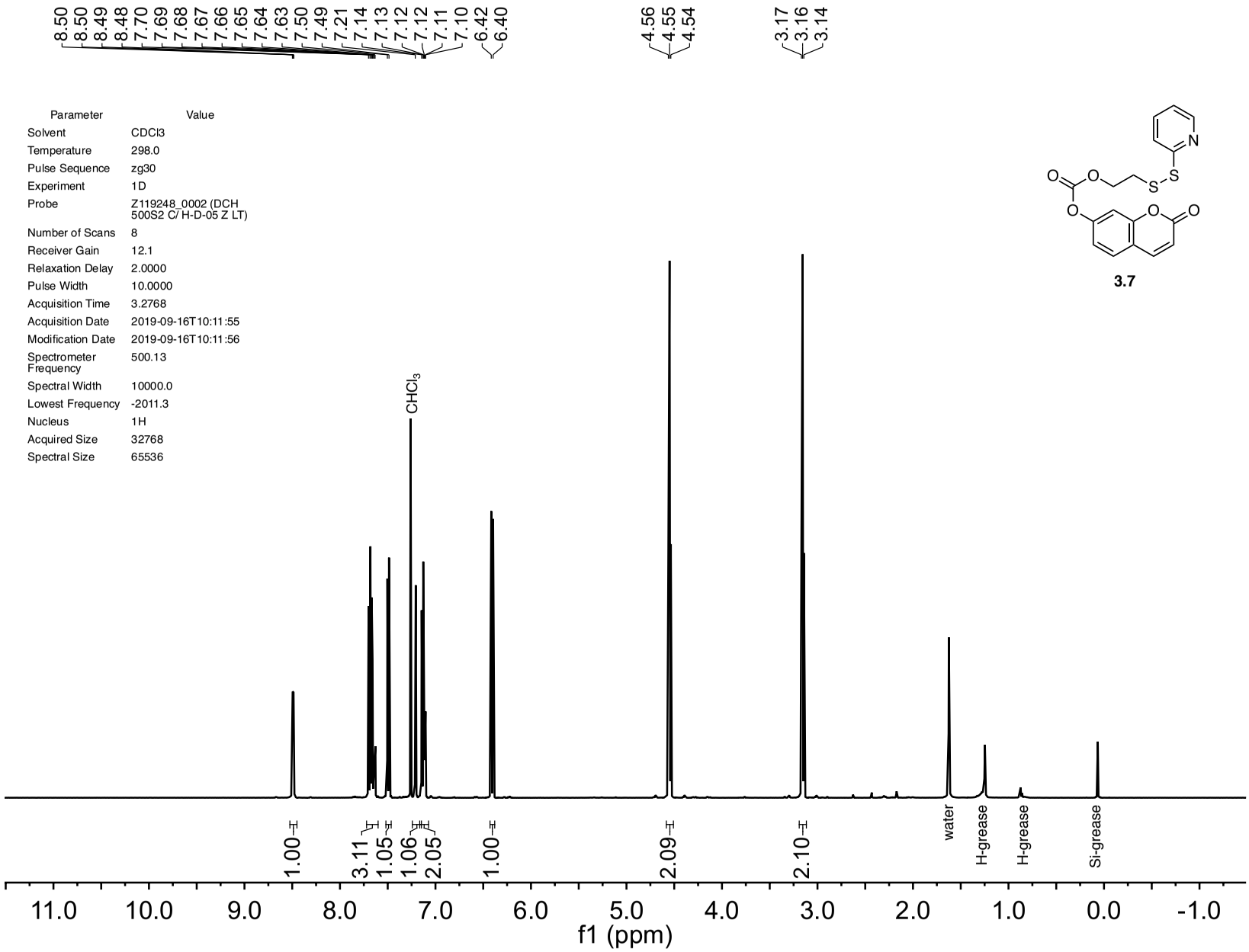
8.50
8.50
8.49
8.48
7.70
7.69
7.68
7.67
7.66
7.65
7.64
7.63
7.50
7.49
7.21
7.14
7.13
7.12
7.12
7.11
7.10
6.42
6.40
4.56
4.55
4.54
3.17
3.16
3.14
Parameter Value
Solvent CDCl3
Temperature 298.0
Pulse Sequence zg30
Experiment 1D
Probe Z119248_0002 (DCH 500S2 C/ H-D-05 Z LT)
Number of Scans 8
Receiver Gain 12.1
Relaxation Delay 2.0000
Pulse Width 10.0000
Acquisition Time 3.2768
Acquisition Date 2019-09-16T10:11:55
Modification Date 2019-09-16T10:11:56
Spectrometer Frequency 500.13
Spectral Width 10000.0
Lowest Frequency -2011.3
Nucleus 1H
Acquired Size 32768
Spectral Size 65536
CHCl3
1.00
3.11
1.05
1.06
2.05
1.00
2.09
2.10
water
H-grease
H-grease
Si-grease
11.0
10.0
9.0
8.0
7.0
6.0
5.0
4.0
3.0
2.0
1.0
0.0
-1.0
f1 (ppm)
3.7

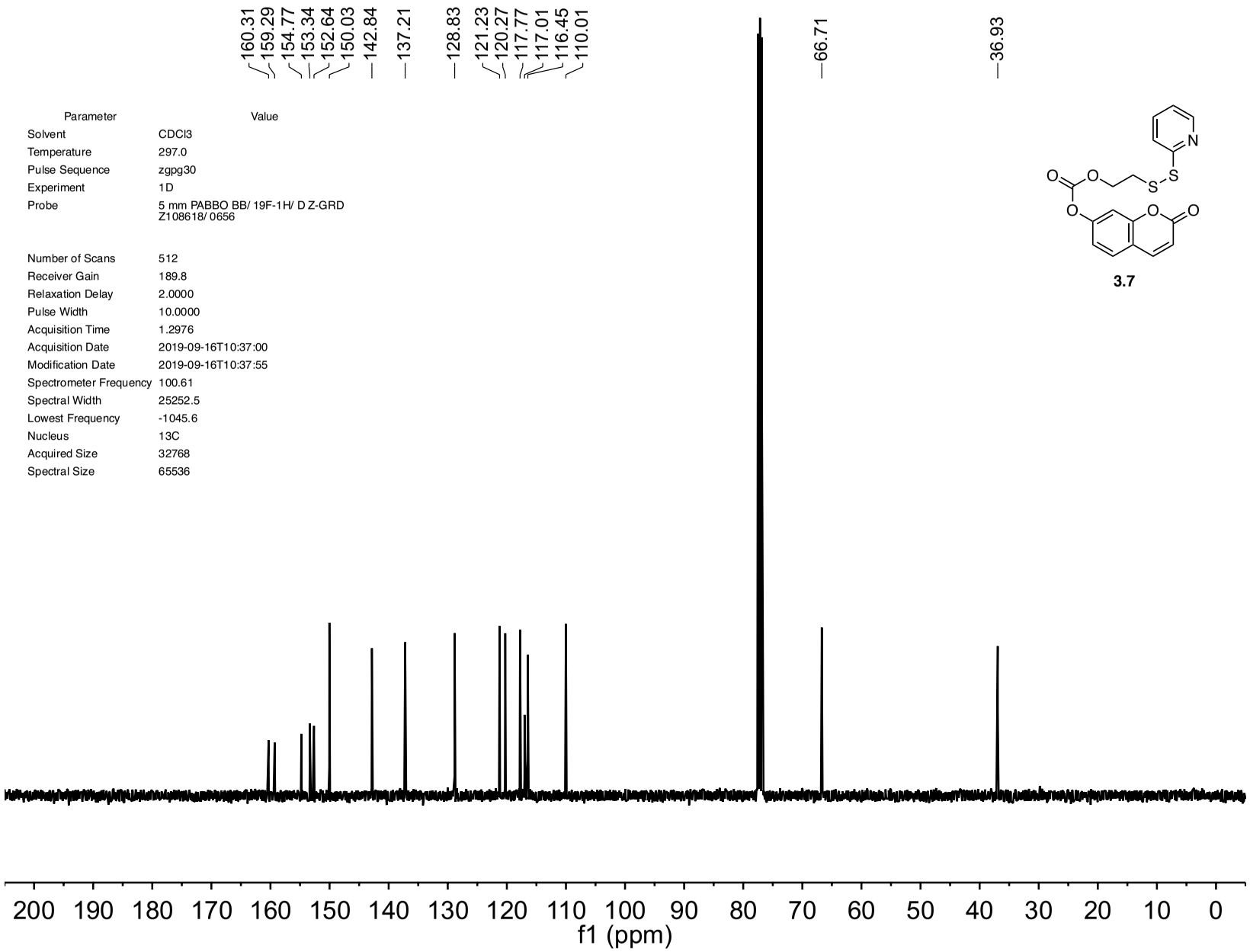

Parameter	Value
Solvent	CDCl3
Temperature	297.0
Pulse Sequence	zgpg30
Experiment	1D
Probe	5 mm PABBO BB/ 19F-1H/ D Z-GRD Z108618/ 0656
Number of Scans	512
Receiver Gain	189.8
Relaxation Delay	2.0000
Pulse Width	10.0000
Acquisition Time	1.2976
Acquisition Date	2019-09-16T10:37:00
Modification Date	2019-09-16T10:37:55
Spectrometer Frequency	100.61
Spectral Width	25252.5
Lowest Frequency	-1045.6
Nucleus	13C
Acquired Size	32768
Spectral Size	65536

3.7

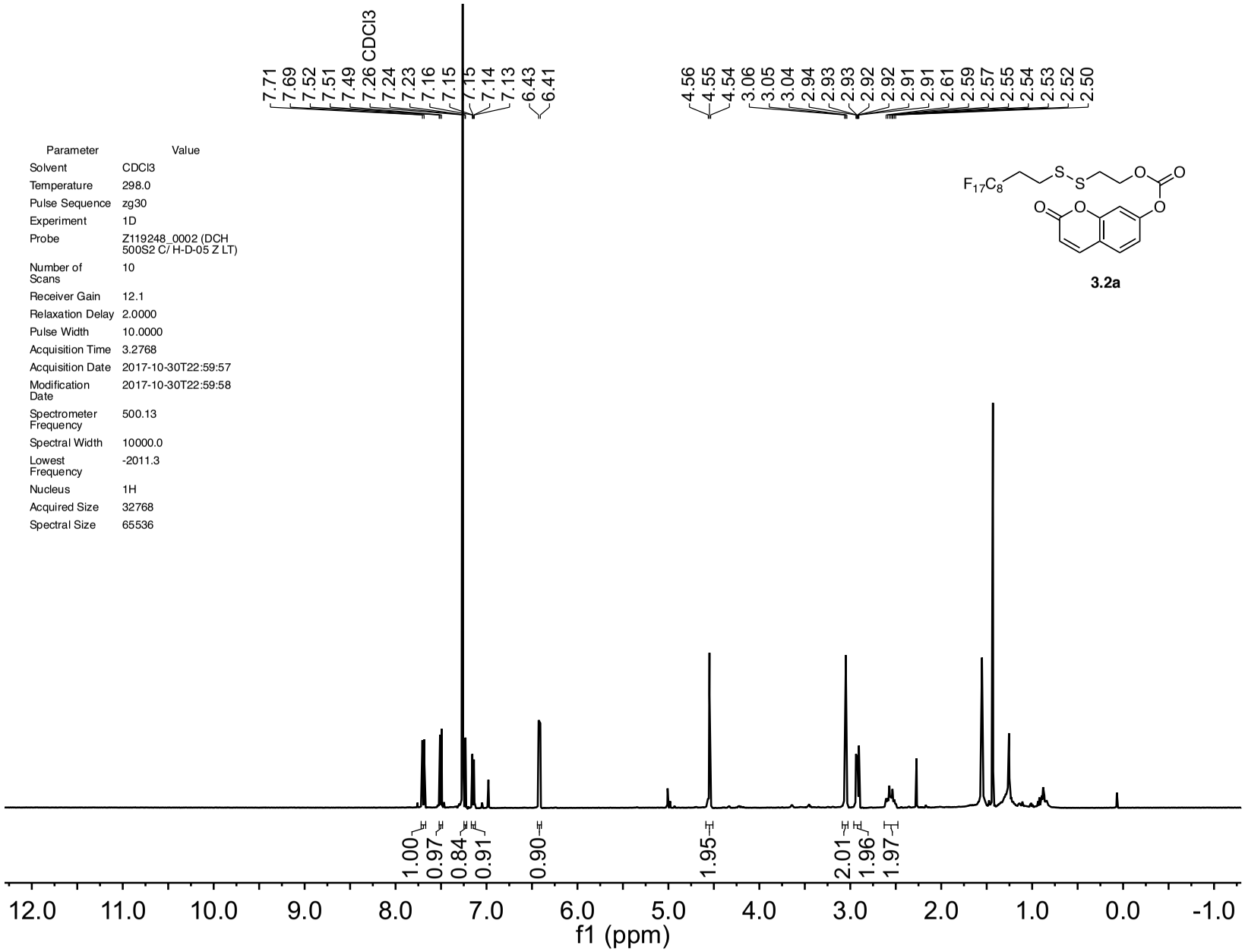

Parameter	Value
Solvent	CDCl3
Temperature	298.0
Pulse Sequence	zg30
Experiment	1D
Probe	Z119248_0002 (DCH 500S2 C/ H-D-05 Z LT)
Number of Scans	10
Receiver Gain	12.1
Relaxation Delay	2.0000
Pulse Width	10.0000
Acquisition Time	3.2768
Acquisition Date	2017-10-30T22:59:57
Modification Date	2017-10-30T22:59:58
Spectrometer Frequency	500.13
Spectral Width	10000.0
Lowest Frequency	-2011.3
Nucleus	1H
Acquired Size	32768
Spectral Size	65536

3.2a

Parameter	Value
Solvent	CDCl3
Temperature	298.9
Pulse Sequence	zgflqn30
Experiment	1D
Probe	5 mm PABBO BB/ 19F-1H/ D Z-GRD Z108618/ 0656
Number of Scans	16
Receiver Gain	189.8
Relaxation Delay	2.0000
Pulse Width	14.5000
Acquisition Time	0.8738
Acquisition Date	2017-07-21T17:48:00
Modification Date	2017-09-21T00:12:58
Spectrometer Frequency	376.50
Spectral Width	150000.0
Lowest Frequency	-75000.0
Nucleus	19F
Acquired Size	131072
Spectral Size	262144

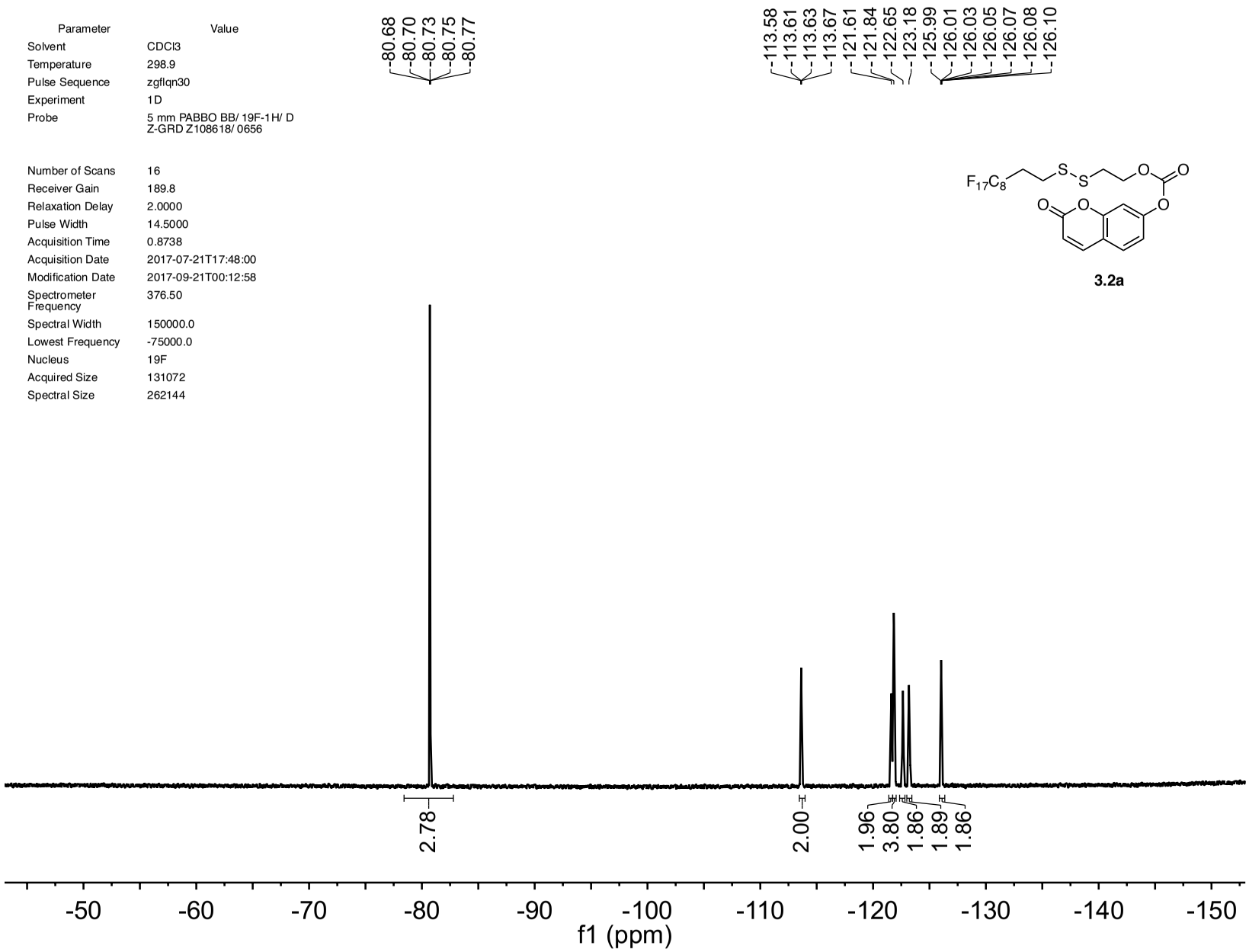

3.2a

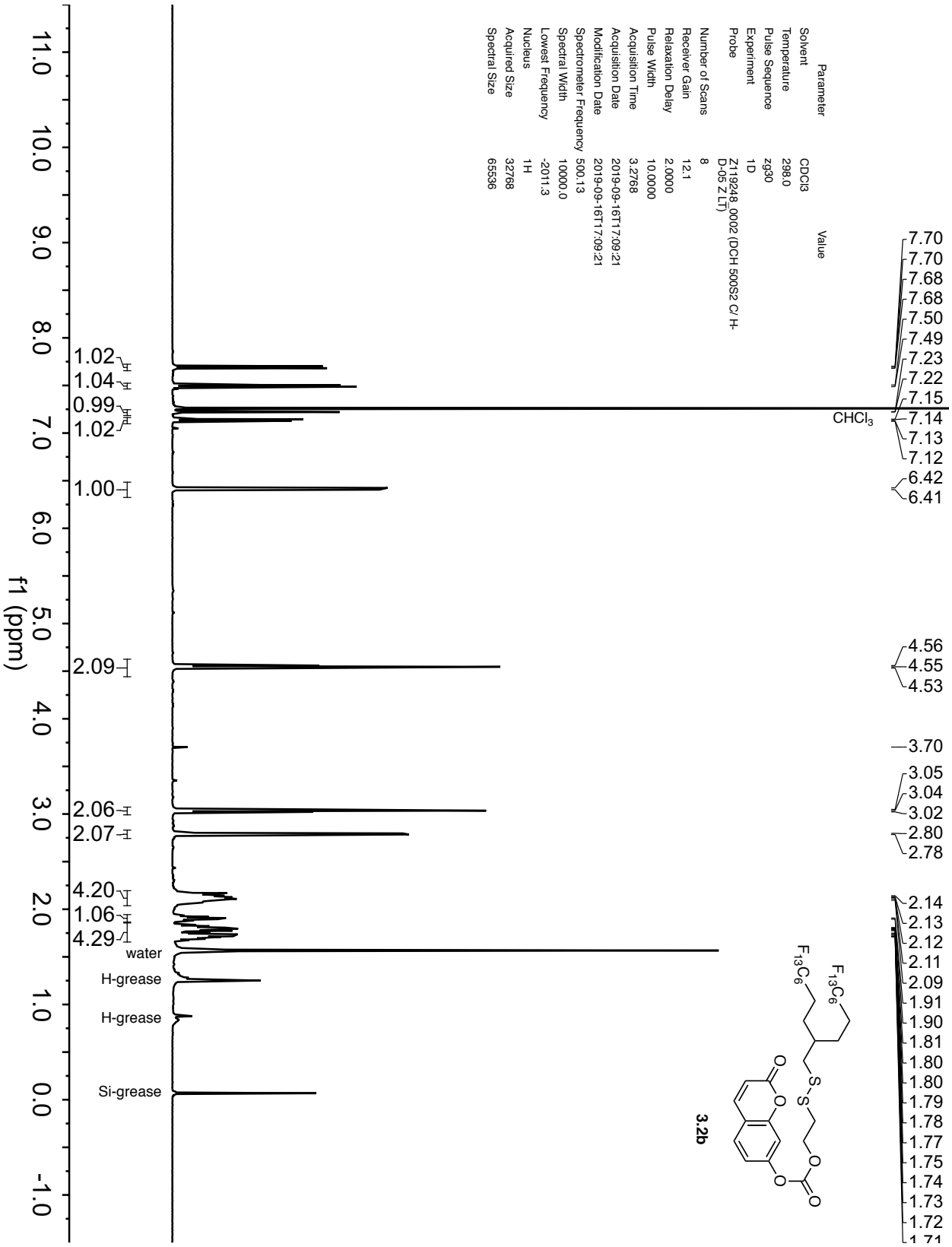
Parameter Value
Solvent CDCl3
Temperature 298.0
Pulse Sequence zg30
Experiment 1D
Probe Z119248_0002 (DCH 500S2 C/ H-D-05 Z LT)
Number of Scans 8
Receiver Gain 12.1
Relaxation Delay 2.0000
Pulse Width 10.0000
Acquisition Time 3.2768
Acquisition Date 2019-09-16T17:09:21
Modification Date 2019-09-16T17:09:21
Spectrometer Frequency 500.13
Spectral Width 10000.0
Lowest Frequency -2011.3
Nucleus 1H
Acquired Size 32768
Spectral Size 65536
CHCl3
water
H-grease
H-grease
Si-grease
3.2b
f1 (ppm)

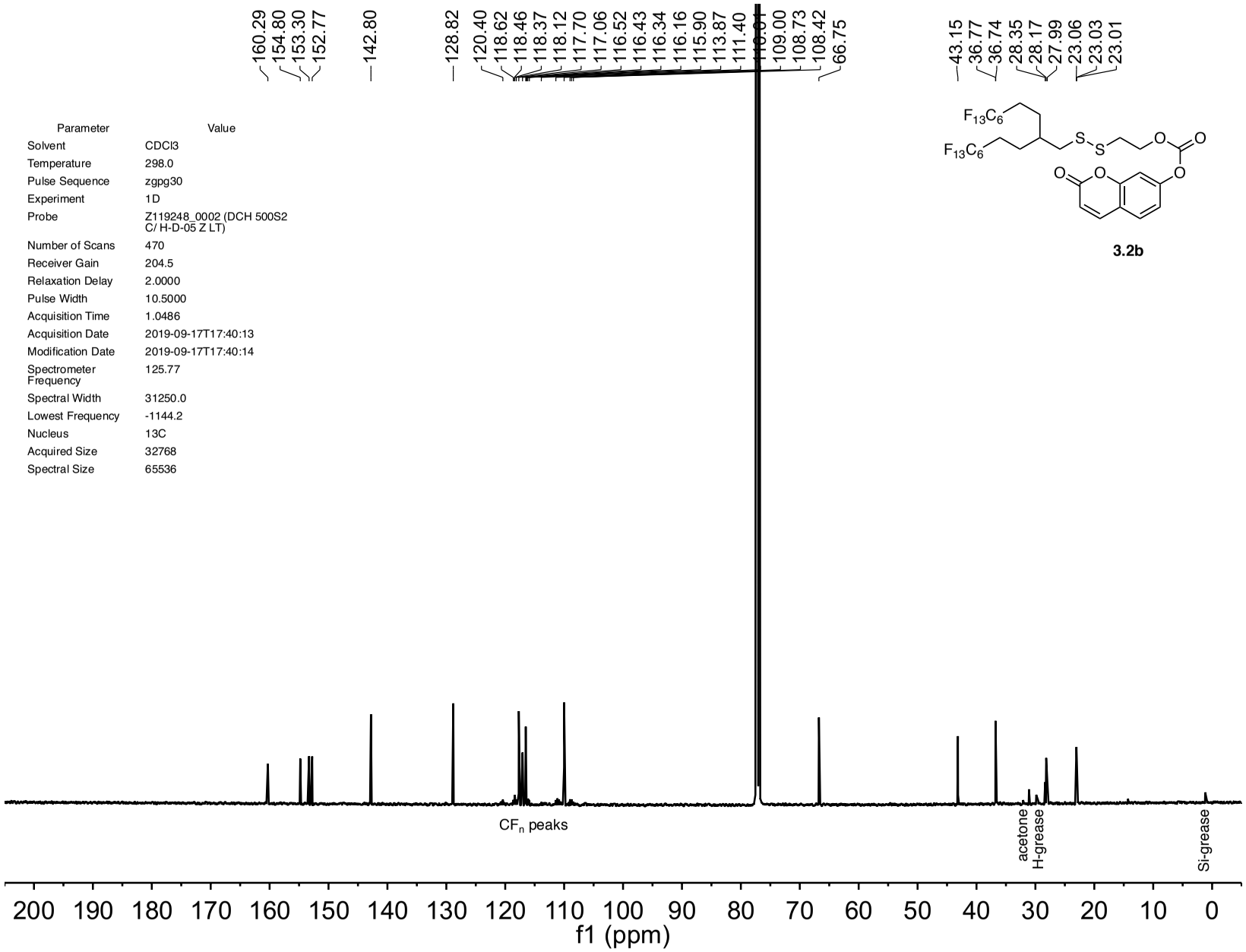

Parameter	Value
Solvent	CDCl3
Temperature	298.0
Pulse Sequence	zgpg30
Experiment	1D
Probe	Z119248_0002 (DCH 500S2 C/ H-D-05 Z LT)
Number of Scans	470
Receiver Gain	204.5
Relaxation Delay	2.0000
Pulse Width	10.5000
Acquisition Time	1.0486
Acquisition Date	2019-09-17T17:40:13
Modification Date	2019-09-17T17:40:14
Spectrometer Frequency	125.77
Spectral Width	31250.0
Lowest Frequency	-1144.2
Nucleus	13C
Acquired Size	32768
Spectral Size	65536

3.2b

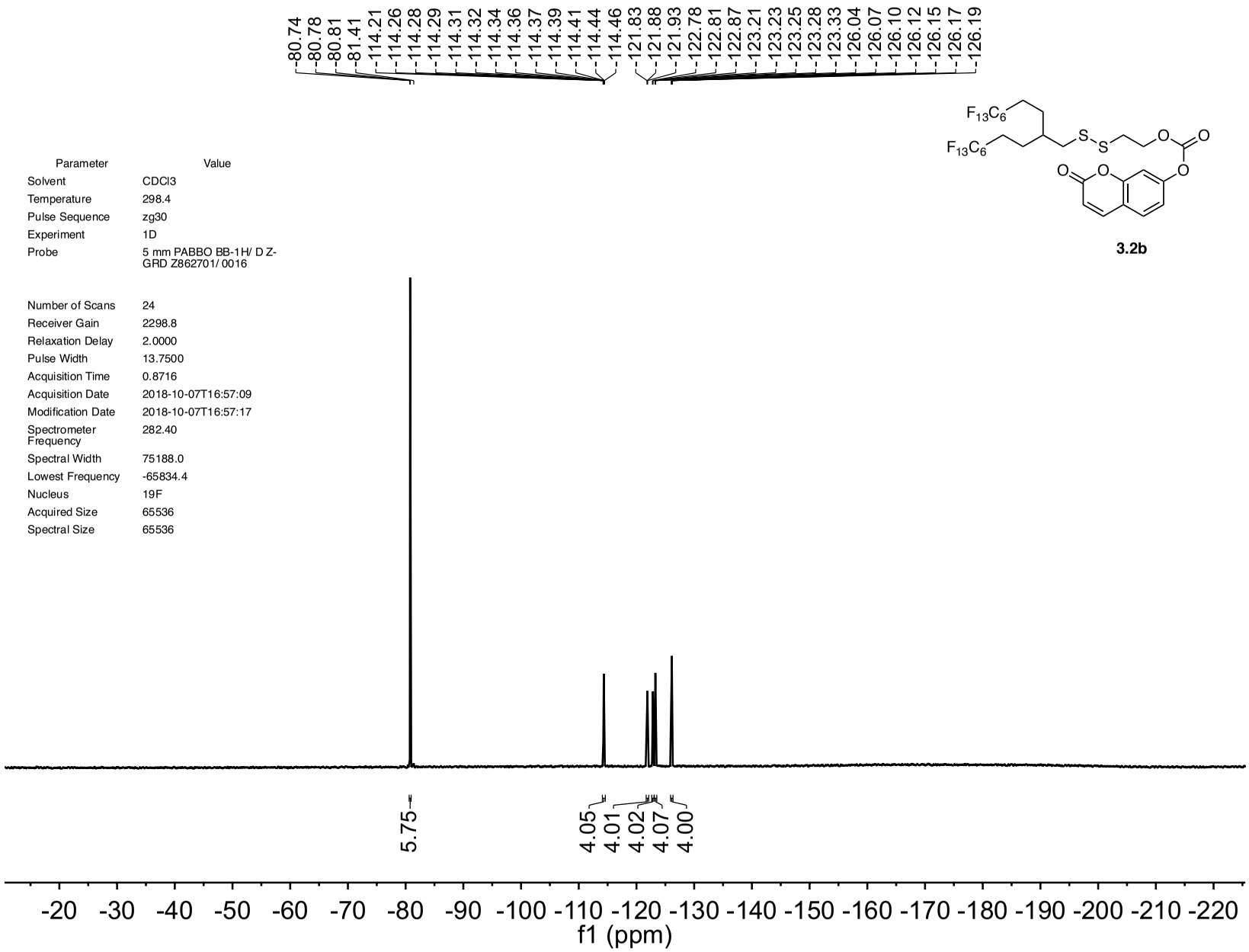

Parameter	Value
Solvent	CDCl3
Temperature	298.4
Pulse Sequence	zg30
Experiment	1D
Probe	5 mm PABBO BB-1H/ D Z-GRD Z862701/ 0016
Number of Scans	24
Receiver Gain	2298.8
Relaxation Delay	2.0000
Pulse Width	13.7500
Acquisition Time	0.8716
Acquisition Date	2018-10-07T16:57:09
Modification Date	2018-10-07T16:57:17
Spectrometer Frequency	282.40
Spectral Width	75188.0
Lowest Frequency	-65834.4
Nucleus	19F
Acquired Size	65536
Spectral Size	65536

3.2b

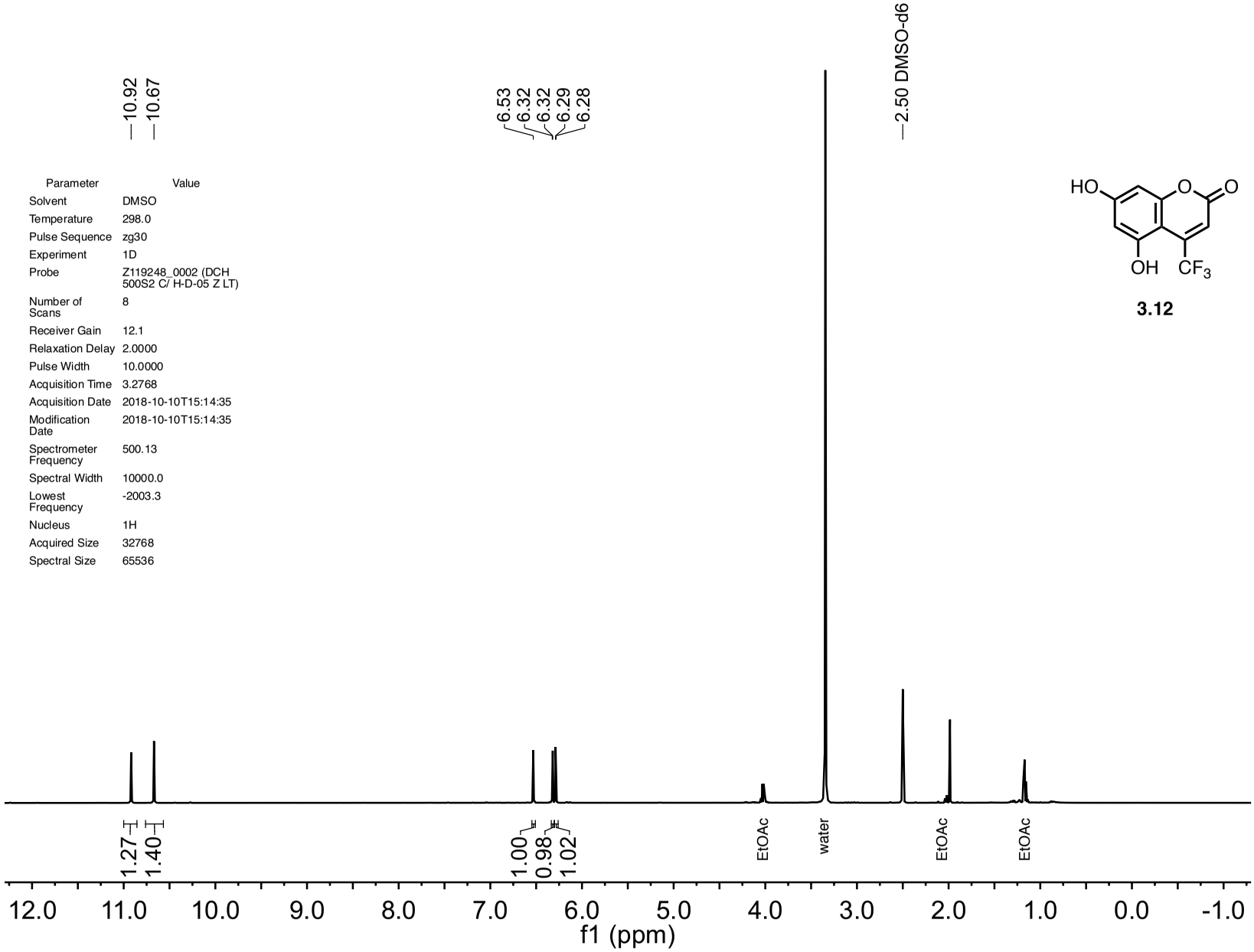

Parameter	Value
Solvent	DMSO
Temperature	298.0
Pulse Sequence	zg30
Experiment	1D
Probe	Z119248_0002 (DCH 500S2 C/ H-D-05 Z LT)
Number of Scans	8
Receiver Gain	12.1
Relaxation Delay	2.0000
Pulse Width	10.0000
Acquisition Time	3.2768
Acquisition Date	2018-10-10T15:14:35
Modification Date	2018-10-10T15:14:35
Spectrometer Frequency	500.13
Spectral Width	10000.0
Lowest Frequency	-2003.3
Nucleus	1H
Acquired Size	32768
Spectral Size	65536

3.12

Parameter	Value
Solvent	Acetone
Temperature	298.0
Pulse Sequence	zg30
Experiment	1D
Probe	Z119248_0002 (DCH 500S2 C/ H-D-05 Z LT)
Number of Scans	8
Receiver Gain	12.1
Relaxation Delay	2.0000
Pulse Width	10.0000
Acquisition Time	3.2768
Acquisition Date	2018-10-31T16:21:41
Modification Date	2018-10-31T16:21:41
Spectrometer Frequency	500.13
Spectral Width	10000.0
Lowest Frequency	-2013.8
Nucleus	1H
Acquired Size	32768
Spectral Size	65536

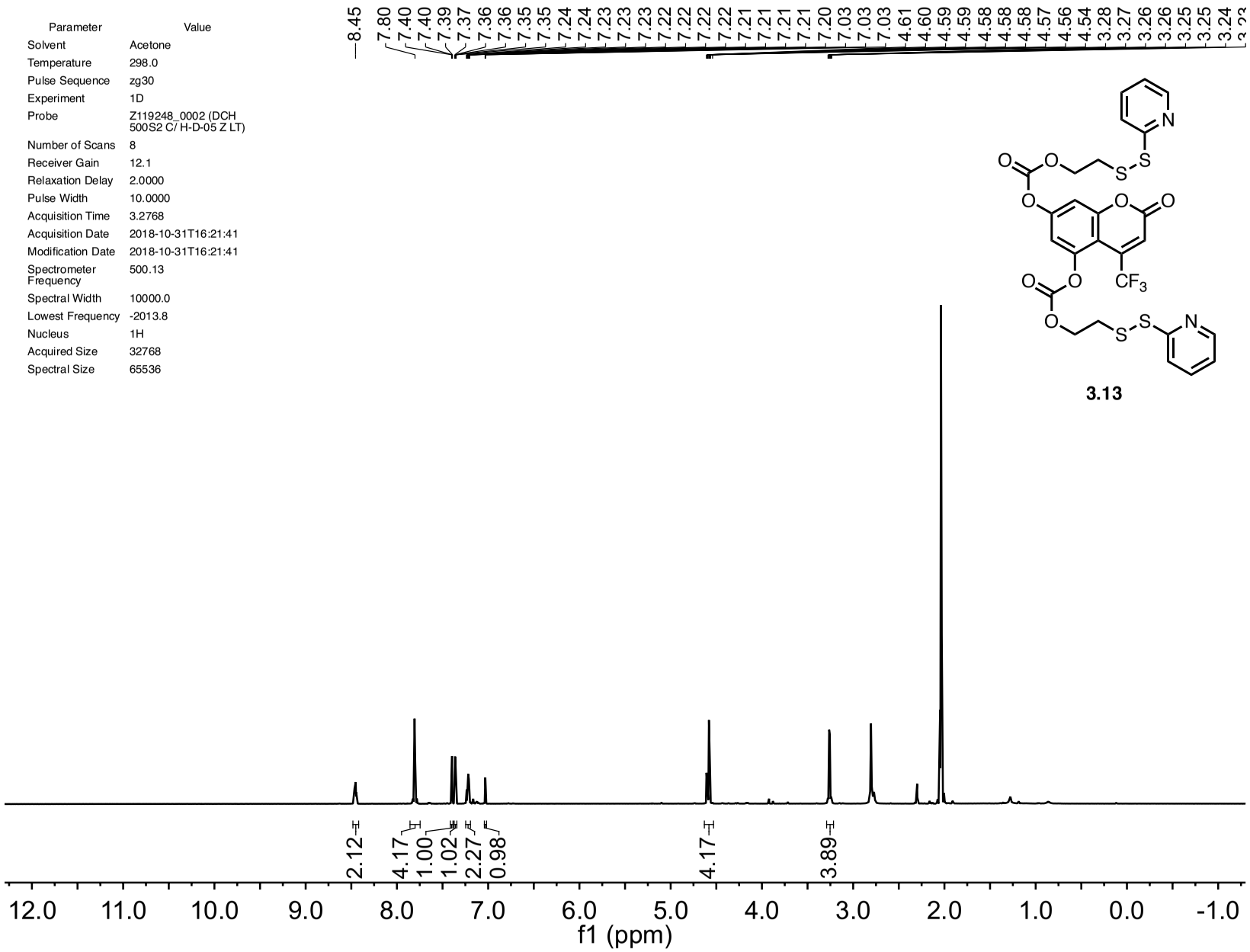

3.13

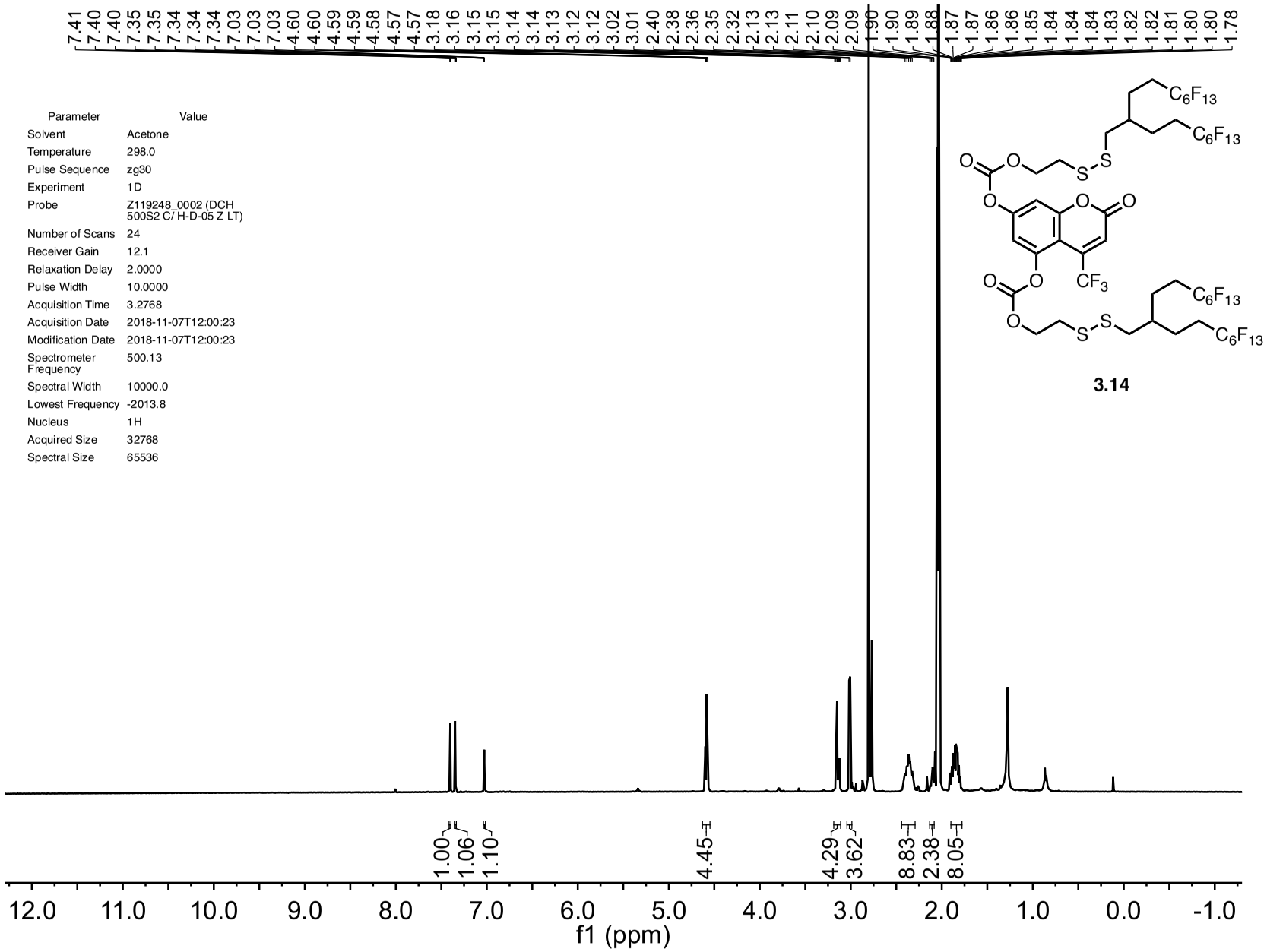

Parameter	Value
Solvent	Acetone
Temperature	298.0
Pulse Sequence	zg30
Experiment	1D
Probe	Z119248_0002 (DCH 500S2 C/ H-D-05 Z LT)
Number of Scans	24
Receiver Gain	12.1
Relaxation Delay	2.0000
Pulse Width	10.0000
Acquisition Time	3.2768
Acquisition Date	2018-11-07T12:00:23
Modification Date	2018-11-07T12:00:23
Spectrometer Frequency	500.13
Spectral Width	10000.0
Lowest Frequency	-2013.8
Nucleus	1H
Acquired Size	32768
Spectral Size	65536

3.14

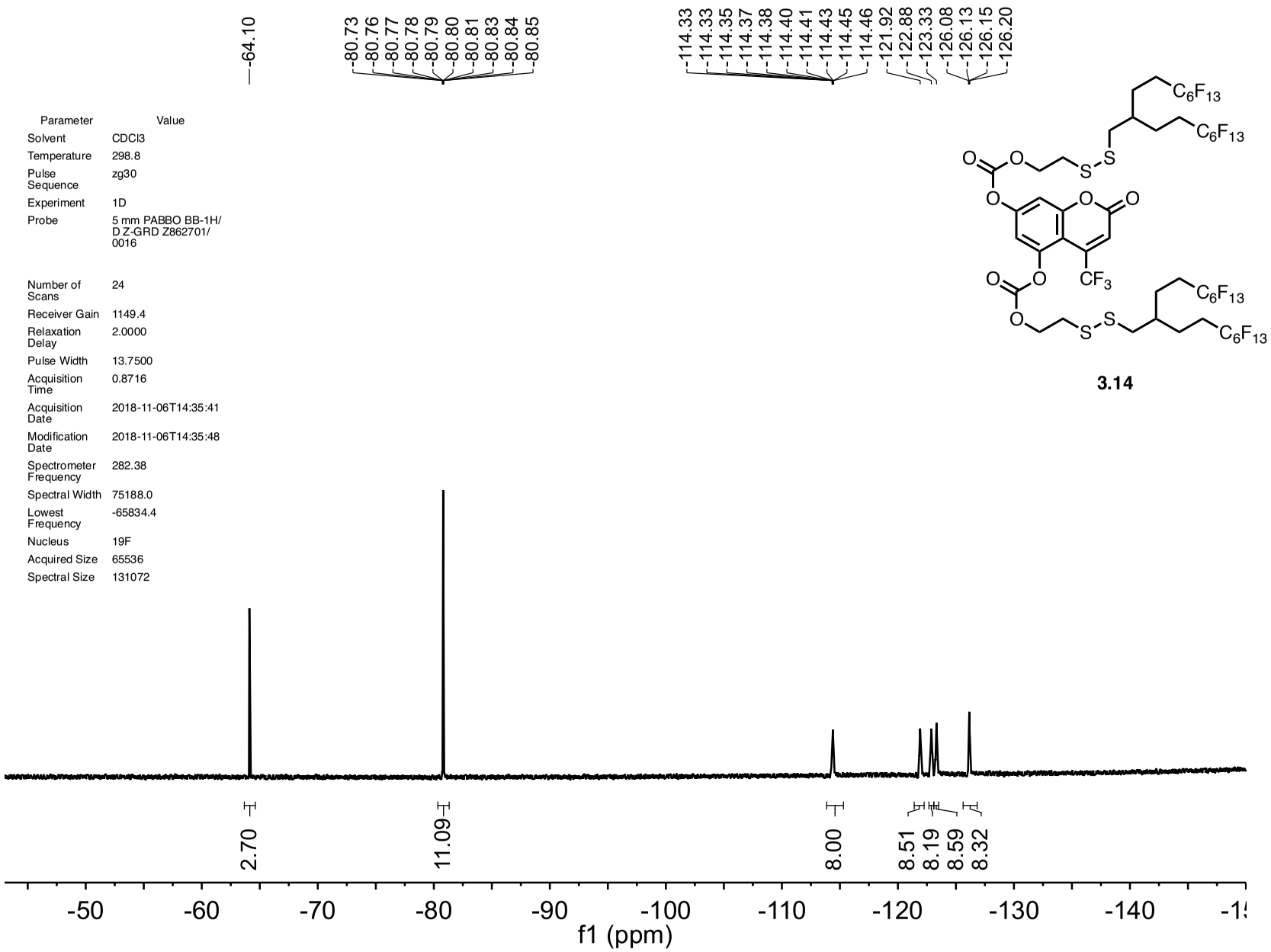
-64.10
-80.73
-80.76
-80.77
-80.78
-80.79
-80.80
-80.81
-80.83
-80.84
-80.85
-114.33
-114.33
-114.35
-114.37
-114.38
-114.40
-114.41
-114.43
-114.45
-114.46
-121.92
-122.88
-123.33
-126.08
-126.13
-126.15
-126.20
Parameter Value
Solvent CDCl3
Temperature 298.8
Pulse Sequence zg30
Experiment 1D
Probe 5 mm PABBO BB-1H/D Z-GRD Z862701/0016
Number of Scans 24
Receiver Gain 1149.4
Relaxation Delay 2.0000
Pulse Width 13.7500
Acquisition Time 0.8716
Acquisition Date 2018-11-06T14:35:41
Modification Date 2018-11-06T14:35:48
Spectrometer Frequency 282.38
Spectral Width 75188.0
Lowest Frequency -65834.4
Nucleus 19F
Acquired Size 65536
Spectral Size 131072
2.70
11.09
8.00
8.51
8.19
8.59
8.32
-50
-60
-70
-80
-90
-100
-110
-120
-130
-140
f1 (ppm)
3.14

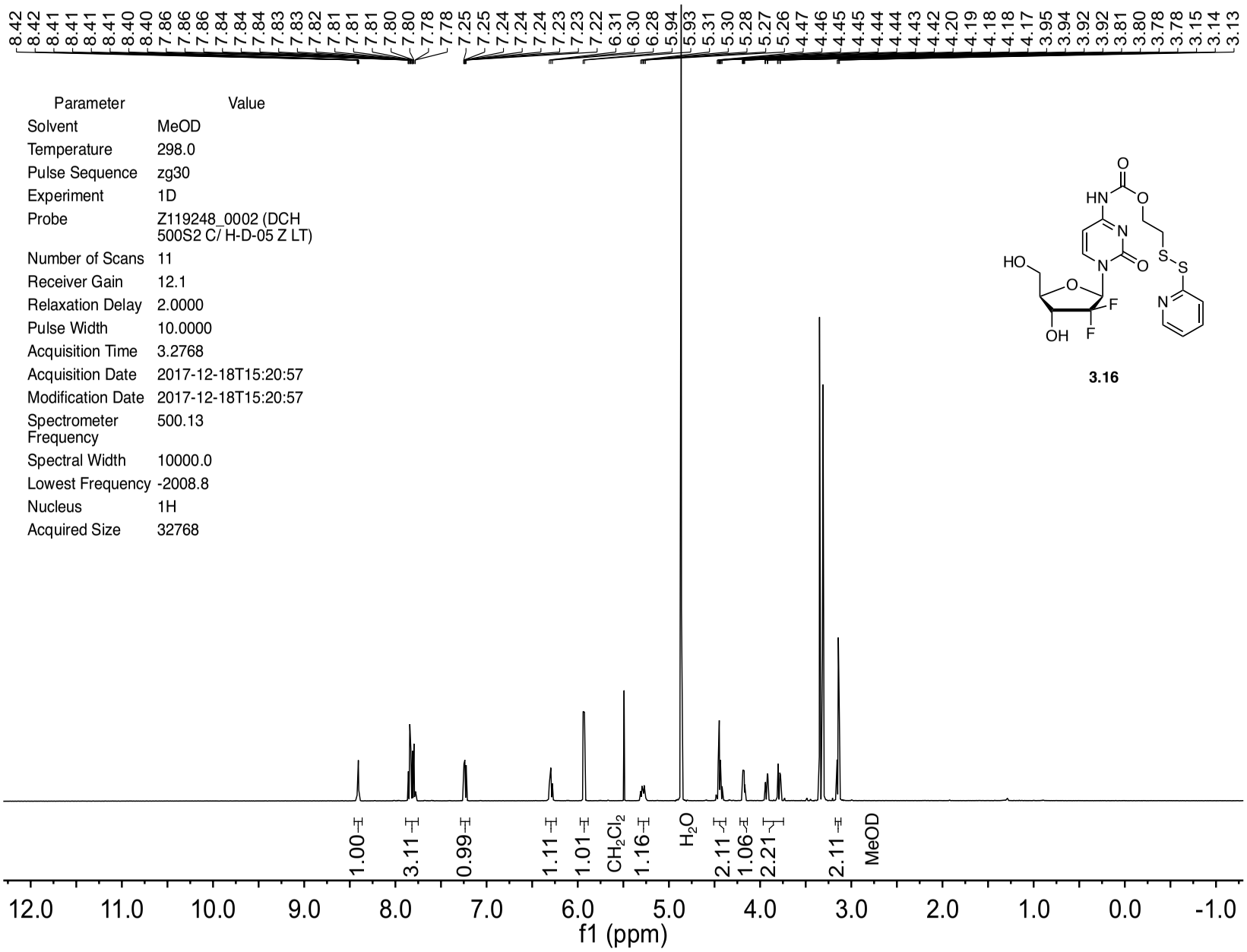
8.42 8.42 8.41 8.41 8.41 8.40 8.40 7.86 7.86 7.84 7.84 7.84 7.83 7.83 7.82 7.81 7.81 7.81 7.80 7.80 7.78 7.78 7.25 7.25 7.24 7.24 7.24 7.23 7.23 7.22 6.31 6.30 6.28 5.94 5.93 5.31 5.30 5.28 5.27 5.26 4.47 4.46 4.45 4.44 4.44 4.43 4.42 4.20 4.19 4.18 4.18 4.17 3.95 3.94 3.92 3.92 3.81 3.80 3.78 3.78 3.15 3.14 3.13
Parameter Value
Solvent MeOD
Temperature 298.0
Pulse Sequence zg30
Experiment 1D
Probe Z119248_0002 (DCH 500S2 C/ H-D-05 Z LT)
Number of Scans 11
Receiver Gain 12.1
Relaxation Delay 2.0000
Pulse Width 10.0000
Acquisition Time 3.2768
Acquisition Date 2017-12-18T15:20:57
Modification Date 2017-12-18T15:20:57
Spectrometer Frequency 500.13
Spectral Width 10000.0
Lowest Frequency -2008.8
Nucleus 1H
Acquired Size 32768
3.16
1.00
3.11
0.99
1.11
1.01
CH2Cl2
1.16
H2O
2.11
1.06
2.21
2.11
MeOD
12.0 11.0 10.0 9.0 8.0 7.0 6.0 5.0 4.0 3.0 2.0 1.0 0.0 -1.0
f1 (ppm)

Parameter	Value
Solvent	MeOD
Temperature	298.5
Pulse Sequence	zgfhigqn.2
Experiment	1D
Probe	5 mm PABBO BB/ 19F-1H/ D Z-GRD Z108618/ 0656
Number of Scans	16
Receiver Gain	189.8
Relaxation Delay	1.0000
Pulse Width	14.5000
Acquisition Time	0.8738
Acquisition Date	2017-12-18T15:44:00
Modification Date	2017-12-18T16:45:00
Spectrometer Frequency	376.46
Spectral Width	150000.0
Lowest Frequency	-112649.8
Nucleus	19F
Acquired Size	131072
Spectral Size	262144

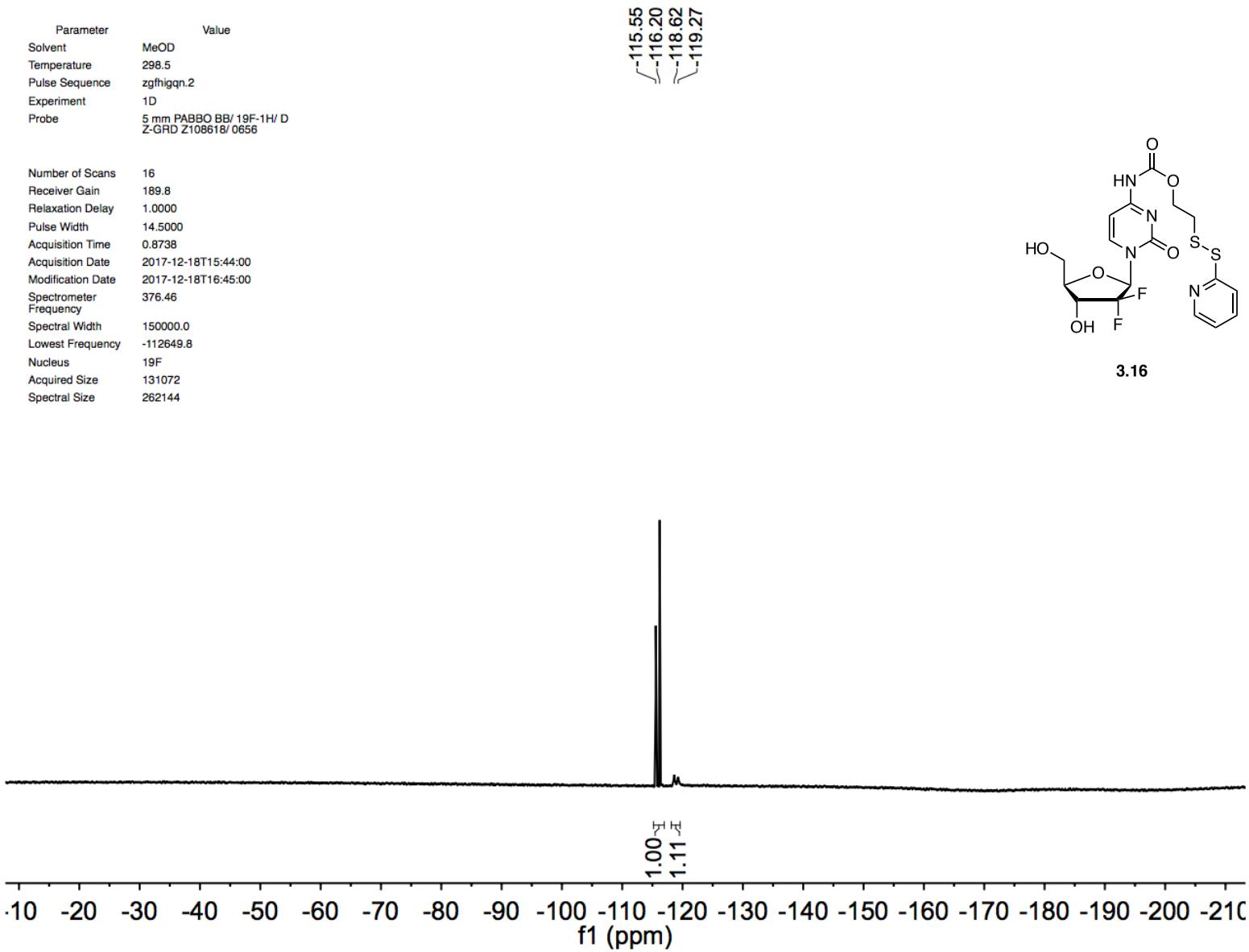

3.16

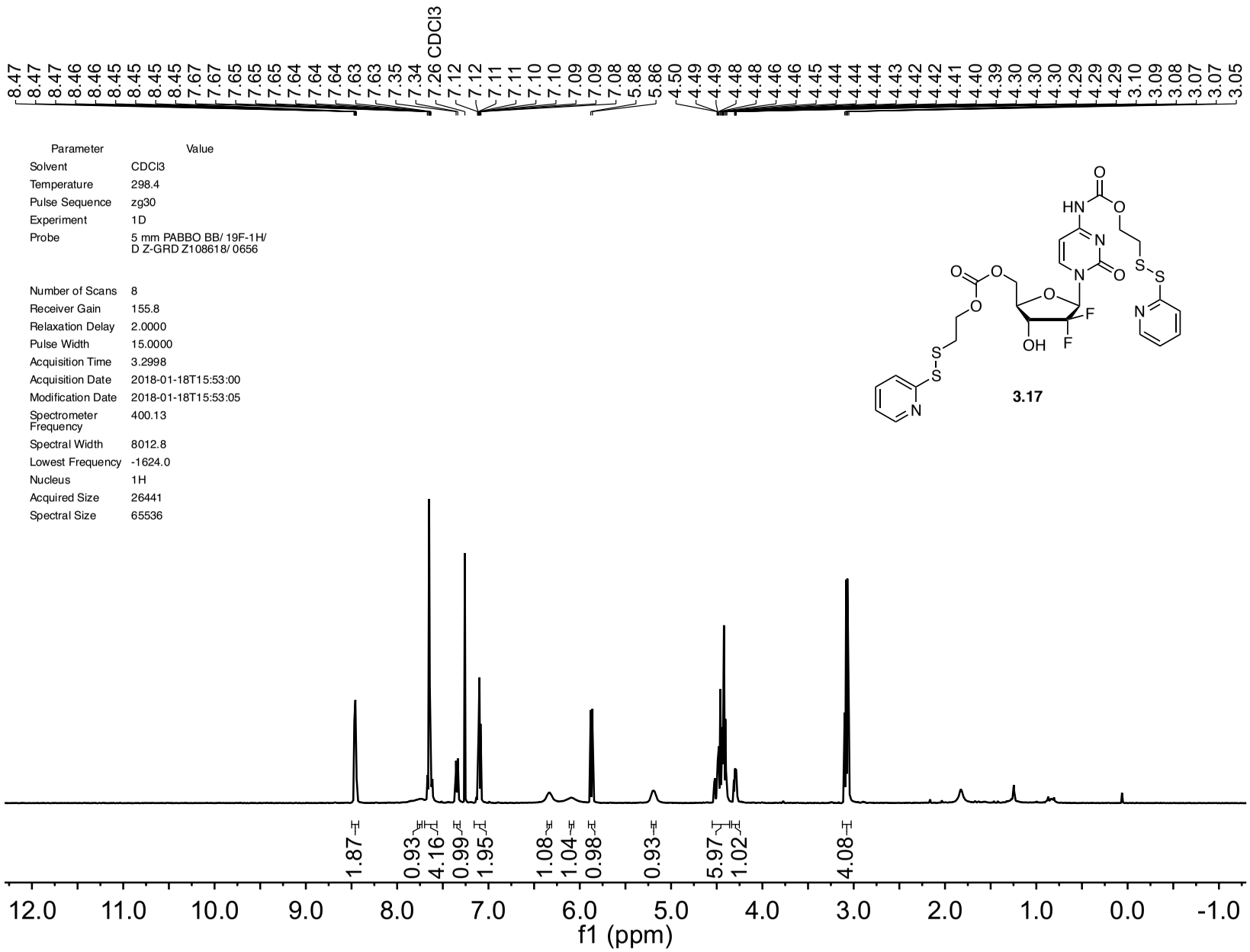
8.47 8.47 8.47 8.46 8.45 8.45 8.45 8.45 7.67 7.67 7.65 7.65 7.65 7.64 7.64 7.64 7.63 7.63 7.35 7.34 7.26 CDCl3 7.12 7.12 7.11 7.11 7.10 7.10 7.09 7.09 7.08 5.88 5.86 4.50 4.49 4.49 4.48 4.48 4.46 4.46 4.45 4.44 4.44 4.44 4.43 4.42 4.42 4.41 4.40 4.39 4.30 4.30 4.29 4.29 4.29 3.10 3.09 3.08 3.07 3.07 3.05
Parameter Value
Solvent CDCl3
Temperature 298.4
Pulse Sequence zg30
Experiment 1D
Probe 5 mm PABBO BB/ 19F-1H/ D Z-GRD Z108618/ 0656
Number of Scans 8
Receiver Gain 155.8
Relaxation Delay 2.0000
Pulse Width 15.0000
Acquisition Time 3.2998
Acquisition Date 2018-01-18T15:53:00
Modification Date 2018-01-18T15:53:05
Spectrometer Frequency 400.13
Spectral Width 8012.8
Lowest Frequency -1624.0
Nucleus 1H
Acquired Size 26441
Spectral Size 65536
3.17
1.87 0.93 4.16 0.99 1.95 1.08 1.04 0.98 0.93 5.97 1.02 4.08
12.0 11.0 10.0 9.0 8.0 7.0 6.0 5.0 4.0 3.0 2.0 1.0 0.0 -1.0
f1 (ppm)

Parameter	Value
Solvent	CDCl3
Temperature	298.5
Pulse Sequence	zgfhigqn.2
Experiment	1D
Probe	5 mm PABBO BB/ 19F-1H/ D Z-GRD Z108618/ 0656
Number of Scans	8
Receiver Gain	189.8
Relaxation Delay	1.0000
Pulse Width	14.5000
Acquisition Time	1.7476
Acquisition Date	2018-01-18T15:55:00
Modification Date	2018-01-18T15:55:14
Spectrometer Frequency	376.46
Spectral Width	75000.0
Lowest Frequency	-75149.8
Nucleus	19F
Acquired Size	131072
Spectral Size	262144

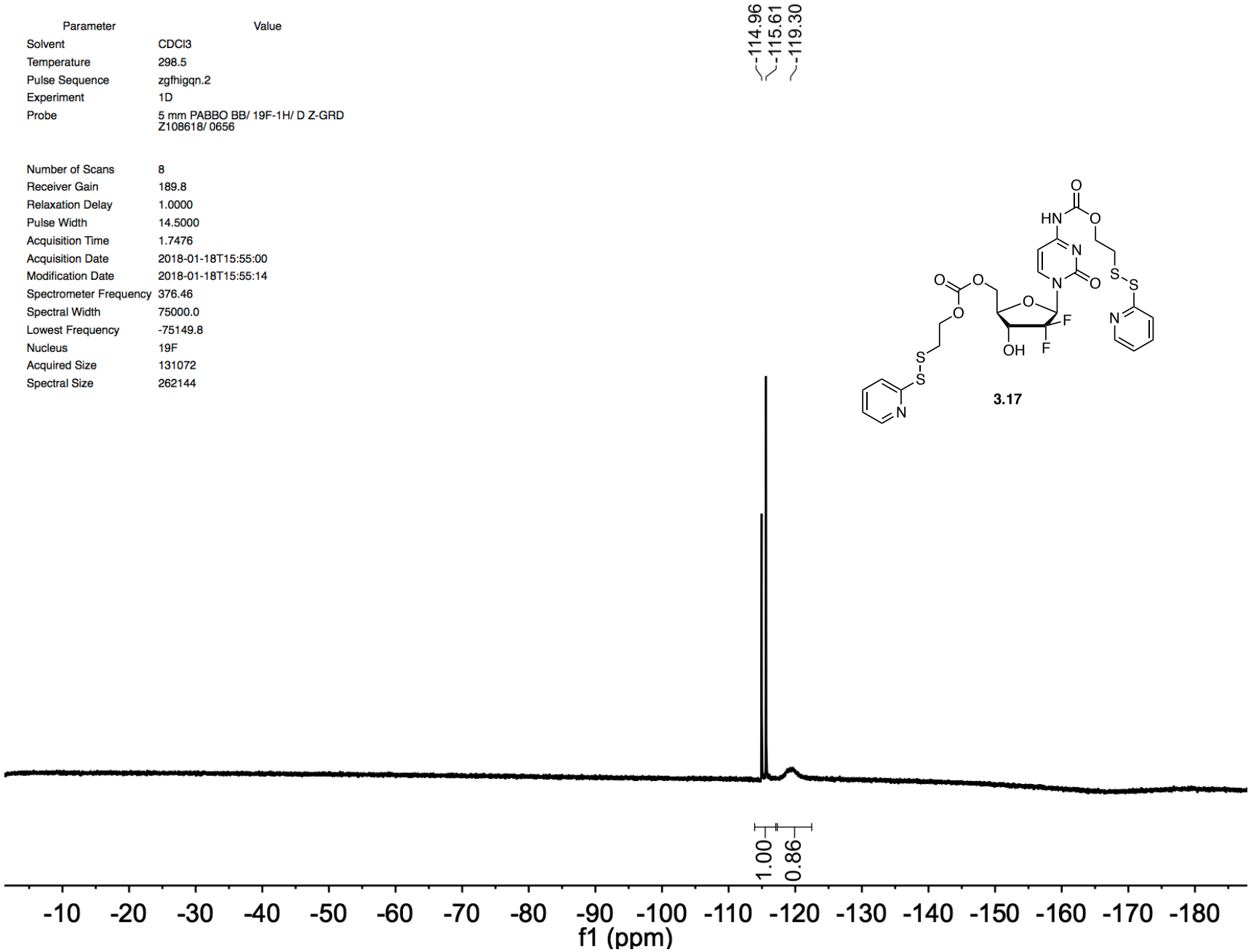

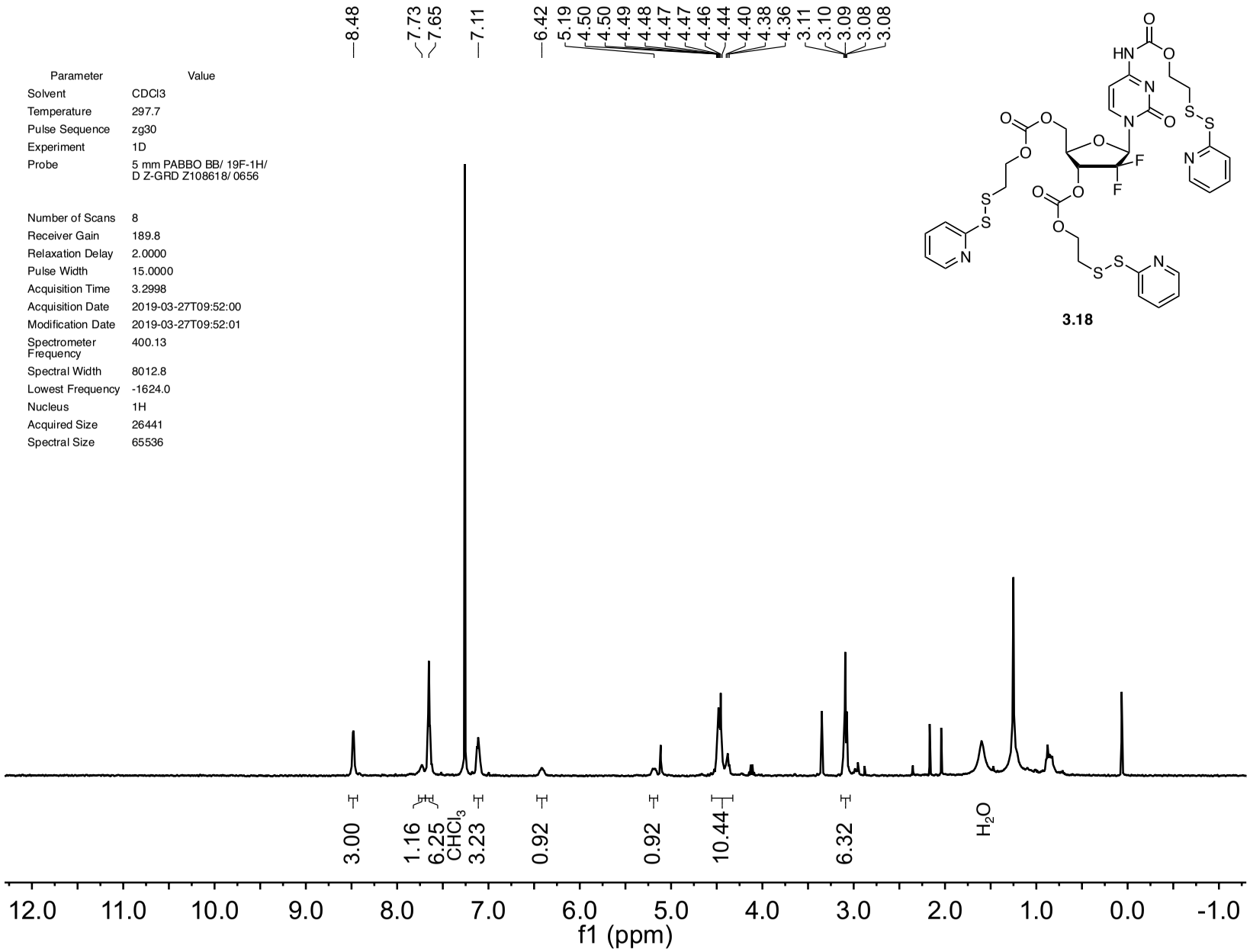

Parameter	Value
Solvent	CDCl3
Temperature	297.7
Pulse Sequence	zg30
Experiment	1D
Probe	5 mm PABBO BB/ 19F-1H/ D Z-GRD Z108618/ 0656
Number of Scans	8
Receiver Gain	189.8
Relaxation Delay	2.0000
Pulse Width	15.0000
Acquisition Time	3.2998
Acquisition Date	2019-03-27T09:52:00
Modification Date	2019-03-27T09:52:01
Spectrometer Frequency	400.13
Spectral Width	8012.8
Lowest Frequency	-1624.0
Nucleus	1H
Acquired Size	26441
Spectral Size	65536

3.18

Parameter	Value
Solvent	CDCl3
Temperature	297.9
Pulse Sequence	zgfhigqn.2
Experiment	1D
Probe	5 mm PABBO BB/ 19F-1H/ D Z-GRD Z108618/ 0656
Number of Scans	24
Receiver Gain	189.8
Relaxation Delay	1.0000
Pulse Width	14.5000
Acquisition Time	0.8738
Acquisition Date	2019-03-27T09:54:00
Modification Date	2019-03-27T09:54:31
Spectrometer Frequency	376.50
Spectral Width	150000.0
Lowest Frequency	-75000.0
Nucleus	19F
Acquired Size	131072
Spectral Size	262144

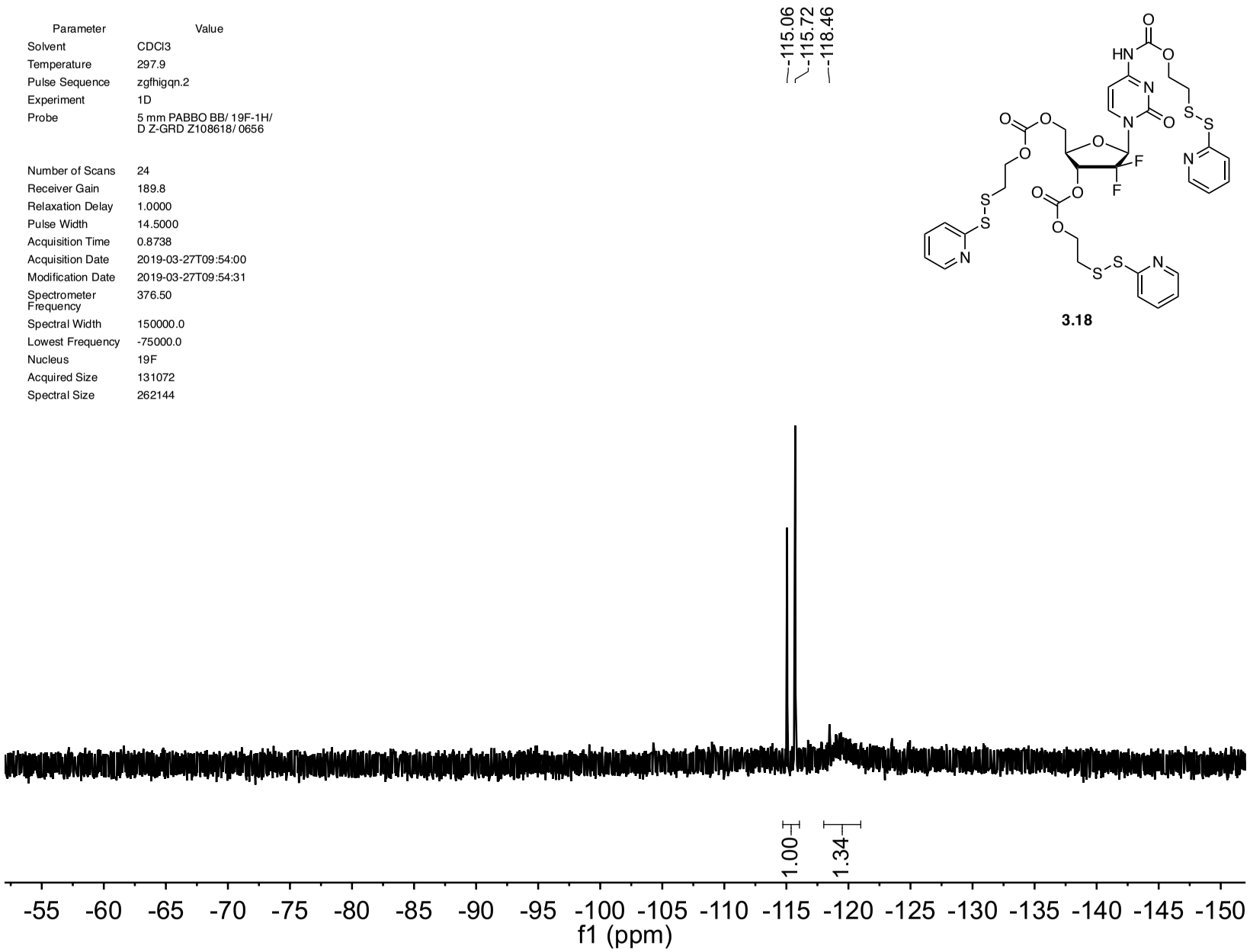

3.18

Parameter	Value
Solvent	MeOD
Temperature	298.3
Pulse Sequence	zg30
Experiment	1D
Probe	5 mm PABBO BB/ 19F-1H/ D Z-GRD Z108618/ 0656
Number of Scans	24
Receiver Gain	189.8
Relaxation Delay	2.0000
Pulse Width	15.0000
Acquisition Time	3.2998
Acquisition Date	2017-12-19T13:26:00
Modification Date	2017-12-19T13:26:32
Spectrometer Frequency	400.13
Spectral Width	8012.8
Lowest Frequency	-1613.2
Nucleus	1H
Acquired Size	26441
Spectral Size	65536

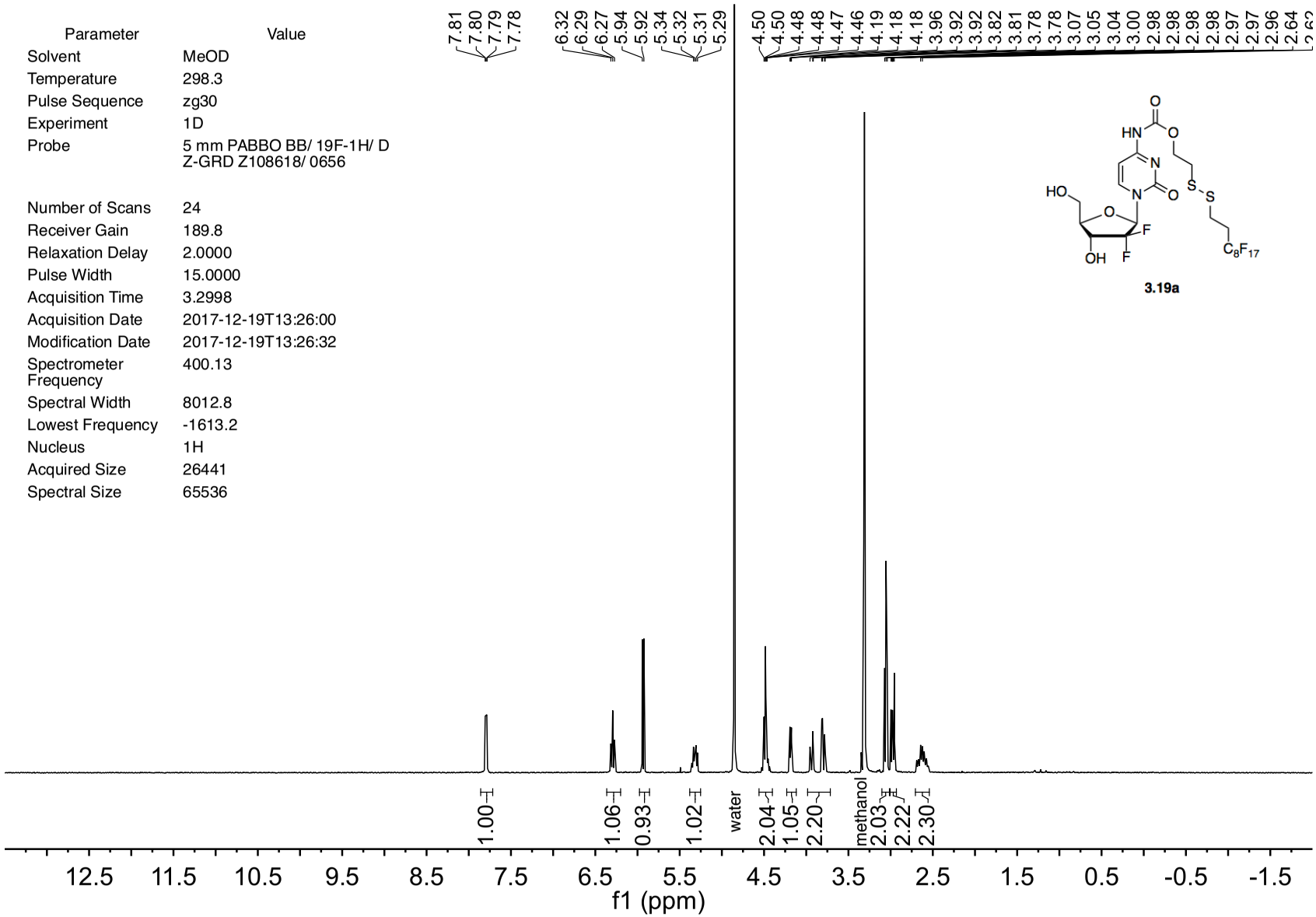

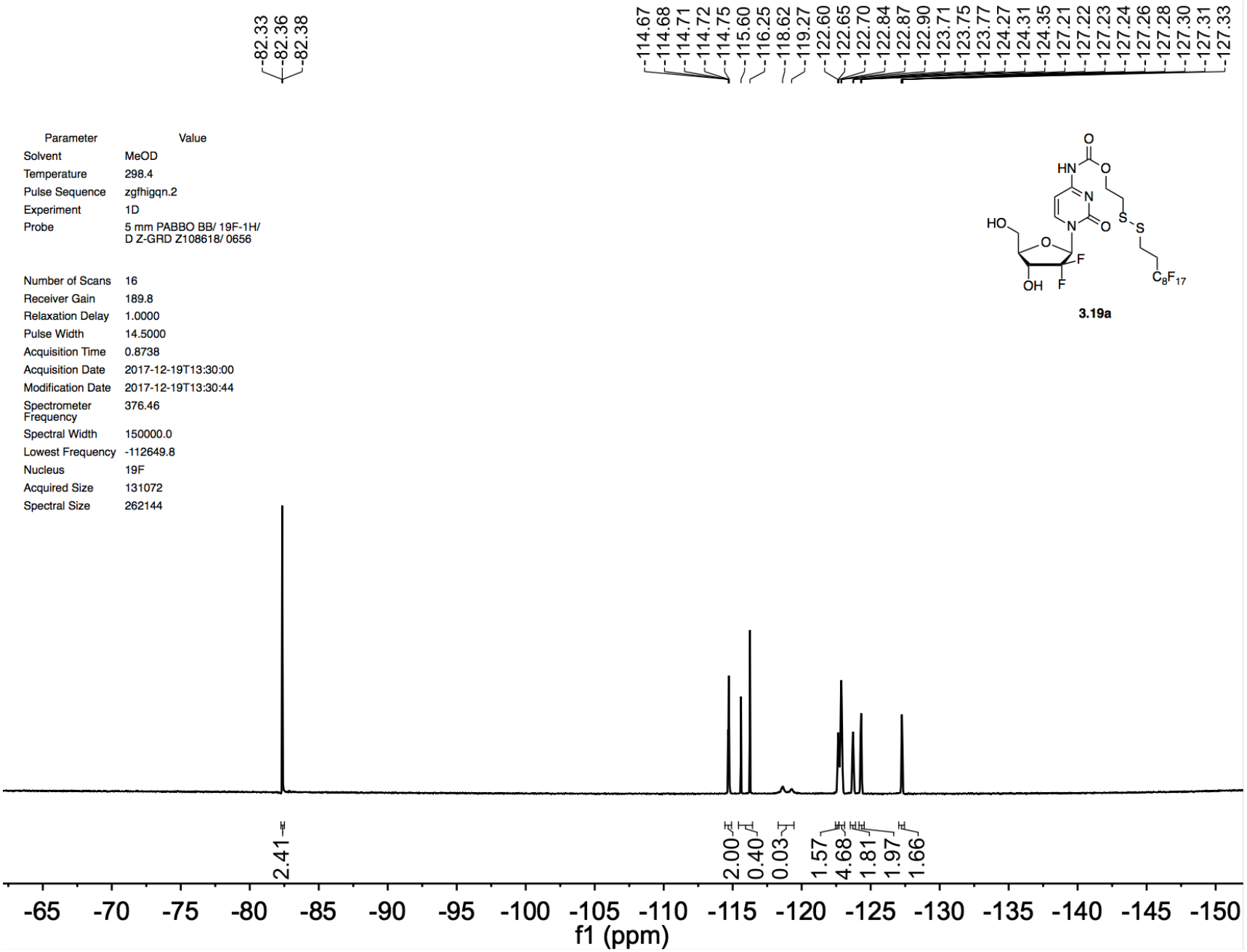
-82.33
-82.36
-82.38
-114.67
-114.68
-114.71
-114.72
-114.75
-115.60
-116.25
-118.62
-119.27
-122.60
-122.65
-122.70
-122.84
-122.87
-122.90
-123.71
-123.75
-123.77
-124.27
-124.31
-124.35
-127.21
-127.22
-127.23
-127.24
-127.26
-127.28
-127.30
-127.31
-127.33
Parameter Value
Solvent MeOD
Temperature 298.4
Pulse Sequence zgfhigqn.2
Experiment 1D
Probe 5 mm PABBO BB/ 19F-1H/ D Z-GRD Z108618/ 0656
Number of Scans 16
Receiver Gain 189.8
Relaxation Delay 1.0000
Pulse Width 14.5000
Acquisition Time 0.8738
Acquisition Date 2017-12-19T13:30:00
Modification Date 2017-12-19T13:30:44
Spectrometer Frequency 376.46
Spectral Width 150000.0
Lowest Frequency -112649.8
Nucleus 19F
Acquired Size 131072
Spectral Size 262144
3.19a
2.41
2.00
0.40
0.03
1.57
4.68
1.81
1.97
1.66
-65 -70 -75 -80 -85 -90 -95 -100 -105 -110 -115 -120 -125 -130 -135 -140 -145 -150
f1 (ppm)

Parameter	Value
Solvent	CDCl3
Temperature	298.0
Pulse Sequence	zg30
Experiment	1D
Probe	Z119248_0002 (DCH 500S2 C/ H-D-05 Z LT)
Number of Scans	8
Receiver Gain	12.1
Relaxation Delay	2.0000
Pulse Width	10.0000
Acquisition Time	3.2768
Acquisition Date	2018-01-23T12:20:17
Modification Date	2018-01-23T12:20:17
Spectrometer Frequency	500.13
Spectral Width	10000.0
Lowest Frequency	-1987.8
Nucleus	1H
Acquired Size	32768
Spectral Size	65536

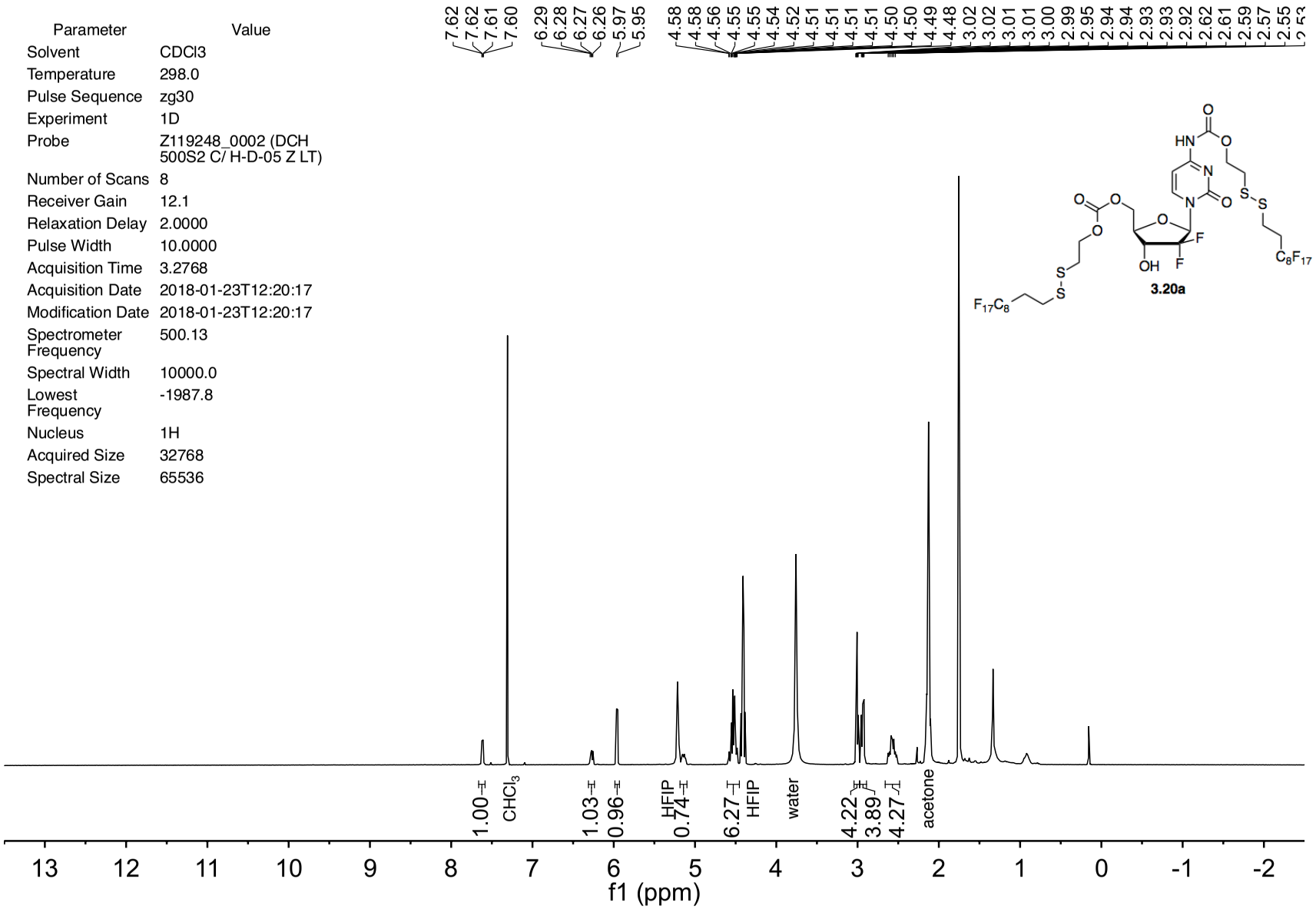

Parameter	Value
Solvent	CDCl3
Temperature	298.3
Pulse Sequence	zgfhigqn.2
Experiment	1D
Probe	5 mm PABBO BB/ 19F-1H/ D Z-GRD Z108618/ 0656
Number of Scans	8
Receiver Gain	53.4
Relaxation Delay	1.0000
Pulse Width	14.5000
Acquisition Time	1.7476
Acquisition Date	2018-01-23T13:16:00
Modification Date	2018-01-23T13:16:32
Spectrometer Frequency	376.46
Spectral Width	75000.0
Lowest Frequency	-75149.8
Nucleus	19F
Acquired Size	131072
Spectral Size	262144

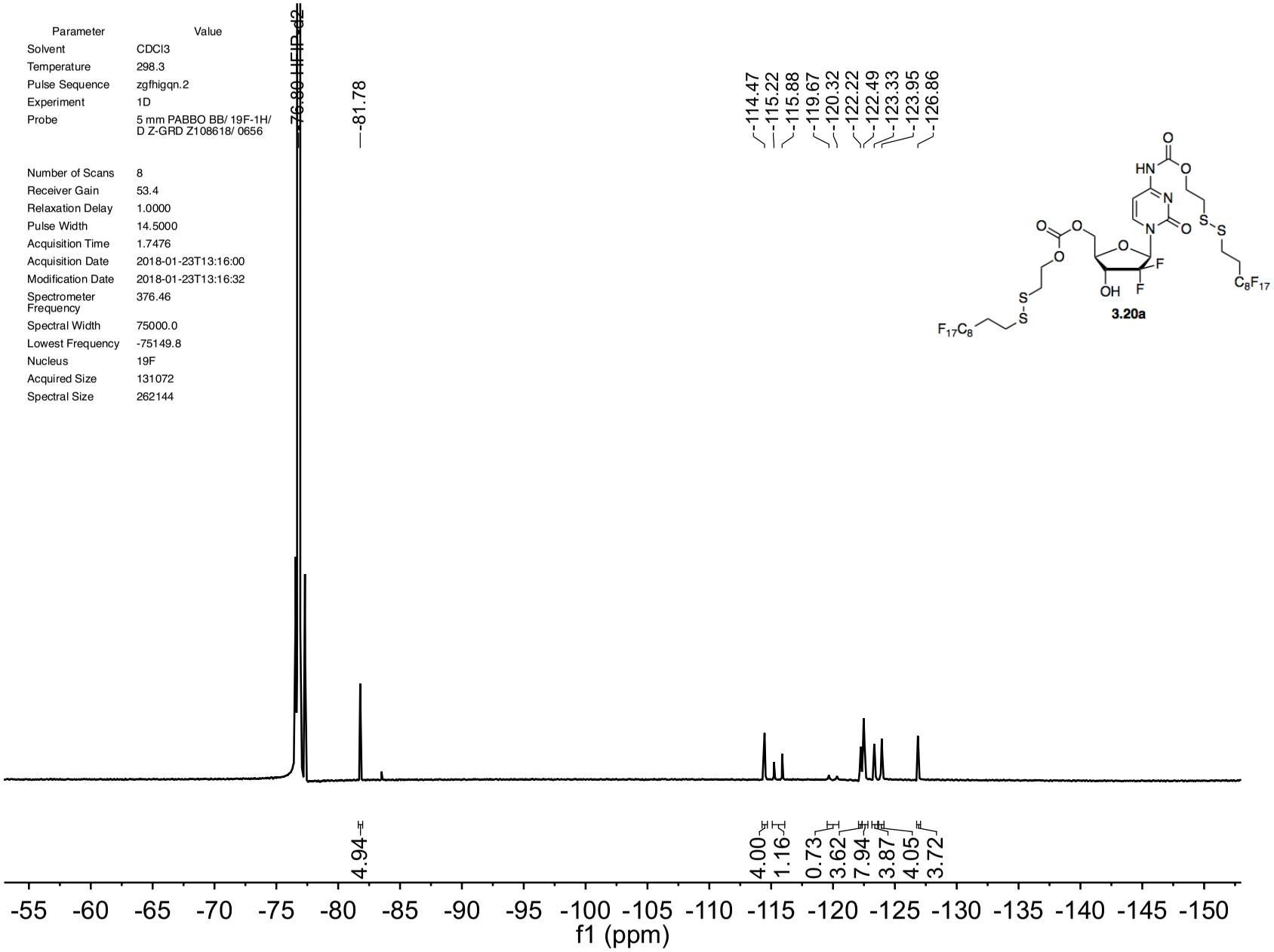

Parameter	Value
Solvent	CDCl3
Temperature	298.4
Pulse Sequence	cosygpmfphpp
Experiment	COSY
Probe	5 mm PABBO BB/ 19F-1H/ D Z-GRD Z108618/ 0656
Number of Scans	2
Receiver Gain	107.8
Relaxation Delay	2.0000
Pulse Width	15.0000
Acquisition Time	0.2847
Acquisition Date	2018-01-23T21 :01:00
Modification Date	2018-01-23T21 :21:31
Spectrometer Frequency	(400.13, 400.13)
Spectral Width	(3597.1, 3597.1)
Lowest Frequency	(-262.9, -263.4)
Nucleus	(1H, 1H)
Acquired Size	(1024, 256)
Spectral Size	(1024, 1024)

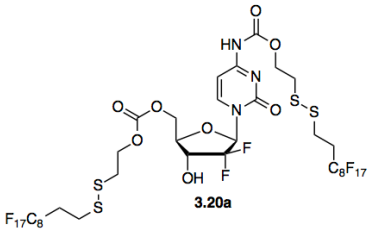

3.20a

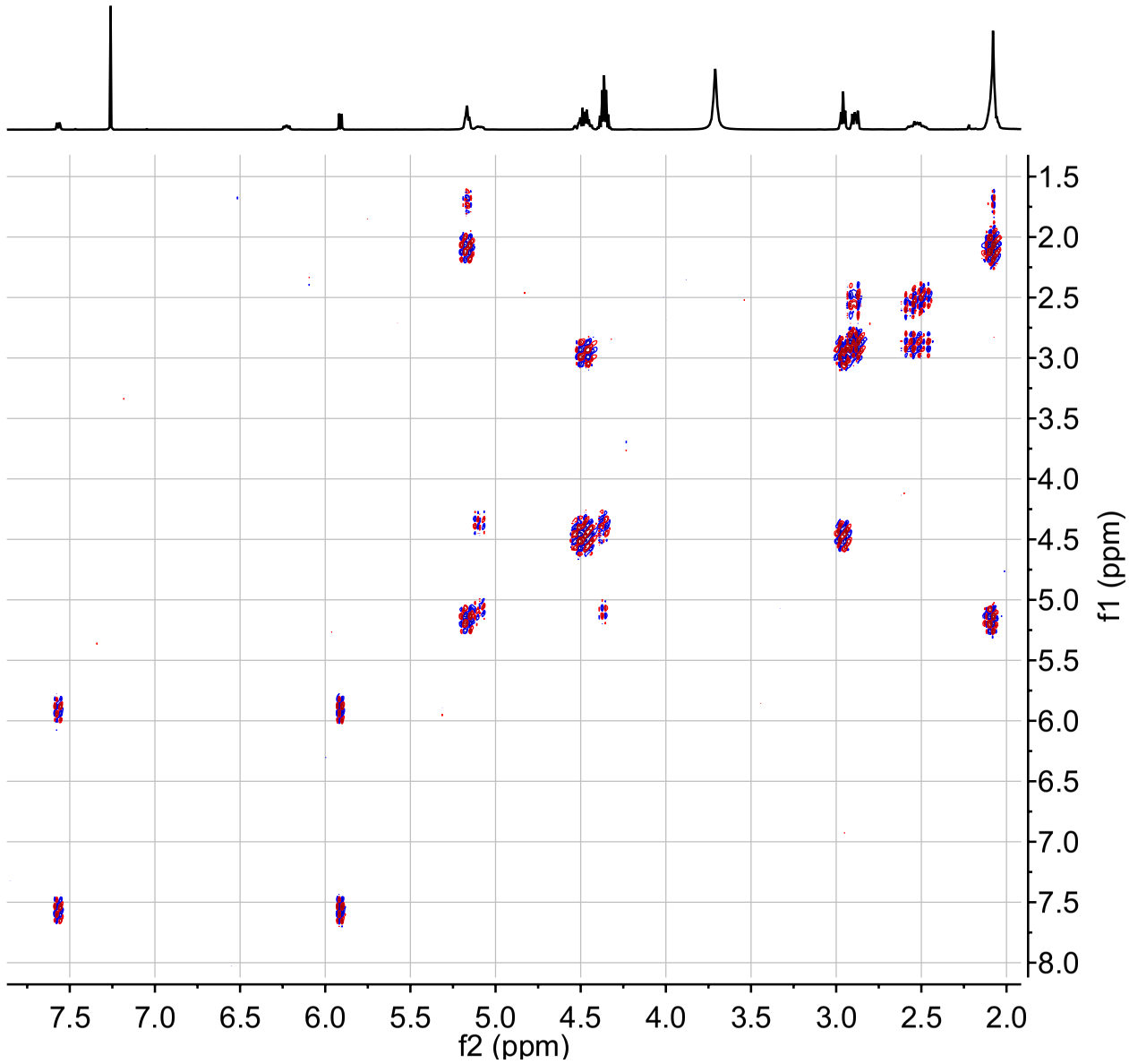

Parameter	Value
Solvent	CDCl3
Temperature	298.0
Pulse Sequence	zg30
Experiment	1D
Probe	Z119248_0002 (DCH 500S2 C/ H-D-05 Z LT)
Number of Scans	8
Receiver Gain	12.1
Relaxation Delay	2.0000
Pulse Width	10.0000
Acquisition Time	3.2768
Acquisition Date	2019-03-10T17:12:00
Modification Date	2019-03-10T17:12:00
Spectrometer Frequency	500.13
Spectral Width	10000.0
Lowest Frequency	-2013.8
Nucleus	1H
Acquired Size	32768
Spectral Size	65536

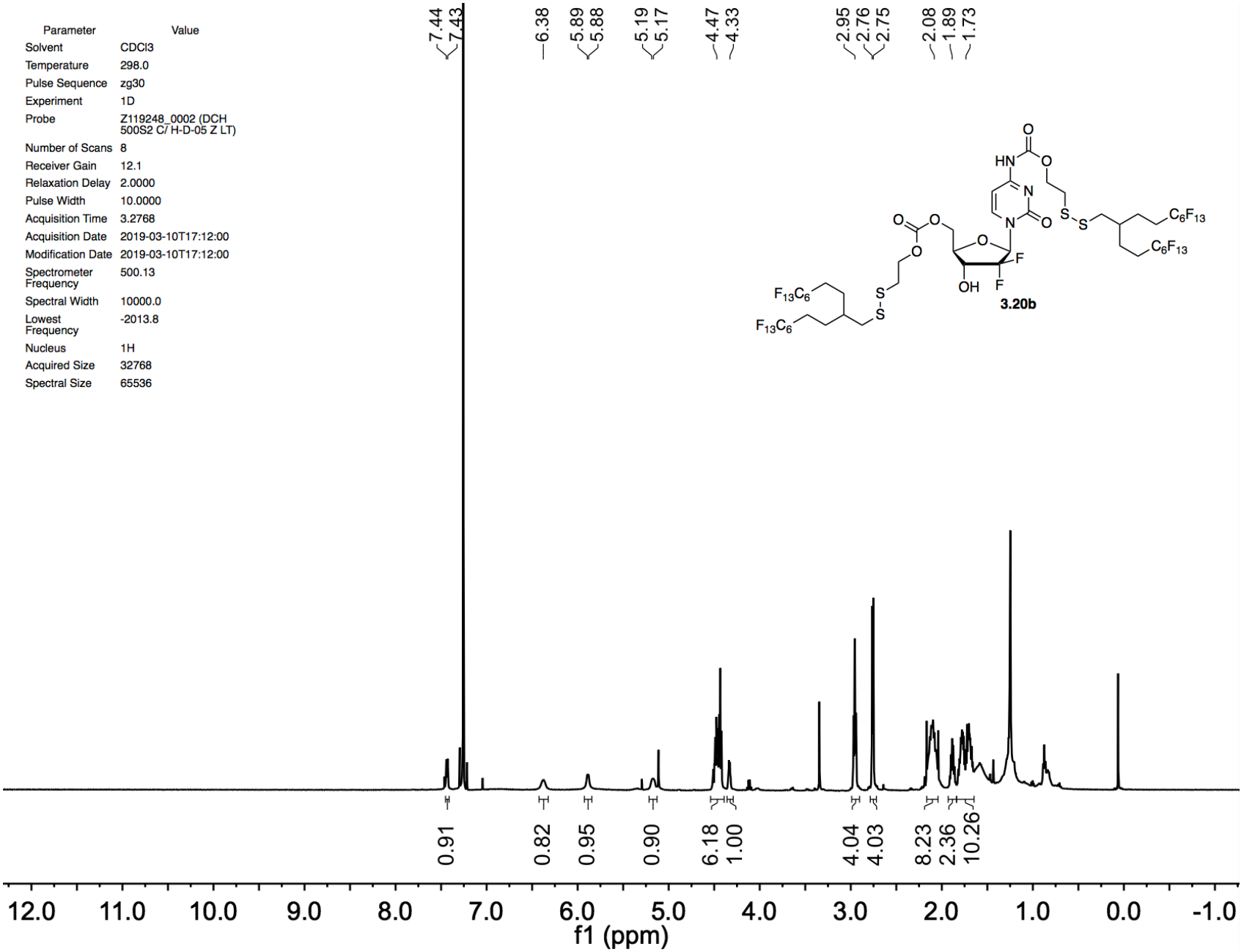

Parameter	Value
Solvent	CDCl3
Temperature	298.1
Pulse Sequence	zgfhigqn.2
Experiment	1D
Probe	5 mm PABBO BB/ 19F-1H/ D Z-GRD Z108618/ 0656
Number of Scans	16
Receiver Gain	189.8
Relaxation Delay	1.0000
Pulse Width	14.5000
Acquisition Time	0.8738
Acquisition Date	2019-03-10T17:18:00
Modification Date	2019-03-10T17:18:50
Spectrometer Frequency	376.46
Spectral Width	150000.0
Lowest Frequency	-112649.8
Nucleus	19F
Acquired Size	131072
Spectral Size	262144

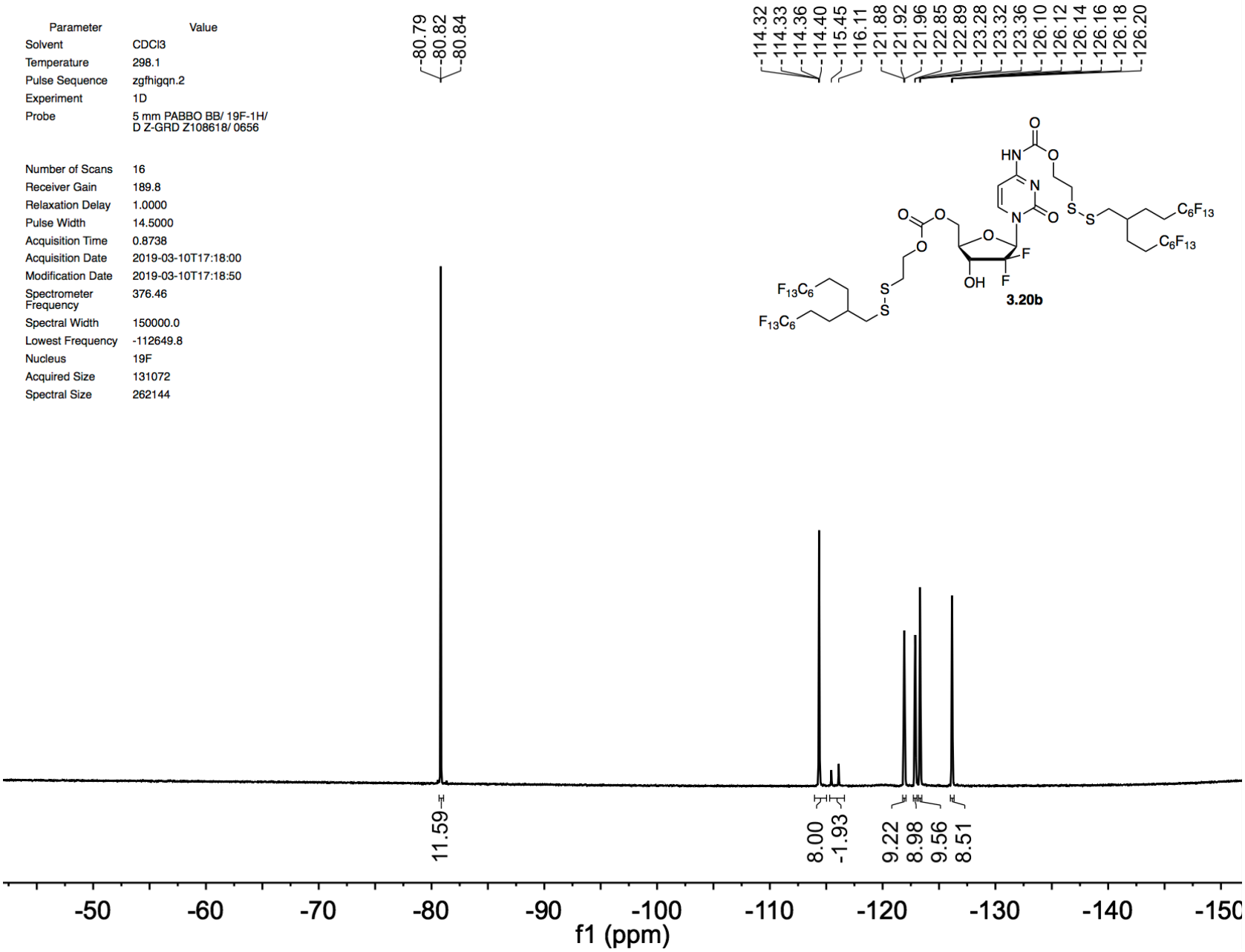

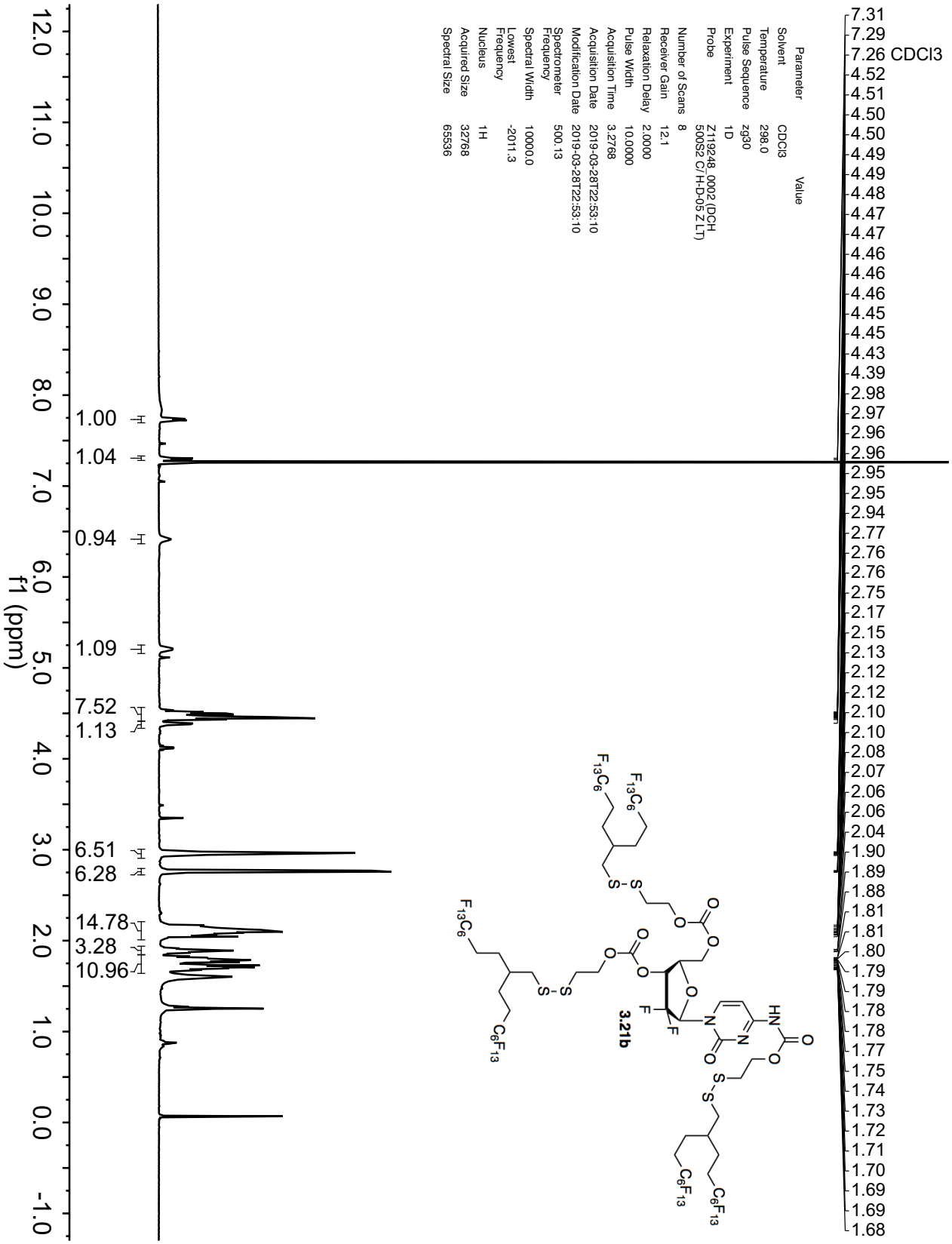
Parameter Value
Solvent CDCl3
Temperature 298.0
Pulse Sequence zg30
Experiment 1D
Probe Z119248_0002 (DCH 500S2 C/ H-D-05 Z LT)
Number of Scans 8
Receiver Gain 12.1
Relaxation Delay 2.0000
Pulse Width 10.0000
Acquisition Time 3.2768
Acquisition Date 2019-03-28T22:53:10
Modification Date 2019-03-28T22:53:10
Spectrometer Frequency 500.13
Spectral Width 10000.0
Lowest Frequency -2011.3
Nucleus 1H
Acquired Size 32768
Spectral Size 65536
CDCl3
3.21b
f1 (ppm)

Parameter	Value
Solvent	CDCl3
Temperature	298.5
Pulse Sequence	zg30
Experiment	1D
Probe	5 mm PABBO BB-1H/ D Z-GRD Z862701/ 0016
Number of Scans	8
Receiver Gain	2298.8
Relaxation Delay	2.0000
Pulse Width	13.7500
Acquisition Time	0.8716
Acquisition Date	2019-03-28T22:09:43
Modification Date	2019-03-28T22:09:50
Spectrometer Frequency	282.38
Spectral Width	75188.0
Lowest Frequency	-65834.4
Nucleus	19F
Acquired Size	65536
Spectral Size	131072

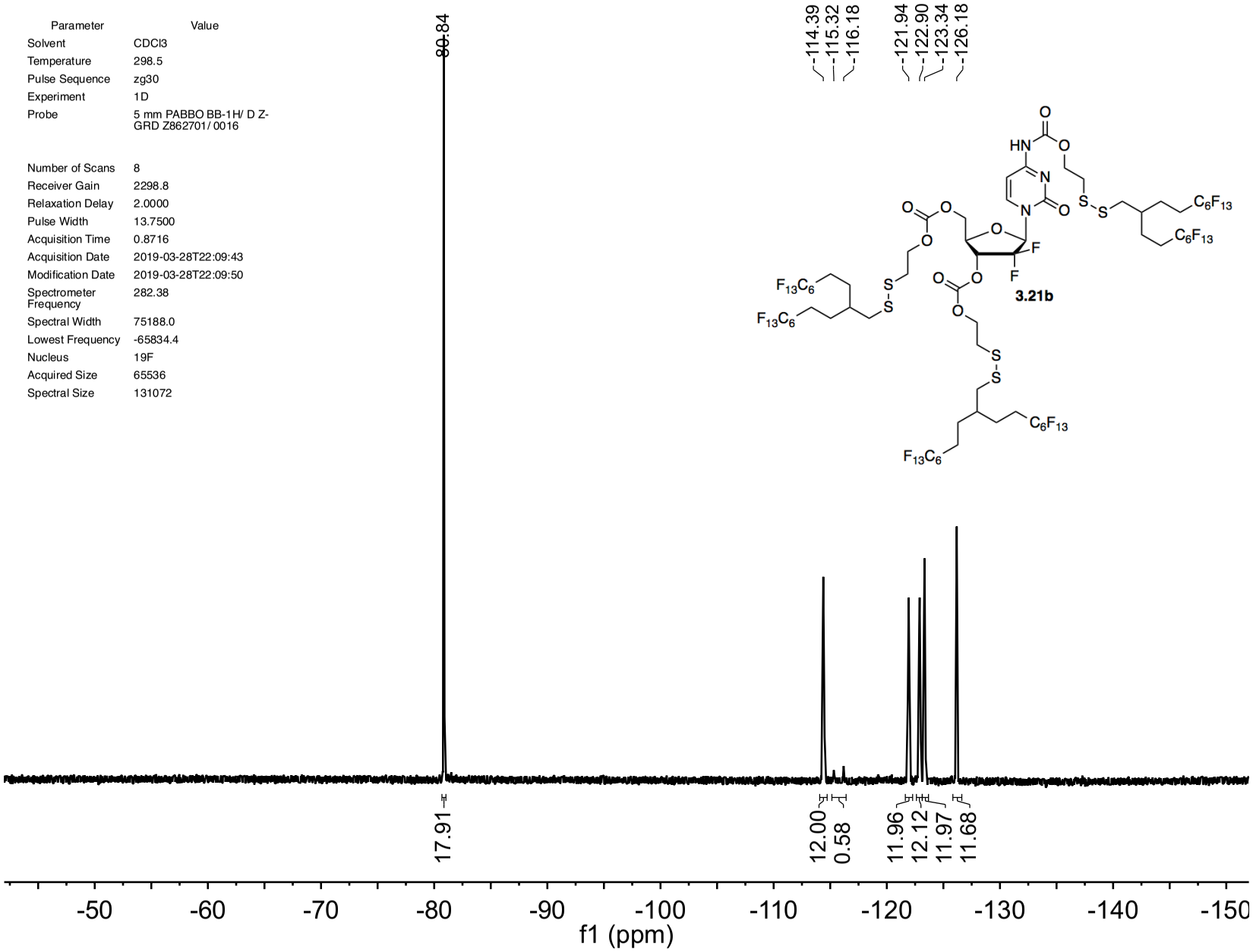

3.6 References

(1) Leriche, G.; Chisholm, L.; Wagner, A. Cleavable Linkers in Chemical Biology. *Bioorg. Med. Chem.* **2012**, *20*, 571–582.

(2) Nadler, A.; Schultz, C. The Power of Fluorogenic Probes. *Angew. Chem.* **2013**, *52*, 2408–2410.

(3) Klymchenko, A. S. Solvatochromic and Fluorogenic Dyes as Environment-Sensitive Probes: Design and Biological Applications. *Acc. Chem. Res.* **2017**, *50*, 366–375.

(4) Grimm, J. B.; Heckman, L. M.; Lavis, L. D. The Chemistry of Small-Molecule Fluorogenic Probes. *Prog. Mol. Biol. Transl. Sci.* **2013**, *113*, 1–34.

(5) Freed, B. K.; Biesecker, J.; Middleton, W. J. Spectral Polarity Index: A New Method for Determining the Relative Polarity of Solvents. *J. Fluor. Chem.* **1990**, *48*, 63–75.

(6) El Bakkari, M.; Fronton, B.; Luguya, R.; Vincent, J.-M. Reversible Fluorous Phase-Switching of Pyridyl-Tagged Porphyrins: Application to the Sensing of Histamine in Water. *J. Fluor. Chem.* **2006**, *127*, 558–564.

(7) Wang, C.; Wu, E.; Wu, X.; Xu, X.; Zhang, G.; Pu, L. Enantioselective Fluorescent Recognition in the Fluorous Phase: Enhanced Reactivity and Expanded Chiral Recognition. *J. Am. Chem. Soc.* **2015**, *137*, 3747–3750.

(8) de Sousa Cavalcante, L.; Monteiro, G. Gemcitabine: Metabolism and Molecular Mechanisms of Action, Sensitivity and Chemoresistance in Pancreatic Cancer. *Eur. J. Pharmacol.* **2014**, *741*, 8–16.

(9) Hodge, L. S.; Taub, M. E.; Tracy, T. S. The Deaminated Metabolite of Gemcitabine, 2’,2’-Difluorodeoxyuridine, Modulates the Rate of Gemcitabine Transport and Intracellular Phosphorylation via Deoxycytidine Kinase. *Drug Metab. Dispos.* **2011**, *39*,

2013–2016.

(10) Moysan, E.; Bastiat, G.; Benoit, J.-P. Gemcitabine versus Modified Gemcitabine: A Review of Several Promising Chemical Modifications. *Mol. Pharm.* **2013**, *10*, 430–444.

(11) Zhang, Y.; Gao, Y.; Wen, X.; Ma, H. Current Prodrug Strategies for Improving Oral Absorption of Nucleoside Analogues. *Asian J. Pharm. Sci.* **2014**, *9* (2), 65–74.

(12) Dubey, R. D.; Saneja, A.; Gupta, P. K.; Gupta, P. N. Recent Advances in Drug Delivery for Improved Therapeutic Efficacy of Gemcitabine. *Eur. J. Pharm. Sci.* **2016**, *93*, 147–162.

(13) Sletten, E. M.; Swager, T. M. Fluorofluorophores: Fluorescent Fluorous Chemical Tools Spanning the Visible Spectrum. *J. Am. Chem. Soc.* **2014**, *136*, 13574–13577.

(14) Kirrane, T. M.; Middleton, W. J. 7-Amino-4-Perfluoroheptylcoumarins: A Novel Class of Perfluorocarbon-Soluble Fluorescent Dyes. *J. Fluor. Chem.* **1993**, *62*, 289–292.

(15) Matsui, M.; Shibata, K.; Muramatsu, H.; Sawada, H.; Nakayama, M. Synthesis, Fluorescence, and Photostabilities of 3-(Perfluoroalkyl)Coumarins. *Chem. Ber.* **1992**, *125*, 467–471.

(16) Matsui, M.; Joglekar, B.; Ishigure, Y.; Shibata, K.; Muramatsu, H.; Murata, Y. Synthesis of 3-Cyano-6-Hydroxy-5-[2-(Perfluoroalkyl)Phenylazo]-2-Pyridones and Their Application for Dye Diffusion Thermal Transfer Printing. *Bull. Chem. Soc. Jpn.* **1993**, *66*, 1790–1794.

(17) Matsui, M. Fluorine-Containing Dyes. *Funct. Dye.* **2006**, 257–266.

(18) Muthuramu, K.; Ramamurthy, V. 7-Alkoxy Coumarins as Fluorescence Probes for Microenvironments. *J. Photochem.* **1984**, *26*, 57–64.

(19) Taneja, L.; Sharma, A. K.; Singh, R. D. Study of Photophysical Properties of Coumarins:

Substituent and Concentration Dependence. *J. Lumin.* **1995**, *63*, 203–214.

(20) Setsukinai, K.; Urano, Y.; Kikuchi, K.; Higuchi, T.; Nagano, T. Fluorescence Switching by O-Dearylation of 7-Aryloxycoumarins. Development of Novel Fluorescence Probes to Detect Reactive Oxygen Species with High Selectivity. *J. Chem. Soc. Perkin Trans. 2* **2000**, *12*, 2453–2457.

(21) Lee, M. H.; Sessler, J. L.; Kim, J. S. Disulfide-Based Multifunctional Conjugates for Targeted Theranostic Drug Delivery. *Acc. Chem. Res.* **2015**, *48*, 2935–2946.

(22) Smith, C. V.; Jones, D. P.; Guenthner, T. M.; Lash, L. H.; Lauterburg, B. H. Compartmentation of Glutathione: Implications for the Study of Toxicity and Disease. *Toxicol. Appl. Pharmacol.* **1996**, *140*, 1–12.

(23) Montero, D.; Tachibana, C.; Rahr Winther, J.; Appenzeller-Herzog, C. Intracellular Glutathione Pools Are Heterogeneously Concentrated. *Redox Biol.* **2013**, *1*, 508–513.

(24) Maiti, S.; Park, N.; Hye Han, J.; Mi Jeon, H.; Hong Lee, J.; Bhuniya, S.; Kang, C.; Seung Kim, J. Gemcitabine−Coumarin−Biotin Conjugates: A Target Specific Theranostic Anticancer Prodrug. *J. Am. Chem. Soc.* **2013**, *135*, 4567–4572.

(25) Satyam, A. Design and Synthesis of Releasable Folate–Drug Conjugates Using a Novel Heterobifunctional Disulfide-Containing Linker. *Bioorg. Med. Chem. Lett.* **2008**, *18*, 3196–3199.

(26) Latorre, A.; Couleaud, P.; Aires, A.; Cortajarena, A. L.; Somoza, A. Multifunctionalization of Magnetic Nanoparticles for Controlled Drug Release: A General Approach. *Eur. J. Med. Chem.* **2014**, *82*, 355–362.

(27) Miller, M. A.; Day, R. A.; Estabrook, D. A.; Sletten, E. M. A Reduction-Sensitive Fluorous Fluorogenic Coumarin. *SynLett* **2020**, *31*, 450–454.

(28) Sherman, W. R.; Robins, E. Fluorescence of Substituted 7-Hydroxycoumarins. *Anal. Chem.* **2002**, *40*, 803–805.

(29) Day, R. A.; Estabrook, D. A.; Logan, J. K.; Sletten, E. M. Fluorous Photosensitizers Enhance Photodynamic Therapy with Perfluorocarbon Nanoemulsions. *Chem. Commun.* **2017**, *53*, 13043–13046.

(30) Estabrook, D. A.; Ennis, A. F.; Day, R. A.; Sletten, E. M. Controlling Nanoemulsion Surface Chemistry with Poly(2-Oxazoline) Amphiphiles. *Chem. Sci.* **2019**, *10*, 3994–4003.

(31) Day, R. A.; Estabrook, D. A.; Wu, C.; Chapman, J. O.; Togle, A. J.; Sletten, E. M. Systematic Study of Perfluorocarbon Nanoemulsions Stabilized by Polymer Amphiphiles. *ACS Appl. Mater. Interfaces* **2020**, *12*, 38887–38898.

(32) Jung, K.; Park, Y.-J.; Ryu, J.-S. Scandium(III) Triflate–Catalyzed Coumarin Synthesis. *Synth. Commun.* **2008**, *38*, 4395–4406.

CHAPTER FOUR

Bioorthogonal complexation: a host-guest approach to the bioorthogonal chemical reporter strategy

4.1 Abstract

The ability to study living systems in their native environment is a major goal in the field of chemical biology. One tool that has been developed for this purpose is the bioorthogonal chemical reporter strategy. This two-step method requires metabolic or genetic incorporation of an unnatural substrate into a biomolecule of interest. The unnatural substrate contains a reactive functional group deemed X. The biomolecule can be detected through a selective covalent reaction between X and a designed partner, Y. The reaction between X and Y is deemed bioorthogonal when X is small, abiotic, and only reactive with Y. Extensive studies have been carried out to improve the rate of the reaction between X and Y. However, this strategy has been challenging in higher organisms due to the balance between rate, size, and the stability of X and Y. The Sletten lab and other labs have addressed this limitation by pursuing an alternative approach to detect unnatural functional groups (X) using non-covalent host-guest chemistry. We have termed this strategy bioorthogonal complexation. Herein, we detail the requirements of bioorthogonal complexation in living systems and provide an overview of the Sletten lab's proof of principle bioorthogonal complexation with a known host. We imagined that perfluoroaromatics, which have previously been incorporated into biomolecules, could make ideal guests for this strategy. Our approach to the design of hosts specific for perfluoroaromatics for bioorthogonal complexation applications is described in the chapters that follow.

4.2 Introduction and discussion

The bioorthogonal chemical reporter strategy is a two-step approach to labeling biomolecules in living systems developed by the Bertozzi group in the early 2000s (Figure 4.1, step 1).[1–3] In the first step, a non-native chemical functional group, deemed the chemical reporter (X), is attached to a target substrate, such as a monosaccharide or amino acid. If designed appropriately, such that the X group is not too large and does not perturb native structure and function, the modified substrate can be incorporated into a biomolecule using the cell's own machinery.

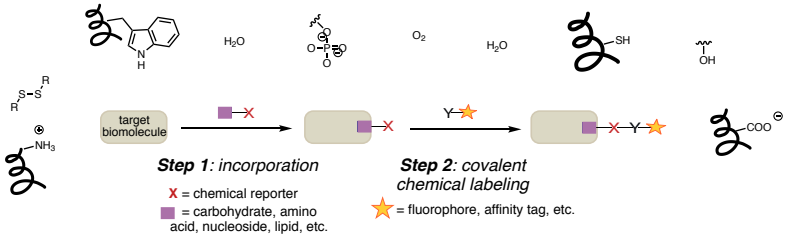

Figure 4.1 The bioorthogonal chemical reporter strategy. Step 1 involves incorporation of unnatural functionality, the chemical reporter (X), into a target biomolecule. Step 2 involves a selective reaction between X and Y to label the target biomolecule with a fluorophore or other payload.

Hijacking the sialic acid biosynthetic pathway is one way to incorporate unnatural functionality into biomolecules (Figure 4.2).[4–6] Unnatural derivatives of D-mannosamine **4.1**, a precursor to sialic acid, can be taken up by cells. The enzymes in the sialic acid biosynthetic pathway are promiscuous enough to tolerate some modification of mannosamine, such that the unnatural derivatives are converted into the corresponding sialic acids and incorporated into cell-surface glycans. In this way, non-native functional groups can be displayed on the cell surface. Larger X groups can be incorporated as unnatural sialic acid derivatives,[7] which enter at a later step in the pathway. In the case of sialic acid, modification on the 5-position **4.2** and 9-position **4.3** are both tolerated. While metabolic incorporation of unnatural carbohydrates is the primary

focus of the work described here, another common approach to installing chemical reporters is through non-canonical amino acids[8] using site-specific amino acid incorporation via amber codon suppression[9–11] or global residue-specific incorporation in auxotrophic cell lines.[12,13]

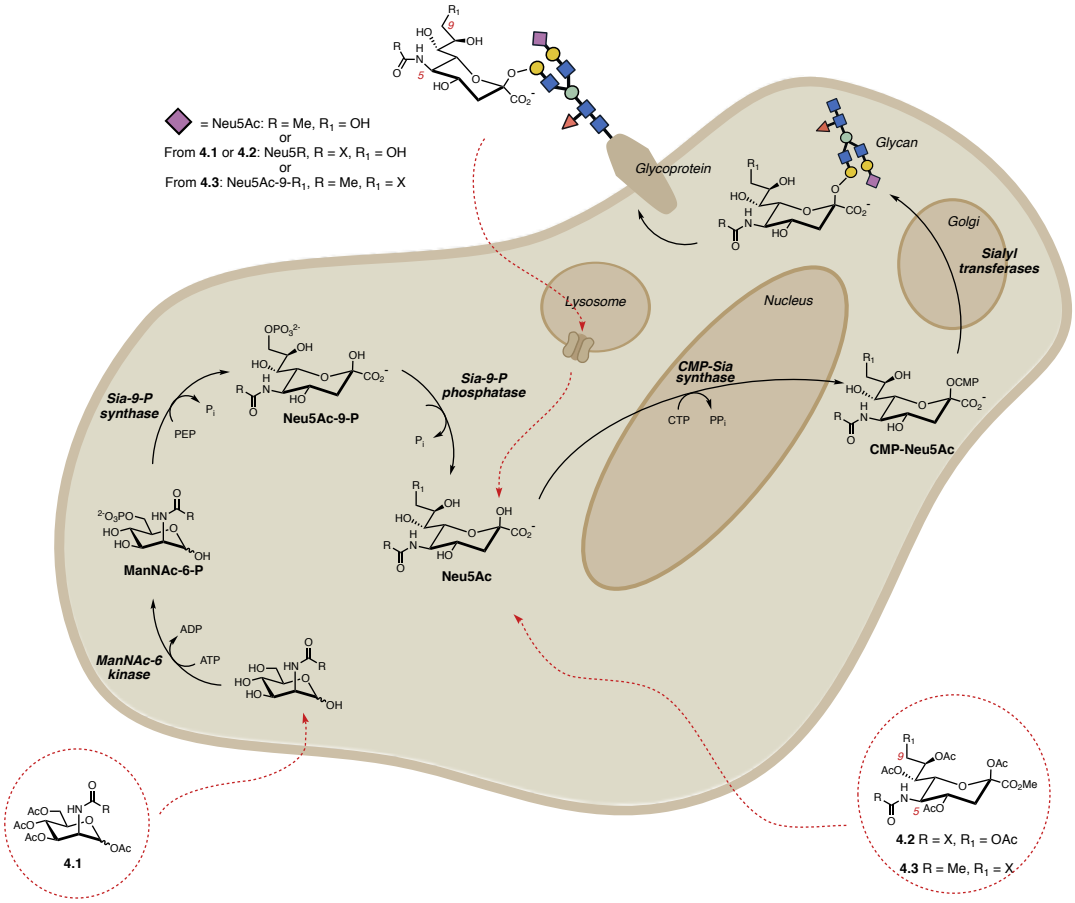

Figure 4.2 The sialic acid biosynthetic pathway. Both unnatural derivatives of mannosamine **4.1** and sialic acid **4.2** and **4.3** can be incorporated into cell-surface glycans through this pathway.[6,14]

In the second step of the bioorthogonal chemical reporter strategy (Figure 4.1, step 2), the unnatural functional group X is detected through a selective covalent reaction with a designed reactive partner, termed Y. The reaction between X and Y allows for labeling of the modified biomolecule with a payload of interest, such as a fluorophore, a radiolabel, or an affinity label.

For the reaction between X and Y to be truly bioorthogonal, the X group must be both small and abiotic. Both X and Y should be stable and non-toxic. They must only react with each

other and not with endogenous biomolecules. The reaction between X and Y must be fast so that biological events that occur on rapid timescales and on low abundance biomolecules can be observed. The rate of the reaction depends heavily on the 2nd order rate constant, *k*, as the concentration of X and Y are inherently low in the complex environment of a cell or organism (Figure 4.4A).

In the past decade, a number of bioorthogonal X and Y pairs have been developed, often focused on increasing the 2nd order rate constant, *k* (Figure 4.3).[3] The first bioorthogonal reaction, the Staudinger ligation, used the azide **4.4** as the X group and a phosphine ester **4.5** as the Y group. In this reaction, an amide product **4.6** is formed through an aza-ylide intermediate.[15] While this reaction was successful in labeling glycoproteins in cells and mice, the reaction is slow (10^{-3} $M^{-1}s^{-1}$), and the phosphine is susceptible to oxidation.[16] To address these concerns, alternative Y groups for the azide were pursued.[17] The azide undergoes a strain-promoted 1,3-dipolar cycloaddition with strained cyclooctynes **4.7** to form triazole products **4.8** with rates up to 1 $M^{-1}s^{-1}$.[18] The efficiency of these reactions is attributed to the strain energy of cyclic alkynes, much of which is released upon reaction with the azide. Many cyclooctynes were developed to both increase the rate of the reaction and improve the hydrophilicity and solubility of the cyclooctyne reagents for copper-free click chemistry in live cells, zebrafish, and mice.[16,19] Strain release has been a guiding principle in the design of other bioorthogonal pairs, such as the reaction between tetrazine **4.11** and strained alkenes, like cyclopropene **4.9**,[20,21] norbornene,[22] or *trans*-cyclooctene **4.10**.[23] The inverse-electron-demand Diels-Alder reaction between tetrazine and *trans*-cyclooctene **4.10** is one of the fastest bioorthogonal reactions reported with a rate of 10^6 $M^{-1}s^{-1}$.[24]

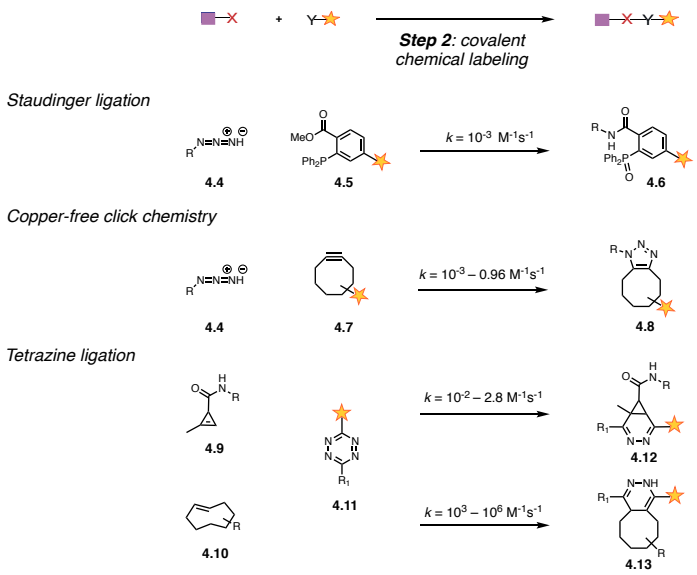

Figure 4.3 Examples of bioorthogonal covalent reactions.

With improved kinetics there is often a compromise on the stability and size of the unnatural functional group X—two key components of bioorthogonality (Figure 4.4A). While the three-atom azide makes an ideal chemical reporter, the cyclooctyne is both larger and less stable. Though the tetrazine ligation is fast, the *trans*-cyclooctene can isomerize to the more stable *cis*-alkene over time.[24–26] Furthermore, though these reactions work well in cells and transparent organisms, they are less successful in mammals. With more complex tissue and greater dilution in larger organisms, higher concentrations of X and Y are required due to the dependence of the rate on the concentration of reagents. With increased concentrations of X and Y, greater background signal can be observed in imaging studies in live mice.[27,28] In practice, translation of the bioorthogonal chemical reporter strategy to higher organisms has been nontrivial.

In the Sletten lab, we have taken an alternative approach to the bioorthogonal chemical reporter strategy (Figure 4.4B). In our approach, the Y component is replaced with a small-molecule host that can selectively bind the unnatural functional group X, or the guest, via strong

non-covalent interactions. With a non-covalent strategy, we take inspiration from the remarkable strong and selective non-covalent interactions that occur naturally in biology.[29–31] The strength of an interaction between host and guest is measured as the binding affinity, K_a, which is equivalent to on rate (k_{on}) divided by the off rate (k_{off}). The k_{on} for non-covalent interactions can approach the rate of diffusion (~$10^{8\text{-}9}$ $M^{-1}s^{-1}$),[32] depending on various factors (viscosity, molecule size, temperature, etc.).[33] Accordingly, non-covalent labeling reagents, like antibodies or hosts in our case, can be used at low concentrations, which minimizes background signal.[3,33,34] An advantage of our approach is that the guest, X, does not need to be reactive—improving the stability of the X group. Additionally, sequential labeling experiments can be performed because of the reversibility of non-covalent interactions.

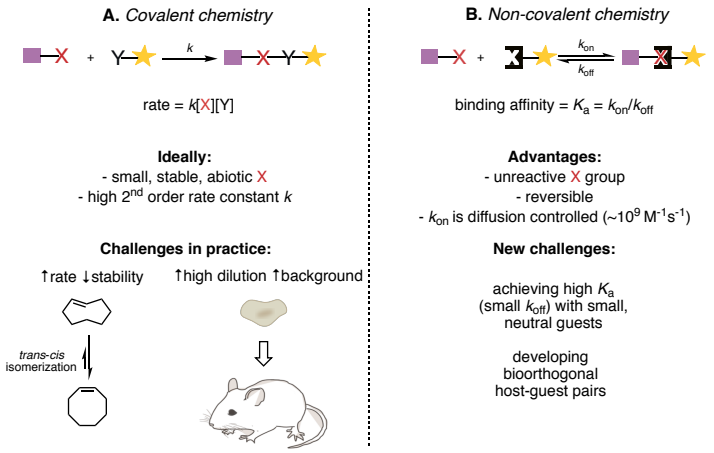

Figure 4.4 Comparison of A) bioorthogonal covalent chemistry and B) bioorthogonal non-covalent complexation.

The field of host-guest chemistry and the idea of mimicking biological non-covalent binding pairs with synthetic systems was pioneered by Cram, Lehn, and Pederson (Figure 4.5).[35–37] They were awarded the Nobel Prize in Chemistry in 1987 for this work.[38–40] Their early work with macrocycles like crown ethers **4.14-4.16**, cryptands **4.17**, and spherands **4.18** helped establish the concepts of complementarity and preorganization (Figure 4.6).[41] Complementarity

is the principle that for a binding event between a host and a guest to occur, the host must possess attractive sites for the guest to bind. The host and the guest must also be size and shape matched to bind strongly. Preorganization is the principle that a stronger binding interaction can be obtained with a rigid host locked in the binding geometry. In a more rigid system, some of the entropic cost of the binding interaction is minimized as the host and the guest do not have to reorient themselves to complex together.[42]

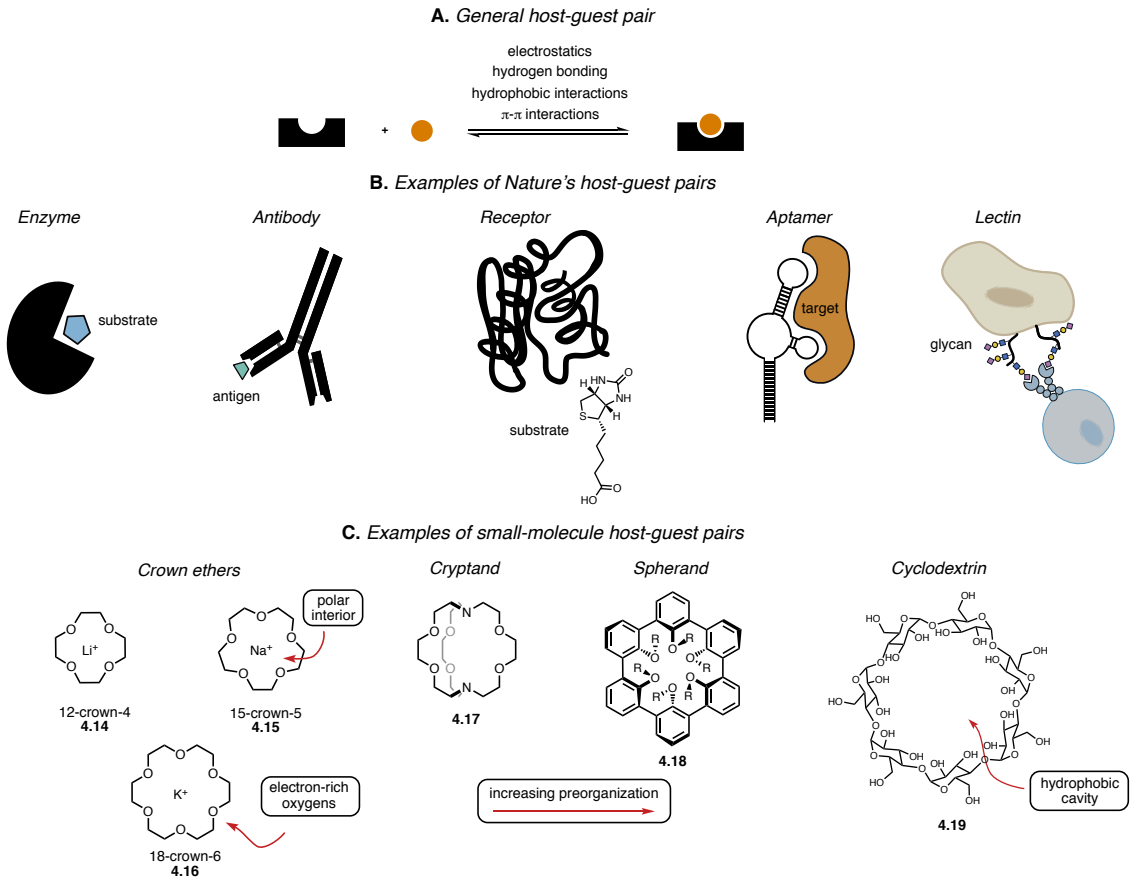

Figure 4.5 Examples of host-guest pairs. A) Generic schematic describing host-guest chemistry. B) Examples of host-guest pairs in biology and synonymous terminology. C) Some examples of small-molecule host-guest pairs.

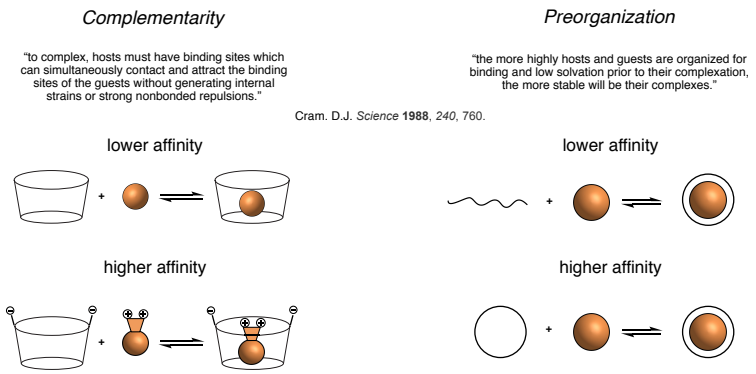

Figure 4.6 Guiding principles of host-guest chemistry as described by Cram. Schematic adapted.[30,35]

These principles have guided the understanding of many host-guest systems with different macrocyclic hosts over the years. Cyclodextrins **4.19** are a class of simple hosts made up of varying number of glucose units. (Figure 4.5C).[43] Interactions between cyclodextrin hosts and their guests are primarily driven by the hydrophobic effect. As such, these interactions are often not very strong ($\leq 10^6$ M^{-1}). Synthetic modification of γ–cyclodextrin (eight glucose units) with carboxylates enhances the complementarity of this host for cationic aminosteroids ($K_a = 10^7$ M^{-1}), as seen in the neuromuscular reversal drug, Sugammadex.[44] However, cyclodextrins also bind endogenous steroids, like cholesterol and estrogen.[45,46] Their lack of selectivity *in vivo* and general low affinity precludes their use in bioorthogonal complexation.

One privileged host that has strikingly high binding affinities is cucurbit[7]uril (CB[7]) **4.20**, a macrocycle composed of seven linked glycoluril units (Figure 4.7).[47,48] This host binds bulky cationic guests, like **4.21**–**4.24**, through ion-dipole interactions and the hydrophobic effect with K_as up to 10^{17} M^{-1}.[49] While this host is rigid, the high-affinity binding is attributed to the combined effect of release of high-energy water molecules from the cavity upon guest binding, desolvation of rigid hydrophobic guests, and direct interactions between CB[7] and the guests.

Due to the release of high-energy waters, this host-guest system has low entropic penalties and breaks the enthalpy/entropy compensation effect.[50]

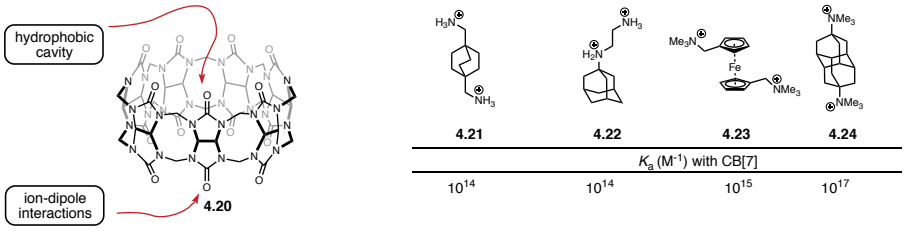

Figure 4.7 Cucurbit[7]uril host **4.20** and some of its high-affinity guests **4.21**–**4.24**.

Others have shown that CB[7][51–53] and multivalent cyclodextrin systems[54] can be used to detect guests in cells and mice. However, systematic studies were lacking; and a guest had not been metabolically incorporated. The Sletten lab demonstrated proof of principle bioorthogonal complexation with cucurbit[7]uril **4.20** by attaching cationic guests to the cell surface (Figure 4.8).[55] In this way, our lab determined the necessary K_a for cell-surface labeling with a small-molecule host to be $\geq 10^8$ M^{-1}. We have also shown that a host-guest system can label the cell surface with lower concentration of reagents than are required for covalent bioorthogonal chemistry. A sialic acid derivative modified with a neutral carborane was incorporated as a guest for CB[7] and some labeling was observed in a hyposialylated cell line. While CB[7] is useful in some contexts, many of its high-affinity charged guests (like **4.21**–**4.24**) cannot be displayed on the cell surface through metabolic incorporation due to their cationic nature and large size.

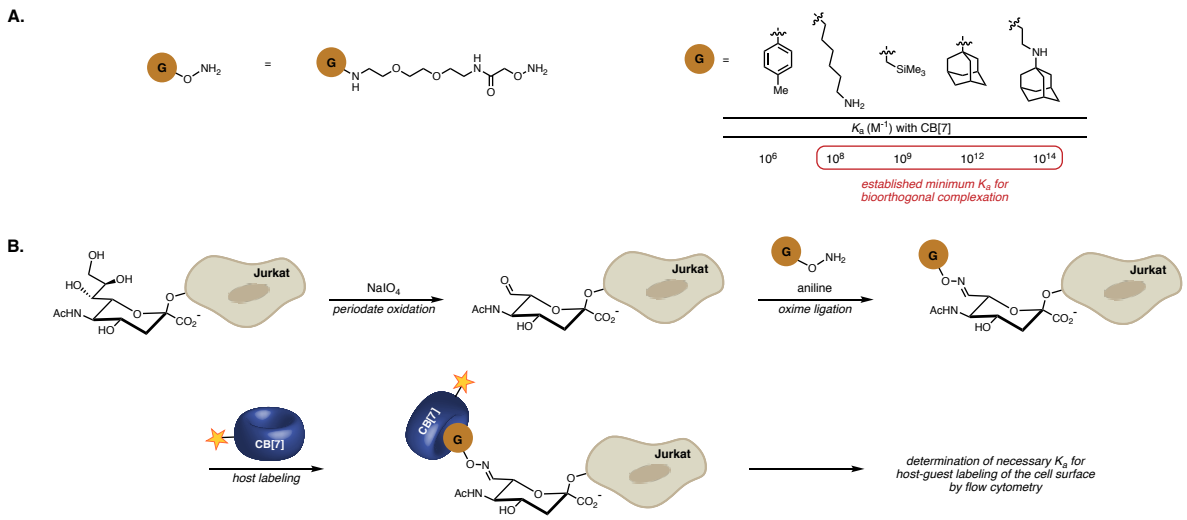

Figure 4.8 Proof of concept bioorthogonal complexation with known host. A) Guest-modified oxime reagents allowed for screening of guests with different K_as without metabolic incorporation. B) Schematic of cell-surface sialic acid oxidation followed by oxime ligation to attach guests and subsequent labeling with CB[7]-fluorophore conjugate.

Ultimately, an ideal host for bioorthogonal complexation would 1) have the binding affinities of CB[7]-guest pairs, 2) bind neutral guests capable of being metabolically incorporated, and 3) not bind any endogenous biomolecules. We would like to have synthetic receptors that could work in tandem with biology's host-guest pairs and other high-affinity hosts, binding guests selectivity in a manner orthogonal to biological and existing synthetic systems. New high-affinity hosts would allow dual labeling experiments, like those that have been performed with different bioorthogonal covalent reactions.[56–59] In some instances, it may be appropriate to use bioorthogonal complexation along with bioorthogonal covalent reactions as well. With numerous tools, chemists may someday be able to mimic the complex binding events and interactions that are all occurring simultaneously in a cell.

Many new host-guest systems have been discovered through screening (Figure 4.9A). To start, a new macrocycle will be synthesized and then a library of possible guests will be screened to find the highest-affinity host-guest pair.[47,60–64] This type of approach can be explanatory over

time and inform the design of even better guests for existing macrocycles.[49] While we are not opposed to this strategy, we envisioned that the requirements of bioorthogonal complexation provided an opportunity for alternative methods of host-guest pair discovery.

We imaged we could take a guest-centric approach to the design of a host-guest system (Figure 4.9B). The ideal guest for bioorthogonal complexation would be 1) abiotic, 2) non-reactive, 3) non-interfering with biology, and 4) neutral and reasonably small such that it can be metabolically incorporated. We hypothesized that perfluoroaromatics fit these requirements.

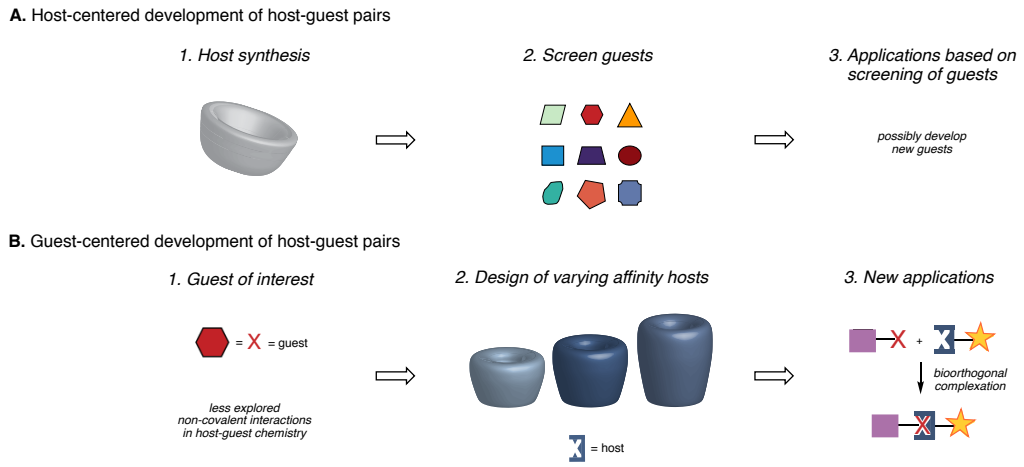

Figure 4.9 Approaches to discover new host-guest pairs. A) Host-centered approach. B) Guest-centered approach described in this dissertation.

Perfluoroaromatics are aromatic compounds where all or most of the hydrogens on a benzene ring have been replaced with fluorine (Figure 4.10A). As described in Chapter 1, fluorine is not found in living tissue.[65] Perfluoroaromatics are also not found in naturally-occurring systems. While perfluoroaromatics can be reactive with nucleophiles under S_NAr type conditions in some environments and solvents, this reactivity can be tuned with substituents.[66–68] Perfluoroaromatics have been previously incorporated into many biomolecules (Figure 4.10B and C), including proteins and peptides as unnatural amino acids.[69–74] One example of a perfluoroaryl azide being metabolically incorporated through a mannosamine derivative has been

reported.[75] This precedent for metabolic incorporation suggested that perfluoroaromatics could make good guests for bioorthogonal complexation.

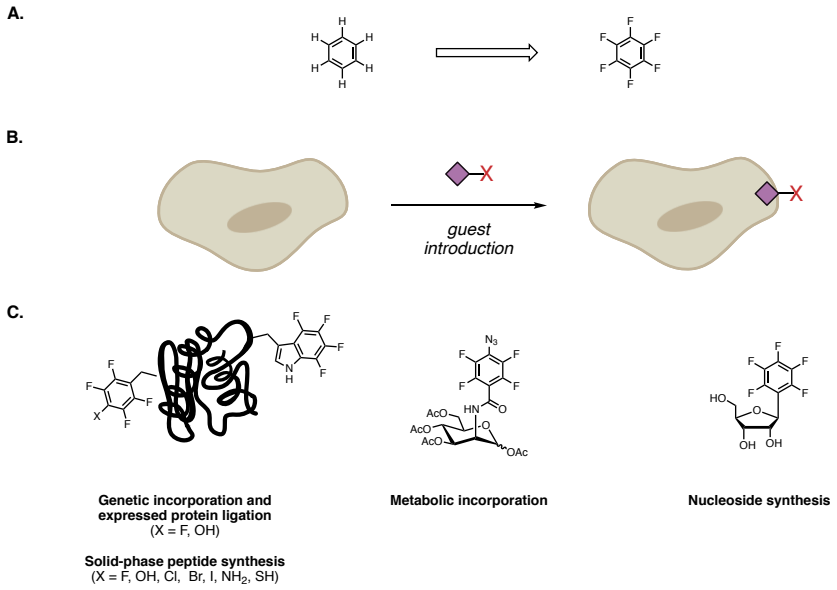

Figure 4.10 Perfluoroaromatics as guests for bioorthogonal complexation. A) Replacement of hydrogen atoms on benzene with fluorine atoms leads to perfluoroaromatic compounds. B) Incorporation of unnatural perfluoroaromatics into biomolecules. C) Perfluorinated phenylalanine and tyrosine analogues have been incorporated into proteins and peptides through amber suppression (X = F[69] or OH[70]), expressed protein ligation (X = OH[71]), and solid-phase peptide synthesis.[72,73] Perfluorinated tryptophan analogues have been incorporated through amber suppression.[74] Perfluoroaryl azide has been metabolically incorporated as a mannosamine derivative.[75] Perfluoroaryl nucleosides have been incorporated into RNA on the solid-phase.[76] Partially perfluorinated aromatic nucleoside analogues have also been described.[77,78]

Perfluoroaromatics have unique electronic character compared to benzene, which we imagined could be exploited in the design of a host specific for perfluoroaromatic guests over other guests. Due to the electronegativity of fluorine, the quadrupole moment of perfluoroaromatics is reversed compared to benzene (Figure 4.11A). As such, perfluoroaromatics and aromatics associate strongly through electrostatics and dispersive interactions.[79,80] Perfluorination of an aryl halide can induce another non-covalent interaction, halogen bonding (Figure 4.11B).[81,82] When a halogen atom is attached to an electron-poor aromatic, an

electropositive spot emerges on the halogen termed the sigma hole. This region of the halogen can interact with Lewis basic sites in a highly direction manner (~180 °C linear relationship).

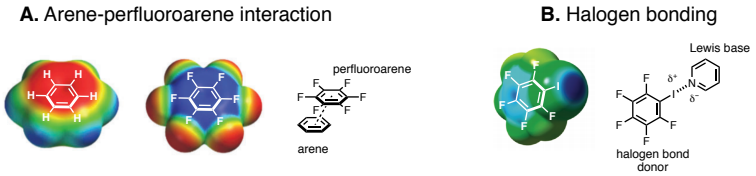

Figure 4.11 Non-covalent interactions induced by perfluorination of aromatic rings. A) Arene-perfluoroarene interactions. B) Halogen bonding.

Though the design of selective hosts for neutral guests is challenging,[61,83] we envisioned that these rare to biology non-covalent interactions could form the basis of a bioorthogonal host for a perfluoroaromatic guest (Figure 4.12A). An electron-rich host would act as the electronic complement to the electron-poor guest. Additional functionality, like a halogen-bond acceptor or hydrogen-bond acceptor,[84] could be incorporated to enforce the host-guest interaction. In collaboration with Dr. Gina Lee, a joint student in the Sletten and Houk lab, we hoped to use computation-guided rational design of a host selective for perfluoroaromatics that could ultimately be used in bioorthogonal complexation. We imagined we could draw inspiration from the extensive fundamental physical organic chemistry of host-guest systems studied in the mid-20th century as we pursue this new application. Our work toward the design and synthesis of a host for perfluoroaromatic guests and progress toward applying this system for bioorthogonal complexation (Figure 4.12B) is detailed in the following three chapters.

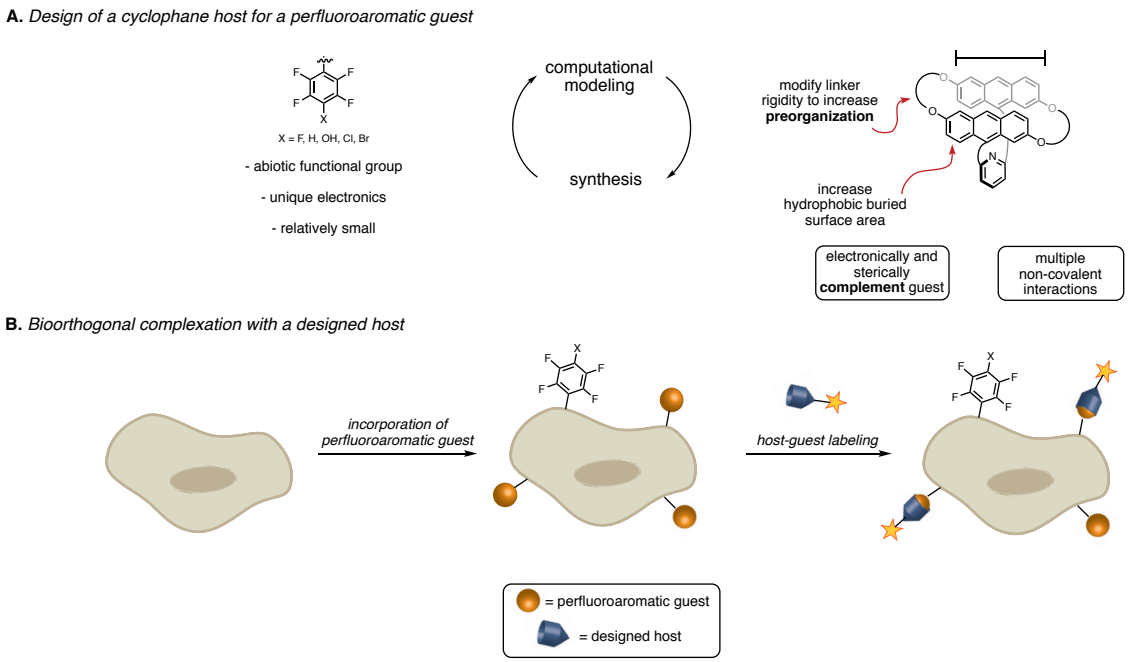

Figure 4.12 Overview of our approach to bioorthogonal host discovery. A) Design of a host for perfluoroaromatics with input from computational modeling and experimentation. B) Metabolic incorporation of a perfluoroaromatic guest and application of the designed host in bioorthogonal complexation.

4.3 Conclusion

The bioorthogonal chemical reporter strategy has enabled studies of many different biological phenomena and facilitated imaging experiments in different types of biomolecules, drug delivery, and biomaterials engineering. Fast, covalent reactions have been the workhorse of these studies. We recognize the limitations of covalent chemistry in some contexts, such as labeling experiments in live mammals. An alternative approach relying on host-guest chemistry is presented. We describe the advantages of bioorthogonal complexation—a non-covalent method for detecting unnatural functional groups in biological contexts. We hypothesize that abiotic perfluoroaromatics could be ideal guests for bioorthogonal complexation due to their unique electronic character and relatively small size. Our approach to the design of a receptor that can selectively bind perfluoroaromatic guests is described here and discussed in depth in the following

chapters. While we have initially focused on perfluoroaromatics due to their distinct non-covalent interactions, we imagine that small perfluorocarbons, like those described in Chapter 1, could make for future guests for bioorthogonal complexation as well.[85]

4.4 References

(1) Prescher, J. A.; Bertozzi, C. R. Chemistry in Living Systems. *Nat. Chem. Biol.* **2005**, *1*, 13–21.

(2) Sletten, E. M.; Bertozzi, C. R. From Mechanism to Mouse: A Tale of Two Bioorthogonal Reactions. *Acc. Chem. Res.* **2011**, *44*, 666–676.

(3) Sletten, E. M.; Bertozzi, C. R. Bioorthogonal Chemistry: Fishing for Selectivity in a Sea of Functionality. *Angew. Chem. Int. Ed.* **2009**, *48*, 6974–6998.

(4) Du, J.; Meledeo, M. A.; Wang, Z.; Khanna, H. S.; Paruchuri, V. D. P.; Yarema, K. J. Metabolic Glycoengineering: Sialic Acid and Beyond. *Glycobiology* **2009**, *19*, 1382–1401.

(5) Oetke, C.; Brossmer, R.; Mantey, L. R.; Hinderlich, S.; Isecke, R.; Reutter, W.; Keppler, O. T.; Pawlita, M. Versatile Biosynthetic Engineering of Sialic Acid in Living Cells Using Synthetic Sialic Acid Analogues. *J. Biol. Chem.* **2002**, *277*, 6688–6695.

(6) Moons, S. J.; Adema, G. J.; Derks, M. T.; Boltje, T. J.; Büll, C. Sialic Acid Glycoengineering Using N-Acetylmannosamine and Sialic Acid Analogs. *Glycobiology* **2019**, *29*, 433–445.

(7) Luchansky, S. J.; Goon, S.; Bertozzi, C. R. Expanding the Diversity of Unnatural Cell-Surface Sialic Acids. *ChemBioChem* **2004**, *5*, 371–374.

(8) Lang, K.; Chin, J. W. Cellular Incorporation of Unnatural Amino Acids and Bioorthogonal Labeling of Proteins. *Chem. Rev.* **2014**, *114*, 4764–4806.

(9) Liu, C. C.; Schultz, P. G. Adding New Chemistries to the Genetic Code. *Annu. Rev. Biochem.* **2010**, *79*, 413–444.

(10) Chin, J. W.; Cropp, T. A.; Anderson, J. C.; Mukherji, M.; Zhang, Z.; Schultz, P. G. An Expanded Eukaryotic Genetic Code. *Science* **2003**, *301*, 964–967.

(11) Wangt, L.; Zhang, Z.; Brock, A.; Schultz, P. G. Addition of the Keto Functional Group to the Genetic Code of Escherichia Coli. *Proc. Natl. Acad. Sci.* **2003**, *100*, 56–61.

(12) Kiick, K. L.; Saxon, E.; Tirrell, D. A.; Bertozzi, C. R. Incorporation of Azides into Recombinant Proteins for Chemoselective Modification by the Staudinger Ligation. *Proc. Natl. Acad. Sci.* **2002**, *99*, 19–24.

(13) Ngo, J. T.; Tirrell, D. A. Noncanonical Amino Acids in the Interrogation of Cellular Protein Synthesis. *Acc. Chem. Res.* **2011**, *44*, 677–685.

(14) Jacobs, C. L.; Goon, S.; Yarema, K. J.; Hinderlich, S.; Hang, H. C.; Chai, D. H.; Bertozzi, C. R. Substrate Specificity of the Sialic Acid Biosynthetic Pathway. *Biochemistry* **2001**, *40*, 12864–12874.

(15) Saxon, E.; Bertozzi, C. R. Cell Surface Engineering by a Modified Staudinger Reaction. *Science* **2000**, *287*, 2007–2010.

(16) Changa, P. V.; Preschera, J. A.; Sletten, E. M.; Baskin, J. M.; Miller, I. A.; Agard, N. J.; Lo, A.; Bertozzi, C. R. Copper-Free Click Chemistry in Living Animals. *Proc. Natl. Acad. Sci.* **2010**, *107*, 1821–1826.

(17) Agard, N. J.; Prescher, J. A.; Bertozzi, C. R. A Strain-Promoted [3 + 2] Azide-Alkyne Cycloaddition for Covalent Modification of Biomolecules in Living Systems. *J. Am. Chem. Soc.* **2004**, *126*, 15046–15047.

(18) Jewett, J. C.; Sletten, E. M.; Bertozzi, C. R. Rapid Cu-Free Click Chemistry with Readily

Synthesized Biarylazacyclooctynones. *J. Am. Chem. Soc.* **2010**, *132*, 3688–3690.

(19) Sletten, E. M.; Bertozzi, C. R. A Hydrophilic Azacyclooctyne for Cu-Free Click Chemistry. *Org. Lett.* **2008**, *10*, 3097–3099.

(20) Patterson, D. M.; Nazarova, L. A.; Xie, B.; Kamber, D. N.; Prescher, J. A. Functionalized Cyclopropenes as Bioorthogonal Chemical Reporters. *J. Am. Chem. Soc.* **2012**, *134*, 18638–18643.

(21) Yang, J.; Šečkute, J.; Cole, C. M.; Devaraj, N. K. Live-Cell Imaging of Cyclopropene Tags with Fluorogenic Tetrazine Cycloadditions. *Angew. Chemie Int. Ed.* **2012**, *51*, 7476–7479.

(22) Devaraj, N. K.; Weissleder, R.; Hilderbrand, S. A. Tetrazine-Based Cycloadditions: Application to Pretargeted Live Cell Imaging. *Bioconjug. Chem.* **2008**, *19*, 2297–2299.

(23) Blackman, M. L.; Royzen, M.; Fox, J. M. Tetrazine Ligation: Fast Bioconjugation Based on Inverse-Electron-Demand Diels-Alder Reactivity. *J. Am. Chem. Soc.* **2008**, *130*, 13518–13519.

(24) Selvaraj, R.; Fox, J. M. Trans-Cyclooctene — a Stable, Voracious Dienophile for Bioorthogonal Labeling. *Curr. Opin. Chem. Biol.* **2013**, *17*, 753–760.

(25) Fang, Y.; Judkins, J. C.; Boyd, S. J.; am Ende, C. W.; Rohlfing, K.; Huang, Z.; Xie, Y.; Johnson, D. S.; Fox, J. M. Studies on the Stability and Stabilization of Trans-Cyclooctenes through Radical Inhibition and Silver (I) Metal Complexation. *Tetrahedron* **2019**, *75*, 4307–4317.

(26) Rossin, R.; Van Den Bosch, S. M.; Ten Hoeve, W.; Carvelli, M.; Versteegen, R. M.; Lub, J.; Robillard, M. S. Highly Reactive Trans-Cyclooctene Tags with Improved Stability for Diels-Alder Chemistry in Living Systems. *Bioconjug. Chem.* **2013**, *24*, 1210–1217.

(27) Rossin, R.; Robillard, M. S. Pretargeted Imaging Using Bioorthogonal Chemistry in Mice. *Curr. Opin. Chem. Biol.* **2014**, *21*, 161–169.

(28) Lee, S. B.; Kim, H. L.; Jeong, H. J.; Lim, S. T.; Sohn, M. H.; Kim, D. W. Mesoporous Silica Nanoparticle Pretargeting for PET Imaging Based on a Rapid Bioorthogonal Reaction in a Living Body. *Angew. Chemie Int. Ed.* **2013**, *52*, 10549–10552.

(29) Houk, K. N.; Leach, A. G.; Kim, S. P.; Zhang, X. Binding Affinities of Host–Guest, Protein–Ligand, and Protein–Transition-State Complexes. *Angew. Chemie Int. Ed.* **2003**, *42*, 4872–4897.

(30) Liu, W.; Samanta, S. K.; Smith, B. D.; Isaacs, L. Synthetic Mimics of Biotin/(Strept)Avidin. *Chem. Soc. Rev.* **2017**, *46*, 2391–2403.

(31) Sela-Culang, I.; Kunik, V.; Ofran, Y. The Structural Basis of Antibody-Antigen Recognition. *Front. Immunol.* **2013**, *4*, 302.

(32) Tang, H.; Fuentealba, D.; Ko, Y. H.; Selvapalam, N.; Kim, K.; Bohne, C. Guest Binding Dynamics with Cucurbit[7]Uril in the Presence of Cations. *J. Am. Chem. Soc.* **2011**, *133*, 20623–20633.

(33) Schreiber, C. L.; Smith, B. D. Molecular Conjugation Using Non-Covalent Click Chemistry. *Nat. Rev. Chem.* **2019**, *3*, 393–400.

(34) Addonizio, C. J.; Gates, B. D.; Webber, M. J. Supramolecular "Click Chemistry" for Targeting in the Body. *Bioconjug. Chem.* **2021**, *32*, 1935–1946.

(35) Anslyn, E. V.; Dougherty, D. A. *Modern Physical Organic Chemstry*; University Science Books: Mill Valley, 2006.

(36) Stoddart, J. F. Chapter 12. Host–Guest Chemistry. *Annu. Reports Sect. "B"* **1988**, *85*, 353–386.

(37) Cram, D. J.; Cram, J. M. Host-Guest Chemistry. *Science (80-.).* **1974**, *183*, 803–809.

(38) Cram, D. J. The Design of Molecular Hosts, Guests, and Their Complexes (Nobel Lecture). *Angew. Chemie Int. Ed.* **1988**, *27*, 1009–1020.

(39) Pedersen, C. J. The Discovery of Crown Ethers (Noble Lecture). *Angew. Chemie Int. Ed.* **1988**, *27*, 1021–1027.

(40) Lehn, J. -M. Supramolecular Chemistry—Scope and Perspectives Molecules, Supermolecules, and Molecular Devices (Nobel Lecture). *Angew. Chemie Int. Ed.* **1988**, *27*, 89–112.

(41) Wittenberg, J. B.; Isaacs, L. Complementarity and Preorganization. In *Supramolecular Chemistry: From Molecules to Nanomaterials*; John Wiley & Sons, Ltd, 2012.

(42) Cram, D. J.; Kaneda, T.; Helgeson, R. C.; Brown, S. B.; Knobler, C. B.; Maverick, E.; Trueblood, K. N. Host-Guest Complexation. 35. Spherands, the First Completely Preorganized Ligand Systems. *J. Am. Chem. Soc.* **1985**, *107*, 3645–3657.

(43) Szejtli, J. Introduction and General Overview of Cyclodextrin Chemistry. *Chem. Rev.* **1998**, *98*, 1743–1753.

(44) Nag, K.; Singh, D. R.; Shetti, A. N.; Kumar, H.; Sivashanmugam, T.; Parthasarathy, S. Sugammadex: A Revolutionary Drug in Neuromuscular Pharmacology. *Anesth. Essays Res.* **2013**, *7*, 302.

(45) Breslow, R.; Zhang, B. Cholesterol Recognition and Binding by Cyclodextrin Dimers. *J. Am. Chem. Soc.* **1996**, *118*, 8495–8496.

(46) Davis, M. E.; Brewster, M. E. Cyclodextrin-Based Pharmaceutics: Past, Present and Future. *Nat. Rev. Drug Discov.* **2004**, *3*, 1023–1035.

(47) Liu, S.; Ruspic, C.; Mukhopadhyay, P.; Chakrabarti, S.; Zavalij, P. Y.; Isaacs, L. The

Cucurbit[n]Uril Family: Prime Components for Self-Sorting Systems. *J. Am. Chem. Soc.* **2005**, *127*, 15959–15967.

(48) Lee, J. W.; Samal, S.; Selvapalam, N.; Kim, H. J.; Kim, K. Cucurbituril Homologues and Derivatives: New Opportunities in Supramolecular Chemistry. *Acc. Chem. Res.* **2003**, *36*, 621–630.

(49) Cao, L.; Šekutor, M.; Zavalij, P. Y.; Mlinarič-Majerski, K.; Glaser, R.; Isaacs, L. Cucurbit[7]Uril·Guest Pair with an Attomolar Dissociation Constant. *Angew. Chemie Int. Ed.* **2014**, *53*, 988–993.

(50) Rekharsky, M. V.; Mori, T.; Yang, C.; Young, H. K.; Selvapalam, N.; Kim, H.; Sobransingh, D.; Kaifer, A. E.; Liu, S.; Isaacs, L.; Chen, W.; Moghaddam, S.; Gilson, M. K.; Kim, O.; Inoue, Y. A Synthetic Host-Guest System Achieves Avidin-Biotin Affinity by Overcoming Enthalpy–Entropy Compensation. *Proc. Natl. Acad. Sci.* **2007**, *104*, 20737–20742.

(51) Kim, K. L.; Sung, G.; Sim, J.; Murray, J.; Li, M.; Lee, A.; Shrinidhi, A.; Park, K. M.; Kim, K. Supramolecular Latching System Based on Ultrastable Synthetic Binding Pairs as Versatile Tools for Protein Imaging. *Nat. Commun.* **2018**, *9*, 1–10.

(52) Sasmal, R.; Das Saha, N.; Pahwa, M.; Rao, S.; Joshi, D.; Inamdar, M. S.; Sheeba, V.; Agasti, S. S. Synthetic Host-Guest Assembly in Cells and Tissues: Fast, Stable, and Selective Bioorthogonal Imaging via Molecular Recognition. *Anal. Chem.* **2018**, *90*, 11305–11314.

(53) Zou, L.; Braegelman, A. S.; Webber, M. J. Spatially Defined Drug Targeting by in Situ Host-Guest Chemistry in a Living Animal. *ACS Cent. Sci.* **2019**, *5*, 1035–1043.

(54) Agasti, S. S.; Liong, M.; Tassa, C.; Chung, H. J.; Shaw, S. Y.; Lee, H.; Weissleder, R.

Supramolecular Host-Guest Interaction for Labeling and Detection of Cellular Biomarkers. *Angew. Chemie Int. Ed.* **2012**, *51*, 450–454.

(55) Kataki-Anastasakou, A.; Hernandez, S.; Sletten, E. M. Cell-Surface Labeling via Bioorthogonal Host-Guest Chemistry. *ACS Chem. Biol.* **2021**, *16*, 2124–2129.

(56) Patterson, D. M.; Prescher, J. A. Orthogonal Bioorthogonal Chemistries. *Curr. Opin. Chem. Biol.* **2015**, *28*, 141–149.

(57) Meineke, B.; Heimgärtner, J.; Eirich, J.; Landreh, M.; Elsässer, S. J. Site-Specific Incorporation of Two NcAAs for Two-Color Bioorthogonal Labeling and Crosslinking of Proteins on Live Mammalian Cells. *Cell Rep.* **2020**, *31*, 107811.

(58) Kamber, D. N.; Nazarova, L. A.; Liang, Y.; Lopez, S. A.; Patterson, D. M.; Shih, H.-W.; Houk, K. N.; Prescher, J. A. Isomeric Cyclopropenes Exhibit Unique Bioorthogonal Reactivities. *J. Am. Chem. Soc* **2013**, *135*.

(59) Hu, Y.; Schomaker, J. M. Recent Developments and Strategies for Mutually Orthogonal Bioorthogonal Reactions. *ChemBioChem* **2021**, *22*, 3254–3262.

(60) Diederich, F.; Dick, K. A New Water-Soluble Macrocyclic Host of the Cyclophane Type: Host-Guest Complexation with Aromatic Guests in Aqueous Solution and Acceleration of the Transport of Arenes through an Aqueous Phase. *J. Am. Chem. Soc.* **1984**, *106*, 8024–8036.

(61) Diederich, F. Complexation of Neutral Molecules by Cyclophane Hosts. *Angew. Chemie Int. Ed.* **1988**, *27*, 362–386.

(62) Yao, H.; Ke, H.; Zhang, X.; Pan, S. J.; Li, M. S.; Yang, L. P.; Schreckenbach, G.; Jiang, W. Molecular Recognition of Hydrophilic Molecules in Water by Combining the Hydrophobic Effect with Hydrogen Bonding. *J. Am. Chem. Soc.* **2018**, *140*, 13466–13477.

(63) Huang, G. B.; Wang, S. H.; Ke, H.; Yang, L. P.; Jiang, W. Selective Recognition of Highly Hydrophilic Molecules in Water by Endo-Functionalized Molecular Tubes. *J. Am. Chem. Soc.* **2016**, *138*, 14550–14553.

(64) Barrans, R. E.; Dougherty, D. A.; Petti, M. A.; Shepodd, T. J. "Hydrophobic" Binding of Water-Soluble Guests by High-Symmetry, Chiral Hosts. An Electron-Rich Receptor Site with a General Affinity for Quaternary Ammonium Compounds and Electron-Deficient .Pi. Systems. *J. Am. Chem. Soc.* **1988**, *110*, 6825–6840.

(65) Harper, D. B.; O'Hagan, O. The Fluorinated Natural Products. *Nat. Prod. Rep.* **1994**, *11*, 123–133.

(66) Zhang, C.; Welborn, M.; Zhu, T.; Yang, N. J.; Santos, M. S.; Van Voorhis, T.; Pentelute, B. L. π-Clamp-Mediated Cysteine Conjugation. *Nat. Chem.* **2015**, *8*, 120–128.

(67) Embaby, A. M.; Schoffelen, S.; Kofoed, C.; Meldal, M.; Diness, F. Rational Tuning of Fluorobenzene Probes for Cysteine-Selective Protein Modification. *Angew. Chemie* **2018**, *130*, 8154–8158.

(68) Zhang, C.; Spokoyny, A. M.; Zou, Y.; Simon, M. D.; Pentelute, B. L. Enzymatic "Click" Ligation: Selective Cysteine Modification in Polypeptides Enabled by Promiscuous Glutathione S-Transferase. *Angew. Chemie Int. Ed.* **2013**, *52*, 14001–14005.

(69) Thorson, J. S.; Chapman, E.; Schultz, P. G. Analysis of Hydrogen Bonding Strengths in Proteins Using Unnatural Amino Acids. *J. Am. Chem. Soc.* **1995**, *117*, 9361–9362.

(70) Liu, X.; Jiang, L.; Li, J.; Wang, L.; Yu, Y.; Zhou, Q.; Lv, X.; Gong, W.; Lu, Y.; Wang, J. Significant Expansion of Fluorescent Protein Sensing Ability through the Genetic Incorporation of Superior Photo-Induced Electron-Transfer Quenchers. *J. Am. Chem. Soc.* **2014**, *136*, 13094–13097.

(71) Seyedsayamdost, M. R.; Yee, C. S.; Stubbe, J. A. Site-Specific Incorporation of Fluorotyrosines into the R2 Subunit of E. Coli Ribonucleotide Reductase by Expressed Protein Ligation. *Nat. Protoc.* **2007**, *2*, 1225–1235.

(72) Pace, C. J.; Gao, J. Exploring and Exploiting Polar−π Interactions with Fluorinated Aromatic Amino Acids. *Acc. Chem. Res.* **2013**, *46*, 907–915.

(73) Qin, L.; Sheridan, C.; Gao, J. Synthesis of Tetrafluorinated Aromatic Amino Acids with Distinct Signatures in 19F NMR. *Org. Lett.* **2012**, *14*, 528–531.

(74) Nowak, M. W.; Kearney, P. C.; Sampson, J. R.; Saks, M. E.; Labarca, C. G.; Silverman, S. K.; Zhong, W.; Thorson, J.; Abelson, J. N.; Davidson, N.; Schultz, P. G.; Dougherty, D. A.; Lester, H. A. Nicotinic Receptor Binding Site Probed with Unnatural Amino Acid Incorporation in Intact Cells. *Science* **1995**, *268*, 439–442.

(75) Sundhoro, M.; Jeon, S.; Park, J.; Ramström, O.; Yan, M. Perfluoroaryl Azide Staudinger Reaction: A Fast and Bioorthogonal Reaction. *Angew. Chemie* **2017**, *129*, 12285–12289.

(76) Živković, A.; Engels, J. W. RNA Recognition by Fluoro-Aromatic Substituted . *Nucleosides, Nucleotides, and Nucleic Acids* **2011**, *24*, 1023–1027.

(77) Parsch, J.; Engels, J. W. C−F···H−C Hydrogen Bonds in Ribonucleic Acids. *J. Am. Chem. Soc.* **2002**, *124*, 5664–5672.

(78) Kool, E. T.; Morales, J. C.; Guckian, K. M. Mimicking the Structure and Function of DNA: Insights into DNA Stability and Replication. *Angew. Chem.* **2000**, *39*, 990–1009.

(79) Smith, C. E.; Smith, P. S.; Thomas, R. L.; Robins, E. G.; Collings, J. C.; Dai, C.; Scott, A. J.; Borwick, S.; Batsanov, A. S.; Watt, S. W.; Clark, S. J.; Viney, C.; Howard, J. A. K.; Clegg, W.; Marder, T. B. Arene-Perfluoroarene Interactions in Crystal Engineering: Structural Preferences in Polyfluorinated Tolans. *J. Mater. Chem.* **2004**, *14*, 413–420.

(80) Lee, G. Y.; Hu, E.; Rheingold, A. L.; Houk, K. N.; Sletten, E. M. Arene-Perfluoroarene Interactions in Solution. *J. Org. Chem.* **2021**, *86*, 8425–8436.

(81) Cavallo, G.; Metrangolo, P.; Milani, R.; Pilati, T.; Priimagi, A.; Resnati, G.; Terraneo, G. The Halogen Bond. *Chem. Rev.* **2016**, *116*, 2478–2601.

(82) Beale, T. M.; Chudzinski, M. G.; Sarwar, M. G.; Taylor, M. S. Halogen Bonding in Solution: Thermodynamics and Applications. *Chem. Soc. Rev* **2013**, *42*, 1667.

(83) Guo, D.-S.; Uzunova, V. D.; Assaf, K. I.; Lazar, A. I.; Liu, Y.; Nau, W. M. Inclusion of Neutral Guests by Water-Soluble Macrocyclic Hosts – a Comparative Thermodynamic Investigation with Cyclodextrins, Calixarenes and Cucurbiturils. *Supramol. Chem.* **2016**, *28*, 384–395.

(84) Metrangolo, P.; Neukirch, H.; Pilati, T.; Resnati, G. Halogen Bonding Based Recognition Processes: A World Parallel to Hydrogen Bonding. *Acc. Chem. Res.* **2005**, *38*, 386–395.

(85) Assaf, K. I.; Nau, W. M. Cucurbiturils as Fluorophilic Receptors. *Supramol. Chem.* **2014**, *26*, 657–669.

CHAPTER FIVE

Naphthalene-based cyclophanes to explore arene-perfluoroarene interactions in host-guest systems

5.1 Abstract

Arene-perfluoroarene interactions have been under studied in directional host-guest systems. Given our interest in abiotic host-guest complexes, we explore this interaction by repurposing Whitlock's rigid naphthalene-based cyclophanes. Through π-π interactions and hydrogen bonding, a dibutylamino-variant of Whitlock's naphthalene-based host is found to interact with a model perfluoroaryl guest, pentafluorophenol, with a $K_a = 10^2$ M^{-1} in $CDCl_3$. Studies with these hosts and various perfluoroaryl guests suggest that the naphthalene-based hosts have a cavity too narrow for accommodating perfluoroaryl guests. Ultimately, this work provides the groundwork for the design of new hosts that better accommodate perfluoroaromatics.

5.2 Introduction

For a host-guest pair to be truly bioorthogonal (i.e. non-interfering with naturally occurring cellular processes and not binding endogenous molecules), the host and guest should interact through abiotic or rare non-covalent interactions. One such interaction, the arene-perfluoroarene interaction, has precedent for driving the association of two species in aqueous media.[1,2] While arene-perfluoroarene interactions have been studied extensively in crystal engineering,[3–5] there are few examples of host-guest systems based on this interaction (Table 5.1). In 1982, Vogtle and coworkers described a biphenyl-based cyclophane **5.1** that was observed to bind perfluoroaromatics such as **5.2** and **5.3**, but not other aromatic guests.[6] However, extensive binding information was not reported. For chromatographic purposes, a

calixarene host **5.4** has been shown to interact with hexafluorobenzene **5.2**.[7] A Pt(II)-cyclophane **5.5** and related metallocyclophanes were found to bind hexafluorobenzene **5.2**.[8] Inclusion complexes between Pd-based coordination cages and perfluoroaromatics have been observed.[9] However, these metal-based hosts are formed through dative bonds and may not remain intact upon dilution in biologically-relevant media. Cucurbit[7]uril (CB[7]) **5.6** binds hexafluorobenzene **5.2** (K_a = 3.6x10^3 M^{-1} in aqueous solution),[10] however this K_a is much lower than many common guests for CB[7], including phenylalanine.

Host	Guest	K_a	ref.
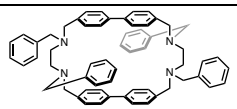 **5.1**	 **5.2**, X = F **5.3**, X = H	not reported "stoichiometrical binding" did not bind C_6H_6, C_6H_{12}, dioxane, or C_6H_5F	*4*
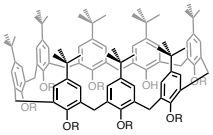 **5.4** R = $(EtO)_2P(O)$	 **5.2**	1.7x10^3 M^{-1} in MeCN: H_2O (86:14)	*5*
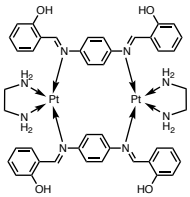 **5.5**	 **5.2**	3.17x 10^4 M^{-1} in DMSO-d_6	*6*
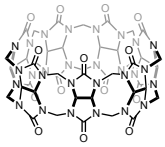 **5.6**	 **5.2**	3.6x10^3 M^{-1} in aqueous solution	*8*

Table 5.1 Examples of hosts that have been reported to bind or complex with perfluoroaromatic guests.

Lacking from these examples is intentional directionality in the design of the host-guest complex. The arene-perfluoroarene interaction is strongest in the parallel slip-stacked orientation, rather than a T-shaped orientation.[11,12] We hypothesized that a rigid and preorganized host capable of accommodating the parallel perfluoroaromatic guest could provide

a high-affinity host-guest pair. We imagined general structure **5.7** composed of electron-rich aromatic walls (region A), which would be complementary to electron-poor perfluoroaryl guests (Figure 5.1A). The walls would be joined by rigid linkers (region B) to preorganize the system in the binding geometry. An additional non-covalent interaction, such as halogen or hydrogen bonding, would be accommodated on the bottom portion of the host structure (region C) to further enhance the binding affinity to the perfluoroaryl guest.

Toward this goal, the Sletten lab became interested in computationally-guided host design. Dr. Gina Lee optimized the *6H*-benzo[c,d]pyrene-based host structure **5.8** to bind bromopentafluorobenzene derivative **5.9** (Figure 5.1B), which had a promising computed binding affinity (K_a = 1.5x10^6 M^{-1} in the gas phase). However, due to the lengthy synthetic route to **5.8**, we thought a simplified host-guest system that could be accessed quickly would allow us to begin to experimentally study arene-perfluoroarene-based host-guest systems, while also validating the lab's computational approaches.

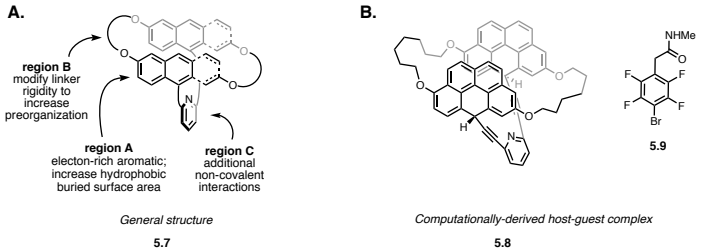

Figure 5.1 Inspiration for design of a cyclophane host. (A) General imagined cyclophane host structure **5.7** for binding perfluoroaromatic guests. (B) Computationally-optimized host structure **5.8** for bromopentafluorobenzene derivative **5.9** designed by Dr. Gina Lee.

With a desire for a simplified system, we were excited by the naphthalene-based cyclophanes **5.10**–**5.13** described by Whitlock and coworkers in the late 1980s and 1990s (Figure 5.2).[13–20] **5.13** was demonstrated to bind an electron-poor aromatic guest 4-nitrophenol **5.14** with a binding affinity reaching up to 10^5 M^{-1} in organic solvent, through a combination of arene-arene

interactions in the vertical (face-to-face) and horizontal (edge-to-face) directions in addition to hydrogen bonding.[18,19] This system possessed some of the criteria we had envisioned would be a part of general structure **5.7**, including electron-rich aromatic walls, rigid diyne side linkers, and a pyridine bottom linker capable of hydrogen bonding to the guest. Given the electronic similarities between 4-nitrophenol **5.14** and pentafluorophenol **5.15**, we imagined that Whitlock's hosts could be repurposed as hosts for pentafluorophenol, a model perfluorinated aromatic guest. Additionally, structures like **5.10–5.13** could be accessed through convergent routes, allowing us to swap out different regions of the host quickly to assess structure-property relationships in arene-perfluoroarene-based host-guest systems.

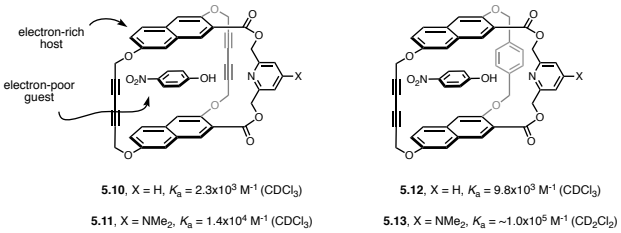

Figure 5.2 Whitlock's naphthalene-based macrocycles **5.10–5.13**: hosts for electron-poor 4-nitrophenol **5.14**.

5.3 Discussion and results

We chose **5.10** as the initial host target due to synthetic accessibility, so that binding studies with perfluorinated guests could be performed quickly. Additionally, perfluorinated aromatics do not readily participate in edge-to-face interactions (C—F to π) with benzene derivatives,[11,12] therefore hosts **5.12** and **5.13** may not be strong hosts for pentafluorophenol **5.15**. We chose **5.10** over **5.11** for a better pK_a match between the pyridine of the host (pyridinium pK_a= 5.2) and the pentafluorophenol guest (pK_a = 5.5), compared to 4-dimethylaminopyridinium (pK_a = 9.2). It is hypothesized that pK_a equalization can play a role in increasing the strength of the hydrogen bond, though this principle has not been fully verified.[21]

Whitlock's host **5.10** was prepared in five steps. We began with the preparation of the tri-substituted naphthalene **5.17** from 3,7-dihydroxy-2-naphthoic acid **5.16** (Scheme 5.1). Following the reported conditions,[18,22] we observed a mixture of species including *C*-alkylation (**5.18**) and over-propargylation (**5.19**), presumably due to intramolecular hydrogen bonding. We found that the use of methyl ester starting material **5.16b** did not improve the regioselectivity or minimize side products. Ultimately, after a small screen of solvents and bases, **5.17** was accessed in pure form after recrystallization.

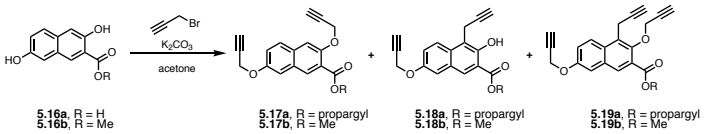

Scheme 5.1 Propargylation of 3,7-dihydroxy-2-naphthoic acid **5.16** under reported conditions.

With grams of tripropargylated naphthalene **5.17** in hand, **5.17** was hydrolyzed readily to **5.20** (Scheme 5.2). **5.20** was activated as the PFPester **5.21** and coupled with pyridine diol **5.22** to form premacrocycle **5.23**. Due to limited solubility, premacrocycle **5.23** could be purified via washing and filtration. Macrocyclization of **5.23** was carried out under modified Eglinton-type conditions. Two isomers of **5.10** were obtained, a more symmetric meso **5.10a** and a less symmetric dl **5.10b**, which could be separated by column chromatography. The structure of the meso isomer **5.10a** was confirmed by x-ray crystallography.

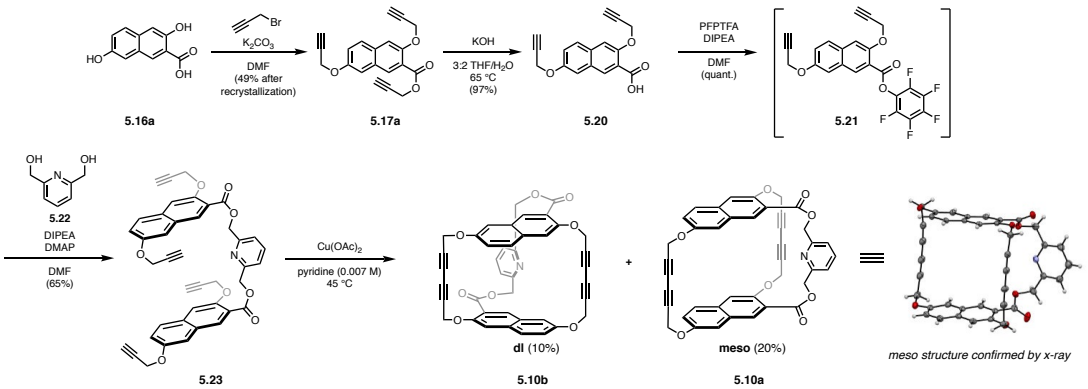

Scheme 5.2 Synthesis of 4H-pyridine naphthalene hosts **5.10a** and **5.10b**.

We began binding studies with meso host **5.10a** as Whitlock and coworkers showed that the meso isomer **5.10a** had a higher binding affinity than **5.10b** to guest 4-nitrophenol **5.14**. **5.10a** was also more soluble than **5.10b**, simplifying preparation for titration experiments. We confirmed that we were able to obtain binding constants of the same order of magnitude as Whitlock with known guest 4-nitrophenol **5.14** (10^3 M^{-1}) (Figure 5.3).[17] We then examined pentafluorophenol **5.15** as a model perfluoroaromatic guest capable of both arene-perfluoroarene interactions and hydrogen bonding interactions with host **5.10a**. Unfortunately, we found that in $CDCl_3$ the perfluorinated phenol guest **5.15** did not have as high of a binding affinity (K_a = 48 M^{-1}) as known guest **5.14** (K_a = 1.1x10^3 M^{-1}). Host **5.10a** also bound phenol **5.24** (K_a = 72 M^{-1}) more strongly than pentafluorophenol **5.15**, suggesting this system would not be ideal in a biological environment due to a possible binding interaction with tyrosine.

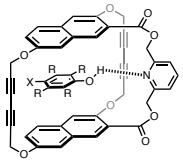

5.10a-guest

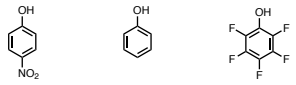

5.14 **5.24** **5.15**

	4-nitrophenol	phenol	pentafluorophenol
K_a ($CDCl_3$)	$1.1 \times 10^3 \pm 7\%$ M^{-1}	$72 \pm 8\%$ M^{-1}	$48 \pm 2\%$ M^{-1}
pK_a	7.1	10	5.5

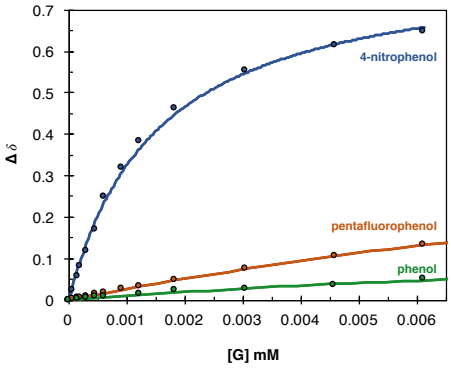

Figure 5.3 Binding affinity between host **5.10a** and 4-nitrophenol **5.14**, pentafluorophenol **5.15**, and phenol **5.24** in $CDCl_3$.

Though the binding affinity between host **5.10a** and pentafluorophenol **5.15** was not large, we wanted to explore alternative guests that did not possess a hydroxyl group. Ultimately hydrogen bonding is not ideal for bioorthogonal complexation due to an abundance of hydrogen bond donors and acceptors within biomolecules and competition with water. However, no interaction between hexafluorobenzene **5.2** and host **5.10a** was observed by ^{1}H NMR. Guests capable of halogen bonding, **5.25**, **5.26**, and **5.27** were also not observed to interact significantly with host **5.10a**. A strong halogen bond requires a linear relationship between the halogen of the halogen bond donor and the halogen bond acceptor,[23] which may not be accessible in the cavity of **5.10a** due to the orientation of the pyridine.

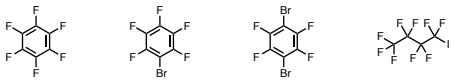

5.2 **5.25** **5.26** **5.27**

Figure 5.4 Guests that did not bind host **5.10a** by ^{1}H NMR in $CDCl_3$.

An alternative approach to screening host-guest pairs is to make modifications to the host. We became interested in post-macrocyclization modifications of region C of host **5.10a** that could alter the binding affinity to pentafluorophenol **5.15**. Whitlock and coworkers had previously showed that *N*-oxide host **5.28a** had a reasonably high K_a (1.1×10^4 M^{-1} in $CDCl_3$) to

guest 4-nitrophenol **5.14**.[17] We imagined this modification could drastically change the binding geometry and perhaps improve the K_a for **5.15**. Despite limited solubility of **5.10a**, *N*-oxide host **5.28a** was synthesized in 43% yield (59% brsm). Unfortunately, the binding affinity of *N*-oxide **5.28a** and pentafluorophenol **5.15** (K_a = 48 M^{-1} in $CDCl_3$) was similar to the K_a with **5.10a**.

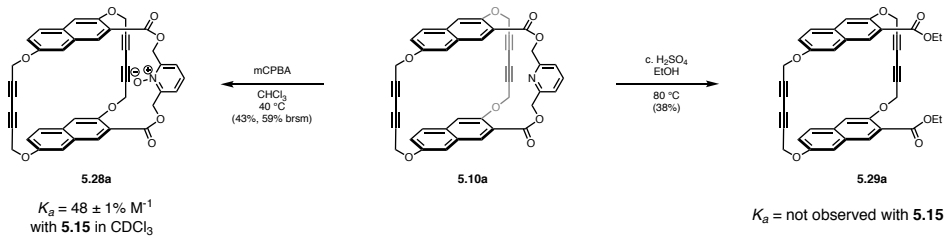

Scheme 5.3 Post-macrocyclization modifications to naphthalene host **5.10a**.

A second post-macrocyclization modification was made by removing the pyridine linker entirely. The pyridine linker of **5.10a** was hydrolyzed in EtOH to form diester naphthalene host **5.29a**. The lack of ABq splitting patterns in the methylene protons by ^{1}H NMR suggests that host **5.29a** is much less rigid than **5.10a** and capable of free rotation. No binding interaction between **5.29a** and pentafluorophenol **5.15** was observed by ^{1}H NMR in $CDCl_3$, suggesting the importance of the pyridine for the rigidity of the host and the necessity of the hydrogen bonding interaction.

To further explore the importance of the hydrogen bonding interaction in this host-guest system, a modification to the pyridine linker was made pre-macrocyclization (Scheme 5.4). This opportunity was also used to add organic solubilizing groups to simplify purification of these hosts and to increase the concentrations accessible for titrations. To access a more electron-rich pyridine diol, 4-chloropyridinediester **5.31** was prepared from chelidamic acid **5.30**. Under microwave conditions, **5.31** was aminated with dibutylamine. The crude diacid **5.32** was treated

with trimethylsilyldiazomethane to reform the diester **5.33** and simplify purification. Finally, the diester **5.33** was reduced to access 4-dibutylaminopyridine diol **5.34**.

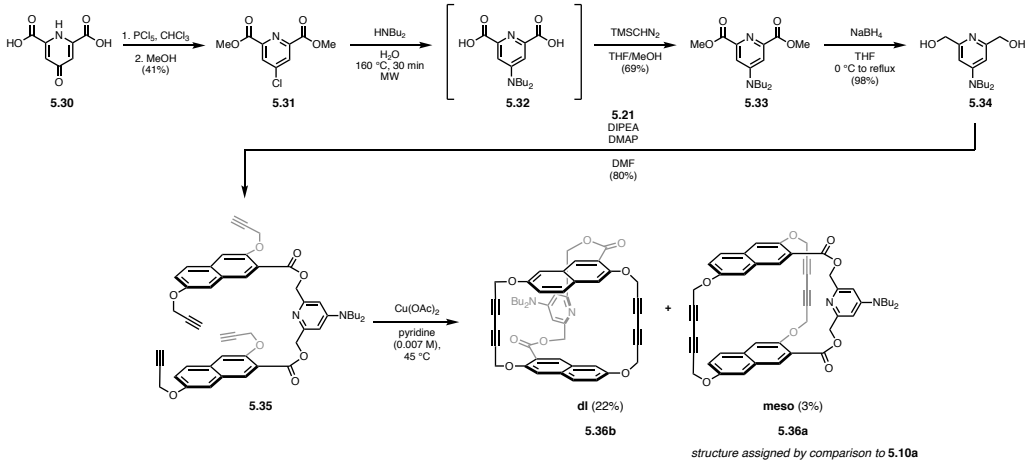

Scheme 5.4 Synthesis of 4-dibutylaminopyridine diol **5.34** and more electron-rich naphthalene hosts **5.36a** and **5.36b**.

Similar to the 4-H-pyr-naphthalene system, **5.34** was esterified with naphthalene PFPester **5.21**. 4-NBu_2-pyr-naphthalene prehost **5.35** was cyclized under oxidative conditions to yield both isomers of the more electron-rich host **5.36**. The meso variant **5.36a** was isolated in low yield due to purification difficulties, but enough material was obtained for preliminary binding studies. The identity of the meso isomer **5.36a** was assigned by ^{1}H NMR comparison to **5.10a** (Figure 5.5).

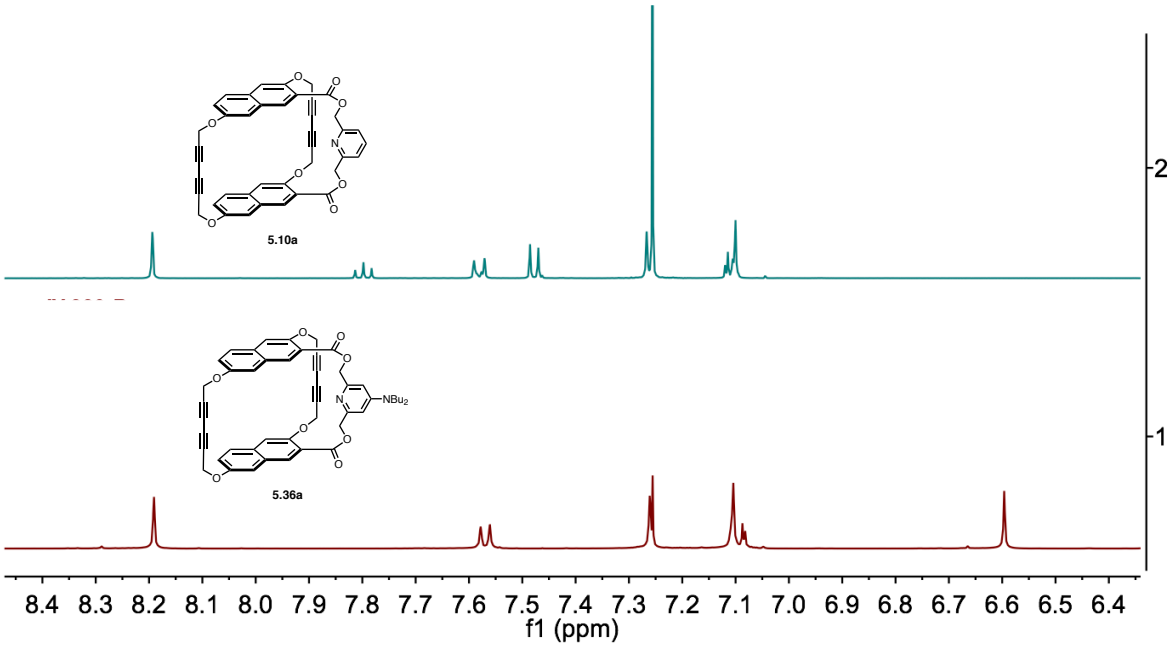

Figure 5.5 Assignment of **5.36a** as the meso isomer by ^{1}H NMR comparison to **5.10a** in $CDCl_3$.

With the more electron-rich host **5.36a**, the K_a with pentafluorophenol **5.15** was found to be an order of magnitude higher than the pyridine-based host **5.10a** (7.0×10^2 vs 48 M^{-1}) (Figure 5.6). An order of magnitude increase in the binding affinity of **5.36a** to 4-nitrophenol **5.14** was also observed (1.1×10^4 vs 1.11×10^3 M^{-1}), consistent with the Whitlock group's work (Figure 5.7).

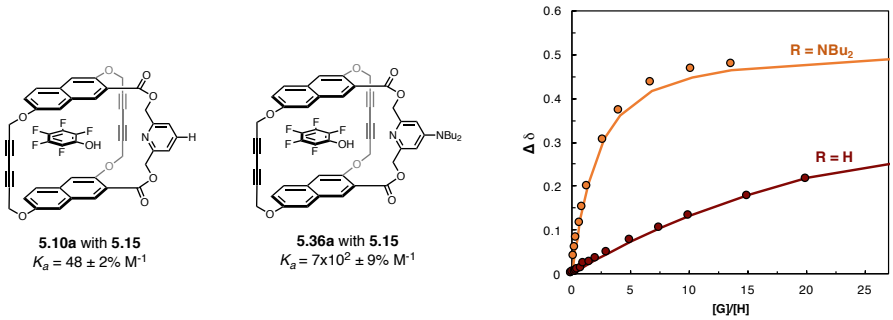

Figure 5.6 Comparison of binding affinity in $CDCl_3$ between host **5.10a** and host **5.36a** With guest pentafluorophenol **5.15**.

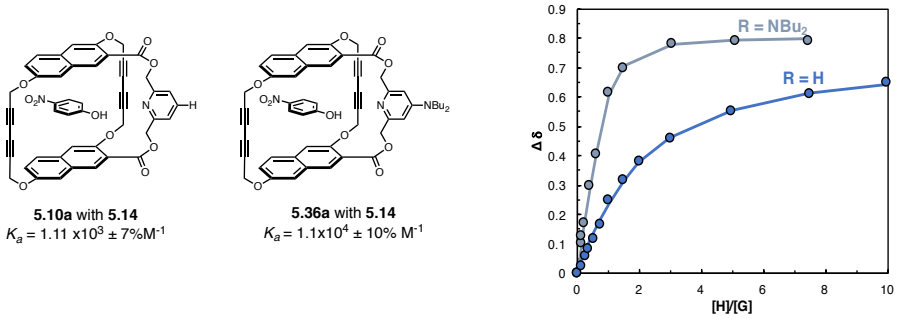

Figure 5.7 Comparison of binding affinity in $CDCl_3$ between host **5.10a** and host **5.36a** with guest 4-nitrophenol **5.14**.

We found that increasing the basicity of the pyridine is a tool to increase the binding affinity of these hosts (**5.10a** → **5.36a**) with pentafluorophenol **5.15**. However, this modification also increases the binding affinity to 4-nitrophenol **5.14**. Our initial hypothesis about pK_a matching to increase hydrogen bonding strength also did not appear to hold in this system. As we were ultimately interested in high-affinity hosts selective for perfluorinated aromatic guests, we sought alternative explanations for the lower binding affinity of perfluorinated aromatics compared to 4-nitrophenol **5.14** with hosts **5.10a** and **5.36a**.

We next considered the size of fluorine compared to hydrogen. The van der Waals radius of fluorine is larger than that of hydrogen (1.47 Å vs. 1.20 Å); as such, perfluoroaromatics are longer and wider than their non-fluorinated aromatic counterparts (Figure 5.8). With this in mind, we considered whether the naphthalene cavity was large enough to accommodate pentafluorophenol **5.15**. Dr. Gina Lee computationally modeled **5.10a** bound to 4-nitrophenol **5.14** and pentafluorophenol **5.15**. From the ball-and-stick structure and the space-filling model, it is evident that the perfluorinated guest does not sit symmetrically in the naphthalene cavity due to repulsive interactions with the diyne side linkers. Given the van der Waals radii of fluorine and carbon (1.7 Å), 3.2 Å spacing would be required for minimal overlap between the fluorine atoms of the guest and the host. Since the pentafluorophenol **5.15** guest is too large to fully enter

the cavity of **5.10a**, the hydrogen bond between the guest and the host is longer (3.04 Å vs 2.48 Å) and weaker for **5.15** than **5.14** (see alternate side view, Figure 5.8). Further improvements to address this size discrepancy will be described in Chapter 6.

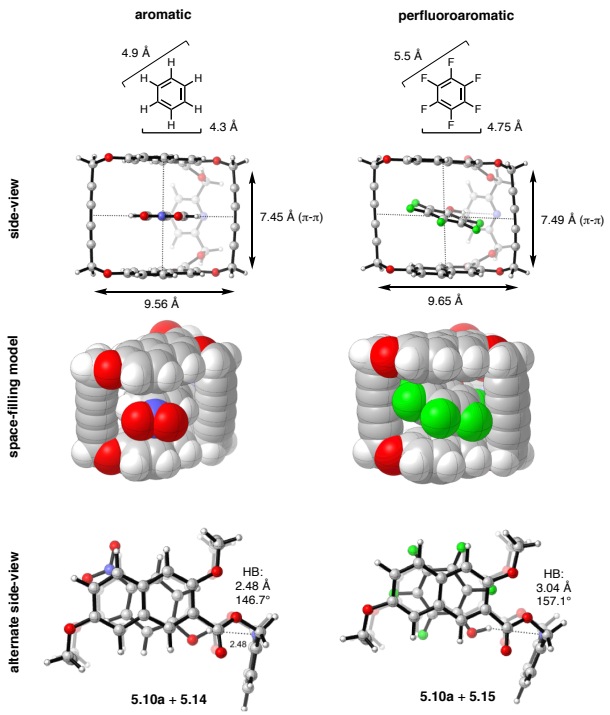

Figure 5.8 Examination of cavity size as a limiting factor for the binding interaction between host **5.10a** and pentafluorophenol **5.15**. Computational modeling was performed by Dr. Gina Lee (B3LYP-d3/6-31G(d)).

5.4 Conclusion

In summary, Whitlock's host **5.10a** was synthesized and repurposed to explore arene-perfluoroarene interactions in host-guest systems. Pentafluorophenol **5.15** was investigated as a model perfluorinated aromatic guest capable of both π-π interactions and hydrogen bonding with the host. Though pentafluorophenol **5.15** is also electron-poor, we found that **5.10a** binds 4-nitrophenol **5.14** with a higher binding affinity than **5.15**. Modification to host **5.10a**, such as increasing the basicity of the host in the form of host **5.23a**, did increase the binding affinity to

pentafluorophenol **5.15** by an order of magnitude. However, selectivity for **5.15** was not observed over other possible aromatic guests. At this point, it seems that a naphthalene-based system is too narrow to accommodate the width of perfluorinated guests like **5.15**. If the guest is too wide, it cannot completely enter the cavity of host **5.10a** or **5.36a**, and the full strength of the hydrogen bonding interaction cannot be realized. Though these naphthalene-based cyclophanes are not the ideal hosts for perfluorinated aromatic guests, they could be repurposed for other electron-poor phenols described by Whitlock or electron-deficient triazines, tetrazines, and dihydrotetrazines. Azoles, which are smaller than pentafluorophenol, could also be screened as possible guests for host **5.36a** for bioorthogonal complexation in the future (Figure 5.9).

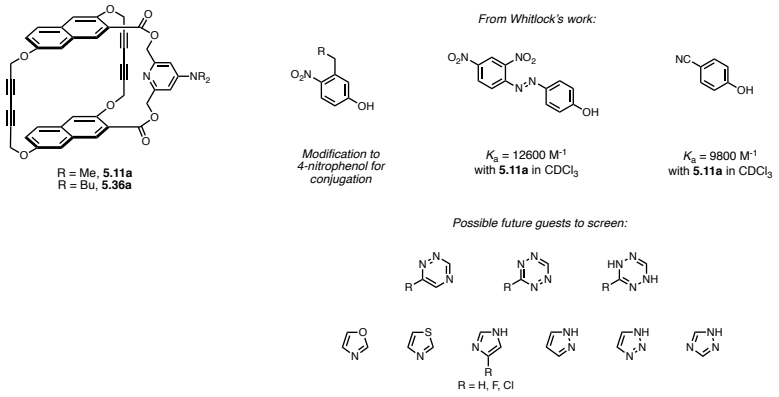

Figure 5.9 Alternative known and hypothesized guests for host **5.11a** or **5.36a**.

5.5 Experimental procedures

Chemical reagents were purchased from Sigma-Aldrich, Alfa Aesar, Fisher Scientific, Acros Organics, Synquest, or TCI and used without purification unless noted otherwise. Anhydrous dimethyl sulfoxide (DMSO) was obtained from a Sure-Seal™ bottle (Aldrich). Anhydrous and deoxygenated solvents dichloromethane (DCM), dimethylformamide (DMF), acetonitrile (MeCN), methanol (MeOH), and tetrahydrofuran (THF) were dispensed from a Grubb's-type Phoenix Solvent Drying System. Thin layer chromatography was performed using Silica Gel 60 F_{254} (EMD Millipore) plates. Flash chromatography was executed with technical grade silica gel with 60 Å pores and 40–63 μm mesh particle size (Sorbtech Technologies). Solvent was removed under reduced pressure with a Büchi Rotovapor with a Welch self-cleaning dry vacuum pump and further dried with a Welch DuoSeal pump. Bath sonication was performed using a Branson 3800 ultrasonic cleaner. NMR spectra were recorded on Bruker AV-500 (^{1}H and ^{13}C) and AV-400 (^{1}H, ^{13}C, and ^{19}F) instruments and processed with MestReNova software. NMR peaks are calibrated using residual undeuterated solvent ($CHCl_3$ at 7.26 ppm ^{1}H NMR, 77.16 ppm ^{13}C NMR). Masses for analytical measurements were taken on a Sartorius MSE6.6S-000-DM Cubis Micro Balance. HRMS (electrospray ionization (ESI)) were collected on a Thermo Scientific Q Exactive™ Plus Hybrid Quadrupole-Orbitrap™ with Dionex UltiMate 3000 RSLCnano System and LRMS (electrospray ionization (ESI)) were collected on an Agilent 1260 Infinity II HPLC-tandem MS system.

5.5.1 General host-guest titration/K_a determination procedures

The host was measured on an analytical microbalance. Host stock solutions were prepared with basified $CDCl_3$. Concentrations of host stock solutions were made below the solubility limit of the host. Guest stock solutions were prepared in basified $CDCl_3$. Preliminary

titrations and the Bindsim program (http://app.supramolecular.org/bindsim/) were used to determine the approximate equivalents of guest needed for saturation. Binding data were fit using Bindfit (http://app.supramolecular.org/bindfit/).[24,25]

5.5.2 Synthetic experimental procedures

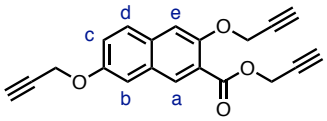

5.17a

Prop-2-yn-1-yl 3,7-bis(prop-2-yn-1-yloxy)-2-naphthoate (5.17a). In a 250 mL flask, 3,7-dihydroxy-2-naphthoic acid **5.16a** (4.15 g, 20.3 mmol, 1.00 equiv), K_2CO_3 (9.5 g, 69 mmol, 3.4 equiv) were dissolved in anhydrous DMF (65 mL, 0.31 M) and stirred for 10 min. Propargyl bromide (80 wt% in toluene, 7.6 mL, 69 mmol, 3.4 equiv) was added. After 22 h, the reaction was filtered and DMF was removed. The crude material was passed through a SiO_2 plug (60% $CHCl_3$/hexanes) and then repeatedly crystallized from $CHCl_3$/heptane to yield the product **5.17a** as a pale yellow crystalline solid (3.15 g, 9.88 mmol, 49% yield). R_f = 0.63 in 40% EtOAc/hexanes. ^{1}H NMR (400 MHz, Acetone-d_6): δ 8.25 (s, 1H, H_a), 7.83 (d, J = 9.0 Hz, 1H, H_e), 7.56 (s, 1H, H_b), 7.50 (d, J = 2.6 Hz, 1H, H_c), 7.29 (dd, J = 9.0, 2.6 Hz, 1H, H_d), 4.98 (d, J = 2.5 Hz, 2H), 4.94 (s, 2H), 4.92 (d, J = 2.4 Hz, 2H), 3.16 – 3.06 (m, 3H). ^{13}C NMR (101 MHz, Acetone-d_6): δ 165.4, 155.9, 153.0, 132.4, 131.9, 129.7, 129.2, 123.4, 122.3, 110.7, 109.2, 79.5, 79.5, 79.0, 77.4, 77.2, 76.5, 57.4, 56.5, 52.9. HRMS (ESI) calcd. for $C_{20}H_{14}O_4Na$ $(M+Na)^+$ 341.0784; found 341.0816.

3,7-bis(prop-2-yn-1-yloxy)-2-naphthoic acid (5.20). In a 100 mL flask equipped with a reflux condenser, **5.17a** (1.88 g, 5.90 mmol, 1.0 equiv) and KOH (511 mg, 9.11 mmol, 1.54 equiv)

were dissolved in THF:H_2O (12 mL:8.5 mL). The reaction was monitored for disappearance of starting material. After 2.5 h, additional KOH (50 mg) was added. After 1 h more, full conversion was observed by TLC and the reaction was cooled to RT. The reaction was diluted with EtOAc and 1M HCl was added. The organic layer was separated, and the aqueous was washed with EtOAc (2x more). The organic layers were dried ($MgSO_4$), filtered, and concentrated to obtain the product **5.20** as a pale yellow solid (1.61 g, 5.74 mmol, 97% yield). ^{1}H NMR (500 MHz, $CDCl_3$): δ 8.71 (s, 1H), 7.73 (d, J = 8.8 Hz, 1H), 7.38 (s, 1H), 7.37 – 7.29 (m, 2H), 5.02 (d, J = 2.4 Hz, 2H), 4.81 (d, J = 2.4 Hz, 2H), 2.68 (t, J = 2.4 Hz, 1H), 2.57 (t, J = 2.4 Hz, 1H). ^{13}C NMR (126 MHz, $CDCl_3$): δ 165.2, 155.4, 151.3, 135.2, 132.2, 129.7, 128.5, 122.9, 118.8, 109.2, 108.7, 78.1, 78.1, 76.9, 76.5, 76.3, 57.8, 56.1.

Perfluorophenyl 3,7-bis(prop-2-yn-1-yloxy)-2-naphthoate (5.21). In a 100 mL flask, **5.20** (716 mg, 2.55 mmol, 1.00 equiv) was dissolved in anhydrous DMF (11 mL, 0.23 M), and DIPEA (0.66 mL, 3.8 mmol, 1.5 equiv) was added. The reaction mixture was cooled to 0 °C, and pentafluorophenyl trifluoroacetate (0.66 mL, 3.8 mmol, 1.5 equiv) was added slowly. The reaction was let warm to RT and stopped after 1.5 h. DMF was removed under a stream of compressed air. The crude reaction mixture was suspended in DCM, filtered, and washed with additional DCM and hexanes. The precipitate **5.21** was collected as a pale yellow solid (638 mg, 1.43 mmol, 56% yield). The filtrate could be further purified by column chromatography (20%→ 40% DCM/hexanes) to yield additional clean material **5.21** (in total 1.13 g, 2.53 mmol, quantitative). Alternatively, the crude **5.21** could be dried and used directly in the next reaction. R_f = 0.57 in 20% EtOAc/hexanes.^{1}H NMR (500 MHz, DMSO-d_6): δ 8.60 (s, 1H), 7.89 (d, J = 9.0 Hz, 1H), 7.67 (s, 1H), 7.62 (d, J = 2.6 Hz, 1H), 7.39 (dd, J = 9.0, 2.6 Hz, 1H), 5.01 (d, J = 2.4

Hz, 2H), 4.92 (d, J = 2.4 Hz, 2H), 3.64 (t, J = 2.3 Hz, 1H), 3.62 (t, J = 2.3 Hz, 1H). ^{13}C NMR (126 MHz, DMSO-d_6): δ 160.9, 154.5, 151.8, 132.7, 132.1, 128.4, 128.1, 122.5, 117.8, 109.9, 108.8, 79.0, 78.8, 78.7, 78.6, 56.6, 55.7. ^{19}F NMR (376 MHz, DMSO-d_6): δ -153.0 – -153.4 (m), -157.7 (t, J = 23.2 Hz), -162.3 – -162.6 (m).

Note: **5.21** was stable upon storage under N_2 at 4 °C for multiple months.

Pyridine-2,6-diylbis(methylene) bis(3,7-bis(prop-2-yn-1-yloxy)-2-naphthoate) (5.23). In a 25 mL flask, **5.21** (888 mg, 1.99 mmol, 2.49 equiv), pyridine diol **5.22** (111 mg, 0.798 mmol, 1.00 equiv), DMAP (25 mg, 0.20 mmol, 0.26 equiv) were dissolved in anhydrous DMF (6.1 mL, 0.13 M). DIPEA (300 µL, 1.72 mmol, 2.16 equiv) was added. Additional DIPEA was added over 3 days, at which point the DMF was removed. The crude product was suspended in MeCN and filtered, rinsing with additional MeCN. The precipitate was suspended in EtOH, sonicated, and filtered to yield the product **5.23** as an off-white solid (344 mg, 0.518 mmol, 65% yield). R_f = 0.58 in 20% acetone/toluene. ^{1}H NMR (400 MHz, $CDCl_3$): δ 8.35 (s, 2H), 7.78 (t, J = 7.8 Hz, 1H), 7.73 – 7.64 (m, 2H), 7.54 (d, J = 7.8 Hz, 2H), 7.33 (s, 2H), 7.27-7.25 (m, 4H), 5.55 (s, 4H), 4.87 (d, J = 2.4 Hz, 4H), 4.78 (d, J = 2.4 Hz, 4H), 2.56-2.54 (m, 4H). ^{13}C NMR (101 MHz, $CDCl_3$): δ 165.8, 156.0, 154.9, 152.6, 137.7, 132.4, 131.8, 128.9, 128.4, 122.3, 121.8, 121.0, 109.9, 108.4, 78.5, 78.4, 76.2, 76.0, 67.4, 57.1, 56.1.

4-H-pyridine naphthalene host (5.10):

In a 500 mL flask, $Cu(OAc)_2$ (2.75 g, 15.1 mmol, 12.6 equiv) was dissolved in pyridine (75 mL) and heated to 45 °C. Prehost **5.23** (797 mg, 1.20 mmol, 1.00 equiv) was dissolved in pyridine (93 mL) and added to the $Cu(OAc)_2$ solution via cannula transfer over 30 min. After 3.5 h, no starting material was observed by TLC. The pyridine was removed, and crude reaction was suspended in $CHCl_3$ and filtered. The filtrate was washed with 1 M HCl and sat. NH_4Cl (2x). The organic layer was dried ($MgSO_4$) and filtered. The crude was evaporated onto SiO_2 from $CHCl_3$ and purified by column chromatography (silica gel, 5%→10%→50% acetone/toluene→100% acetone). Both isomers of the host were obtained.

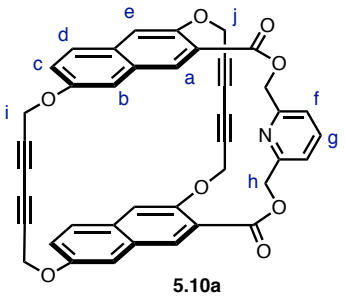

Isomer 1 (meso) 10a: The structure of isomer 1 was confirmed to be the meso isomer by x-ray crystallography. Isomer 1 **10a** was isolated as an off-white solid (152 mg, 0.241 mmol, 20% yield). R_f = 0.41 in 20% acetone/toluene. ^{1}H NMR (400 MHz, $CDCl_3$): δ 8.20 (s, 2H, H_a), 7.82 (t, J = 7.7 Hz, 1H, H_g), 7.62 – 7.54 (m, 2H), 7.50 (d, J = 7.7 Hz, 2H, H_f), 7.27 (s, 2H, H_b), 7.15 – 7.06 (m, 4H), 5.54 (ABq, J_{AB} = 12.0 Hz, 4H, H_j), 4.93 (ABq, J_{AB} = 16.0 Hz, 4H), 4.87 (ABq, J_{AB} = 16.0 Hz, 4H). HRMS (ESI) calcd. for $C_{41}H_{26}NO_8$ $(M+H)^+$ 660.1653; found 660.1701.

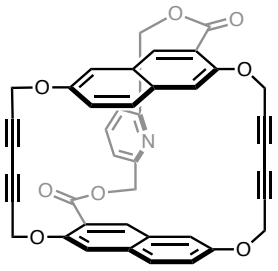

5.10b

Isomer 2 (dl) 5.10b: 5.10b was an off-white solid (80 mg, 0.12 mmol, 10%). R_f = 0.29 in 20% acetone/toluene. ^{1}H NMR (500 MHz, $CDCl_3$): δ 8.26 (s, 2H), 7.89 (t, J = 7.7 Hz, 1H), 7.67 – 7.48 (m, 4H), 7.17 – 6.98 (m, 4H), 5.73 (d, J = 11.5 Hz, 4H), 5.16 (d, J = 11.5 Hz, 4H), 5.00 (ABq, J_{AB} =17.5 Hz, 4H), 4.83 (s, 4H). HRMS (ESI) calcd. for $C_{41}H_{26}NO_8$ $(M+H)^+$ 660.1653; found 660.1697.

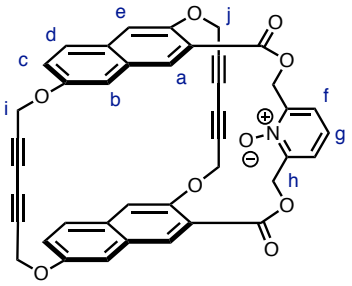

5.28a

Naphthalene-pyridine-*N*-oxide-meso host (5.28a). In a 100 mL pear flask, **5.10a** (33.4 mg, 0.051 mmol, 1.00 equiv) was suspended in basified $CHCl_3$ (29 mL, 1.8 mM) and heated to 40 °C. mCPBA (15.3 mg, 0.089 mmol, 1.75 equiv) was added in portions, and the opaque solution became more transparent. After 17 h, additional mCPBA (10 mg) was added. After 2 days, the reaction was quenched with 10% Na_2SO_3. The organic layer was separated, washed with saturated sodium bicarbonate, and dried ($MgSO_4$). The crude product was evaporated onto basic alumina and purified by column chromatography (basic alumina, 80% EtOAc/hexanes→100% EtOAc→1% MeOH/EtOAc). The product **5.28a** was isolated as a solid (14.8 mg, 0.022 mmol,

43% yield). R_f = 0.26 in 5% MeOH/DCM. ^{1}H NMR (500 MHz, $CDCl_3$): δ 8.30, (s, 2H, H_a), 7.73 (d, J = 7.9 Hz, 2H, H_f), 7.55 (d, J = 8.9 Hz, 2H, H_c), 7.28 (t, J = 7.9 Hz, 1H, H_g), 7.22 (s, 2H, H_b), 7.16 (d, J = 2.6 Hz, 2H, H_e), 7.11 (dd, J = 8.8, 2.6 Hz, 2H, H_d), 5.68 – 5.56 (m, 4H, H_h), 4.99 – 4.77 (m, 8H, $H_{i/j}$). LRMS (ESI) calc. for $C_{41}H_{26}NO_9$ $(M+H)^+$ 676.1602; found 676.2.

Naphthalene-diester-meso host (5.29a). 5.10a (21.9 mg, 0.0332 mmol, 1.00 equiv) was suspended in absolute EtOH (15 mL, 2.2 mM) in a 50 mL flask equipped with a reflux condenser. Conc. H_2SO_4 (1.5 mL) was added, and the reaction was heated to 80 °C. After 16 h, the reaction was cooled to RT. $CHCl_3$ and water were added. The organic layer was separated and the aqueous layer was extracted with $CHCl_3$ (2x more). The combined organic layers were dried (Na_2SO_4), filtered, and concentrated. The crude material was evaporated onto SiO_2 and purified by column chromatography (silica gel, 40% →60%→80% EtOAc/hexanes→100% EtOAc). The product **5.29a** was isolated as a solid (7.7 mg, 0.013 mmol, 38% yield). R_f = 0.77 in 50% EtOAc/hexanes. ^{1}H NMR (500 MHz, Acetone-d_6): δ 8.06 (s, 2H), 7.64 (d, J = 9.0 Hz, 2H), 7.42 (s, 2H), 7.38 (d, J = 2.6 Hz, 2H), 7.16 (dd, J = 9.0, 2.6 Hz, 2H), 5.09 (d, J = 15.1 Hz, 8H), 4.31 (q, J = 7.1 Hz, 4H), 1.35 (t, J = 7.1 Hz, 6H). HRMS (ESI) calc. for $C_{38}H_{29}O_8$ $(M+H)^+$ 613.1857; found 613.1889.

Dimethyl 4-chloropyridine-2,6-dicarboxylate (5.31). Based on a modified literature procedure,[26] chelidamic acid **5.30** (5.0 g, 27 mmol, 1.0 equiv) was dissolved in $CHCl_3$ (60 mL, 0.45 M) in a flame-dried 500 mL flask attached to a reflux condenser. PCl_5 (25 g, 120 mmol, 4.4 equiv) was added slowly, and the reaction was heated to reflux. The reaction was monitored by LCMS. After 3 days, the reaction was cooled to 0 °C and a base trap was attached. Anhydrous

MeOH (30 mL) was added and the reaction was stirred for 1 day. Sat. aqueous sodium bicarbonate was added to the reaction while stirring. The layers were separated and the aqueous layer was extracted with $CHCl_3$ (3x). The crude material was evaporated onto SiO_2 and purified by column chromatography (30%→50%→70% EtOAc/hexanes). The product **5.31** was isolated as a white solid (2.52 g, 11.0 mmol, 41% yield). R_f = 0.53 in 50% EtOAc/hexanes ^{1}H NMR (500 MHz, DMSO-d_6): δ 8.32 (s, 2H), 3.93 (s, 3H). The spectral data were consistent with the literature report. Small amounts of dimethyl 4-methoxypyridine-2,6-dicarboxylate and dimethyl 4-hydroxypyridine-2,6-dicarboxylate were observed by mass with, but could be easily separated from the product.

Dimethyl 4-(dibutylamino)pyridine-2,6-dicarboxylate (5.33). To three 30 mL microwave vials was added **5.31** (350 mg, 1.52 mmol, 1.00 equiv), dibutyl amine (7 mL, 42 mmol, 28 equiv), and water (7 mL, 0.22 M) per vial. The reaction was heated in the microwave to 160 °C for 30 min at 300W. The three vials were combined (4.57 mmol SM total), and the aqueous layer was extracted with EtOAc (4x). The organic layer was concentrated and placed on high vacuum until the crude diacid **5.32** was a powdery solid. The crude was dissolved in THF/MeOH (50 mL:15 mL). Trimethylsilyldiazomethane (2M in hexanes, 9.2 mL, 18.4 mmol, 4.0 equiv) was added slowly. Additional trimethylsilyldiazomethane (2 mL) was added after 17 h. Once esterification was complete as observed by LCMS, the reaction was poured in H_2O and extracted with EtOAc (4x). The organics were dried ($MgSO_4$), filtered, and concentrated to a yellow solid. The crude was evaporated onto SiO_2 and purified by column chromatography (30%→40%→50%→60% EtOAc/hexanes). The product **5.33** was isolated as a white solid (1.02 g, 3.16 mmol, 69% yield). R_f = 0.37 in 50% EtOAc/hexanes. ^{1}H NMR (500 MHz, $CDCl_3$): δ

7.45 (s, 2H), 3.98 (s, 6H), 3.44 – 3.30 (m, 4H), 1.64 – 1.55 (m, 4H), 1.39 (h, J = 7.4 Hz, 4H), 0.98 (t, J = 7.4 Hz, 6H). ^{13}C NMR (126 MHz, $CDCl_3$): δ 166.5, 154.3, 148.6, 110.2, 53.2, 50.4, 29.1, 20.3, 14.0. HRMS (ESI) calcd. for $C_{17}H_{27}N_2O_4$ $(M+H)^+$: 323.1966; found 323.2135.

(4-(dibutylamino)pyridine-2,6-diyl)dimethanol (5.34). In a 100 mL flame-dried flask equipped with a reflux condenser, **5.33** (611 mg, 1.90 mmol, 1.00 equiv) and $NaBH_4$ (300 mg, 7.93 mmol, 4.17 equiv) were suspended in anhydrous THF (10 mL, 0.19 M), and the reaction was heated to reflux. After 22 h, the reaction was cooled to RT and H_2O (20 mL) was added slowly while stirring. The reaction mixture was poured into a sep funnel, and the aqueous was extracted with 5% MeOH/DCM (3x). The opaque organic layer was dried ($MgSO_4$), filtered, and concentrated. The crude was dried extensively to yield the product **5.34** as a white solid (495 mg, 1.86 mmol, 98% yield). R_f = 0.33 in 8:1.5:1 EtOAc/MeOH/H_2O. ^{1}H NMR (500 MHz, DMSO-d_6): δ 6.51 (s, 2H), 5.15 (s, 2H), 4.35 (s, 4H), 3.33 (s, 1H), 3.32 – 3.23 (m, 4H), 1.57 – 1.44 (m, 4H), 1.32 (h, J = 7.4 Hz, 4H), 0.92 (t, J = 7.3 Hz, 6H). ^{13}C NMR (126 MHz, DMSO-d_6): δ 160.8, 153.3, 100.4, 64.3, 49.2, 28.9, 19.6, 13.8. HRMS (ESI) calcd. for $C_{17}H_{27}N_2O_4$ $(M+H)^+$: 267.2067; found 267.2076.

(4-(dibutylamino)pyridine-2,6-diyl)bis(methylene) bis(3,7-bis(prop-2-yn-1-yloxy)-2-naphthoate) (5.35). In a 50 mL flask, naphthalene PFPester **5.21** (~1.1 g, 2.5 mmol, 2.5 equiv), diol **5.34** (266 mg, 1.00 mmol, 1.00 equiv), and DMAP (122 mg, 1.00 mmol, 1.00 equiv) were dissolved in anhydrous DMF (7.7 mL, 0.13 M). DIPEA (0.37 mL, 2.1 mmol, 2.1 equiv) was added. After 3 days, additional DMAP (50 mg) was added and the reaction was heated to 40 °C. The DMF was removed, and the crude product was evaporated onto SiO_2. The crude product was purified by column chromatography (silica gel, 20%→30%→45%→60%→80%

EtOAc/hexanes). The product **5.35** was isolated as a pale yellow solid (630 mg, 0.797 mmol, 80% yield). R_f = 0.37 in 40% EtOAc/hexanes. ^{1}H NMR (400 MHz, Acetone-d_6): δ 8.34 (s, 2H), 7.82 (d, J = 8.8 Hz, 2H), 7.54 (s, 2H), 7.47 (d, J = 2.5 Hz, 2H), 7.28 (dd, J = 9.0, 2.6 Hz, 2H), 6.74 (s, 2H), 5.35 (s, 4H), 4.94 (d, J = 2.4 Hz, 4H), 4.91 (d, J = 2.4 Hz, 4H), 3.46 – 3.34 (m, 4H), 3.10 (td, J = 2.4, 0.5 Hz, 4H), 1.57 (p, J = 7.5 Hz, 4H), 1.35 – 1.21 (m, 4H), 0.79 (t, J = 7.4 Hz, 6H). ^{13}C NMR (126 MHz, Acetone-d_6): δ 166.1, 156.9, 155.8, 154.9, 153.1, 132.3, 132.0, 129.8, 129.2, 124.1, 122.1, 110.8, 109.2, 103.6, 79.6, 79.5, 77.5, 77.2, 68.0, 57.5, 56.5, 50.7, one C under solvent peak, 20.7, 14.1. HRMS (ESI) calc. for $C_{49}H_{47}N_2O_8$ $(M+H)^+$ 791.3327; found 791.3533.

4-NBu$_2$-pyridine-naphthalene host (5.36). In a 250 mL flask, $Cu(OAc)_2$ (1.75 g, 9.64 mmol, 12.5 equiv) was dissolved in pyridine (60 mL) and heated to 45 °C. Prehost **5.35** (610 mg, 0.771 mmol, 1.00 equiv) was dissolved in pyridine (50 mL) and added to the $Cu(OAc)_2$ solution via addition funnel over 1.5 h. After 2 h more, pyridine was removed. The crude material was suspended in $CHCl_3$ and sat. NH_4Cl was added. The aqueous layer was extracted with $CHCl_3$ (2x more). The combined organic layers were washed with 1M HCl (1x) and brine (1x). The organic layers were dried ($MgSO_4$), filtered, and concentrated. The crude product was evaporated onto SiO_2 and purified by column chromatography (silica gel, 1:1:1 →1:2:2→1:5:5 hexanes/$CHCl_3$/EtOAc→$CHCl_3$→EtOAc→MeOH). Isomer 2 **5.36b** was isolated as a white powdery solid (133 mg, 0.169 mmol, 22% yield). Impure isomer 1 was isolated from the flushes. Some of this material was purified by preparatory thin layer chromatography (60% EtOAc/hexanes) and isomer 1 **5.36aa** was isolated as a white solid (20 mg, 0.025 mmol, 3% yield).

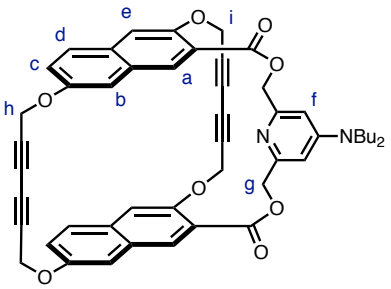

5.36a

Isomer 1 5.36a R_f = 0.42 in 1:1:1 hexanes/$CHCl_3$/EtOAc. ^{1}H NMR (500 MHz, $CDCl_3$): δ 8.20 (s, 2H, H_a), 7.57 (d, J = 8.6 Hz, 2H), 7.27 (s, 2H, H_b), 7.15 – 7.05 (m, 4H), 6.60 (s, 2H, H_f), 5.38 (ABq, J_{AB} = 10.0 Hz, 4H), 4.93 (ABq, J_{AB} = 15.0 Hz, 4H), 4.87 (ABq, J_{AB} = 20.0 Hz, 4H), 3.39 – 3.28 (m, 4H), 1.68 – 1.57 (m, 4H), 1.40 (h, J = 7.4 Hz, 4H), 0.99 (t, J = 7.3 Hz, 6H). ^{13}C NMR (126 MHz, $CDCl_3$): δ 165.6, 155.4, 154.1, 154.2, 152.3, 131.6, 131.5, 129.6, 128.6, 124.6, 121.8, 114.3, 107.9, 106.1, 74.1, 74.0, 71.1, 70.8, 68.4, 59.3, 55.0, 50.3, 29.3, 20.4, 14.1. HRMS (ESI) calc. for $C_{49}H_{43}N_2O_8$ $(M+H)^+$ 787.3014; found 787.3047.

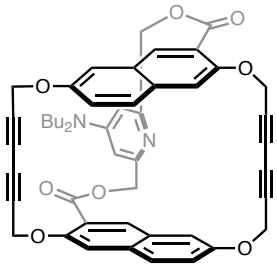

5.36b

Isomer 2 5.36b R_f = 0.61 in 1:1:1 hexanes/$CHCl_3$/EtOAc. ^{1}H NMR (400 MHz, DMSO-d_6): δ 8.33 (s, 2H), 7.63 (d, J = 9.0 Hz, 2H), 7.53 – 7.39 (m, 4H), 7.10 (dd, J = 9.0, 2.5 Hz, 2H), 6.81 (s, 2H), 5.37 (d, J = 11.5 Hz, 2H), 5.29 – 4.87 (m, 10H), 3.38 (t, J = 7.7 Hz, 4H), 1.57 (p, J = 7.6 Hz, 4H), 1.38 (h, J = 7.3 Hz, 4H), 0.96 (t, J = 7.3 Hz, 6H). ^{13}C NMR (101 MHz, DMSO-d_6): δ 164.0, 155.0, 153.5, 153.3, 150.6, 131.2, 130.8, 128.7, 127.7, 122.1, 121.6, 108.9, 107.9, 106.4,

76.0, 75.6, 70.2, 69.7, 68.0, 55.0, 49.2, one C under solvent peak, 28.8, 19.6, 13.9. HRMS (ESI) calc. for $C_{49}H_{43}N_2O_8$ $(M+H)^+$ 787.3014; found 787.3157.

5.5.3 NMR titrations

Complex of **5.10a** and **5.15** in $CDCl_3$ (mam-III-196)

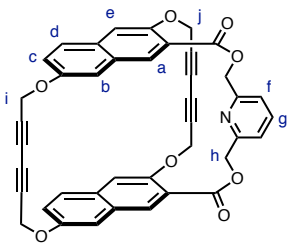

Host: **5.10a**

[H] = 0.61 mM

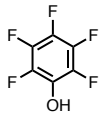

Guest: **5.15**

[G] = 0 - 61 mM

proton	K_a (bindfit)
a	48 ± 3%
g	47 ± 3%
global fitting	48 ± 2%

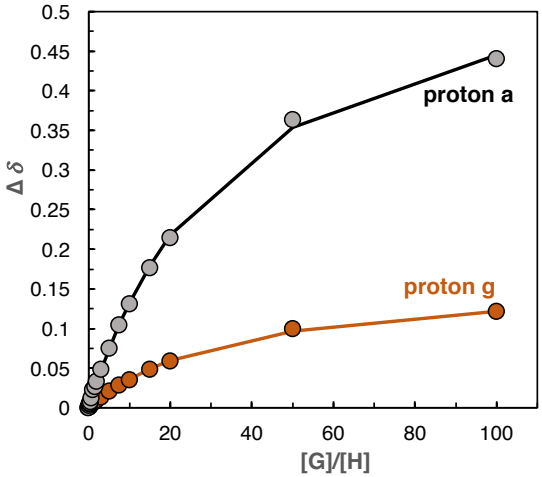

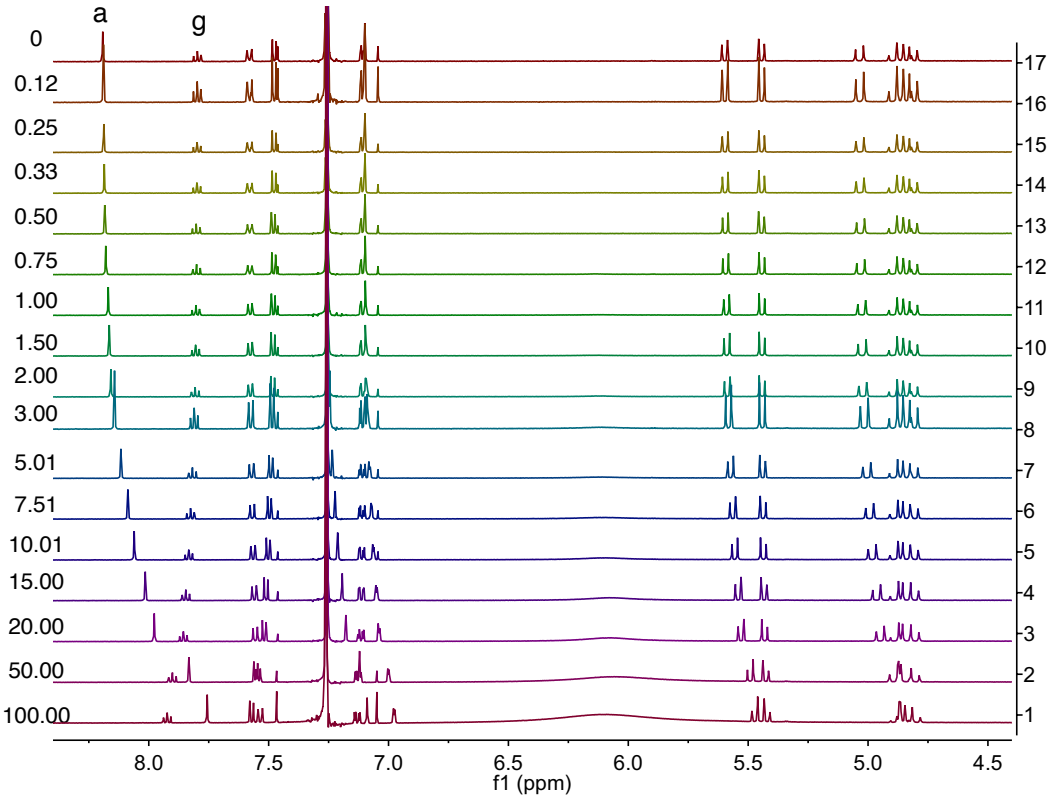

^{19}F NMR of complex of **5.10a** and **5.15** in $CDCl_3$, aligned with TFA external standards (mam-III-196)

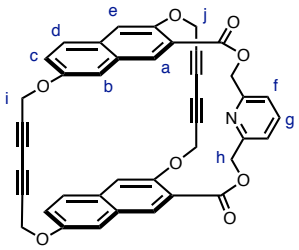

Host: **5.10a**

[H] = 0.61 mM

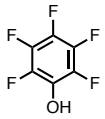

Guest: **5.15**

[G] = 0 - 61 mM

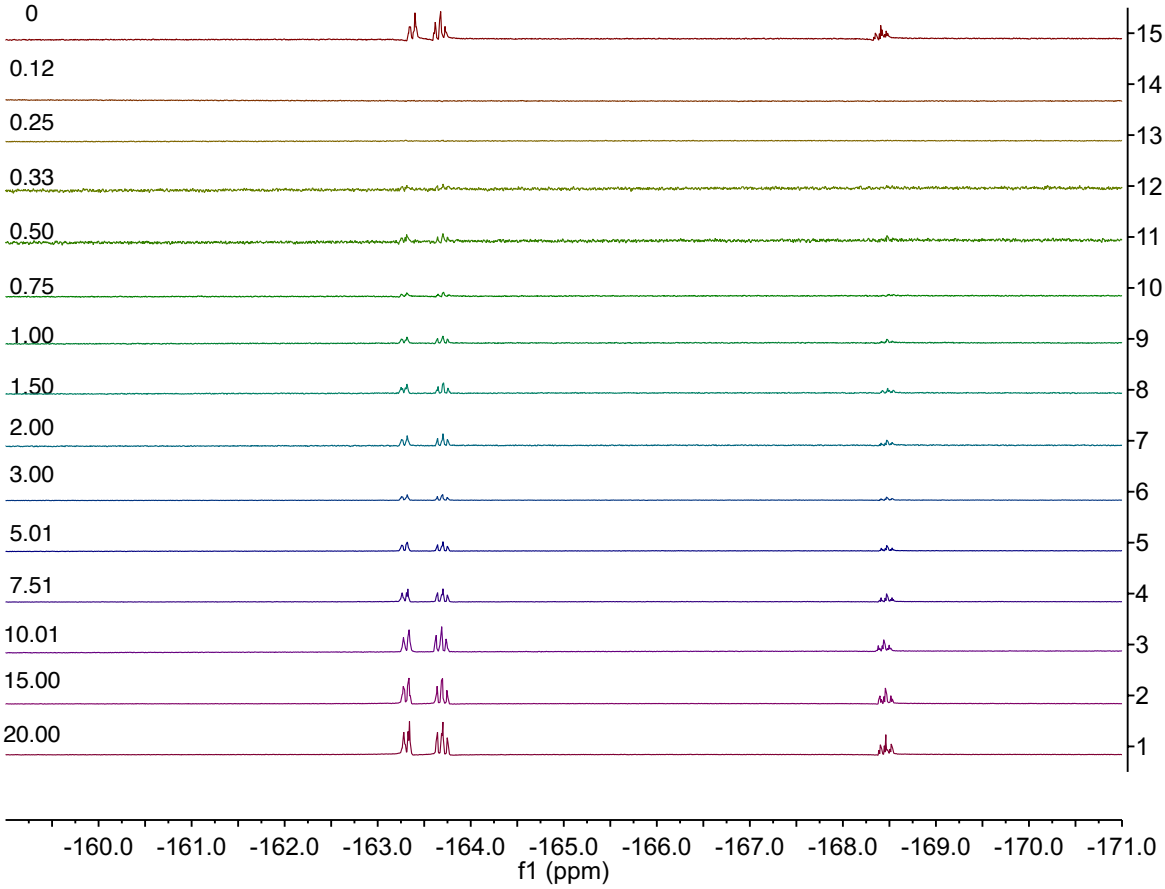

^{19}F NMR of complex of **5.15** and model hydrogen bond acceptors in $CDCl_3$, aligned with TFA external standards (mam-III-200)

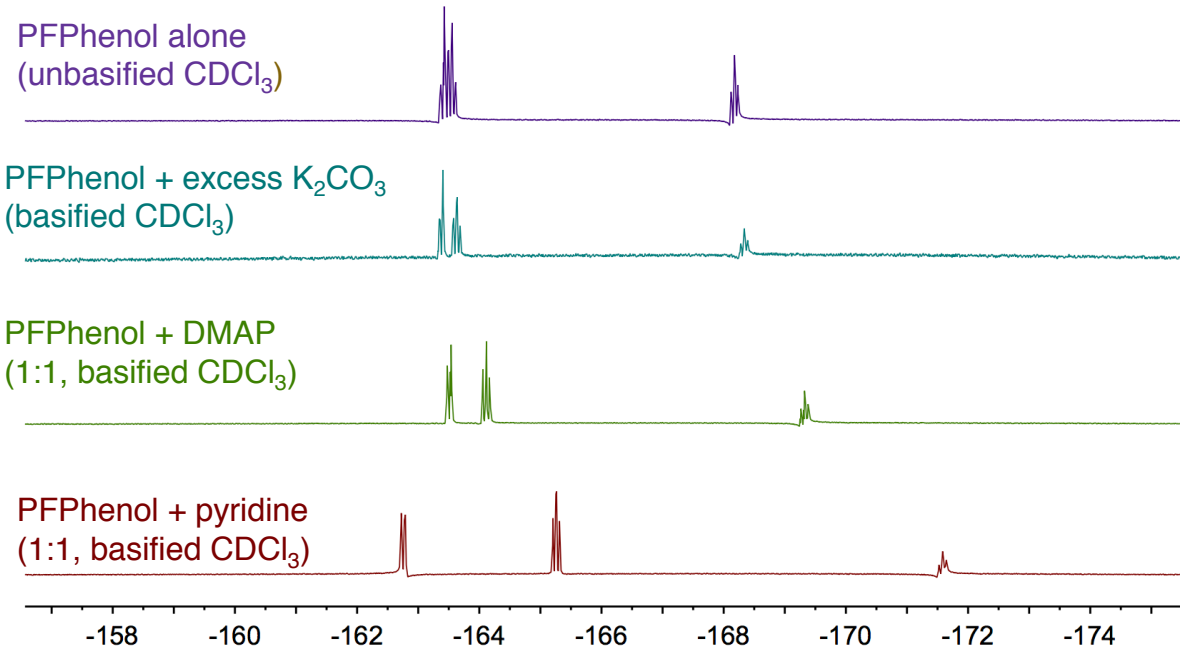

Complex of **5.10a** and **TFA** in $CDCl_3$ (mam-III-210)

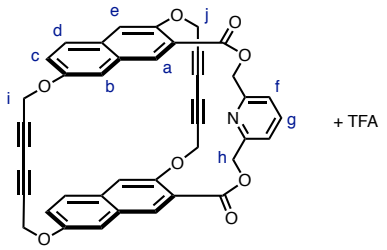

Host: **5.10a**

[H] = 0.61 mM

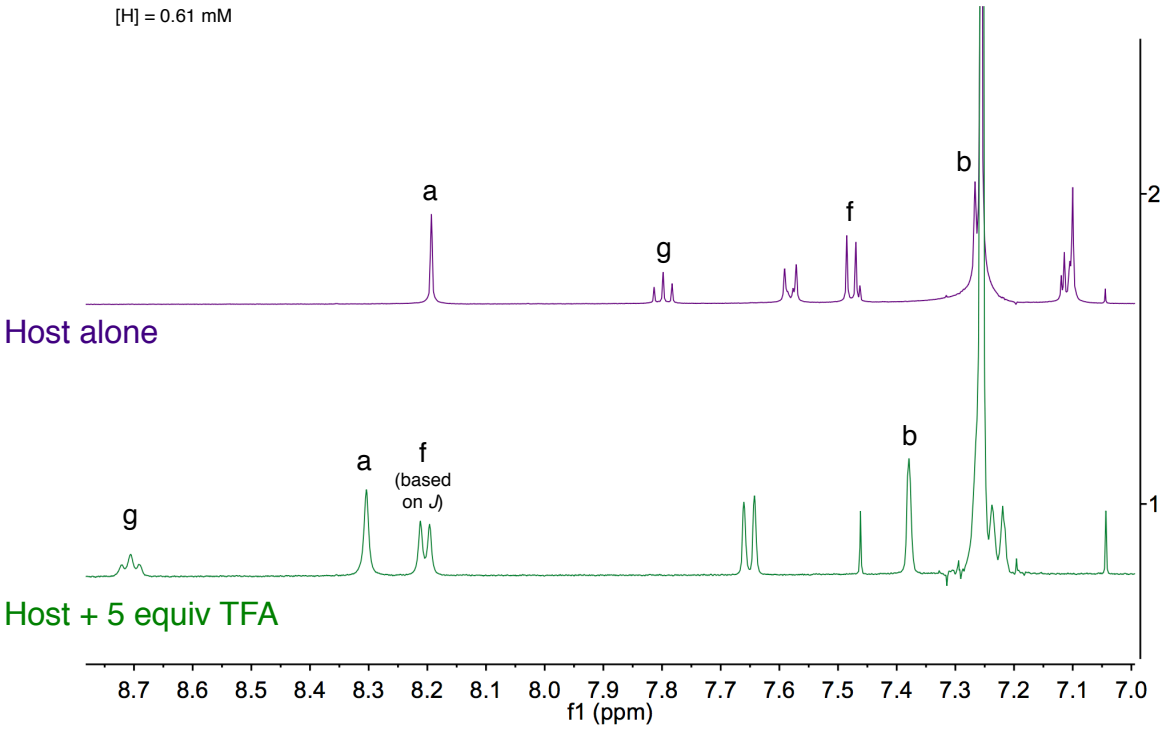

H_a and H_b shift opposite direction upon protonation compared to when bound to guest

Complex of **5.10a** and **5.14** in $CDCl_3$ (mam-III-175)

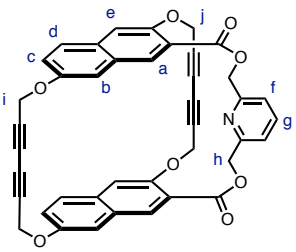

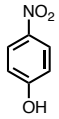

Host: **5.10a**

[H] = 0.61 mM

Guest: **5.14**

[G] = 0 - 6.1 mM

proton	K_a (bindfit)
a	1050 ± 7%
g	3907 ± 35%
global fitting	1117 ± 7%

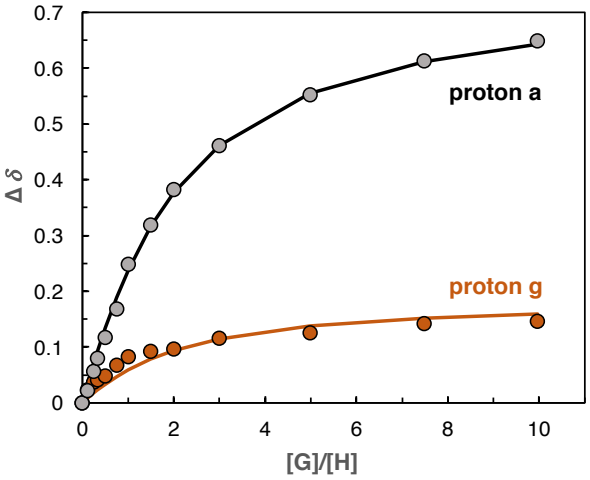

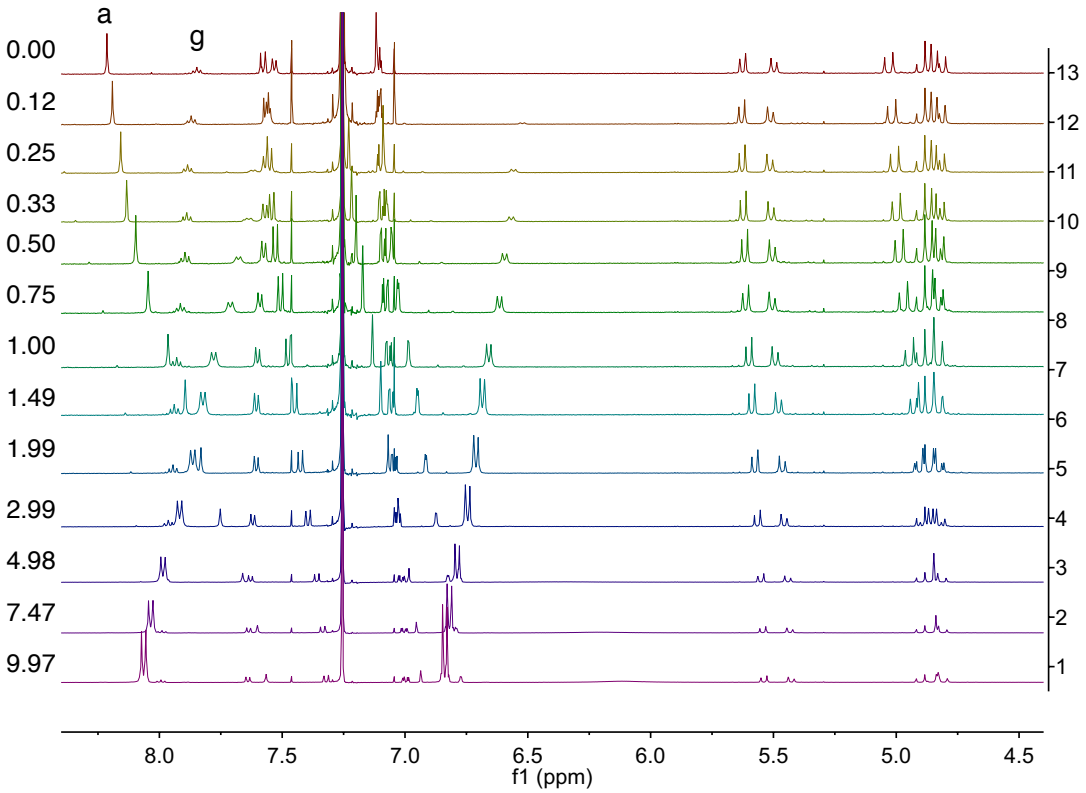

Complex of **5.10a** and **5.24** in $CDCl_3$ (mam-III-228)

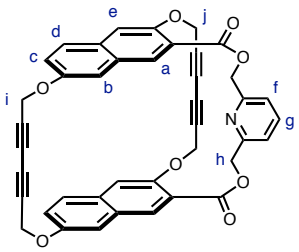

Host: **5.10a**

[H] = 0.61 mM

Guest: **5.24**

[G] = 0 - 60 mM

proton	K_a (bindfit)
a	72 ± 8%
g	Fails to fit
global fitting	72 ± 8%

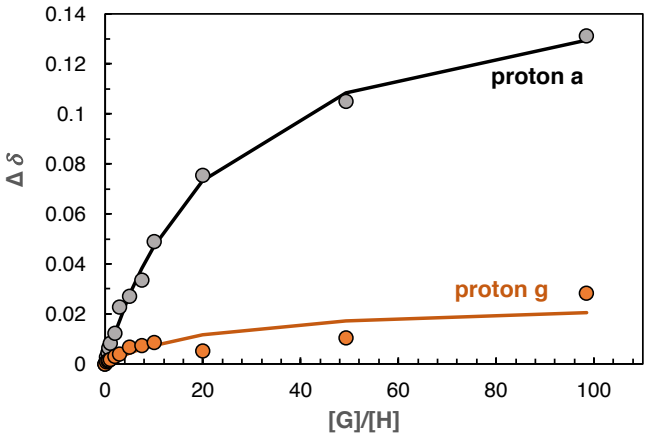

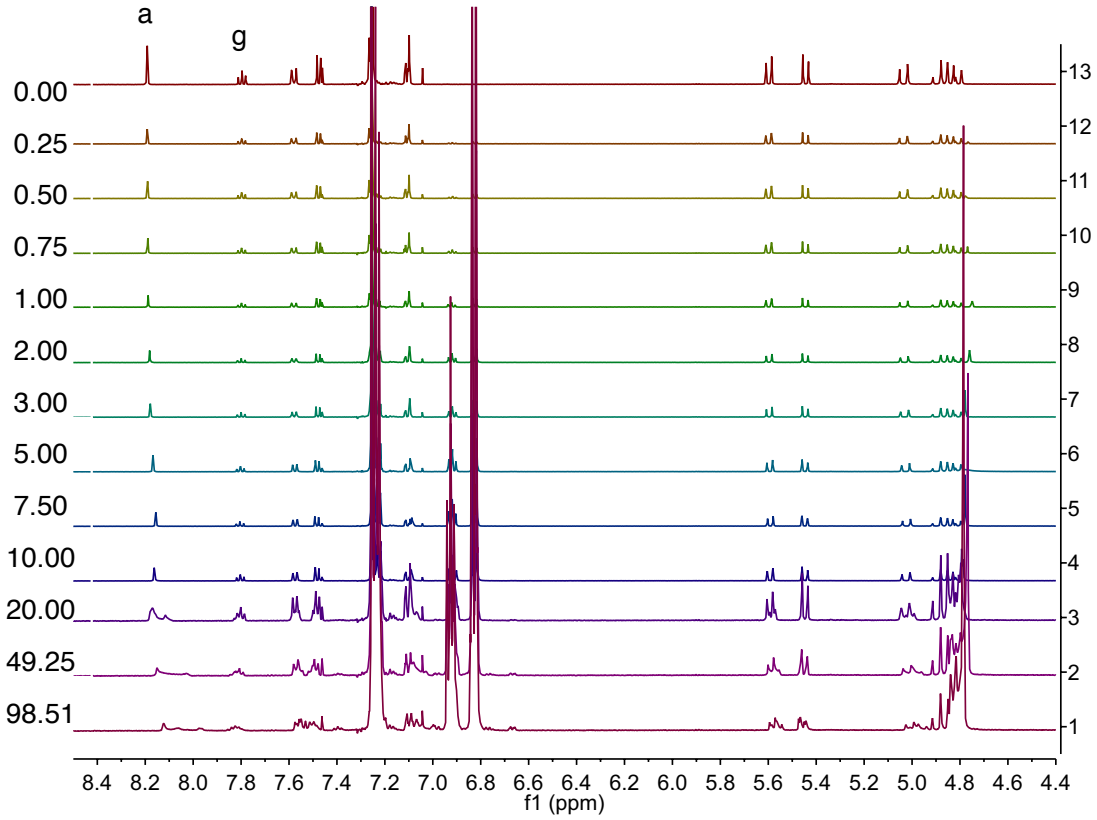

Complex of **5.10a** and **5.2** in $CDCl_3$ (mam-III-124)

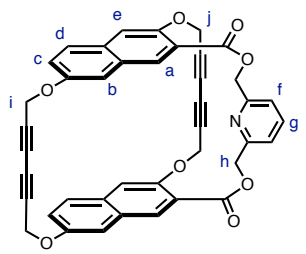

Host: **5.10a**

[H] = 1.36 mM

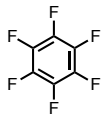

Guest: **5.2**

[G] = 0 - 6.8 mM

^{19}F NMR

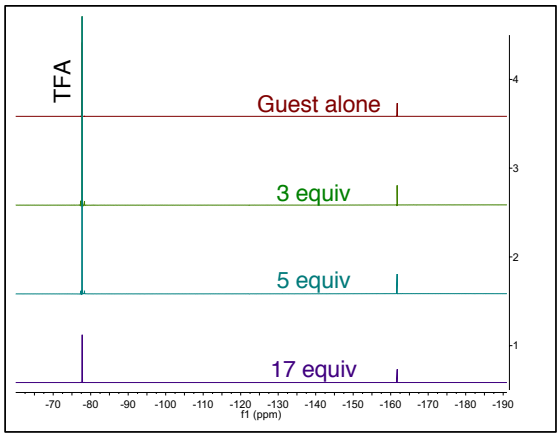

No observable binding up to 17 equiv

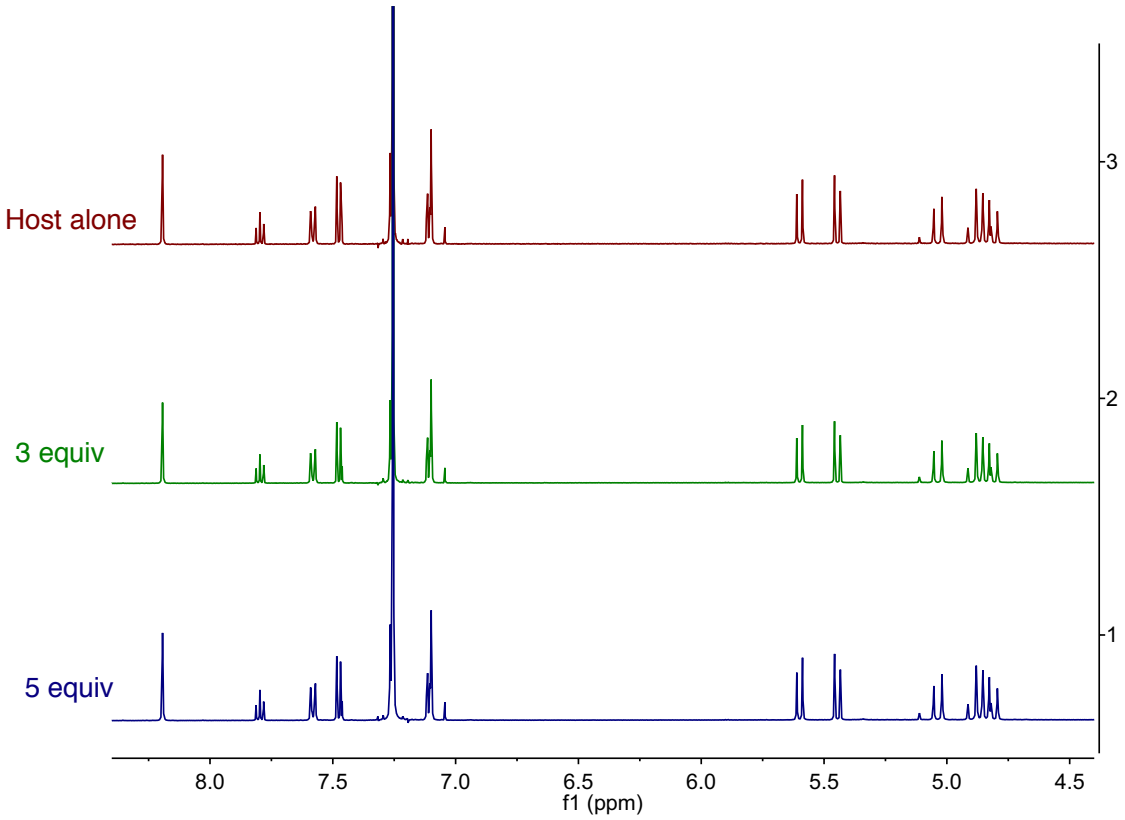

Complex of **5.10a** and **5.25** in $CDCl_3$ (mam-III-212)

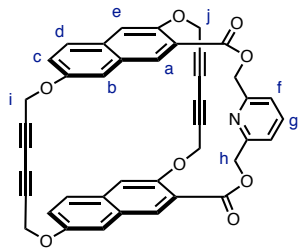

Host: **5.10a**

[H] = 0.61 mM

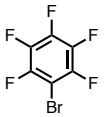

Guest: **5.25**

^{19}F NMR

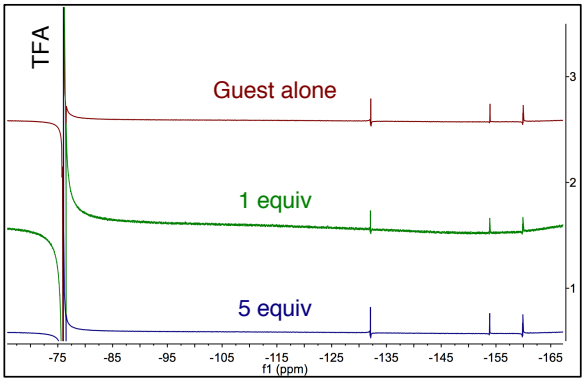

No observable binding up to 5 equiv

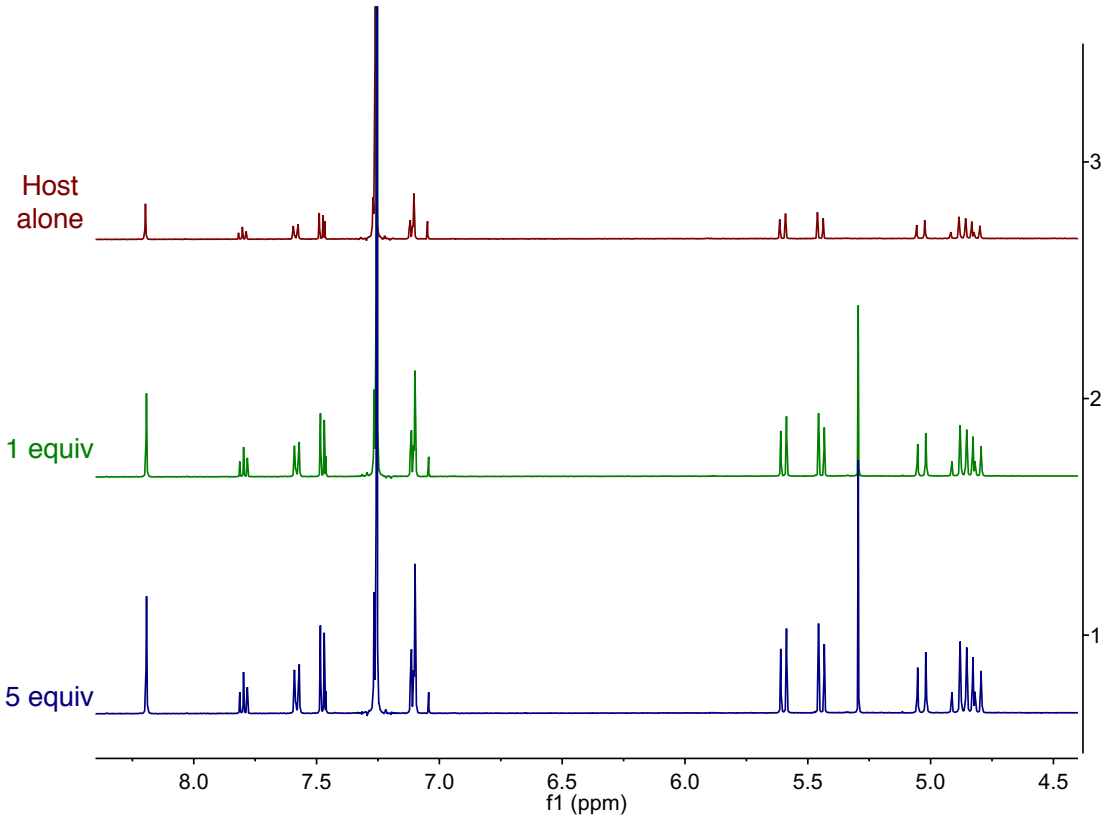

Complex of **5.10a** and **5.26** in $CDCl_3$ (mam-III-202)

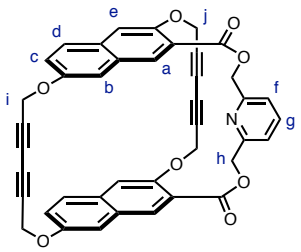

Host: **5.10a**

[H] = 0.61 mM

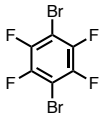

Guest: **5.26**

^{19}F NMR

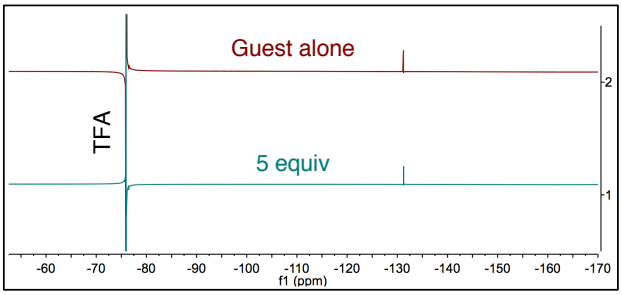

No observable binding up to 5 equiv

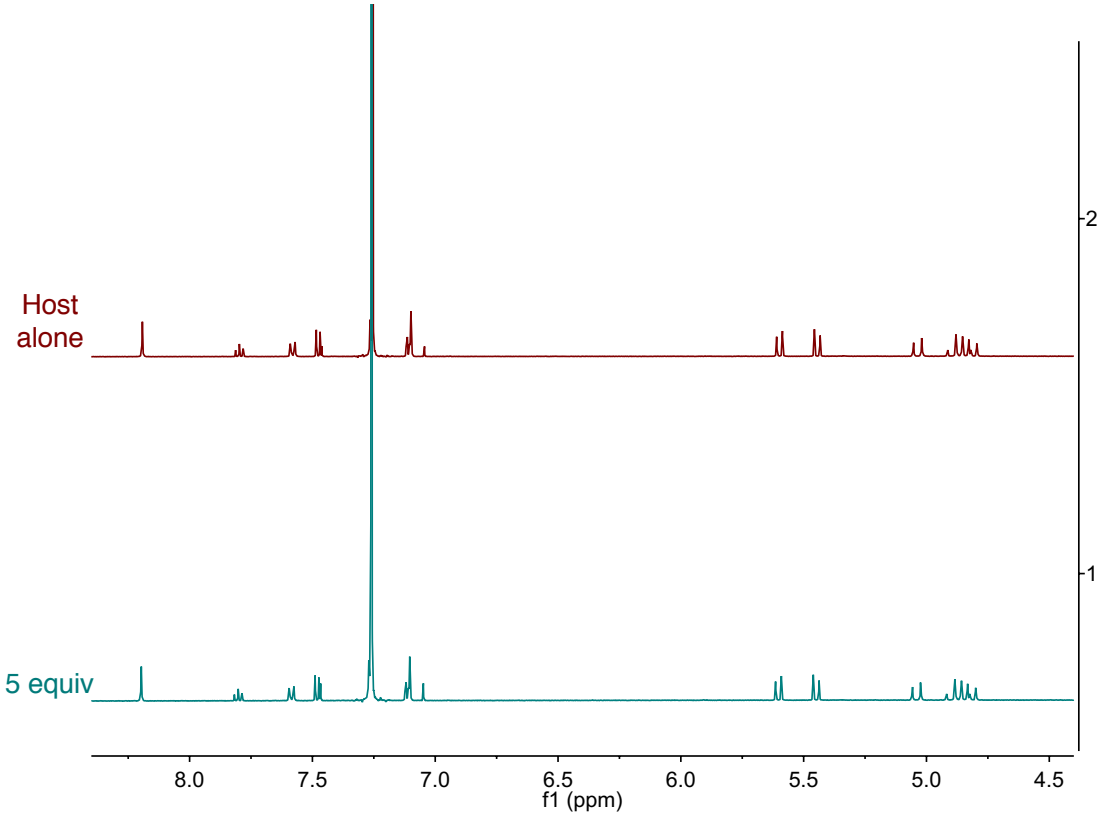

Complex of **5.10a** and **5.27** in $CDCl_3$ (mam-III-214)

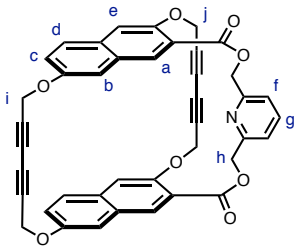

Host: **5.10a**

[H] = 0.61 mM

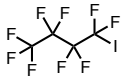

Guest: **5.27**

^{19}F NMR

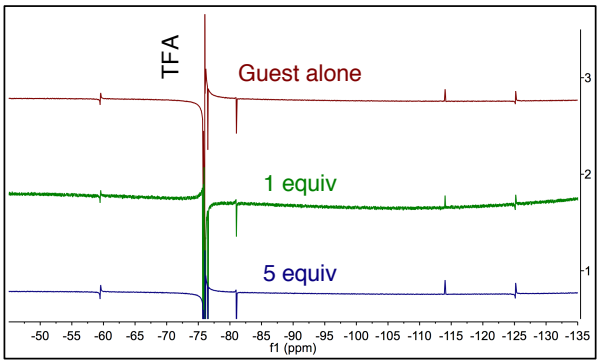

No observable binding up to 5 equiv

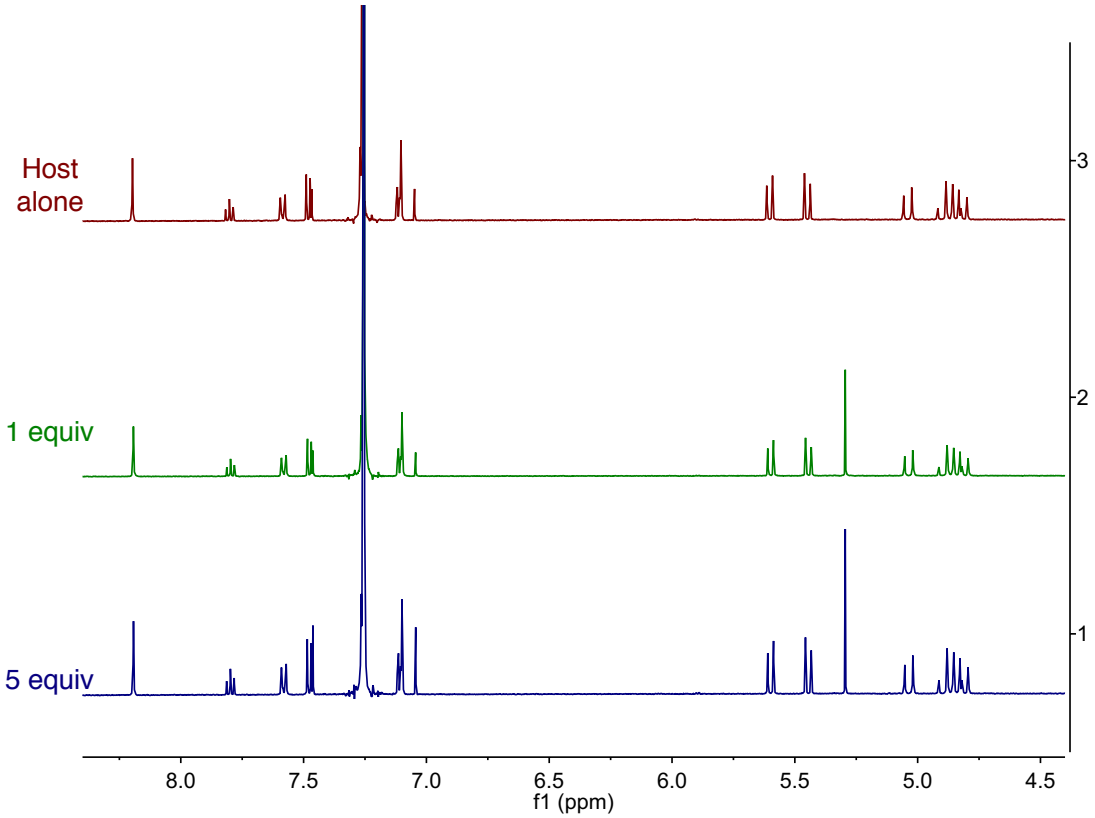

Complex of **5.28a** and **5.15** in $CDCl_3$ (mam-III-238)

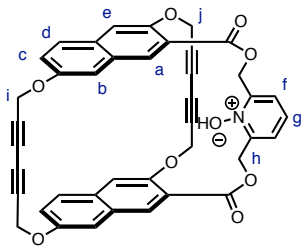

Host: **5.28a**

[H] = 0.60 mM

Guest: **5.15**

[G] = 0 - 60 mM

proton	K_a (bindfit)
a	50 ± 2%
b	49 ± 3%
g	44 ± 2%
global fitting	48 ± 1%

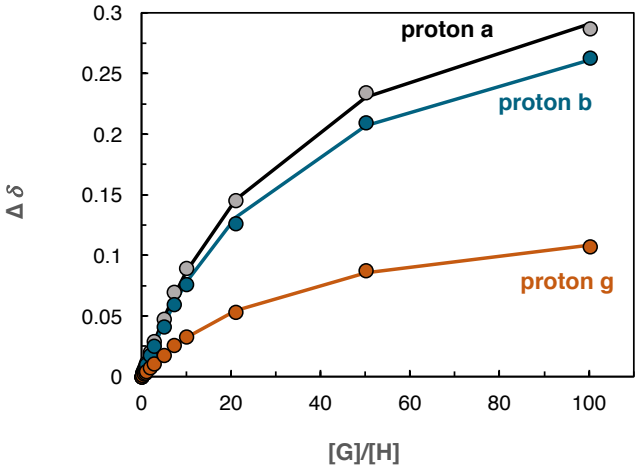

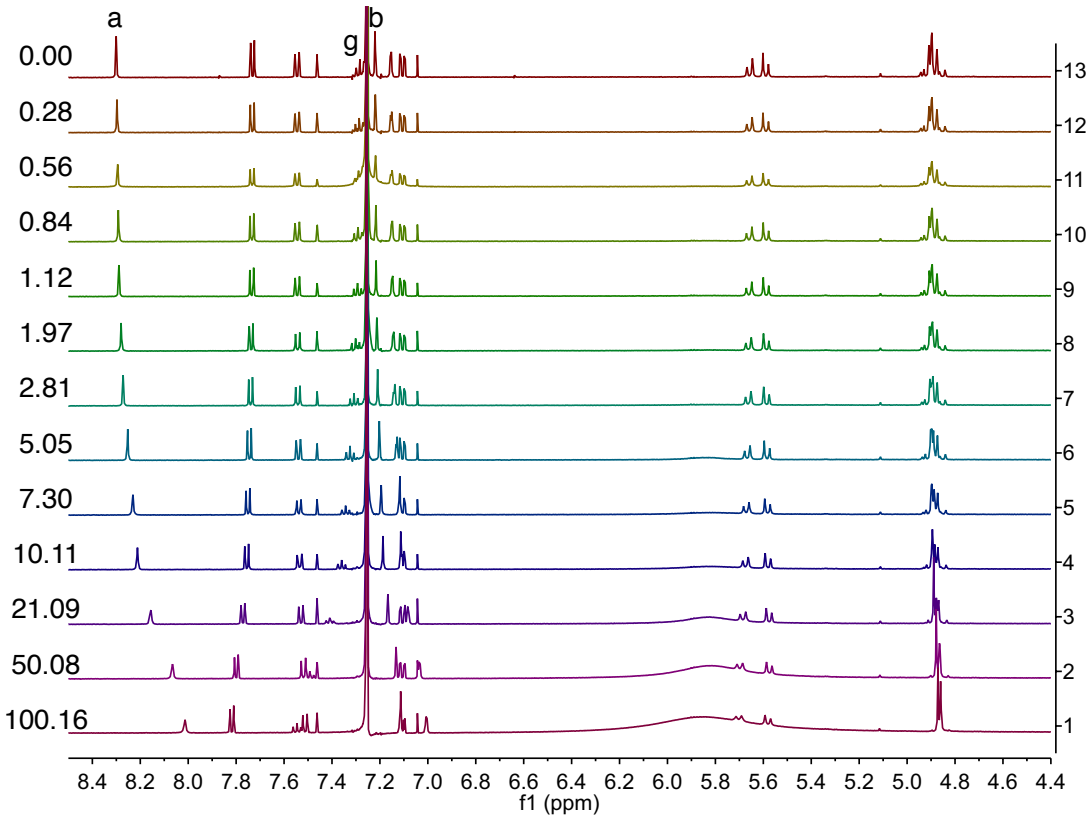

Complex of **5.29a** and **5.15** in $CDCl_3$ (mam-III-251)

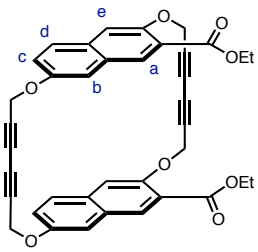

Host: **5.29a**

[H] = 0.60 mM

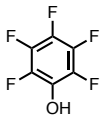

Guest: **5.15**

[G] = 0 - 60 mM

No observable binding up to 100 equiv

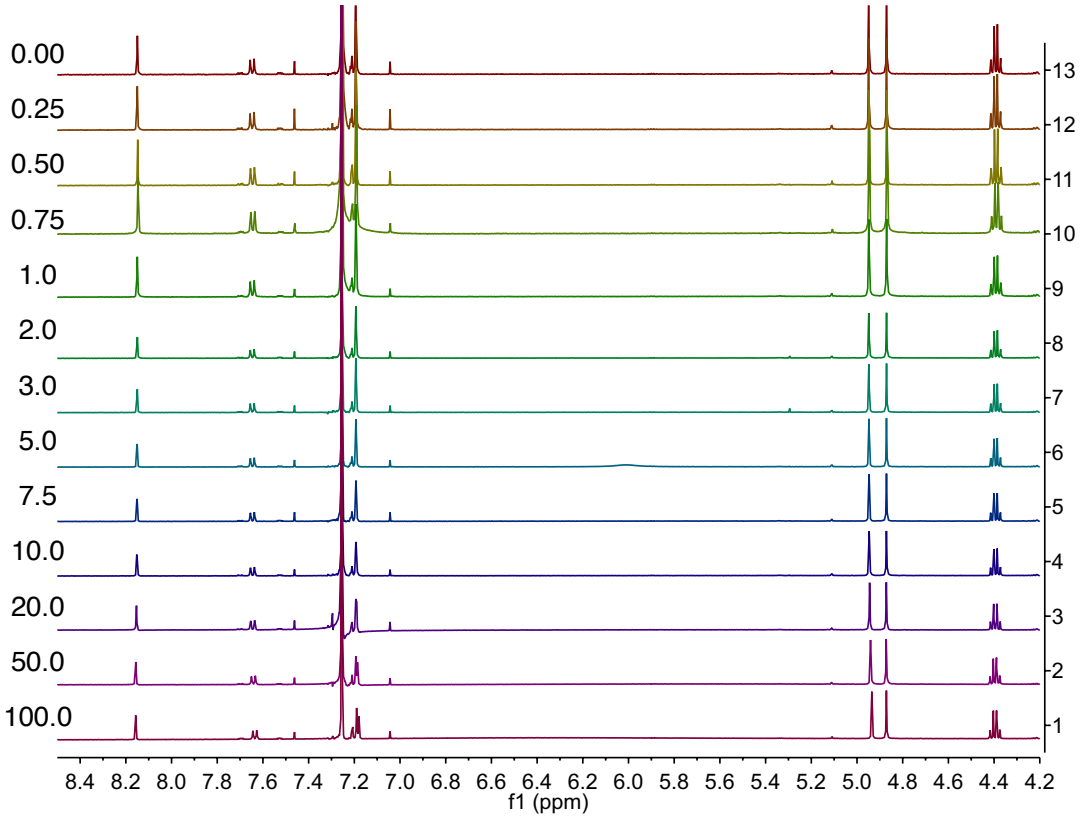

Complex of **5.36a** and **5.15** in $CDCl_3$ (mam-IV-236)

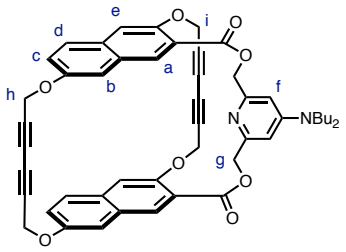

Host: **5.36a**

[H] = 0.98 mM

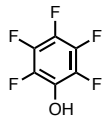

Guest: **5.15**

[G] = 0 - 27 mM

proton	K_a (bindfit)
a	741 ± 16%
c/d/e	538 ± 9%
b	668 ± 13%
f	n/a
global fitting	703 ± 9%

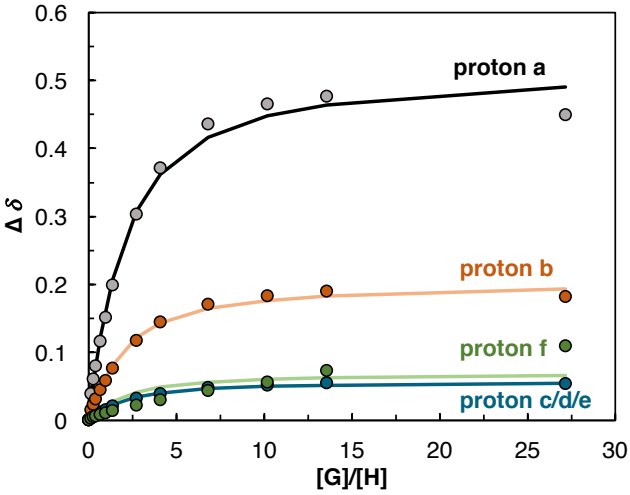

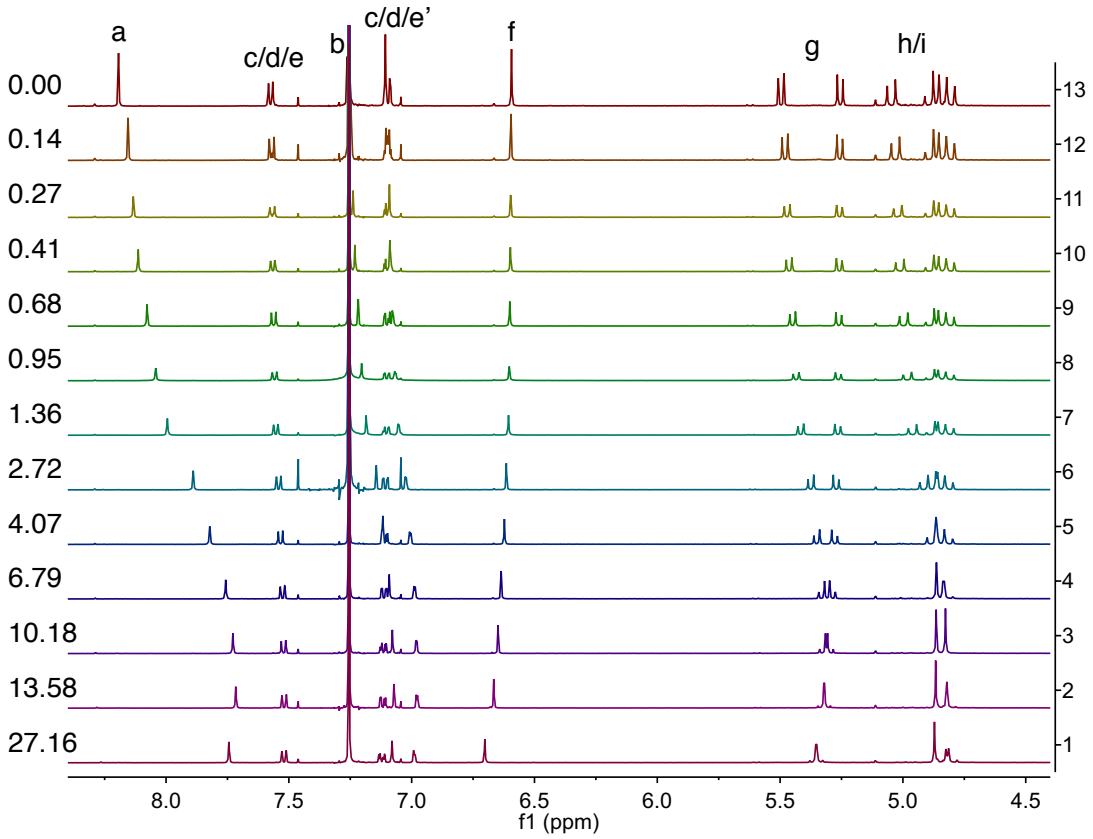

Complex of **5.36a** and **5.14** in $CDCl_3$ (mam-IV-250)

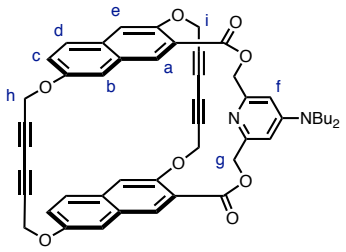

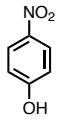

Host: **5.36a**

[H] = 0.98 mM

Guest: **5.14**

[G] = 0 - 9.1 mM

proton	K_a (bindfit)
a	11831 ± 28%
c/d/e	9935 ± 25%
b	10381 ± 25%
f	14623 ± 35%
g	15665 ± 38%
global fitting	11486 ± 10%

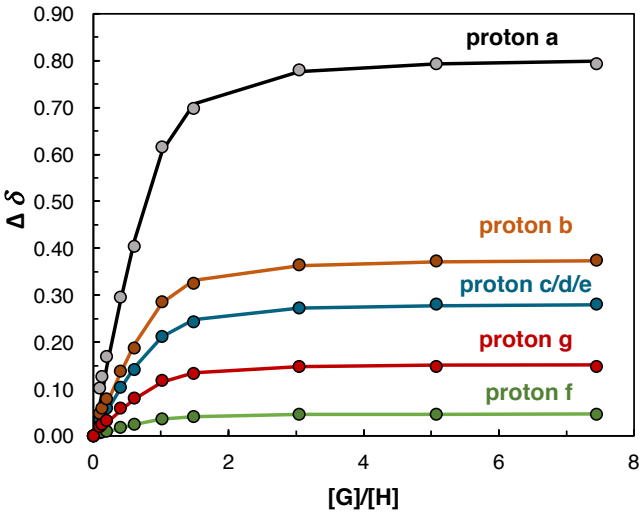

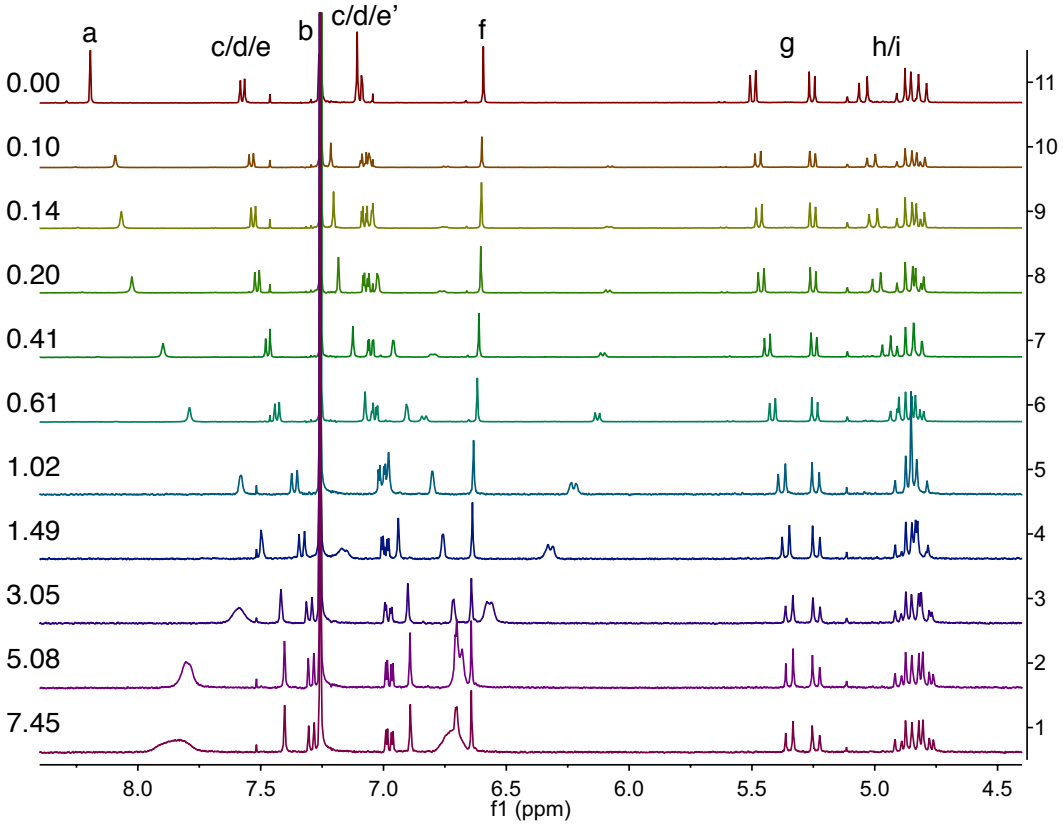

5.5.4 NMR spectra

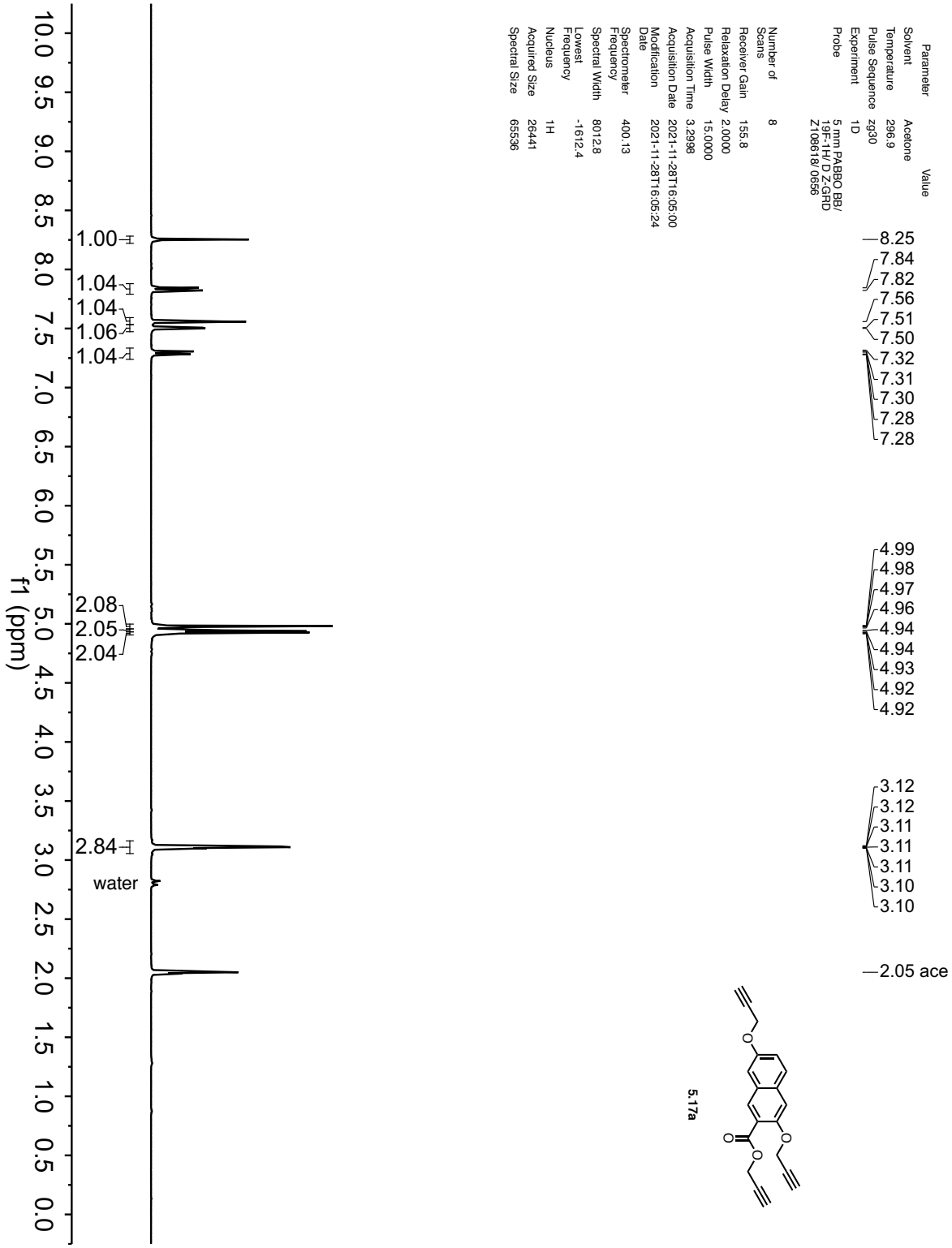

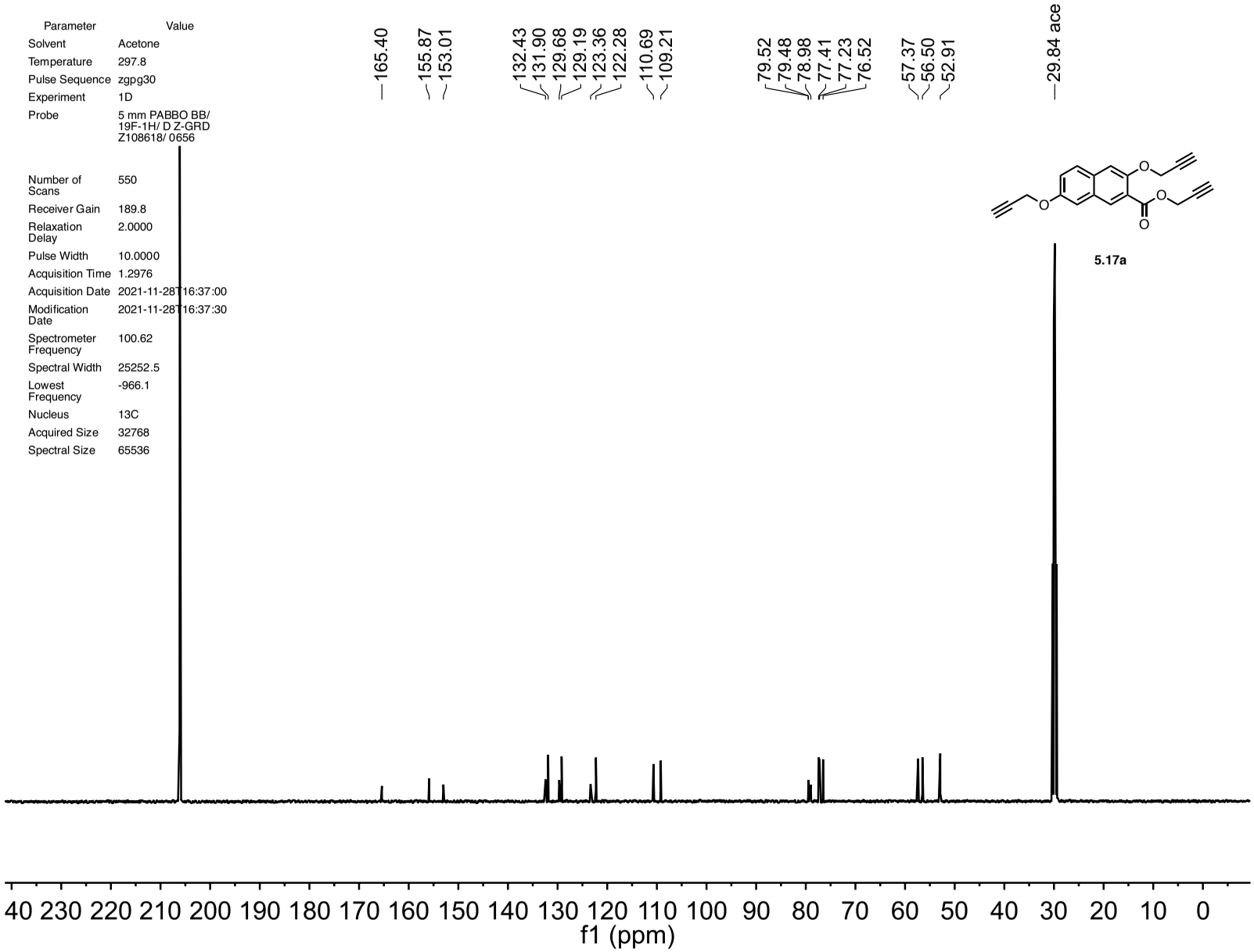
Parameter Value
Solvent Acetone
Temperature 297.8
Pulse Sequence zgpg30
Experiment 1D
Probe 5 mm PABBO BB/ 19F-1H/ D Z-GRD Z108618/ 0656
Number of Scans 550
Receiver Gain 189.8
Relaxation Delay 2.0000
Pulse Width 10.0000
Acquisition Time 1.2976
Acquisition Date 2021-11-28T16:37:00
Modification Date 2021-11-28T16:37:30
Spectrometer Frequency 100.62
Spectral Width 25252.5
Lowest Frequency -966.1
Nucleus 13C
Acquired Size 32768
Spectral Size 65536
165.40
155.87
153.01
132.43
131.90
129.68
129.19
123.36
122.28
110.69
109.21
79.52
79.48
78.98
77.41
77.23
76.52
57.37
56.50
52.91
29.84 ace
5.17a
40 230 220 210 200 190 180 170 160 150 140 130 120 110 100 90 80 70 60 50 40 30 20 10 0
f1 (ppm)

Parameter	Value
Solvent	Acetone
Temperature	297.0
Pulse Sequence	cosygpmfphpp
Experiment	COSY
Probe	5 mm PABBO BB/ 19F-1H/ D Z-GRD Z108618/ 0656
Number of Scans	6
Receiver Gain	122.3
Relaxation Delay	2.0000
Pulse Width	15.0000
Acquisition Time	0.3052
Acquisition Date	2021-11-28T23:34:00
Modification Date	2021-11-29T00:35:16
Spectrometer Frequency	(400.13, 400.13)
Spectral Width	(3355.7, 3355.7)
Lowest Frequency	(219.8, 219.8)
Nucleus	(1H, 1H)
Acquired Size	(1024, 256)
Spectral Size	(1024, 1024)

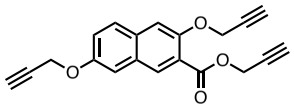

5.17a

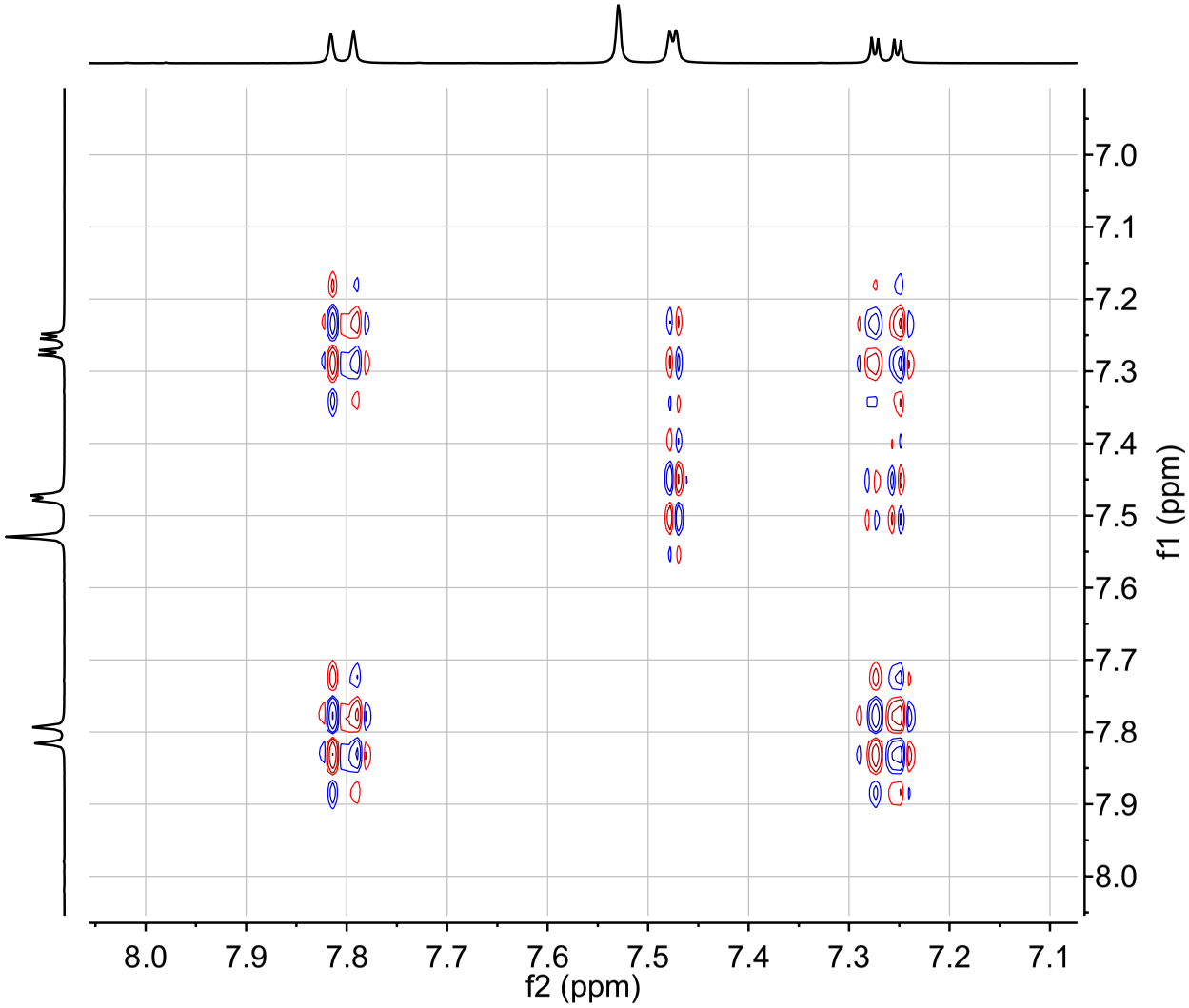

Parameter	Value
Solvent	Acetone
Temperature	297.2
Pulse Sequence	hsqcedetgpsisp2.3
Experiment	HSQC-EDITED
Probe	5 mm PABBO BB/ 19F-1H/ D Z-GRD Z108618/ 0656
Number of Scans	10
Receiver Gain	189.8
Relaxation Delay	2.0610
Pulse Width	15.0000
Acquisition Time	0.1526
Acquisition Date	2021-11-28T19:49:00
Modification Date	2021-11-28T23:32:18
Spectrometer Frequency	(400.13, 100.62)
Spectral Width	(3355.7, 25000.0)
Lowest Frequency	(219.8, -1560.3)
Nucleus	(1H, 13C)
Acquired Size	(512, 596)
Spectral Size	(512, 1024)

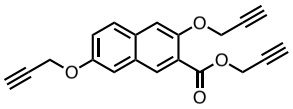

5.17a

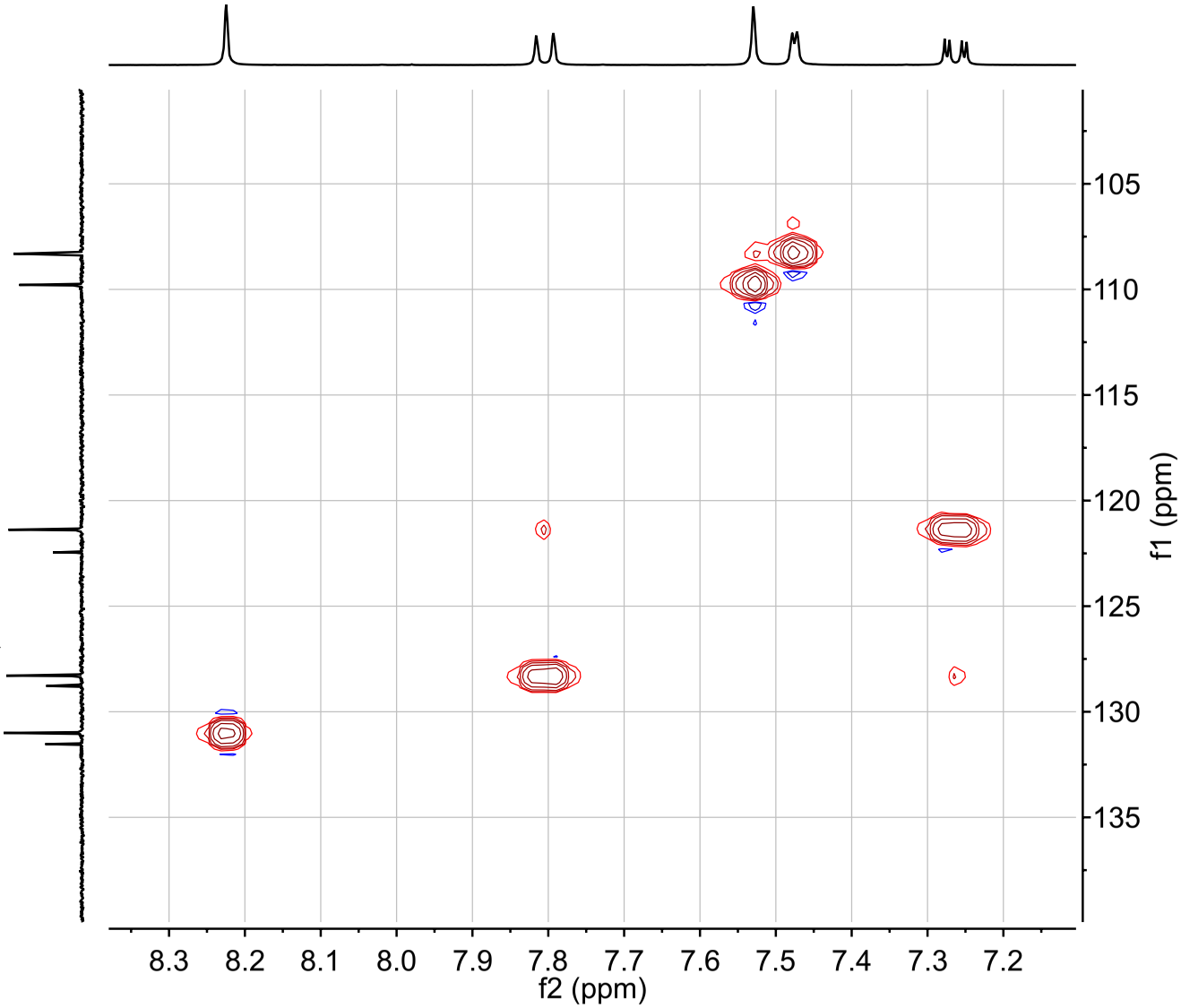

Parameter	Value
Solvent	CDCl3
Temperature	298.0
Pulse Sequence	zg30
Experiment	1D
Probe	Z119248_0002 (DCH 500S2 C/ H-D-05 Z LT)
Number of Scans	16
Receiver Gain	12.1
Relaxation Delay	2.0000
Pulse Width	10.0000
Acquisition Time	3.2768
Acquisition Date	2020-09-21T18:26:25
Modification Date	2020-09-21T18:26:25
Spectrometer Frequency	500.13
Spectral Width	10000.0
Lowest Frequency	-2011.3
Nucleus	1H
Acquired Size	32768
Spectral Size	65536

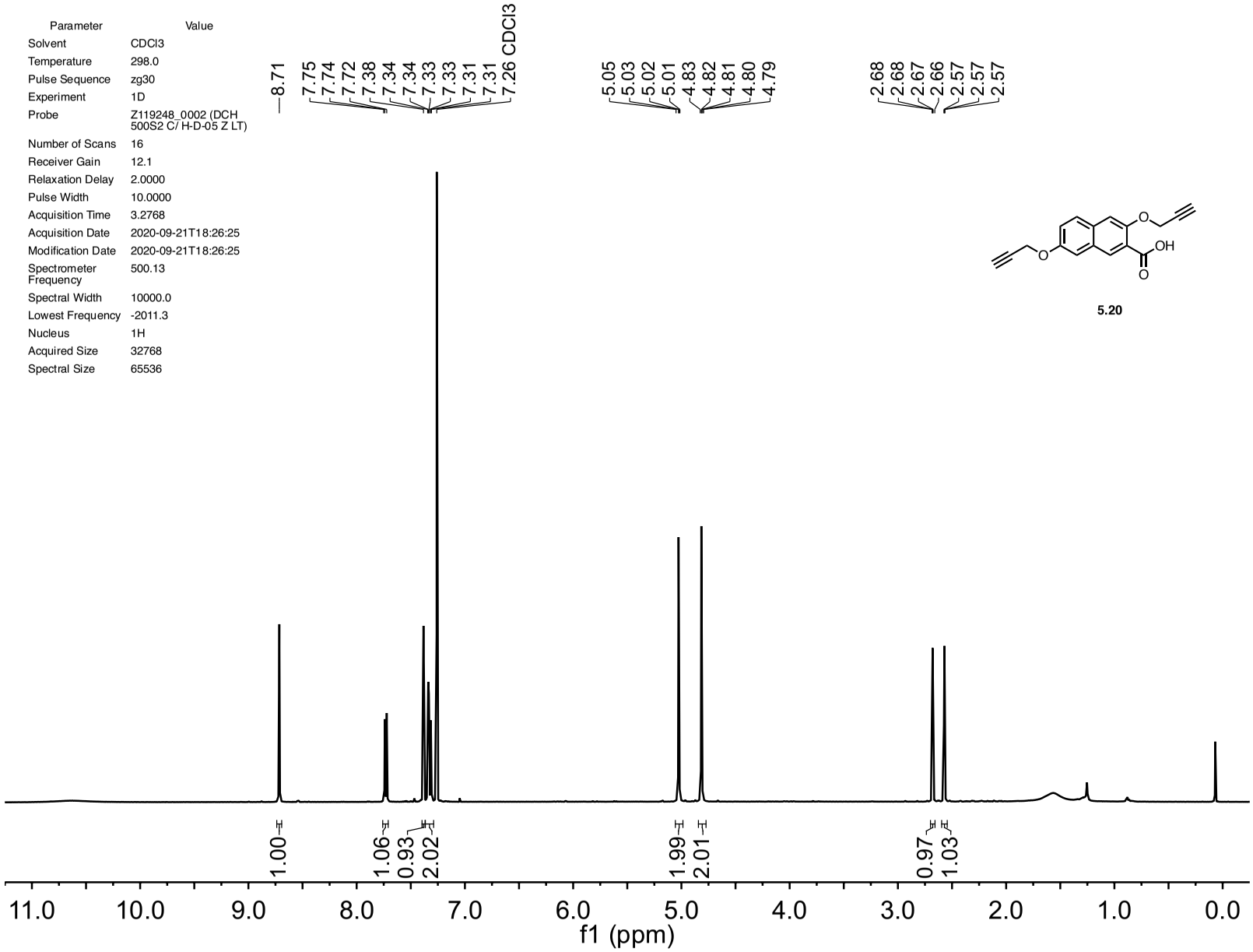

5.20

Parameter	Value
Solvent	CDCl3
Temperature	298.0
Pulse Sequence	zgpg30
Experiment	1D
Probe	Z119248_0002 (DCH 500S2 C/ H-D-05 Z LT)
Number of Scans	300
Receiver Gain	204.5
Relaxation Delay	2.0000
Pulse Width	10.5000
Acquisition Time	1.0486
Acquisition Date	2020-09-21T18:45:27
Modification Date	2020-09-21T18:45:27
Spectrometer Frequency	125.77
Spectral Width	31250.0
Lowest Frequency	-1144.7
Nucleus	13C
Acquired Size	32768
Spectral Size	65536

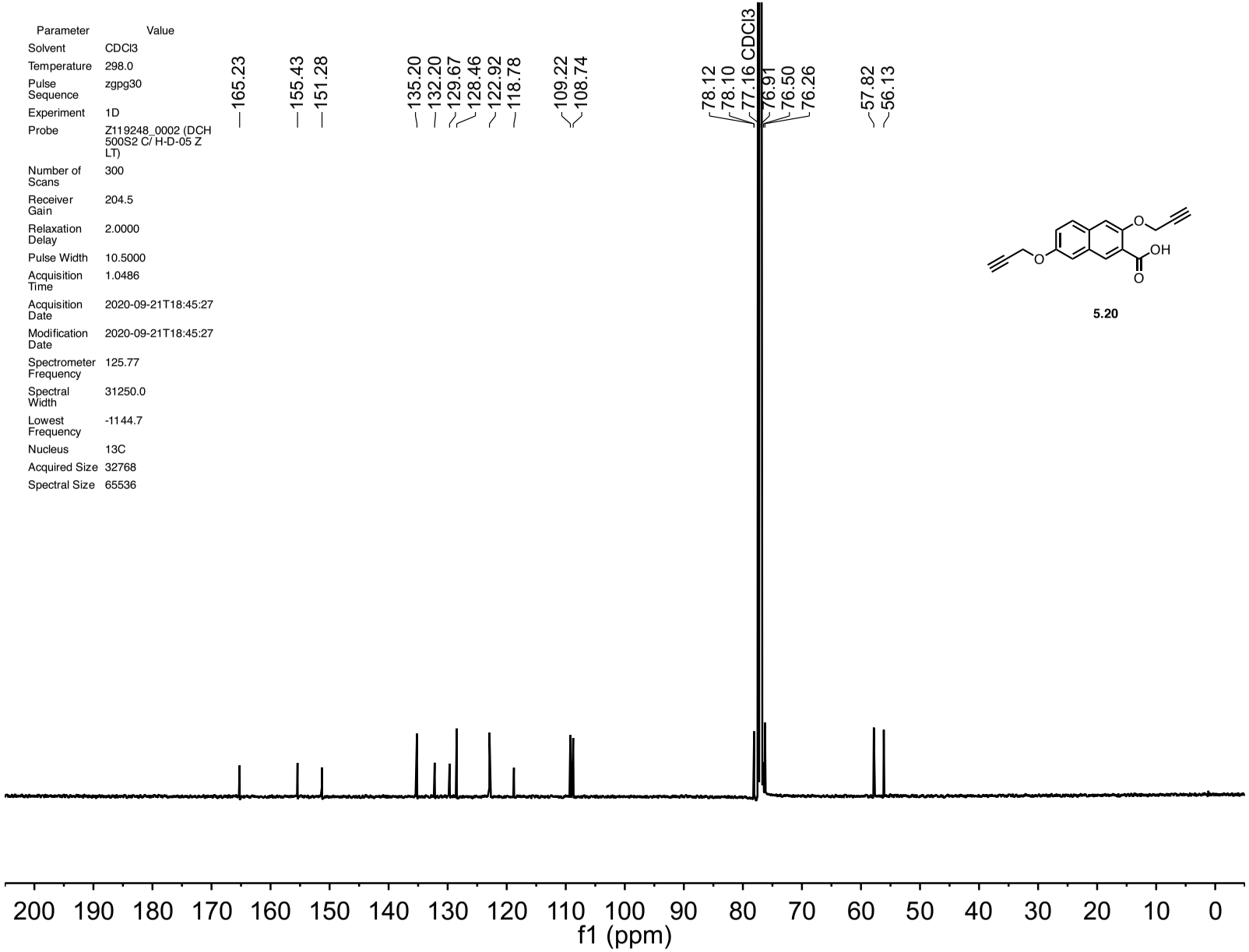

5.20

Parameter	Value
Solvent	DMSO
Temperature	298.0
Pulse Sequence	zg30
Experiment	1D
Probe	Z119248_0002 (DCH 500S2 C/ H-D-05 Z LT)
Number of Scans	8
Receiver Gain	12.1
Relaxation Delay	2.0000
Pulse Width	10.0000
Acquisition Time	3.2768
Acquisition Date	2020-10-13T16:33:12
Modification Date	2020-10-13T16:33:12
Spectrometer Frequency	500.13
Spectral Width	10000.0
Lowest Frequency	-2003.3
Nucleus	1H
Acquired Size	32768
Spectral Size	65536

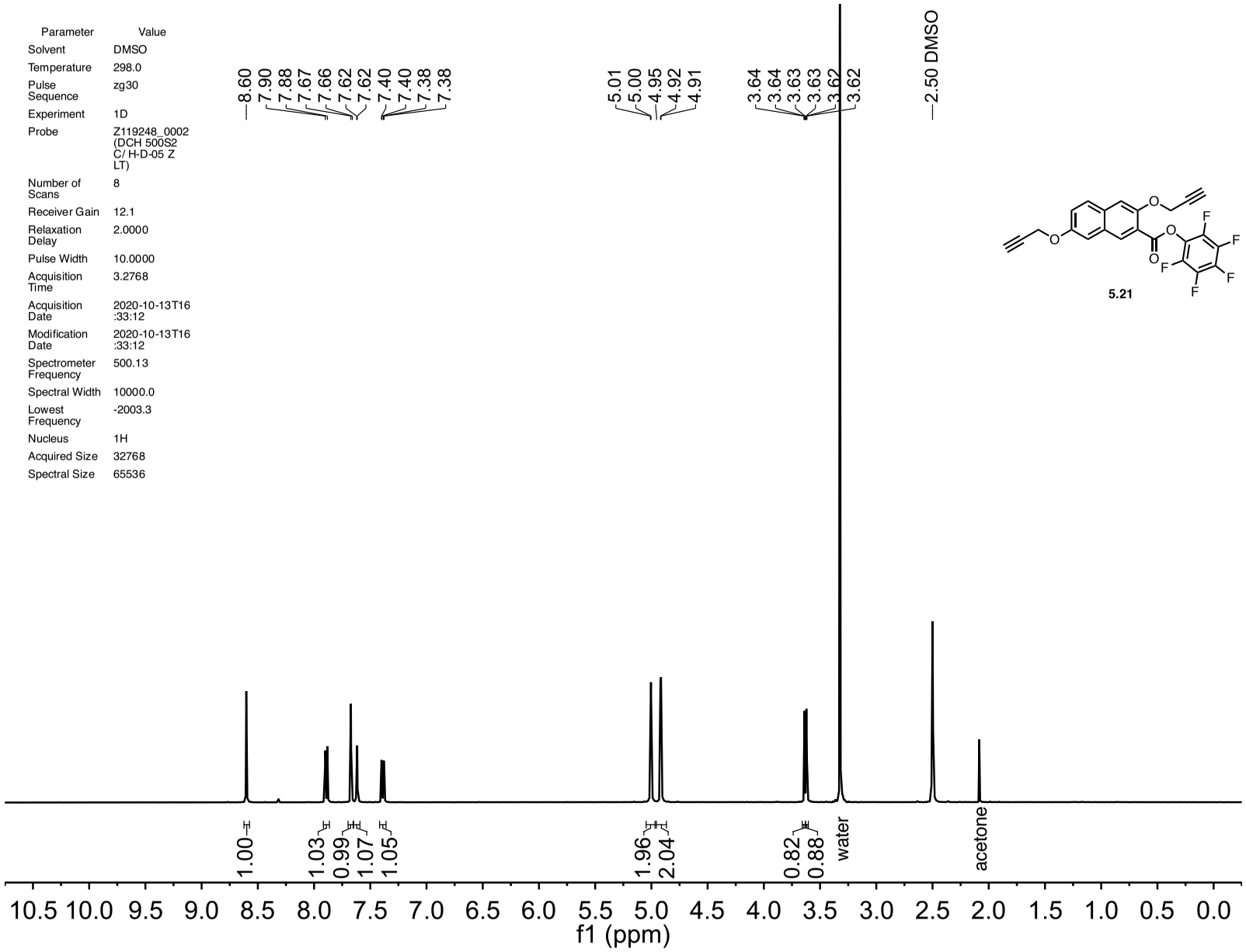

5.21

Parameter	Value
Solvent	DMSO
Temperature	298.0
Pulse Sequence	zgpg30
Experiment	1D
Probe	Z119248_0002 (DCH 500S2 C/ H-D-05 Z LT)
Number of Scans	250
Receiver Gain	204.5
Relaxation Delay	2.0000
Pulse Width	10.5000
Acquisition Time	1.0486
Acquisition Date	2020-10-14T19 :33:04
Modification Date	2020-10-14T19 :33:05
Spectrometer Frequency	125.77
Spectral Width	31250.0
Lowest Frequency	-1220.4
Nucleus	13C
Acquired Size	32768

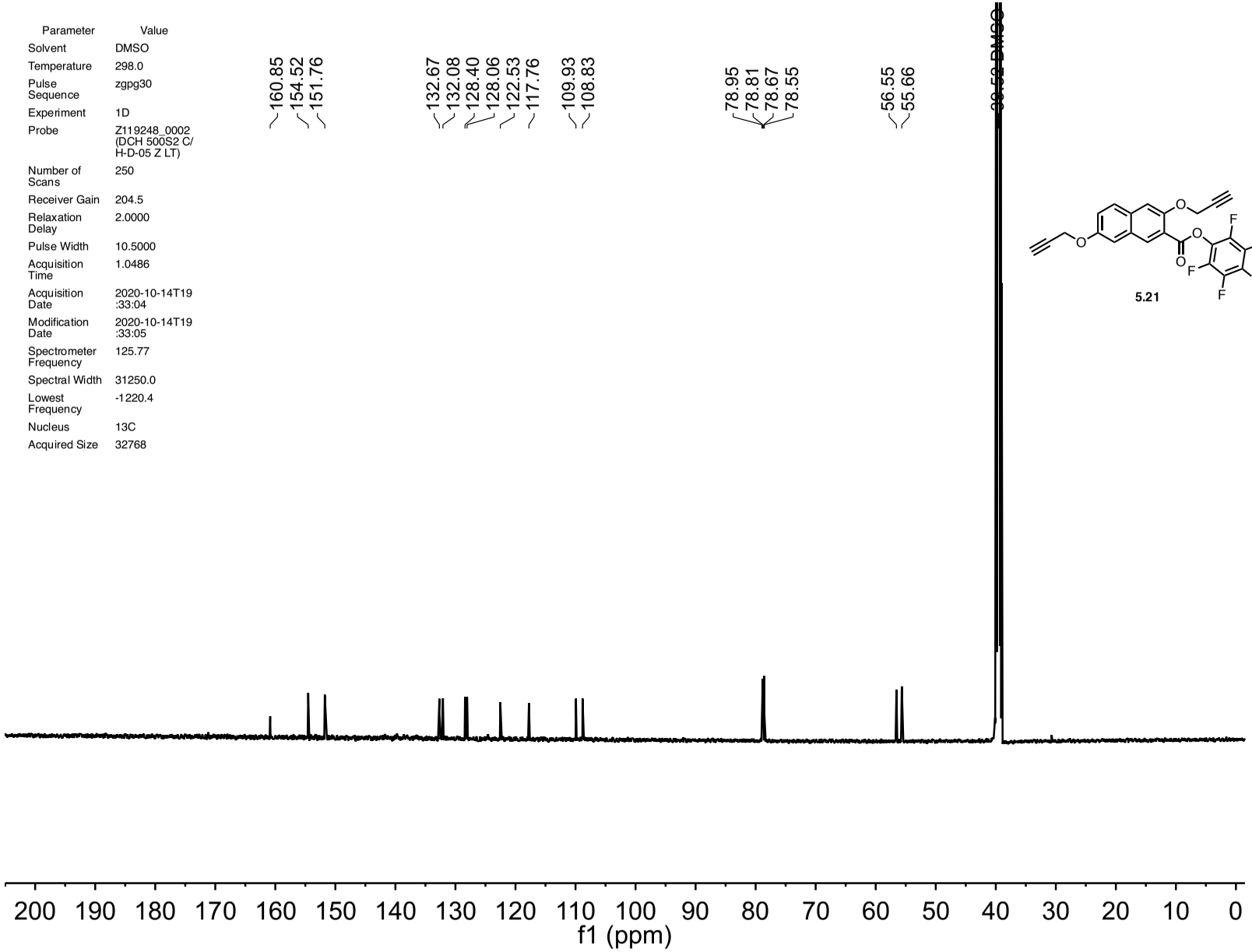

5.21

Parameter	Value
Solvent	DMSO
Temperature	296.9
Pulse Sequence	zgfhigqn.2
Experiment	1D
Probe	5 mm PABBO BB/ 19F-1H/ D Z-GRD Z108618/ 0656
Number of Scans	8
Receiver Gain	189.8
Relaxation Delay	1.0000
Pulse Width	14.5000
Acquisition Time	1.7476
Acquisition Date	2020-10-13T21:15:00
Modification Date	2020-10-13T21:15:14
Spectrometer Frequency	376.46
Spectral Width	75000.0
Lowest Frequency	-75149.8
Nucleus	19F
Acquired Size	131072
Spectral Size	262144

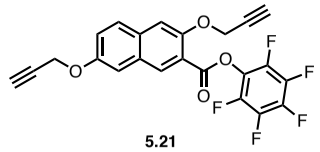

5.21

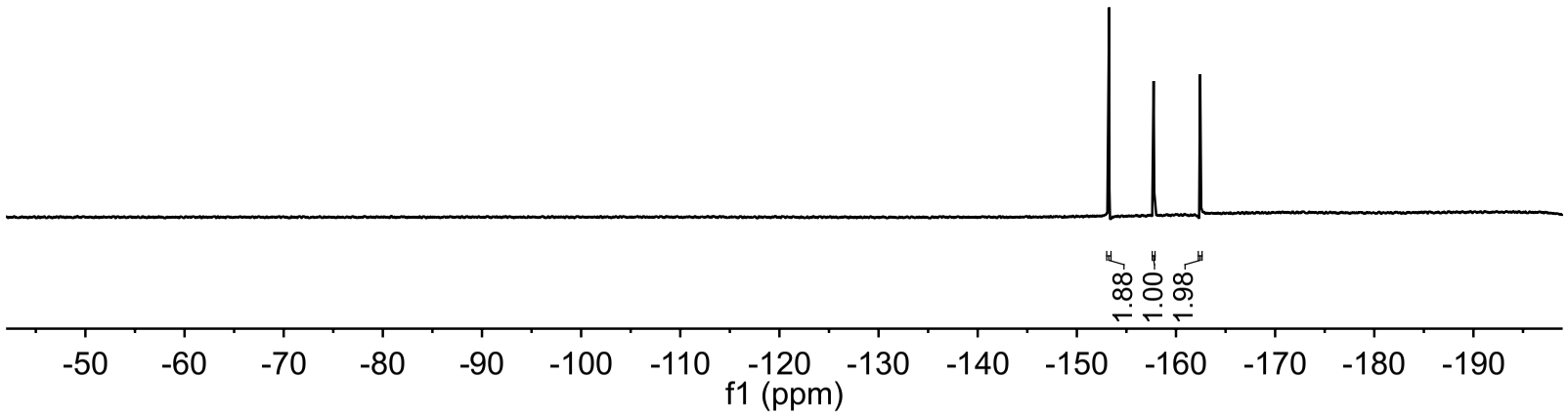

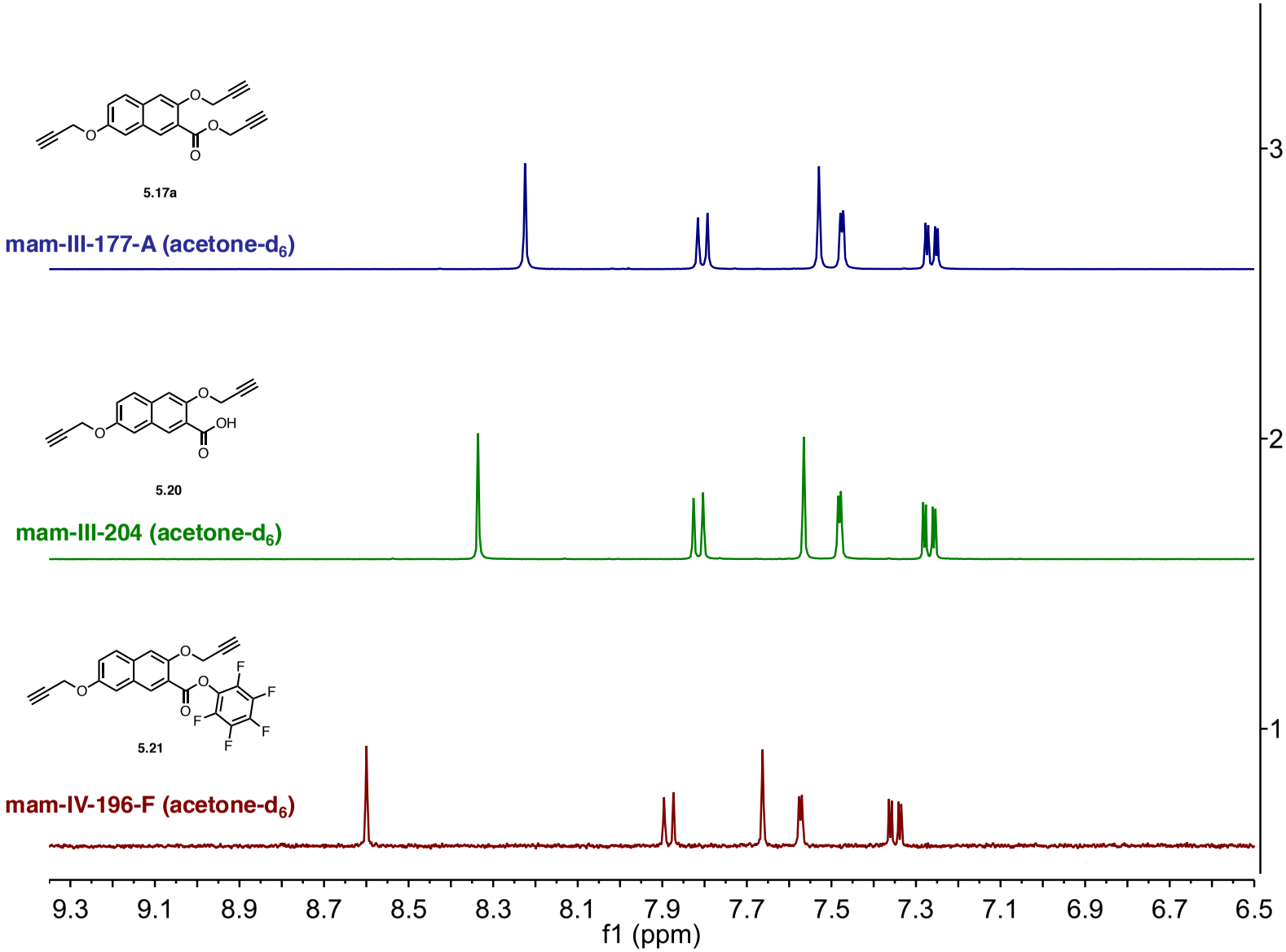
5.17a
mam-III-177-A (acetone-d6)
5.20
mam-III-204 (acetone-d6)
5.21
mam-IV-196-F (acetone-d6)
3
2
1
9.3
9.1
8.9
8.7
8.5
8.3
8.1
7.9
7.7
7.5
7.3
7.1
6.9
6.7
6.5
f1 (ppm)

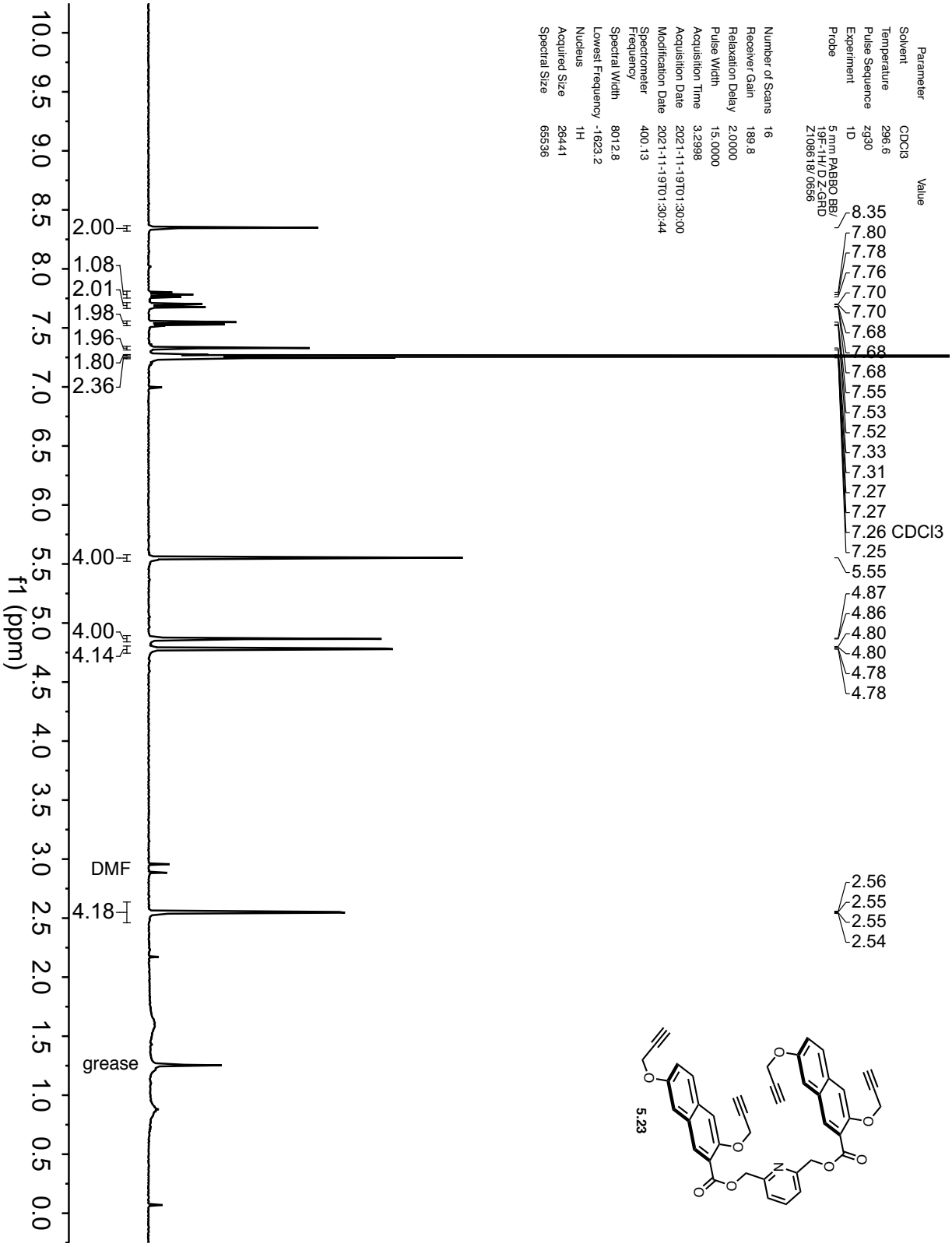
Parameter Value
Solvent CDCl3
Temperature 296.6
Pulse Sequence zg30
Experiment 1D
Probe 5 mm PABBO BB/ 19F-1H/ D Z-GRD Z108618/ 0656
Number of Scans 16
Receiver Gain 189.8
Relaxation Delay 2.0000
Pulse Width 15.0000
Acquisition Time 3.2998
Acquisition Date 2021-11-19T01:30:00
Modification Date 2021-11-19T01:30:44
Spectrometer Frequency 400.13
Spectral Width 8012.8
Lowest Frequency -1623.2
Nucleus 1H
Acquired Size 26441
Spectral Size 65536
8.35
7.80
7.78
7.76
7.70
7.70
7.68
7.68
7.68
7.55
7.53
7.52
7.33
7.31
7.27
7.27
7.26 CDCl3
7.25
5.55
4.87
4.86
4.80
4.80
4.78
4.78
2.56
2.55
2.55
2.54
2.00
1.08
2.01
1.98
1.96
1.80
2.36
4.00
4.00
4.14
DMF
4.18
grease
f1 (ppm)
10.0 9.5 9.0 8.5 8.0 7.5 7.0 6.5 6.0 5.5 5.0 4.5 4.0 3.5 3.0 2.5 2.0 1.5 1.0 0.5 0.0
5.23

Parameter	Value
Solvent	CDCl3
Temperature	297.2
Pulse Sequence	zgpg30
Experiment	1D
Probe	5 mm PABBO BB/ 19F-1H/ D Z-GRD Z108618/ 0656
Number of Scans	2000
Receiver Gain	189.8
Relaxation Delay	2.0000
Pulse Width	10.0000
Acquisition Time	1.2976
Acquisition Date	2021-11-19T03:24:00
Modification Date	2021-11-19T03:24:02
Spectrometer Frequency	100.62
Spectral Width	25252.5
Lowest Frequency	-1042.5
Nucleus	13C
Acquired Size	32768
Spectral Size	65536

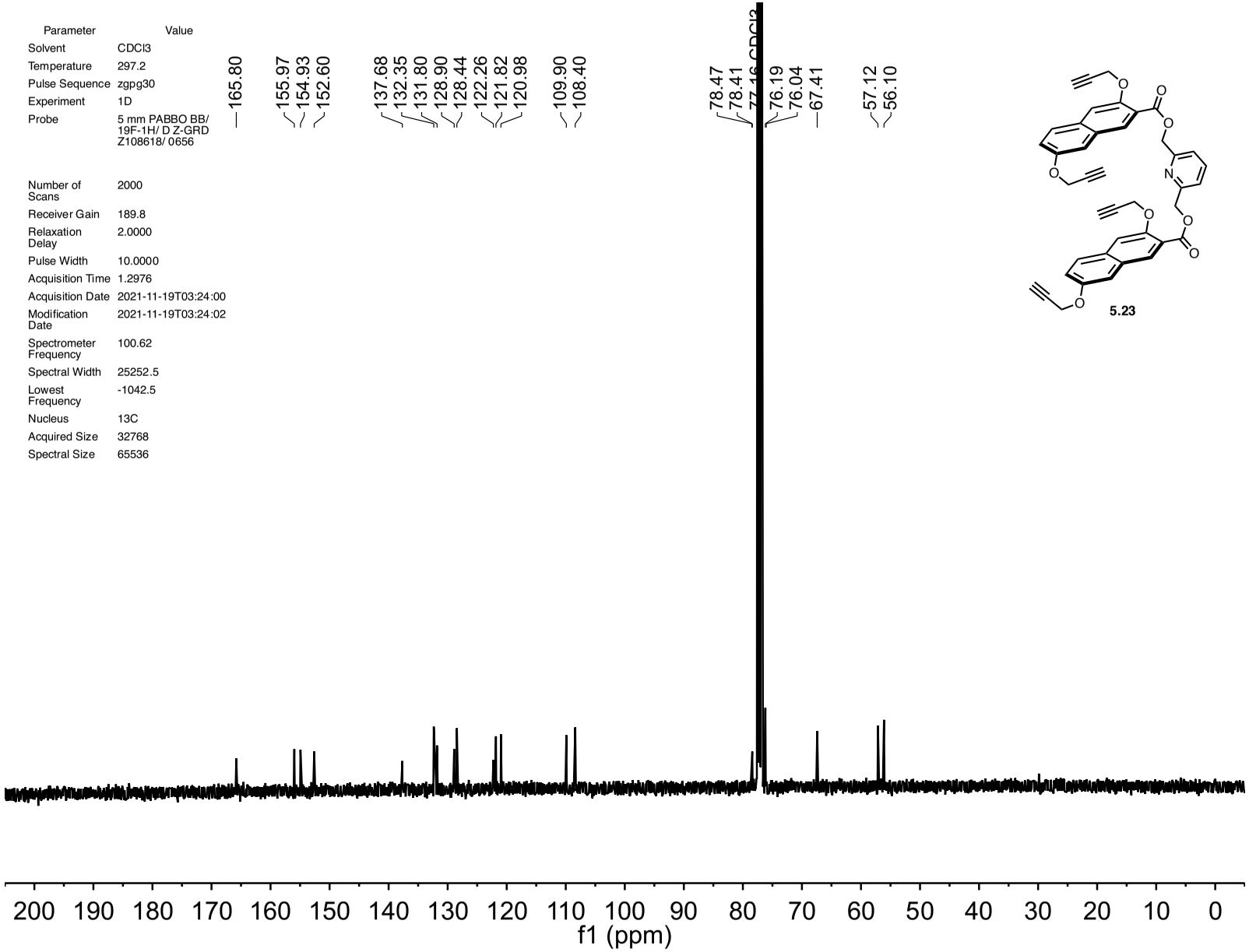

Parameter	Value
Title	mam-III-156-D-check
Solvent	CDCl3
Temperature	297.5
Pulse Sequence	zg30
Experiment	1D
Probe	5 mm PABBO BB/ 19F-1H/ D Z-GRD Z108618/ 0656
Number of Scans	16
Receiver Gain	189.8
Relaxation Delay	2.0000
Pulse Width	15.0000
Acquisition Time	3.2998
Acquisition Date	2019-04-21T15:46:00
Modification Date	2019-04-21T15:46:30
Spectrometer Frequency	400.13
Spectral Width	8012.8
Lowest Frequency	-1623.2
Nucleus	1H
Acquired Size	26441
Spectral Size	65536

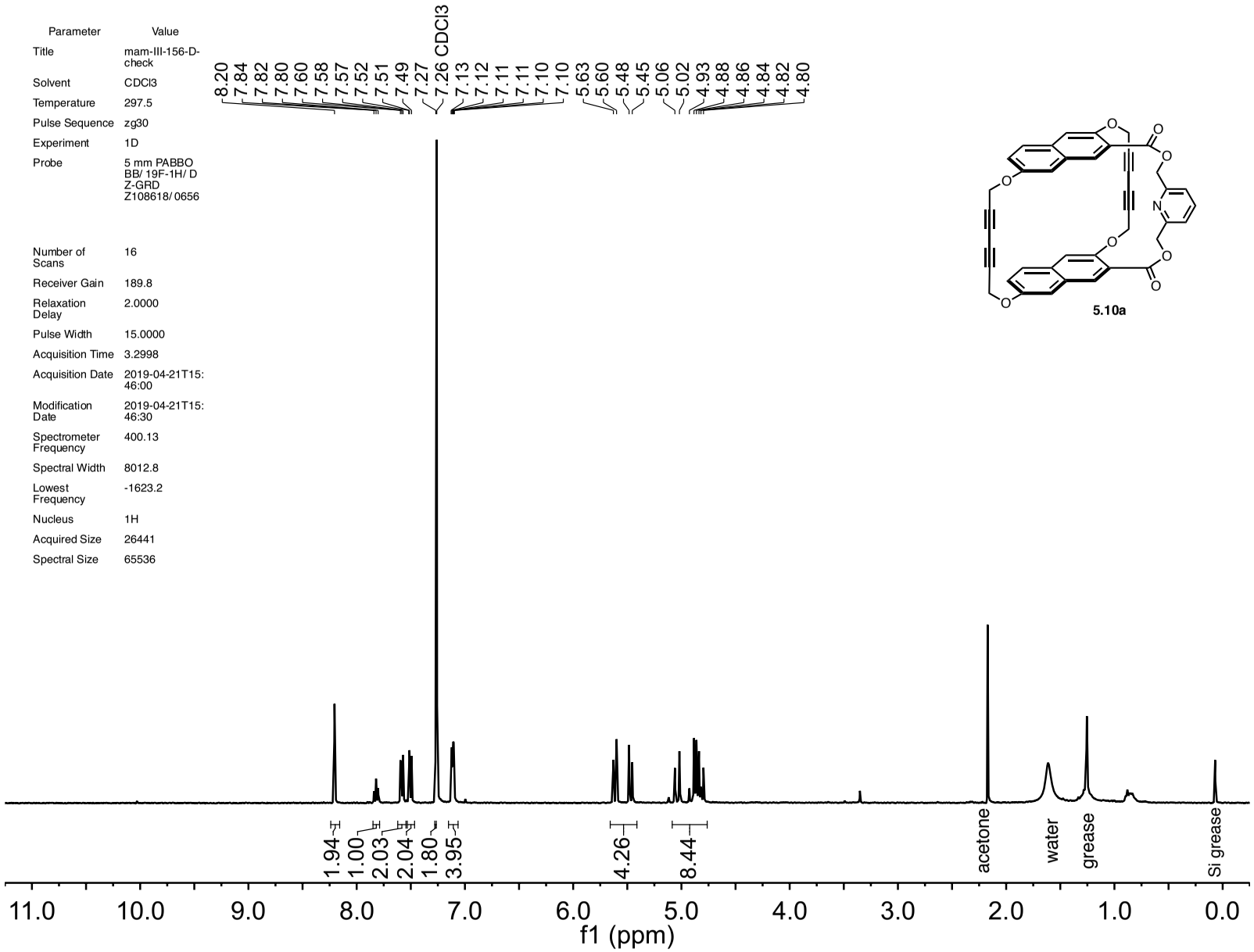

5.10a

Current Data Parameters
NAME mam-III-194-C
EXPNO 1
PROCNO 1

F2 - Acquisition Parameters
Date_ 20190423
Time 11.07 h
INSTRUM av500
PROBHD Z119248_0002 (
PULPROG zg30
TD 65536
SOLVENT CDCl3
NS 16
DS 0
SWH 10000.000 Hz
FIDRES 0.305176 Hz
AQ 3.2767999 sec
RG 12.14
DW 50.000 usec
DE 10.00 usec
TE 298.0 K
D1 2.00000000 sec
TD0 1
SFO1 500.1330008 MHz
NUC1 1H
P1 10.00 usec
PLW1 13.50000000 W

F2 - Processing parameters
SI 65536
SF 500.1300122 MHz
WDW EM
SSB 0
LB 0.30 Hz
GB 0
PC 1.00

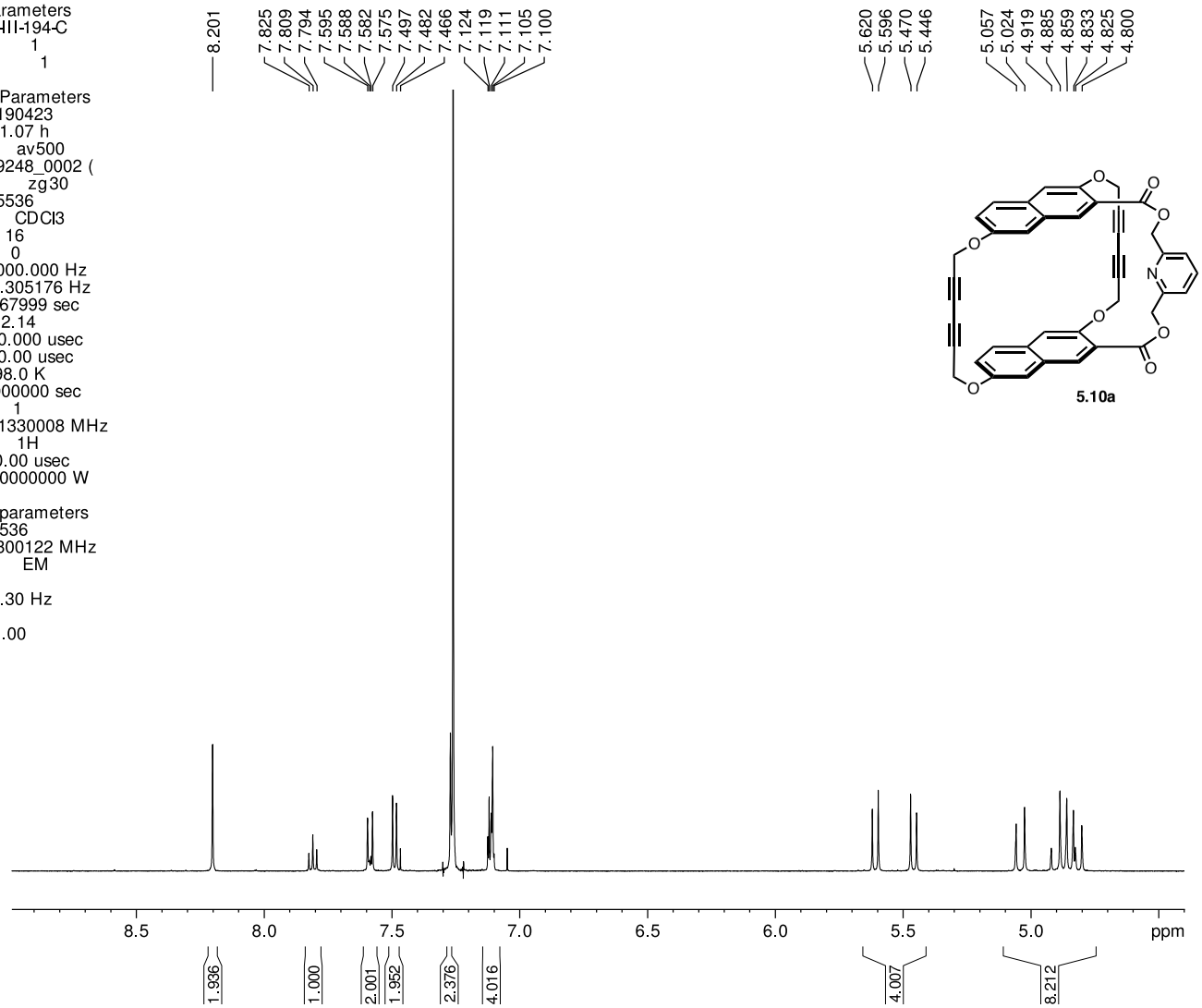

Parameter	Value
Title	mam-III-156-D-check
Solvent	CDCl3
Temperature	297.4
Pulse Sequence	cosygpmfphpp
Experiment	COSY
Probe	5 mm PABBO BB/ 19F-1H/ D Z-GRD Z108618/ 0656
Number of Scans	2
Receiver Gain	137.2
Relaxation Delay	2.0000
Pulse Width	15.0000
Acquisition Time	0.2662
Acquisition Date	2019-04-21T15:48:00
Modification Date	2019-04-21T16:08:21
Spectrometer Frequency	(400.13, 400.13)
Spectral Width	(3846.2, 3846.2)
Lowest Frequency	(-275.7, -278.4)
Nucleus	(1H, 1H)
Acquired Size	(1024, 256)
Spectral Size	(1024, 1024)

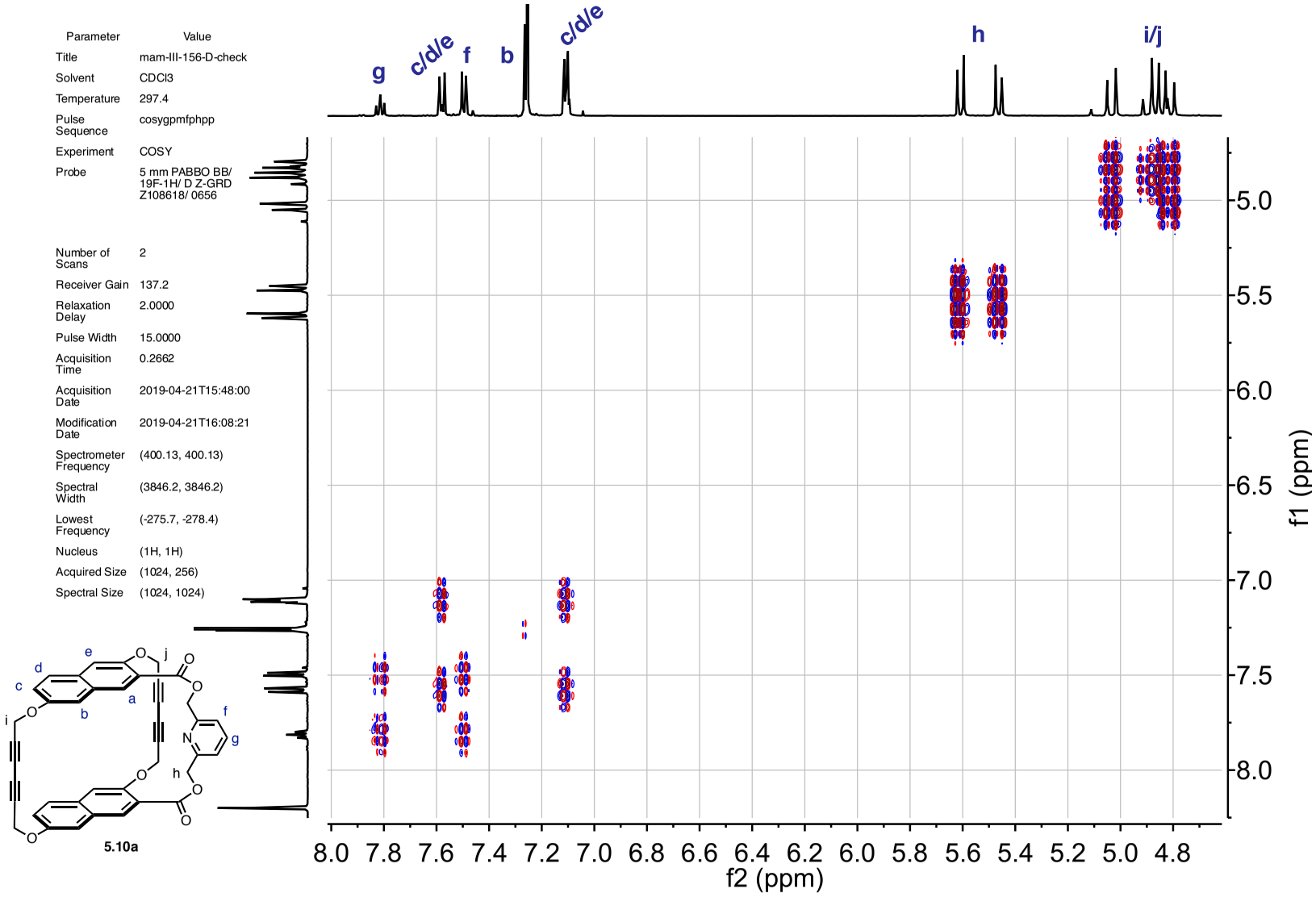

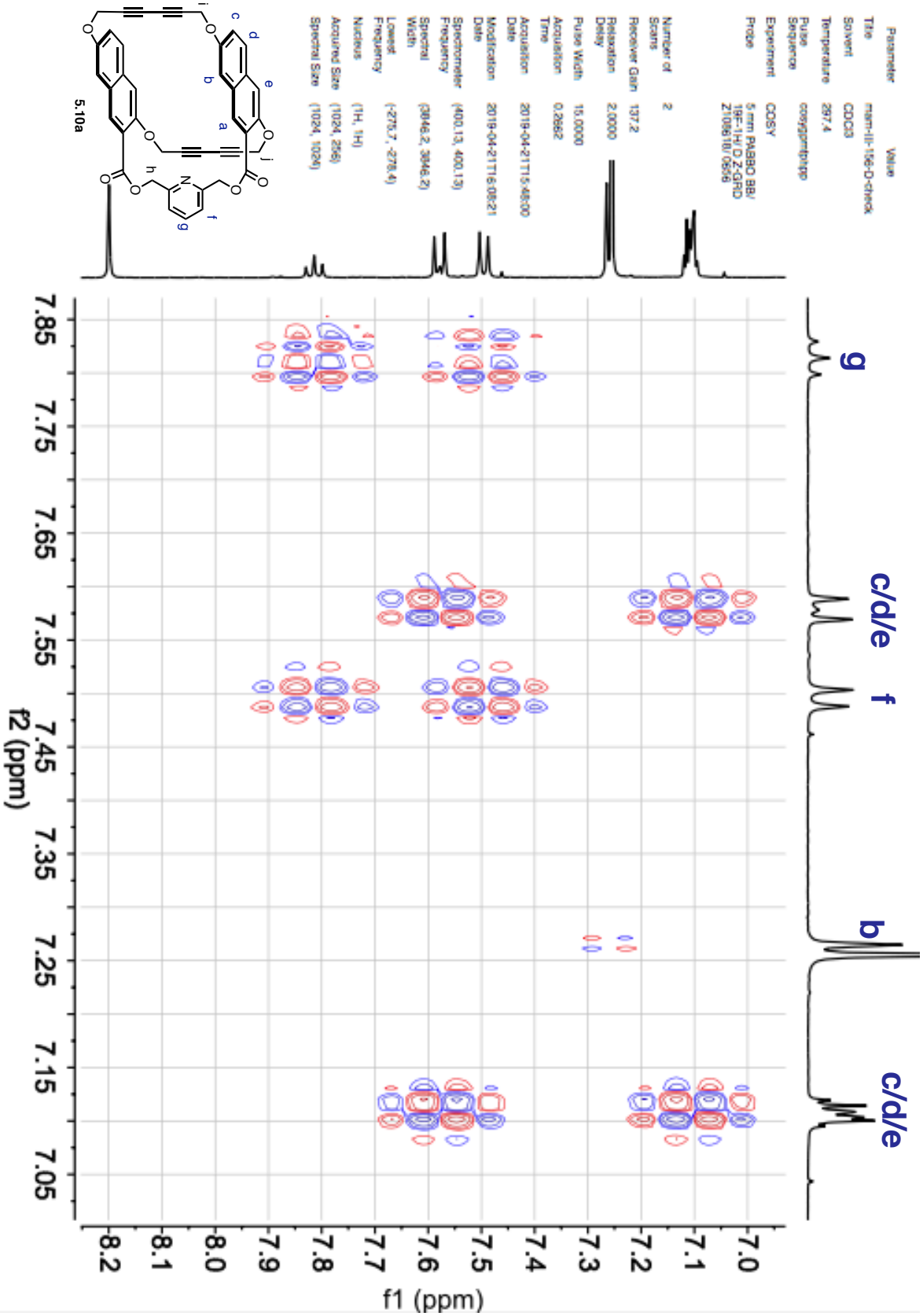
Parameter Value
Title mam-III-156-D-check
Solvent CDCl3
Temperature 297.4
Pulse Sequence cosygpmfqfpp
Experiment COSY
Probe 5 mm PABBO BB/ 19F-1H/ D Z-GRD Z108610/ 0656
Number of Scans 2
Receiver Gain 137.2
Relaxation Delay 2.0000
Pulse Width 15.0000
Acquisition Time 0.2662
Acquisition Date 2019-04-21T15:48:00
Modification Date 2019-04-21T16:08:21
Spectrometer Frequency (400.13, 400.13)
Spectral Width (3846.2, 3846.2)
Lowest Frequency (-276.7, -278.4)
Nucleus (1H, 1H)
Acquired Size (1024, 256)
Spectral Size (1024, 1024)
5.10a
g
c/d/e
f
b
c/d/e
f2 (ppm)
f1 (ppm)

Parameter	Value
Title	mam-III-188-D.1.fid
Solvent	CDCl3
Temperature	298.0
Pulse Sequence	zg30
Experiment	1D
Probe	Z119248_0002 (DCH 500S2 C/ H-D-05 Z LT)
Number of Scans	16
Receiver Gain	12.1
Relaxation Delay	2.0000
Pulse Width	10.0000
Acquisition Time	3.2768
Acquisition Date	2019-04-24T17:37:56
Modification Date	2019-04-24T17:37:56
Spectrometer Frequency	500.13
Spectral Width	10000.0
Lowest Frequency	-2011.3
Nucleus	1H
Acquired Size	32768
Spectral Size	65536

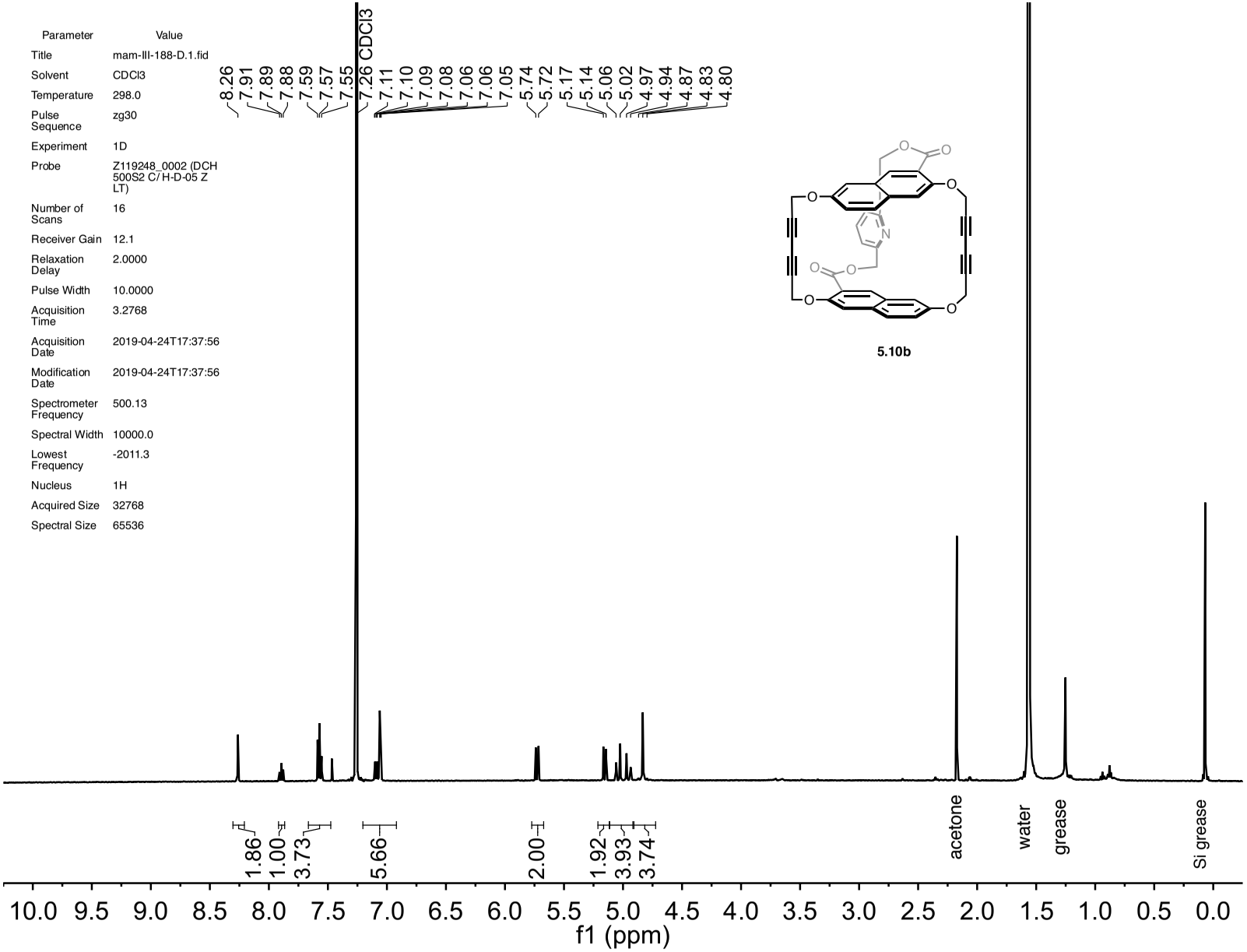

5.10b

Current Data Parameters
NAME mam-III-188-D
EXPNO 1
PROCNO 1

F2 - Acquisition Parameters
Date_ 20190424
Time 17.37 h
INSTRUM av500
PROBHD Z119248_0002 (
PULPROG zg30
TD 65536
SOLVENT CDCl3
NS 16
DS 0
SWH 10000.000 Hz
FIDRES 0.305176 Hz
AQ 3.2767999 sec
RG 12.14
DW 50.000 usec
DE 10.00 usec
TE 298.0 K
D1 2.00000000 sec
TD0 1
SFO1 500.1330008 MHz
NUC1 1H
P1 10.00 usec
PLW1 13.50000000 W

F2 - Processing parameters
SI 65536
SF 500.1300146 MHz
WDW EM
SSB 0
LB 0.30 Hz
GB 0
PC 1.00

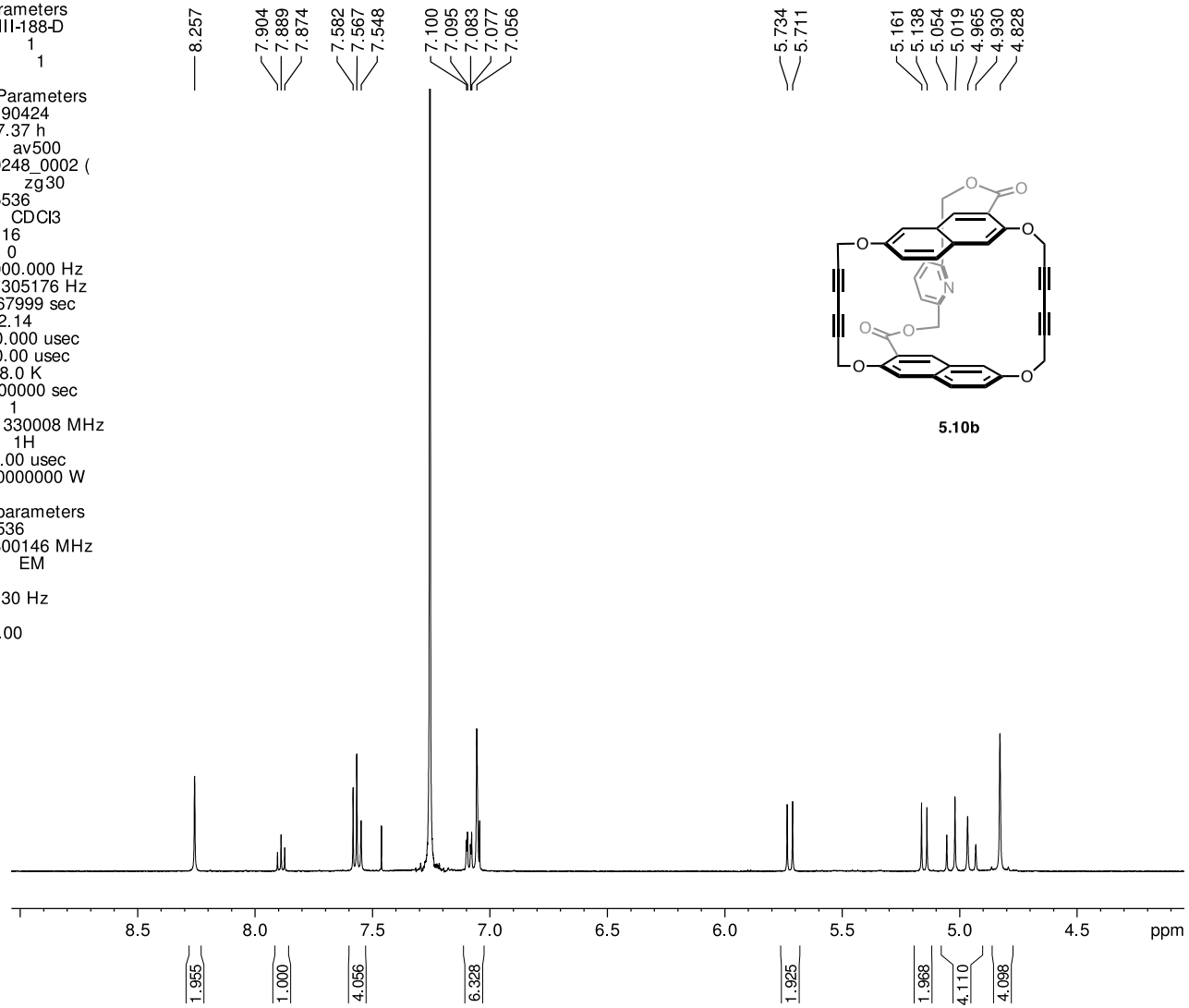

5.10b

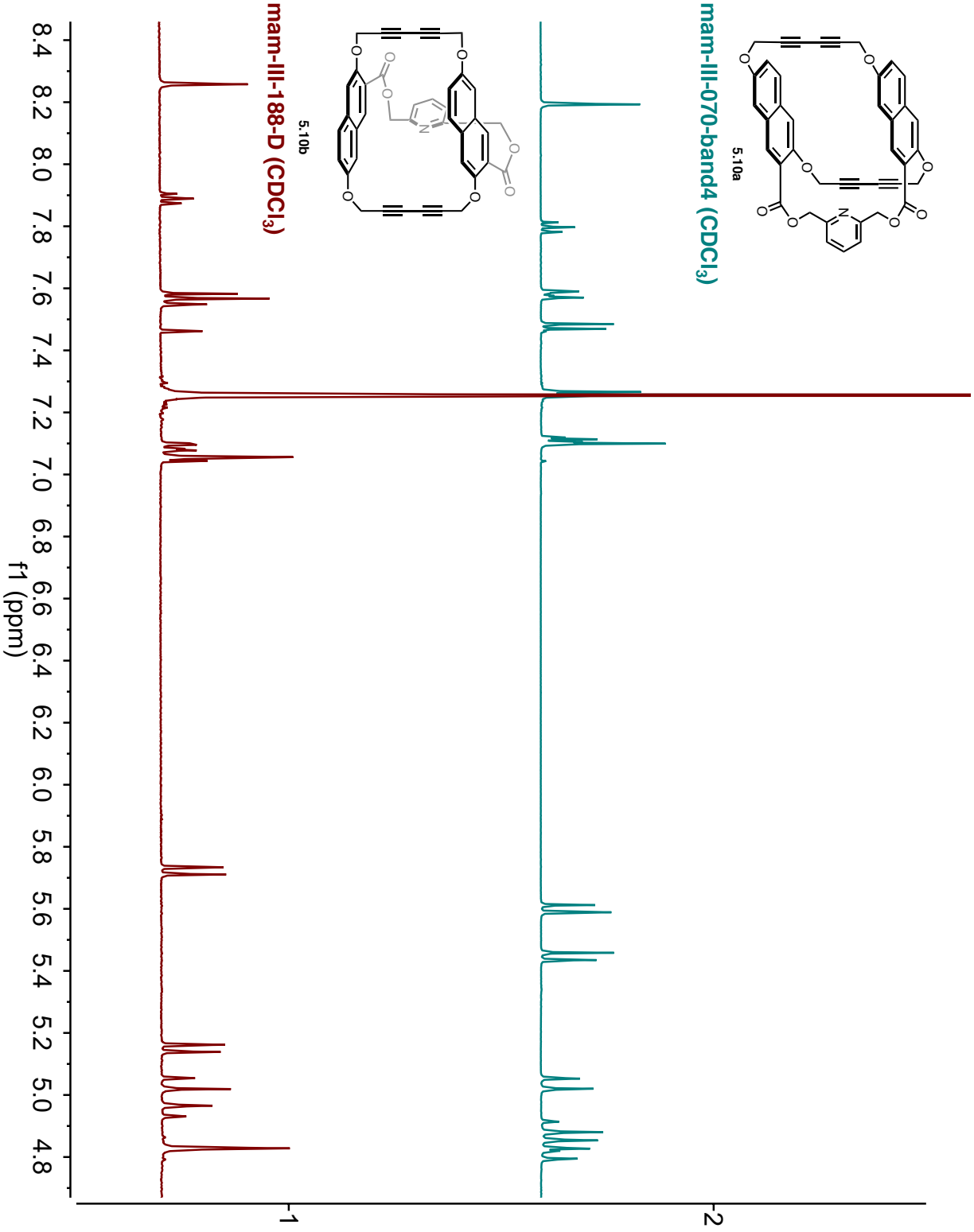
5.10a
mam-III-070-band4 (CDCl3)
5.10b
mam-III-188-D (CDCl3)
8.4
8.2
8.0
7.8
7.6
7.4
7.2
7.0
6.8
6.6
6.4
6.2
6.0
5.8
5.6
5.4
5.2
5.0
4.8
f1 (ppm)
2
1

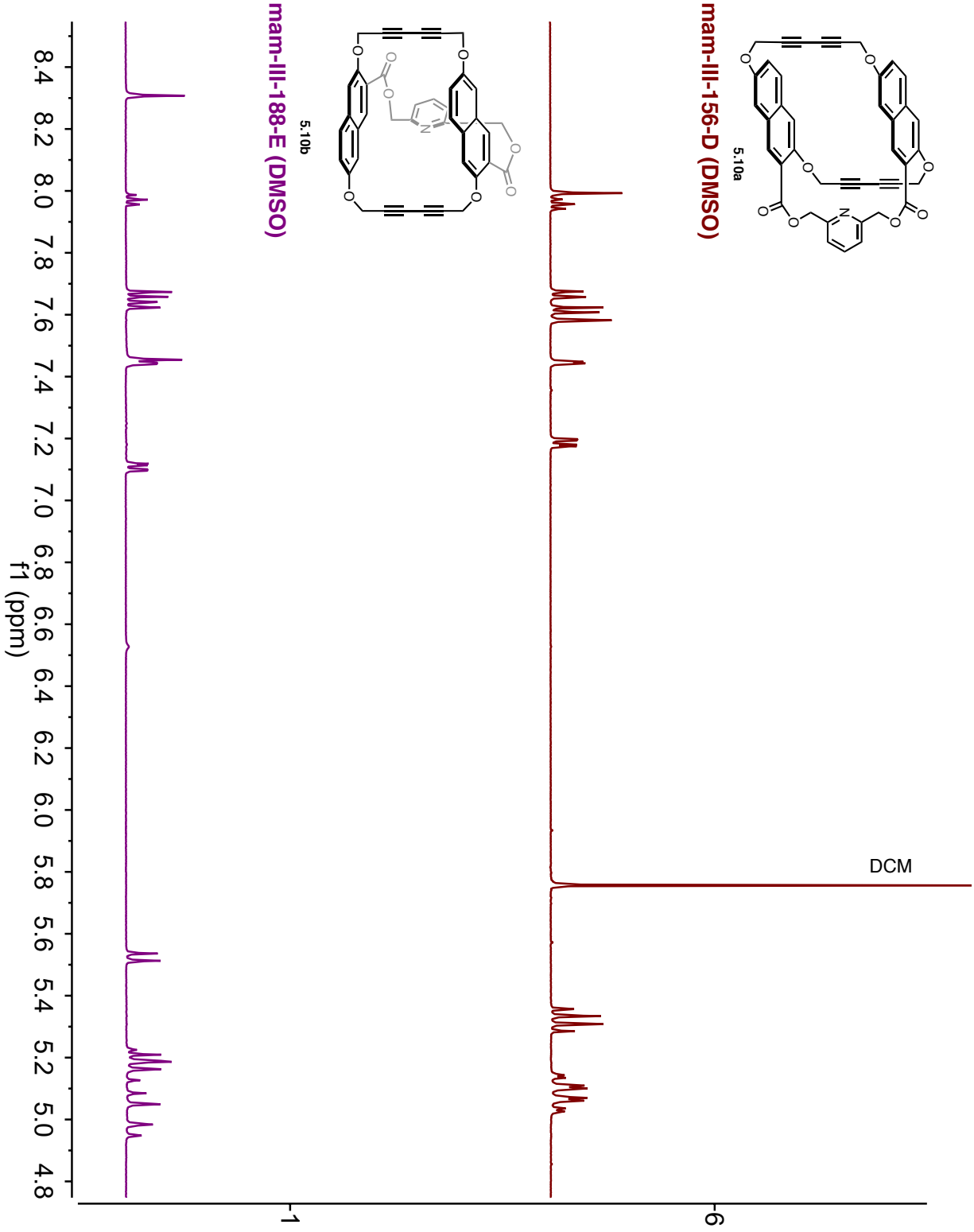
mam-III-156-D (DMSO)
5.10a
DCM
6
mam-III-188-E (DMSO)
5.10b
1
8.4
8.2
8.0
7.8
7.6
7.4
7.2
7.0
6.8
6.6
6.4
6.2
6.0
5.8
5.6
5.4
5.2
5.0
4.8
f1 (ppm)

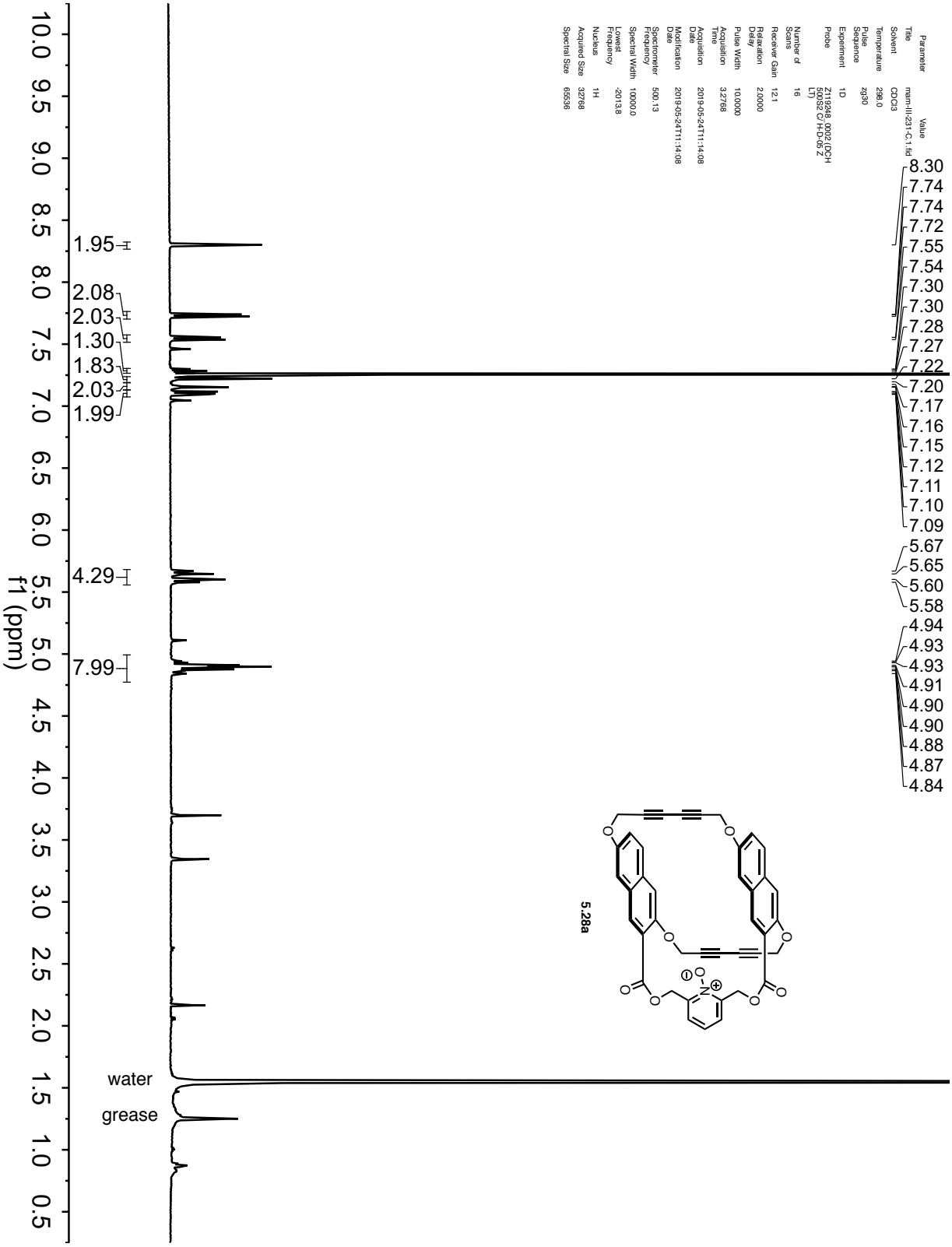
Parameter
Value
Title
mam-III-231-C.1.fid
Solvent
CDCl3
Temperature
298.0
Pulse Sequence
zg30
Experiment
1D
Probe
Z119248_0002 (DCH 500S2 Cr H-D-05 Z LT)
Number of Scans
16
Receiver Gain
12.1
Relaxation Delay
2.0000
Pulse Width
10.0000
Acquisition Time
3.2768
Acquisition Date
2019-05-24T11:14:08
Modification Date
2019-05-24T11:14:08
Spectrometer Frequency
500.13
Spectral Width
10000.0
Lowest Frequency
-2013.8
Nucleus
1H
Acquired Size
32768
Spectral Size
65536
8.30
7.74
7.74
7.72
7.55
7.54
7.30
7.30
7.28
7.27
7.22
7.20
7.17
7.16
7.15
7.12
7.11
7.10
7.09
5.67
5.65
5.60
5.58
4.94
4.93
4.93
4.91
4.90
4.90
4.88
4.87
4.84
5.28a
1.95
2.08
2.03
1.30
1.83
2.03
1.99
4.29
7.99
water
grease
f1 (ppm)
10.0
9.5
9.0
8.5
8.0
7.5
7.0
6.5
6.0
5.5
5.0
4.5
4.0
3.5
3.0
2.5
2.0
1.5
1.0
0.5

Parameter	Value
Title	mam-III-244-C.1.fid
Solvent	Acetone
Temperature	298.0
Pulse Sequence	zg30
Experiment	1D
Probe	Z119248_0002 (DCH 500S2 C/ H-D-05 Z LT)
Number of Scans	8
Receiver Gain	12.1
Relaxation Delay	2.0000
Pulse Width	10.0000
Acquisition Time	3.2768
Acquisition Date	2019-05-30T15:36:33
Modification Date	2019-05-30T15:36:33
Spectrometer Frequency	500.13
Spectral Width	10000.0
Lowest Frequency	-2007.8
Nucleus	1H
Acquired Size	32768
Spectral Size	65536

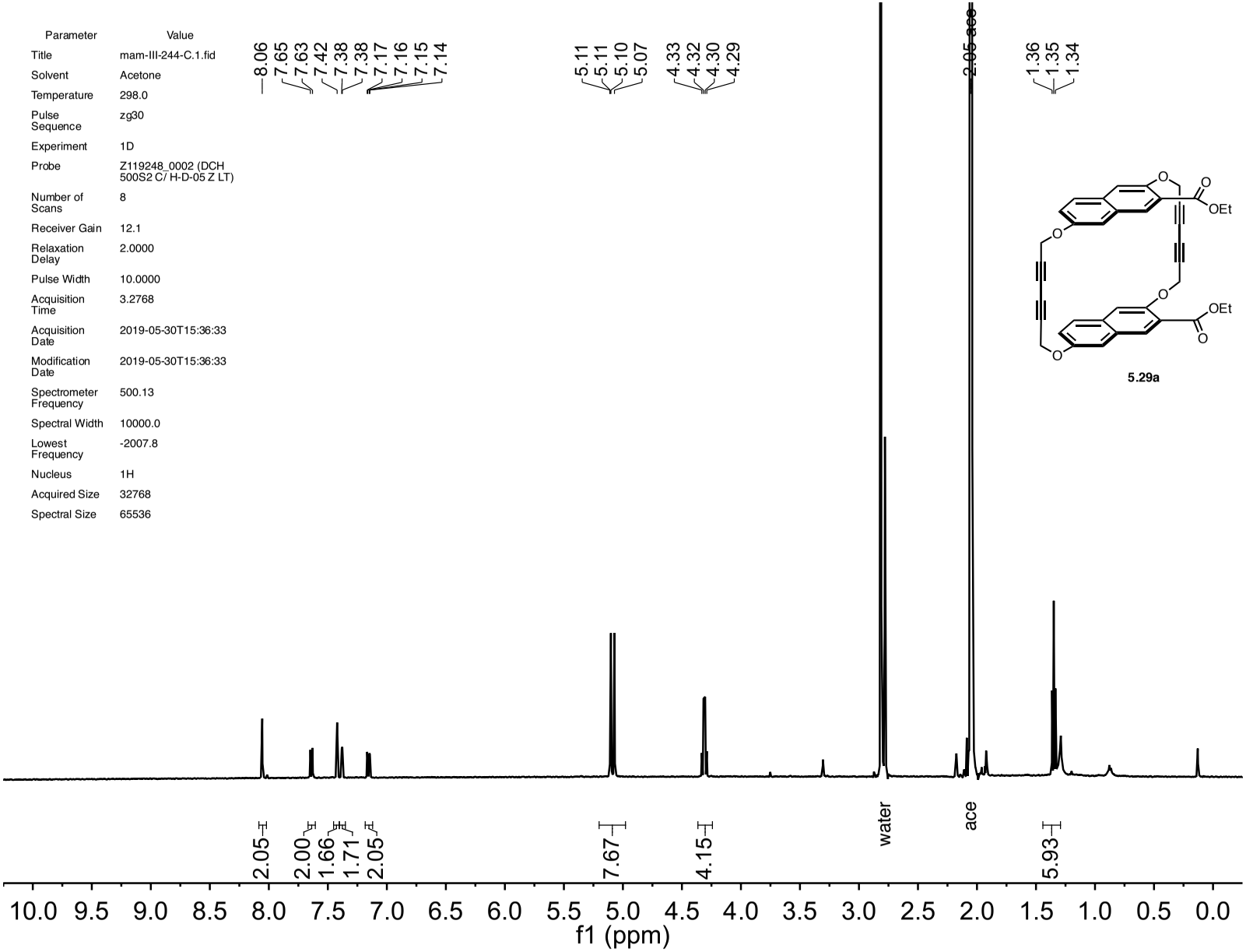

5.29a

Parameter	Value
Title	mam-IV-196-A
Solvent	Acetone
Temperature	296.7
Pulse Sequence	zg30
Experiment	1D
Probe	5 mm PABBO BB/ 19F-1H/ D Z-GRD Z108618/ 0656
Number of Scans	16
Receiver Gain	189.8
Relaxation Delay	2.0000
Pulse Width	15.0000
Acquisition Time	3.2998
Acquisition Date	2021-11-30T10:15:00
Modification Date	2021-11-30T10:15:27
Spectrometer Frequency	400.13
Spectral Width	8012.8
Lowest Frequency	-1612.4
Nucleus	1H
Acquired Size	26441
Spectral Size	65536

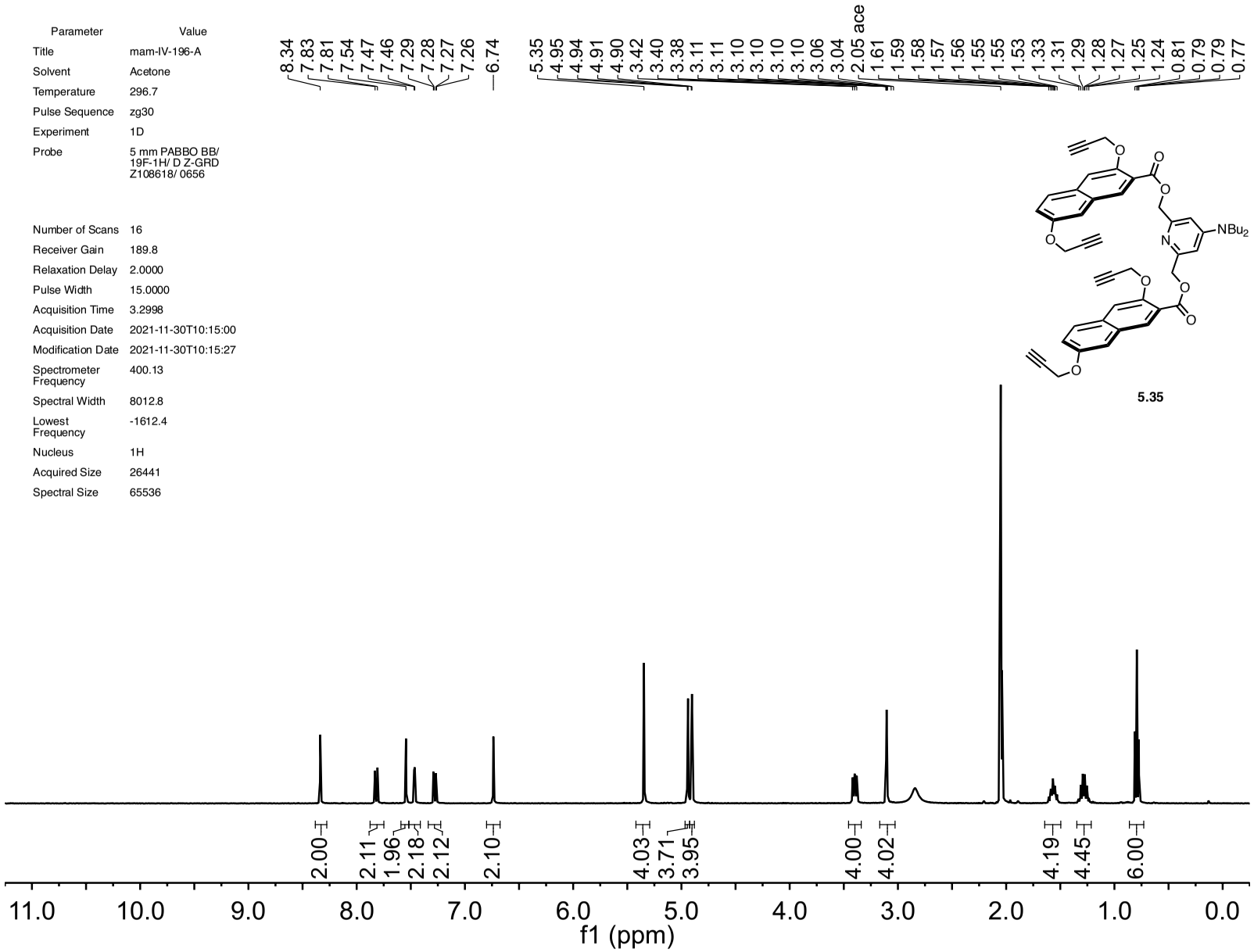

5.35

Parameter	Value
Title	mam-IV-196-A-13C.13.fid
Solvent	Acetone
Temperature	298.0
Pulse Sequence	zgpg30
Experiment	1D
Probe	Z119248_0002 (DCH 500S2 C/ H-D-05 Z LT)
Number of Scans	750
Receiver Gain	204.5
Relaxation Delay	2.0000
Pulse Width	10.5000
Acquisition Time	1.0486
Acquisition Date	2021-11-30T11:24:57
Modification Date	2021-11-30T11:24:57
Spectrometer Frequency	125.77
Spectral Width	31250.0
Lowest Frequency	-1050.0
Nucleus	13C
Acquired Size	32768
Spectral Size	65536

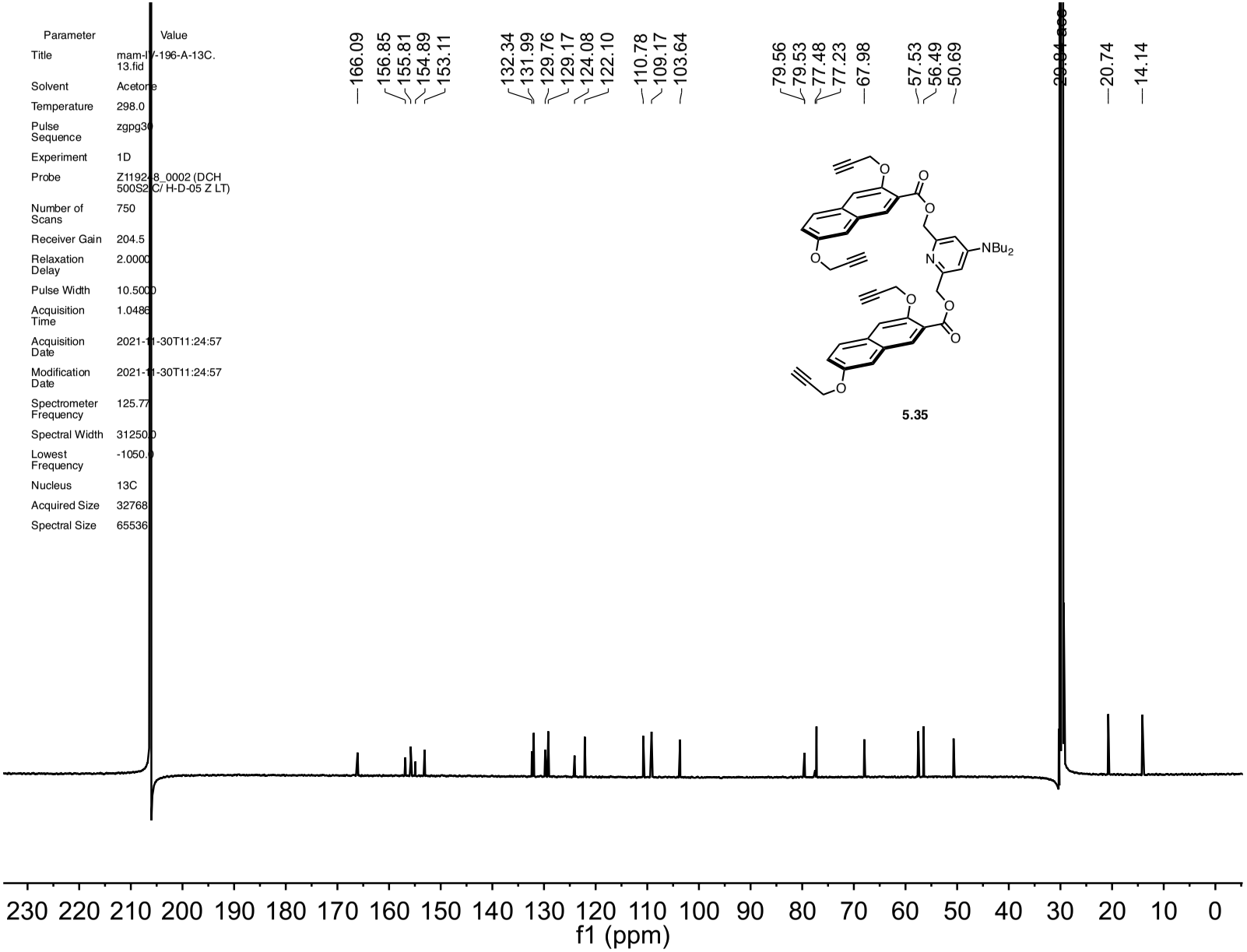

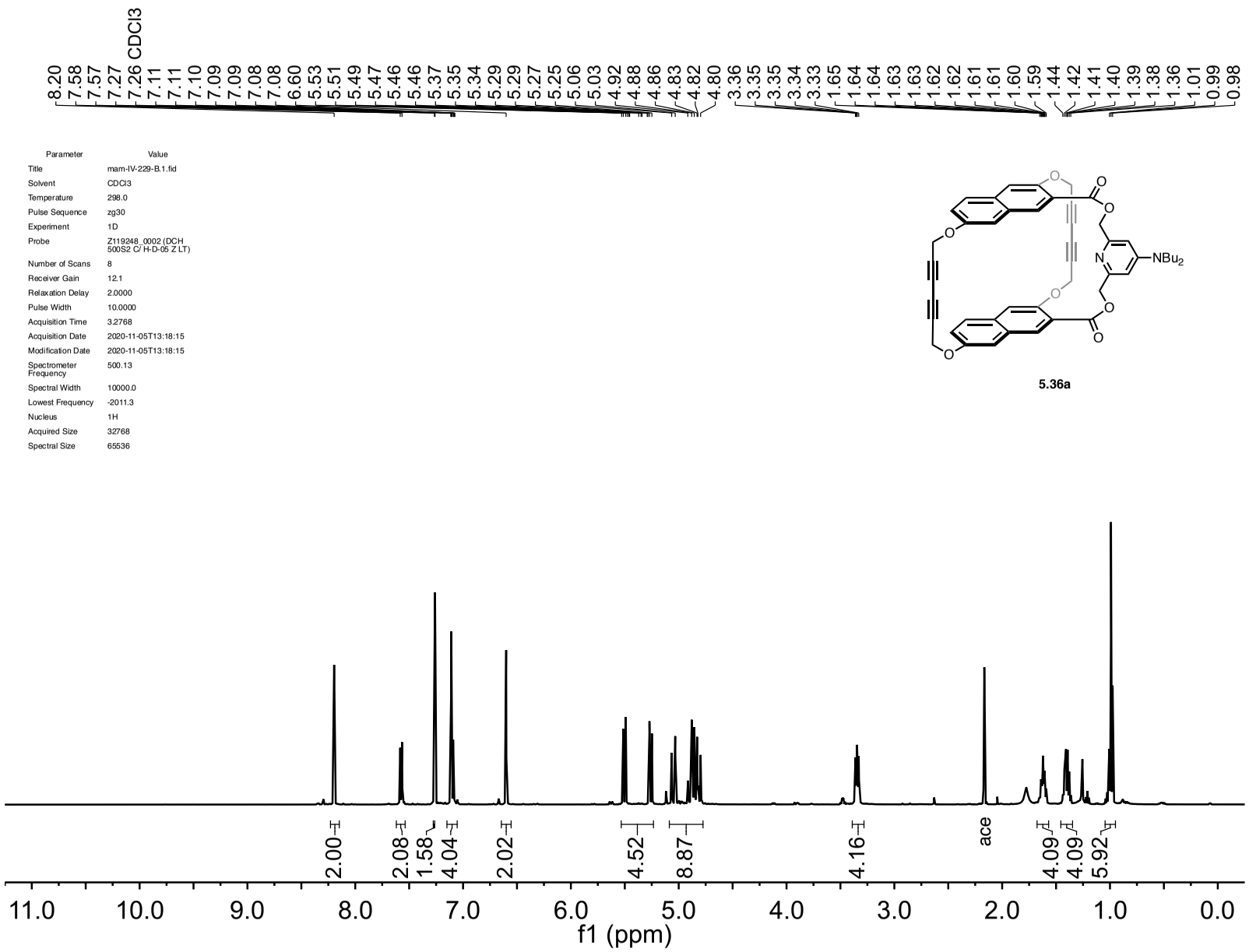

Parameter	Value
Title	mam-IV-229-B.1.fid
Solvent	CDCl3
Temperature	298.0
Pulse Sequence	zg30
Experiment	1D
Probe	Z119248_0002 (DCH 500S2 C/ H-D-05 Z LT)
Number of Scans	8
Receiver Gain	12.1
Relaxation Delay	2.0000
Pulse Width	10.0000
Acquisition Time	3.2768
Acquisition Date	2020-11-05T13:18:15
Modification Date	2020-11-05T13:18:15
Spectrometer Frequency	500.13
Spectral Width	10000.0
Lowest Frequency	-2011.3
Nucleus	1H
Acquired Size	32768
Spectral Size	65536

5.36a

Parameter	Value
Title	mam-IV-229-B-cosy.13.fid
Solvent	CDCl3
Temperature	298.0
Pulse Sequence	zgpg30
Experiment	1D
Probe	Z119248_0002 (DCH 500S2 C/ H-D-05 Z LT)
Number of Scans	64
Receiver Gain	204.5
Relaxation Delay	2.0000
Pulse Width	10.5000
Acquisition Time	1.0486
Acquisition Date	2020-11-07T16:06:31
Modification Date	2020-11-07T16:06:32
Spectrometer Frequency	125.77
Spectral Width	31250.0
Lowest Frequency	-1147.5
Nucleus	13C
Acquired Size	32768
Spectral Size	65536

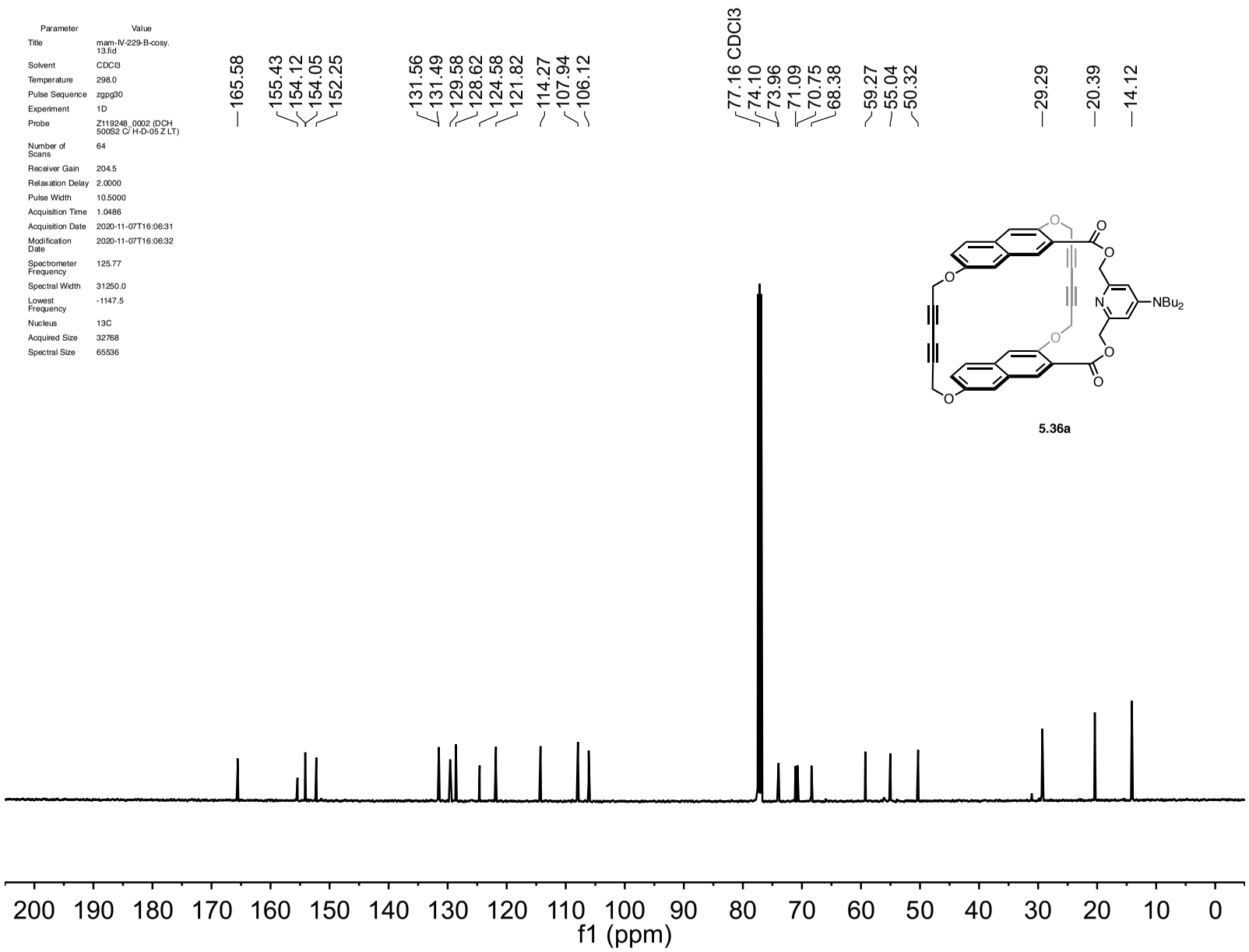

Parameter	Value
Title	Nov27-2021-sletten.50.fid
Solvent	DMSO
Temperature	296.8
Pulse Sequence	zg30
Experiment	1D
Probe	5 mm PABBO BB/ 19F-1H/ D Z-GRD Z108618/ 0656
Number of Scans	16
Receiver Gain	189.8
Relaxation Delay	2.0000
Pulse Width	15.0000
Acquisition Time	3.2998
Acquisition Date	2021-11-27T20:21:00
Modification Date	2021-11-27T20:21:52
Spectrometer Frequency	400.13
Spectral Width	8012.8
Lowest Frequency	-1608.8
Nucleus	1H
Acquired Size	26441
Spectral Size	65536

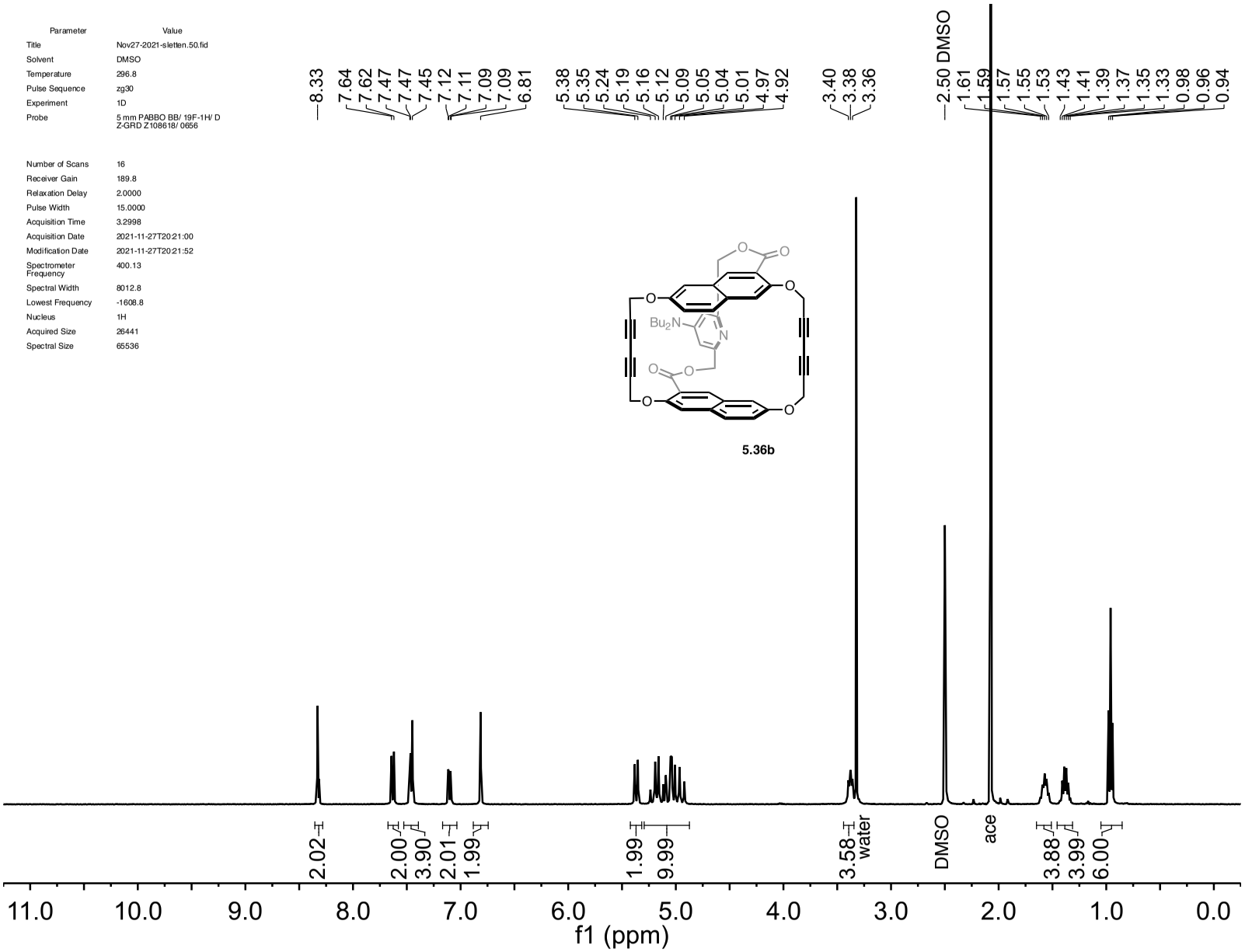

5.36b

Parameter	Value
Title	mam-IV-212-A
Solvent	DMSO
Temperature	298.0
Pulse Sequence	zgpg30
Experiment	1D
Probe	5 mm PABBO BB/ 19F-1H/ D Z-GRD Z108618/ 0656
Number of Scans	4000
Receiver Gain	189.8
Relaxation Delay	2.0000
Pulse Width	10.0000
Acquisition Time	1.2976
Acquisition Date	2021-11-28T00:07:00
Modification Date	2021-11-28T00:07:07
Spectrometer Frequency	100.62
Spectral Width	25252.5
Lowest Frequency	-1103.9
Nucleus	13C
Acquired Size	32768
Spectral Size	65536

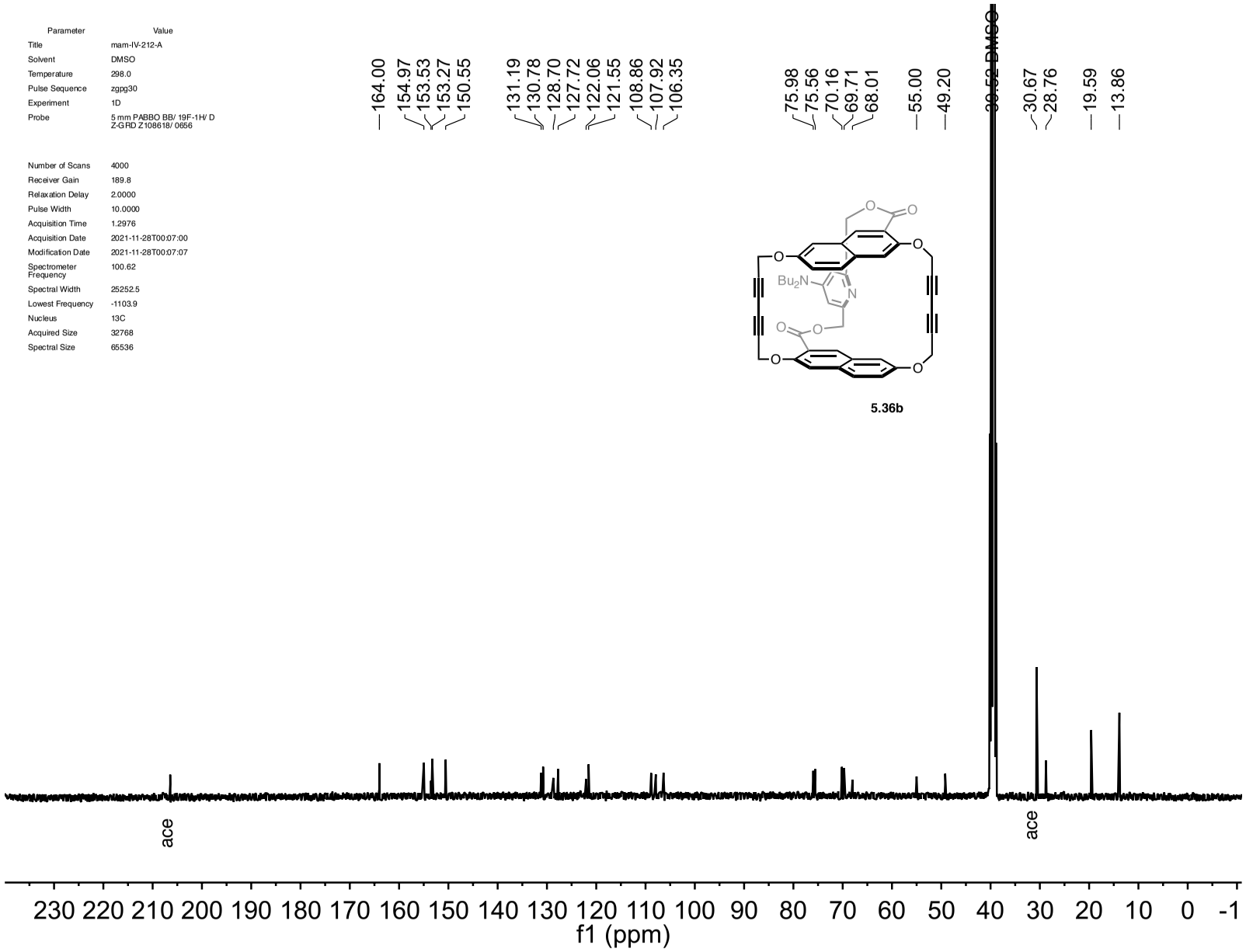

5.36b

Parameter	Value
Title	mam-IV-212-A
Solvent	DMSO
Temperature	296.8
Pulse Sequence	noesygpphpp
Experiment	NOESY
Probe	5 mm PABBO BB/ 19F-1H/ D Z-GRD Z108618/ 0656
Number of Scans	6
Receiver Gain	94.6
Relaxation Delay	2.0000
Pulse Width	15.0000
Acquisition Time	0.2867
Acquisition Date	2021-11-28T14:06:00
Modification Date	2021-11-28T15:25:17
Spectrometer Frequency	(400.13, 400.13)
Spectral Width	(3571.4, 3571.4)
Lowest Frequency	(35.6, 35.6)
Nucleus	(1H, 1H)
Acquired Size	(1024, 256)
Spectral Size	(1024, 1024)

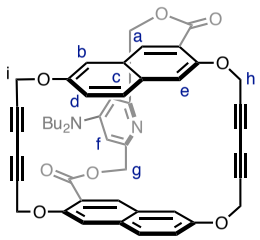

5.36b

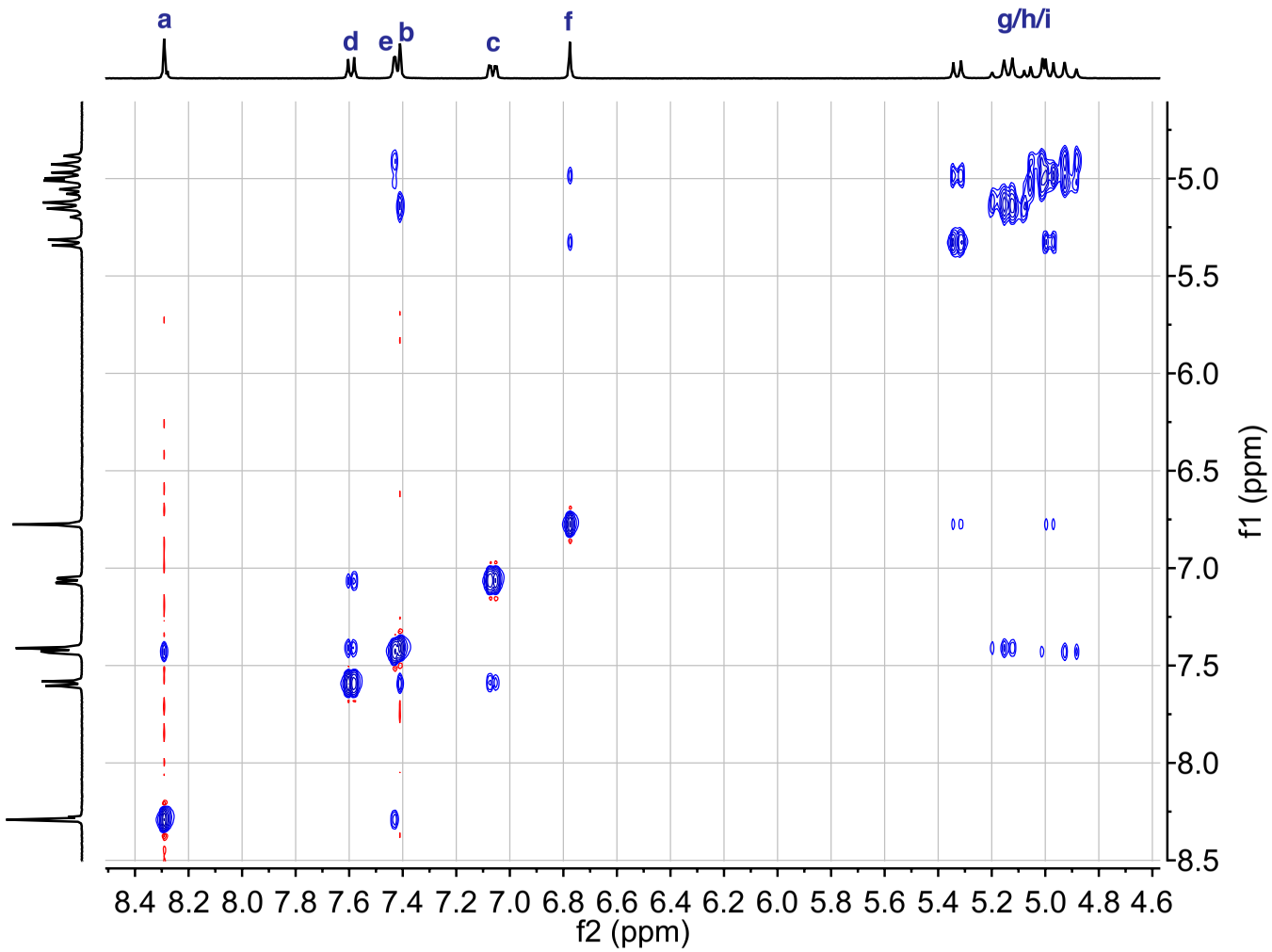

5.6 References

(1) Pace, C. J.; Zheng, H.; Mylvaganam, R.; Kim, D.; Gao, J. Stacked Fluoroaromatics as Supramolecular Synthons for Programming Protein Dimerization Specificity. *Angew. Chemie Int. Ed.* **2012**, *51*, 103–107.

(2) Zhang, C.; Welborn, M.; Zhu, T.; Yang, N. J.; Santos, M. S.; Van Voorhis, T.; Pentelute, B. L. π-Clamp-Mediated Cysteine Conjugation. *Nat. Chem.* **2015**, *8*, 120–128.

(3) Smith, C. E.; Smith, P. S.; Thomas, R. L.; Robins, E. G.; Collings, J. C.; Dai, C.; Scott, A. J.; Borwick, S.; Batsanov, A. S.; Watt, S. W.; Clark, S. J.; Viney, C.; Howard, J. A. K.; Clegg, W.; Marder, T. B. Arene-Perfluoroarene Interactions in Crystal Engineering: Structural Preferences in Polyfluorinated Tolans. *J. Mater. Chem.* **2004**, *14*, 413–420.

(4) Sharber, S. A.; Mullin, W. J.; Thomas, S. W. Bridging the Void: Halogen Bonding and Aromatic Interactions to Program Luminescence and Electronic Properties of π-Conjugated Materials in the Solid State. *Chem. Mater.* **2021**, *33*, 6640–6661.

(5) Corpinot, M. K.; Bučar, D. K. A Practical Guide to the Design of Molecular Crystals. *Cryst. Growth Des.* **2018**, *19*, 1426–1453.

(6) Roos, E.; Walter Siebert, B.; Edwin, J.; Priizkow, H.; Siebert, I. W.; Edwin, J.; Pritzkow, H. Selective Inclusion of Uncharged Guest Molecules by Neutral Hosts with Fence-Shaped Side Arms. *Angew. Chem. Int. Ed.* **1982**, *21*, 147–148.

(7) Kalchenko, O. I.; Lipkowski, J.; Kalchenko, V. I.; Vysotsky, M. A.; Markovsky, L. N. Effect of Octakis(Diethoxyphosphoryloxy)-Tert-Butyl-Calix[8]Arene in Mobile Phase on the Reversed-Phase Retention Behavior of Aromatic Compounds: Host-Guest Complex Formation and Stability Constants Determination. *J. Chromatogr. Sci.* **1998**, *36*, 269–273.

(8) Kumari, N.; Prajapati, R.; Mishra, L. Reactivity of M(En)Cl2 (M = PdII/PtII, En = 1,2-

Diaminoethane) with N,N′-Bis(Salicylidene)-p-Phenylenediamine: Binding with Hexafluorobenzene. *Polyhedron* **2008**, *27*, 241–248.

(9) Takezawa, H.; Murase, T.; Resnati, G.; Metrangolo, P.; Fujita, M. Halogen-Bond-Assisted Guest Inclusion in a Synthetic Cavity. *Angew. Chem. Int. Ed.* **2015**, *127*, 8531–8534.

(10) Assaf, K. I.; Nau, W. M. Cucurbiturils as Fluorophilic Receptors. *Supramol. Chem.* **2014**, *26*, 657–669.

(11) Tsuzuki, S.; Uchimaru, T.; Mikami, M. Intermolecular Interaction between Hexafluorobenzene and Benzene: Ab Initio Calculations Including CCSD(T) Level Electron Correlation Correction. *J. Phys. Chem. A* **2006**, *110*, 2027–2033.

(12) Lee, G. Y.; Hu, E.; Rheingold, A. L.; Houk, K. N.; Sletten, E. M. Arene-Perfluoroarene Interactions in Solution. *J. Org. Chem.* **2021**, *86*, 8425–8436.

(13) Sheridan, R. E.; Whitlock, H. W. Concave Functionality: Design of a Phenol Sticky Host. *J. Am. Chem. Soc.* **1986**, *108*, 7120–7121.

(14) Miller, S. P.; Whitlock, H. W. Novel Cyclophane-Based Hosts with Functionally Neutral Cavities. *J. Am. Chem. Soc.* **1984**, *106*, 1492–1494.

(15) Sheridan, R. E.; Whitlock, H. W. Concave Functionality: Some Exceptionally Large Binding Constants of Phenol Sticky Hosts. *J. Am. Chem. Soc.* **1988**, *110*, 4071–4073.

(16) Haeg, M. E.; Whitlock, B. J.; Whitlock, H. W. Anthraquinone-Based Cyclophane Hosts: Synthesis and Complexation Studies. *J. Am. Chem. Soc.* **1989**, *111*, 692–696.

(17) Neder, K. M.; Whitlock, H. W. Importance of Hydrogen Bond Acceptor Ability in Design of Host Molecules Capable of Molecular Recognition. *J. Am. Chem. Soc.* **1990**, *112*, 9412–9414.

(18) Whitlock, B. J.; Whitlock, H. W. Concave Functionality: Design Criteria for Nonaqueous

Binding Sites. *J. Am. Chem. Soc.* **1990**, *112*, 3910–3915.

(19) Cochran, J. E.; Parrott, T. J.; Whitlock, B. J.; Whitlock, H. W. Pi Hydrogen Bonds as a Design Principal in Molecular Recognition. *J. Am. Chem. Soc.* **1992**, *114*, 2269–2270.

(20) Cloninger, M. J.; Whitlock, H. W. A Synthetic Receptor Which Uses Multiple Edge−Face Interactions To Bind Aromatic Guests. *J. Org. Chem.* **1998**, *63*, 6153–6159.

(21) Gilli, P.; Pretto, L.; Bertolasi, V.; Gilli, G. Predicting Hydrogen-Bond Strengths from Acid-Base Molecular Properties. the pKa Slide Rule: Toward the Solution of a Long-Lasting Problem. *Acc. Chem. Res.* **2009**, *42*, 33–44.

(22) Brown & Howard, A. B.; Whitlock, W. W. Syntheses and Synthetic Studies of 2-Hydroxy-5-(Propargyloxy)Benzoic Acid. *Synth. Commun.* **1993**, *23*, 23–34.

(23) Cavallo, G.; Metrangolo, P.; Milani, R.; Pilati, T.; Priimagi, A.; Resnati, G.; Terraneo, G. The Halogen Bond. *Chem. Rev.* **2016**, *116*, 2478–2601.

(24) Thordarson, P. Determining Association Constants from Titration Experiments in Supramolecular Chemistry. *Chem. Soc. Rev.* **2011**, *40*, 1305–1323.

(25) Brynn Hibbert, D.; Thordarson, P. The Death of the Job Plot, Transparency, Open Science and Online Tools, Uncertainty Estimation Methods and Other Developments in Supramolecular Chemistry Data Analysis. *Chem. Commun.* **2016**, *52*, 12792–12805.

(26) (a) Lamture, J. B.; Hong Zhou, Z.; Suresh Kumar, A.; Wensel, T. G. Luminescence Properties of Terbium(III) Complexes with 4-Substituted Dipicolinic Acid Analogs. *Inorg. Chem.* **2002**, *34*, 864–869. (b) Kovacs, D.; Kocsi, D.; Wells, J. A. L.; Kiraev, S. R.; Borbas, K. E. Electron Transfer Pathways in Photoexcited Lanthanide(III) Complexes of Picolinate Ligands. *Dalt. Trans.* **2021**, *50*, 4244–4254.

CHAPTER SIX

A phenanthrene-based cyclophane as a receptor for pentafluorophenol-based guests

6.1 Abstract

Rational design of hosts that selectively bind one guest over other small molecules is a challenge in the field of host-guest chemistry. Perfluoroaromatics are distinct from their hydrocarbon counterparts due to the high electronegativity of fluorine. The distinct electronic character of abiotic perfluoroaromatics provides an attractive feature on which to design a receptor selective for electron-poor perfluoroaromatics over other aromatic compounds. If this selective host can be achieved, we hope to apply this host-guest system for cell-surface labeling of abiotic guests. Here, a phenanthrene-based cyclophane is designed to bind a model perfluorinated aromatic guest, pentafluorophenol. Upon synthesis, we found that this phenanthrene-based host binds both pentafluorophenol and tetrafluoro-4-hydroxy-*N*-pentylbenzamide with $K_a = 10^3$ and 10^4 M^{-1} respectively. We explore the importance of arene-perfluoroarene interactions and hydrogen bonding interactions to the overall binding affinity of this system. Ultimately, these studies will inform future iterations of cyclophane hosts based on arene-perfluoroarene interactions and hydrogen bonding.

6.2 Introduction

The design of high-affinity hosts for specific guests is challenging.[1] Historically, hosts have been synthesized and then screened against panels of guests to find high-affinity host-guest pairs.[2–6] As described in Chapter 4, bioorthogonal complexation is a term that describes the use of specific, high-affinity host-guest pairs for binding and labeling of unnatural guests incorporated on the cell surface. For the host-guest pair to be truly bioorthogonal, the host must not bind or interact with other endogenous biomolecules and metabolites. Because of the

perfluoroaromatics' unique electron-poor character, distinct from most electron-neutral or electron-rich aromatic amino acids, we imagined they would be ideal guests for bioorthogonal complexation. Our interest in using perfluoroaromatics as guests for bioorthogonal complexation provided an opportunity to address challenges in the field of rational host design for a specific guests of interest.

We envisioned that we could apply the knowledge gained from our attempts to repurpose Whitlock's naphthalene-based host (Chapter 5) into our design plan for an improved receptor for perfluoroaromatics. We found that the size of the naphthalene host cavity was too narrow to accommodate the width of a perfluoroaromatic guest, like pentafluorophenol **6.1**. We considered new hosts with a larger cavities composed of tricyclic aromatics, such as anthracene, carbazole, fluorene, acridinium, or phenanthrene (Figure 6.1A). The aromatic component needed to be stable and synthetically accessible. Ideally, this expanded host would be otherwise similar in configuration to the naphthalene-based host described in Chapter 5.

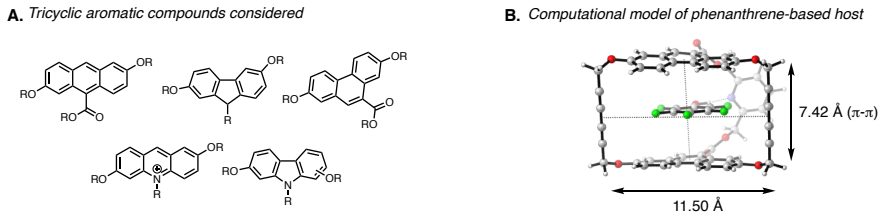

Figure 6.1 Design of an expanded cyclophane. A) Tricyclic aromatics considered as the aromatic walls of an expanded host. B) Computational model of phenanthrene-based host complexed with pentafluorophenol **1** provided by Dr. Gina Lee (B3LYP-d3/6-31G(d)).

Phenanthrene, with two Clar π-sextets, is more stable than anthracene (one Clar sextet) by ~4–8 kcal/mol.[7] This stability could lend itself to the stability of a phenanthrene-based host. Additionally, computational analyses suggested that a phenanthrene-based host would provide both the necessary length and configuration to accommodate a perfluoroaryl guest (Figure 6.1B).

While phenanthrene has been demonstrated as a guest in a number of arene-arene-based host-guest complexes,[8,9] there are limited hosts based on a phenanthrene scaffold.[10–14] Existing reports of phenanthrene-based macrocycles are often lacking in host-guest binding studies.[15] A phenanthrene host comparable to naphthalene host **5.36a** would require the synthesis of a trisubstituted phenanthrene building block such as **6.3**.

6.3 Discussion and results

Retrosynthetically, aryl halide **6.4** and boronic acid **6.5** would be needed to access the phenanthrene component of expanded host **6.2a** (Scheme 6.1). These building blocks were accessed from 2-(3-methoxyphenyl)acetic acid **6.6** and 2-bromo-5-methoxybenzaldehyde **6.7** respectively (Scheme 6.2). A microwave-assisted Suzuki-Aldol cascade reaction between **6.4** and **6.5** provided the trisubstituted phenanthrene core **6.9** in 64% yield on multi-gram scale. This approach ensures the methoxy substituents are symmetric, unlike other phenanthrene syntheses, which can suffer from poor regioselectivity.[16,17] Despite reported procedures, we found that the addition of DavePhos ligand made no significant difference in the yield.[18]

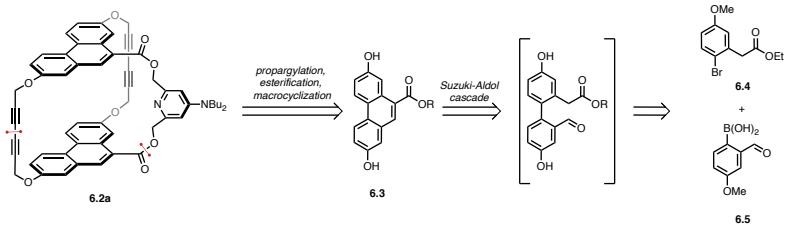

Scheme 6.1 Retrosynthesis of phenanthrene-based host **6.2a**.

Dimethoxy phenanthrene ester **6.9** was carefully deprotected with boron tribromide to provide ester **6.3a**. If not monitored closely, some hydrolysis to phenanthrene acid **6.3b** could be observed; however **6.3b** could be re-esterified or used directly if needed. **6.3a** was then treated with propargyl bromide to access dipropargyl-substituted ester **6.10** (Scheme 6.3). Minimal *C*-

propargylation of the phenanthrene diol **6.3** was observed, unlike in the naphthalene-based system (Chapter 5). Dipropargylphenanthrene ester **6.10** was hydrolyzed to access carboxylic acid **6.11**. Higher temperatures led to undesired Claisen-type rearrangement products.

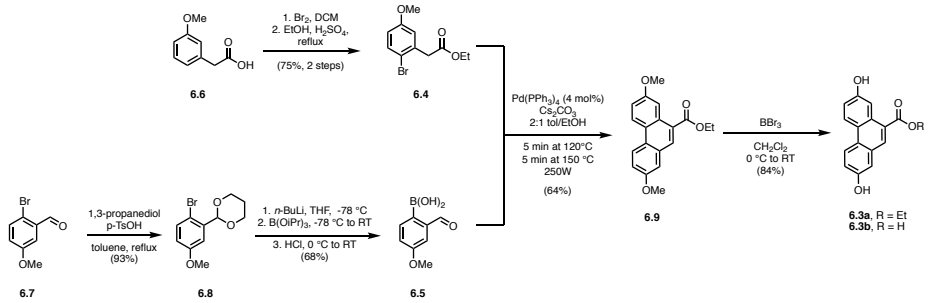

Scheme 6.2 Synthesis of trisubstituted phenanthrene **6.3**.

Phenanthrene acid **6.11** was activated as the PFP ester **6.12** and treated with 4-dibutylaminopyridine diol **6.13** to access premacrocycle **6.14** in good yield. A modified Eglinton reaction furnished two isomers of the final phenanthrene macrocycle, which could be separated by column chromatography (Figure 6.2). Single crystals were difficult to obtain of **6.2a** or **6.2b**, and a publication-quality x-ray structure was unable to be obtained to confirm isomer assignment. However, the less polar isomer was found to bind pentafluorophenol **6.1** more strongly than the more polar isomer (**K_a** = 3.8x10^3 ± 3% vs 2.9x10^3 ± 5% M^{-1}, Figure 6.3). Whitlock reported that the meso isomer of naphthalene host **5.10a** bound 4-nitrophenol **6.15** and other guests more strongly than dl-isomer of the naphthalene host **5.10b** (K_a = 2340 vs 1156 M^{-1}).[19] For these reasons, the less polar isomer has been tentatively assigned as the more symmetric meso isomer **6.2a**. Further binding studies were carried out with **6.2a** in $CDCl_3$.

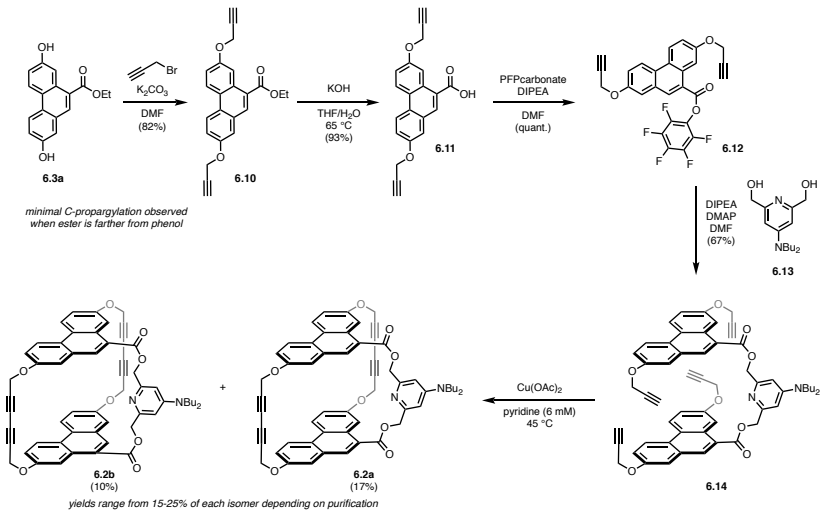

Scheme 6.3 Synthesis of phenanthrene macrocycles **6.2a** and **6.2b**.

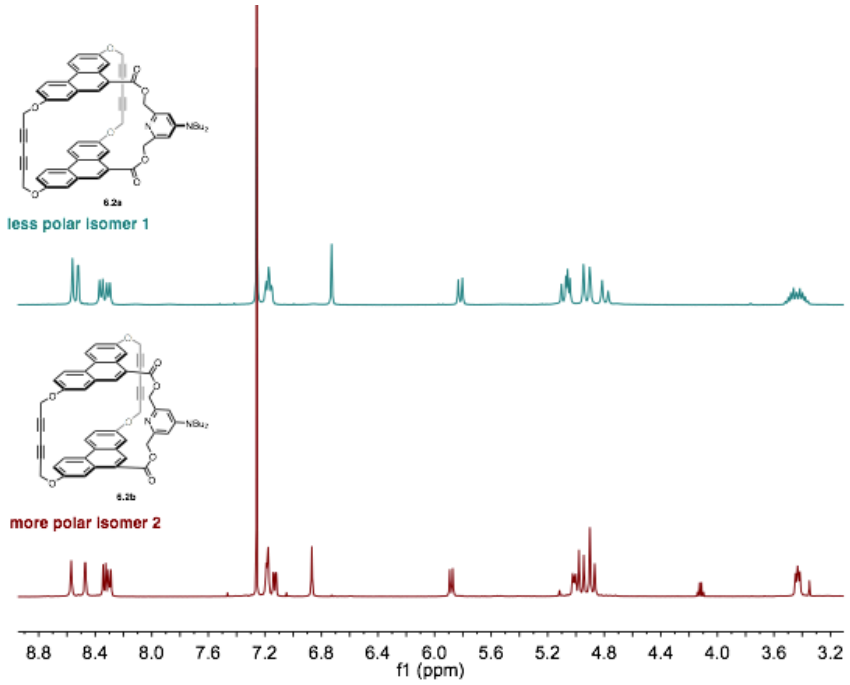

Figure 6.2 ^{1}H NMR comparison of phenanthrene hosts **6.2a** and **6.2b** in $CDCl_3$. Structures are tentatively assigned and should be further confirmed by x-ray crystallography.

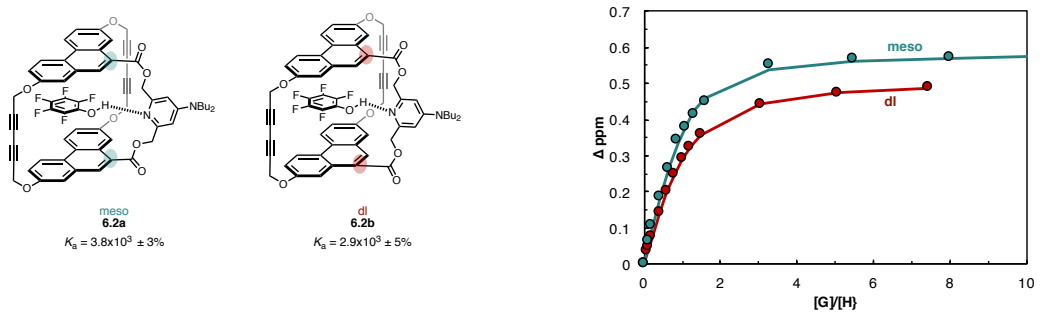

Figure 6.3 Comparison of binding affinities between hosts **6.2a** and **6.2b** with guest pentafluorophenol **6.1** in $CDCl_3$.

We were excited to find that expanded phenanthrene host **6.2a** binds pentafluorophenol **6.1** more strongly than the comparable naphthalene host **5.36a** by an order of magnitude (K_a = 3.8x10^3 M^{-1} ± 3% vs. 7.0x10^2 ± 9% M^{-1}, Figure 6.4). This difference supports the hypothesis that the phenanthrene-sized cavity is wide enough to accommodate perfluoroaryl guests. In future work, characterization of the host-guest interaction via ^{1}H-^{19}F NOESY (>300 MHz) would be insightful.

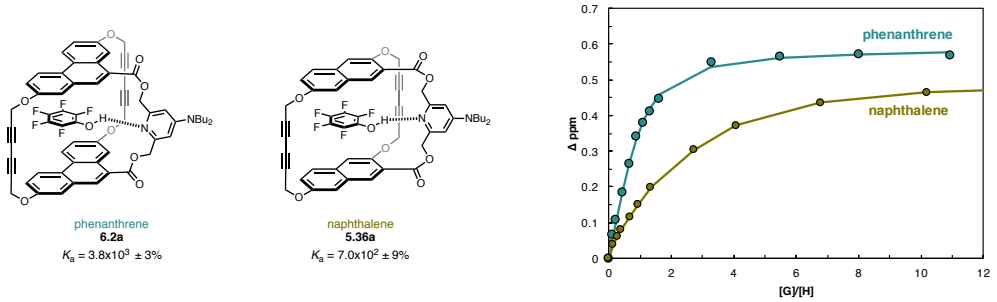

Figure 6.4 Effect of aromatic size on K_a: comparing phenanthrene host **6.2a** to naphthalene host **5.36a** complexed with pentafluorophenol **6.1** in $CDCl_3$.

While phenanthrene host **6.2a** does bind 4-nitrophenol **6.15** quite strongly (K_a = 2.5x10^4 ± 13% M^{-1}), it still binds pentafluorophenol guest **6.1** two orders of magnitude more strongly than phenol guest **6.16**, an organic-soluble substitute for tyrosine (K_a = 3.8x10^3 M^{-1} vs. 14.2 ± 0.9% M^{-1}) (Figure 6.5). This difference in K_a suggests that phenanthrene host **6.2a** may be able

to discriminate between perfluoroaromatics and biologically relevant aromatic species, which is important for bioorthogonal complexation.

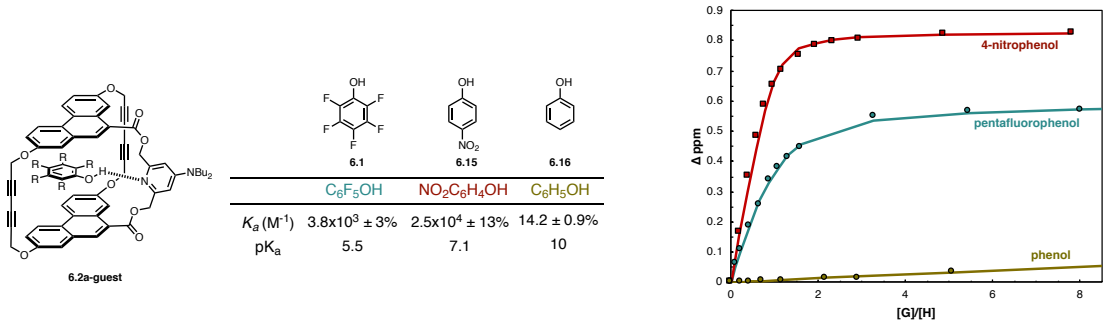

Figure 6.5 Comparison of binding interaction with host **6.2a** and phenolic guests pentafluorophenol **6.1**, 4-nitrophenol **6.15**, and phenol **6.16** in $CDCl_3$.

To explore the importance of the arene-perfluoroarene interaction to the overall binding affinity, titrations with host **6.2a** and other perfluorinated guests were performed (Figure 6.6A). With perfluorinated aromatic guests lacking classical hydrogen bond donors (hexafluorobenzene **6.17**, pentafluorobenzene **6.18**, and chloropentafluorobenzene **6.19**, minimal interaction was observed with host **6.2a** (K_a = <10 M^{-1}). Pentafluoroaniline **6.20**, which is capable of hydrogen bonding, did not bind host **6.2a** very strongly (K_a = 28.2 ± 2% M^{-1}). This low binding affinity for a perfluoroaromatic capable of hydrogen bonding is not well understood. We speculate that pentafluoroaniline (pK_a of the conjugate acid = 2.1 in 95.6% ethanol)[20] itself, rather than the conjugate acid, may not be the ideal hydrogen bonding partner for 4-dibutylaminopyridine.

We hypothesized that by removing the hydrogen-bonding capability of the host rather than the hydrogen-bonding ability of the guest, we would observe a similar dependence of the K_a on the hydrogen-bonding interaction (Figure 6.6B). Erika Aguiluz Ramirez prepared a control host **6.21a**, where a benzene ring replaces the pyridine of the linker. Kaitlin Hartung studied the interaction between control host **6.21a** and pentafluorophenol guest **6.1** by ^{1}H NMR in $CDCl_3$

and obtained a K_a = 9.5 ± 1% M^{-1} for this complex. This K_a is larger, but within the same order of magnitude as the interaction between host **6.2a** and hexafluorobenzene **6.17** (Figure 6.6C).

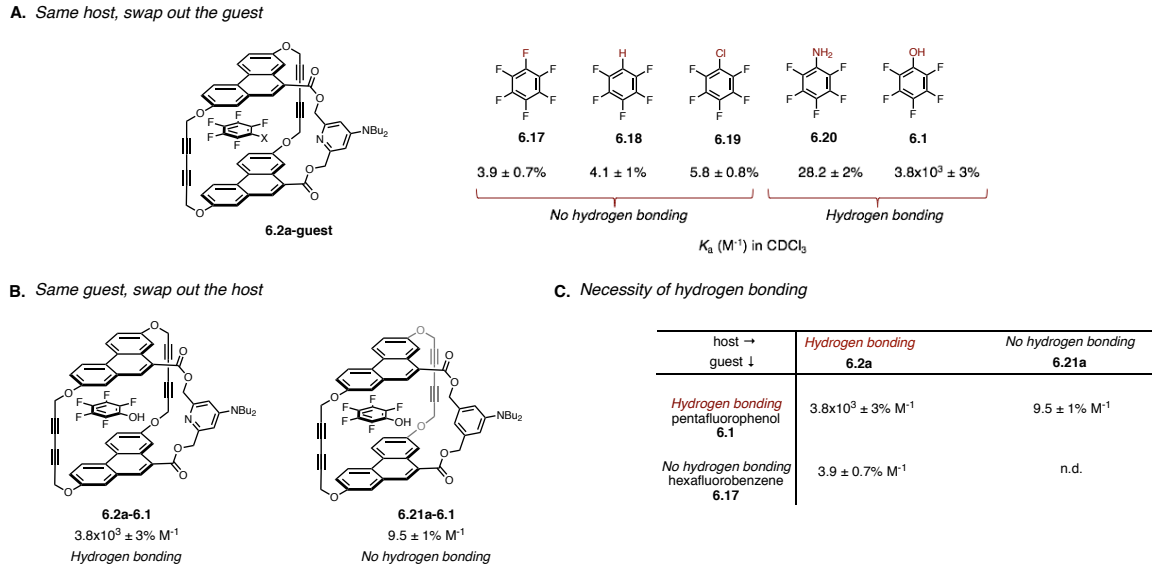

Figure 6.6 Exploration of the importance of the hydrogen-bonding interaction to the overall binding affinity. A) Complexation of host **6.2** with various perfluorinated aromatic guests in $CDCl_3$. B) Comparison of complexation strength between host **6.2a** and control host **6.20a** with guest pentafluorophenol **6.1** in $CDCl_3$. C) Summary of the importance of hydrogen bonding to this host-guest complex.

Given the low binding affinities of hexafluorobenzene **6.17**, pentafluorobenzene **6.18**, and chloropentafluorobenzene **6.19** with host **6.2a**, and the low binding affinity between control host **6.21a** and pentafluorobenzene **6.1**, it seems that the hydrogen bonding interaction is driving the complexation event in $CDCl_3$. It should be noted that these effects are observed in organic solvent. It is possible that the K_a between variants of host **6.2a** and guest **6.17**-**6.19** could be stronger in water.

We sought further explanation for the higher K_a with host **6.2a** and guest 4-nitrophenol **6.15** compared to pentafluorophenol **6.1**. One explanation could be steric effects due to fluorine substitution in both *ortho* positions of pentafluorophenol guest **6.1**. In the future, it could be interesting to study perfluoroaromatics like 3,5-difluorophenol **6.22** or 3,4,5-trifluorophenol **6.23**

to assess this hypothesis. Another explanation could be possible substituent effects between the nitro group of guest **6.15** and the C-H bonds of the phenanthrene portion of the host.

To explore the importance of substituent effects, Dr. Gina Lee prepared two additional perfluorinated aromatic guests, 2,3,5,6-tetrafluoro-4-hydroxy-*N*-pentylbenzamide **6.24** and tetrafluoro-4-nitrophenol **6.25** (Figure 6.7). In collaboration with Dr. Lee, I found that host **6.2a** forms a more stable complex with amide guest **6.25** than pentafluorophenol guest **6.1** by an order of magnitude in $CDCl_3$ ($K_a = 3.2\text{x}10^4 \pm 13\%\ M^{-1}$). This result suggests there may be some favorable interaction between the carbonyl of the amide with the phenanthrene C-H bonds, similar to the nitro group of guest **6.15**. We note that a larger change in ppm (Δppm) over the course of the titration is not always indicative of higher K_a (Table 6.1, H_a, entry 1, 2, and 5).

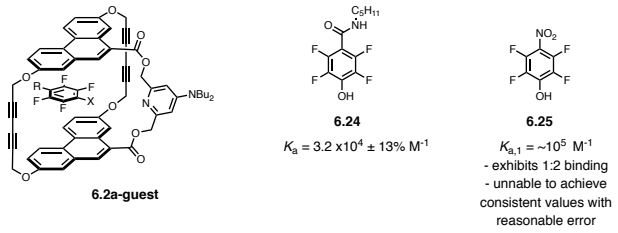

Figure 6.7 Binding affinity between host **6.2a** and custom perfluorinated phenol guests **6.24** and **6.25** in $CDCl_3$.

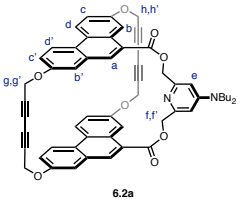

	Complex	ΔH_a	ΔH_b	$\Delta H_{d,d'}$	ΔH_e	$\Delta H_{f,f'}$
1	**6.2a**-pentafluorophenol **6.1**	0.5701	0.4315	0.1563	0.0825	0.1721
2	**6.2a**-4-nitrophenol **6.15**	0.8258	0.5494	0.2338	0.0360	0.1866
3	**6.2a**-phenol **6.16**	0.3072	0.1444	0.1179	-[1]	<0.002
4	**6.2a**-hexafluorobenzene **6.17**	0.1035	0.0286	0.0990	0.0143	0.0467
5	**6.2a**-tetrafluorohydroxy-benzamide **6.24**	0.4631	0.3315	0.1258	0.0974	0.1000
6	**6.2a**-pentafluorobenzene **6.18**	0.1107	0.0472	0.0816	0.0112	0.0409
7	**6.2a**-chloropentafluorobenzene **6.19**	0.1294	0.0329	0.1299	0.0210	0.0543
8	**6.2a**-pentafluoroaniline **6.20**	0.3027	0.1494	0.1909	<0.002	0.1255
9	**6.2a**-pentafluorophenol **6.1**	0.4839	0.3218	0.1081	0.1790	0.1337

Table 6.1 Summary of Δppm for host-guest complexes with **6.2a** and **6.2b** with 1:1 binding in $CDCl_3$. [1]For phenol guest **6.16**, proton H_e was not used because it overlaps with guest peaks. Guest tetrafluoro-4-nitrophenol **6.25** was not included as it displayed apparent 1:2 binding.

Unfortunately, a reliable K_a between host **6.2a** and tetrafluoro-4-nitrophenol **6.25** was not able to be obtained with reasonable error (<30%) (Figure 6.7). Complexation between host **6.2a** and **6.25** appears to be quite strong (K_a = >10^5 M^{-1}) in $CDCl_3$ and seems to exhibits 1:2 binding. One contribution to the large error was that **6.25** was difficult to accurately weigh on a microbalance, presumably because **6.25** is hygroscopic[21] and/or melts near room temperature. Furthermore, **6.25** may have some radical anion character.[22,23] A partially fluorinated nitrophenol may be less problematic.[24]

All the binding data with host **6.2a** and **6.2b** are summarized in Table 6.2. With **6.24** and **6.25** as additional phenolic guests, there does seem to be some correlation between an increase in K_a between the host and the guest and lower pK_a of the guest (Figure 6.8A). Moving forward, pentafluorothiophenol **6.26** (pK_a = 2.68) [25,26] could be an interesting guest to examine given its similar pK_a to tetrafluoro-4-nitrophenol **6.25** (pK_a = 2.81).[27] However, **6.26** may not be as good of a hydrogen bond donor as the corresponding phenol **6.1**, and binding studies could be complicated by disulfide formation. Tetrafluoro-4-cyanophenol **6.27** (predicted pK_a = 3.36) could also be an additional intermediate point between **6.24** and pentafluorophenol **6.1**. Hydrogen bond length, which is indicative of hydrogen bond strength, could be a more accurate parameter to correlate with K_a through computation or crystal structure data of these host-guest complexes. It may also be informative to compare K_a with Hammett constants, but more perfluorinated guests with different *para* substituents would be needed for that analysis.

Host	Guest	K_a (M^{-1}) Trial 1	K_a (M^{-1}) Trial 2	$K_{a,\ avg}$ (M^{-1})
6.2a	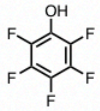 **6.1**	4248 ± 5% 0.1 to 10.9 equiv mam-IV-238	3353 ± 4% 0.25 to 9.81 equiv GL-IV-251	3.8×10^3 ± 3%
6.2a	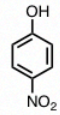 **6.15**	25870 ± 14% 0.2 to 7.81 equiv mam-V-182	25071 ± 21% 0.1 to 10.76 equiv mam-IV-240	2.5×10^4 ± 13%
6.2a	 **6.16**	15.3 ± 1% 0.2 to 102 equiv mam-IV-274	13.3 ± 0.9% 8.6 to 171 equiv GL-IV-253	14.2 ± 0.9%
6.2a	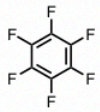 **6.17**	3.9 ± 0.8% 0.58 to 117 equiv mam-IV-276	3.79 ± 1% 25 to 500 equiv GL-IV-254	3.9 ± 0.7%
6.2a	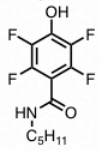 **6.24**	30910 ± 19% 0.05 to 1.9 equiv mam-VI-014	32318 ± 18% 0.05 to 2.0 equiv mam-VI-028	3.2×10^4 ± 13%
6.2a	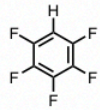 **6.18**	4.1 ± 1% 0.5 to 108 mam-IV-280	n.d.	n/a
6.2a	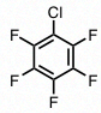 **6.19**	5.8 ± 0.8% 0.5 to 108 mam-IV-278	n.d.	n/a
6.2a	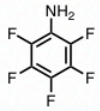 **6.20**	28.2 ± 2% 0.4 to 110 mam-IV-257	n.d	n/a
6.2b	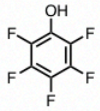 **6.1**	2870 ± 5% 0.1 to 7.43 mam-IV-244	n.d.	n/a

Table 6.2 Summary of K_as in $CDCl_3$ between host **6.2a** or **6.2b** and guests described in this chapter.

A.

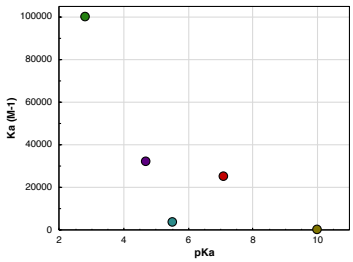

Guest	pK_a
phenol **6.16**	10
4-nitrophenol **6.15**	7.1
pentafluorophenol **6.1**	5.5
4-CONHpentyl-tetrafluorophenol **6.24**	4.69[1]
4-NO_2-tetrafluorophenol **6.25**[2]	2.81

B.

Guest	pK_a
pentafluorobenzenesulfonamide **6.28**	8.3
3,5-difluorophenol **6.30**	8.3
2,6-difluorophenol **6.29**	7.34
2,3,5,6-tetrafluorophenol **6.31**	5.67
4-propionyl-2,6-difluorophenol **6.32**	5.4
pentachlorophenol **6.33**	4.7
4-cyanotetrafluorophenol **6.27**	3.36[1]
pentafluorothiophenol **6.26**	2.68

Figure 6.8 Exploring the relevance of pKa of the guest to the overall binding affinity. A) Comparing K_a and pK_a of measured guests with host **6.2a**. B) Reported pK_as of other perhalogenated phenols that could be studied to understand the importance of pK_a in this system. [1]Predicted pK_a from Scifinder (Advanced Chemistry Development (ACD/Labs) Software V11.02). [2]K_a for tetrafluoro-4-nitrophenol **6.25** is an approximate value based on multiple titrations with large error.

As we think about future biological applications of this system, some alterations to both the host and the guest will be necessary. First, the guest will need to be able to be conjugated to a biomolecule of interest, such as a carbohydrate. Here, we show through binding studies with amide guest **6.24** that conjugation can occur through an amide linkage without decreasing the binding affinity. However, at physiological pH, pentafluorophenol **6.1** and amide derivative **6.24** will be deprotonated. It could be informative to study the complexation of **6.2a** and the sodium salt of pentafluorophenol **6.1**. An alternative solution could be to study other perfluoroaromatic guests such as pentafluorobenzenesulfonamide **6.28** (pK_a = 8.30),[28] 2,6-difluorophenol **6.29** (pK_a = 7.34),[28,29] 3,5-difluorophenol **6.30** (pK_a = 8.3),[30] 2,3,5,6-tetrafluorophenol **6.31** (pK_a = 5.67),[28] or 4-propionyl-2,6-difluorophenol **6.32** (pK_a = 5.4).[29] The former three guests **6.28-6.30** could be particularly interesting for our purposes as they have similar pK_as to 4-nitrophenol **6.15** and would remain protonated at physiological pH.

In addition to our ultimate goal of bioorthogonal complexation, an alternative application of host **6.2a** could be for sequestration of polychlorinated aromatic contaminants, like pentachlorophenol **6.33** (pK_a = 4.7).[31] **6.33** was used as a wood preservative and pesticide and is

now considered a "reasonably anticipated" human carcinogen.[32] Binding studies with **6.33** would also provide information on the size complementarity and specificity of phenanthrene host **6.2a** for perfluoroaromatics over other perhalogenated aromatic compounds.

Modifications to phenanthrene host **6.2a** such that it can be studied in the described applications will be detailed in Chapter 7. These modifications may also enable translation of this system from organic solvent to more polar solutions and aqueous media. If the host can be made water-soluble, the binding affinity to guests of interest should increase further due to the hydrophobic effect.[33]

6.4 Conclusion

In this chapter, we described the synthesis of an expanded, rigid host **6.2a** based on a phenanthrene scaffold. This host was found to act as a receptor for pentafluorophenol **6.1** with millimolar affinity. This value is similar to K_as that have been described in the literature for hexafluorobenzene guest (Chapter 5, Table 1). Phenanthrene host **6.2a** bound custom perfluorinated aromatic guest, tetrafluoro-4-hydroxy-*N*-pentylbenzamide **6.24**, with an order of magnitude higher binding affinity (10^4 M^{-1}). Binding studies presented here suggest that the K_a can be tuned through substitution at the *para* position of the perfluoroaryl phenol guests, but hydrogen bonding is necessary for a reasonable K_a in organic solvent. Phenanthrene host **6.2a** also preferentially bound pentafluorophenol **6.1** and amide variant **6.24** over phenol, a possible biologically-relevant aromatic guest, which is promising for future applications in living systems. While we have developed a host with an improved binding affinity for pentafluorophenol over the naphthalene-based system described in Chapter 5, ultimately, we would like to have a host for perfluoroaromatics with a larger than micromolar binding affinity ($>10^6$ M^{-1}). For this high K_a to be achieved, a water-soluble variant of host **6.2a** would be

beneficial. We would also like to enhance the contribution of the arene-perfluoroarene interaction to the overall K_a of the host-guest complex. To achieve this goal, we plan to expand the aromatic portion of the host in future iterations of this system.

6.5 Experimental Procedures

Chemical reagents were purchased from Sigma-Aldrich, Alfa Aesar, Fisher Scientific, Acros Organics, Synquest, or TCI and used without purification unless noted otherwise. Anhydrous dimethyl sulfoxide (DMSO) was obtained from a Sure-Seal™ bottle (Aldrich). Anhydrous and deoxygenated solvents dichloromethane (DCM), dimethylformamide (DMF), acetonitrile (MeCN), methanol (MeOH), and tetrahydrofuran (THF) were dispensed from a Grubb's-type Phoenix Solvent Drying System. Thin layer chromatography was performed using Silica Gel 60 F_{254} (EMD Millipore) plates. Flash chromatography was executed with technical grade silica gel with 60 Å pores and 40–63 μm mesh particle size (Sorbtech Technologies). Solvent was removed under reduced pressure with a Büchi Rotovapor with a Welch self-cleaning dry vacuum pump and further dried with a Welch DuoSeal pump. Bath sonication was performed using a Branson 3800 ultrasonic cleaner. NMR spectra were recorded on Bruker AV-500 (^{1}H and ^{13}C) and AV-400 (^{1}H, ^{13}C, and ^{19}F) instruments and processed with MestReNova software. NMR peaks are calibrated using residual undeuterated solvent ($CHCl_3$ at 7.26 ppm ^{1}H NMR, 77.16 ppm ^{13}C NMR). Masses for analytical measurements were taken on a Sartorius MSE6.6S-000-DM Cubis Micro Balance. HRMS (electrospray ionization (ESI)) were collected on a Thermo Scientific Q Exactive™ Plus Hybrid Quadrupole-Orbitrap™ with Dionex UltiMate 3000 RSLCnano System and LRMS (electrospray ionization (ESI)) were collected on an Agilent 1260 Infinity II HPLC-tandem MS system.

6.5.1 General host-guest titration/K_a determination procedures

The host was measured on an analytical microbalance. Host stock solutions were prepared with basified $CDCl_3$. Concentrations of host stock solutions were made below the solubility limit of the host. Guest stock solutions were prepared in basified $CDCl_3$. Preliminary titrations and the Bindsim program (http://app.supramolecular.org/bindsim/) were used to determine the approximate equivalents of guest needed for saturation. Ideally, >70% saturation was achieved. Binding data were fit using Bindfit (http://app.supramolecular.org/bindfit/).[34,35] In some cases, it was necessary to allow the samples to equilibrate before NMRs were taken to improve peak resolution and minimize broadening. Samples were performed in duplicate where indicated.

6.5.2 Equations for average K_a value determination from duplicate experiments

Equation 1: $K_{a,avg} = \frac{K_{a,1}+K_{a,2}}{2}$

Equation 2: $\Delta K_{a,avg} = \frac{1}{2}\sqrt{(\Delta K_{a,1})^2 + (\Delta K_{a,2})^2}$

6.5.3 Synthetic experimental procedures

2-(2-bromo-5-methoxyphenyl)-1,3-dioxane (6.8). Based on a modified literature procedure, 2-bromo-5-methoxybenzaldehyde **6.7** (20 g, 93 mmol, 1.0 equiv) and TsOH (1.8 g, 9.5 mmol, 0.10 equiv) were added to a 1 L three-necked flask equipped with a condenser and a Dean-Stark trap. Toluene (370 mL, 0.250 M) and 1,3-propanediol (13.4 mL, 185 mmol, 1.99 equiv) were added. The reaction was heated to reflux for 3.5 h. The reaction was cooled to RT and then washed with brine (3x). The crude was dried (Na_2SO_4), filtered, and concentrated. The crude was purified by column chromatography (silica gel, 5% EtOAc/hexanes→10% EtOAc/hexanes) to yield the

product **6.8** as a pale yellow oil (23.6 g, 86.4. mmol, 93% yield). R_f= 0.42 in 15% EtOAc/hexanes. ^{1}H NMR (400 MHz, $CDCl_3$): δ 7.40 (d, J = 8.8 Hz, 1H), 7.24 (d, J = 3.2 Hz, 1H), 6.77 (dd, J = 8.8, 3.2 Hz, 1H), 5.72 (s, 1H), 4.27 (ddt, J = 10.5, 5.0, 1.3 Hz, 2H), 4.09 – 3.97 (m, 2H), 3.81 (s, 3H), 2.25 (dtt, J = 13.6, 12.5, 5.1 Hz, 1H), 1.46 (dtt, J = 13.6, 2.7, 1.4 Hz, 1H). The spectral data were consistent with the literature report.[36]

(2-formyl-4-methoxyphenyl)boronic acid (6.5). Based on a modified literature procedure,[36] **6.7** (18.9 g, 69.0 mmol, 1 equiv) was dissolved in anhydrous THF (200 mL, 0.35 M) and cooled to -78 °C. n-BuLi (1.6 M, 48 mL, 76 mmol, 1.1 equiv) was added slowly via cannula. After 1 h, triisopropyl borate (19.9 mL, 86 mmol, 1.25 equiv) was added at -78 °C, and then the reaction was allowed to warm to RT. After 2 h, the reaction was cooled to 0 °C and 2M HCl (~200 mL) was added slowly and stirred for 1 h. The reaction mixture was collected by filtration, after rinsing with H_2O, hexanes, and cold Et_2O. Additional precipitate was recovered by a second filtration of the filtrate and further rinsing with H_2O and cold acetone. **6.5** was isolated in total as a white solid (8.5 g, 47 mmol, 68%). ^{1}H NMR (400 MHz, DMSO-d_6): δ 10.22 (s, 1H, CHO), 8.26 (s, 2H, $B(OH)_2$), 7.61 (d, J = 8.2 Hz, 1H), 7.38 (d, J = 2.6 Hz, 1H), 7.20 (dd, J = 8.2, 2.7 Hz, 1H), 3.83 (s, 3H, OCH_3). The spectral data were consistent with the literature report.[36]

Ethyl 2-(2-bromo-5-methoxyphenyl)acetate (6.4). Based on a modified literature procedure,[37] In a 250 mL three-necked flask, 2-(3-methoxyphenyl)acetic acid **6.6** (9.0 g, 54 mmol, 1.0 equiv) was dissolved in anhydrous DCM (90 mL, 0.60 M) and cooled to 0 °C. Br_2 (2.9 mL, 57 mmol, 1.05 equiv) was added slowly, and the reaction was allowed to warm to RT. After 19 h, the reaction was discolored with 0.1 M aqueous $Na_2S_2O_3$ (~100 mL) and extracted with DCM (3x).

The organic layers were dried ($MgSO_4$), filtered, and concentrated under reduced pressure. The crude material was then dissolved in absolute EtOH (180 mL, 0.3 M) and conc. H_2SO_4 (2.7 mL) was added. The reaction was heated to 80 °C for 14 h. After cooling to RT, the reaction mixture was extracted with H_2O and DCM (2x). The organic layer was washed with brine (2x), dried ($MgSO_4$), filtered, and concentrated under reduced pressure. The crude material was purified by column chromatography (1%→3%→5%→10% EtOAc/hexanes), resulting in **6.4** as a colorless oil (11.1 g, 40.6 mmol, 75% yield). R_f = 0.33 in 15% EtOAc/hexanes. ^{1}H NMR (500 MHz, $CDCl_3$): δ 7.44 (d, J = 8.7 Hz, 1H), 6.85 (d, J = 3.0 Hz, 1H), 6.71 (dd, J = 8.8, 3.1 Hz, 1H), 4.19 (q, J = 7.1 Hz, 2H), 3.79 (s, 3H), 3.74 (s, 2H), 1.27 (s, 3H). The spectral data were consistent with the literature report.[38]

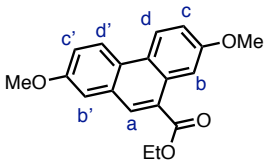

6.9

Ethyl 2,7-dimethoxyphenanthrene-9-carboxylate (6.9). Based on a modified literature procedure,[18] aryl halide **6.4** (650 mg, 2.38 mmol, 1.0 equiv), boronic acid **6.5** (600 mg, 3.33 mmol, 1.40 equiv), Cs_2CO_3 (2.33 g, 7.15 mmol, 3.00 equiv), and $Pd(PPh_3)_4$ (110 mg, 0.095 mmol, 0.04 equiv) were added to a 30 mL microwave vial equipped with a stir bar. The vial was evacuated and purged with N_2, and then degassed toluene (14 mL, 0.17 M) was added. The mixture was briefly stirred and then placed in the microwave for 5 min at 120 °C then 150 °C for 5 min. This was procedure was replicated 4x more, and the crude material was all combined. The crude was sonicated and filtered through celite, rinsing with EtOAc. The crude was passed through a silica plug and then recrystallized from hot acetone. The yellow crystals were washed with hexanes and small amounts of Et_2O. Repeated crystallizations led to **6.9** as yellow crystals

(4.73 g, 15.2 mmol, 64% yield). R_f= 0.37 in 10% Acetone/hexanes. ^{1}H NMR (500 MHz, Acetone-d_6): δ 8.69 (d, J = 9.2 Hz, 1H, $H_{d,d'}$), 8.65 (d, J = 9.1 Hz, 1H, $H_{d,d'}$), 8.52 (s, 1H, H_a), 8.45 (d, J = 2.7 Hz, 1H, $H_{b,b'}$), 7.54 (d, J = 2.7 Hz, 1H, $H_{b,b'}$), 7.39 (dd, J = 9.1, 2.7 Hz, 1H, $H_{c,c'}$), 7.34 (dd, J = 9.1, 2.7 Hz, 1H, $H_{c,c'}$), 4.49 (q, J = 7.1 Hz, 2H), 3.96 (d, J = 13.3 Hz, 6H), 1.47 (t, J = 7.1 Hz, 3H). ^{13}C NMR (126 MHz, Acetone-d_6): δ 206.2, 168.0, 159.2, 159.0, 133.2, 131.4, 130.4, 127.5, 127.0, 126.2, 125.0, 124.8, 120.9, 118.2, 110.3, 108.0, 61.7, 55.9, 55.6, 14.7. HRMS (ESI) calcd. for $C_{19}H_{19}O_4$ $(M+H)^+$: calc. 311.1278; found 311.1288.

Ethyl 2,7-dihydroxyphenanthrene-9-carboxylate (6.3a). Dimethoxyphenanthrene ester **6.9** (1.00 g, 3.22 mmol, 1.00 equiv) was dissolved in CH_2Cl_2 (17 mL, 0.19 M). The reaction mixture was cooled to 0 °C, and BBr_3 (1.20 mL, 12.6 mmol, 3.93 mmol) was added carefully. The reaction was let warm to RT and monitored for disappearance of starting material and formation of diol ester **6.3a** and diol acid **6.3b**. After 2.5 h, the reaction was quenched with absolute EtOH (~30 mL). The reaction mixture was concentrated (a base trap was used between the rotovap pump and the flask) and evaporated onto SiO_2. The crude product was purified by column chromatography (silica gel, 40%→50%→60% EtOAc/Hexanes). The product **6.3a** was isolated as a yellow crystalline solid (761 mg, 2.70 mmol, 84%). R_f = 0.32 in 40% acetone/hexanes. ^{1}H NMR (500 MHz, Methanol-d_4): δ 8.53 (d, J = 9.1 Hz, 1H), 8.51 – 8.47 (m, 1H), 8.25 (s, 1H), 8.18 (d, J = 2.6 Hz, 1H), 7.29 – 7.23 (m, 2H), 7.19 (dd, J = 9.0, 2.6 Hz, 1H), 4.47 (q, J = 7.1 Hz, 2H), 1.48 (t, J = 7.1 Hz, 3H). ^{13}C NMR (126 MHz, Methanol-d_4): δ 169.4, 156.9, 156.8, 132.8, 131.7, 130.6, 127.4, 127.2, 126.0, 124.9, 124.7, 120.8, 118.4, 113.3, 110.8, 62.2, 14.7. HRMS (ESI) calcd. for $C_{17}H_{13}O_4$ $(M-H)^-$: calc. 281.0819; found 281.0893

Ethyl 2,7-bis(prop-2-yn-1-yloxy)phenanthrene-9-carboxylate (6.10). To phenanthrene ester diol **6.3a** (2.0 g, 7.1 mmol, 1.0 equiv) and K_2CO_3 (2.94 g, 21.3 mmol, 3.00 equiv) was added anhydrous DMF (22 mL, 0.32 M). The solution was stirred for 30 min and then propargyl bromide (80 wt% in toluene, 2.4 mL, 22 mmol, 3.1 equiv) was added and the reaction was stirred vigorously. The reaction was done in duplicate, and the crude reaction mixture of both was combined after 21 h. The DMF was removed and the crude was evaporated onto silica. The crude material was purified by column chromatography (silica gel, 10%→20%→30%→50% acetone/hexanes) to yield **6.10** as a yellow solid (4.0 g, 11 mmol, 82%). R_f = 0.62 in 40% EtOAc/hexanes. ^{1}H NMR (500 MHz, $CDCl_3$): δ 8.55 (dd, J = 6.0, 3.2 Hz, 2H), 8.53 – 8.49 (m, 1H), 8.47 (s, 1H), 7.43 – 7.39 (m, 2H), 7.37 (dd, J = 9.2, 2.7 Hz, 1H), 4.88 (d, J = 2.4 Hz, 2H), 4.86 (d, J = 2.4 Hz, 2H), 4.52 (q, J = 7.2 Hz, 2H), 2.59 – 2.56 (m, 2H), 1.51 (t, J = 7.1 Hz, 3H). ^{13}C NMR (126 MHz, $CDCl_3$): δ 167.8, 156.4, 155.9, 132.8, 130.4, 129.7, 127.5, 126.3, 125.9, 124.2, 124.1, 120.4, 118.1, 111.1, 108.5, 78.6, 78.5, 76.1, 75.7, 61.4, 56.2, 56.1, 14.6. HRMS (ESI) calcd. for $C_{23}H_{19}O_4$ $(M+H)^+$: 359.1278; found 359.1279.

2,7-bis(prop-2-yn-1-yloxy)phenanthrene-9-carboxylic acid (6.11). To a 250 mL flask was added **6.10** (1.88 g, 5.25 mmol, 1.00 equiv) and powdered KOH (883 mg, 15.7 mmol, 3.00 equiv). THF (26 mL, 0.20 M) and H_2O (15 mL, 0.35 M) were added. The reaction was heated to 65 °C. The reaction was monitored for conversion by TLC, and additional KOH (500 mg) was added at 3 h and 18 h. When the starting material was not observed by TLC, the reaction was cooled to RT. The crude reaction mixture was diluted with EtOAc (100 mL) and 1 M HCl was added. The organic layer was separated and the aqueous layer was further extracted with EtOAc (3x). The organics were dried ($MgSO_4$), filtered, and concentrated to yield the product **6.11** as a

yellow powdery solid (1.73 g, 5.24 mmol, quantitative). ^{1}H NMR (400 MHz, DMSO-d_6): δ 13.21 (s, 1H), 8.77 (d, J = 9.3 Hz, 1H), 8.72 (d, J = 9.2 Hz, 1H), 8.52 – 8.43 (m, 2H), 7.67 (d, J = 2.7 Hz, 1H), 7.43 (ddd, J = 10.3, 9.1, 2.8 Hz, 2H), 4.97 (d, J = 2.4 Hz, 2H), 4.94 (d, J = 2.4 Hz, 2H), 3.63 (t, J = 2.3 Hz, 1H), 3.62 – 3.59 (m, 1H).^{13}C NMR (126 MHz, DMSO-d_6): δ 168.6, 155.7, 155.5, 132.1, 130.0, 129.1, 126.4, 126.4, 125.2, 124.6, 124.3, 119.8, 117.0, 111.4, 109.4, 79.1, 78.5, 78.5, one C missing, 55.7, 55.6. HRMS (ESI) calcd. for $C_{21}H_{13}O_4$ $(M-H)^-$: 329.081924; found 329.0800.

Perfluorophenyl 2,7-bis(prop-2-yn-1-yloxy)phenanthrene-9-carboxylate (6.12). See prep included with the synthesis of **6.14**. R_f = 0.31 in 20% acetone/hexanes. ^{1}H NMR (500 MHz, Acetone-d_6): δ 9.01 (s, 1H), 8.83 (d, J = 9.2 Hz, 1H), 8.78 (d, J = 9.2 Hz, 1H), 8.55 (d, J = 2.8 Hz, 1H), 7.78 (d, J = 2.8 Hz, 1H), 7.56 (dd, J = 9.1, 2.7 Hz, 1H), 7.49 (dd, J = 9.2, 2.7 Hz, 1H), 5.02 (d, J = 2.4 Hz, 2H), 4.97 (d, J = 2.4 Hz, 2H), 3.17 (t, J = 2.4 Hz, 1H), 3.12 (t, J = 2.4 Hz, 1H). ^{19}F NMR (376 MHz, Acetone-d_6): δ -154.46 – -154.94 (m), -160.13 (t, J = 21.2 Hz), -164.29 – -165.03 (m).

(4-(dibutylamino)pyridine-2,6-diyl)bis(methylene) bis(2,7-bis(prop-2-yn-1-yloxy)phenanthrene-9-carboxylate) (6.14). To a flame-dried 250 mL flask was added **6.11** (2.0 g, 6.1 mmol, 1.0 equiv) and bis(perfluorophenyl) carbonate (2.86 g, 7.26 mmol, 1.19 equiv). Anhydrous DMF (30 mL, 0.20 M) was added, and the solution was cooled to 0 °C. DIPEA (1.3 mL, 7.5 mmol, 1.2 equiv) was added, and the reaction was allowed to warm to room temperature. After 1 h, the reaction was concentrated under reduced pressure and placed on high vacuum overnight to yield **6.12** as a yellow solid. Diol **6.13** (645 mg, 2.42 mmol, 0.397 equiv) and DMAP (295 mg, 2.42 mmol, 0.397 equiv) were added to the phenanthrene PFPester **6.12**.

The reaction mixture was redissolved in DMF (20 mL, 0.31 M), and additional DIPEA (890 uL, 5.1 mmol, 0.84 equiv) was added. The reaction was monitored by LCMS, and after 3 days the solvent was removed under reduced pressure. The crude was evaporated onto silica from acetone and purified by column chromatography (silica gel, 20% acetone/hexanes→80% acetone/hexanes) to remove excess **6.12**. Partially pure product **6.14** was collected and recrystallized from acetone and heptane. The yellow precipitate was washed with heptane to yield **6.14** (1.45 g, 1.62 mmol, 67% yield). R_f = 0.6 in 50% EtOAc/hexanes. ^{1}H NMR (500 MHz, DMSO-d_6): δ 8.74 (d, J = 9.3 Hz, 2H), 8.70 (d, J = 9.2 Hz, 2H), 8.59 (s, 2H), 8.41 (d, J = 2.7 Hz, 2H), 7.63 (d, J = 2.7 Hz, 2H), 7.44 (dd, J = 9.1, 2.7 Hz, 2H), 7.40 (dd, J = 9.2, 2.7 Hz, 2H), 6.67 (s, 2H), 5.44 (s, 4H), 4.93 (d, J = 2.4 Hz, 4H), 4.89 (d, J = 2.4 Hz, 4H), 3.61 (t, J = 2.3 Hz, 2H), 3.57 (t, J = 2.3 Hz, 2H), 3.26 (t, J = 7.8 Hz, 4H), 1.44 – 1.35 (m, 4H), 1.09 (h, J = 7.4 Hz, 4H), 0.59 (t, J = 7.4 Hz, 6H). ^{13}C NMR (126 MHz, DMSO-d_6): δ 166.5, 155.8, 155.7, 155.5, 153.4, 132.5, 129.8, 128.7, 126.5, 125.3, 125.2, 124.6, 124.3, 120.1, 117.2, 111.4, 108.9, 102.7, 79.0, 79.0, 78.5, 78.4, 67.2, 55.7, 55.6, 49.4, 28.6, 19.4, 13.5. HRMS (ESI) calcd. for $C_{57}H_{51}N_2O_8$ $(M+H)^+$: 891.363976; found 891.3801.

Phenanthrene-NBu$_2$ host (6.2). Prehost **6.14** (1.45 g, 1.63 mmol, 1.0 equiv) was dissolved in pyridine (140 mL, 0.01 M). Over 2 h, **6.14** was added to a solution of $Cu(OAc)_2$ (3.7 g, 20.4 mmol, 12.5 equiv) in pyridine (140 mL) at 45 °C. After 4 h, the pyridine was removed under reduced pressure. The crude was suspended in $CHCl_3$ and filtered to remove oligomeric precipitate. The $CHCl_3$ organics were washed with 1 M HCl. The aqueous was extracted with $CHCl_3$ (3x), and the combined organics were washed with saturated aq NH_4Cl (1x). The crude was dried ($MgSO_4$), filtered, and concentrated. The crude was evaporated on silica and purified

by column chromatography (silica gel, 30%→40%→50%→60%→70%→80% EtOAc/hexanes→100% EtOAc). The less polar isomer (isomer 1) **6.2a** was isolated as an off-white solid (217 mg, 0.245 mmol, 17% yield). Fractions containing a mixture of isomers were repurified with a more polar gradient to yield isomer 2 **6.2b** (124 mg, 0.140 mmol, 10% yield) as an off-white solid).

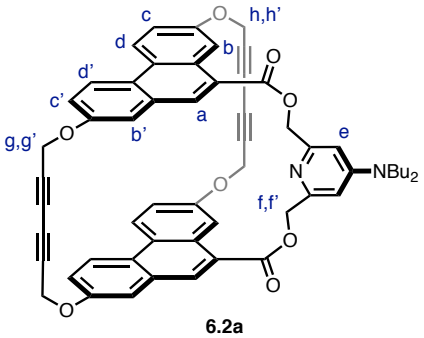

6.2a

PhenanthreneNBu$_2$ host isomer 1 (6.2a): R_f = 0.36 in 50% EtOAc/hexanes. ^{1}H NMR (500 MHz, $CDCl_3$): δ 8.56 (s, 2H, H_a), 8.52 (d, J = 2.3 Hz, 2H, H_b), 8.36 (d, J = 9.1 Hz, 2H, $H_{d,d'}$), 8.31 (d, J = 9.0 Hz, 2H, $H_{d,d'}$), 7.25 (d, 2H, under $CHCl_3$ peak, $H_{b'}$), 7.17 (td, J = 8.9, 2.6 Hz, 4H $H_{c,c'}$), 6.73 (s, 2H, H_e), 5.82 (d, J = 11.8 Hz, 2H), 5.17 – 4.70 (m, 10H), 3.44 (ddt, J = 38.9, 15.0, 7.7 Hz, 4H), 1.79 – 1.67 (m, 4H), 1.52 – 1.42 (m, 4H), 1.05 (t, J = 7.3 Hz, 6H). ^{13}C NMR (126 MHz, $CDCl_3$): δ 167.1, 155.9, 155.1, 155.0, 154.1, 133.6, 130.4, 129.8, 127.3, 126.0, 125.2, 124.0, 123.8, 120.9, 118.2, 109.7, 109.5, 106.0, 74.8, 73.2, 71.4, 70.4, 68.4, 55.5, 55.4, 50.4, 29.4, 20.5, 14.1. ^{1}H NMR (500 MHz, CD_2Cl_2): δ 8.49 (s, 2H, H_a), 8.48 (d, J = 2.8 Hz, 2H, H_b), 8.40 (d, J = 9.1 Hz, 2H, $H_{d,d'}$), 8.34 (d, J = 9.1 Hz, 2H, $H_{d,d'}$), 7.30 (d, J = 2.7 Hz, 2H, H_b), 7.20 (dt, J = 9.1, 2.9 Hz, 4H, $H_{c,c'}$), 6.74 (s, 2H, H_e), 5.70 (d, J = 11.6 Hz, 2H, $H_{f,f'}$), 5.07 (d, J = 11.8 Hz, 2H, $H_{f,f'}$), 5.03 – 4.84 (m, 8H), 3.45 (td, J = 7.1, 2.0 Hz, 4H), 1.73 (p, J = 7.7 Hz, 4H), 1.53 – 1.43 (m, 4H), 1.06 (t, J = 7.3 Hz, 6H). ^{13}C NMR (126 MHz, CD_2Cl_2): δ 167.4, 156.0, 155.5, 155.3, 154.4, 133.4, 130.7, 129.9, 127.4, 126.1, 125.9, 124.3, 124.3, 121.1, 117.9, 109.9, 109.6,

106.3, 75.0, 74.0, 71.0, 70.4, 68.8, 55.8, 55.6, 50.7, 29.6, 20.7, 14.2. HRMS (ESI) calcd. for $C_{57}H_{47}N_2O_8$ $(M+H)^+$: 887.3326; found 887.3443.

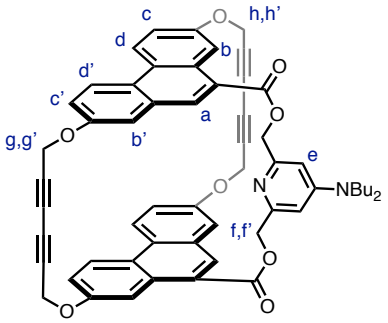

6.2b

PhenanthreneNBu$_2$ host isomer 2 (6.2b). R_f = 0.14 in 50% EtOAc/hexanes. ^{1}H NMR (500 MHz, $CDCl_3$): δ 8.57 (s, 2H, H_a), 8.47 (d, J = 2.7 Hz, 2H, H_b), 8.34 (d, J = 9.2 Hz, 2H, $H_{d,d'}$), 8.30 (d, J = 9.7 Hz, 2H, $H_{d,d'}$), 7.20 – 7.18 (m, 4H, $H_{b'}$ and $H_{c,c'}$), 7.13 (dd, J = 9.0, 2.7 Hz, 2H, $H_{c,c'}$), 6.87 (s, 2H, H_e), 5.88 (d, J = 10.9 Hz, 2H), 5.06 – 4.82 (m, 10H), 3.48 – 3.40 (m, 4H), 1.76 (p, J = 7.7 Hz, 4H), 1.50 (h, J = 7.5 Hz, 4H), 1.10 (t, J = 7.3 Hz, 6H). ^{13}C NMR (126 MHz, $CDCl_3$): δ 167.0, 155.6, 155.2, 154.7, 154.0, 133.7, 130.2, 129.8, 127.4, 125.9, 125.1, 124.0, 124.0, 121.2, 118.7, 109.4, 107.8, 107.7, 73.8, 73.8, one C missing, 70.6, 68.6, 55.0, 54.8, 50.6, 29.3, 20.5, 14.1. HRMS (ESI) calcd. for $C_{57}H_{47}N_2O_8$ $(M+H)^+$: 887.3326; found 887.3455.

6.5.4 NMR titrations

Complex of **6.2a** and **6.1** in $CDCl_3$ (mam-IV-238)

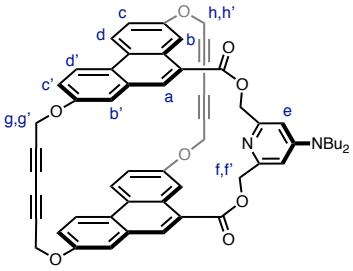

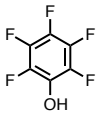

Host: **6.2a**

[H] = 0.93 mM

Guest: **6.1**

[G] = 0 - 10.1 mM

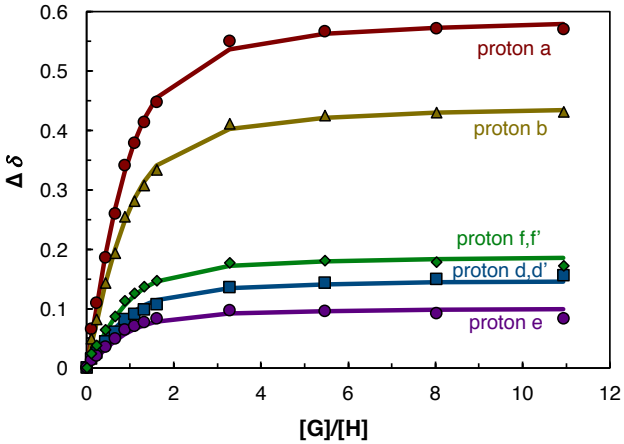

proton	K_a (bindfit)
a	4253 ± 10%
b	4033 ± 10%
d,d'	2627 ± 9%
e	11674 ± 46%
f,f'	6088 ± 19%
global fitting	4248 ± 5%

Trial 1 (mam-IV-238) 0.1 to 10.9	Trial 2 (GL-IV-251) 0.25 to 9.81
4248 ± 5%	3353 ± 4%

$K_{a,avg}$ = 3.8x10^3 ± 3%

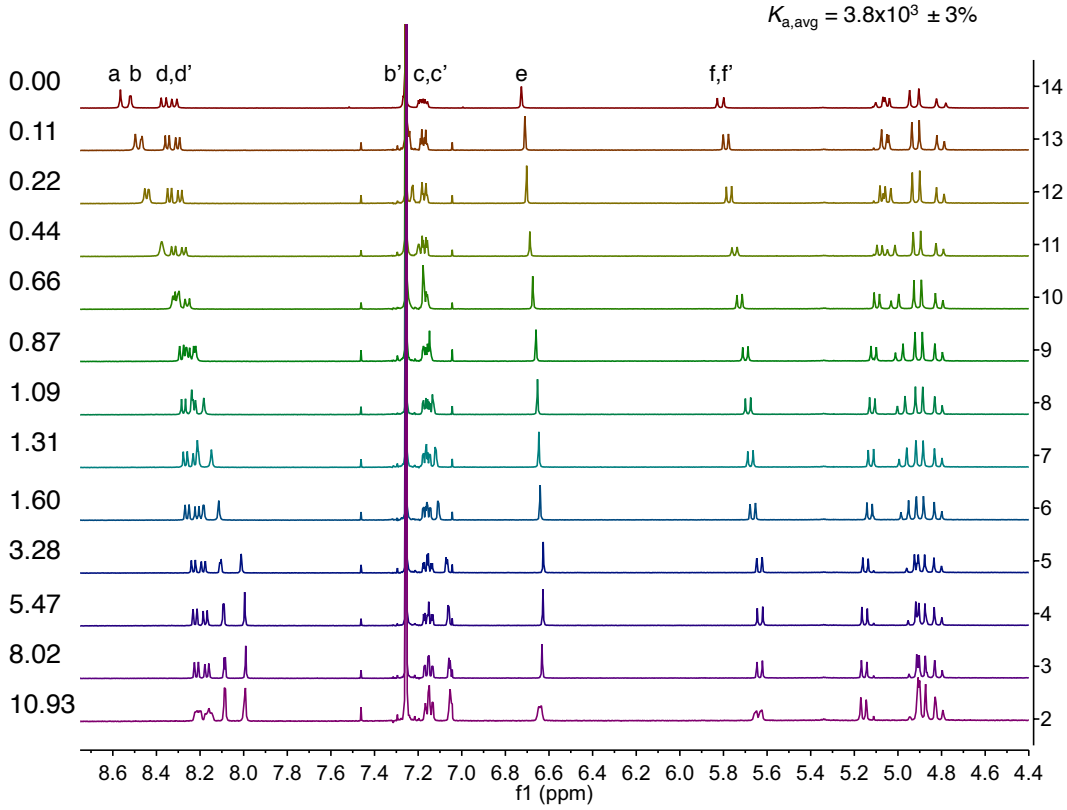

Complex of **6.2a** and **6.1** in $CDCl_3$: Example error calculation

Trial 1 (mam-IV-238)	Trial 2 (GL-IV-251)
4248 ± 5%	3353 ± 4%
$\Delta K_{a1} = 212$	$\Delta K_{a2} = 134$

Equation 1: $K_{a,avg} = \frac{K_{a,1}+K_{a,2}}{2} = 3800.5$

Equation 2: $\Delta K_{a,avg} = \frac{1}{2}\sqrt{(\Delta K_{a,1})^2 + (\Delta K_{a,2})^2} = 125$

$K_{a,avg} = 3.8\text{x}10^3 \pm 3\%\ M^{-1}$

Complex of **6.2b** and **6.1** in $CDCl_3$ (mam-IV-244)

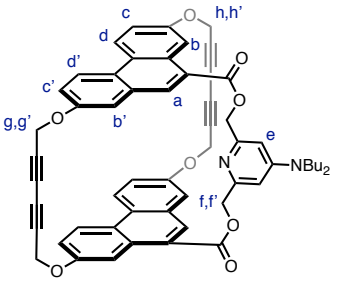

Host: **6.2b**
[H] = 1 mM

Guest: **6.1**
[G] = 0 - 7.4 mM

proton	K_a (bindfit)
a	2849 ± 13%
b	2798 ± 13%
d,d'	1947 ± 8%
e	4008 ± 15%
f,f'	2443 ± 12%
global fitting	2870 ± 5%

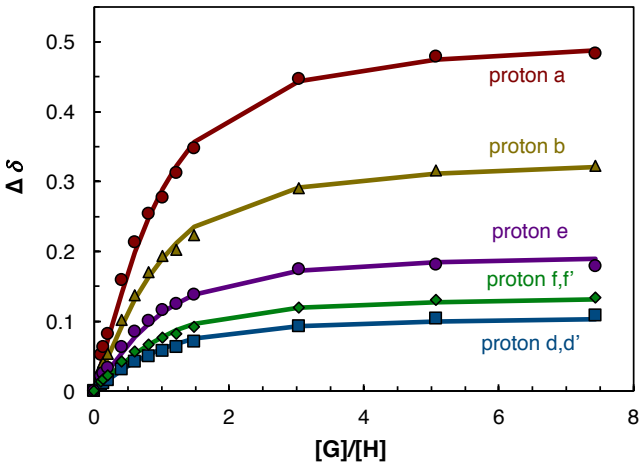

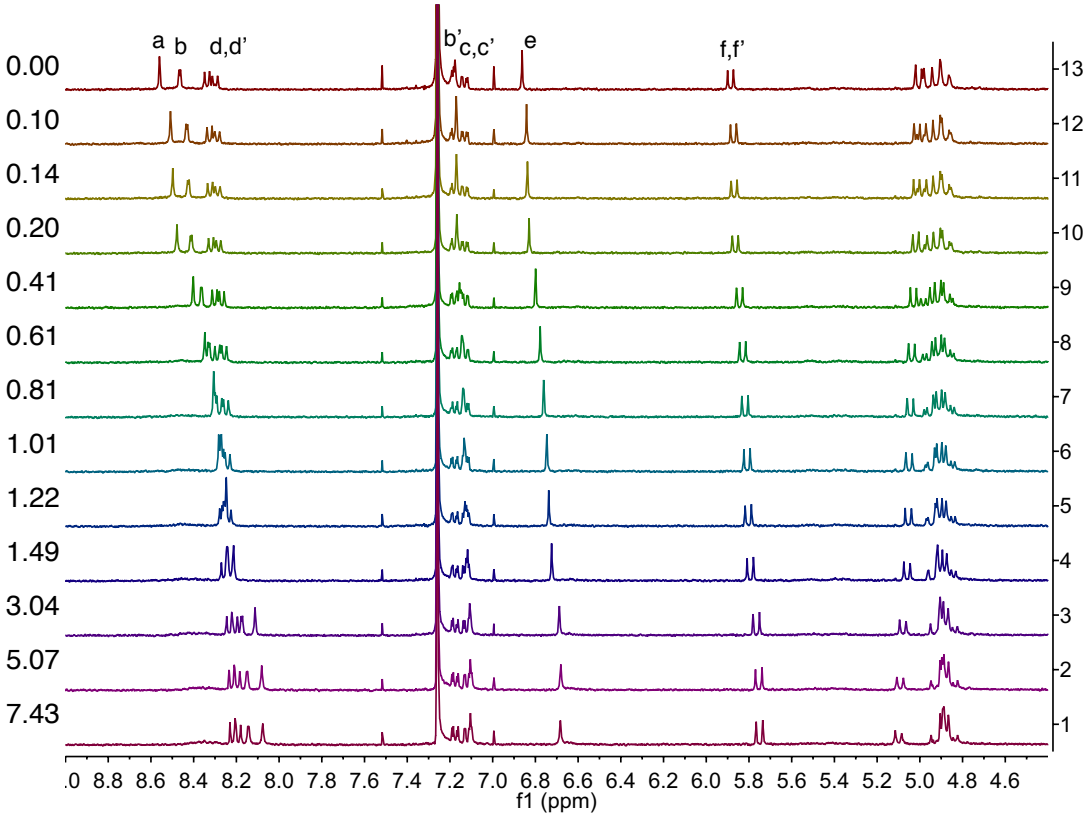

Complex of **6.2a** and **6.15** in $CDCl_3$ (mam-V-182)

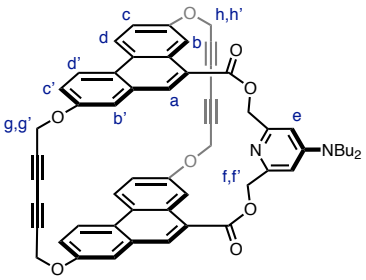

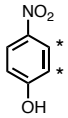

Host: **6.2a**

[H] = 0.87 mM

Guest: **6.15**

[G] = 0 - 6.8 mM

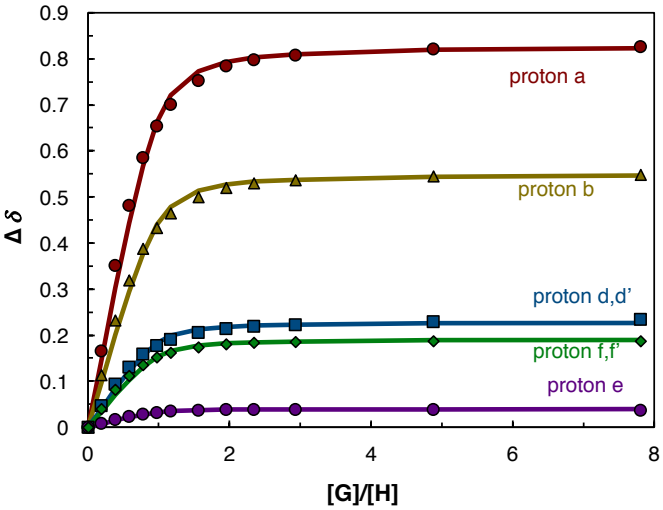

proton	K_a (bindfit)
a	26239 ± 38%
b	25553 ± 38%
d,d'	19628 ± 32%
e	75640 ± 104%
f,f'	31758 ± 45%
global fitting (all)	25870 ± 14%

Trial 1 (mam-V-182) 0.20 to 7.81 equiv	Trial 2 (mam-IV-240) 0.1 to 10.76 equiv
25870 ± 14%	25071 ± 21%

$K_{a,avg} = 2.5 \times 10^4 \pm 13\%$

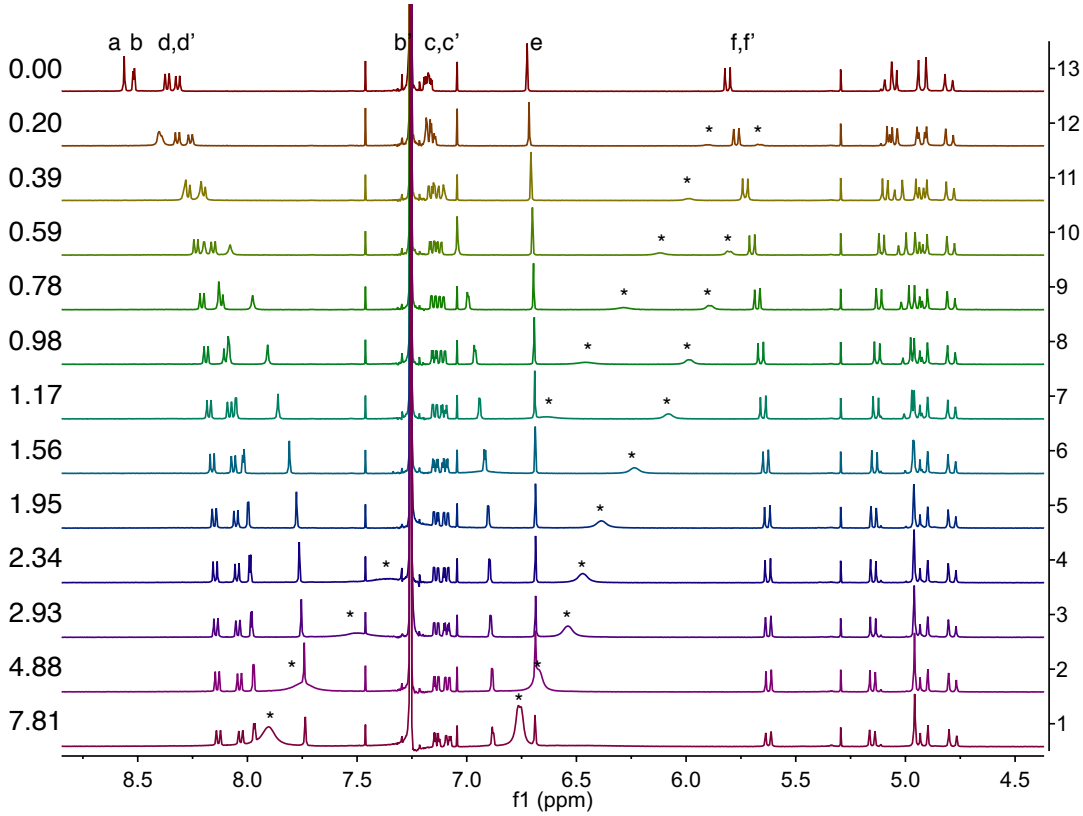

Complex of **6.2a** and **6.16** in $CDCl_3$ (mam-IV-274)

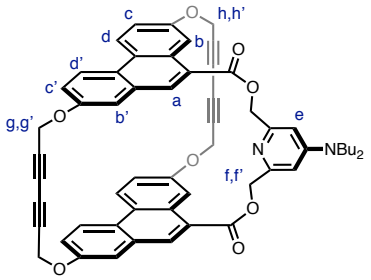

Host: **6.2a**

[H] = 0.93 mM

Guest: **6.16**

[G] = 0 - 96 mM

proton	K_a (bindfit)
a	15.8 ± 3%
b	13.7 ± 3%
d,d'	14.1 ± 2 %
global fitting (all)	15.3 ± 1%

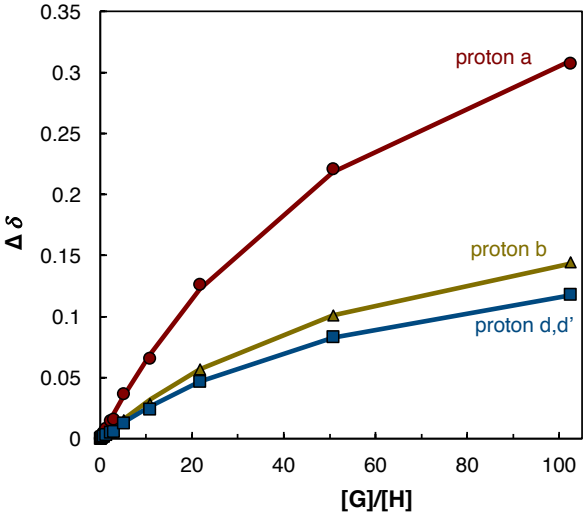

Trial 1 (mam-IV-274) 0.2 to 102 equiv	Trial 2 (GL-IV-253) 8.6 to 171 equiv
15.3 ± 1%	13.3 ± 0.9%

$K_{a,avg}$ = 14.2 ± 0.9%

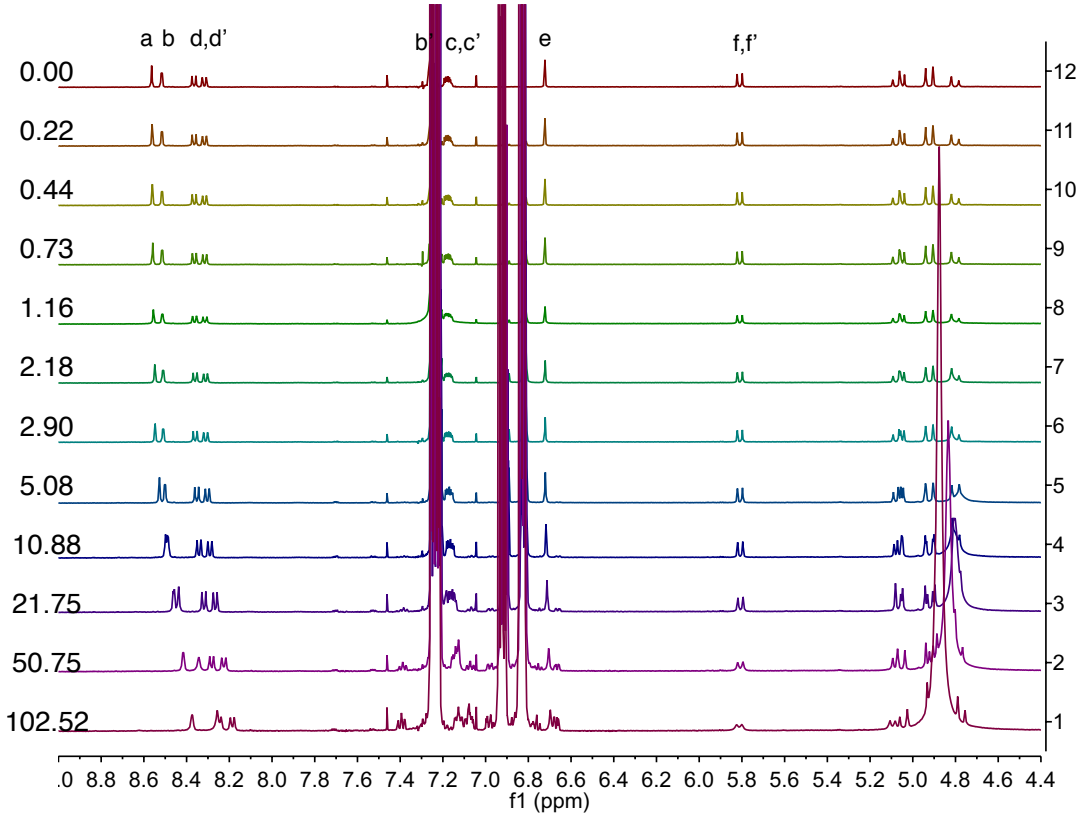

Complex of **6.2a** and **6.17** in $CDCl_3$ (mam-IV-276)

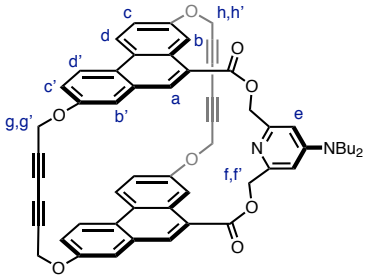

Host: **6.2a**

[H] = 0.93 mM

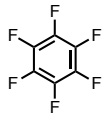

Guest: **6.17**

[G] = 0 - 109 mM

proton	K_a (bindfit)
a	4.26 ± 2%
d,d'	3.76 ± 1%
e	8.06 ± 14%
global fitting (all)	4.05 ± 1%

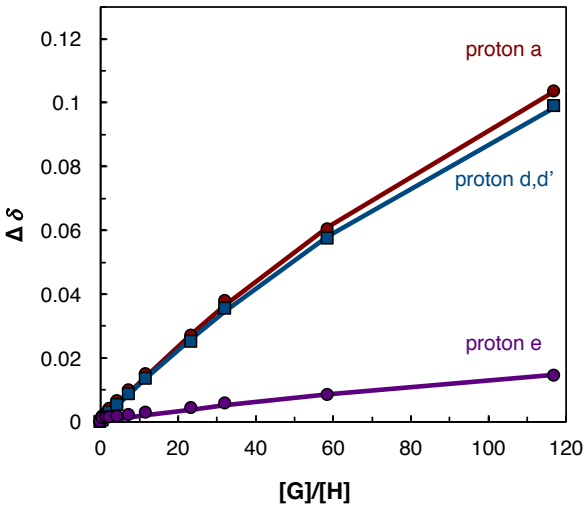

Trial 1 (mam-IV-276) 0.58 to 117 equiv	Trial 2 (GL-IV-254) 25 to 500 equiv
4.05 ± 1%	3.79 ± 1%

$K_{a,avg}$ = 3.9 ± 0.7%

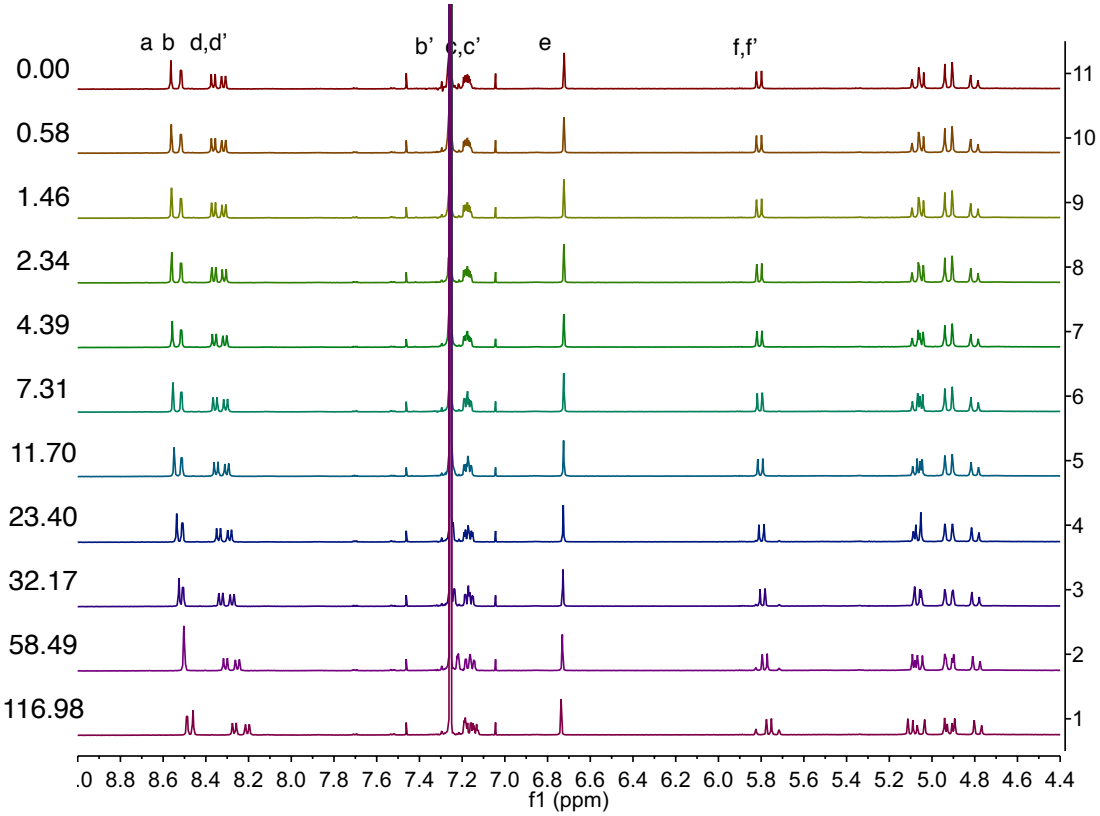

Complex of **6.2a** and **6.18** in $CDCl_3$ (mam-IV-280)

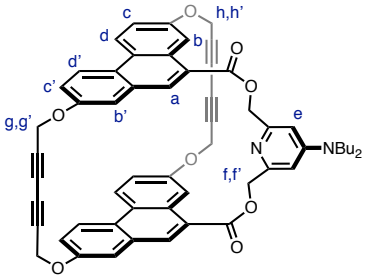

Host: **6.2a**

[H] = 0.93 mM

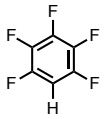

Guest: **6.18**

[G] = 0 - 100 mM

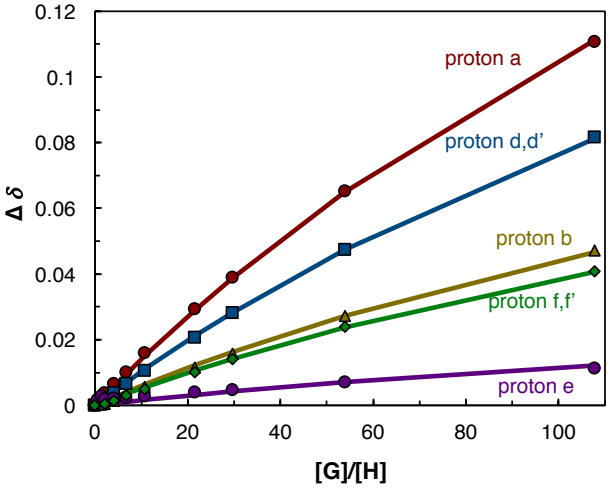

proton	K_a (bindfit)
a	4.6 ± 1%
b	3.0 ± 3%
d,d'	3.7 ± 1%
e	19.6 ± 37%
f,f'	3.4 ± 3%
global fitting (all)	4.1 ± 1%

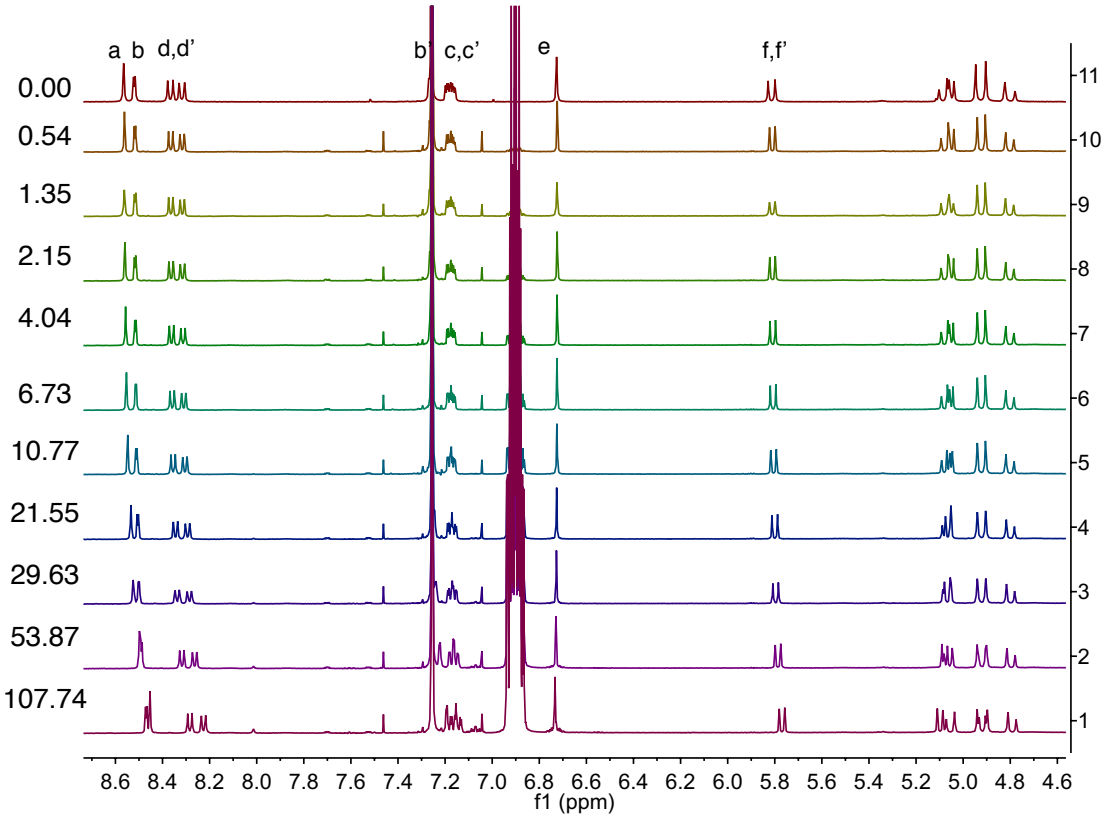

Complex of **6.2a** and **6.19** in $CDCl_3$ (mam-IV-278)

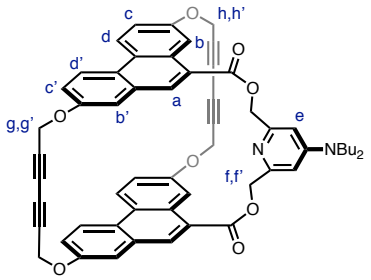

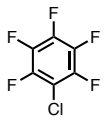

Host: **6.2a**
[H] = 0.93 mM

Guest: **6.19**
[G] = 0 - 100 mM

proton	K_a (bindfit)
a	6.1 ± 2%
b	4.2 ± 3%
d,d'	5.5 ± 1%
e	9.5 ± 11%
f,f'	5.3 ± 2%
global fitting (all)	5.75 ± 0.79%

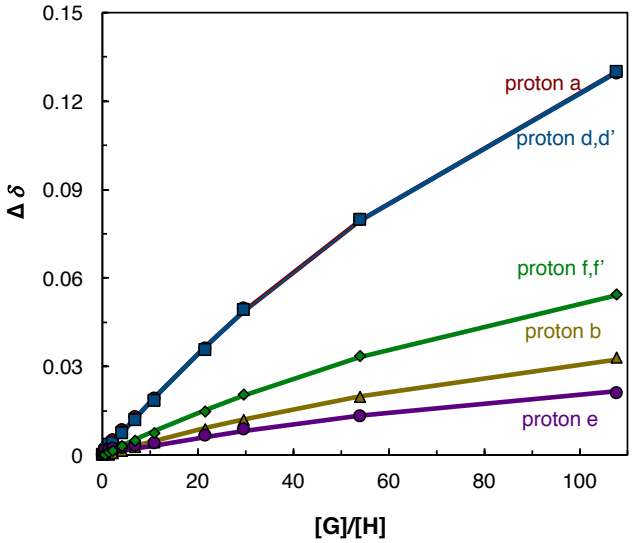

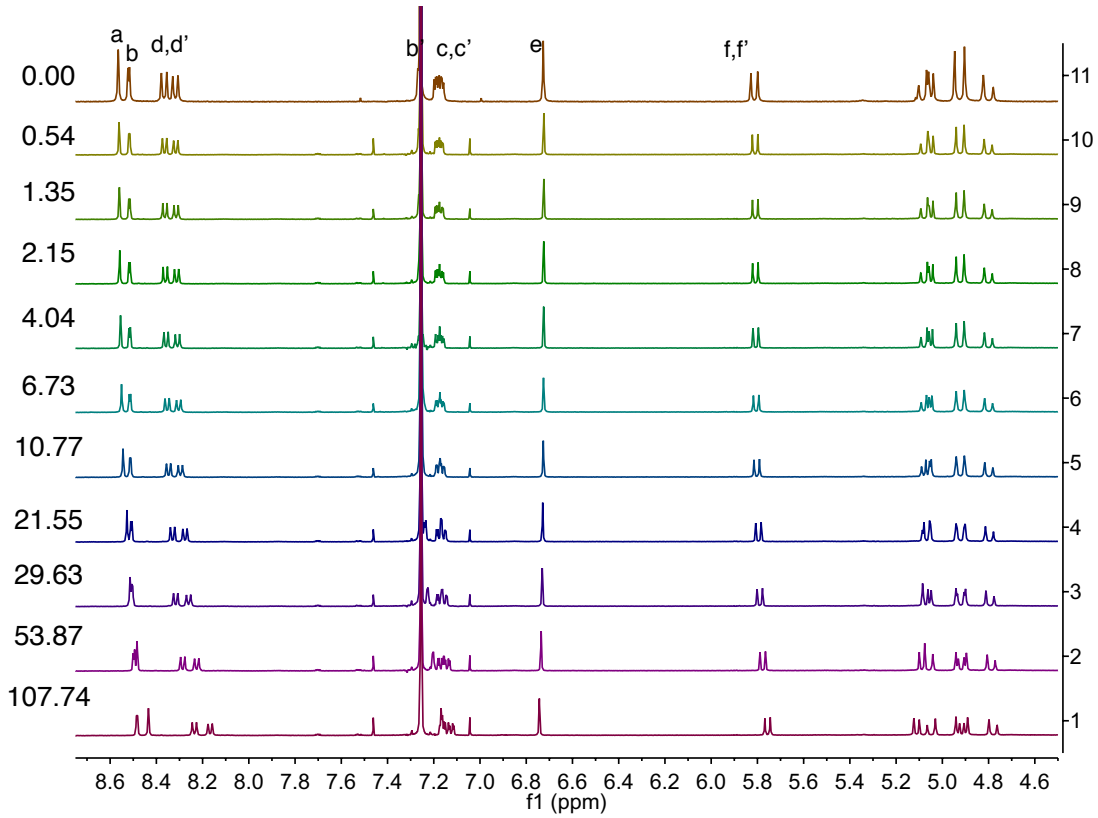

Complex of **6.2a** and **6.20** in $CDCl_3$ (mam-IV-257)

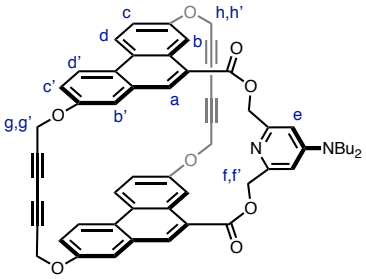

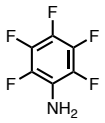

Host: **6.2a**

[H] = 0.93 mM

Guest: **6.20**

[G] = 0 - 102 mM

proton	K_a (bindfit)
a	28 ± 4%
b	29 ± 6%
d,d'	26 ± 3%
f,f'	33 ± 9%
global fitting (all)	28.2 ± 2%

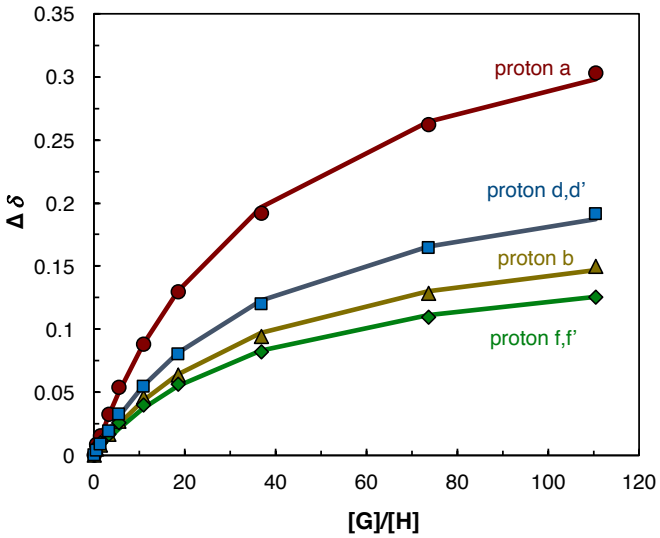

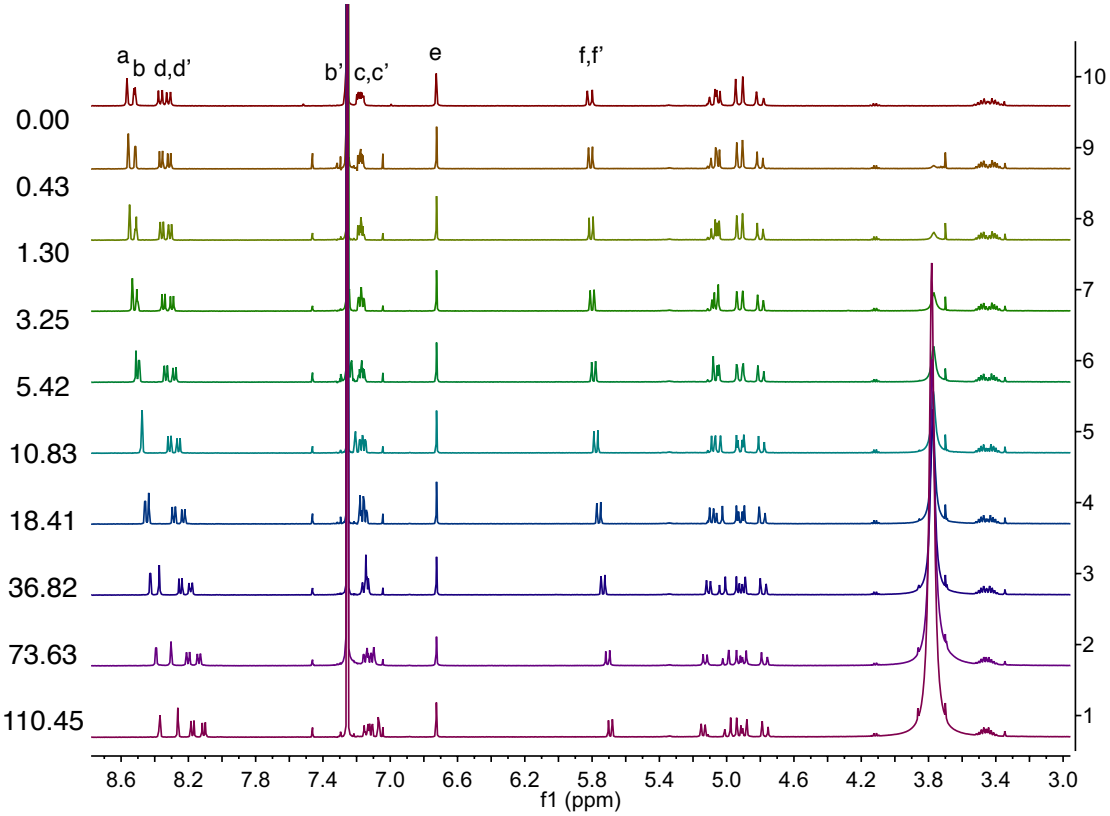

Complex of **6.2a** and **6.24** in $CDCl_3$ (mam-VI-014)

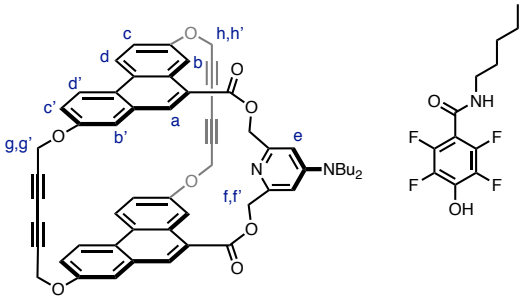

Host: **6.2a**

[H] = 0.93 mM

Guest: **6.24**

[G] = 0 - 1.79 mM

proton	K_a (bindfit)
a	30625 ± 49%
b	28162 ± 41%
d,d'	18469 ± 25%
e	120172 ± 223%
f,f'	68837 ± 124%
Global fitting (a,b,d)	29133 ± 22%
global fitting (all)	30910 ± 19%

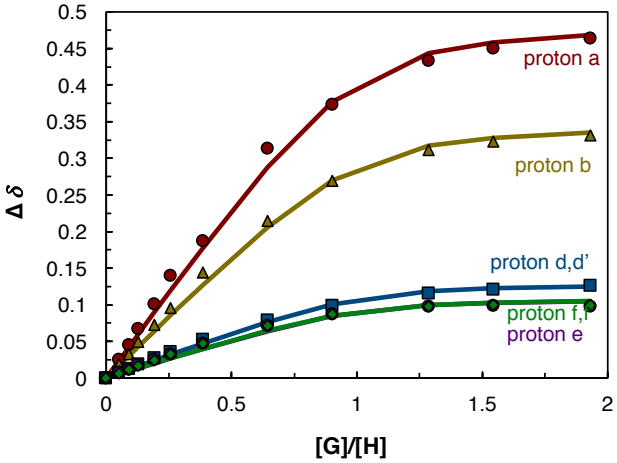

Trial 1 (mam-VI-014) 0.05 to 1.9 equiv	Trial 2 (mam-VI-028) 0.05 to 2.0 equiv
30910 ± 19%	32318 ± 18%

$K_{a,avg} = 3.2 \times 10^4 \pm 13\%$

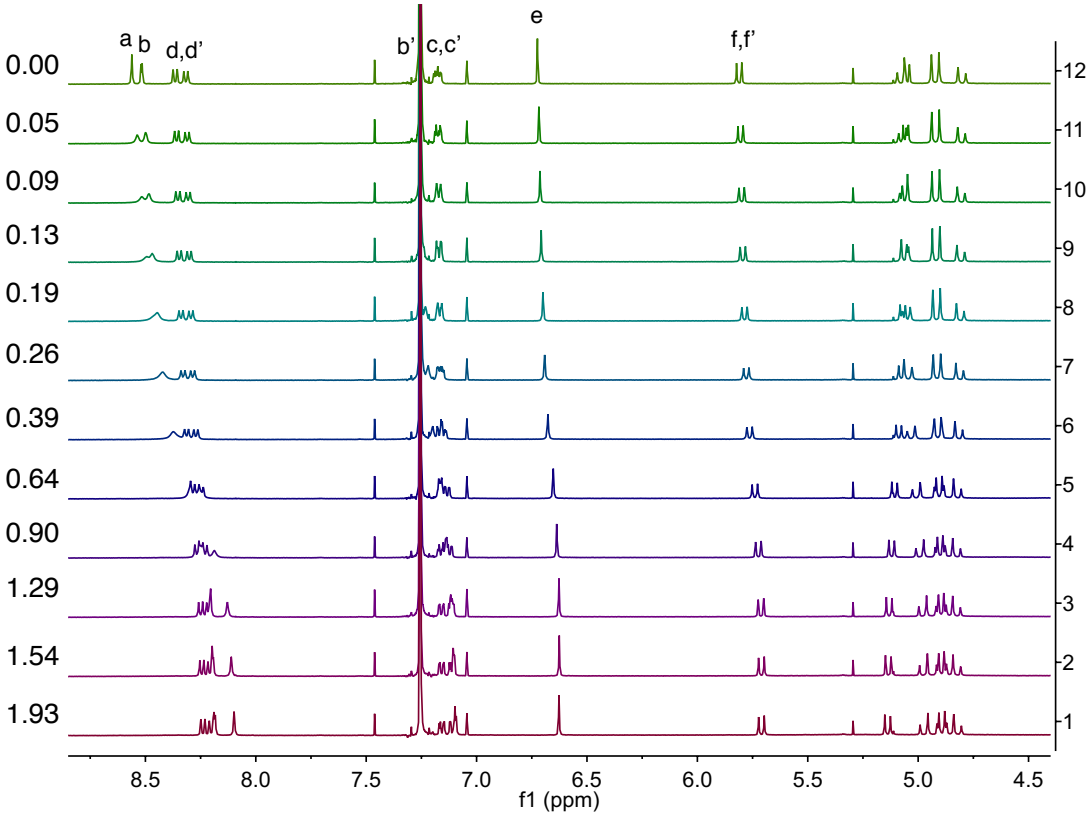

^{19}F NMR of complex of **6.2a** and **6.24** in $CDCl_3$, aligned with 1,2-difluorobenzene (mam-VI-014)

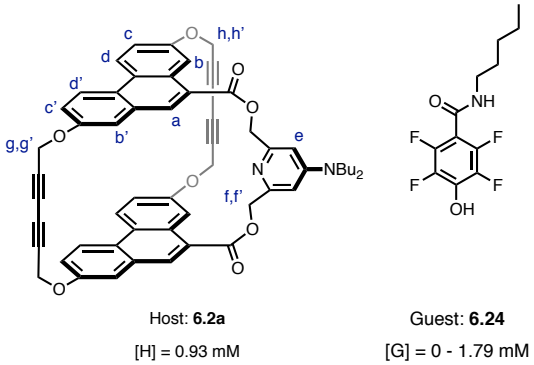

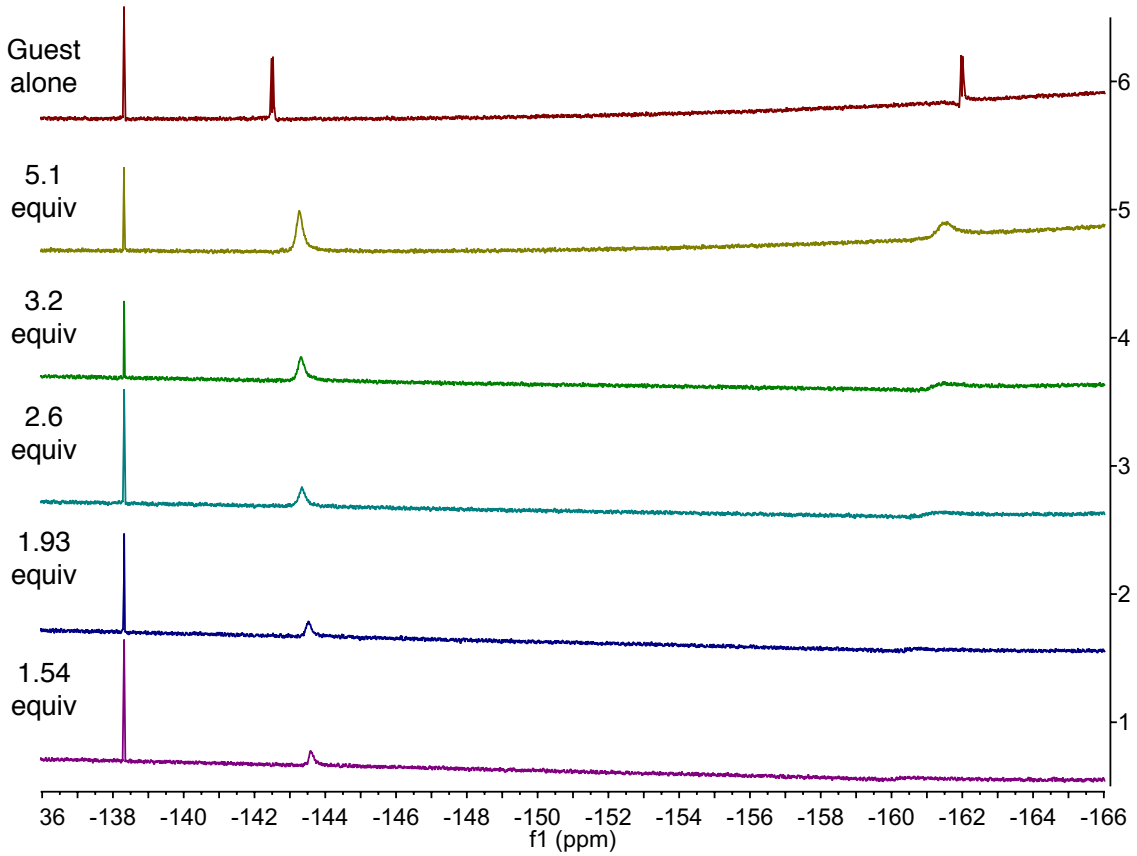

Complex of **6.2a** and **6.25** in $CDCl_3$ (mam-VI-088): displays 1:2 binding

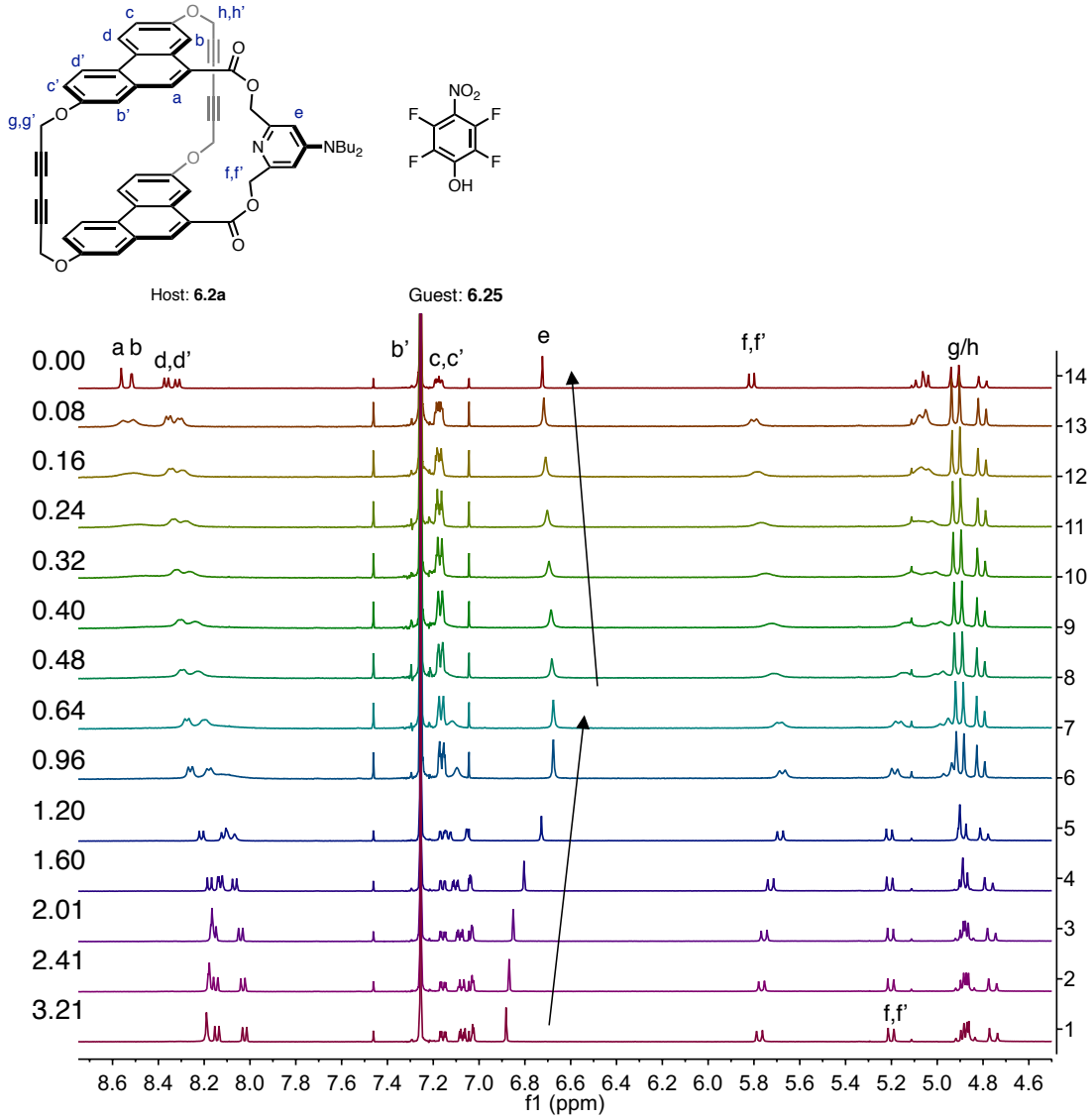

reference	equiv	K_a	protons used
GL_04_143	0.09 to 13.51	170000 ± 18.4%, 7200 ± 15.1%	d,e,f
GL_04_239	0.08 to 3.12	267276 ± 19%, 24146 ± 14%	d,e,f
GL_04_250	0.08 to 3.12	280000 ± 13.6%, 7700 ± 5.84%	d,e,f
mam-VI-060	0.038 to 3.07	1035323 ± 140%, 61598 ± 131%	d,e,f,g/h
mam-VI-074	0.038 to 3.07	998931 ± 71%, 18078 ± 43% (glovebox)	d,e,f,g/h
mam-VI-088, 7 h	0.08 to 3.12	680518 ± 67%, 46741 ± 55 % (glovebox)	d,e,f
mam-VI-088, 22 h	0.08 to 3.12	570012 ± 75%, 45496 ± 54% (glovebox)	e,f,g/h
mam-VI-090, 7 h	0.08 to 3.12	763510 ± 62%, 38558 ± 48% (glovebox)	e,f,g/h

^{19}F NMR of complex of **6.2a** and **6.25** in $CDCl_3$, aligned with 1,2-difluorobenzene standards (mam-VI-090)

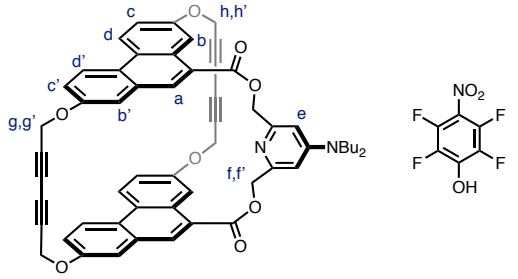

Host: **6.2a**

Guest: **6.25**

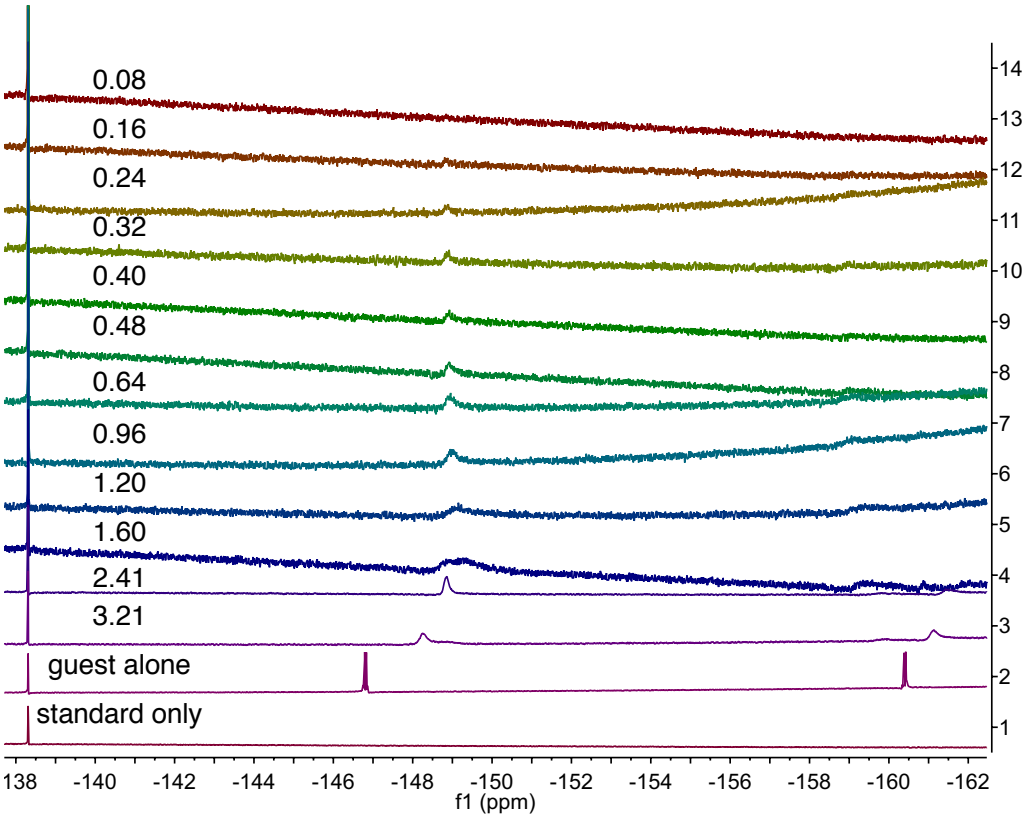

6.5.5 NMR spectra

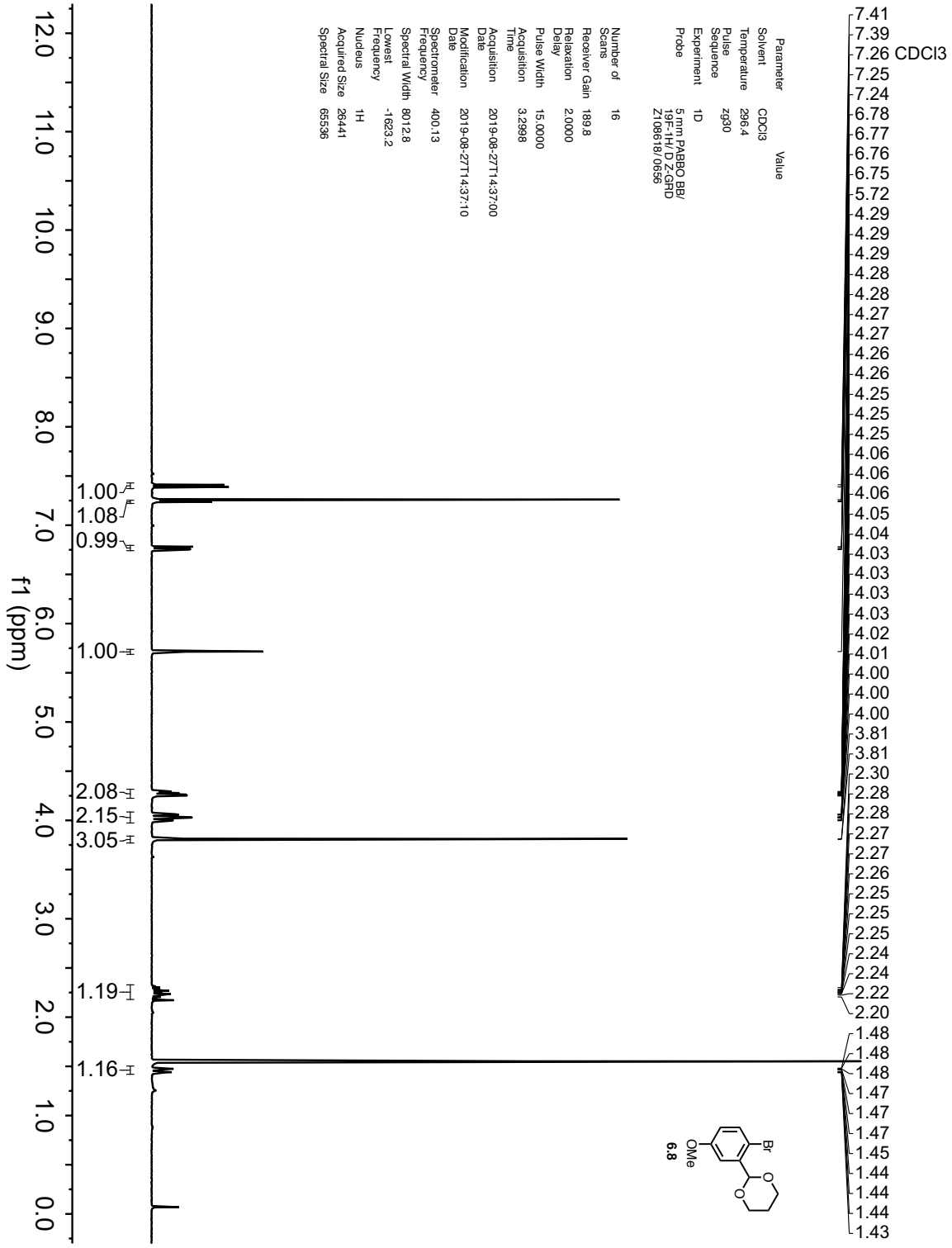

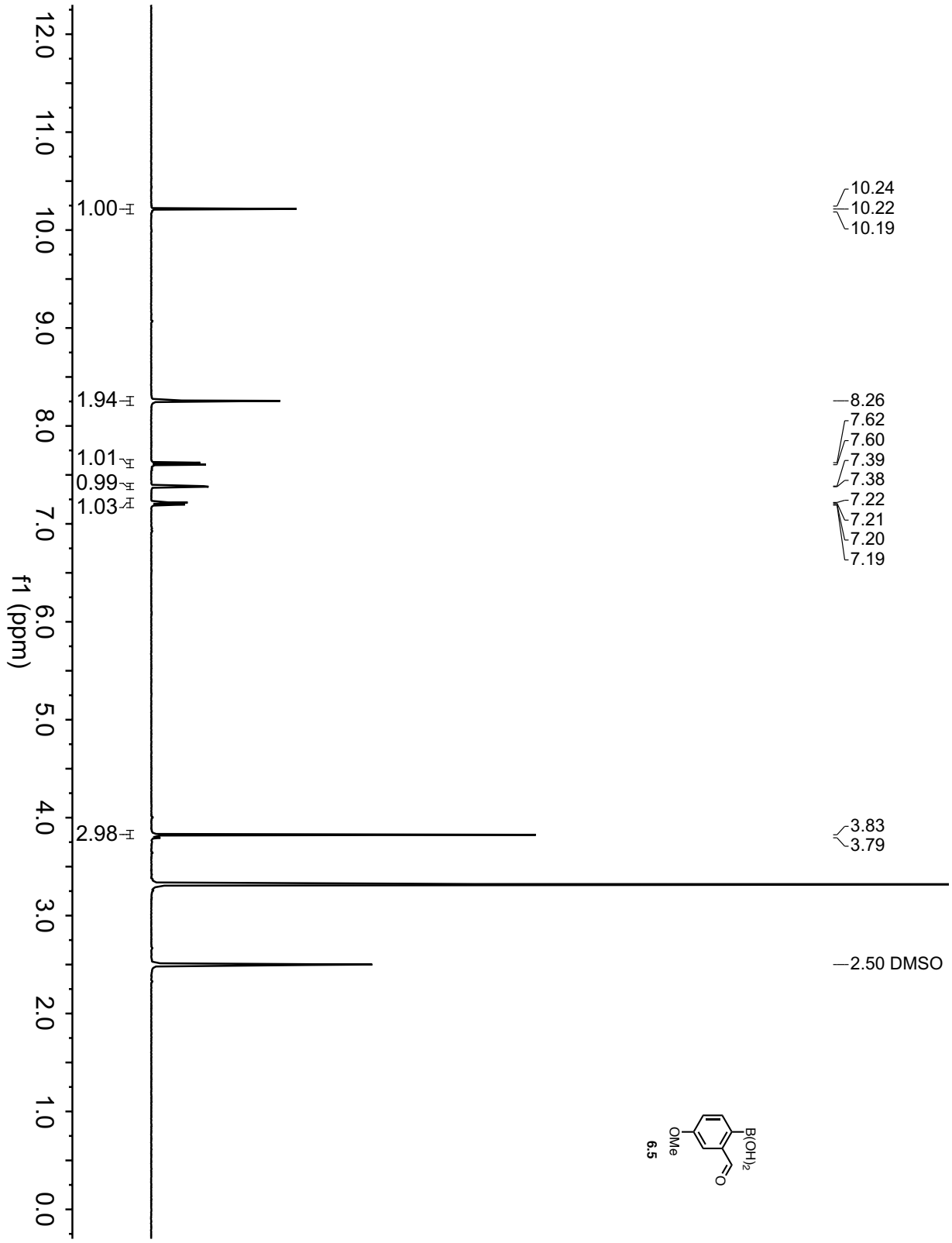
10.24
10.22
10.19
8.26
7.62
7.60
7.39
7.38
7.22
7.21
7.20
7.19
3.83
3.79
2.50 DMSO
1.00
1.94
1.01
0.99
1.03
2.98
12.0
11.0
10.0
9.0
8.0
7.0
6.0
5.0
4.0
3.0
2.0
1.0
0.0
f1 (ppm)
B(OH)2
OMe
O
6.5

Parameter	Value
Solvent	CDCl3
Temperature	298.0
Pulse Sequence	zg30
Experiment	1D
Probe	Z119248_0002 (DCH 500S2 C/ H-D-05 Z LT)
Number of Scans	8
Receiver Gain	12.1
Relaxation Delay	2.0000
Pulse Width	10.0000
Acquisition Time	3.2768
Acquisition Date	2019-08-29T12:03:39
Modification Date	2019-08-29T12:03:39
Spectrometer Frequency	500.13
Spectral Width	10000.0
Lowest Frequency	-2011.3
Nucleus	1H
Acquired Size	32768
Spectral Size	65536

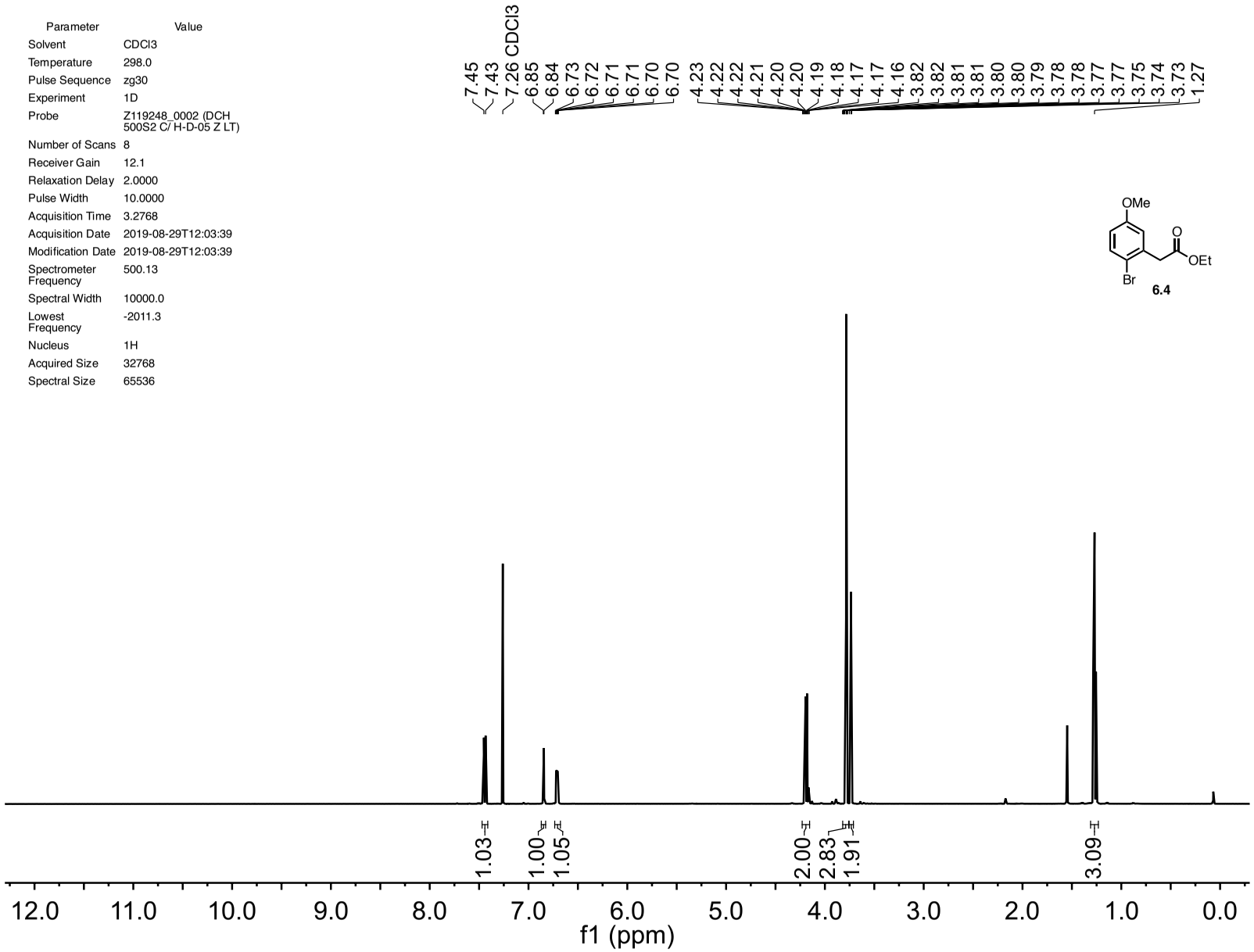

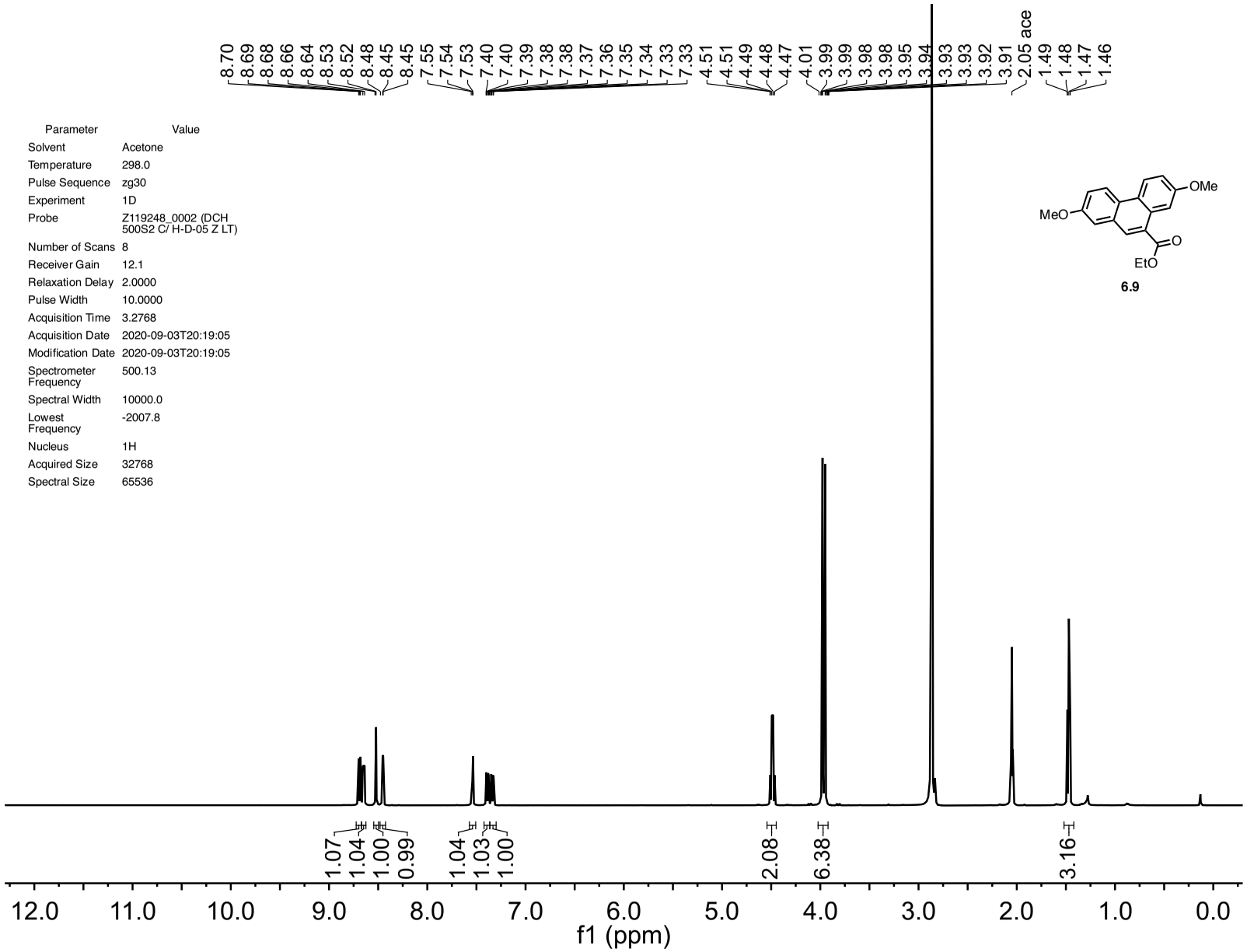

Parameter	Value
Solvent	Acetone
Temperature	298.0
Pulse Sequence	zg30
Experiment	1D
Probe	Z119248_0002 (DCH 500S2 C/ H-D-05 Z LT)
Number of Scans	8
Receiver Gain	12.1
Relaxation Delay	2.0000
Pulse Width	10.0000
Acquisition Time	3.2768
Acquisition Date	2020-09-03T20:19:05
Modification Date	2020-09-03T20:19:05
Spectrometer Frequency	500.13
Spectral Width	10000.0
Lowest Frequency	-2007.8
Nucleus	1H
Acquired Size	32768
Spectral Size	65536

6.9

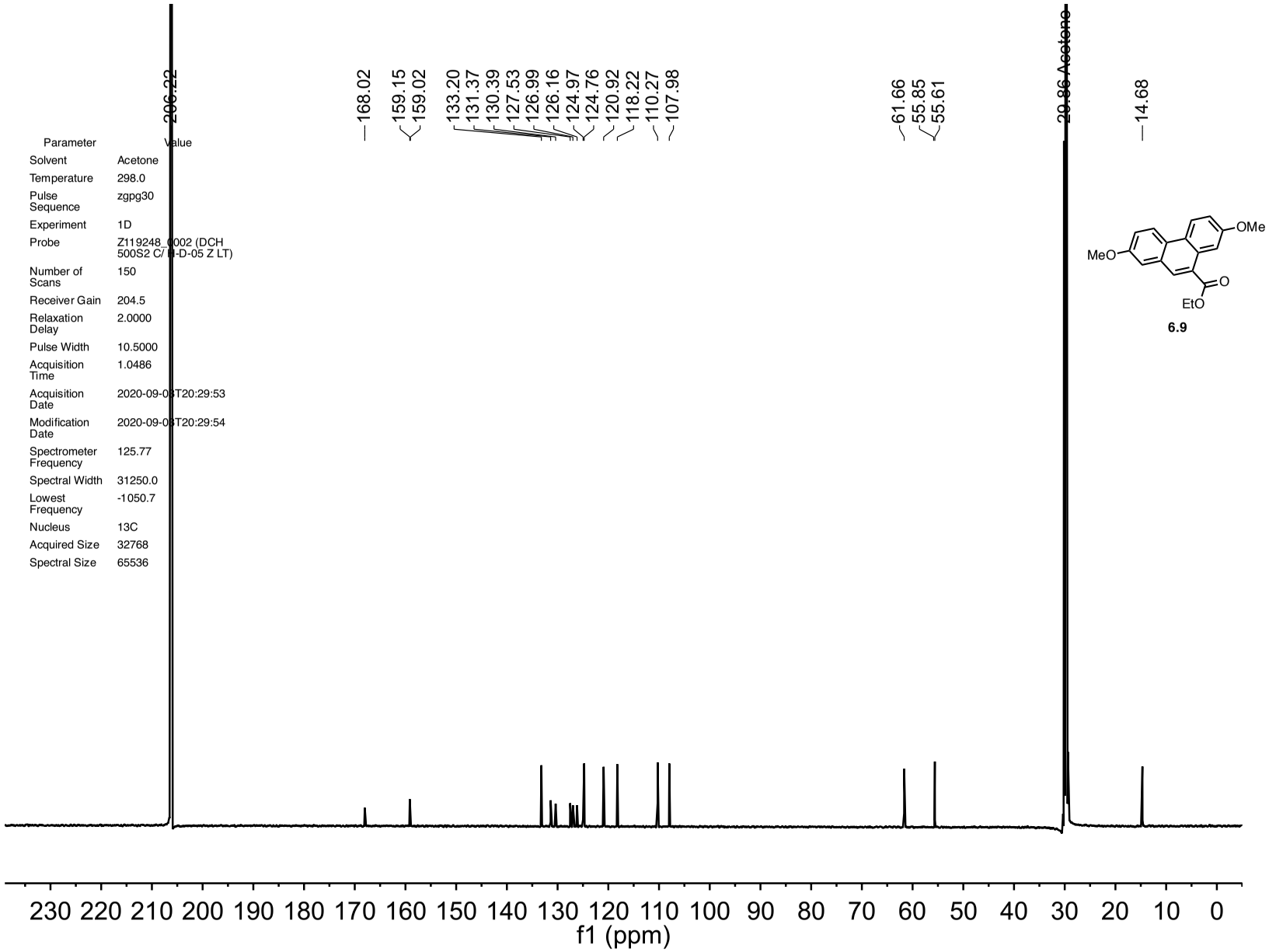

Parameter	Value
Solvent	Acetone
Temperature	298.0
Pulse Sequence	zgpg30
Experiment	1D
Probe	Z119248_0002 (DCH 500S2 C/H-D-05 Z LT)
Number of Scans	150
Receiver Gain	204.5
Relaxation Delay	2.0000
Pulse Width	10.5000
Acquisition Time	1.0486
Acquisition Date	2020-09-03T20:29:53
Modification Date	2020-09-03T20:29:54
Spectrometer Frequency	125.77
Spectral Width	31250.0
Lowest Frequency	-1050.7
Nucleus	13C
Acquired Size	32768
Spectral Size	65536

6.9

COSY (acetone-d_6)

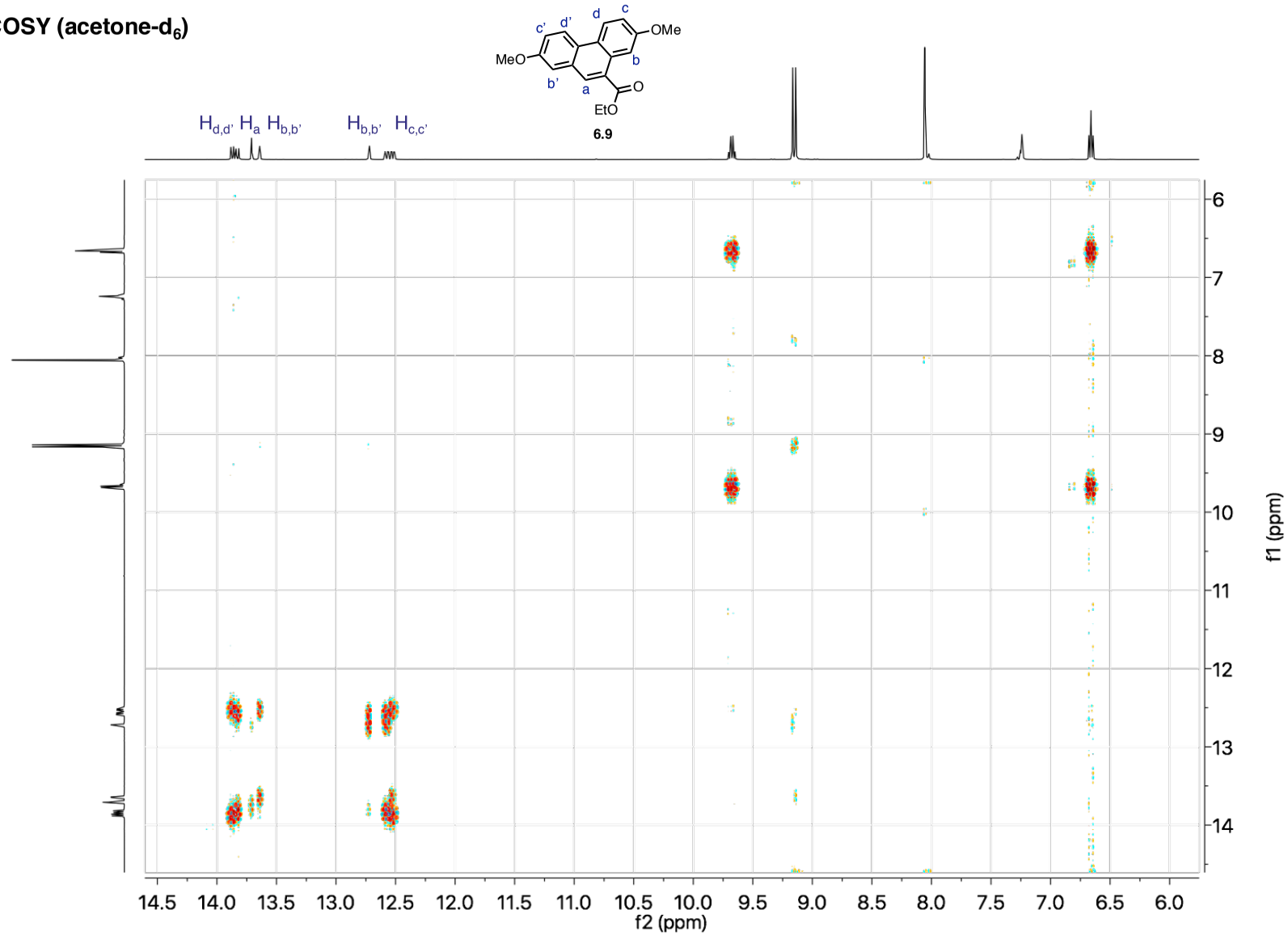

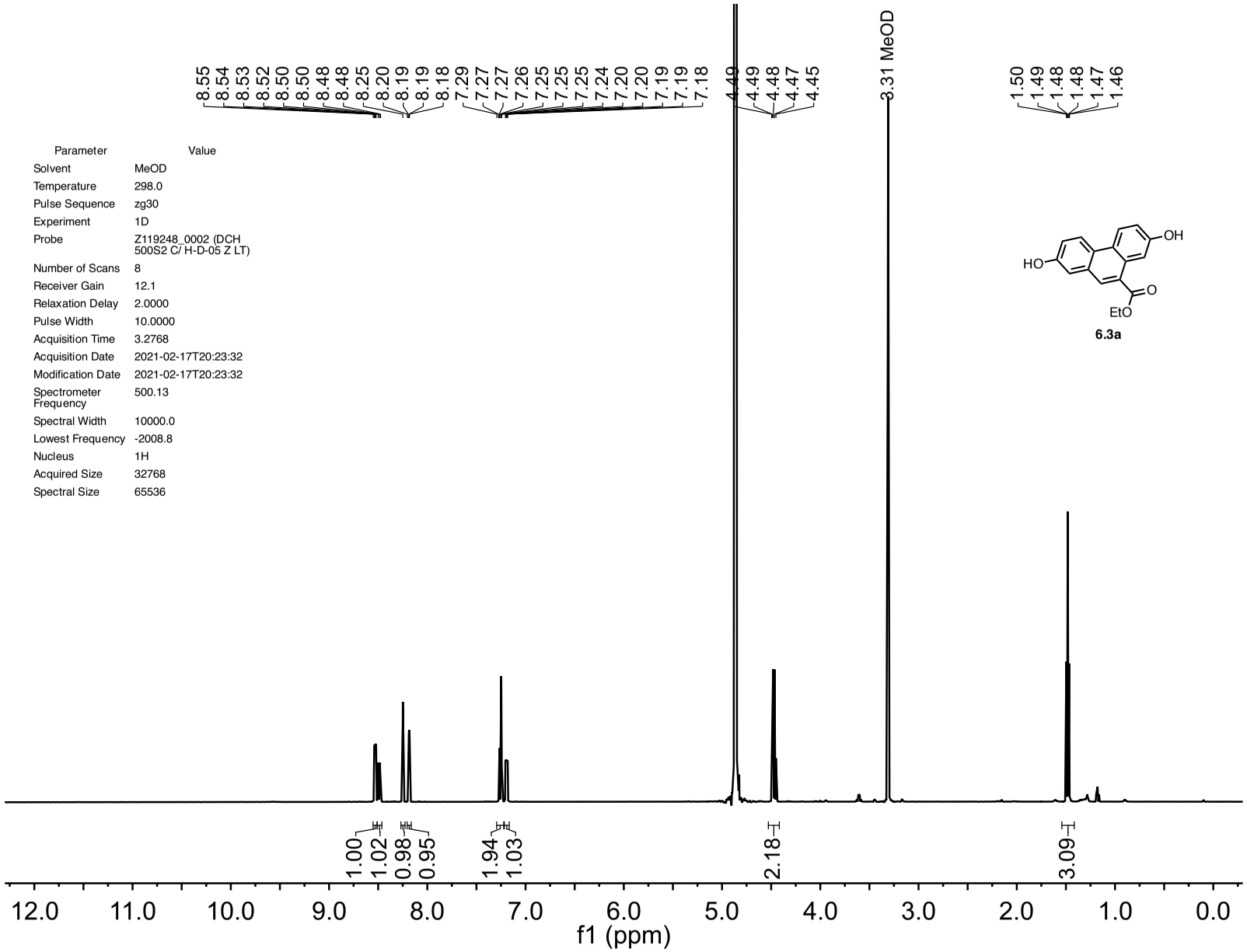

Parameter	Value
Solvent	MeOD
Temperature	298.0
Pulse Sequence	zg30
Experiment	1D
Probe	Z119248_0002 (DCH 500S2 C/ H-D-05 Z LT)
Number of Scans	8
Receiver Gain	12.1
Relaxation Delay	2.0000
Pulse Width	10.0000
Acquisition Time	3.2768
Acquisition Date	2021-02-17T20:23:32
Modification Date	2021-02-17T20:23:32
Spectrometer Frequency	500.13
Spectral Width	10000.0
Lowest Frequency	-2008.8
Nucleus	1H
Acquired Size	32768
Spectral Size	65536

6.3a

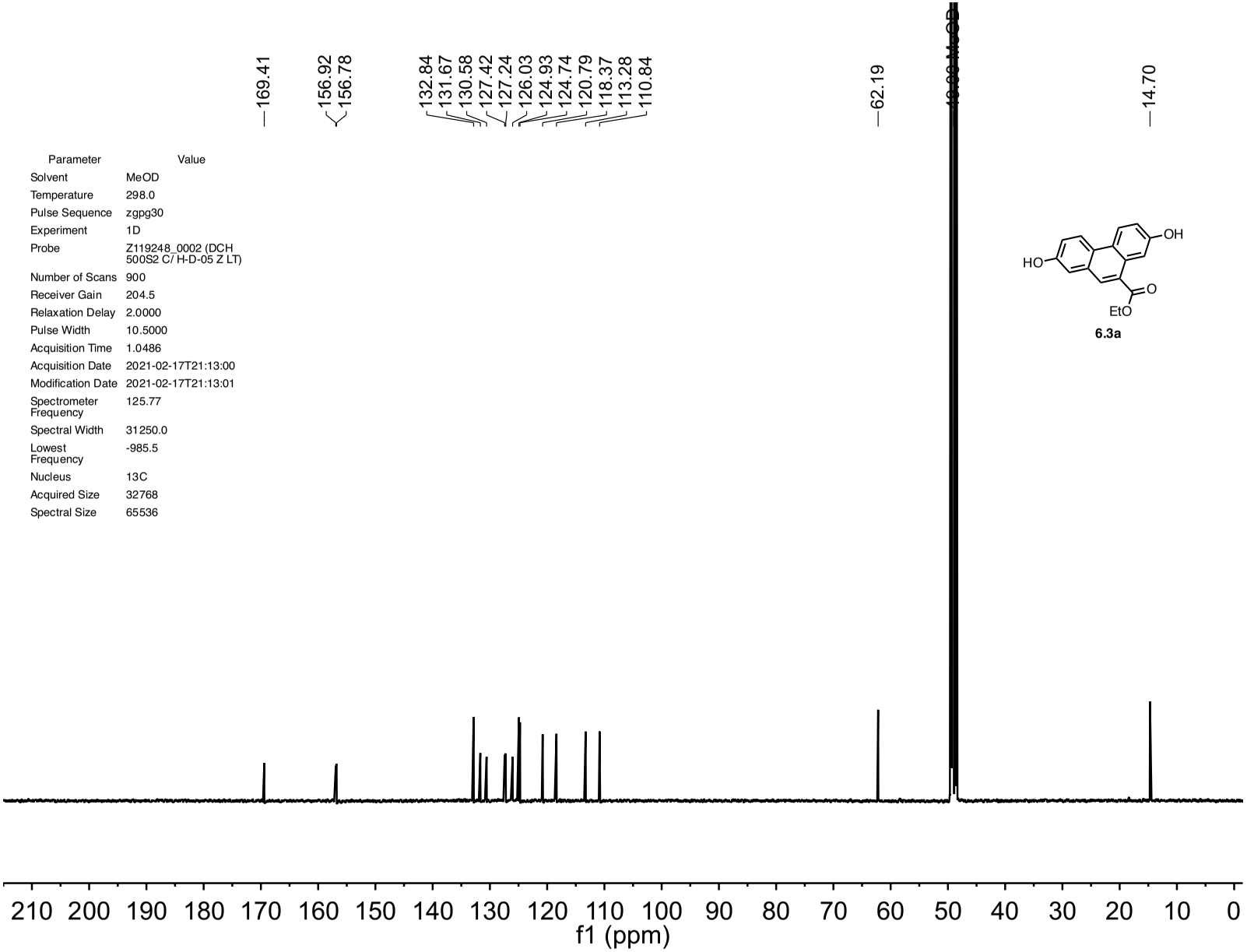

Parameter	Value
Solvent	MeOD
Temperature	298.0
Pulse Sequence	zgpg30
Experiment	1D
Probe	Z119248_0002 (DCH 500S2 C/ H-D-05 Z LT)
Number of Scans	900
Receiver Gain	204.5
Relaxation Delay	2.0000
Pulse Width	10.5000
Acquisition Time	1.0486
Acquisition Date	2021-02-17T21:13:00
Modification Date	2021-02-17T21:13:01
Spectrometer Frequency	125.77
Spectral Width	31250.0
Lowest Frequency	-985.5
Nucleus	13C
Acquired Size	32768
Spectral Size	65536

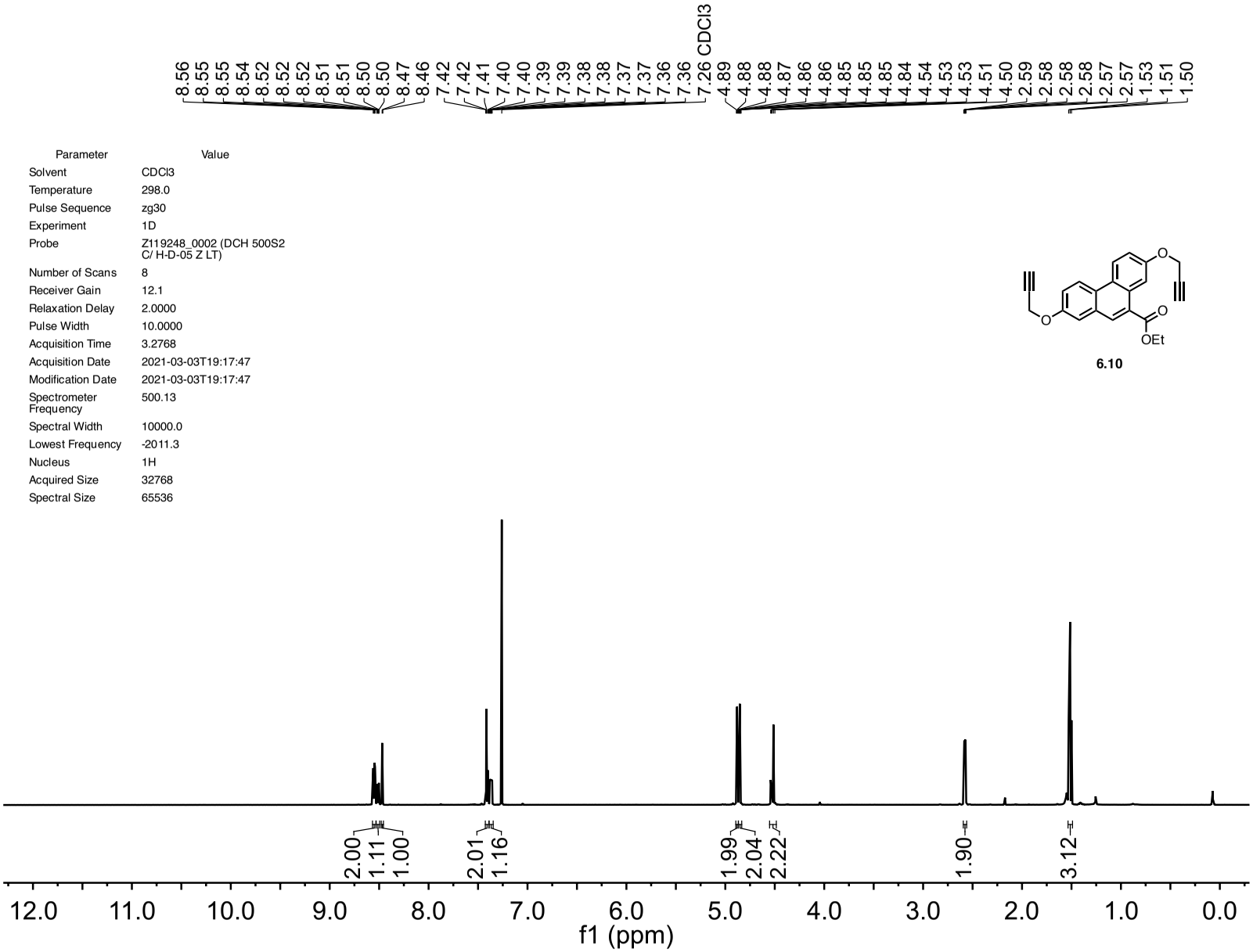

Parameter	Value
Solvent	CDCl3
Temperature	298.0
Pulse Sequence	zg30
Experiment	1D
Probe	Z119248_0002 (DCH 500S2 C/ H-D-05 Z LT)
Number of Scans	8
Receiver Gain	12.1
Relaxation Delay	2.0000
Pulse Width	10.0000
Acquisition Time	3.2768
Acquisition Date	2021-03-03T19:17:47
Modification Date	2021-03-03T19:17:47
Spectrometer Frequency	500.13
Spectral Width	10000.0
Lowest Frequency	-2011.3
Nucleus	1H
Acquired Size	32768
Spectral Size	65536

6.10

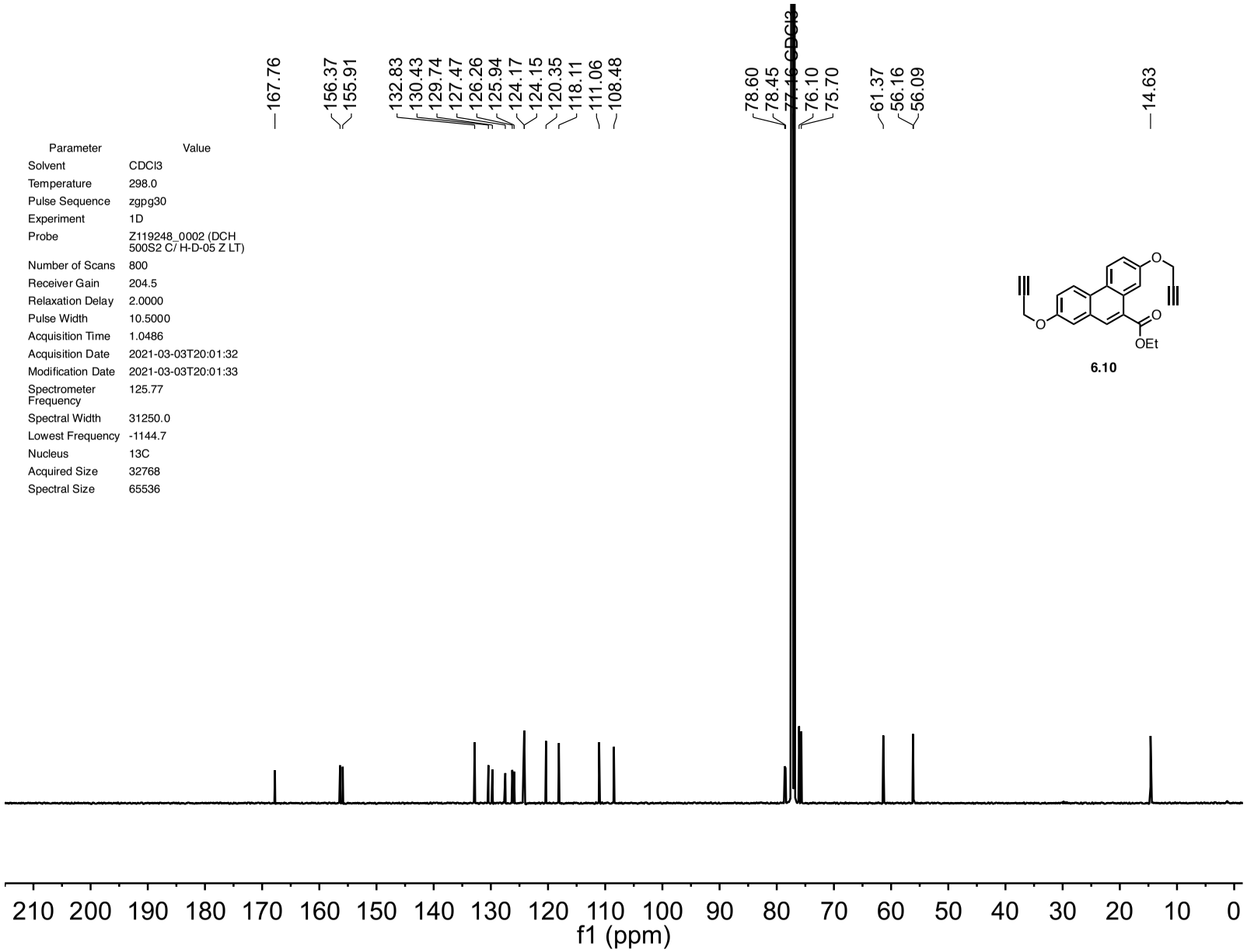

Parameter	Value
Solvent	CDCl3
Temperature	298.0
Pulse Sequence	zgpg30
Experiment	1D
Probe	Z119248_0002 (DCH 500S2 C/ H-D-05 Z LT)
Number of Scans	800
Receiver Gain	204.5
Relaxation Delay	2.0000
Pulse Width	10.5000
Acquisition Time	1.0486
Acquisition Date	2021-03-03T20:01:32
Modification Date	2021-03-03T20:01:33
Spectrometer Frequency	125.77
Spectral Width	31250.0
Lowest Frequency	-1144.7
Nucleus	13C
Acquired Size	32768
Spectral Size	65536

6.10

Parameter	Value
Title	mam-IV-128-precip
Solvent	DMSO
Temperature	296.9
Pulse Sequence	zg30
Experiment	1D
Probe	5 mm PABBO BB/ 19F-1H/ D Z-GRD Z108618/ 0656
Number of Scans	24
Receiver Gain	189.8
Relaxation Delay	2.0000
Pulse Width	15.0000
Acquisition Time	3.2998
Acquisition Date	2021-11-22T13:51:00
Modification Date	2021-11-22T13:51:43
Spectrometer Frequency	400.13
Spectral Width	8012.8
Lowest Frequency	-1608.8
Nucleus	1H
Acquired Size	26441
Spectral Size	65536

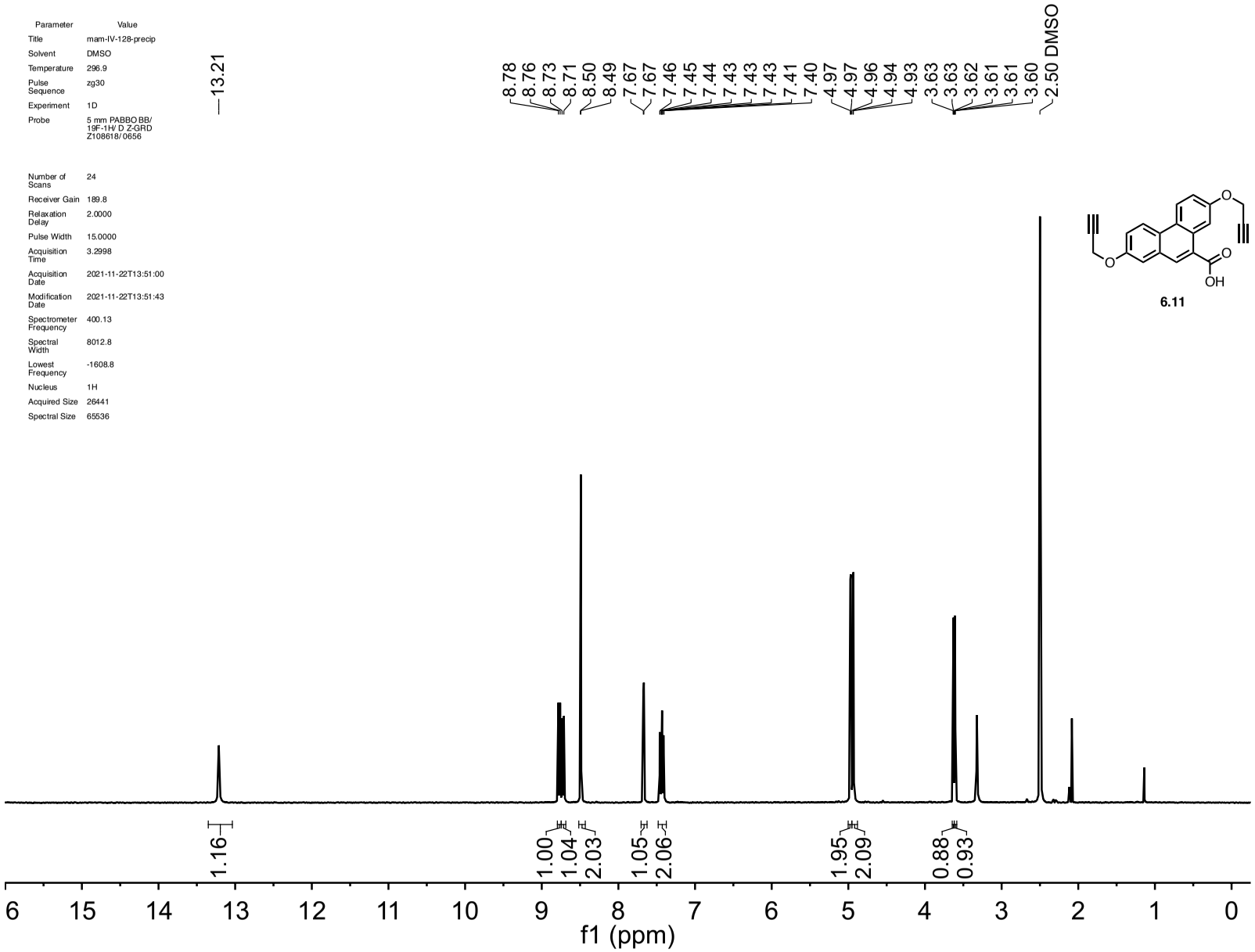

6.11

Parameter	Value
Title	mam-IV-128-G-dmso-carbon.1.fid
Solvent	DMSO
Temperature	298.0
Pulse Sequence	zgpg30
Experiment	1D
Probe	Z119248_0002 (DCH 500S2 C/H-D-05 Z LT)
Number of Scans	2000
Receiver Gain	204.5
Relaxation Delay	2.0000
Pulse Width	10.5000
Acquisition Time	1.0486
Acquisition Date	2021-11-27T19:43:37
Modification Date	2021-11-27T19:43:37
Spectrometer Frequency	125.77
Spectral Width	31250.0
Lowest Frequency	-1220.7
Nucleus	13C
Acquired Size	32768
Spectral Size	65536

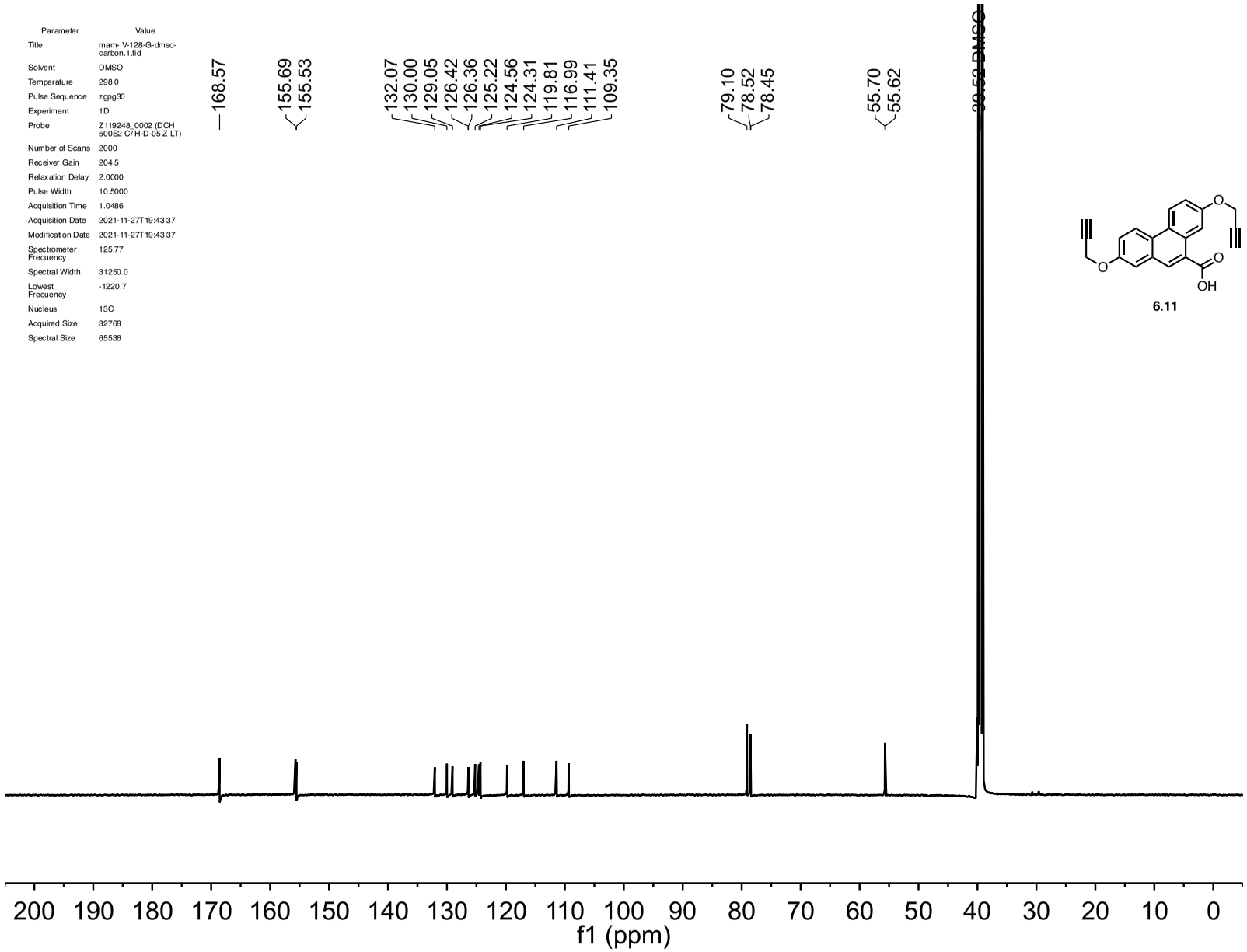

6.11

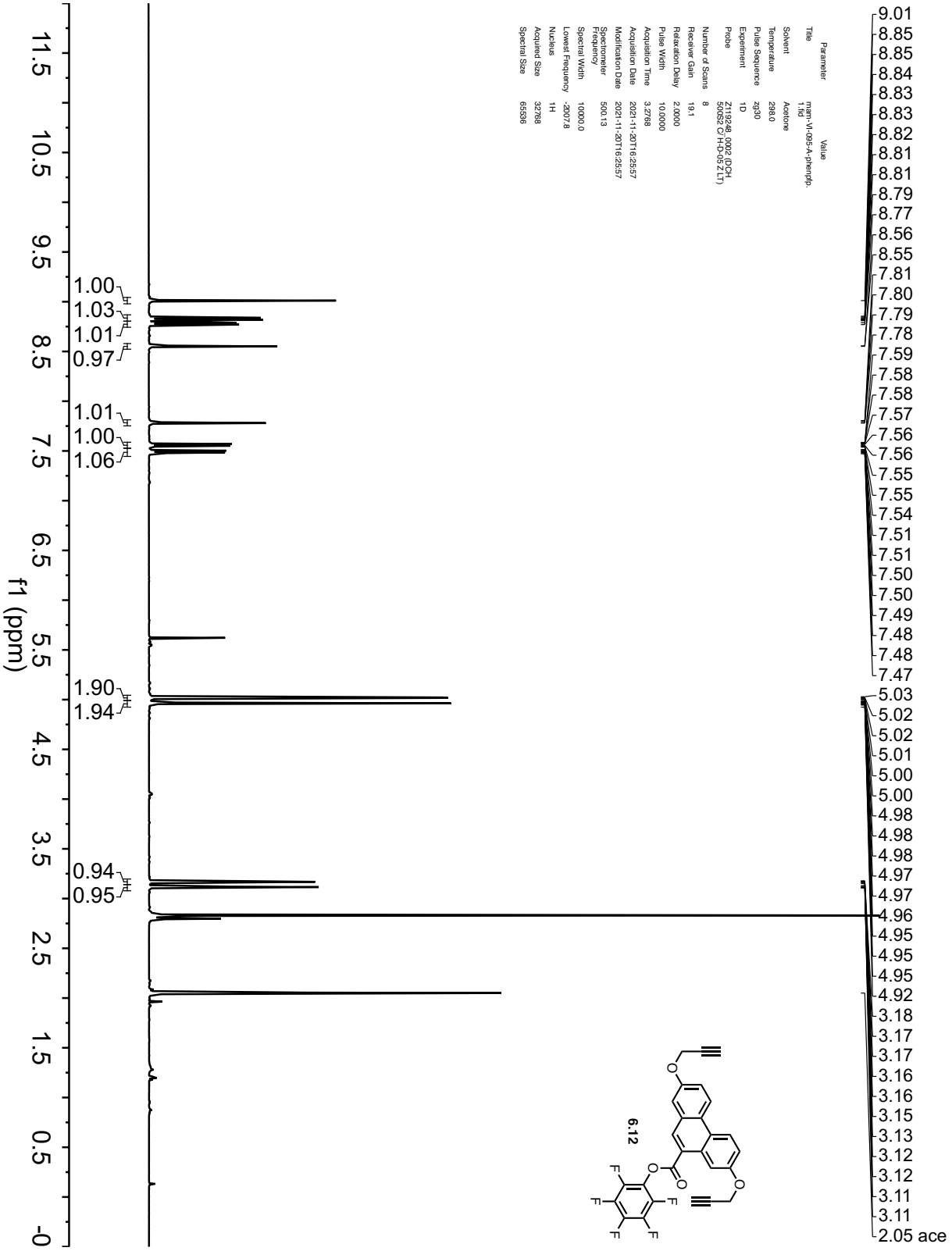
Parameter Value
Title mam-VI-095-A-phenylp. 1.fid
Solvent Acetone
Temperature 298.0
Pulse Sequence zg30
Experiment 1D
Probe Z119248_0002 (DCH 50052 C/ H-D-05 Z LT)
Number of Scans 8
Receiver Gain 19.1
Relaxation Delay 2.0000
Pulse Width 10.0000
Acquisition Time 3.2768
Acquisition Date 2021-11-20T16:25:57
Modification Date 2021-11-20T16:25:57
Spectrometer Frequency 500.13
Spectral Width 10000.0
Lowest Frequency -2007.8
Nucleus 1H
Acquired Size 32768
Spectral Size 65536
6.12
f1 (ppm)
1.00
1.03
1.01
0.97
1.01
1.00
1.06
1.90
1.94
0.94
0.95
9.01
8.85
8.85
8.84
8.83
8.83
8.82
8.81
8.81
8.79
8.77
8.56
8.55
7.81
7.80
7.79
7.78
7.59
7.58
7.58
7.57
7.56
7.56
7.55
7.55
7.54
7.51
7.51
7.50
7.50
7.49
7.48
7.48
7.47
5.03
5.02
5.02
5.01
5.00
5.00
4.98
4.98
4.98
4.97
4.97
4.96
4.95
4.95
4.95
4.92
3.18
3.17
3.17
3.16
3.16
3.15
3.13
3.12
3.12
3.11
3.11
2.05 ace

Parameter	Value
Title	mam-VI-095-A
Solvent	Acetone
Temperature	297.0
Pulse Sequence	zgfhigqn.2
Experiment	1D
Probe	5 mm PABBO BB/ 19F-1H/ D Z-GRD Z108618/ 0656

Number of Scans	24
Receiver Gain	189.8
Relaxation Delay	1.0000
Pulse Width	14.5000
Acquisition Time	0.8738
Acquisition Date	2021-11-27T12:47:00
Modification Date	2021-11-27T12:47:39
Spectrometer Frequency	376.50
Spectral Width	150000.0
Lowest Frequency	-75000.0
Nucleus	19F
Acquired Size	131072
Spectral Size	262144

-154.64
-154.65
-154.67
-154.69
-154.71
-154.72
-154.73
-160.07
-160.13
-160.18
-164.57
-164.58
-164.59
-164.61
-164.64
-164.65
-164.66
-164.70
-164.71
-164.72

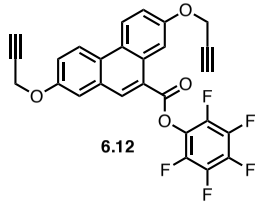

6.12

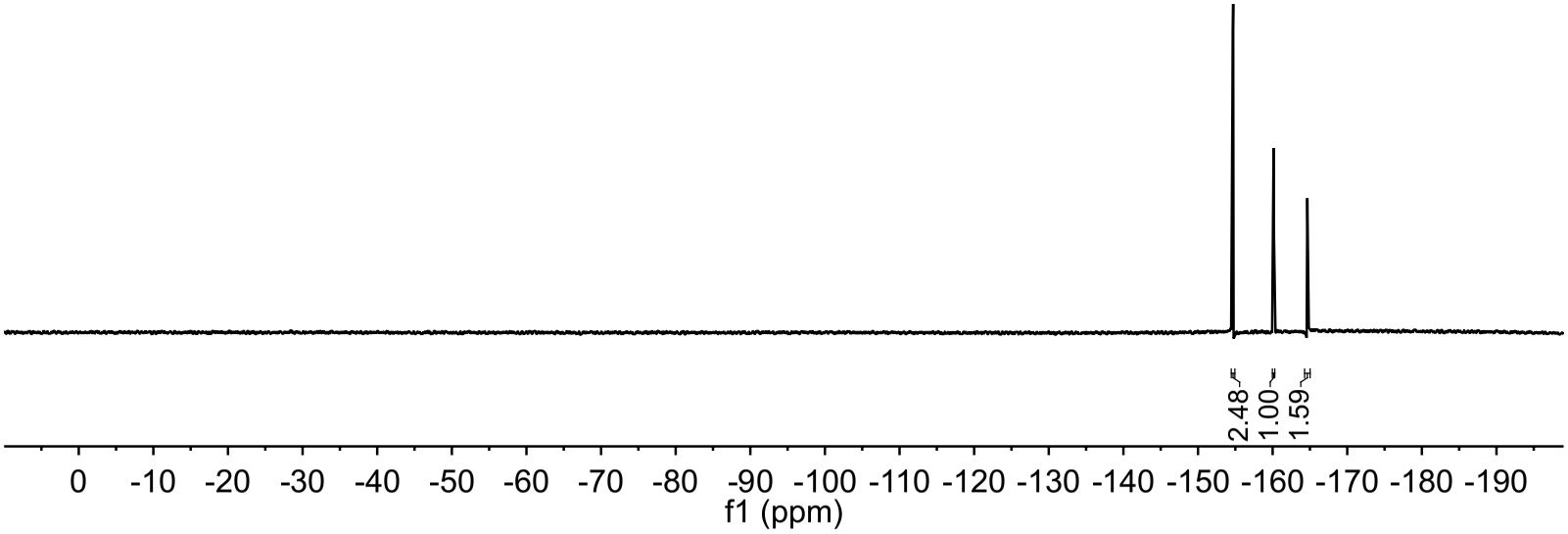

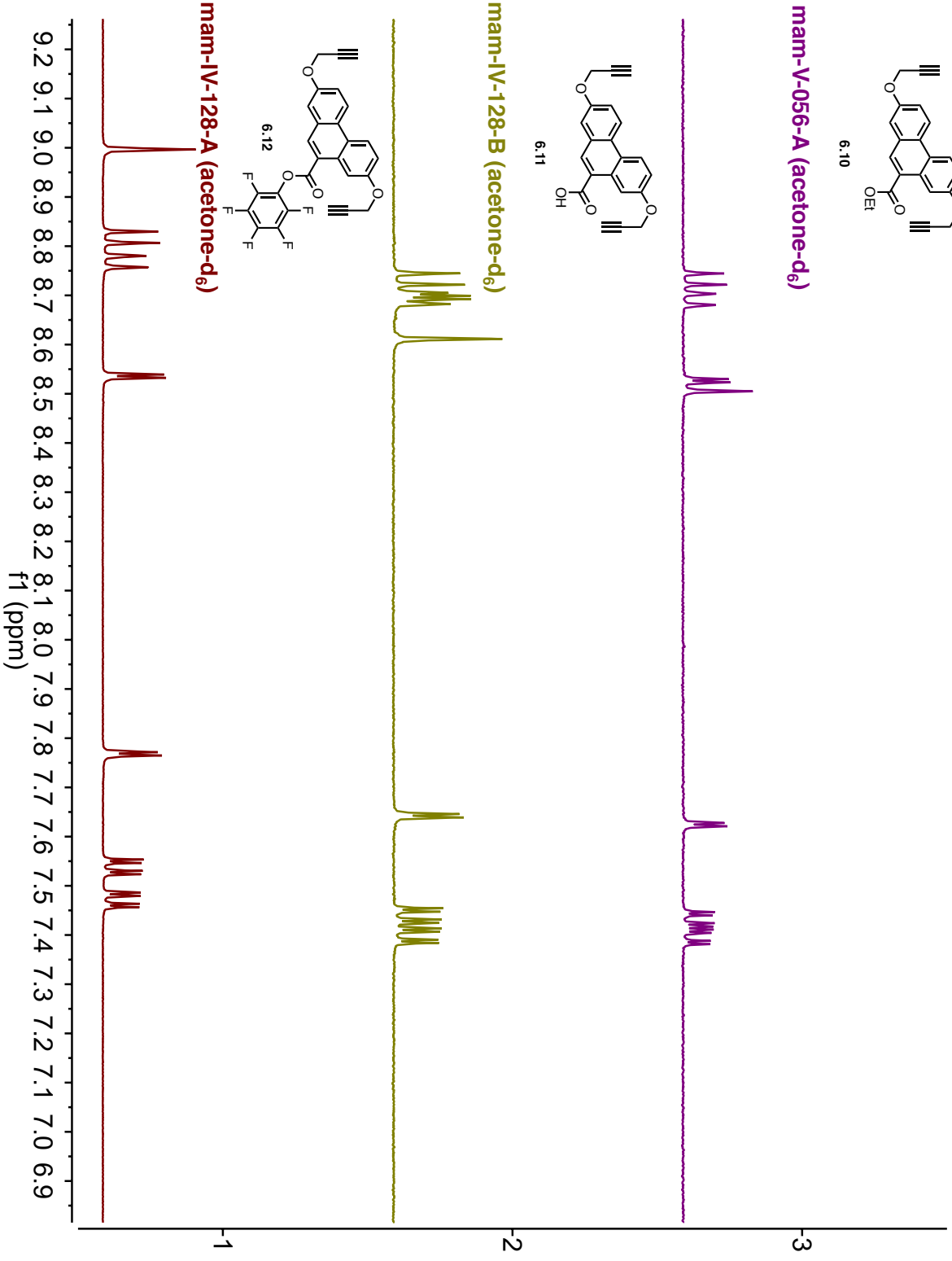
6.10
mam-V-056-A (acetone-d6)
6.11
mam-IV-128-B (acetone-d6)
6.12
mam-IV-128-A (acetone-d6)
f1 (ppm)

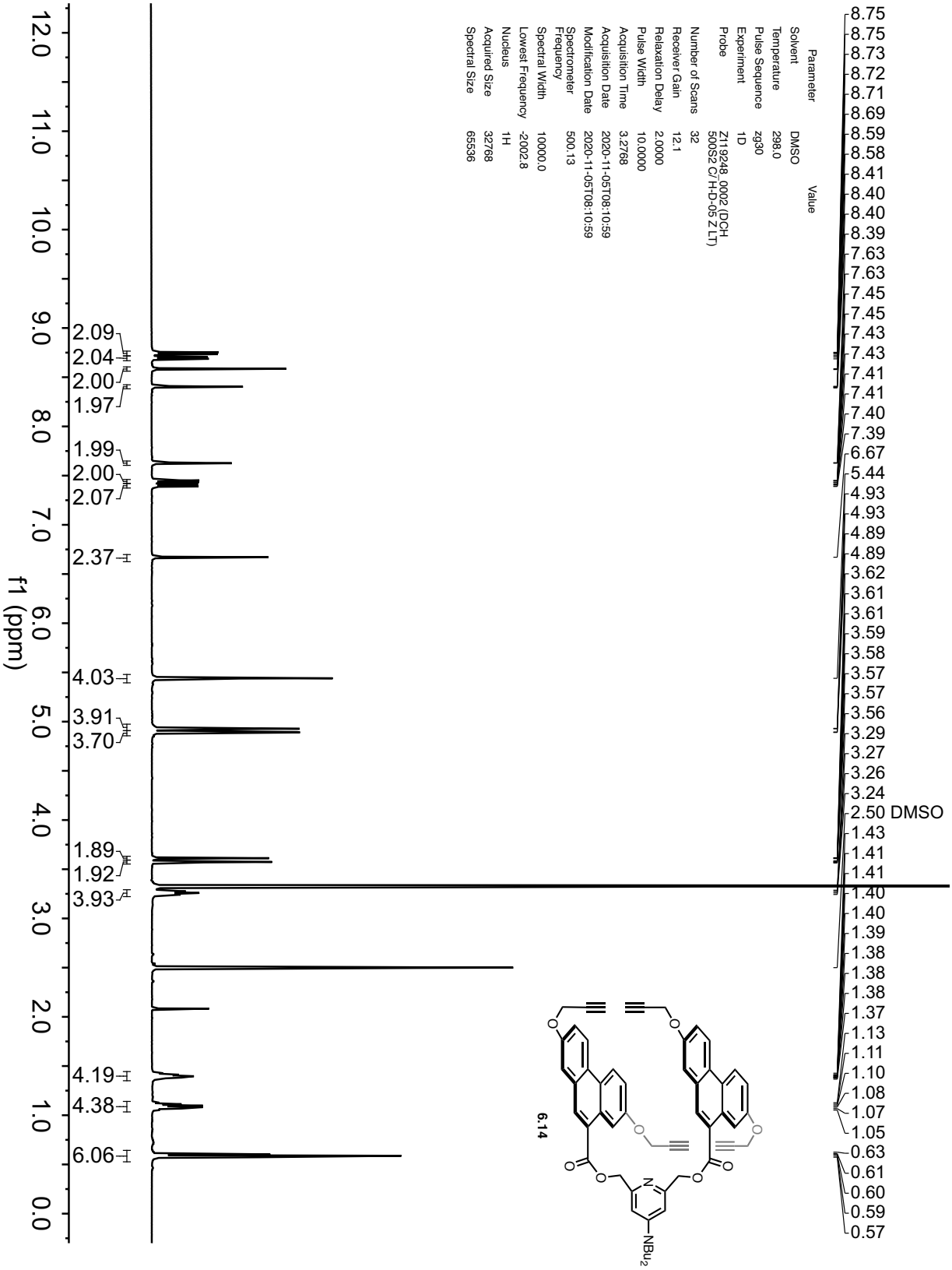
Parameter Value
Solvent DMSO
Temperature 298.0
Pulse Sequence zg30
Experiment 1D
Probe Z119248_0002 (DCH 500S2 C/ H-D-05 Z LT)
Number of Scans 32
Receiver Gain 12.1
Relaxation Delay 2.0000
Pulse Width 10.0000
Acquisition Time 3.2768
Acquisition Date 2020-11-05T08:10:59
Modification Date 2020-11-05T08:10:59
Spectrometer Frequency 500.13
Spectral Width 10000.0
Lowest Frequency -2002.8
Nucleus 1H
Acquired Size 32768
Spectral Size 65536
8.75 8.75 8.73 8.72 8.71 8.69 8.59 8.58 8.41 8.40 8.40 8.39 7.63 7.63 7.45 7.45 7.43 7.43 7.41 7.41 7.40 7.39 6.67 5.44 4.93 4.93 4.89 4.89 3.62 3.61 3.61 3.59 3.58 3.57 3.57 3.56 3.29 3.27 3.26 3.24 2.50 DMSO 1.43 1.41 1.41 1.40 1.40 1.39 1.38 1.38 1.38 1.37 1.13 1.11 1.10 1.08 1.07 1.05 0.63 0.61 0.60 0.59 0.57
2.09 2.04 2.00 1.97 1.99 2.00 2.07 2.37 4.03 3.91 3.70 1.89 1.92 3.93 4.19 4.38 6.06
12.0 11.0 10.0 9.0 8.0 7.0 6.0 5.0 4.0 3.0 2.0 1.0 0.0
f1 (ppm)
6.14
NBu2

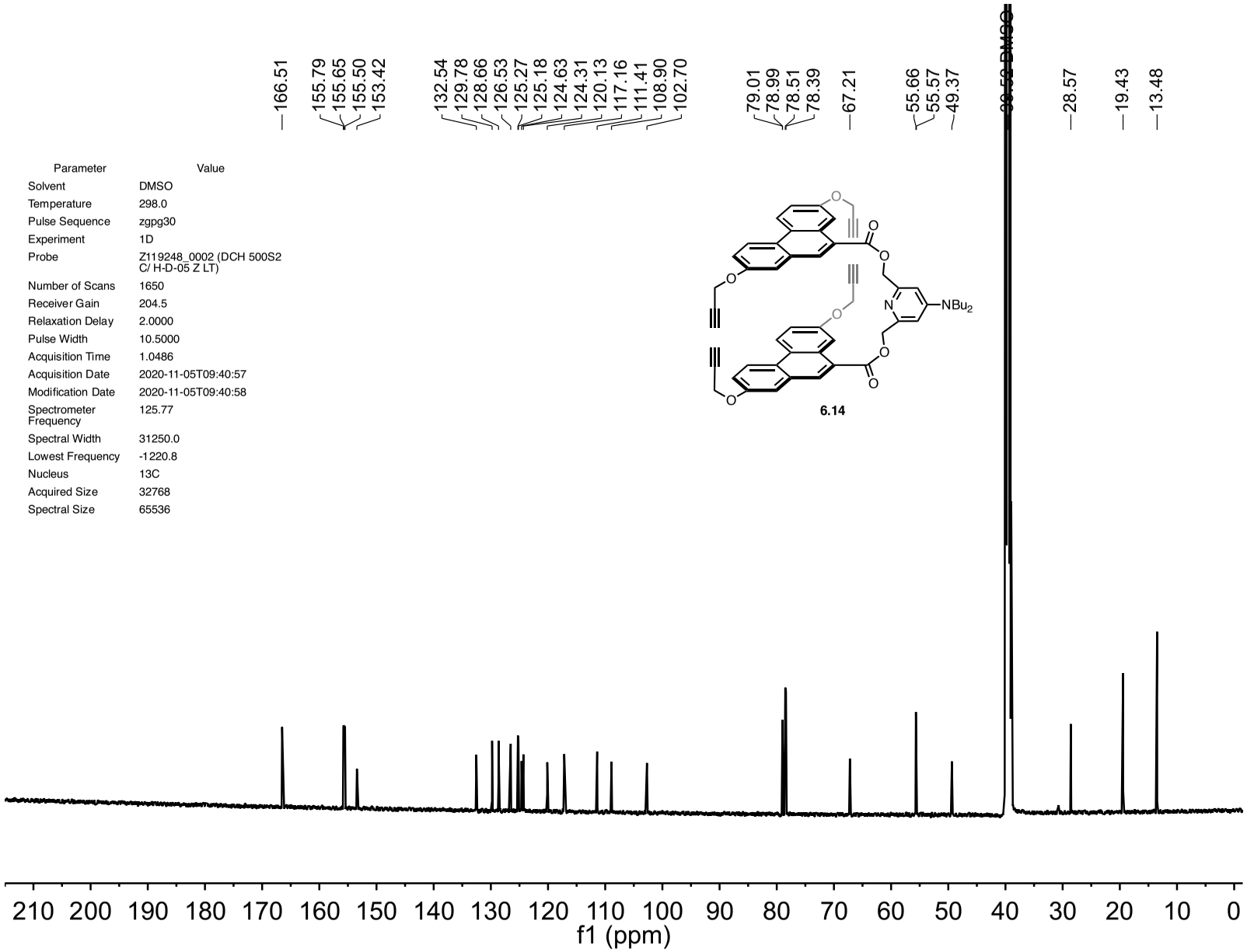

Parameter	Value
Solvent	DMSO
Temperature	298.0
Pulse Sequence	zgpg30
Experiment	1D
Probe	Z119248_0002 (DCH 500S2 C/ H-D-05 Z LT)
Number of Scans	1650
Receiver Gain	204.5
Relaxation Delay	2.0000
Pulse Width	10.5000
Acquisition Time	1.0486
Acquisition Date	2020-11-05T09:40:57
Modification Date	2020-11-05T09:40:58
Spectrometer Frequency	125.77
Spectral Width	31250.0
Lowest Frequency	-1220.8
Nucleus	13C
Acquired Size	32768
Spectral Size	65536

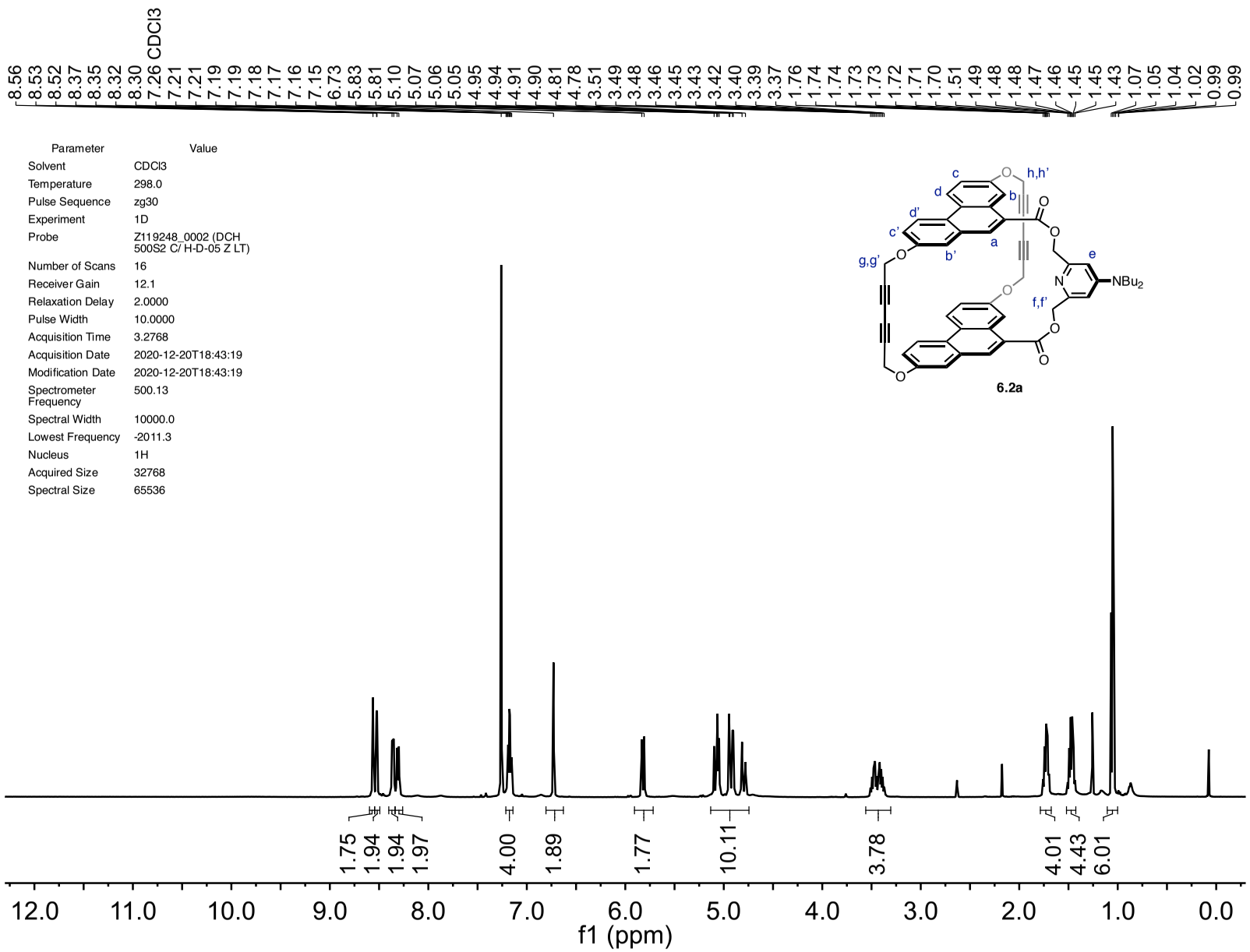

Parameter	Value
Solvent	CDCl3
Temperature	298.0
Pulse Sequence	zg30
Experiment	1D
Probe	Z119248_0002 (DCH 500S2 C/ H-D-05 Z LT)
Number of Scans	16
Receiver Gain	12.1
Relaxation Delay	2.0000
Pulse Width	10.0000
Acquisition Time	3.2768
Acquisition Date	2020-12-20T18:43:19
Modification Date	2020-12-20T18:43:19
Spectrometer Frequency	500.13
Spectral Width	10000.0
Lowest Frequency	-2011.3
Nucleus	1H
Acquired Size	32768
Spectral Size	65536

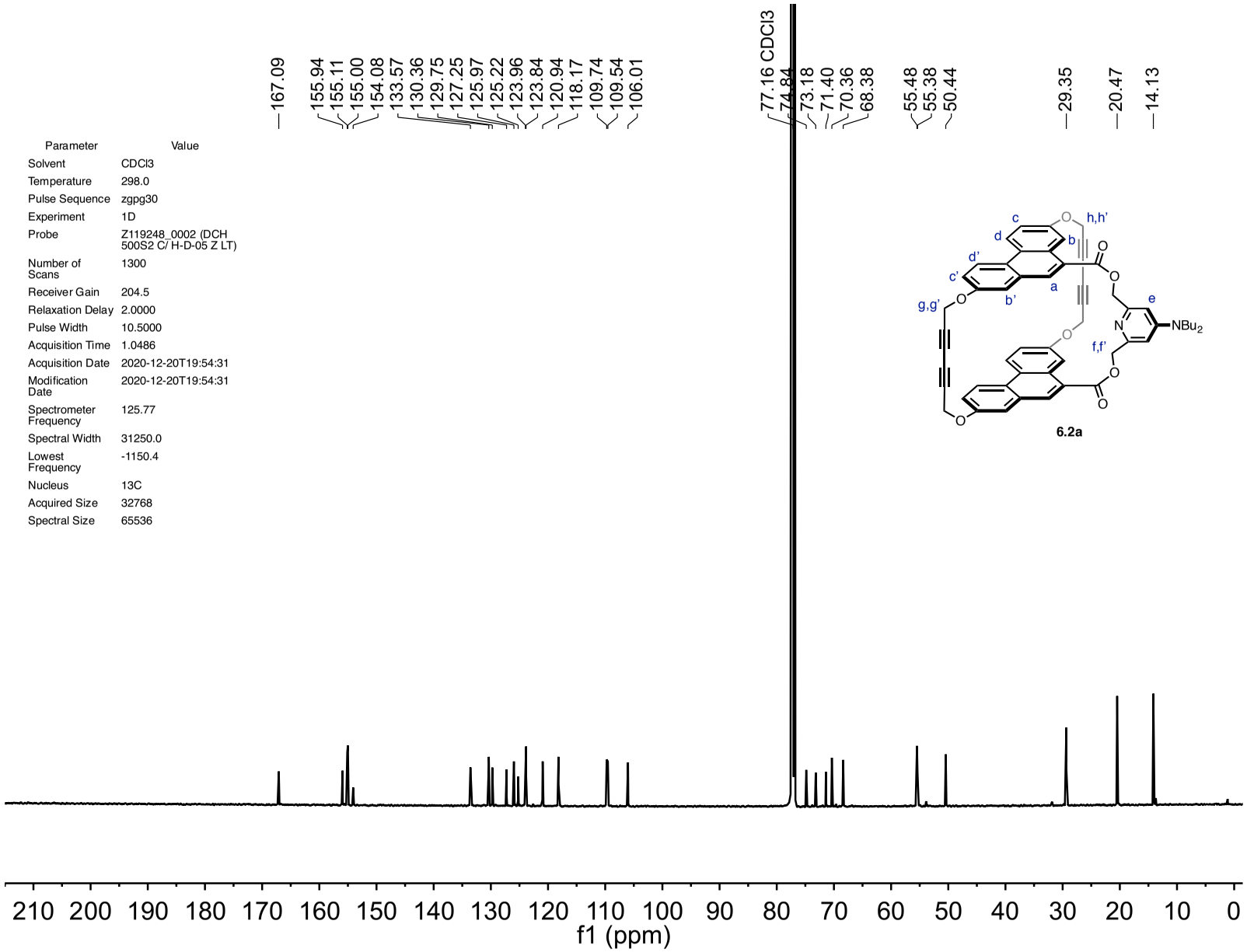

Parameter	Value
Solvent	CDCl3
Temperature	298.0
Pulse Sequence	zgpg30
Experiment	1D
Probe	Z119248_0002 (DCH 500S2 C/ H-D-05 Z LT)
Number of Scans	1300
Receiver Gain	204.5
Relaxation Delay	2.0000
Pulse Width	10.5000
Acquisition Time	1.0486
Acquisition Date	2020-12-20T19:54:31
Modification Date	2020-12-20T19:54:31
Spectrometer Frequency	125.77
Spectral Width	31250.0
Lowest Frequency	-1150.4
Nucleus	13C
Acquired Size	32768
Spectral Size	65536

Parameter	Value
Title	mam-V-060-cosy.2.ser
Solvent	CDCl3
Temperature	298.0
Pulse Sequence	cosygpmfph
Experiment	COSY
Probe	Z119248_0002 (DCH 500S2 C/ H-D-05 Z LT)
Number of Scans	6
Receiver Gain	12.1
Relaxation Delay	2.0000
Pulse Width	10.0000
Acquisition Time	0.1704
Acquisition Date	2021-11-28T14:27:22
Modification Date	2021-11-28T15:23:13
Spectrometer Frequency	(500.13, 500.13)
Spectral Width	(6009.6, 6009.6)
Lowest Frequency	(-520.7, -532.6)
Nucleus	(1H, 1H)
Acquired Size	(1024, 256)
Spectral Size	(1024, 1024)

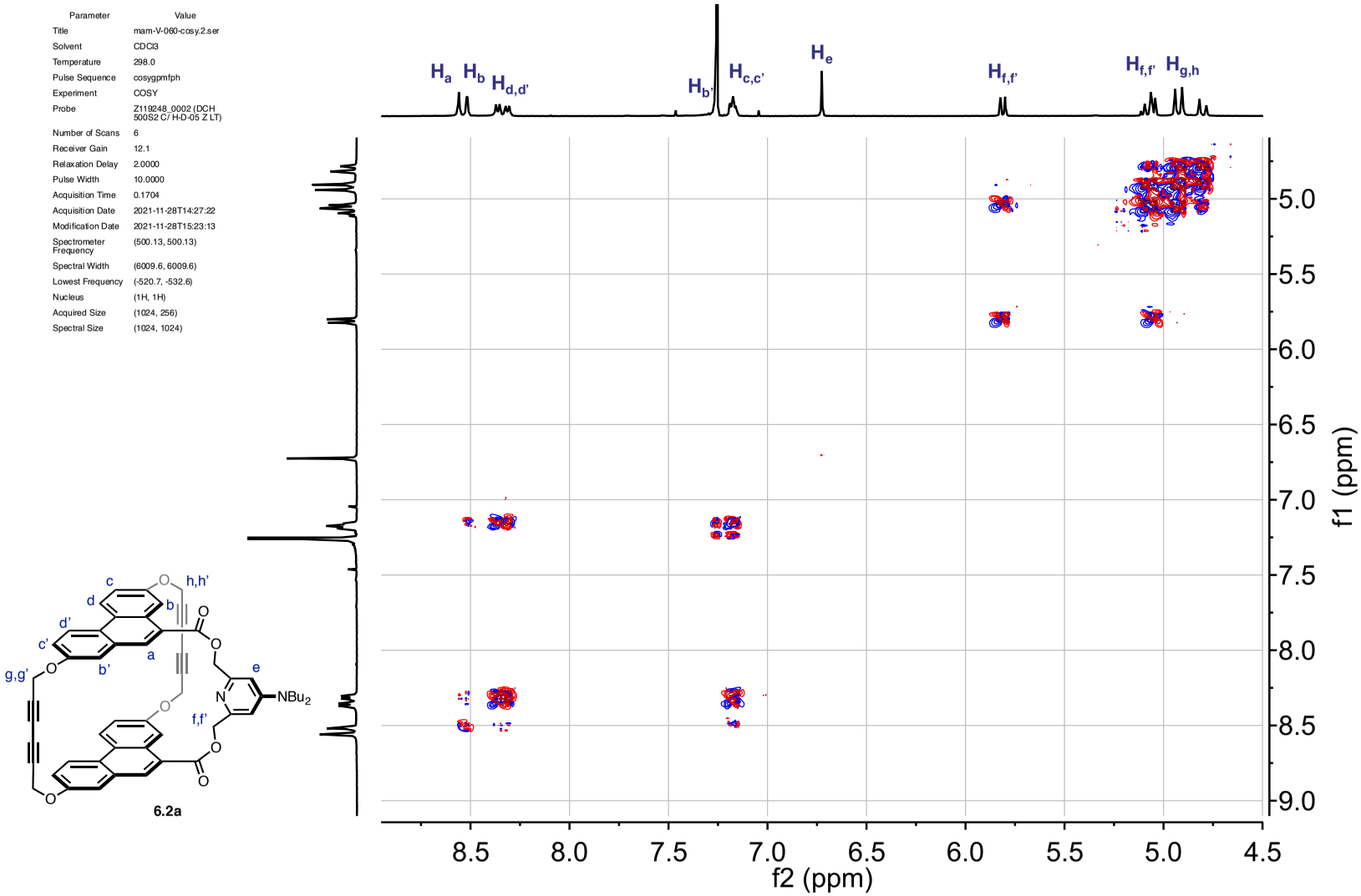

6.2a

Parameter	Value
Title	mam-V-060-cosy.2.ser
Solvent	CDCl3
Temperature	298.0
Pulse Sequence	cosygpmfph
Experiment	COSY
Probe	Z119248_0002 (DCH 500S2 C/ H-D-05 Z LT)
Number of Scans	6
Receiver Gain	12.1
Relaxation Delay	2.0000
Pulse Width	10.0000
Acquisition Time	0.1704
Acquisition Date	2021-11-28T14:27:22
Modification Date	2021-11-28T15:23:13
Spectrometer Frequency	(500.13, 500.13)
Spectral Width	(6009.6, 6009.6)
Lowest Frequency	(-520.7, -532.6)
Nucleus	(1H, 1H)
Acquired Size	(1024, 256)
Spectral Size	(1024, 1024)

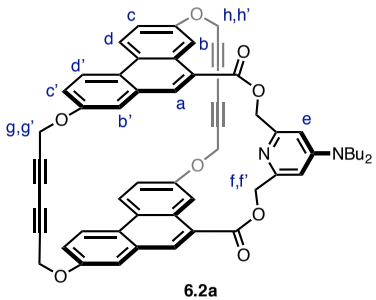

6.2a

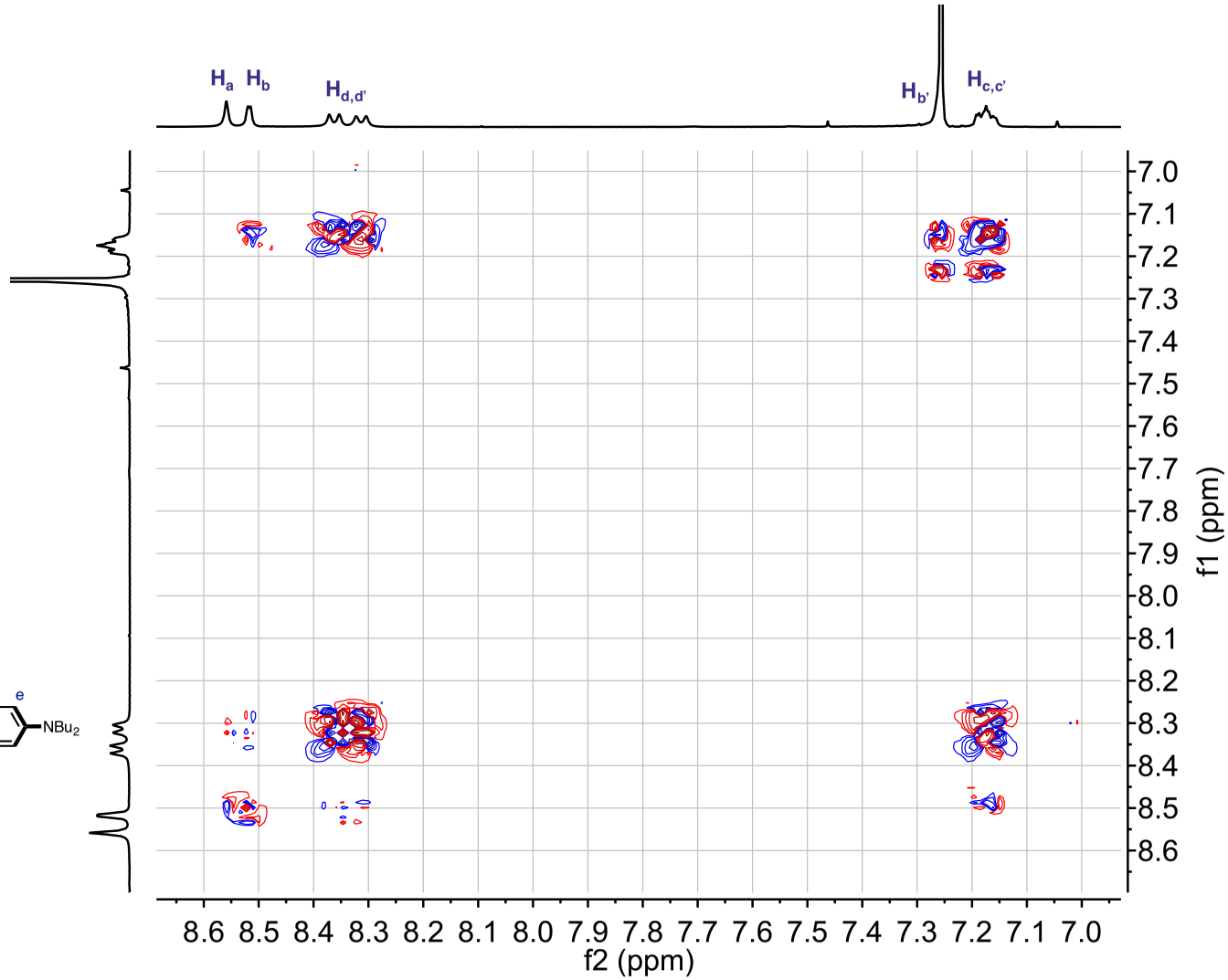

Parameter	Value
Title	mam-V-060-2d.2.ser
Solvent	CDCl3
Temperature	298.0
Pulse Sequence	noesygpph
Experiment	NOESY
Probe	Z119248_0002 (DCH 500S2 C/ H-D-05 Z LT)
Number of Scans	8
Receiver Gain	14.7
Relaxation Delay	2.0000
Pulse Width	10.0000
Acquisition Time	0.1704
Acquisition Date	2021-11-28T19:27:50
Modification Date	2021-11-28T21:07:37
Spectrometer Frequency	(500.13, 500.13)
Spectral Width	(6009.6, 6009.6)
Lowest Frequency	(-517.7, -517.7)
Nucleus	(1H, 1H)
Acquired Size	(1024, 256)
Spectral Size	(1024, 1024)

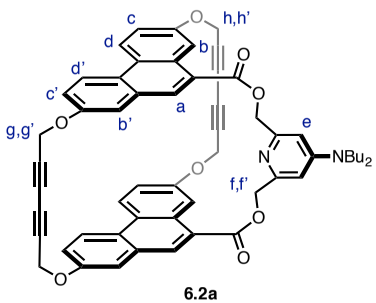

6.2a

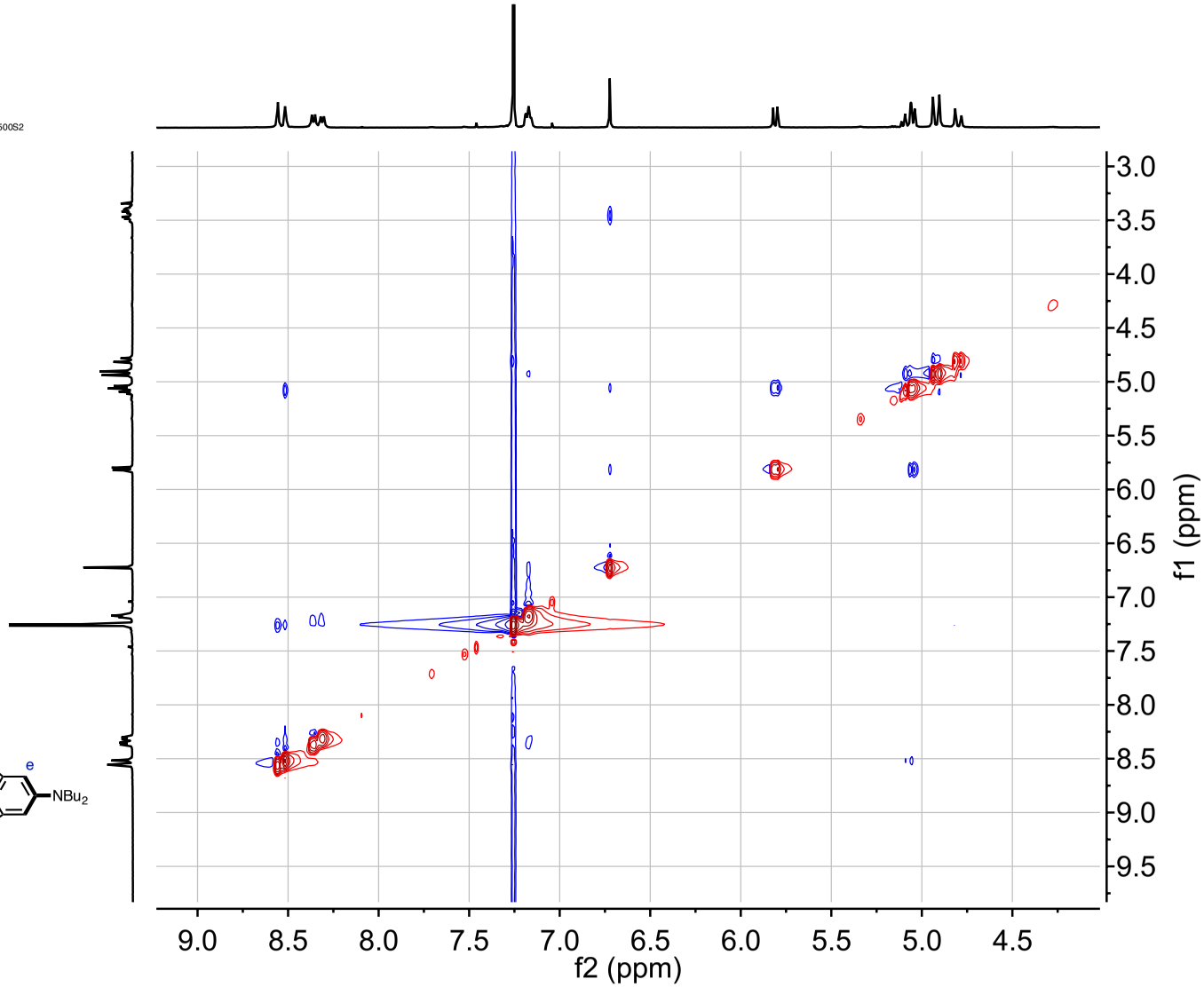

Parameter	Value
Title	mam-V-060-2d.4.ser
Solvent	CDCl3
Temperature	298.0
Pulse Sequence	hsqcedetgp
Experiment	HSQC-EDITED
Probe	Z119248_0002 (DCH 500S2 C/ H-D-05 Z LT)
Number of Scans	20
Receiver Gain	204.5
Relaxation Delay	1.5000
Pulse Width	10.0000
Acquisition Time	0.1704
Acquisition Date	2021-11-28T22:00:59
Modification Date	2021-11-29T00:24:42
Spectrometer Frequency	(500.13, 125.77)
Spectral Width	(6009.6, 27624.3)
Lowest Frequency	(-517.7, -37.0)
Nucleus	(1H, 13C)
Acquired Size	(1024, 256)
Spectral Size	(1024, 1024)

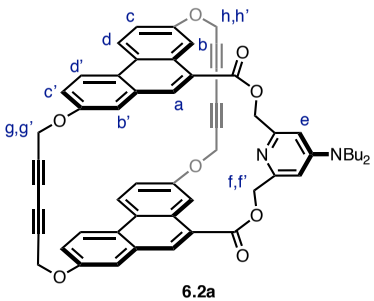

6.2a

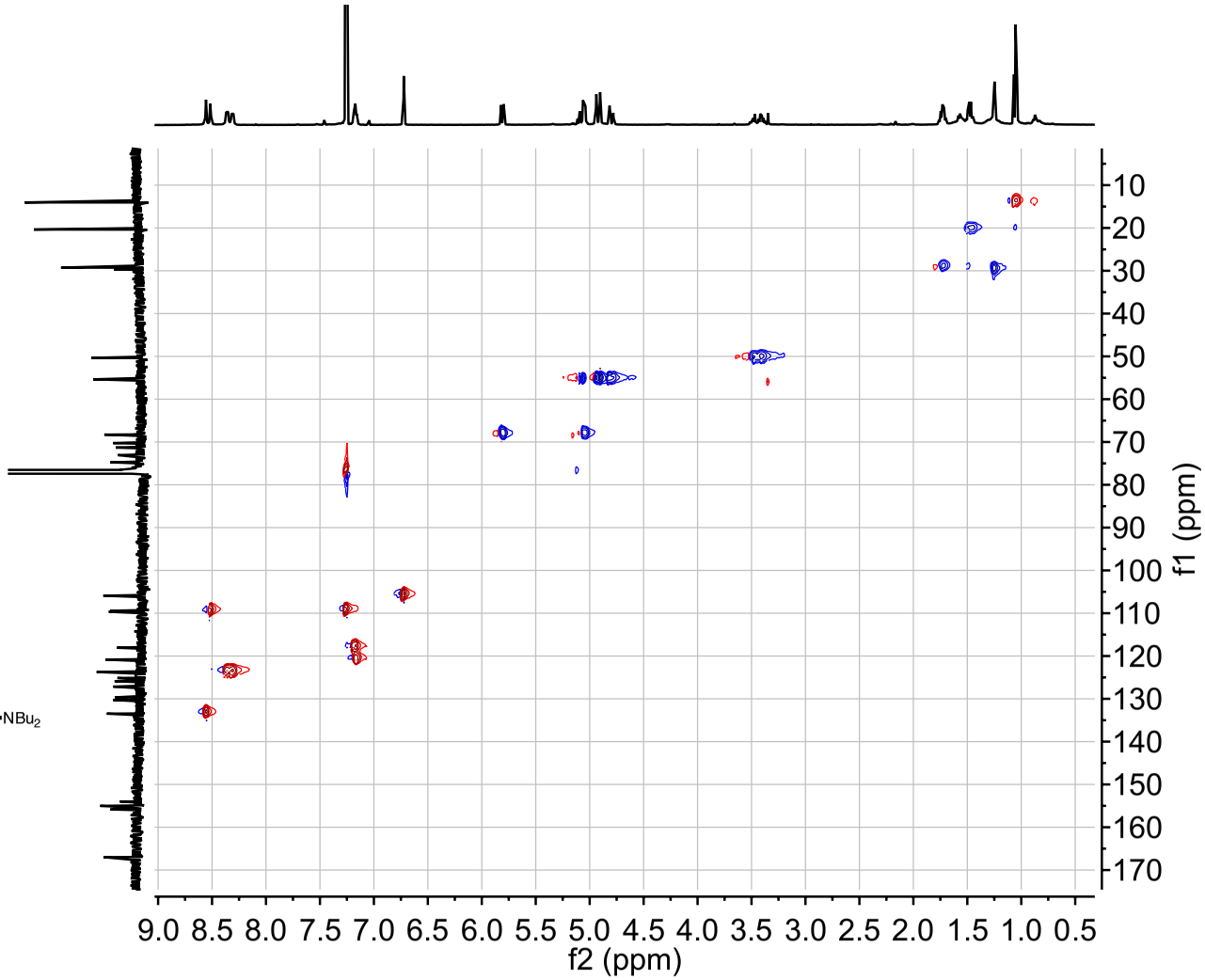

Parameter	Value
Title	mam-V-060-2d.4.ser
Solvent	CDCl3
Temperature	298.0
Pulse Sequence	hsqcedetgp
Experiment	HSQC-EDITED
Probe	Z119248_0002 (DCH 500S2 C/ H-D-05 Z LT)
Number of Scans	20
Receiver Gain	204.5
Relaxation Delay	1.5000
Pulse Width	10.0000
Acquisition Time	0.1704
Acquisition Date	2021-11-28T22:00:59
Modification Date	2021-11-29T00:24:42
Spectrometer Frequency	(500.13, 125.77)
Spectral Width	(6009.6, 27624.3)
Lowest Frequency	(-517.7, -37.0)
Nucleus	(1H, 13C)
Acquired Size	(1024, 256)
Spectral Size	(1024, 1024)

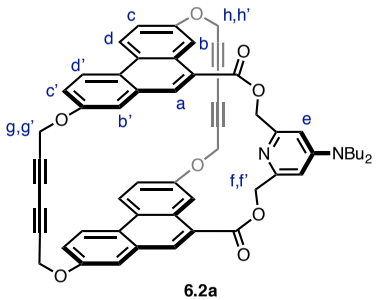

6.2a

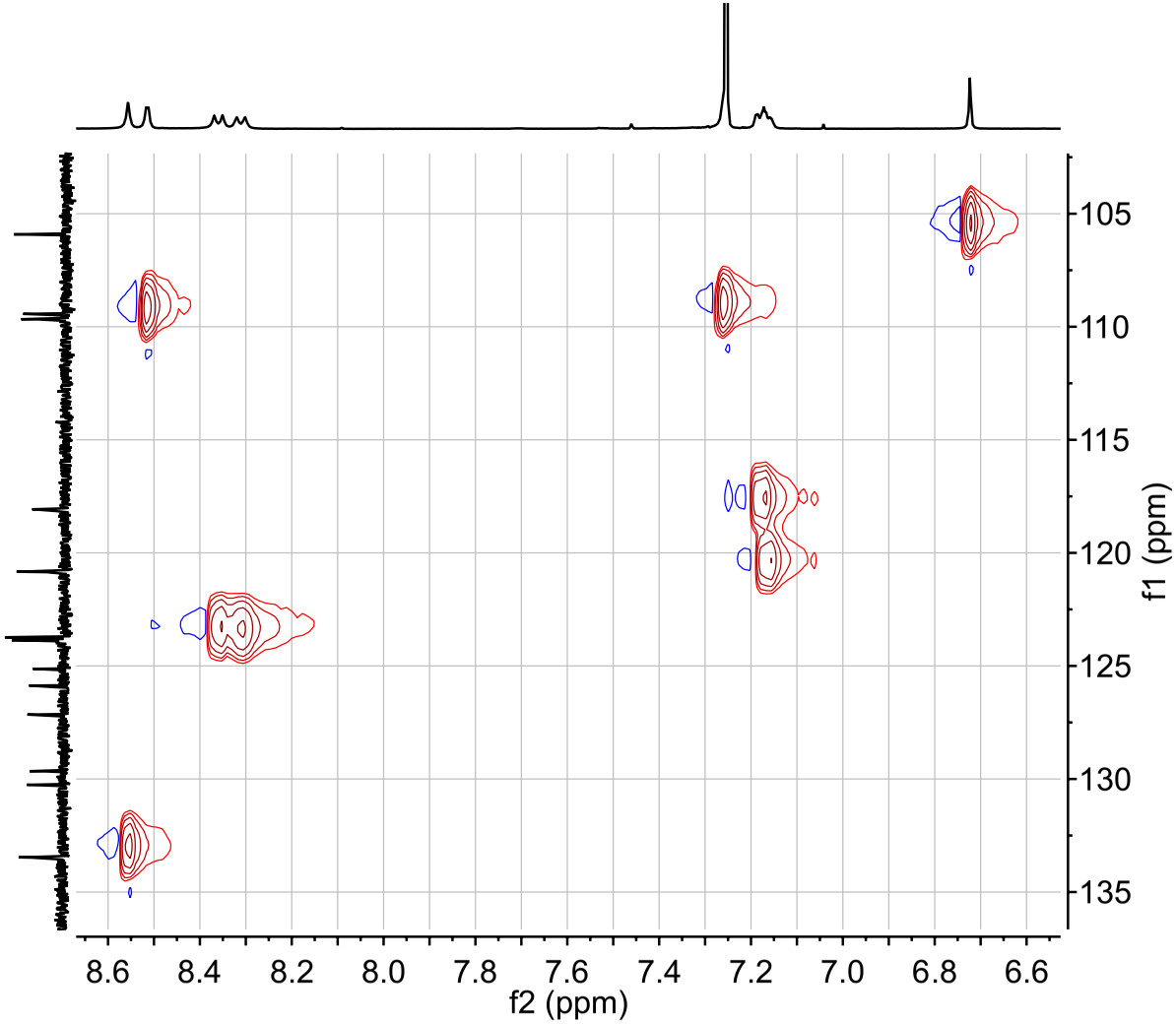

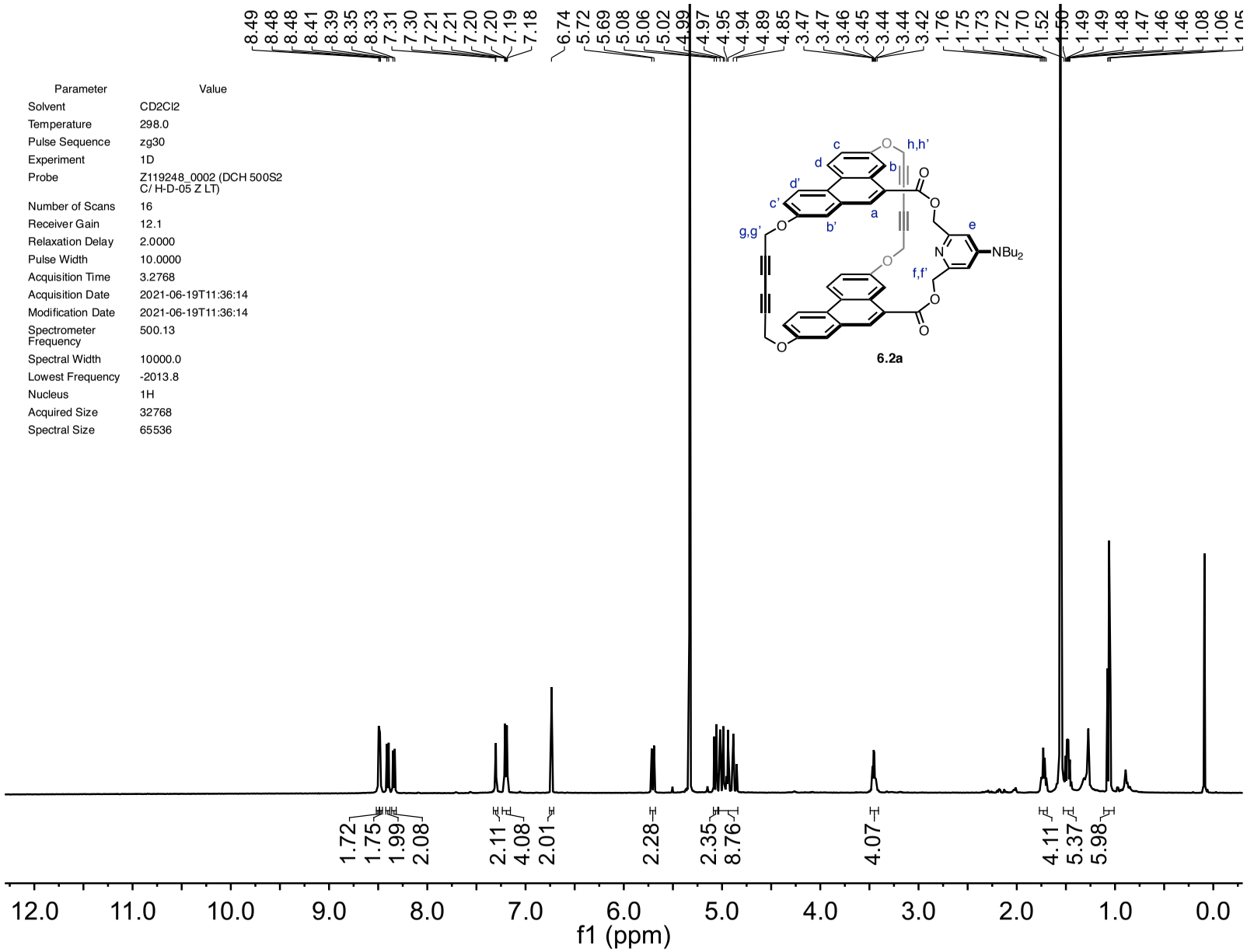

Parameter	Value
Solvent	CD2Cl2
Temperature	298.0
Pulse Sequence	zg30
Experiment	1D
Probe	Z119248_0002 (DCH 500S2 C/ H-D-05 Z LT)
Number of Scans	16
Receiver Gain	12.1
Relaxation Delay	2.0000
Pulse Width	10.0000
Acquisition Time	3.2768
Acquisition Date	2021-06-19T11:36:14
Modification Date	2021-06-19T11:36:14
Spectrometer Frequency	500.13
Spectral Width	10000.0
Lowest Frequency	-2013.8
Nucleus	1H
Acquired Size	32768
Spectral Size	65536

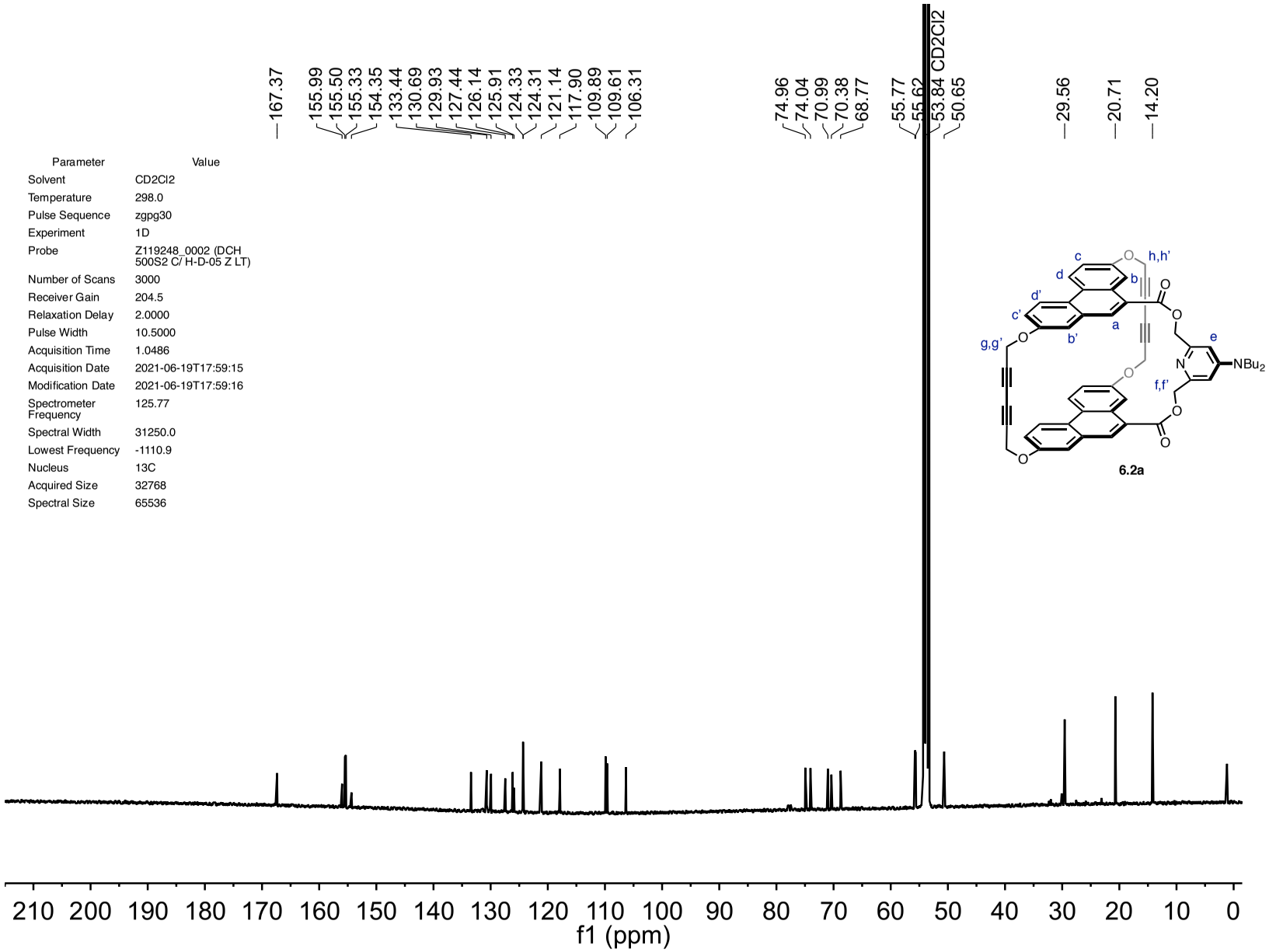

Parameter	Value
Solvent	CD2Cl2
Temperature	298.0
Pulse Sequence	zgpg30
Experiment	1D
Probe	Z119248_0002 (DCH 500S2 C/ H-D-05 Z LT)
Number of Scans	3000
Receiver Gain	204.5
Relaxation Delay	2.0000
Pulse Width	10.5000
Acquisition Time	1.0486
Acquisition Date	2021-06-19T17:59:15
Modification Date	2021-06-19T17:59:16
Spectrometer Frequency	125.77
Spectral Width	31250.0
Lowest Frequency	-1110.9
Nucleus	13C
Acquired Size	32768
Spectral Size	65536

Parameter	Value
Title	mam-V-142-dcm
Solvent	CD2Cl2
Temperature	297.1
Pulse Sequence	cosygpmfphpp
Experiment	COSY
Probe	5 mm PABBO BB/ 19F-1H/ D Z-GRD Z108618/ 0656
Number of Scans	4
Receiver Gain	137.2
Relaxation Delay	2.0000
Pulse Width	15.0000
Acquisition Time	0.2540
Acquisition Date	2021-06-19T18:51:00
Modification Date	2021-06-19T19:31:07
Spectrometer Frequency	(400.13, 400.13)
Spectral Width	(4032.3, 4032.3)
Lowest Frequency	(-292.6, -286.0)
Nucleus	(1H, 1H)
Acquired Size	(1024, 256)
Spectral Size	(1024, 1024)

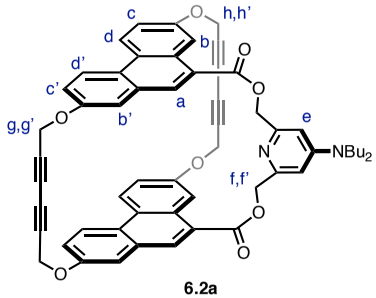

6.2a

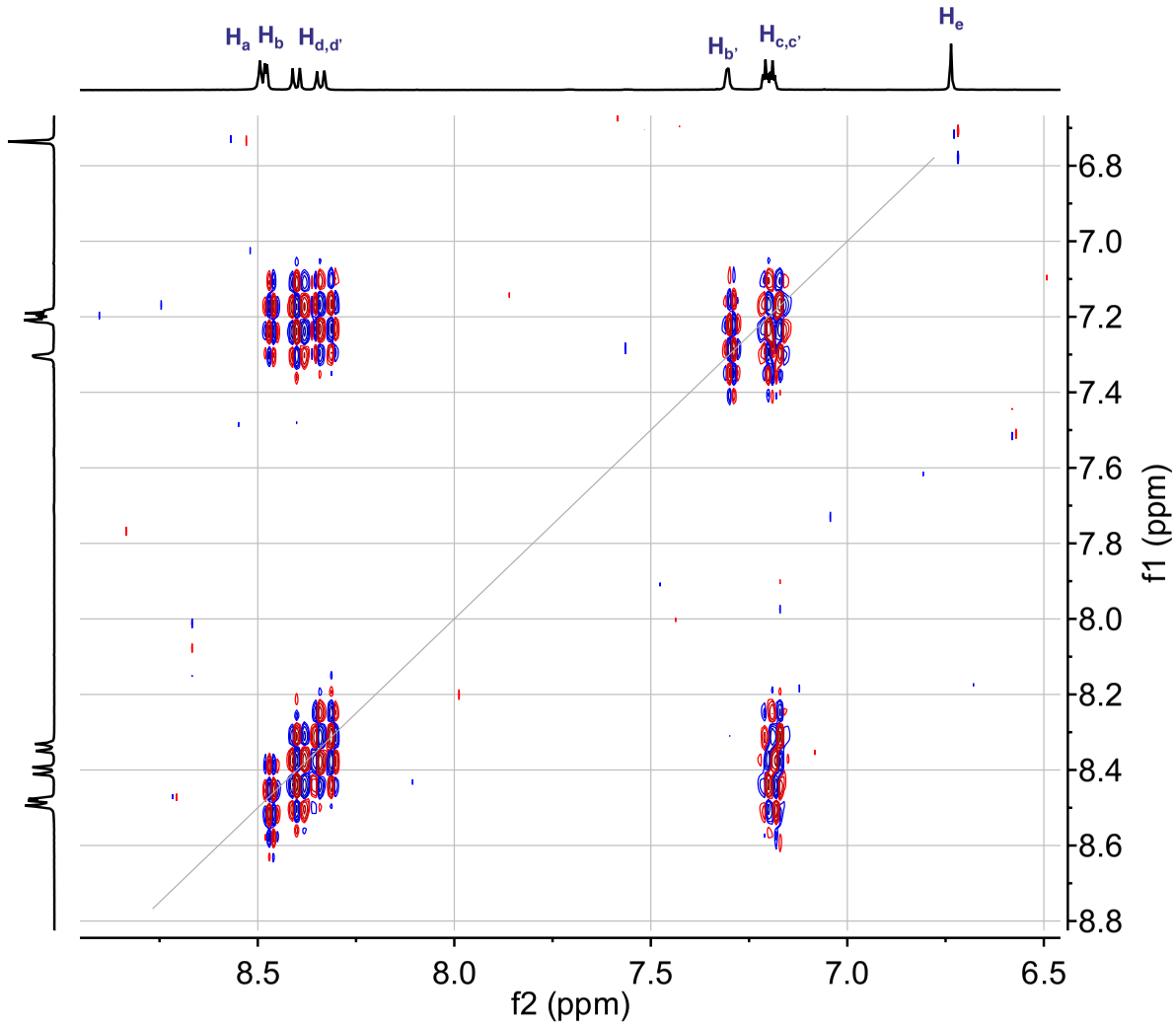

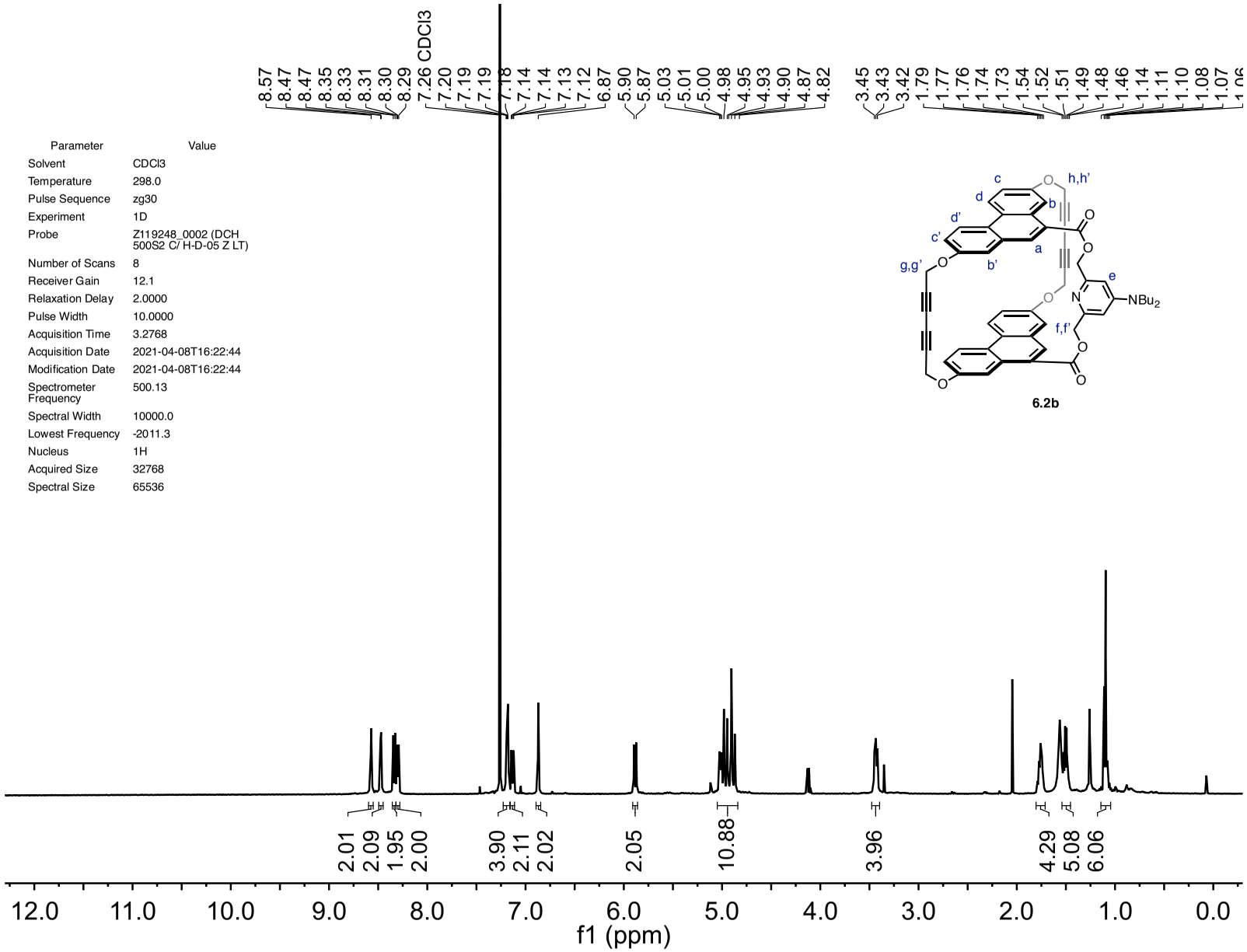

Parameter	Value
Solvent	CDCl3
Temperature	298.0
Pulse Sequence	zg30
Experiment	1D
Probe	Z119248_0002 (DCH 500S2 C/ H-D-05 Z LT)
Number of Scans	8
Receiver Gain	12.1
Relaxation Delay	2.0000
Pulse Width	10.0000
Acquisition Time	3.2768
Acquisition Date	2021-04-08T16:22:44
Modification Date	2021-04-08T16:22:44
Spectrometer Frequency	500.13
Spectral Width	10000.0
Lowest Frequency	-2011.3
Nucleus	1H
Acquired Size	32768
Spectral Size	65536

6.2b

Parameter	Value
Title	mam-V-52-E-cdcl3.13.fid
Solvent	CDCl3
Temperature	298.0
Pulse Sequence	zgpg30
Experiment	1D
Probe	Z119248_0002 (DCH 500S2 C/ H-D-05 Z LT)
Number of Scans	1720
Receiver Gain	204.5
Relaxation Delay	2.0000
Pulse Width	10.5000
Acquisition Time	1.0486
Acquisition Date	2021-11-27T17:48:10
Modification Date	2021-11-27T17:48:10
Spectrometer Frequency	125.77
Spectral Width	31250.0
Lowest Frequency	-1145.1
Nucleus	13C
Acquired Size	32768
Spectral Size	65536

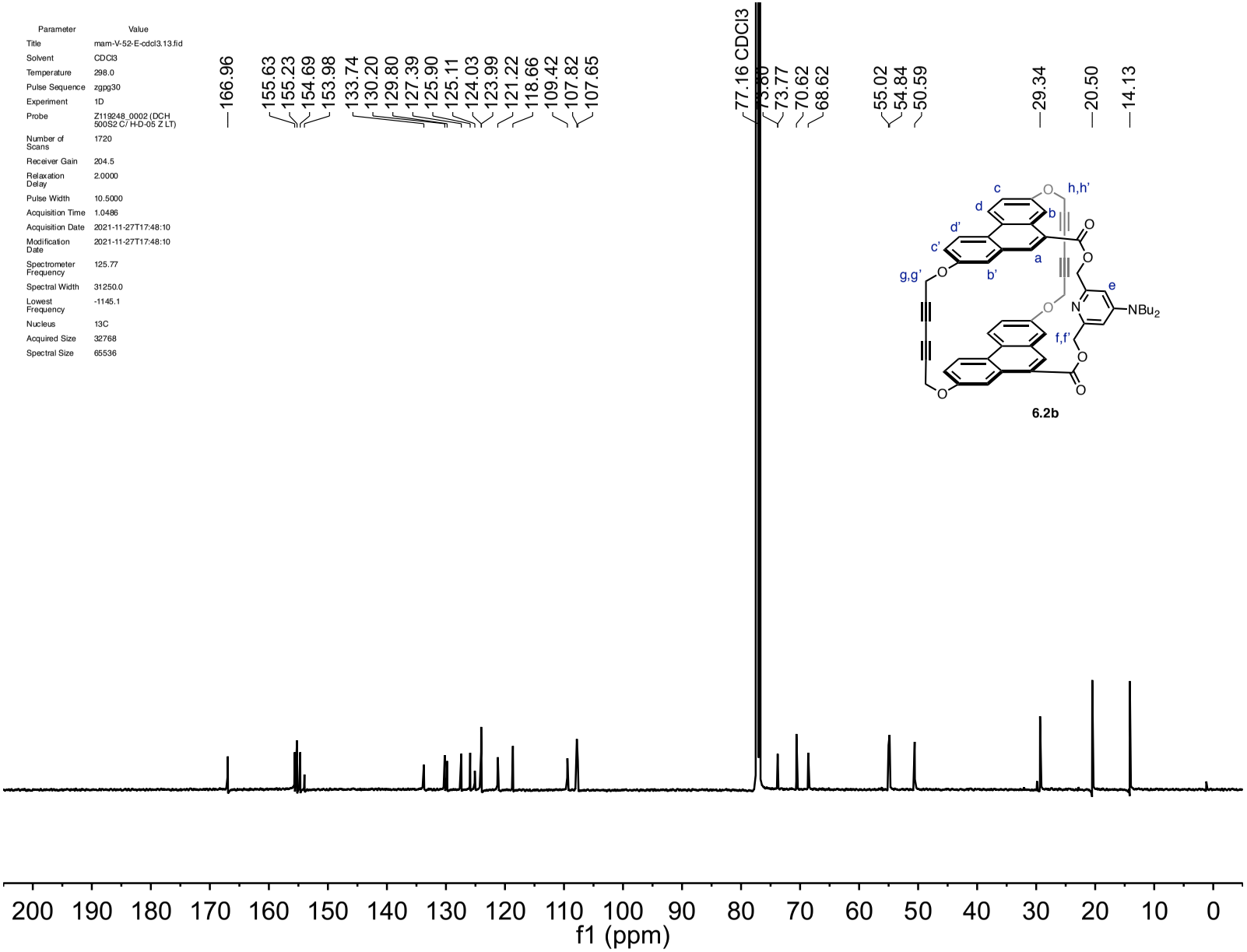

Parameter	Value
Title	mam-V-052-E
Solvent	CDCl3
Temperature	297.0
Pulse Sequence	cosygpmfphpp
Experiment	COSY
Probe	5 mm PABBO BB/ 19F-1H/ D Z-GRD Z108618/ 0656

Number of Scans	6
Receiver Gain	122.3
Relaxation Delay	2.0000
Pulse Width	15.0000
Acquisition Time	0.2499
Acquisition Date	2021-11-27T17:56:00
Modification Date	2021-11-27T18:55:00
Spectrometer Frequency	(400.13, 400.13)
Spectral Width	(4098.4, 4098.4)
Lowest Frequency	(-284.7, -284.7)
Nucleus	(1H, 1H)
Acquired Size	(1024, 256)
Spectral Size	(1024, 1024)

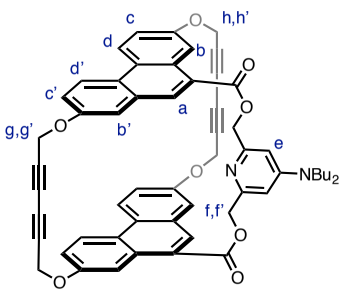

6.2b

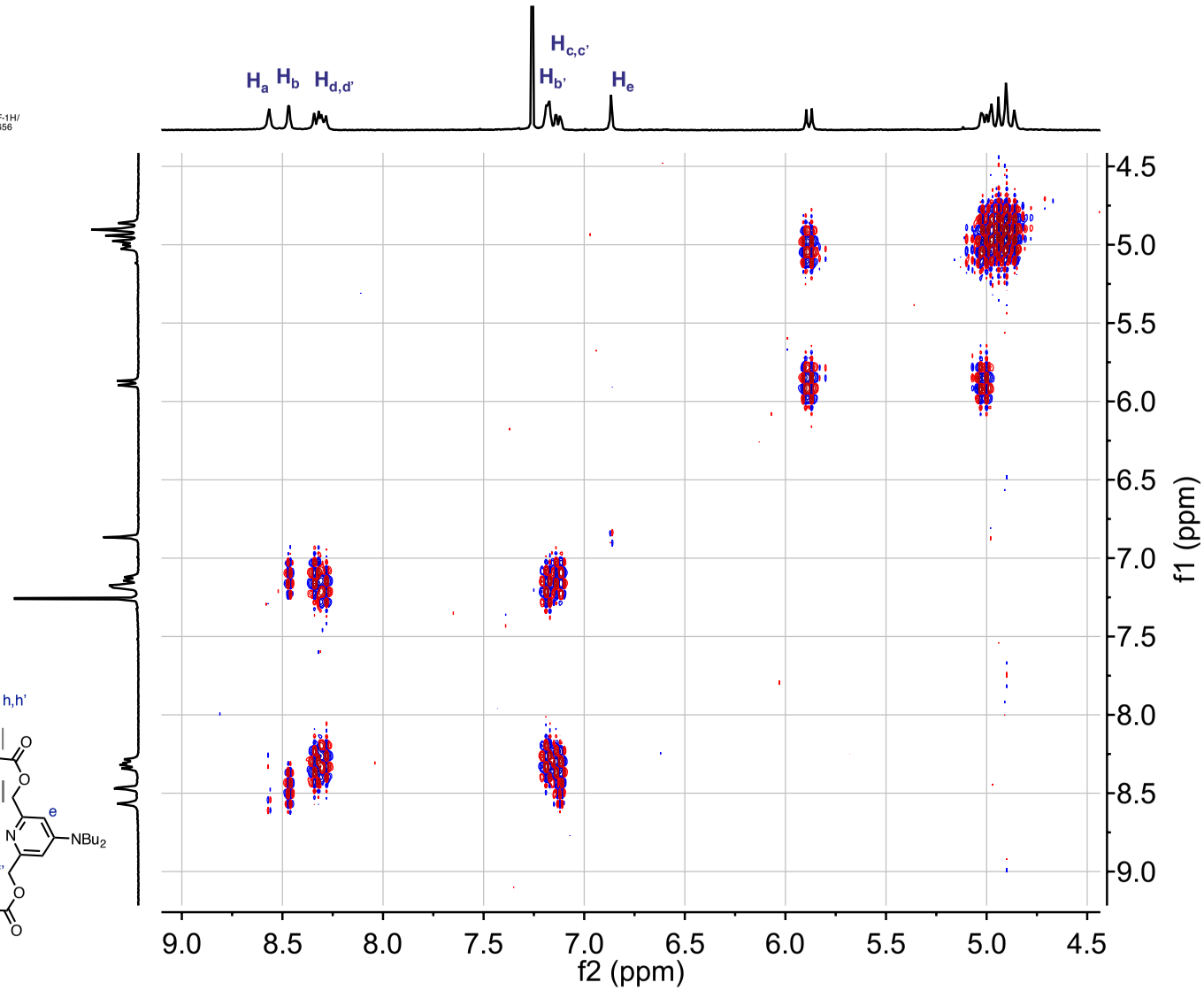

6.6 References

(1) Gunasekara, R. W.; Zhao, Y. Rationally Designed Cooperatively Enhanced Receptors To Magnify Host−Guest Binding in Water. *J. Am. Chem. Soc* **2015**, *137*, 843–849.

(2) Cao, L.; Šekutor, M.; Zavalij, P. Y.; Mlinarič-Majerski, K.; Glaser, R.; Isaacs, L. Cucurbit[7]Uril·Guest Pair with an Attomolar Dissociation Constant. *Angew. Chemie Int. Ed.* **2014**, *53*, 988–993.

(3) Yang, L. P.; Wang, X.; Yao, H.; Jiang, W. Naphthotubes: Macrocyclic Hosts with a Biomimetic Cavity Feature. *Acc. Chem. Res.* **2019**, *53*, 198–208.

(4) Yao, H.; Ke, H.; Zhang, X.; Pan, S. J.; Li, M. S.; Yang, L. P.; Schreckenbach, G.; Jiang, W. Molecular Recognition of Hydrophilic Molecules in Water by Combining the Hydrophobic Effect with Hydrogen Bonding. *J. Am. Chem. Soc.* **2018**, *140*, 13466–13477.

(5) Barrans, R. E.; Dougherty, D. A.; Petti, M. A.; Shepodd, T. J. "Hydrophobic" Binding of Water-Soluble Guests by High-Symmetry, Chiral Hosts. An Electron-Rich Receptor Site with a General Affinity for Quaternary Ammonium Compounds and Electron-Deficient .Pi. Systems. *J. Am. Chem. Soc.* **2002**, *110*, 6825–6840.

(6) Diederich, F.; Dick, K. A New Water-Soluble Macrocyclic Host of the Cyclophane Type: Host-Guest Complexation with Aromatic Guests in Aqueous Solution and Acceleration of the Transport of Arenes through an Aqueous Phase. *J. Am. Chem. Soc.* **1984**, *106*, 8024–8036.

(7) Poater, J.; Duran, M.; Solà, M. Aromaticity Determines the Relative Stability of Kinked vs. Straight Topologies in Polycyclic Aromatic Hydrocarbons. *Front. Chem.* **2018**, *6*, 561.

(8) Spenst, P.; Würthner, F. A Perylene Bisimide Cyclophane as a "Turn-On" and "Turn-Off" Fluorescence Probe. *Angew. Chemie* **2015**, *127*, 10303–10306.

(9) Dale, E. J.; Vermeulen, N. A.; Thomas, A. A.; Barnes, J. C.; Juríček, M.; Blackburn, A. K.; Strutt, N. L.; Sarjeant, A. A.; Stern, C. L.; Denmark, S. E.; Stoddart, J. F. ExCage. *J. Am. Chem. Soc.* **2014**, *136*, 10669–10682.

(10) Luis Castedo, I. Ben; Saá, J. M.; Seijas, J. A.; Suau, R.; Tojo, G. 4,5-O-Substituted Phenanthrenes from Cyclophanes. The Total Synthesis of Cannithrene II. *J. Org. Chem.* **2002**, *50*, 2236–2240.

(11) Jessup, P. J.; Reiss, J. A. Cyclophanes. VIII. An Attempted Preparation of [7]Circulene from [2,2](3,6)Phenanthro(2,7)Naphthalenophane-1,11-Diene. *Aust. J. Chem.* **1977**, *30*, 851–857.

(12) He, Z.; Xu, X.; Zheng, X.; Ming, T.; Miao, Q. Conjugated Macrocycles of Phenanthrene: A New Segment of [6,6]-Carbon Nanotube and Solution-Processed Organic Semiconductors. *Chem. Sci.* **2013**, *4*, 4525–4531.

(13) Vaijnath Phulwale, B.; Mishra, S. K.; Neč, M.; Mazal, C. Phenanthrylene-Butadiynylene and Phenanthrylene-Thienylene Macrocycles: Synthesis, Structure, and Properties. *J. Org. Chem* **2016**, *81*, 6244–6252.

(14) Luo, Z.; Yang, X.; Cai, K.; Fu, X.; Zhang, D.; Ma, Y.; Zhao, D. Toward Möbius and Tubular Cyclopolyarene Nanorings via Arylbutadiyne Macrocycles. *Angew. Chem.* **2020**, *132*, 14964–14970.

(15) Cui, S.; Huang, Q.; Wang, J.; Jia, H.; Huang, P.; Wang, S.; Du, P. From Planar Macrocycle to Cylindrical Molecule: Synthesis and Properties of a Phenanthrene-Based Coronal Nanohoop as a Segment of [6,6]Carbon Nanotube. *Org. Lett.* **2019**, *21*, 5917–5921.

(16) Wassmundt, F. W.; Kiesman, W. F. Soluble Catalysts for Improved Pschorr Cyclizations.

J. Org. Chem. **2002**, *60*, 196–201.

(17) Almeida, J. F.; Castedo, L.; Fernández, D.; Neo, A. G.; Romero, V.; Tojo, G. Base-Induced Photocyclization of 1,2-Diaryl-1-Tosylethenes. A Mechanistically Novel Approach to Phenanthrenes and Phenanthrenoids. *Org. Lett.* **2003**, *5*, 4939–4941.

(18) Ha Kim, Y.; Lee, H.; Joon Kim, Y.; Tae Kim, B.; Heo, J.-N. Direct One-Pot Synthesis of Phenanthrenes via Suzuki-Miyaura Coupling/Aldol Condensation Cascade Reaction. *J. Org. Chem* **2008**, *73*, 495–501.

(19) Neder, K. M.; Whitlock, H. W. Importance of Hydrogen Bond Acceptor Ability in Design of Host Molecules Capable of Molecular Recognition. *J. Am. Chem. Soc.* **1990**, *112*, 9412–9414.

(20) Kexki, W. Z.; Denisow, G. S. NMR Study of Pentafluoroaniline - Hydrogen Bonding and Proton Exchange. *Spectrosc. Lett.* **1991**, *24*, 1363–1372.

(21) Birchall, J. M.; Haszeldine, R. N.; Nikokavouras, J.; Wilks, E. S. Polyfluoroarenes. Part XV. Diazo-Oxides and Related Compounds. *J. Chem. Soc. C Org.* **1971**, No. 0, 562–566.

(22) Shoute, L. C. T.; Mittal, J. P.; Neta, P. Fluoride Elimination upon Reaction of Pentafluoroaniline with H, and OH Radicals in Aqueous Solution. *J. Phys. Chem.* **1996**, *100*, 11355–11359.

(23) Shoute, L. C. T.; Mittal, J. P.; Neta, P. Reduction and Defluorination of Pentafluorophenol in Aqueous Solutions. *J. Phys. Chem.* **1996**, *100*, 3016–3019.

(24) Chapman, E.; Bryan, M. C.; Wong, C. H. Mechanistic Studies of β-Arylsulfotransferase IV. *Proc. Natl. Acad. Sci.* **2003**, *100*, 910–915.

(25) Jencks, W. P.; Salvesen, K.; Hobden, F. W.; Johnston, E. F.; Weldon, L. P.; Wilson, C. L.; Chem Soc, J.; Lienhard, G. E.; Jencks, W. P.; Amer Chem, J. Equilibrium Deuterium

Isotope Effects on the Ionization of Thiol Acids. *J. Am. Chem. Soc.* **2002**, *93*, 4433–4436.

(26) Robson, P.; Stacey, M.; Stephens, R.; Tatlow, J. C. Aromatic Polyfluoro-Compounds. Part VI. Penta- and 2,3,5,6-Tetra-Fluorothiophenol. *J. Chem. Soc.* **1960**, *178*, 4754–4760.

(27) Psciuk, B. T.; Prémont-Schwarz, M.; Koeppe, B.; Keinan, S.; Xiao, D.; Nibbering, E. T. J.; Batista, V. S. Correlating Photoacidity to Hydrogen-Bond Structure by Using the Local O-H Stretching Probe in Hydrogen-Bonded Complexes of Aromatic Alcohols. *J. Phys. Chem. A* **2015**, *119*, 4800–4812.

(28) Parman, E.; Toom, L.; Selberg, S.; Leito, I. Determination of pKa Values of Fluorocompounds in Water Using 19F NMR. *J. Phys. Org. Chem.* **2019**, *32*, e3940.

(29) Sigala, P. A.; Kraut, D. A.; Caaveiro, J. M. M.; Pybus, B.; Ruben, E. A.; Ringe, D.; Petsko, G. A.; Herschlag, D. Testing Geometrical Discrimination within an Enzyme Active Site: Constrained Hydrogen Bonding in the Ketosteroid Isomerase Oxyanion Hole. *J. Am. Chem. Soc.* **2008**, *130*, 13696–13708.

(30) Hanoian, P.; Sigala, P. A.; Herschlag, D.; Hammes-Schiffer, S. Hydrogen Bonding in the Active Site of Ketosteroid Isomerase: Electronic Inductive Effects and Hydrogen Bond Coupling. *Biochemistry* **2010**, *49*, 10339–10348.

(31) World Health Organization. *Pentachlorophenol in Drinking-Water Background Document for Development of WHO Guidelines for Drinking-Water Quality*; 2003.

(32) Erickson, B. E. The End of Pentachlorophenol Is Near. *C&EN* **2021**.

(33) Lee, G. Y.; Hu, E.; Rheingold, A. L.; Houk, K. N.; Sletten, E. M. Arene-Perfluoroarene Interactions in Solution. *J. Org. Chem.* **2021**, *86*, 8425–8436.

(34) Thordarson, P. Determining Association Constants from Titration Experiments in Supramolecular Chemistry. *Chem. Soc. Rev.* **2011**, *40*, 1305–1323.

(35) Brynn Hibbert, D.; Thordarson, P. The Death of the Job Plot, Transparency, Open Science and Online Tools, Uncertainty Estimation Methods and Other Developments in Supramolecular Chemistry Data Analysis. *Chem. Commun.* **2016**, *52*, 12792–12805.

(36) Speicher, A.; Groh, M.; Hennrich, M.; Huynh, A.-M. Syntheses of Macrocyclic Bis(Bibenzyl) Compounds Derived from Perrottetin E. *Eur. J. Org. Chem.* **2010**, *2010*, 6760–6778.

(37) Adams, H.; Gilmore, N. J.; Jones, S.; Muldowney, M. P.; Von Reuss, S. H.; Vemula, R. Asymmetric Synthesis of Corsifuran A by an Enantioselective Oxazaborolidine Reduction. *Org. Lett.* **2008**, *10*, 1457–1460.

(38) Muratake, H.; Natsume, M. Synthetic Study of Hetisine-Type Aconite Alkaloids. Part 1: Preparation of Tetracyclic Intermediate Containing the C14–C20 Bond. *Tetrahedron* **2006**, *62*, 7056–7070.

CHAPTER SEVEN

Towards bioorthogonal complexation: modifications to a phenanthrene-based cyclophane for detecting pentafluorophenol-based guests on cell surfaces

7.1 Abstract

Bioorthogonal complexation requires that the host is soluble in biologically-relevant media and is able to bind unnatural functionality on cell surfaces. Progress towards this goal through modification of an arene-perfluoroarene-based host-guest complex is detailed in this Chapter. We describe synthetic modifications to a phenanthrene-based cyclophane that ultimately will allow for conjugation of the host to a multivalent water-compatible bead. We find that *O*-propargyl modifications to the host pyridine linker region decrease the binding affinity and explore alternative chemistries based on functionalized piperazines. Progress toward the synthesis of unnatural perfluoroaryl-modified mannosamine and sialic acid analogues is described as well. Ultimately, this work may enable formation of multivalent phenanthrene-based beads to bind and detect tetrafluorophenol functionality on cell surfaces.

7.2 Introduction

Our ultimate goal of biorthogonal complexation requires that a macrocyclic host can bind and detect unnatural functionality incorporated on cell surfaces in a selective manner. A number of requirements of the host and the guest must be met for this type of detection to occur. First, the host must be soluble in water. The host should be stable in water and in the presence of biomolecules and should not bind endogenous small molecules. Second, the Sletten lab has recently shown that a K_a of at least 10^8 M^{-1} is required to efficiently label guests on cell surfaces using a known host, cucurbit[7]uril.[1] Third, the guest needs to be incorporated on the cell surface, ideally through the sialic acid biosynthetic pathway or salvage pathway.

In Chapter 6, we developed a phenanthrene-based host **6.2a**, which can bind pentafluorophenol **7.1** and amide variant of pentafluorophenol **7.2** with binding affinities in organic solvent in the range of a single lectin carbohydrate recognition domain-carbohydrate interaction (10^3 M^{-1}).[2,3] In nature[4] and in synthetic systems,[5,6] multivalency, achieved through multivalent ligands and/or oligomeric receptors, can increase the functional binding affinity between a host/receptor and a guest/ligand. Though the K_a of the complex between phenanthrene **6.2a** and **7.1**/**7.2** should increase in water due to the hydrophobic effect,[7] a multivalent host of **6.2a** could further improve the K_a into the desired range for cell-surface labeling. Rather than attempt to solubilize host **6.2a** with individual water-solubilizing groups, we imagined that attaching multiple phenanthrene hosts to a PEG or poly(amide)-based bead or particle (Figure 7.1A). In this manner, we could address the requirements of water solubility and increase the overall K_a at the same time.

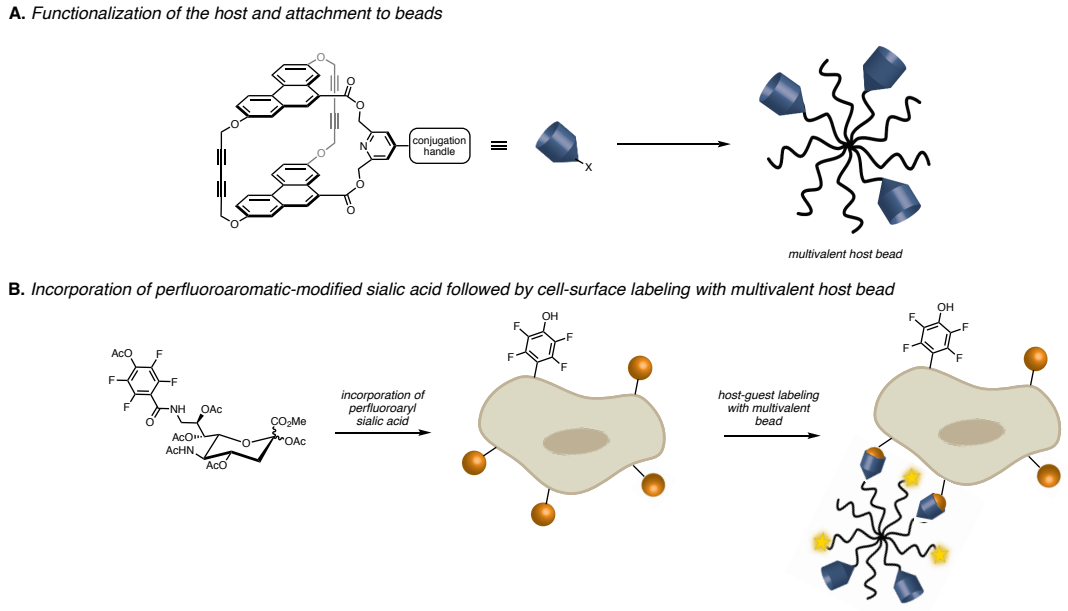

Figure 7.1 General scheme for multivalent bioorthogonal complexation with a variant of host **6.2a** to detect perfluoroaryl guests on cell surfaces.

For the third requirement, we imagined that perfluoroaryl-modified sialic acids could be incorporated into cell-surface glycans (Figure 7.1B), as a similar functional group has been incorporated into A549 cells as acetylated-*N*-4-azidotetrafluorophenyl-D-mannosamine **7.3**.[8] Non-fluorinated aromatics **7.4,**[9] and aryl azides **7.5** and **7.6**,[10,11] and dinitro aromatics **7.7**[12,13] have also been synthesized and incorporated as D-mannosamine and sialic acid derivatives (Figure 7.2).

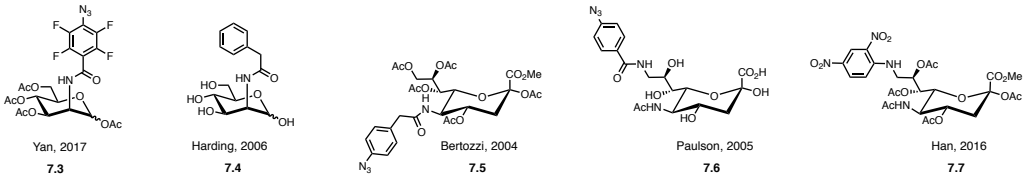

Figure 7.2 Unnatural sialic acids with aromatic modifications that have been incorporated into cell-surface glycans.

7.3 Results and discussion: functionalized host

Towards functionalizing host **6.2a** to be attached to beads or other payloads, we imagined that modifying the pyridine linker would be fairly simple and various conjugation strategies could be explored. Altogether, this modification needed 1) to have orthogonal functional groups to those already present in the synthesis and final host structure, 2) be compatible with the macrocyclization, and 3) to not decrease the K_a.

An azide attached to the host would be a simple conjugation strategy to any bead or particle modified with a strained cyclic alkyne. However, since the macrocycle **6.2a** is itself formed through a copper-catalyzed alkyne-alkyne coupling, an azide would not be a tolerated in this cyclization. The azide could be installed post-macrocyclization, but this approach requires additional steps. Ideally, the synthesis of a functionalized host could be convergent. Common

conjugation handles, like free amines, free alcohols, or carboxylic acids could also be problematic in the reduction and/or premacrocycle formation steps.

Seeking an orthogonal functional handle, we focused on protected alkynes. We began with 4-*O*-propargyl-pyridinediester **7.9**, which was simple to access from **7.8**. To determine if this modification altered the K_a, **7.9** was coupled with 2-ethylhexylazide **7.10** to add a solubilizing group. Triazole diester product **7.11** was reduced to the diol **7.12** and coupled to phenanthrene PFPester **6.12** resulting in prehost **7.13** in 49% yield. The prehost **7.13** was cyclized to yield both isomers of this host **7.14a** (24%) and **7.14b** (19%).

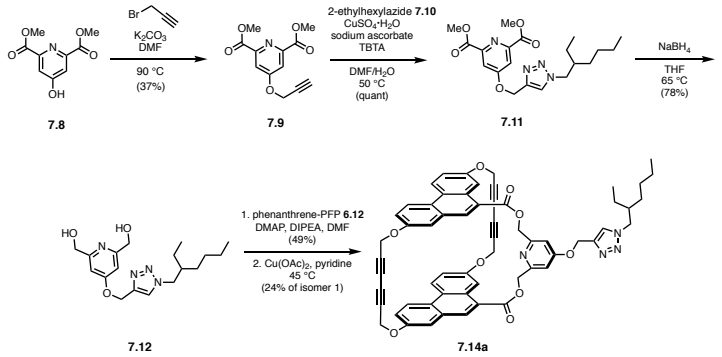

Scheme 7.1 Synthesis of *O*-propargyl phenanthrene host **7.14a**.

7.14a was assigned as the more symmetric isomer by comparison to **6.2a**. *O*-propargyl phenanthrene host **7.14a** had a diminished binding affinity ($K_a = 8.0\text{x}10^2 \pm 2\%$) for pentafluorophenol guest **7.1** when compared to the dibutyl amine-modified structure **6.2a** ($K_a = 3.8\text{x}10^3 \pm 3\%$) in $CDCl_3$. These studies were done concurrently with the work described in Chapter 6, Figure 6.6 and provide further evidence of the importance of the hydrogen bonding interaction to the overall K_a.

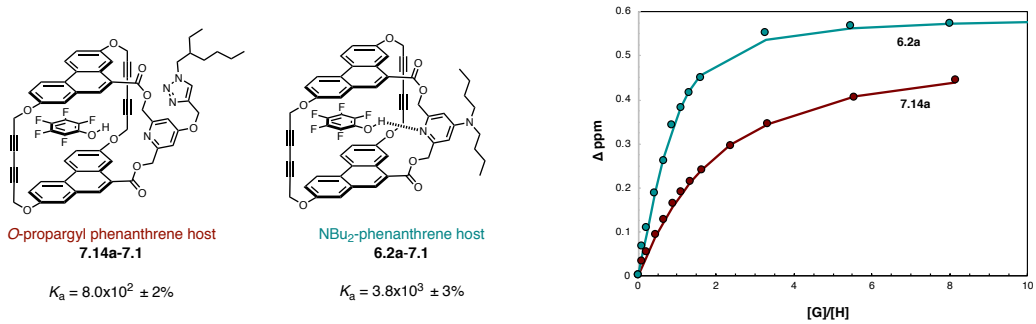

Figure 7.3 Comparison of binding affinities between pentafluorophenol guest **7.1** and *O*-propargyl host **7.14a** and NBu_2 host **6.2a** in $CDCl_3$.

We then focused on functionalized amines, which would be more similar to the dibutyl amine functional group in host **6.2a**. In Chapter 5, conditions for microwave-assisted amination of 4-chloro-2,6-diesterpyridine **7.15** with 30 equivalents of simple dialkylamines to access products like **7.16** were described. However, similar reactions with *N*-propargyl butylamine **7.17** resulted in low yields of the desired product **7.18**, along with 4-butylaminopyridine diester **7.19** (Figure 7.4A).

Next, functionalized cyclic amines were explored due to their increased nucleophilicity.[14] We intended to find reaction conditions that were mild and did not cause ester hydrolysis to avoid the use of trimethylsilyl diazomethane. Ideally, fewer equivalents of the functionalized amine could be used as well. Test reactions with 4-chloropyridine **7.15** and only ten equivalents of methyl piperazine resulted in minimal ester hydrolysis and good conversion to **7.20** at 100 °C in the microwave (Figure 7.4B). TIPS-alkyne functionalized piperazine **7.21** was synthesized in three steps. Using the conditions optimized for methyl piperazine, the desired product **7.22** was isolated in 45% yield, along with two major similar side products that were not explicitly identified. In the future, 4-fluoro-2,6-diesterpyridine could be used which may allow for lower reaction temperatures and less side reactivity.

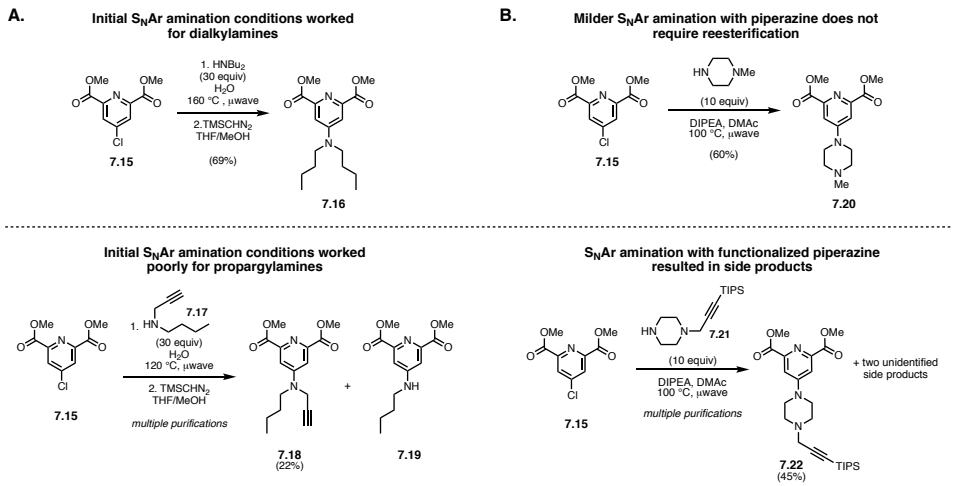

Figure 7.4 Synthetic approaches to diester pyridines with functionalized amines at the 4-position. A) Initial S_NAr reaction conditions with dialkylamines and functionalized linear secondary amines. B) S_NAr conditions with cyclic amines.

With less than optimal yields from S_NAr reactions, we found that **7.22** could be accessed through Buchwald-Hartwig amination in comparable yield (30%) with only slight excess of the TIPS-alkyne functionalized piperazine **7.21**. Conversion to **7.22** under Buchwald-Hartwig conditions was greater than 50% by LCMS, however extensive purification to remove *rac*-BINAP and oxidized *rac*-BINAP resulted in the low isolated yield. The functionalized diester **7.22** was then reduced to the diol **7.23** in low isolated yield (37%). Low isolated yields in the reduction step with both **7.22** and **7.20** were due to poor conversion and difficulty isolating highly polar pyridine diols cleanly.

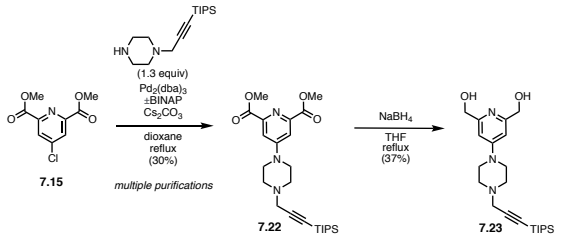

Scheme 7.2 Buchwald-Hartwig amination with TIPS-propargyl-piperazine **7.21** and reduction to diol **7.23**.

Amidst these challenges, the route was altered such that the reduction is carried out first to yield **7.24** (Scheme 7.3), followed by immediate acetylation to **7.25**. Acetylated pyridine diol **7.25** can then be aminated with TIPS-propargyl piperazine **7.21** under Buchwald-Hartwig conditions in moderate yield (51%), though purification of **7.26** is still not trivial. **7.26** can be deacetylated to yield the final diol **7.23** cleanly.

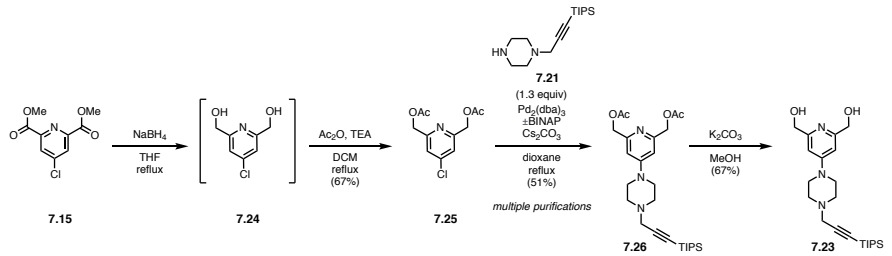

Scheme 7.3 Alternative route to functionalized diol **7.23**.

Functionalized piperazine pyridine diol **7.23** was coupled with naphthalene PFPester **5.21** to yield the functionalized prehost **7.27**. Functionalized naphthalene prehost **7.27** was cyclized to the naphthalene host **7.28** with full conversion, suggesting that the protected alkyne functionality is tolerated under the macrocyclization reaction conditions. The two isomers of functionalized naphthalene host **7.28a** and **7.28b** could be not be readily separated. The functionalized phenanthrene prehost **7.29** was synthesized similarly in 90% yield (Scheme 7.4).

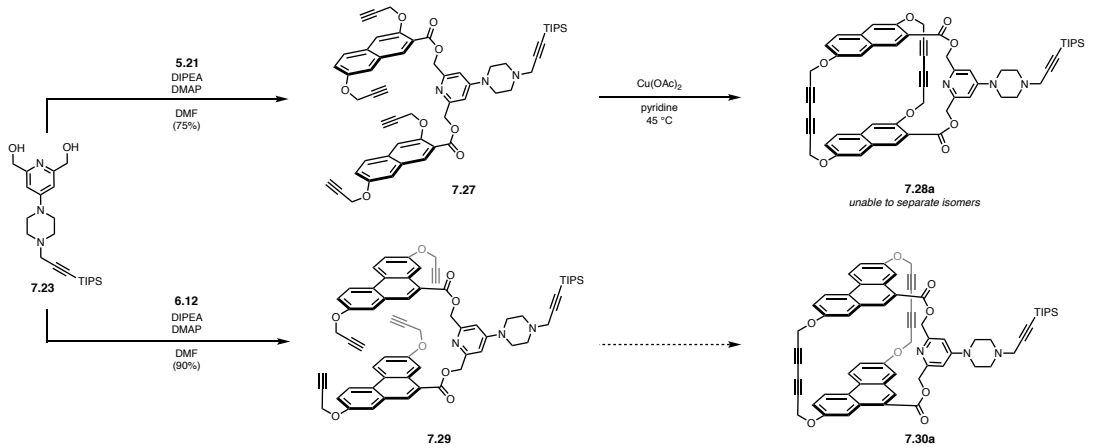

Scheme 7.4 Synthesis of TIPS-propargyl functionalized host variants from diol **7.23**.

Moving forward, a control host, Me-pip-phenanthrene host **7.31a**, will be synthesized from **7.20.** The binding affinity between **7.31a** and pentafluorophenol **7.1** will be determined and compared to that of NBu_2-phenanthrene host **6.2a** to ensure this modification does not drastically decrease the K_a (Scheme 7.5) . For the conjugatable host, the TIPS-pip-phenanthrene host **7.30a** will need to be deprotected to yield the terminal alkyne host **7.32a** (Scheme 7.6). Conditions will have to be optimized for copper-azide-alkyne cycloaddition (CuAAC) to conjugate this host to azide-modified beads **7.33**. A balance of host to bead will have to be determined to ensure the bead does not become too hydrophobic for applications *in cellulo*. A fluorophore modified with a strained alkyne can then be attached to the host modified beads **7.34** through SPAAC to form **7.35** (Scheme 7.6).

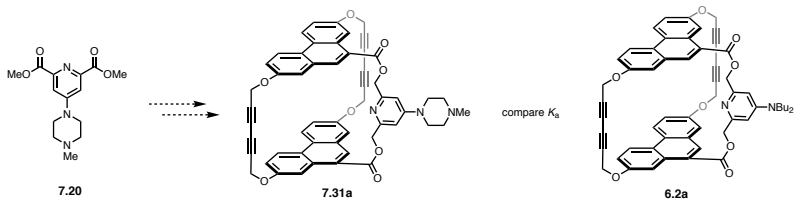

Scheme 7.5 Synthesis of a methyl piperazine control host **7.31a** and comparison to NBu_2-phenanthrene **6.2a**.

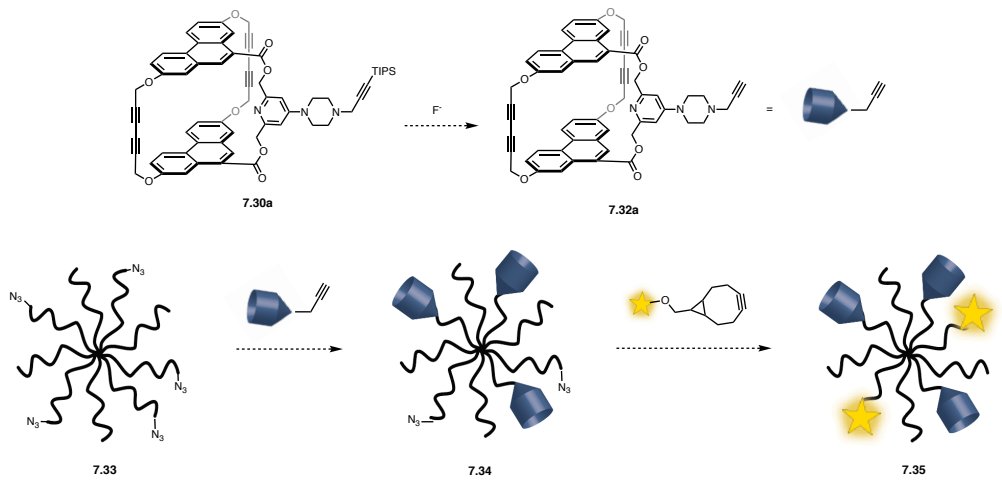

Scheme 7.6 Deprotection of functionalized TIPS-pip-phenanthrene host **7.30a** and conjugation to azide-modified beads.

7.4 Results and discussion: functionalized guest

For guest incorporation, I began with the synthesis of a D-mannosamine analogue modified with a tetrafluorophenol moiety **7.36** (Scheme 7.7). Erika Ramirez also synthesized the pentafluorophenyl mannosamine derivative **7.37** as a future control. This structure is similar to the tetrafluorophenylazide derivative **7.3** that was incorporated by the Yan group.[8] Dr. Anna Kataki-Anastasakou found that analogue **7.36** was not incorporated into a hypo-sialylated cell line, BJAB-K20,[15] through a lectin-binding assay (Figure 7.5).

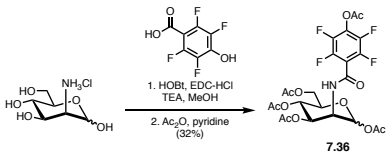

Scheme 7.7 Synthesis of tetrafluorophenol-modified mannosamine **7.36**.

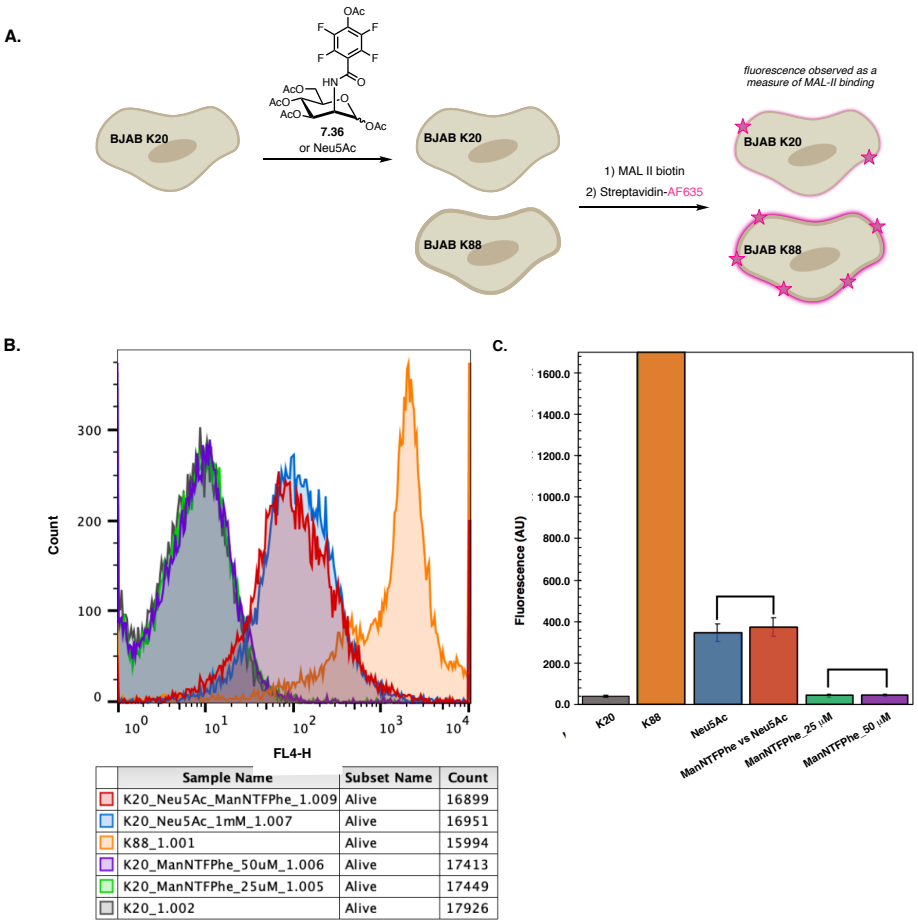

	Sample Name	Subset Name	Count
	K20_Neu5Ac_ManNTFPhe_1.009	Alive	16899
	K20_Neu5Ac_1mM_1.007	Alive	16951
	K88_1.001	Alive	15994
	K20_ManNTFPhe_50uM_1.006	Alive	17413
	K20_ManNTFPhe_25uM_1.005	Alive	17449
	K20_1.002	Alive	17926

Figure 7.5 Attempt at metabolic incorporation of tetrafluorophenol-modified mannosamine **7.36** assessed via lectin binding assay. Experiment was performed by Dr. Anna Kataki-Anastasakou. A) Mannosamine derivative **7.36** (25 μM and 50 μM) and sialic acid Neu5Ac (1 mM) were incubated with cells for 3 days in 90% nutridoma/FBS supplemented RPMI. Incorporation was assessed by cell labeling with MAL II biotin (0.01 mg/mL) followed by incubation with Streptavidin-AF635 (0.005 mg/mL). Metabolic incorporation of **7.36** was assessed in hypo-sialylated BJAB K20 cells with wild-type BJAB K88 cells as a positive control for normal levels of sialylation. Fluorescence recovery by sialic acid incorporation was tested using Neu5Ac (1 mM) as a positive control. B) Representative histograms of Streptavidin-AF635 fluorescence after incubation with MAL II biotin C) Analysis of triplicate experiments of Streptavidin-AF635 fluorescence after incubation with MAL II biotin.

A broader range of functional groups have been incorporated via sialic acid derivatives, bypassing the bottleneck enzymatic step in the sialic acid biosynthetic pathway, phosphorylation of ManNAc derivatives by ManNAc 6-kinase.[11,16] Both 9- and 5-modified sialic acid derivatives have been described.[17] We focused on 9-tetrafluorophenol sialic acid as a target (Scheme 7.8). A PFPester of 2,3,5,6-tetrafluoro-4-hydroxybenzoic acid **7.39** was prepared. We chose not to

acetylate the phenol at this point, as that would convert **7.39** into an acetylation reagent as well. 9-azido sialic acid methyl ester **7.40** was reduced to amine **7.41** and PFPester **7.39** was added immediately. Post amide-coupling the reaction mixture was acetylated to yield **7.42**. These reactions were low yielding, and **7.42** could not be isolated cleanly after HPLC. Preliminary incorporation studies with impure **7.42** in BJAB K20 cells were performed by Caitlyn Fick with limited success (Figure 7.6).

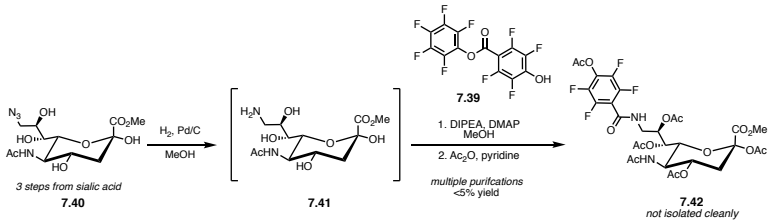

Scheme 7.8 Synthesis of acetylated 9-tetrafluorophenol-modified sialic acid **7.42**.

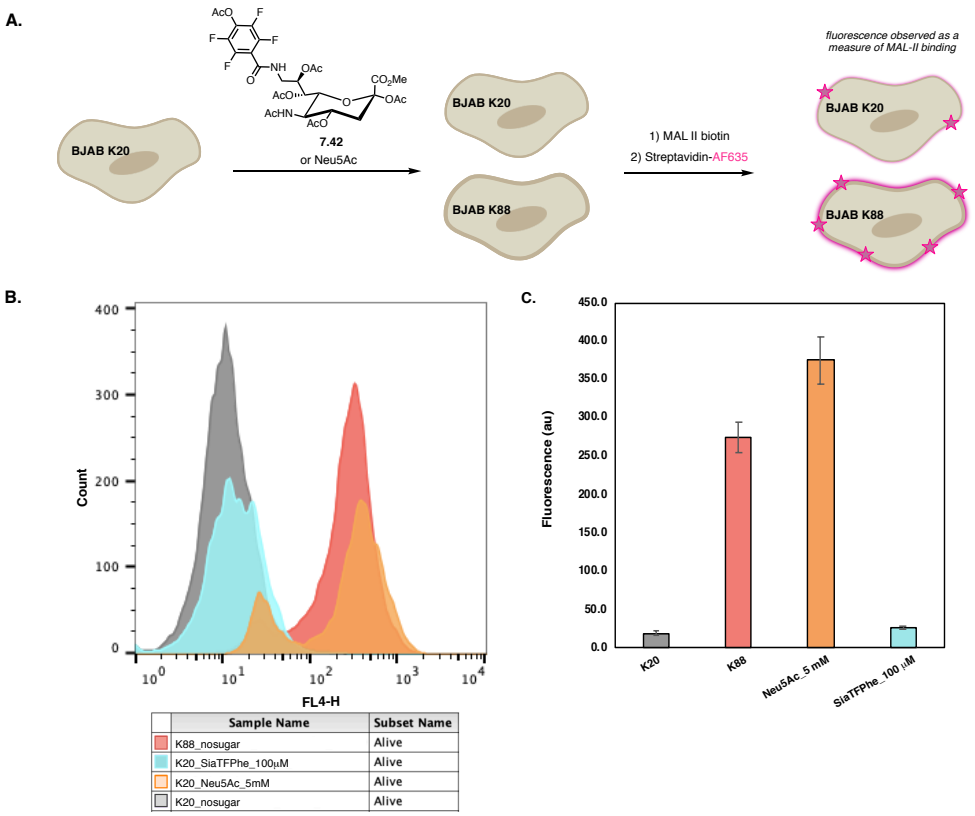

Figure 7.6 Attempt at metabolic incorporation of impure tetrafluorophenol-modified sialic acid **7.42** assessed via lectin binding assay. Experiment was performed by Caitlyn Fick. A) Sialic acid derivative **7.42** (100 μM) and sialic acid Neu5Ac (5 mM) were incubated with cells for 3 days in 90% nutridoma/FBS supplemented RPMI. Incorporation was assessed by cell labeling with MAL II biotin (0.01 mg/mL) followed by incubation with Streptavidin-AF635 (0.005 mg/mL). Metabolic incorporation of **7.42** was assessed in hypo-sialylated BJAB K20 cells with wild-type BJAB K88 cells as a positive control for normal levels of sialylation. Fluorescence recovery by sialic acid incorporation was tested using Neu5Ac (5 mM) as a positive control. B) Representative histograms of Streptavidin-AF635 fluorescence after incubation with MAL II biotin. C) Analysis of triplicate experiments of Streptavidin-AF635 fluorescence after incubation with MAL II biotin.

Given that amide couplings with 9-aminosialic acid are often low yielding with non-perfluoroaromatic carboxylic acid coupling partners (9-45% yield),[10,18] we considered alternative methods to access perfluoroaryl-modified sialic acid derivatives. We imagined that a traceless Staudinger ligation with the appropriate phosphine ester and 9-azido-sialic acid could be used to access **7.42**. The traceless Staudinger ligation has been used previously to access mannosamine

analogues.[19] Attempts to synthesize the desired phosphine reagent **7.44** from (2-hydroxyphenyl)diphenylphosphine **7.43** and PFPester **7.39** were unfruitful, however the control 2-(diphenylphosphaneyl)phenyl-pentafluorobenzoate **7.45** was synthesized from pentafluorobenzoyl chloride. A test reaction with acetylated 9-azidosialic acid **7.46** and phosphine **7.45** showed some conversion to the desired amide product **7.47**, suggesting this approach could be useful with some optimization of the purification. 9-Pentafluorophenyl-modified sialic acid **7.47** could be used to assess whether the hydroxyl group of the intended guest on **7.42** is interfering with incorporation and can act as a control sugar for future cell-surface binding studies.

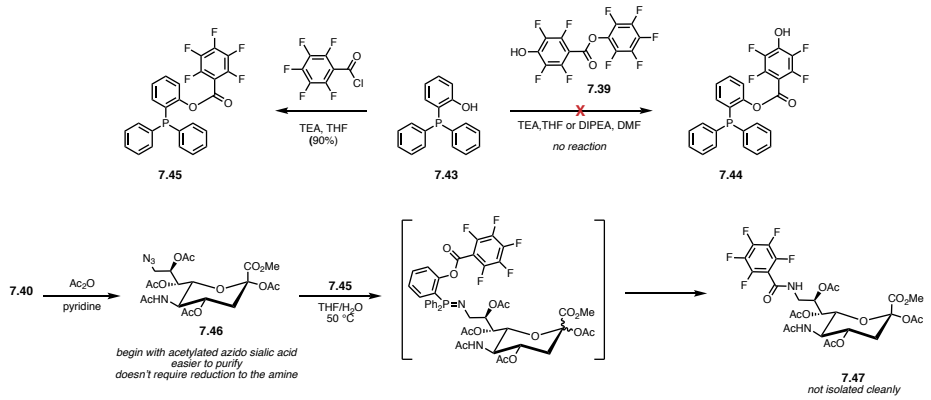

Scheme 7.9 Traceless Staudinger strategy to access perfluoroaryl-modified sialic acids **7.47** and **7.42**.

While our preliminary incorporation studies with tetrafluorophenol-modified mannosamine **7.36** and sialic acid **7.42** have not been successful, it remains unclear whether these derivatives are being incorporated or the lectins used in lectin binding assays are unable to recognize these bulkier perfluorinated analogues. One way to probe this question will be to perform similar assays with control pentafluorophenyl sialic acid **7.47** or use different lectins. Alternative methods, such as the DMB assay, will also be used to assess analogue incorporation. We may find improved yields for amide couplings with the NHS ester of tetrafluoro-4-

hydroxybenzoic acid rather than the PFPester **7.39**. When all synthetic steps described here can be scaled up and the final sialic acid derivatives isolated pristinely, we will have more confidence in the results of the incorporation studies.

It should be noted that other electron-poor aromatics have been successfully incorporated as sialic acid analogues. 9-amino-2,4-dinitrobenzene-modified sialic acid **7.7** was incorporated in B16F10 cells and five other cell lines.[13] However, the authors noted that this modification was more resistant to sialidase-mediated hydrolysis. In our quest to incorporate perfluoroaromatics through the sialic acid biosynthetic pathway, modification of the 5-position of sialic acid, linking the guest to sialic acid through other functional groups like carbamates,[20] or alternative cell lines may be explored.

7.5 Conclusion

In this chapter, we describe the design of conjugatable variants of phenanthrene-host **6.2a** to enable the binding of tetrafluorophenol functionality in biologically relevant environments. Initially, we explored *O*-alkyl modifications to the pyridine region of the host. *O*-propargyl-phenanthrene host **7.14a** was synthesized and found to bind pentafluorophenol **7.1** with a lower K_a than **6.2a** the original host described in Chapter 6. In hopes of retaining or improving the initial K_a, both linear and cyclic functionalized amines are explored for modification of the 4-pyridine position of the host. With TIPS-propargyl piperazine **7.21**, Buchwald-Hartwig amination was used to prepare the functionalized pyridine diol linker **7.23** in moderate yield. In the future, this chemistry can be used to access TIPS-propargyl phenanthrene host **7.30a**, which may eventually be coupled to PEG or poly(amide)-based beads to form multivalent host beads **7.35**.

For the guest incorporation, a tetrafluorophenol mannosamine derivative **7.36** was synthesized. However, preliminary studies in a sialic acid-deficient cell line showed minimal incorporation of this analogue. The synthesis of a tetrafluorophenol sialic acid **7.42** derivative was not successful, but an alternative traceless Staudinger ligation approach is described. With additional unnatural sialic acid, further investigation into the metabolic incorporation of **7.42** and control pentafluorophenyl sialic acid **7.47** will be possible. If **7.42** cannot be incorporated, arene-perfluoroarene host-guest complexation on cell surfaces can be explored through conjugation of the tetrafluorophenol moiety to the cell surface through lysine modification or the oxime ligation. Ultimately, these modifications to the phenanthrene-based host will provide further understanding of the extent that the arene-perfluoroarene interaction is strengthened in an aqueous environment, while enabling a rendition of bioorthogonal complexation through multivalent labeling.

7.6 Experimental Procedures

Chemical reagents were purchased from Sigma-Aldrich, Alfa Aesar, Fisher Scientific, Acros Organics, Synquest, or TCI and used without purification unless noted otherwise. Anhydrous dimethyl sulfoxide (DMSO) was obtained from a Sure-Seal™ bottle (Aldrich). Anhydrous and deoxygenated solvents dichloromethane (DCM), dimethylformamide (DMF), acetonitrile (MeCN), methanol (MeOH), and tetrahydrofuran (THF) were dispensed from a Grubb's-type Phoenix Solvent Drying System. Thin layer chromatography was performed using Silica Gel 60 F_{254} (EMD Millipore) plates. Flash chromatography was executed with technical grade silica gel with 60 Å pores and 40–63 μm mesh particle size (Sorbtech Technologies). Solvent was removed under reduced pressure with a Büchi Rotovapor with a Welch self-cleaning dry vacuum pump and further dried with a Welch DuoSeal pump. Bath sonication was

performed using a Branson 3800 ultrasonic cleaner. NMR spectra were recorded on Bruker AV-500 (^{1}H and ^{13}C) and AV-400 (^{1}H, ^{13}C, and ^{19}F) instruments and processed with MestReNova software. NMR peaks are calibrated using residual undeuterated solvent ($CHCl_3$ at 7.26 ppm ^{1}H NMR, 77.16 ppm ^{13}C NMR). Masses for analytical measurements were taken on a Sartorius MSE6.6S-000-DM Cubis Micro Balance. HRMS (electrospray ionization (ESI)) were collected on a Thermo Scientific Q Exactive™ Plus Hybrid Quadrupole-Orbitrap™ with Dionex UltiMate 3000 RSLCnano System and LRMS (electrospray ionization (ESI)) were collected on an Agilent 1260 Infinity II HPLC-tandem MS system.

7.6.1 General host-guest titration/K_a determination procedures

The host was measured on an analytical microbalance. Host stock solutions were prepared with basified $CDCl_3$. Concentrations of host stock solutions were made below the solubility limit of the host. Guest stock solutions were prepared in basified $CDCl_3$. Preliminary titrations and the Bindsim program (http://app.supramolecular.org/bindsim/) were used to determine the approximate equivalents of guest needed for saturation. Ideally, >70% saturation was achieved. Binding data were fit using Bindfit (http://app.supramolecular.org/bindfit/).[21,22] In some cases, it was necessary to allow the samples to equilibrate before NMRs were taken to improve peak resolution and minimize broadening. Titrations were performed in duplicate.

7.6.2 Equations for average K_a value determination from duplicate experiments

Equation 1: $K_{a,avg} = \frac{K_{a,1}+K_{a,2}}{2}$

Equation 2: $\Delta K_{a,avg} = \frac{1}{2}\sqrt{(\Delta K_{a,1})^2 + (\Delta K_{a,2})^2}$

7.6.3 General cell culture procedures

BJAB K88 and K20 cells were a gift from the Kohler lab (UT Southwestern)— with permission from Michael Pawlita and Tim Waterboer (DKFZ)— and were cultured in RPMI 1640 media (Genessee #25-506H) supplemented with 10% fetal bovine serum (FBS) (Corning, lot# 35016109) and 1% penicillin-streptomycin (PS) (Life Technologies, cat# 15070063). For metabolic incorporation experiments, BJAB K88 and K20 cells were grown in minimal media using 1% Nutridoma-SP (Roche #11011375001) in basal RPMI 1640. Cells were gradually weaned off FBS over four passages using 10, 40, 70, 90% of 1% nutridoma reagent in FBS-supplemented RPMI 1640, without inhibition of growth for up to two months.

Cells were incubated at 37℃, 5% CO_2, throughout culturing, in HERACell 150i CO_2 incubators. Cells were pelleted through use of Sorvall ST 40R centrifuge. All cell work was performed in 1300 Series A2 biosafety cabinets.

For metabolic incorporation experiments MAL (Maackia Amurensis) II Biotin (Vector Labs #B-1265) was used. During experiments, cells were incubated on ice (0 ºC) with gentle rocking in the dark. Flow cytometry was performed on a BDBiosciences FACSCalibur equipped with 488 nm and 635 nm lasers. Streptavidin-AlexaFluor™635 (Fisher Scientific #S32364) fluorescence was measured on the FL4 channel. Propidium iodide (Biotium #40016) fluorescence was measured on the FL2 channel.

7.6.4 Synthetic experimental procedures

Dimethyl 4-(prop-2-yn-1-yloxy)pyridine-2,6-dicarboxylate (7.9). 7.9 was prepared following a modified literature procedure.[23,24] 4-hydroxypyridine diester **7.8** (548 mg, 2.60 mmol, 1.00

equiv) and K_2CO_3 (718 mg, 5.19 mmol, 2.00 equiv) were dissolved in DMF (11 mL, 0.24 M). Propargyl bromide (0.32 mL, 2.86 mmol, 1.1 equiv) was added, and the reaction mixture was heated to 90 °C. After 19 h, the reaction was cooled to RT and filtered. The crude was evaporated onto SiO_2 and purified by column chromatography (silica gel, 50% EtOAc/hexanes). The product **7.9** was isolated as a white solid (240 mg, 0.963 mmol, 37% yield). R_f = 0.5 in 60% EtOAc/hexanes. ^{1}H NMR (500 MHz, DMSO-d_6): δ 7.82 (s, 2H), 5.12 (d, J = 2.4 Hz, 2H), 3.91 (s, 6H), 3.75 (t, J = 2.4 Hz, 1H). LRMS (ESI) calcd. for $C_{12}H_{12}NO_5$ $(M+H)^+$: 205.0710; found 250.0.

Note: Propargyl ester side products were also isolated.

2-ethylhexyl azide (7.10). Ethylhexyl bromide (0.53 mL, 3.0 mmol, 1.0 equiv) and NaN_3 (975 mg, 15.0 mmol, 5.0 equiv) were dissolved in DMF (3 mL, 1.0 M) and heated to 70 °C for 13 h. The reaction was cooled to RT and poured into H_2O and EtOAc. The aqueous layer was extracted with EtOAc (3x). The combined organics were dried ($MgSO_4$), filtered, and concentrated. Full conversion was observed by ^{1}H NMR. The product **7.10** was volatile and was used as a solution in DMF. ^{1}H NMR (400 MHz, $CDCl_3$): δ 3.23 (d, J = 6.0 Hz, 2H), 1.53 – 1.44 (m, 1H), 1.42 – 1.20 (m, 8H), 0.95 – 0.82 (m, 6H). Spectra are consistent with literature reports.[25,26]

dimethyl 4-((1-(2-ethylhexyl)-1H-1,2,3-triazol-4-yl)methoxy)pyridine-2,6-dicarboxylate (7.11). dimethyl 4-(prop-2-yn-1-yloxy)pyridine-2,6-dicarboxylate **7.9** (175 mg, 0.702 mmol, 1.00 equiv) and 2-ethylhexylazide **7.10** in DMF (~218 mg, 1.4 mmol, 2.0 equiv) were added to a scintillation vial. $CuSO_4$-$5H_2O$ (5.3 mg, 0.021 mmol. 0.03 equiv), TBTA (11.2 mg, 0.0211

mmol, 0.03 equiv), and sodium ascorbate (25 mg, 0.140 mmol, 0.20 equiv) were added. The reaction contents were dissolved in DMF (5 mL) and H_2O (2 mL), and heated to 50 °C for 19 h. The solvent was removed under vacuum, and the crude product was evaporated onto SiO_2. The crude product was purified by column chromatography (silica gel, 50%→75% EtOAc/hexanes) to yield the product as a white solid **7.11** (300 mg, quantitative) which was used without further purification. R_f = 0.37 in 60% EtOAc/hexanes. ^{1}H NMR (400 MHz, $CDCl_3$): δ 7.92 (s, 2H), 7.61 (s, 1H), 5.38 (s, 2H), 4.29 (d, J = 6.9 Hz, 2H), 4.01 (s, 6H), 1.95 – 1.85 (m, 1H), 1.34 – 1.22 (m, 8H), 0.91 (dd, J = 14.8, 7.2 Hz, 6H). LRMS (ESI) calcd. for $C_{20}H_{29}N_4O_5$ $(M+H)^+$: 405.2; found 405.4.

(4-((1-(2-ethylhexyl)-1*H*-1,2,3-triazol-4-yl)methoxy)pyridine-2,6-diyl)dimethanol (7.12). To a 15 mL flask equipped with a reflux condenser, was added **7.11** (~280 mg, 0.692 mmol, 1.00 equiv). Anhydrous THF (4 mL, 0.17 M) was added, followed by $NaBH_4$ (105 mg, 2.77 mmol, 4.0 equiv). The reaction mixture was heated to 65 °C, and turned from yellow to red. After 18 h, the reaction mixture was colorless and was cooled to RT. H_2O was added slowly with stirring. The reaction mixture was poured into a sep funnel and extracted with 5% MeOH/DCM (3x). The combined organic layers were dried ($MgSO_4$), filtered, and concentrated. The product **7.12** was isolated as a sticky white solid (189 mg, 0.542 mmol, 78% yield) and used without further purification. ^{1}H NMR (500 MHz, $CDCl_3$): δ 7.57 (s, 1H), 6.82 (s, 2H), 5.27 (s, 2H), 4.70 (s, 4H), 4.27 (d, J = 6.9 Hz, 2H), 1.94 – 1.84 (m, 1H), 1.36 – 1.16 (m, 8H), 0.95 – 0.81 (m, 6H). ^{13}C NMR (126 MHz, $CDCl_3$): δ 165.86, 160.8, 142.8, 123.5, 105.8, 64.5, 62.0, 53.9, 40.5, 30.5, 28.6, 23.8, 23.0, 14.1, 10.6. HRMS (ESI) calcd. for $C_{18}H_{29}N_4O_3$ $(M+H)^+$: 349.2234; found 349.2299.

(4-((1-(2-ethylhexyl)-1*H*-1,2,3-triazol-4-yl)methoxy)pyridine-2,6-diyl)bis(methylene) bis(2,7-bis(prop-2-yn-1-yloxy)phenanthrene-9-carboxylate) (7.13). In a 15 ml flask, pyridine diol **7.12** (177 mg, 0.508 mmol, 1.00 equiv), phenanthrenePFP **6.12** (630 mg, 1.27 mmol, 2.5 equiv), and DMAP (62 mg, 0.508 mmol, 1.00 equiv) were dissolved in anhydrous DMF (4 mL, 0.13 M). DIPEA (0.19 mL, 1.07 mmol, 2.1 equiv) was added. After 2 days, DMF was evaporated under a stream of compressed air. The crude product was evaporated onto SiO_2 and purified by column chromatography (silica gel, 20%→30%→50%→60%→80% EtOAc/hexanes). The product was collected and concentrated and then precipitated from acetone/heptane to yield the product **7.13** as a pale yellow solid (244 mg, 0.251 mmol, 49% yield). R_f = 0.57 in 60% EtOAc/hexanes. ^{1}H NMR (500 MHz, $CDCl_3$): δ 8.56 (s, 2H), 8.54 (d, J = 2.7 Hz, 2H), 8.45 (d, J = 9.2 Hz, 2H), 8.43 – 8.38 (m, 2H), 7.54 (s, 1H), 7.38 – 7.29 (m, 6H), 7.14 (s, 2H), 5.60 (s, 4H), 5.32 (s, 2H), 4.84 (d, J = 2.4 Hz, 4H), 4.77 (d, J = 2.4 Hz, 4H), 4.17 (d, J = 7.0 Hz, 2H), 2.59 – 2.53 (m, 4H), 1.85 – 1.77 (m, 1H), 1.29 – 1.13 (m, 8H), 0.86 – 0.80 (m, 6H). ^{13}C NMR (126 MHz, $CDCl_3$): δ 167.1, 166.2, 157.8, 156.4, 155.8, 142.5, 133.6, 130.2, 129.6, 127.5, 125.8, 125.1, 124.2, 124.0, 123.6, 120.6, 118.0, 111.0, 108.4, 108.0, 78.6, 78.5, 76.1, 75.7, 66.8, 62.2, 56.1, 53.9, 40.4, 30.4, 28.5, 23.8, 22.9, 14.1, 10.5. LRMS (ESI) calcd. for $C_{18}H_{29}N_4O_3$ $(M+H)^+$: 973.4; found 973.6.

4-*O*-propargyl-pyridine functionalized phenanthrene host (7.14).

Prehost **7.13** (240 mg, 0.247 mmol, 1.0 equiv) was dissolved in pyridine (21 mL, 0.01 M). Over 45 min, **7.13** was added to a solution of $Cu(OAc)_2$ (560 mg, 3.08 mmol, 12.5 equiv) in pyridine (140 mL) at 45 °C. After 2.5 h, the pyridine was removed under reduced pressure. The crude product was suspended in $CHCl_3$ (~100 mL). The organics were washed with 1 M HCl (~100

mL). The aqueous layer was extracted with $CHCl_3$ (3x50mL), and the combined organics were washed with saturated aq NH_4Cl (1x). The organic layers were dried ($MgSO_4$), filtered, and concentrated. The crude product was evaporated on SiO_2 and purified by column chromatography (silica gel, 40%→50%→60%→80% EtOAc/hexanes). The less polar isomer (isomer 1) **7.14a** was isolated as a pale yellow solid (57 mg, 0.059 mmol, 24% yield). The more polar isomer **7.14b** was isolated as a pale yellow solid (45 mg, 0.046 mmol, 19% yield).

Isomer 1 (7.14a): R_f = 0.55 in 75% EtOAc/hexanes. ^{1}H NMR (500 MHz, $CDCl_3$): δ 8.57 – 8.45 (m, 4H), 8.37 (d, J = 9.1 Hz, 2H), 8.32 (d, J = 9.1 Hz, 2H), 7.70 (s, 1H), 7.25 (d, J = 2.8 Hz, 2H), 7.23 (s, 2H), 7.18 (dd, J = 9.1, 2.7 Hz, 4H), 5.86 (d, J = 12.0 Hz, 2H), 5.47 (s, 2H), 5.14 (d, J = 12.0 Hz, 2H), 5.08 – 4.78 (m, 8H), 4.34 (d, J = 6.9 Hz, 2H), 1.99 – 1.92 (m, 1H), 1.42 – 1.26 (m, 8H), 1.01 – 0.85 (m, 6H). ^{13}C NMR (126 MHz, $CDCl_3$): δ 166.9, 165.8, 157.5, 155.2, 155.1, 142.8, 133.5, 130.4, 129.7, 127.3, 125.9, 125.2, 124.0, 124.0, 123.6, 121.1, 118.2, 110.5, 109.6, 109.2, 74.7, 73.4, 71.3, 70.4, 67.5, 62.3, 55.4, 55.4, 54.0, 40.6, 30.6, 28.7, 23.9, 23.0, 14.2, 10.7. HRMS (ESI) calcd. for $C_{60}H_{49}N_4O_9$ $(M+H)^+$: 969.3494; found 969.3573.

Isomer 2 (7.14b): R_f = 0.34 in 75% EtOAc/hexanes. ^{1}H NMR (500 MHz, $CDCl_3$): δ 8.59 (s, 2H), 8.45 (s, 2H), 8.34 (d, J = 9.1 Hz, 2H), 8.30 (d, J = 9.0 Hz, 2H), 7.72 (s, 1H), 7.21 (s, 2H), 7.19 (d, J = 2.5 Hz, 2H), 7.14 (dd, J = 9.0, 2.7 Hz, 4H), 5.93 (d, J = 11.3 Hz, 2H), 5.46 (s, 2H), 5.08 – 4.84 (m, 10H), 4.36 (d, J = 6.8 Hz, 2H), 2.00 – 1.94 (m, 1H), 1.45 – 1.29 (m, 8H), 0.98 (t, J = 7.4 Hz, 3H), 0.96 – 0.90 (m, 3H).

***N*-(prop-2-yn-1-yl)butan-1-amine (7.17).** A 250 mL flask was charged with butyl amine (100 mL, 1.0 mol, 10 equiv) and cooled to 0 °C. Propargyl bromide (11 mL, 100 mol, 1.0 equiv) was

added via addition funnel over 20 min. The reaction mixture was diluted with Et_2O and poured into 1M NaOH. The organic layer was separated. The aqueous layer was extracted with Et_2O (2x), dried (Na_2SO_4), filtered and concentrated. The crude red product was then distilled via vacuum transfer to provide the product **7.17** as a clear liquid (5.27 g, 47 mmol, 47% yield). ^{1}H NMR (400 MHz, $CDCl_3$): δ 3.42 (d, J = 2.4 Hz, 2H), 2.74 – 2.62 (m, 2H), 2.20 (t, J = 2.4 Hz, 1H), 1.54 – 1.41 (m, 2H), 1.43 – 1.29 (m, 2H), 0.92 (t, J = 7.3 Hz, 3H). LRMS (ESI) calcd. for $C_7H_{14}N$ $(M+H)^+$: 112.1; found 112.0.

Dimethyl 4-(butyl(prop-2-yn-1-yl)amino)pyridine-2,6-dicarboxylate (7.18). To a 30 mL microwave vial was added 4-chloropyridinediester **7.15** (293 mg, 1.28 mmol, 1.0 equiv), amine **7.17** (4.26 g, 38.3 mmol, 30 equiv), and H_2O (5.8 mL, 0.22 M). The reaction mixture was heated in the microwave for 1h at 120 °C. The reaction mixture was dried under a stream of compressed air overnight. The crude mixture was re-dissolved in THF (20 mL, 0.06 M) and MeOH (6 mL, 0.21 M) and trimethylsilyldiazomethane (2M in hexanes, 2.6 mL, 5.2 mmol, 4.1 equiv) was added carefully. The reaction was monitored by LCMS, and additional trimethylsilyldiazomethane was added as needed. The reaction was quenched with AcOH and poured into H_2O. The reaction mixture was extracted with EtOAc (4x), dried ($MgSO_4$), filtered, and concentrated. The crude product was evaporated onto SiO_2 and purified by column chromatography (silica gel, 40%→50% EtOAc/hexanes). The product **7.18** was isolated as a white solid. Partially pure product was also isolated and further purified by preparatory thin layer chromatography (silica gel, 50% EtOAc/hexanes). In total the product **7.18** was isolated in 22% yield (86 mg, 0.28 mmol). R_f = 0.23 in 40% EtOAc/hexanes. ^{1}H NMR (400 MHz, $CDCl_3$): δ 7.59 (s, 2H), 4.13 (d, J = 2.5 Hz, 2H), 3.98 (s, 6H), 3.54 – 3.44 (m, 2H), 2.28 (t, J = 2.4 Hz, 1H),

1.72 – 1.60 (m, 2H), 1.39 (h, J = 7.4 Hz, 2H), 0.97 (t, J = 7.3 Hz, 3H). ^{13}C NMR (101 MHz, $CDCl_3$): δ 166.2, 154.3, 148.8, 111.1, 77.8, 73.3, 53.2, 50.9, 39.9, 29.3, 20.2, 13.9. LRMS (ESI) calcd. for $C_{16}H_{21}N_2O_4$ $(M+H)^+$: 305.1496; found 305.0

Note: A small amount of dimethyl 4-(butylamino)pyridine-2,6-dicarboxylate **7.19** was also isolated from the column.

Dimethyl 4-(4-methylpiperazin-1-yl)pyridine-2,6-dicarboxylate (7.20). In a 30 mL microwave vial, 4-chloropyrdinedimethylester **7.15** (300 mg, 1.30 mmol, 1.0 equiv) was dissolved in DMAc (10 ml, 0.13 M). Methyl piperazine (1.45 mL, 13 mmol, 10 equiv) and DIPEA (2.3 mL, 13 mmol, 10 equiv) were added. The reaction was heated in the microwave for 45 min at 100 °C. The solvent was removed under a stream of compressed air. The crude product was evaporated onto SiO_2 and purified by column chromatography (silica gel, 10% MeOH/DCM) to yield the product **7.20** as a beige crystalline solid (210 mg, 0.716 mmol, 55% yield).R_f = 0.29 in 10% MeOH/DCM. ^{1}H NMR (400 MHz, $CDCl_3$): δ 7.66 (s, 2H), 3.98 (s, 6H), 3.55 – 3.46 (m, 4H), 2.60 – 2.51 (m, 4H), 2.36 (s, 3H). ^{13}C NMR (101 MHz, $CDCl_3$): δ 166.18, 156.27, 149.07, 111.77, 54.45, 53.24, 46.17, 46.03. HRMS (ESI) calcd. for $C_{14}H_{20}N_3O_4$ $(M+H)^+$: 294.1449; found 294.1508

Dimethyl 4-(4-(3-(triisopropylsilyl)prop-2-yn-1-yl)piperazin-1-yl)pyridine-2,6-dicarboxylate (7.22). To a 30 mL microwave vial was added 4-chloropyridine diester **7.15** (82 mg, 0.356 mmol, 1.0 equiv), amine **7.21** (1.0 g, 3.6 mmol, 10 equiv), DIPEA (0.62 mL, 3.6 mmol, 10 equiv), and DMAc (4.1 mL, 0.09 M). The reaction was stirred to dissolve the starting material completely, and then heated to 100 °C in the microwave for 30 min. The solvent was removed under a stream of compressed air overnight. The crude reaction mixture was evaporated

onto SiO_2 and purified by column chromatography (50%→75%EtOAc/hexanes). The partially pure product **7.22** was isolated as a yellow solid (110 mg). The product was further purified by preparatory thin layer chromatography (silica gel, 65% EtOAc/hexanes) to yield the product **7.22** as a white solid (79 mg, 0.17 mmol, 47% yield). R_f = 0.32 in 70% EtOAc/hexanes. ^{1}H NMR (500 MHz, $CDCl_3$): δ 7.67 (s, 2H), 3.98 (s, 6H), 3.55 (t, J = 5.1 Hz, 4H), 3.47 (s, 2H), 2.72 (t, J = 5.0 Hz, 4H), 1.19 – 0.80 (m, 21H). ^{13}C NMR (101 MHz, $CDCl_3$): δ 166.17, 156.27, 149.08, 111.89, 101.31, 87.26, 53.23, 50.86, 48.01, 46.15, 18.75, 11.31. HRMS (ESI) calcd. for $C_{25}H_{40}N_3O_4Si$ $(M+H)^+$: 474.2783; found 474.2816.

Note: Two other side products with similar polarity, which seemed like possible amide formation, were isolated from the reaction mixture, but could not be definitively identified by mass and NMR.

(3-bromoprop-1-yn-1-yl)triisopropylsilane (7.48). 7.48 was prepared as described in the literature. Spectra are consistent with literature reports. ^{1}H NMR (300 MHz, $CDCl_3$): δ 3.95 (s, 2H), 1.07 (s, 21H).[27]

***tert*-butyl 4-(3-(triisopropylsilyl)prop-2-yn-1-yl)piperazine-1-carboxylate (7.49).** In a 100 mL flask, *N*-Bocpiperazine (780 mg, 4.19 mmol, 1.0 equiv) and K_2CO_3 (753 mg, 5.45 mmol, 1.3 equiv) were dissolved in DMF (25 mL, 0.17 M). The reaction mixture was cooled to 0 °C, and (3-bromoprop-1-yn-1-yl)triisopropylsilane **7.48** (1.5 g, 5.45 mmol, 1.3 equiv) was added. The reaction was let warm to RT overnight, then filtered and concentrated. The crude was evaporated onto SiO_2 and purified by column chromatography (10%→20%→30% EtOAc/hexanes). The product **7.49** was isolated as yellow oil (1.19 g, 3.13 mmol, 75% yield). R_f = 0.41 in 30%

EtOAc/hexanes. ^{1}H NMR (500 MHz, $CDCl_3$): δ 3.46 (t, J = 5.0 Hz, 4H), 3.40 (s, 2H), 2.52 (t, J = 5.1 Hz, 4H), 1.46 (s, 9H), 1.15 – 0.97 (m, 21H). ^{13}C NMR (101 MHz, $CDCl_3$): δ 154.9, 102.0, 86.6, 79.8, 51.6 (2C), 48.2, 28.6, 18.8, 11.4. HRMS (ESI) calcd. for $C_{21}H_{40}N_2O_2Si$ $(M+H)^+$: 381.2932; found 381.3078.

1-(3-(triisopropylsilyl)prop-2-yn-1-yl)piperazine (7.21). In a 250 mL flask, **7.49** (2.45 g, 6.44 mmol, 1.00 equiv) was dissolved in anhydrous DCM (130 mL, 0.05M). TFA (14 mL, 0.46 M) was added. After 5.5 h, the reaction was poured into H_2O and the organic layer was separated. The organic layer was washed with sat. sodium bicarbonate (2x), dried ($MgSO_4$), and concentrated. In a small amount of DCM, K_2CO_3 was added to **7.49**, and the mixture was stirred overnight, filtered, and concentrated. The product **7.49** was isolated as a yellow oil (1.62 g, 5.77 mmol, 90% yield). ^{1}H NMR (400 MHz, $CDCl_3$): δ 3.37 (s, 2H), 2.92 (t, J = 4.9 Hz, 4H), 2.55 (t, J = 4.8 Hz, 4H), 1.07 (s, 21H). ^{13}C NMR (101 MHz, $CDCl_3$): δ 102.5, 86.2, 53.2, 48.7, 46.2, 18.8, 11.4. HRMS (ESI) calcd. for $C_{16}H_{33}NSi$ $(M+H)^+$: 281.2408; found 281.2494.

(4-chloropyridine-2,6-diyl)bis(methylene) diacetate (7.25). In a 100 mL flask equipped with a reflux condenser, 4-chloropyridine diester **7.15** (500 mg, 2.18 mmol, 1.00 equiv) was dissolved in anhydrous THF (20 mL, 0.1 M) and $NaBH_4$ (330 mg, 8.71 mmol, 4.00 equiv) was added. The reaction was heated to 60 °C overnight and the cooled to RT and concentrated. The reaction mixture was resuspended in anhydrous DCM (20 mL, 0.1 M). Acetic anhydride (3 mL) and TEA (3 mL) were added, and the reaction was heated to reflux overnight. The reaction was cooled to RT and diluted with DCM. The organics were washed with sat. sodium bicarbonate (1x), dried ($MgSO_4$), and concentrated. The crude product was evaporated onto SiO_2 and purified by column

chromatography (20% EtOAc/hexanes) to yield **7.25** as an off-white solid (376 mg, 1.46 mmol, 67% yield). R_f = 0.38 in 30% EtOAc/hexanes. ^{1}H NMR (400 MHz, $CDCl_3$): δ 7.29 (s, 2H), 5.18 (s, 4H), 2.18 (s, 6H). ^{13}C NMR (101 MHz, $CDCl_3$): δ 170.5, 157.5, 145.7, 121.0, 66.2, 21.0. HRMS (ESI) calcd. for $C_{11}H_{13}ClNO_4$ $(M+H)^+$: 258.0528; found 258.0588.

(4-(4-(3-(triisopropylsilyl)prop-2-yn-1-yl)piperazin-1-yl)pyridine-2,6-diyl)bis(methylene) diacetate (7.26). To an oven-dried vial was added **7.25** (121 mg, 0.47 mmol, 1.0 equiv), amine **7.21** (171 mg, 0.61 mmol, 1.3 equiv), Cs_2CO_3 (381 mg, 1.2 mmol, 2.6 equiv), *rac*-BINAP (35 mg, 0.056 mmol, 0.12 equiv), and $Pd_2(dba)_3$ (26 mg, 0.028 mmol, 0.06 equiv). Degassed dioxane was added to the vial and it was sealed under N_2. The reaction mixture was heated to 110 °C. After 2 days, the reaction mixture was cooled to RT and filtered through celite, rinsing with EtOAc. The crude product was evaporated onto SiO_2 and purified by column chromatography (silica gel, 80% EtOAc/hexanes→100%EtOAc). The almost pure product was isolated (183 mg) as a yellow oil. To remove small amounts of oxidized *rac*-BINAP, the material was further purified by column chromatography (silica gel, 10%→20% acetone/hexanes). The pure product **7.26** was isolated as a pale yellow oil that solidifies upon extensive drying (121 mg, 0.241 mmol, 51% yield). R_f = 0.6 in 40% acetone/hexanes. ^{1}H NMR (400 MHz, $CDCl_3$): δ 6.68 (s, 2H), 5.10 (s, 4H), 3.46 (s, 2H), 3.42 (t, J = 5.2 Hz, 4H), 2.70 (t, J = 5.1 Hz, 4H), 2.15 (s, 6H), 1.06 (s, 21H). ^{13}C NMR (101 MHz, $CDCl_3$): δ 170.8, 156.4, 156.2, 106.0, 101.6, 86.9, 67.6, 51.1, 48.1, 46.2, 21.2, 18.8, 11.3. HRMS (ESI) calcd. for $C_{27}H_{44}N_3O_4Si$ $(M+H)^+$: 502.3096; found 502.3212.

Note: *In the future, the second column can be skipped. Mostly pure **7.26** can be used in the next step/deacetylation and purified from oxidized *rac*-BINAP at that point. # On larger scale, conversion was decreased. Higher catalyst loading may be required.

(4-(4-(3-(triisopropylsilyl)prop-2-yn-1-yl)piperazin-1-yl)pyridine-2,6-diyl)dimethanol (7.23). 7.26 (~305 mg, 0.608 mmol, 1.00 equiv) was dissolved in anhydrous MeOH (6 mL, 0.1 M). K_2CO_3 (252 mg, 1.82 mmol, 3.0 equiv) was added, and the reaction was stirred at RT. After 40 min, no starting material was observed by TLC. The reaction mixture was diluted with H_2O. The solution was washed with $CHCl_3$ (5x), and the combined organic layers were dried ($MgSO_4$) and concentrated. The crude product was evaporated onto SiO_2 and purified by column chromatography (5% →10% →20%→30% MeOH/DCM). The product **7.23** was isolated as a pale yellow foam (170 mg, 0.407 mmol, 67% yield). R_f = 0.26 in 20% MeOH/DCM. ^{1}H NMR (500 MHz, $CDCl_3$): δ 6.58 (s, 2H), 4.66 (s, 4H), 3.51 – 3.38 (m, 6H), 2.73 – 2.65 (m, 4H), 1.05 (s, 22H). ^{13}C NMR (126 MHz, $CDCl_3$): δ 158.6, 156.5, 103.7, 101.5, 87.0, 64.3, 51.0, 48.0, 46.3, 18.8, 11.3. HRMS (ESI) calcd. for $C_{23}H_{40}N_3O_2Si$ $(M+H)^+$: 418.2885; found 418.2966.

(4-(4-methylpiperazin-1-yl)pyridine-2,6-diyl)bis(methylene) diacetate (7.50). To a 25 mL flask equipped with a reflux condenser, was added **7.20** (124 mg, 0.423 mmol, 1.00 equiv). Anhydrous THF (2 mL, 0.21 M) was added, followed by $NaBH_4$ (96 mg, 2.5 mmol, 6.0 equiv). The reaction mixture was heated to 60 °C. After 18 h, the reaction was cooled to 0 °C and quenched with MeOH. The reaction mixture was concentrated and resuspended in anhydrous DCM (2 mL, 0.21 M). Acetic anhydride (0.6 mL) and dry TEA (0.9 mL) were added and the reaction was heated to reflux overnight. The reaction mixture was diluted with more DCM and

washed with saturated sodium bicarbonate. The organic layers were dried ($MgSO_4$) and concentrated. The crude product was purified by column chromatography (silica gel, 100% DCM →5% MeOH/DCM→10% MeOH/DCM) to yield the product **7.50** (51 mg, 0.16 mmol, 38%). R_f = 0.35 in 10% MeOH/DCM. ^{1}H NMR (400 MHz, $CDCl_3$): δ 6.64 (s, 2H), 5.07 (s, 4H), 3.44 – 3.30 (m, 4H), 2.55 (t, J = 5.2 Hz, 4H), 2.33 (s, 3H), 2.11 (s, 6H). ^{13}C NMR (101 MHz, $CDCl_3$): δ 170.7, 156.3, 156.2, 105.9, 67.3, 54.2, 45.8, 45.8, 21.1. HRMS (ESI) calcd. for $C_{16}H_{24}N_3O_4$ $(M+H)^+$: 322.1762; found 322.1786.

(4-(4-(3-(triisopropylsilyl)prop-2-yn-1-yl)piperazin-1-yl)pyridine-2,6-diyl)bis(methylene) bis(3,7-bis(prop-2-yn-1-yloxy)-2-naphthoate) (7.27). To a vial containing diol **7.23** (63 mg, 0.151 mmol, 1.00 equiv) was added naphthalene PFPester **5.21** (168 mg, 0.377 mmol, 2.5 equiv) and DMAP (18 mg, 0.15 mmol, 1.0 equiv). Anhydrous DMF (2 mL, 0.076 M) and DIPEA (0.60 mL, 0.35 mmol, 2.3 equiv) were added. The reaction was stirred for 3 days, and then DMF was removed under a stream of compressed air. The crude product was evaporated onto SiO_2, and purified by column chromatography (silica gel, 50% →60%→80% EtOAc/hexanes →100% EtOAc). The product **7.27** was isolated (93 mg). Additional mixed fractions of desired **7.27** and mono-ester product were purified by preparatory thin layer chromatography. In total, the product **7.27** was concentrated from heptane to a white fluffy solid (107 mg, 0.114 mmol, 75% yield). R_f = 0.42 in 70% EtOAc/hexanes. ^{1}H NMR (500 MHz, $CDCl_3$): δ 8.33 (s, 2H), 7.69 (d, J = 8.8 Hz, 2H), 7.35 (s, 2H), 7.26 – 7.21 (m, 4H), 6.91 (s, 2H), 5.45 (s, 4H), 4.86 (d, J = 2.4 Hz, 4H), 4.76 (d, J = 2.4 Hz, 4H), 3.53 – 3.38 (m, 6H), 2.70 (t, J = 5.1 Hz, 4H), 2.55 (t, J = 2.4 Hz, 2H), 2.53 (t, J = 2.4 Hz, 2H), 1.04 (d, J = 3.0 Hz, 21H). ^{13}C NMR (101 MHz, $CDCl_3$): δ 165.9, 156.6, 156.4, 154.9, 152.6, 132.4, 131.7, 128.9, 128.4, 122.5, 121.8, 110.0, 108.4, 105.7, 101.6, 87.0,

78.5, 78.4, 76.3, 76.1, 67.8, 57.1, 56.1, 51.2, 48.1, 46.2, 18.8, 11.3. HRMS (ESI) calcd. for $C_{57}H_{60}N_3O_8Si$ $(M+H)^+$: 942.4144; found 942.4272.

(4-(4-(3-(triisopropylsilyl)prop-2-yn-1-yl)piperazin-1-yl)pyridine-2,6-diyl)bis(methylene) bis(2,7-bis(prop-2-yn-1-yloxy)phenanthrene-9-carboxylate) (7.29). In a 25 mL flask, diol **7.23** (170 mg, 0.407 mmol, 1.00 equiv), phenanthrene PFPester **6.12** (606 mg, 1.22 mmol, 3.0 equiv), and DMAP (50 mg, 0.41 mmol, 1.00 equiv) were dissolved in DMF (4 mL, 0.1 M). DIPEA (0.15 mL, 0.855 mmol, 2.1 equiv) was added. After 22 h, the reaction was concentrated. The crude product was evaporated onto SiO_2 and purified by column chromatography (silica gel, 30% →50%→60% EtOAc/hexanes). Excess phenanthrene PFPester was recovered. The product **7.29** was isolated as a pale yellow foam (381 mg, 0.366 mmol, 90% yield). R_f = 0.32 in 60% EtOAc/hexanes. ^{1}H NMR (500 MHz, $CDCl_3$): δ 8.48 (d, J = 2.7 Hz, 2H), 8.46 (s, 2H), 8.42 (d, J = 9.2 Hz, 2H), 8.37 (d, J = 9.2 Hz, 2H), 7.30 (ddd, J = 9.1, 7.1, 2.7 Hz, 4H), 7.18 (d, J = 2.7 Hz, 2H), 6.89 (s, 2H), 5.53 (s, 4H), 4.81 (d, J = 2.4 Hz, 4H), 4.69 (d, J = 2.4 Hz, 4H), 3.50 – 3.42 (m, 6H), 2.70 (t, J = 5.1 Hz, 4H), 2.58 – 2.52 (m, 4H), 1.09 – 0.97 (m, 21H). ^{13}C NMR (126 MHz, $CDCl_3$): δ 167.3, 156.6, 156.4, 156.3, 155.7, 133.4, 130.2, 129.5, 127.4, 125.7, 125.4, 124.0, 123.9, 120.5, 117.9, 110.7, 108.4, 106.4, 101.4, 87.1, 78.7, 78.4, 76.1, 75.7, 67.6, 56.1, 56.0, 51.1, 48.0, 46.1, 18.8, 11.3. HRMS (ESI) calcd. for $C_{65}H_{63}N_3O_8Si$ $(M+H)^+$: 1042.4457; found 1042.4553.

1,3,4,6-Tetra-*O*-acety-*N*-4-acetoxy-2,3,5,6-tetrafluorophenyl-D-mannosamine (7.36). In a 15 mL flask, mannosamine-HCl (100 mg, 0.464 mmol, 1.0 equiv) was dissolved in anhydrous MeOH (3.3 mL, 0.14 M). TEA (0.13 mL, 0.928 mmol, 2.0 equiv) was added, and the solution

was stirred vigorously to dissolve the sugar. 2,3,5,6-tetrafluoro-4-hydroxybenzoic acid (146 mg, 0.696 mmol, 1.5 equiv) was added, and the solution was cooled to 0 °C. HOBt (65 mg, 0.464 mmol, 1.0 equiv) and EDC-HCl (89 mg, 0.464 mmol, 1.0 equiv) were added. After 48 h, the solution was concentrated and evaporated onto SiO_2. The crude product was purified by column chromatography (silica gel, 20% →40% MeOH/EtOAc). The product was collected and dissolved in pyridine (2 mL) and acetic anhydride (1 mL). The reaction was stirred overnight, the solvent was removed, and then the crude product was evaporated onto SiO_2. The crude product was purified by column chromatography (silica gel, 30% →40%→50% EtOAc/hexanes) to provide **7.36** as a white foamy (86 mg, 0.148 mmol, 32% yield). ^{1}H NMR (500 MHz, $CDCl_3$): δ 6.57 (d, J = 9.2 Hz, 1H, H_{a1}), 6.51 (d, J = 9.0 Hz, 0.6H, H_{a2}), 6.14 (d, J = 1.8 Hz, 1H, NH_1), 5.93 (d, J = 1.8 Hz, 0.6H, NH_2), 5.39 (dd, J = 10.2, 4.4 Hz, 1H, H_{c1}), 5.26 (t, J = 10.0 Hz, 1H, H_{d1}), 5.19 (t, J = 9.8 Hz, 0.6H, H_{d2}), 5.13 (dd, J = 10.0, 4.0 Hz, 0.6H, H_{c2}), 4.96 (ddd, J = 9.0, 4.0, 1.7 Hz, 0.6H, H_{b2}), 4.83 (ddd, J = 9.2, 4.4, 1.9 Hz, H_{b1}), 4.29 – 4.21 (m, 1.6H, H_{f1+2}), 4.11 – 4.00 (m, 1H + 1.6H, H_{e1} +$H_{f'1+2}$), 3.83 (ddd, J = 9.8, 5.0, 2.4 Hz, 0.6, H_{e2}), 2.42 (s, 1.5H), 2.42 (s, 3H), 2.20 (s, 3H), 2.12 (s, 1.5H), 2.07 (s, 1.5H), 2.06 (s, 7.5H), 2.03 (s, 1.5H), 2.03 (s, 3H). ^{13}C NMR (126 MHz, $CDCl_3$): δ one anomer 170.7, 170.3, 169.60, 168.2, 166.3, 158.0, 143.3 (C-F), 140.01 (C-F), 131.2, 112.6, 91.3, 70.4, 69.0, 65.2, 62.0, 50.2, 21.0, 20.8, 20.7, 20.7, 20.1. ^{19}F NMR (376 MHz, $CDCl_3$): δ -140.70 – -140.88 (m, anomer 1), -140.88 – -141.04 (m, anomer 2), -150.65 – -150.84 (m, anomer 1), -150.84 – -151.02 (m, anomer 2). HRMS (ESI) calcd. for $C_{23}H_{24}F_4NO_{12}$ $(M+Na)^+$: 604.1048; found 604.1092.

Perfluorophenyl 2,3,5,6-tetrafluoro-4-hydroxybenzoate (7.39). 2,3,5,6-tetrafluoro-4-hydroxybenzoic acid (700 mg, 4.76 mmol, 1.0 equiv) and bis(perfluorophenyl) carbonate (2.25

g, 5.71 mmol, 1.2 equiv) were dissolved in anhydrous DMF (24 mL, 0.2 M). The solution was cooled to 0 °C, and DIPEA (1.0 mL, 5.7 mmol, 1.2 equiv) was added. The DMF was removed under a stream of compressed air overnight. The crude product was evaporated onto SiO_2 and purified by column chromatography (silica gel, 5% MeOH/DCM→10% MeOH/DCM). The DIPEA salt of **7.39** was isolated (1.1846 g). To isolate the free protonated phenol, **7.39** was repurified (silica gel, 80% EtOAc/hexanes + 0.1% AcOH). **7.39** was isolated as white solid (513 mg, 1.36 mmol, 29%). R_f= 0.2 in 10% MeOH/DCM. ^{19}F NMR (376 MHz, $CDCl_3$): δ -136.4, -151.9, 156.8, -161.28, -161.7. LRMS (ESI) calcd. for $C_{13}F_9O_3$ $(M-H)^-$: 375.0; found 375.0.

2-(diphenylphosphaneyl)phenyl 2,3,4,5,6-pentafluorobenzoate (7.45). In a 25 ml flask, 2-(diphenylphosphaneyl)phenol **7.43** (212 mg, 0.761 mmol, 1.0 equiv) was dissolved in anhydrous THF (5 mL, 0.15 M). Triethylamine (0.16 mL, 1.14 mmol, 1.5 equiv) was added, and the reaction mixture was stirred for 30 min. Then, perfluorobenzoylchloride (0.14 mL, 0.99 mmol, 1.3 equiv) was added. After 5.5 h, the reaction mixture was poured into water and extracted with Et_2O (4x). The combined organics were dried ($MgSO_4$), filtered, and concentrated. The crude product was evaporated onto SiO_2 and purified by column chromatography (silica gel, 5% acetone/pentane) to yield the product **7.45** as a colorless oil (334 mg, 0.707 mmol, 93% yield). R_f = 0.42 in 10% EtOAc/hexanes. ^{1}H NMR (400 MHz, Acetone-d_6): δ 7.55 (ddd, J = 7.9, 7.2, 1.7 Hz, 1H), 7.48 – 7.20 (m, 12H), 6.99 (ddd, J = 7.7, 4.2, 1.6 Hz, 1H).^{13}C NMR (101 MHz, Acetone-d_6): δ 135.1, 134.7, 134.5, 131.4, 130.0, 129.6, 129.5, 128.1, 123.5. ^{31}P NMR (162 MHz, Acetone-d_6): δ -11.73. ^{19}F NMR (376 MHz, Acetone-d_6): δ -133.0, -144.6, -157.8. HRMS (ESI) calcd. for $C_{25}H_{15}F_5O_2P$ $(M+H)^+$: 473.0725; found 473.0861.

7.6.5 NMR titrations

Complex of **7.14a** and **7.1** in $CDCl_3$ (mam-V-008)

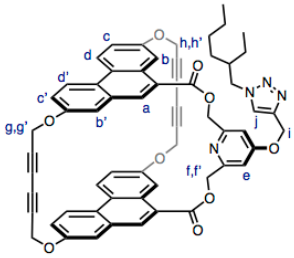

Host: **7.14a**
[H] = 0.93 mM

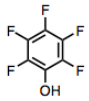

Guest: **7.1**
[G] = 0 - 7.5 mM

proton	K_a (bindfit)
a	809 ± 4%
b	778 ± 4%
d,d'	799 ± 5%
j	274 ± 5%
i	324 ± 4%
f,f'	814 ± 4%
global fitting	795 ± 3%

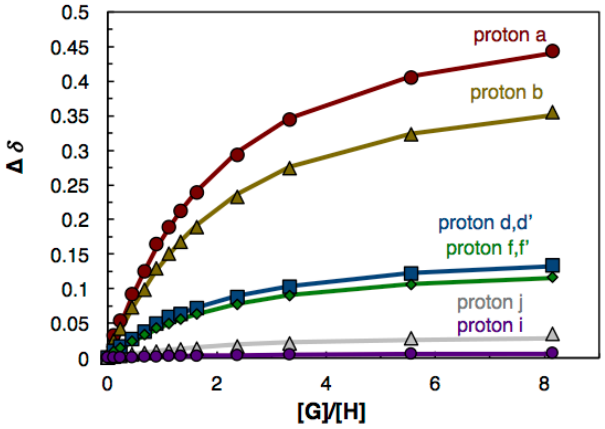

Trial 1 (mam-V-008) 0.1 to 8.1	Trial 2 (mam-V-009) 0.1 to 8.1
795 ± 3%	808 ± 2%

$K_{a,avg}$ = 8.0x10^2 ± 2%

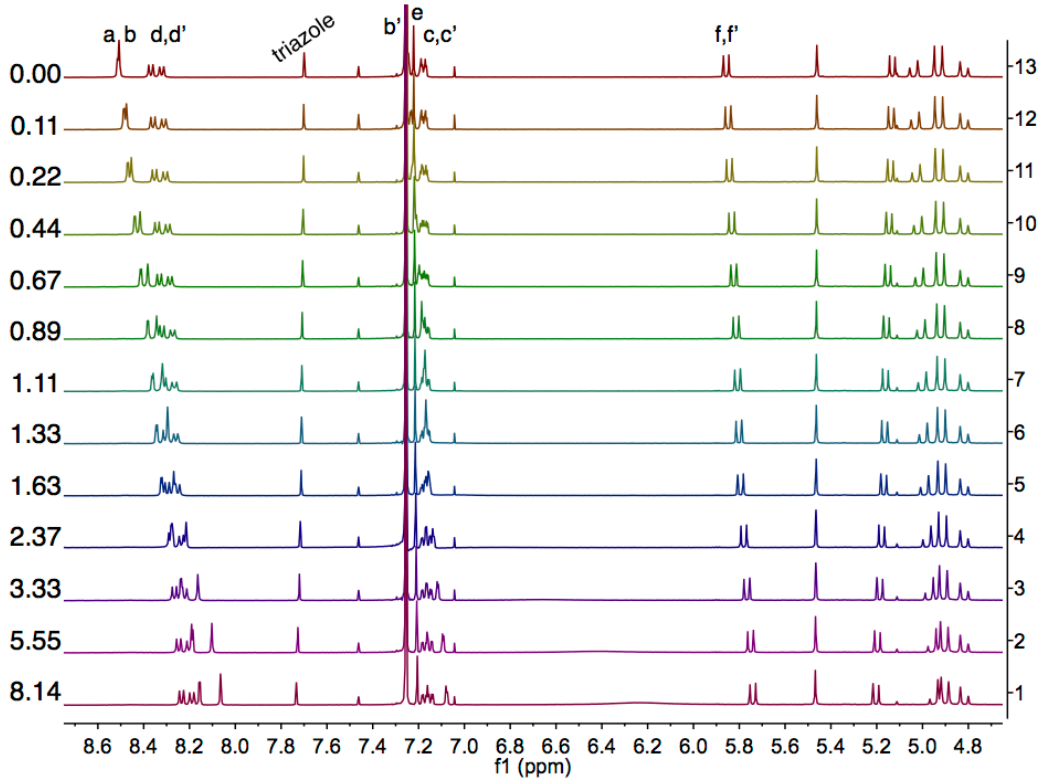

Complex of **7.14a** and **7.1** in $CDCl_3$: Example error calculation

Trial 1 (mam-IV-238)	**Trial 2 (GL-IV-251)**
795 ± 3%	808 ± 2%
$\Delta K_{a1} = 23.85$	$\Delta K_{a2} = 16.16$

Equation 1: $K_{a,avg} = \frac{K_{a,1}+K_{a,2}}{2} = 801.5$

Equation 2: $\Delta K_{a,avg} = \frac{1}{2}\sqrt{(\Delta K_{a,1})^2 + (\Delta K_{a,2})^2} = 14.4$

$K_{a,avg} = 8.0\text{x}10^2\ M^{-1} \pm 2\%$

7.6.6 NMR spectra

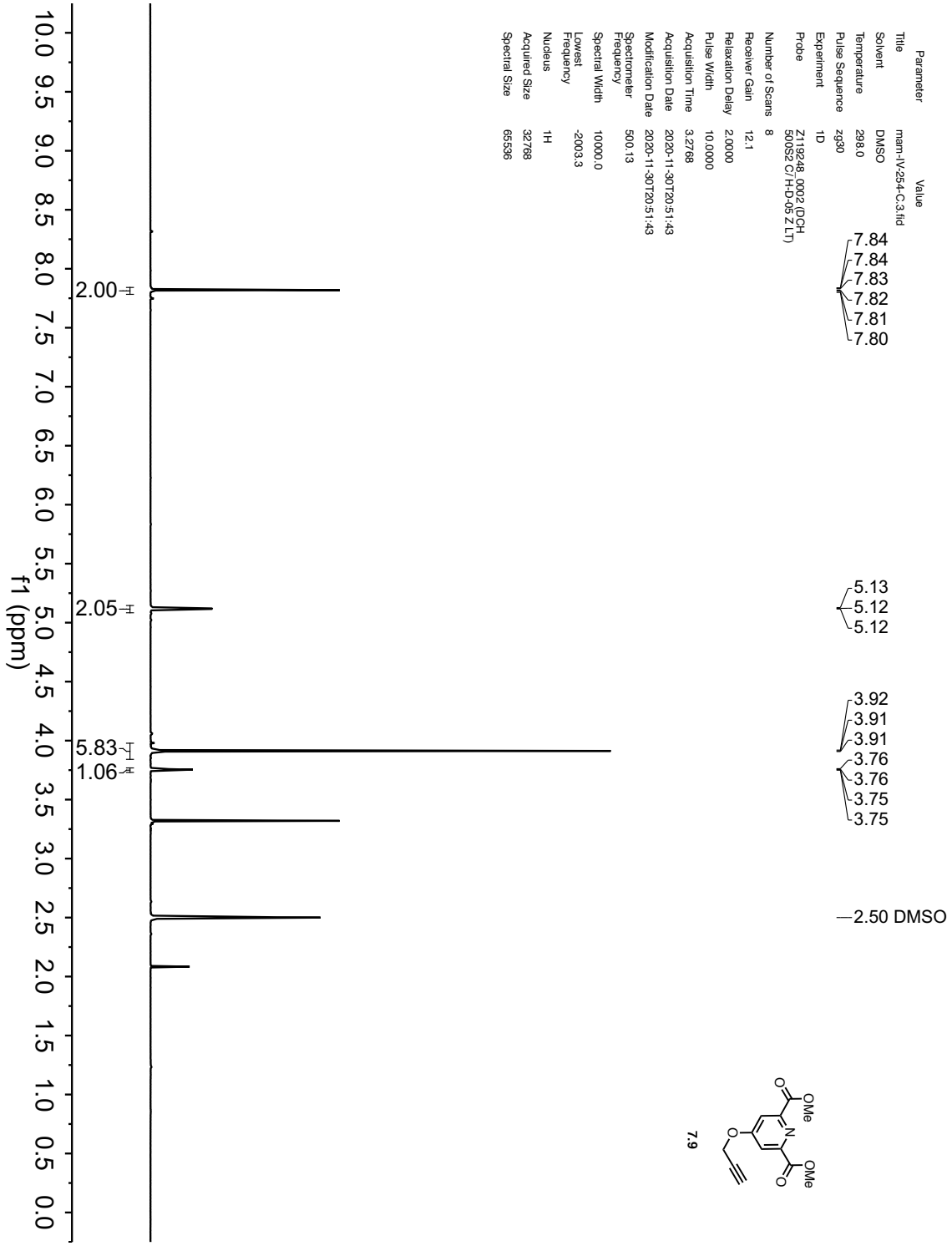

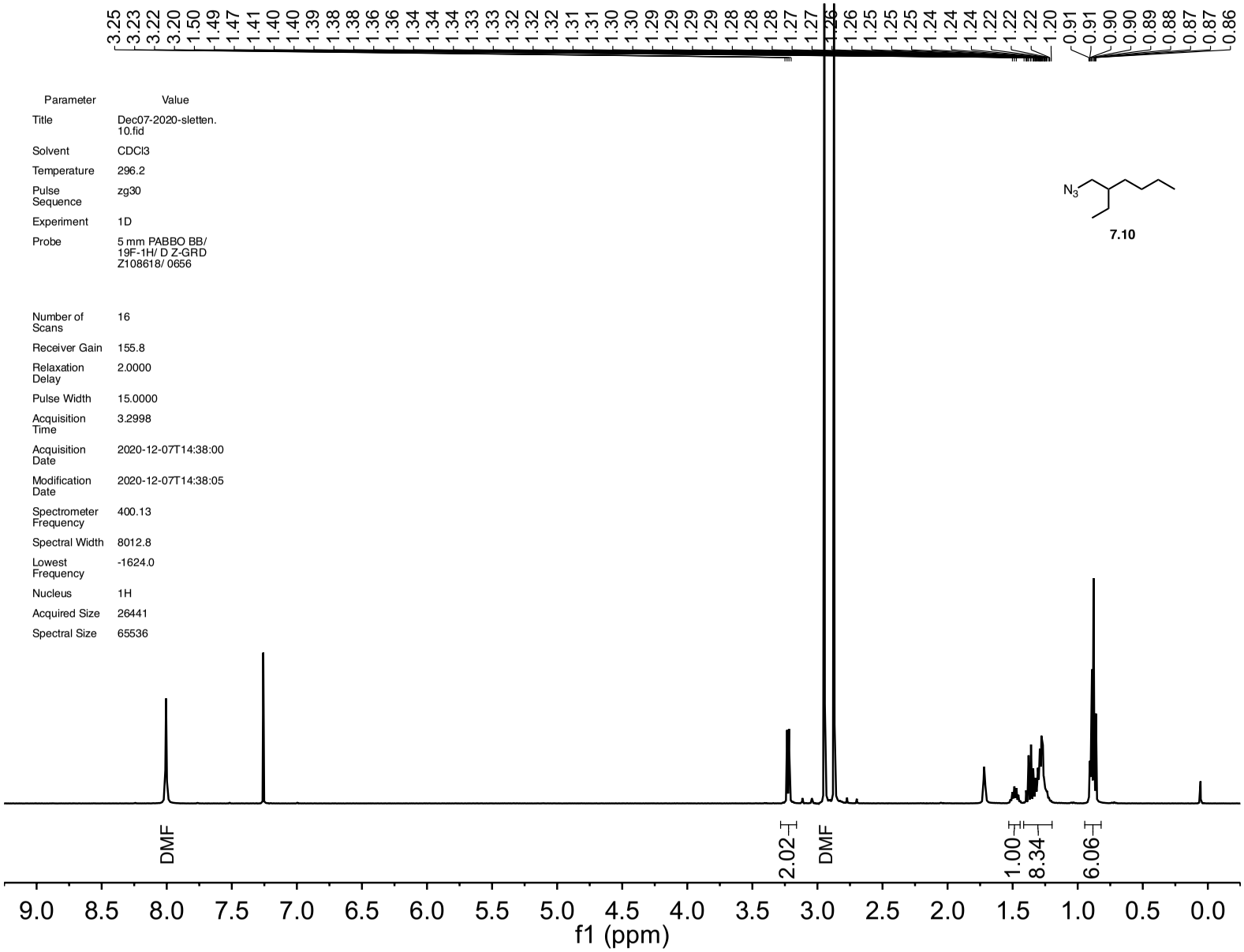

Parameter	Value
Title	Dec07-2020-sletten.10.fid
Solvent	CDCl3
Temperature	296.2
Pulse Sequence	zg30
Experiment	1D
Probe	5 mm PABBO BB/ 19F-1H/ D Z-GRD Z108618/ 0656
Number of Scans	16
Receiver Gain	155.8
Relaxation Delay	2.0000
Pulse Width	15.0000
Acquisition Time	3.2998
Acquisition Date	2020-12-07T14:38:00
Modification Date	2020-12-07T14:38:05
Spectrometer Frequency	400.13
Spectral Width	8012.8
Lowest Frequency	-1624.0
Nucleus	1H
Acquired Size	26441
Spectral Size	65536

Parameter	Value
Title	mam-IV-285
Solvent	CDCl3
Temperature	296.0
Pulse Sequence	zg30
Experiment	1D
Probe	5 mm PABBO BB/ 19F-1H/ D Z-GRD Z108618/ 0656
Number of Scans	8
Receiver Gain	189.8
Relaxation Delay	2.0000
Pulse Width	15.0000
Acquisition Time	3.2998
Acquisition Date	2021-01-13T12:44:00
Modification Date	2021-01-13T12:44:10
Spectrometer Frequency	400.13
Spectral Width	8012.8
Lowest Frequency	-1623.2
Nucleus	1H
Acquired Size	26441
Spectral Size	65536

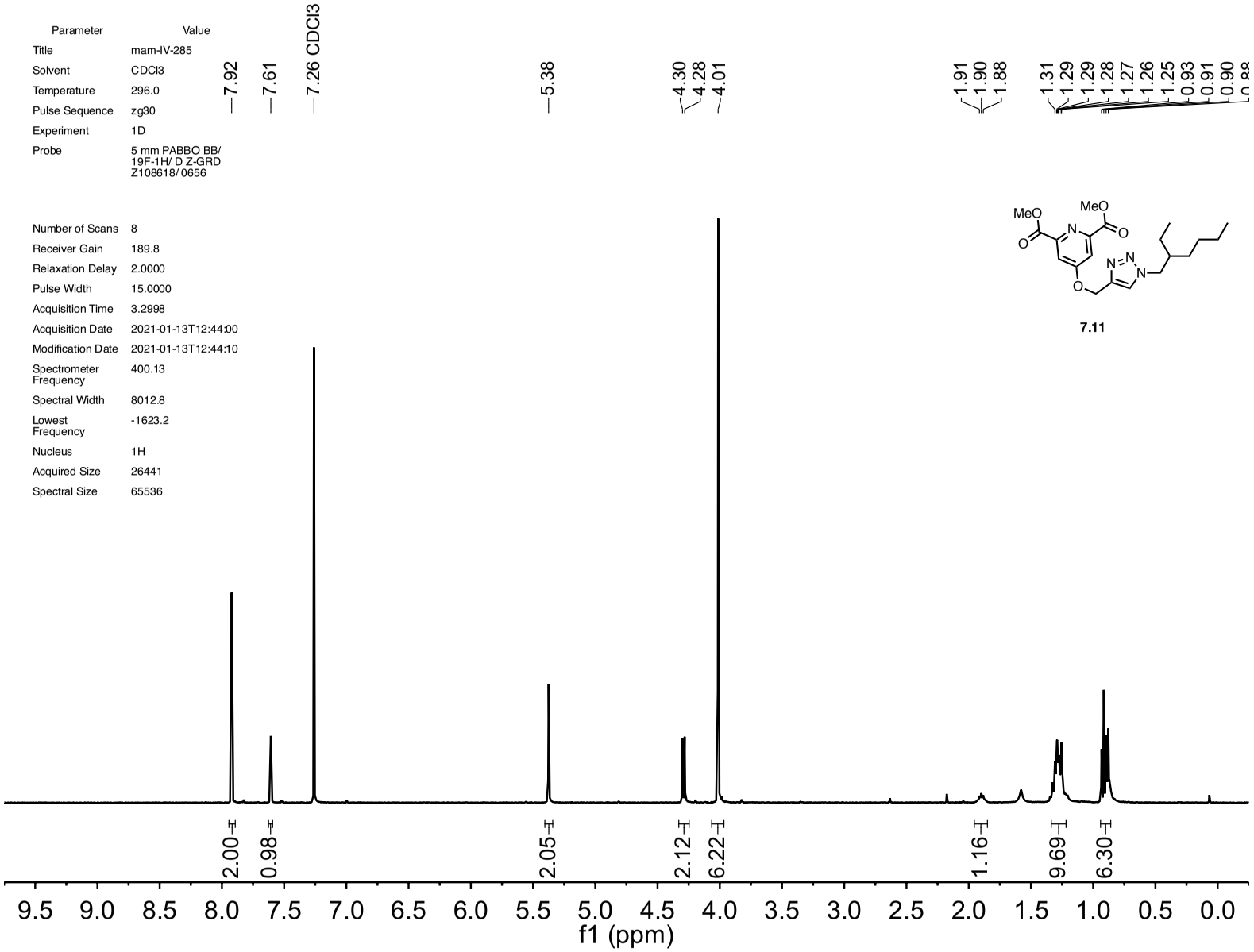

7.11

Parameter	Value
Title	mam-IV-291
Solvent	CDCl3
Temperature	298.0
Pulse Sequence	zg30
Experiment	1D
Probe	Z119248_0002 (DCH 500S2 C/ H-D-05 Z LT)
Number of Scans	8
Receiver Gain	12.1
Relaxation Delay	2.0000
Pulse Width	10.0000
Acquisition Time	3.2768
Acquisition Date	2021-11-27T12: 42:48
Modification Date	2021-11-27T12: 42:48
Spectrometer Frequency	500.13
Spectral Width	10000.0
Lowest Frequency	-2011.3
Nucleus	1H
Acquired Size	32768
Spectral Size	65536

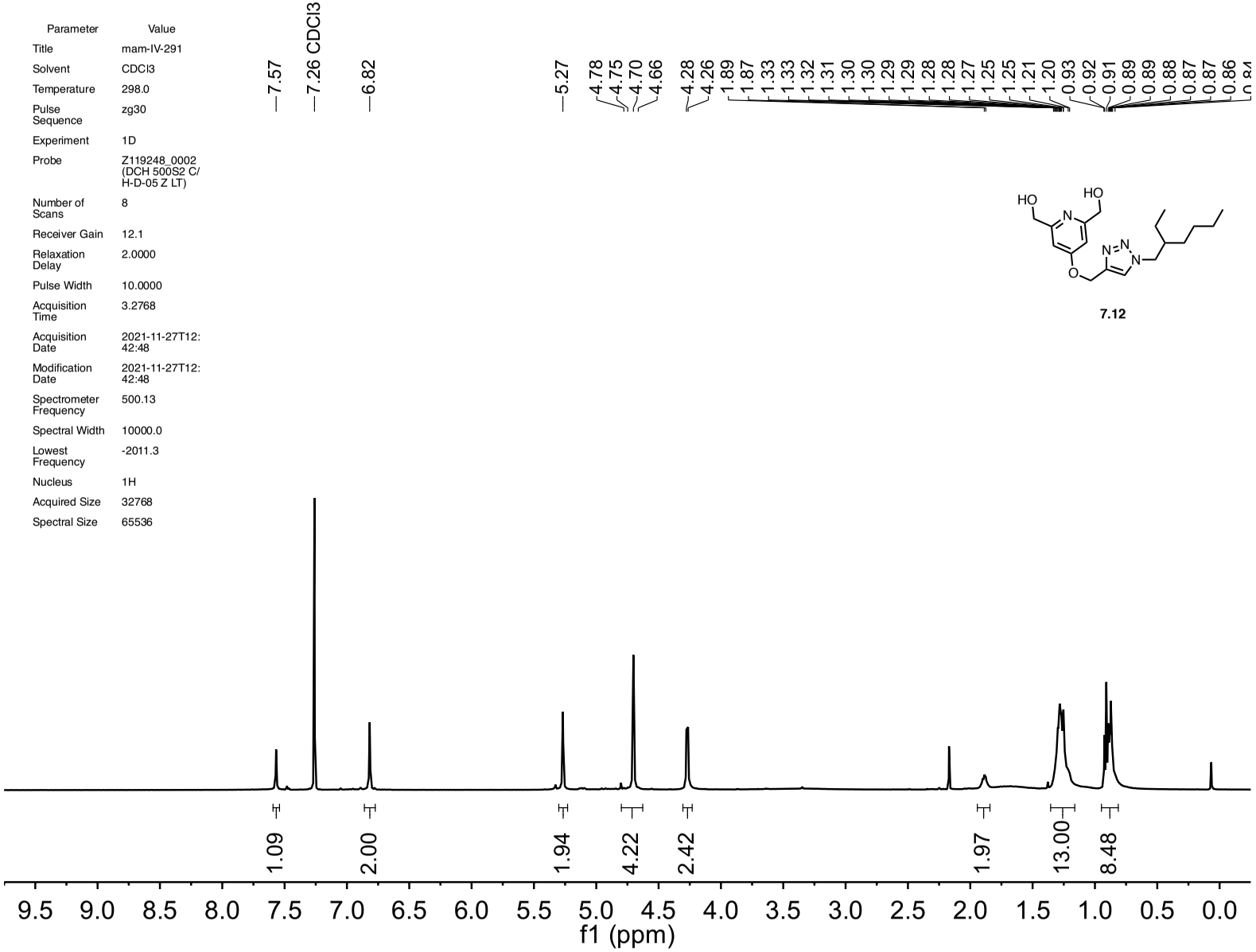

7.12

Parameter	Value
Title	mam-IV-291-cdcl3.13.fid
Solvent	CDCl3
Temperature	298.0
Pulse Sequence	zgpg30
Experiment	1D
Probe	Z119248_0002 (DCH 500S2 C/H-D-05 Z LT)
Number of Scans	1000
Receiver Gain	204.5
Relaxation Delay	2.0000
Pulse Width	10.5000
Acquisition Time	1.0486
Acquisition Date	2021-11-22T12:55:55
Modification Date	2021-11-22T12:55:55
Spectrometer Frequency	125.77
Spectral Width	31250.0
Lowest Frequency	-1145.9
Nucleus	13C
Acquired Size	32768
Spectral Size	65536

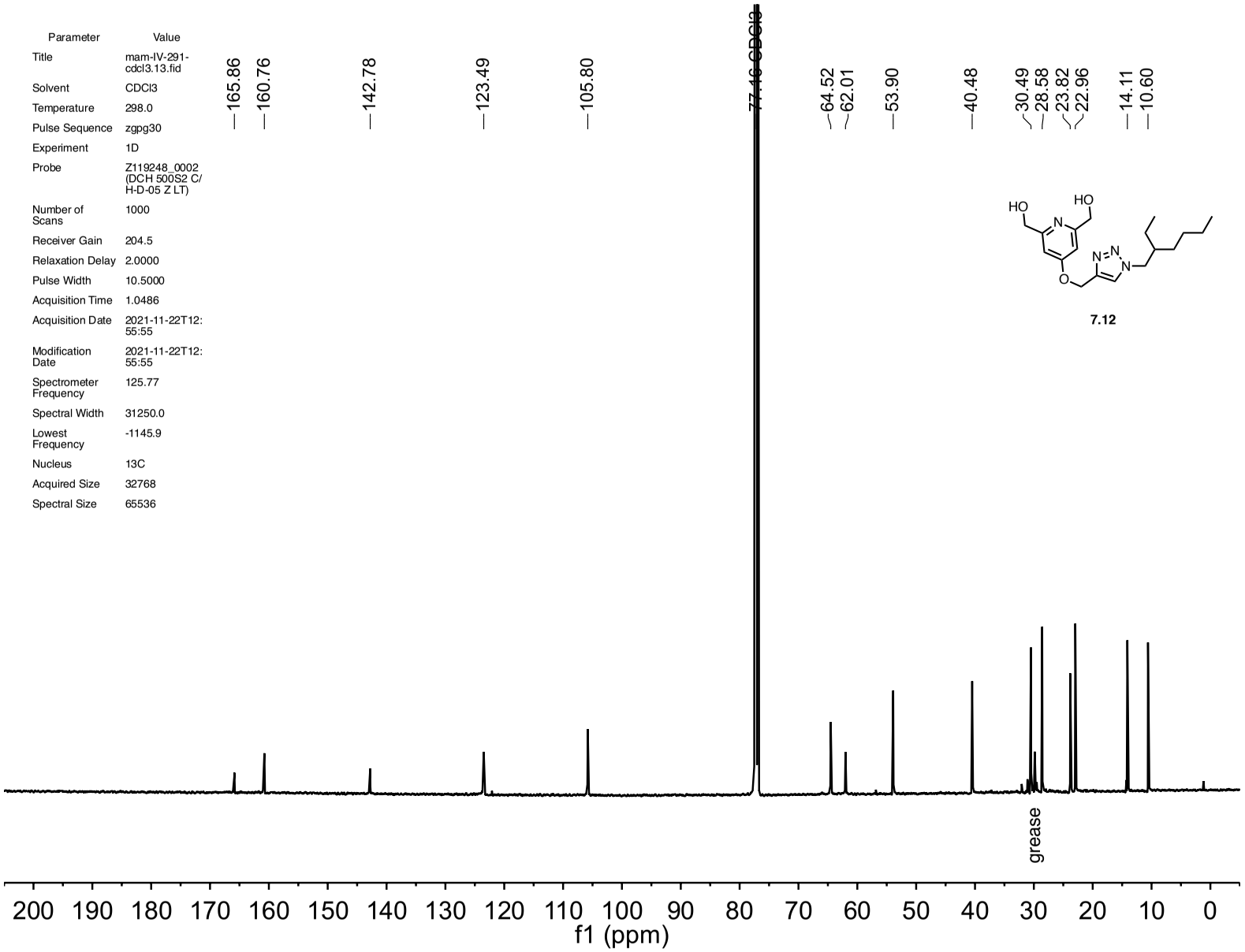

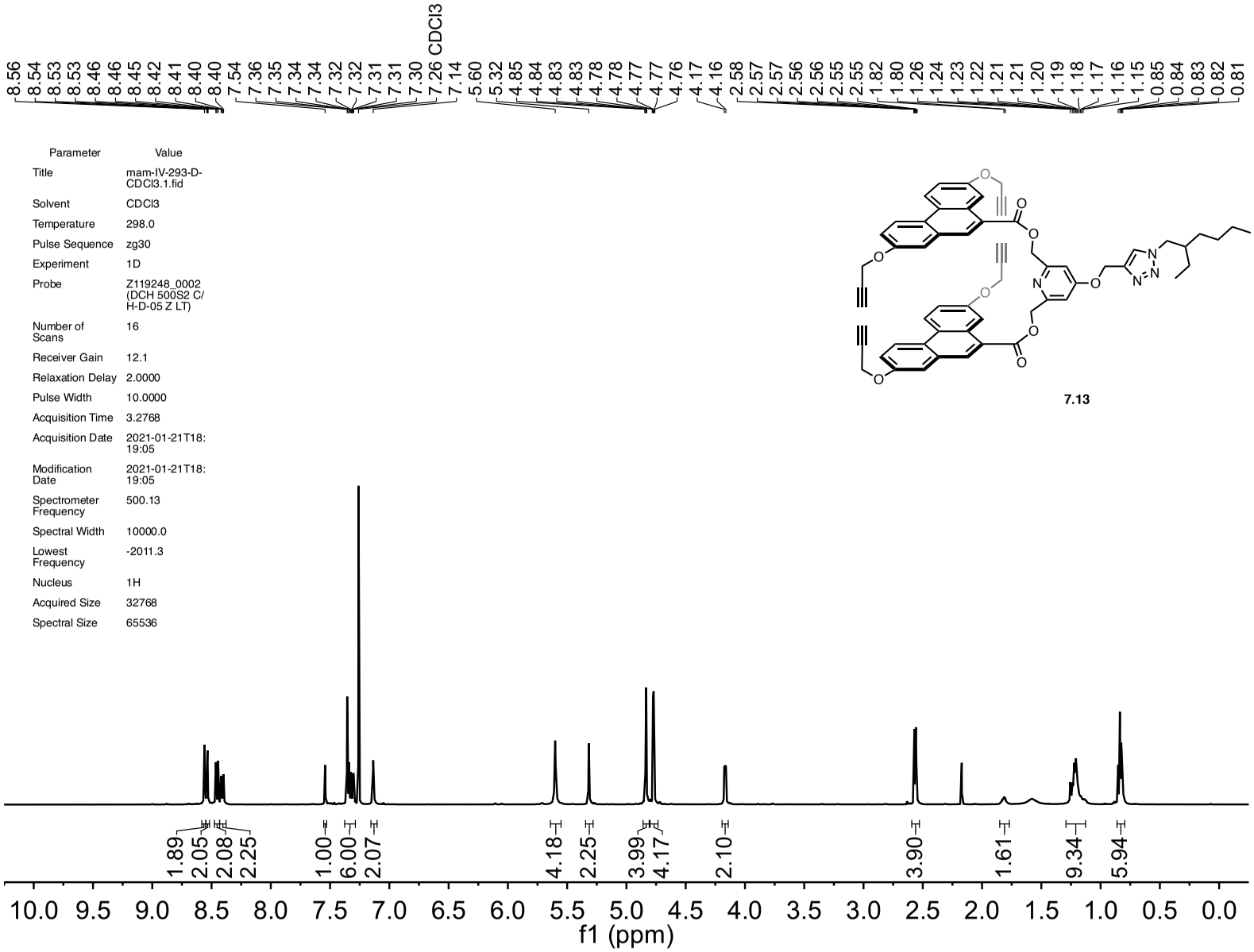

Parameter	Value
Title	mam-IV-293-D-CDCl3.1.fid
Solvent	CDCl3
Temperature	298.0
Pulse Sequence	zg30
Experiment	1D
Probe	Z119248_0002 (DCH 500S2 C/H-D-05 Z LT)
Number of Scans	16
Receiver Gain	12.1
Relaxation Delay	2.0000
Pulse Width	10.0000
Acquisition Time	3.2768
Acquisition Date	2021-01-21T18:19:05
Modification Date	2021-01-21T18:19:05
Spectrometer Frequency	500.13
Spectral Width	10000.0
Lowest Frequency	-2011.3
Nucleus	1H
Acquired Size	32768
Spectral Size	65536

7.13

Parameter	Value
Title	mam-IV-293-D-CDCl3.13.fid
Solvent	CDCl3
Temperature	298.0
Pulse Sequence	zgpg30
Experiment	1D
Probe	Z119248_0002 (DCH 500S2 C/ H-D-05 Z LT)
Number of Scans	950
Receiver Gain	204.5
Relaxation Delay	2.0000
Pulse Width	10.5000
Acquisition Time	1.0486
Acquisition Date	2021-01-21T19:11:55
Modification Date	2021-01-21T19:11:55
Spectrometer Frequency	125.77
Spectral Width	31250.0
Lowest Frequency	-1145.1
Nucleus	13C
Acquired Size	32768
Spectral Size	65536

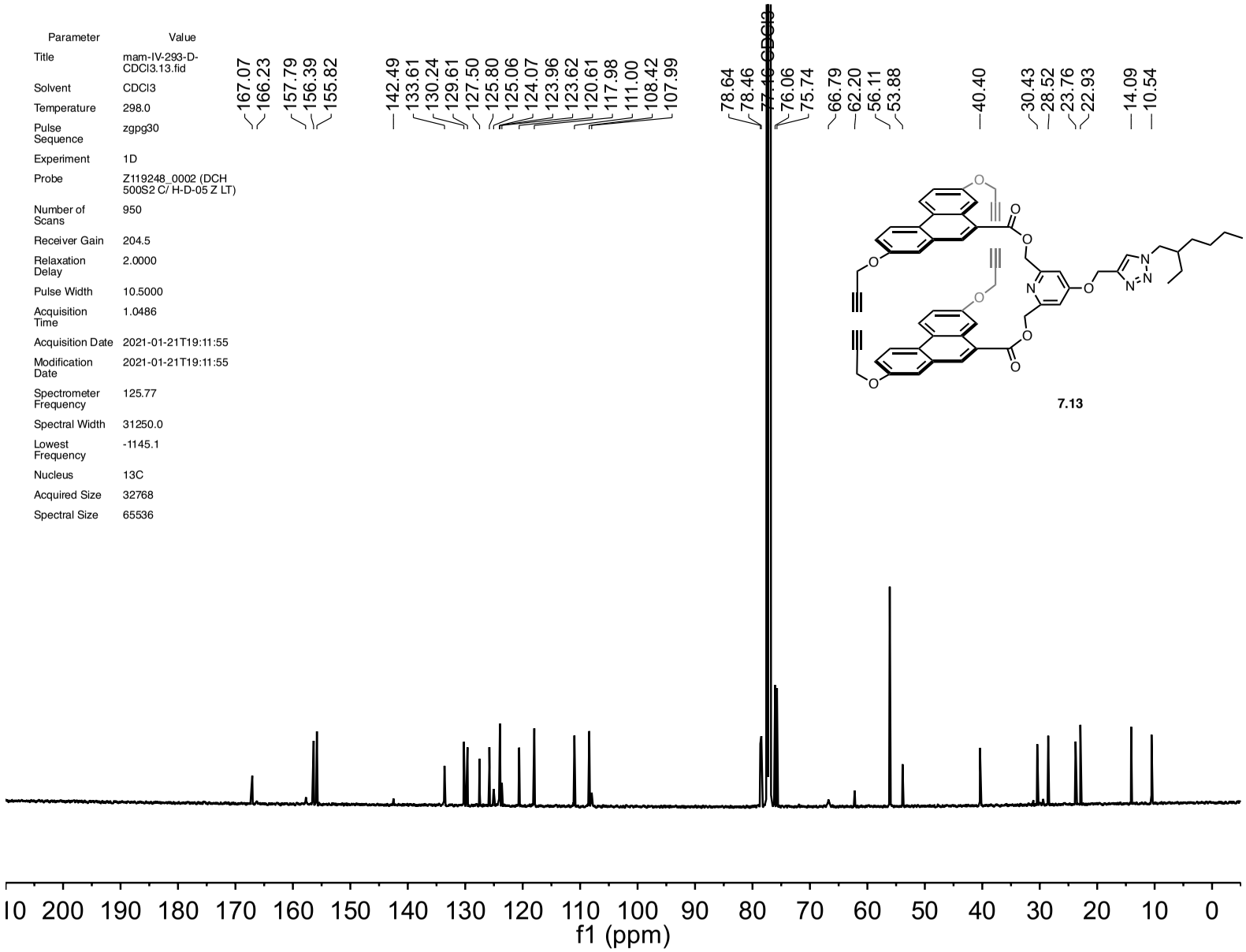

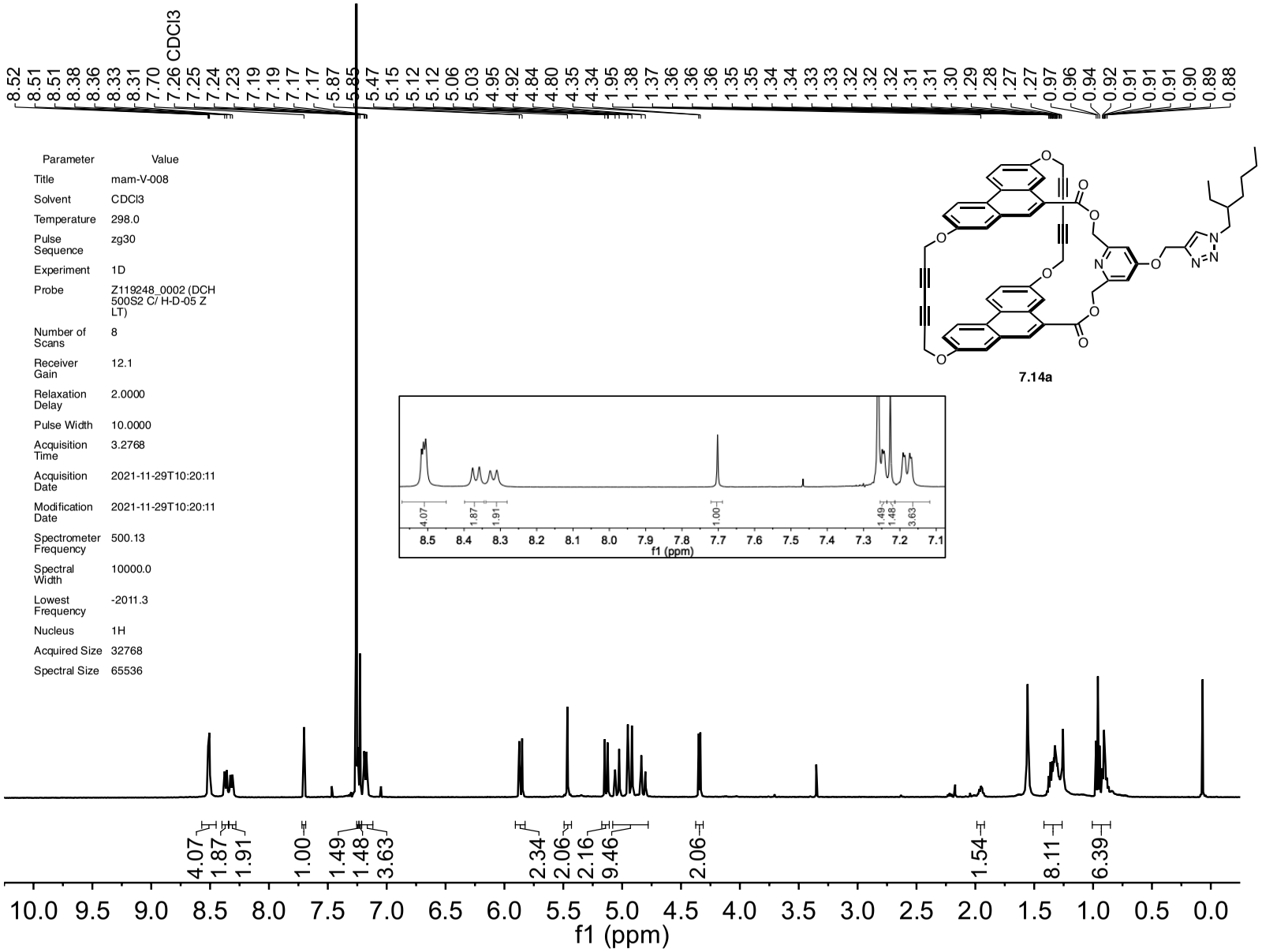

Parameter	Value
Title	mam-V-008
Solvent	CDCl3
Temperature	298.0
Pulse Sequence	zg30
Experiment	1D
Probe	Z119248_0002 (DCH 500S2 C/ H-D-05 Z LT)
Number of Scans	8
Receiver Gain	12.1
Relaxation Delay	2.0000
Pulse Width	10.0000
Acquisition Time	3.2768
Acquisition Date	2021-11-29T10:20:11
Modification Date	2021-11-29T10:20:11
Spectrometer Frequency	500.13
Spectral Width	10000.0
Lowest Frequency	-2011.3
Nucleus	1H
Acquired Size	32768
Spectral Size	65536

7.14a

Parameter	Value
Title	mam-V-008-carbon.13.fid
Solvent	CDCl3
Temperature	298.0
Pulse Sequence	zgpg30
Experiment	1D
Probe	Z119248_0002 (DCH 500S2 C/ H-D-05 Z LT)
Number of Scans	1560
Receiver Gain	204.5
Relaxation Delay	2.0000
Pulse Width	10.5000
Acquisition Time	1.0486
Acquisition Date	2021-11-29T11:43:20
Modification Date	2021-11-29T11:43:21
Spectrometer Frequency	125.77
Spectral Width	31250.0
Lowest Frequency	-1144.5
Nucleus	13C
Acquired Size	32768
Spectral Size	65536

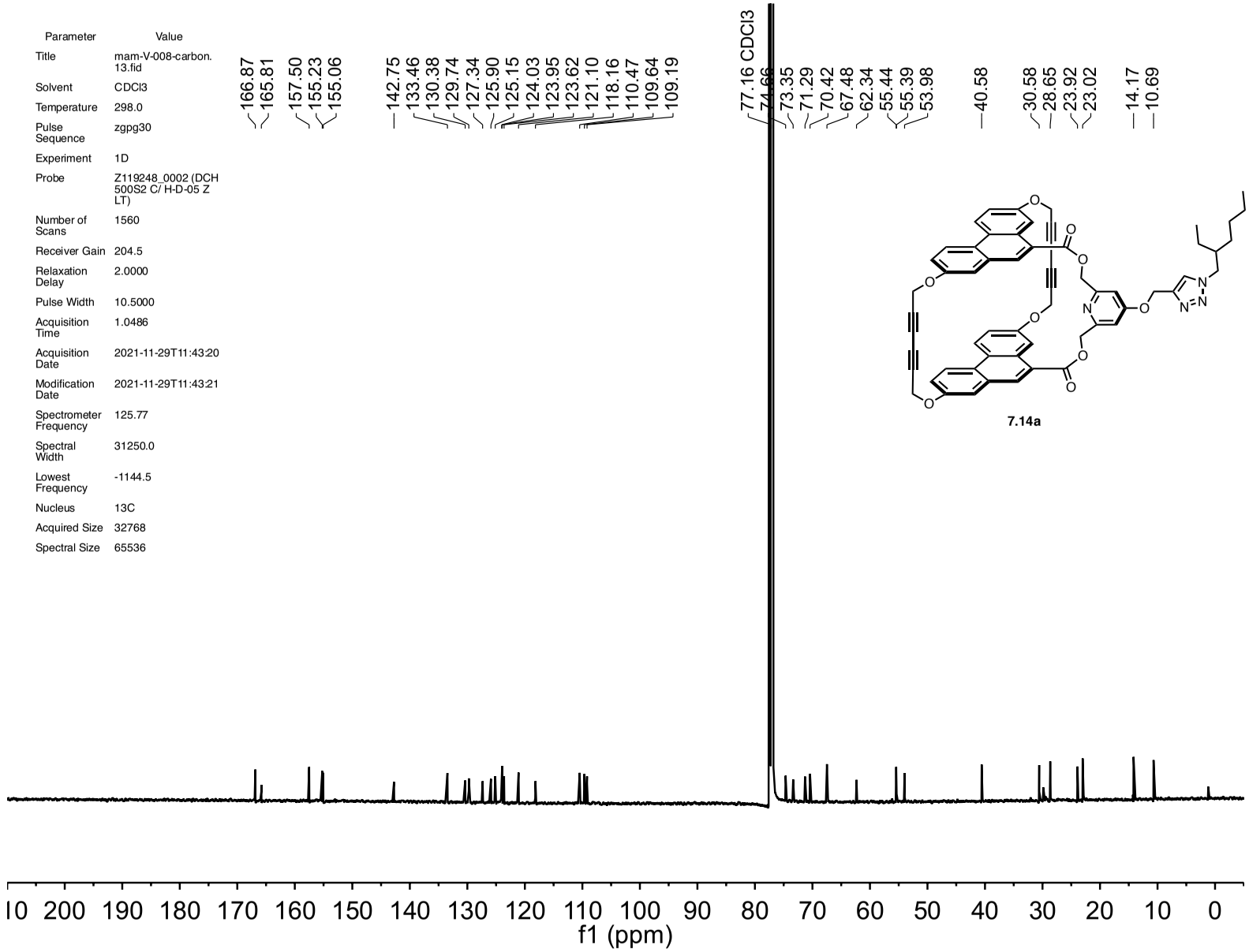

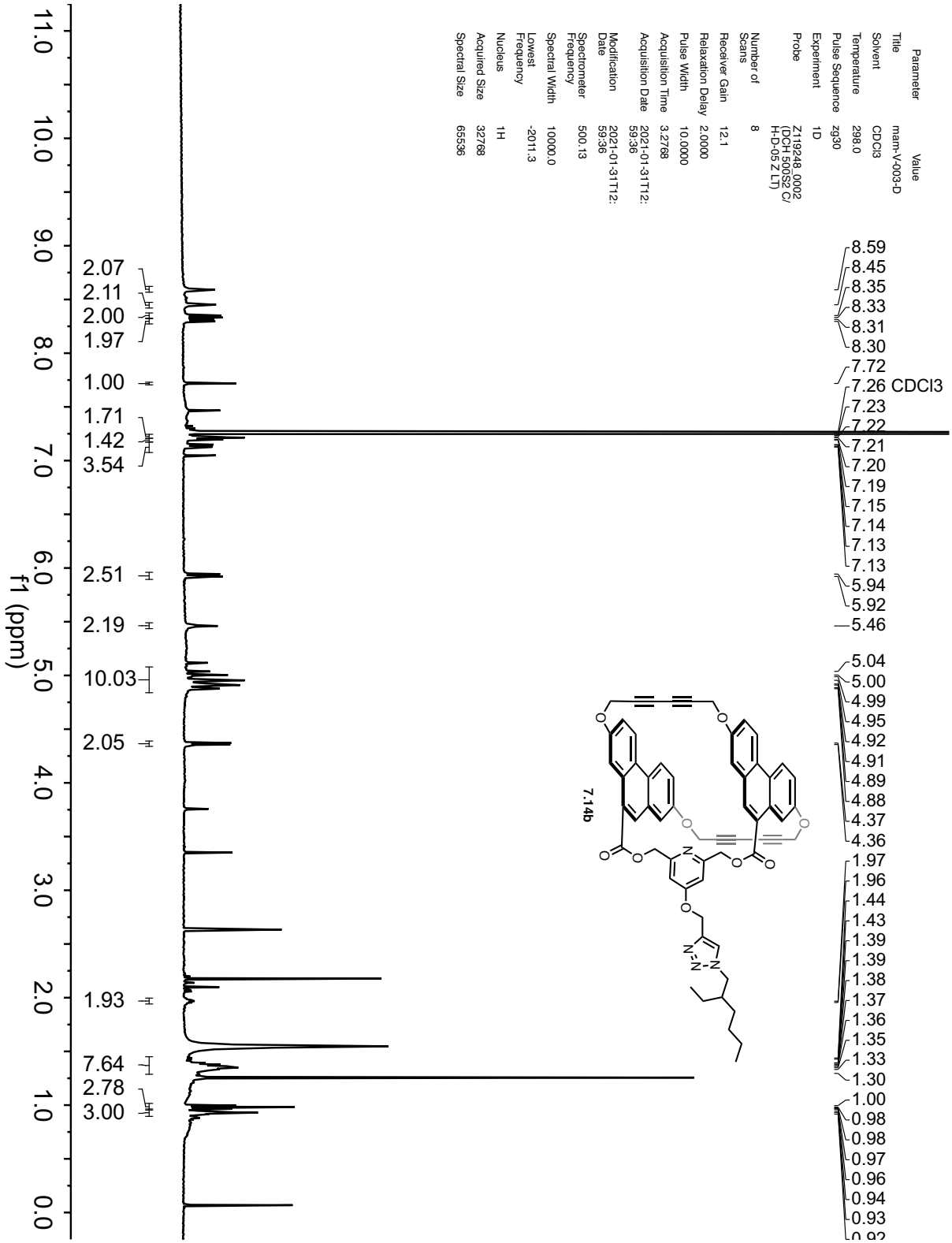
Parameter Value
Title mam-V-003-D
Solvent CDCl3
Temperature 298.0
Pulse Sequence zg30
Experiment 1D
Probe Z119248_0002 (DCH 500S2 C/H-D-05 Z LT)
Number of Scans 8
Receiver Gain 12.1
Relaxation Delay 2.0000
Pulse Width 10.0000
Acquisition Time 3.2768
Acquisition Date 2021-01-31T12:59:36
Modification Date 2021-01-31T12:59:36
Spectrometer Frequency 500.13
Spectral Width 10000.0
Lowest Frequency -2011.3
Nucleus 1H
Acquired Size 32768
Spectral Size 65536
8.59
8.45
8.35
8.33
8.31
8.30
7.72
7.26 CDCl3
7.23
7.22
7.21
7.20
7.19
7.15
7.14
7.13
7.13
5.94
5.92
5.46
5.04
5.00
4.99
4.95
4.92
4.91
4.89
4.88
4.37
4.36
1.97
1.96
1.44
1.43
1.39
1.39
1.38
1.37
1.36
1.35
1.33
1.30
1.00
0.98
0.98
0.97
0.96
0.94
0.93
0.92
7.14b
2.07
2.11
2.00
1.97
1.00
1.71
1.42
3.54
2.51
2.19
10.03
2.05
1.93
7.64
2.78
3.00
11.0
10.0
9.0
8.0
7.0
6.0
5.0
4.0
3.0
2.0
1.0
0.0
f1 (ppm)

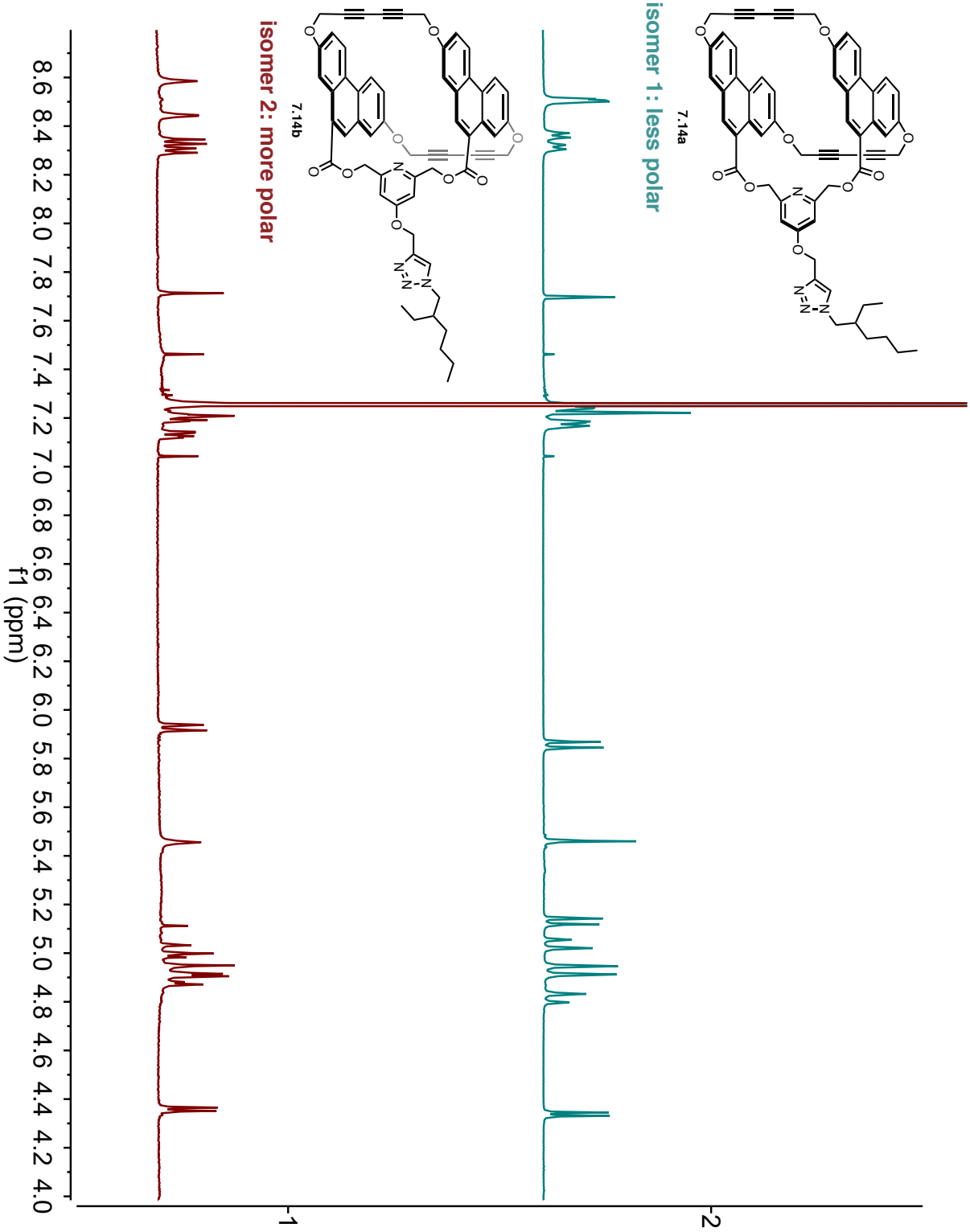
7.14a
isomer 1: less polar
7.14b
isomer 2: more polar
2
1
8.6 8.4 8.2 8.0 7.8 7.6 7.4 7.2 7.0 6.8 6.6 6.4 6.2 6.0 5.8 5.6 5.4 5.2 5.0 4.8 4.6 4.4 4.2 4.0
f1 (ppm)

Assignment of *O*-propargyl hosts **7.14** by comparison to NBu_2 hosts **6.2**

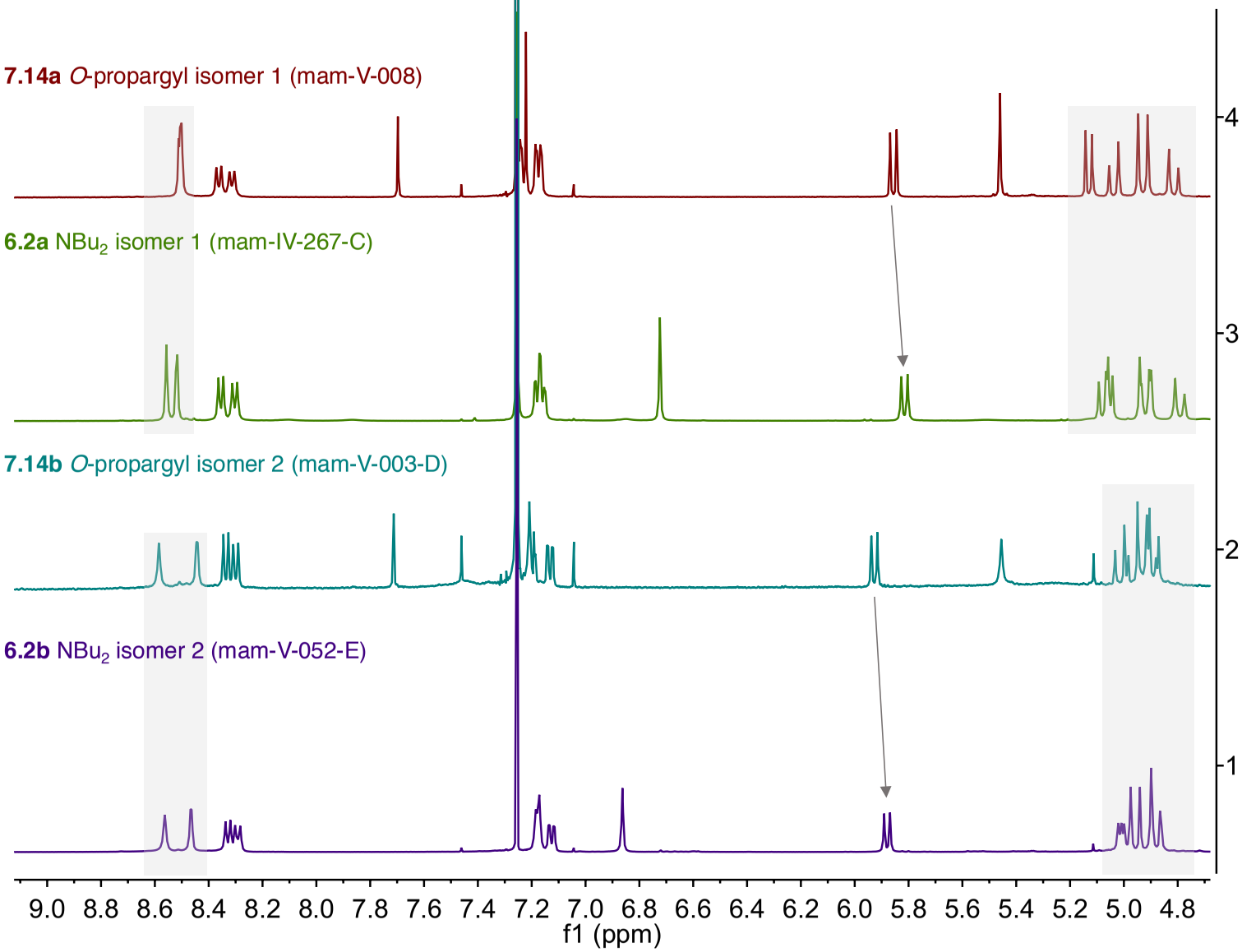

Parameter	Value
Title	Apr28-2021-sletten.31.fid
Solvent	CDCl3
Temperature	296.2
Pulse Sequence	zg30
Experiment	1D
Probe	5 mm PABBO BB/19F-1H/ D Z-GRD Z108618/ 0656
Number of Scans	8
Receiver Gain	155.8
Relaxation Delay	2.0000
Pulse Width	15.0000
Acquisition Time	3.2998
Acquisition Date	2021-04-28T13:22:00
Modification Date	2021-04-28T13:22:29
Spectrometer Frequency	400.13
Spectral Width	8012.8
Lowest Frequency	-1623.2
Nucleus	1H
Acquired Size	26441
Spectral Size	65536

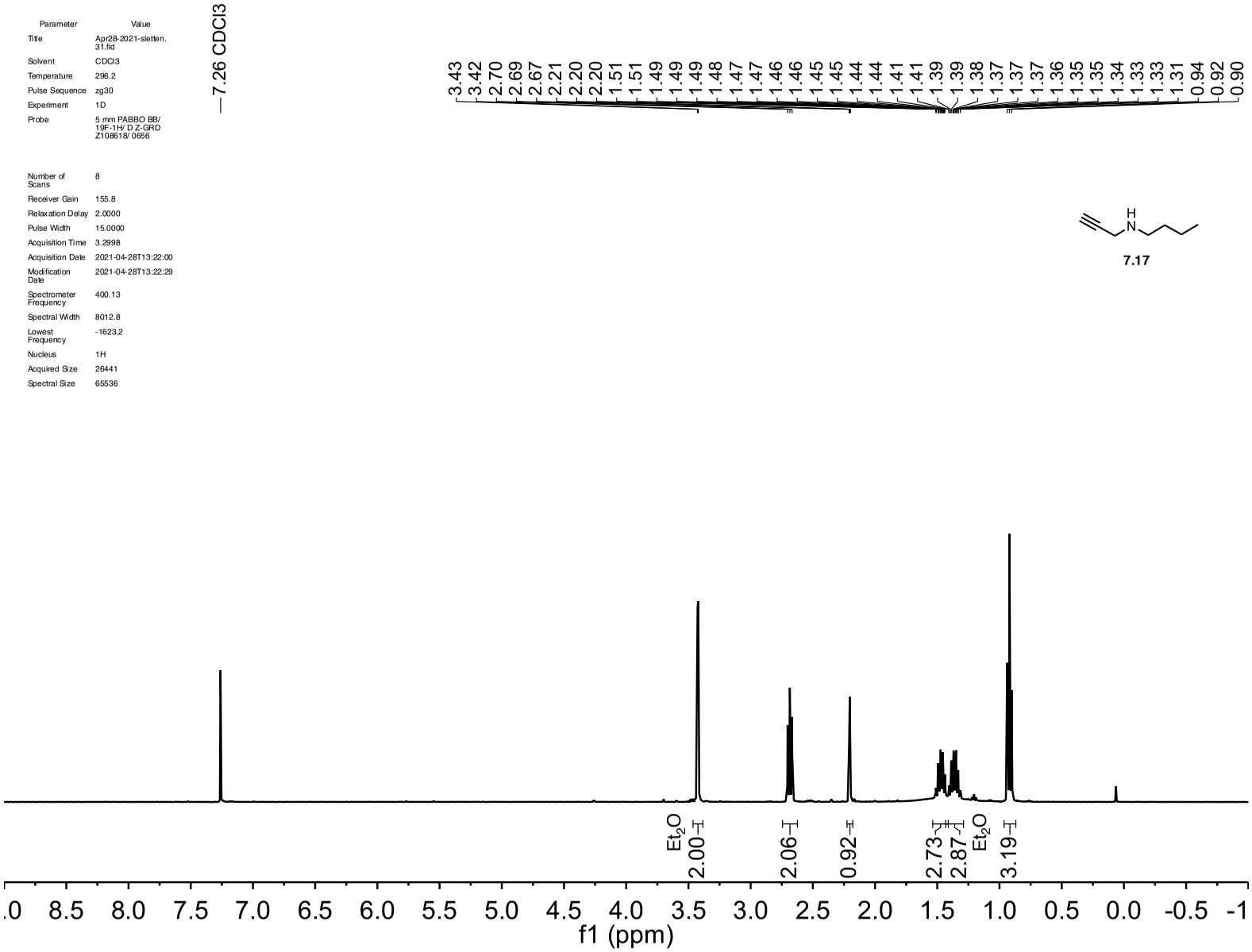

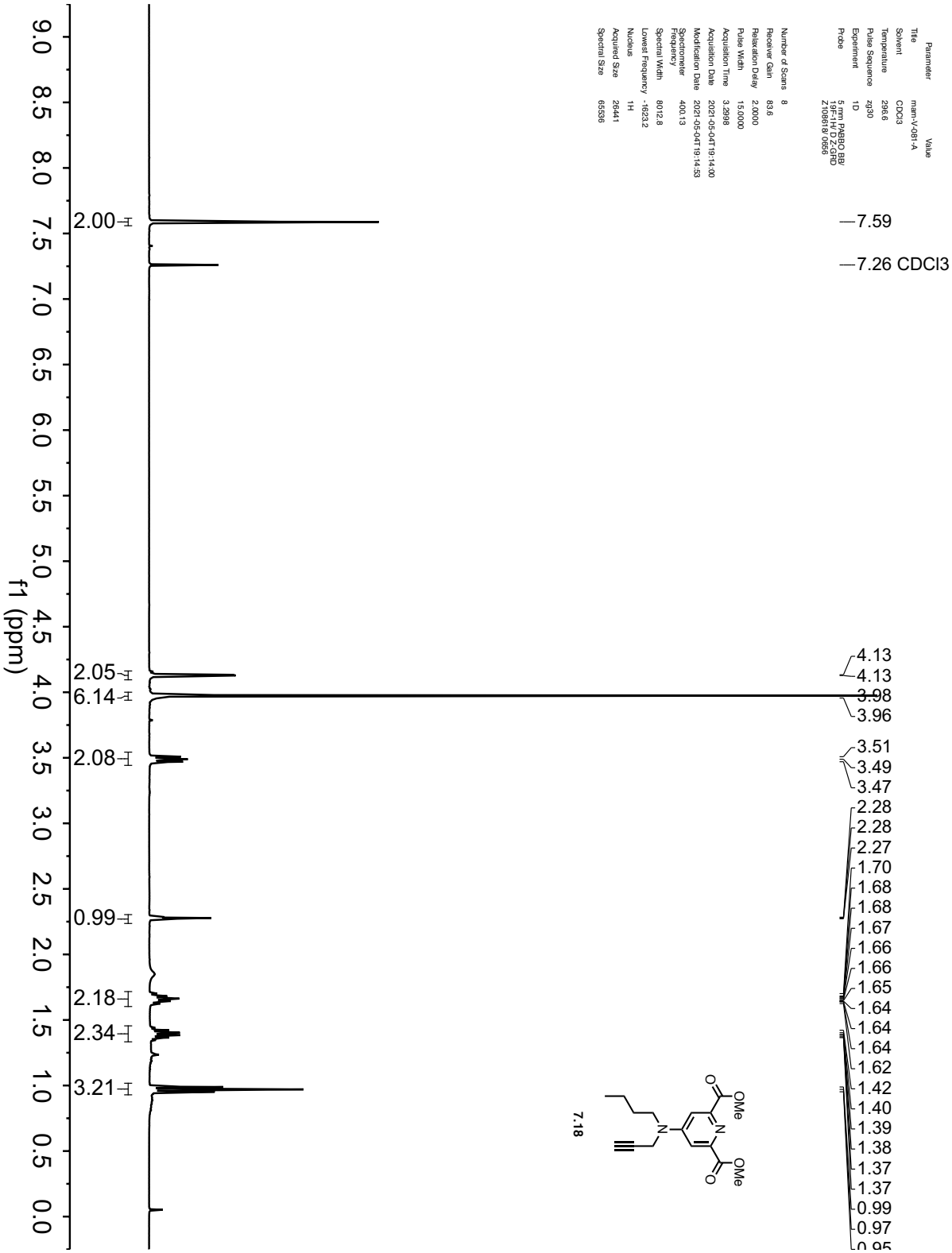
Parameter Value
Title mam-V-081-A
Solvent CDCl3
Temperature 296.6
Pulse Sequence zg30
Experiment 1D
Probe 5 mm PABBO BB/ 19F-1H D Z-GRD Z108618/ 0666
Number of Scans 8
Receiver Gain 83.6
Relaxation Delay 2.0000
Pulse Width 15.0000
Acquisition Time 3.2998
Acquisition Date 2021-05-04T19:14:00
Modification Date 2021-05-04T19:14:53
Spectrometer Frequency 400.13
Spectral Width 8012.8
Lowest Frequency -1623.2
Nucleus 1H
Acquired Size 26441
Spectral Size 65536
7.59
7.26 CDCl3
4.13
4.13
3.98
3.96
3.51
3.49
3.47
2.28
2.28
2.27
1.70
1.68
1.68
1.67
1.66
1.66
1.65
1.64
1.64
1.64
1.62
1.42
1.40
1.39
1.38
1.37
1.37
0.99
0.97
0.95
2.00
2.05
6.14
2.08
0.99
2.18
2.34
3.21
f1 (ppm)
9.0 8.5 8.0 7.5 7.0 6.5 6.0 5.5 5.0 4.5 4.0 3.5 3.0 2.5 2.0 1.5 1.0 0.5 0.0
OMe
OMe
N
N
O
O
7.18

Parameter	Value
Title	mam-V-081-A
Solvent	CDCl3
Temperature	297.5
Pulse Sequence	zgpg30
Experiment	1D
Probe	5 mm PABBO BB/ 19F-1H/ D Z-GRD Z108618/ 0656
Number of Scans	500
Receiver Gain	189.8
Relaxation Delay	2.0000
Pulse Width	10.0000
Acquisition Time	1.2976
Acquisition Date	2021-05-04T20:05:00
Modification Date	2021-05-04T20:05:57
Spectrometer Frequency	100.62
Spectral Width	25252.5
Lowest Frequency	-1045.9
Nucleus	13C
Acquired Size	32768
Spectral Size	65536

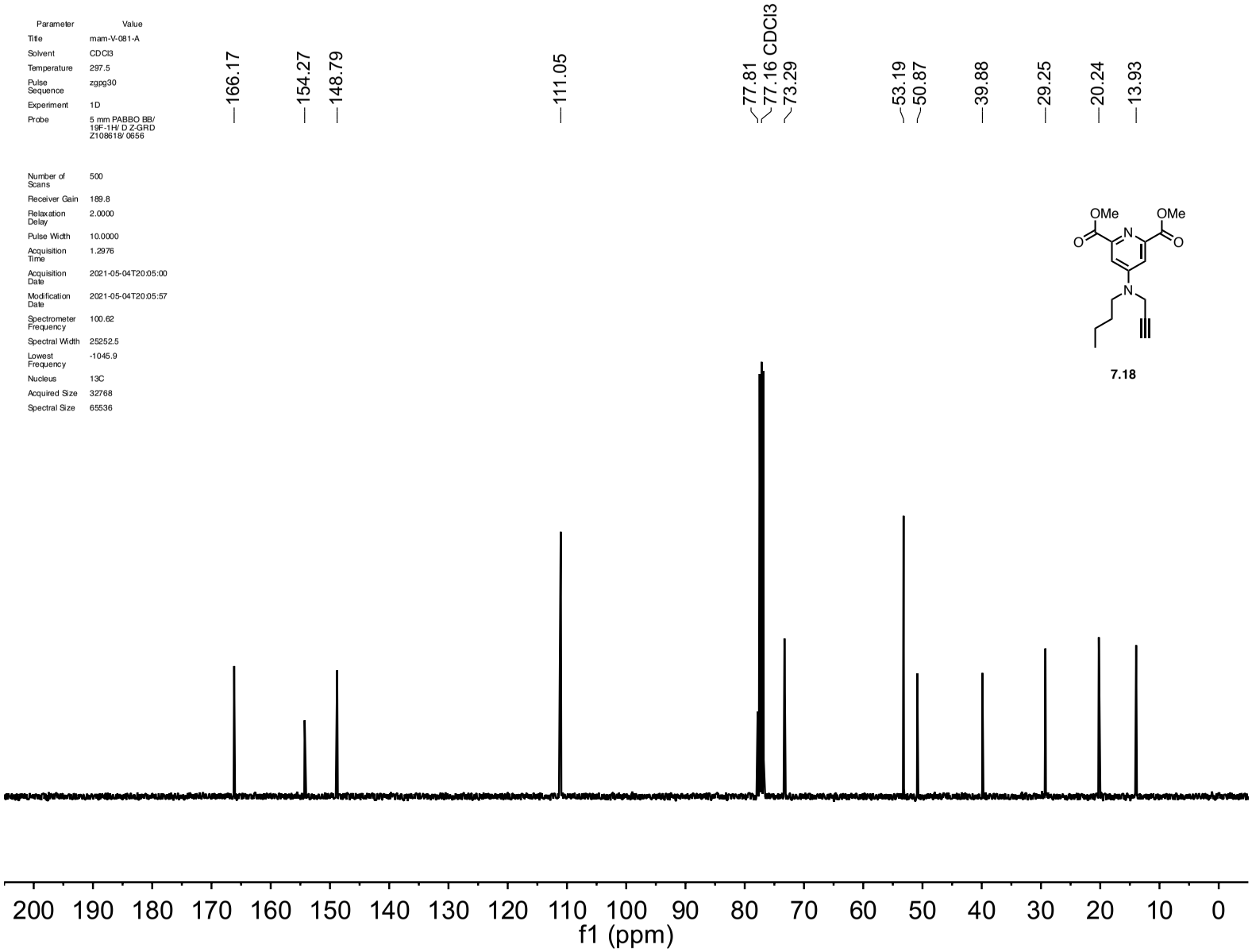

Parameter	Value
Solvent	CDCl3
Temperature	297.8
Pulse Sequence	zg30
Experiment	1D
Probe	5 mm PABBO BB/ 19F-1H/ D Z-GRD Z108618/ 0656
Number of Scans	8
Receiver Gain	189.8
Relaxation Delay	2.0000
Pulse Width	15.0000
Acquisition Time	3.2998
Acquisition Date	2021-07-27T17:54:00
Modification Date	2021-07-27T17:54:50
Spectrometer Frequency	400.13
Spectral Width	8012.8
Lowest Frequency	-1623.2
Nucleus	1H
Acquired Size	26441
Spectral Size	65536

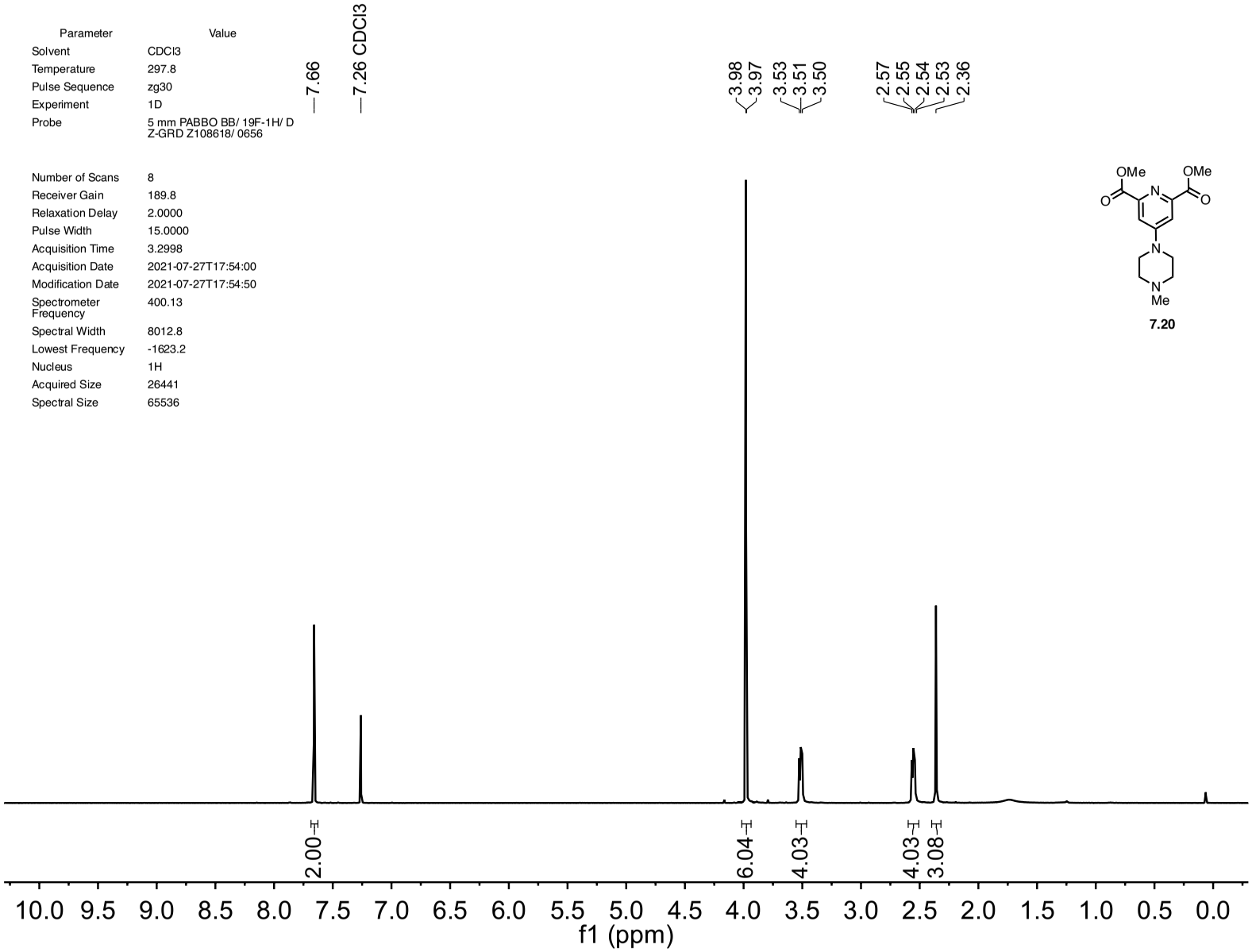

7.20

Parameter	Value
Solvent	CDCl3
Temperature	298.5
Pulse Sequence	zgpg30
Experiment	1D
Probe	5 mm PABBO BB/ 19F-1H/ D Z-GRD Z108618/ 0656
Number of Scans	550
Receiver Gain	189.8
Relaxation Delay	2.0000
Pulse Width	10.0000
Acquisition Time	1.2976
Acquisition Date	2021-07-27T18:27:00
Modification Date	2021-07-27T18:27:05
Spectrometer Frequency	100.62
Spectral Width	25252.5
Lowest Frequency	-1043.0
Nucleus	13C
Acquired Size	32768
Spectral Size	65536

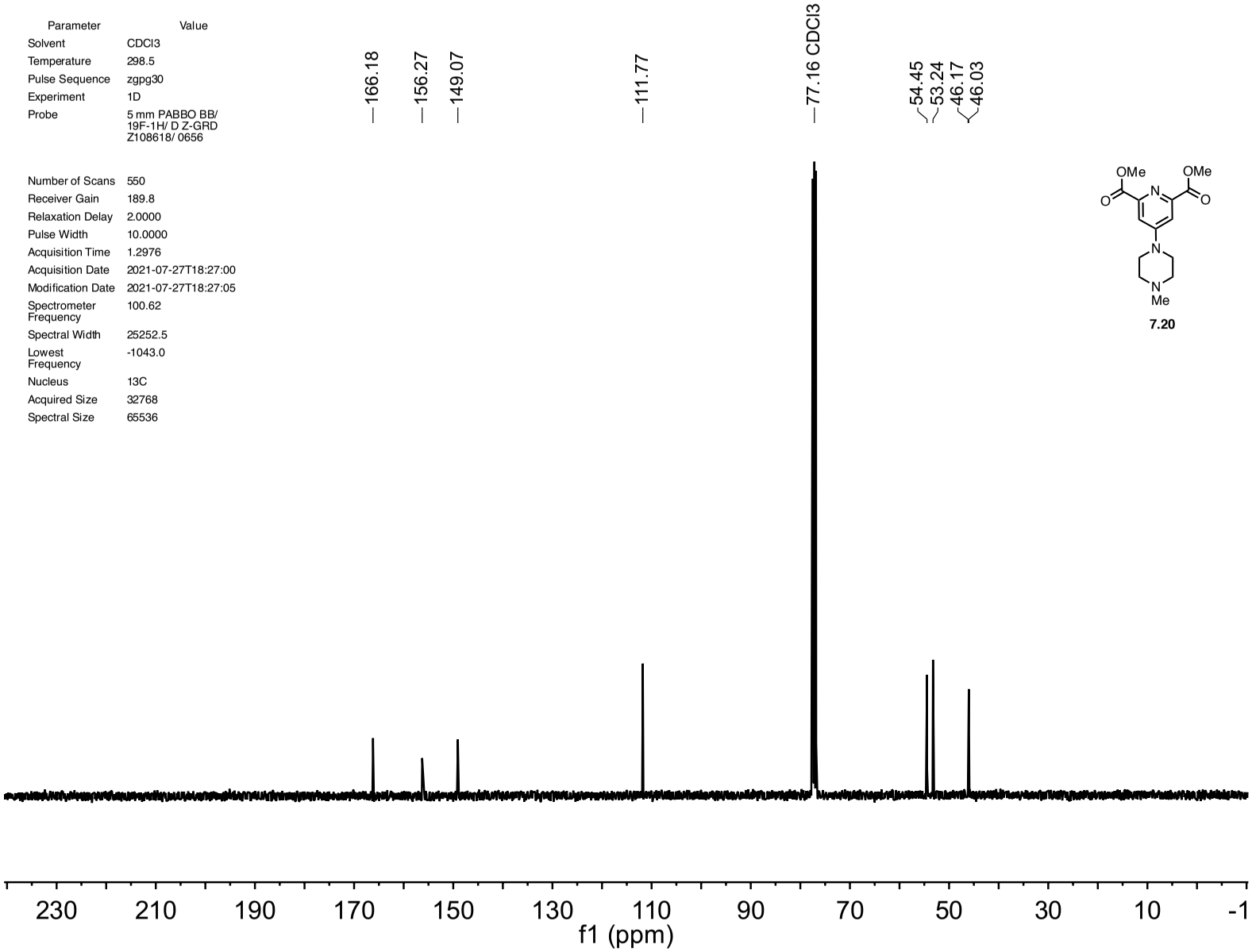

7.20

Parameter	Value
Solvent	CDCl3
Temperature	300.0
Pulse Sequence	zg30
Experiment	1D
Probe	5 mm PABBO BB-1H/ D Z-GRD Z862701/ 0016
Number of Scans	16
Receiver Gain	574.7
Relaxation Delay	2.0000
Pulse Width	15.0000
Acquisition Time	5.4658
Acquisition Date	2021-08-25T09:56:00
Modification Date	2021-08-25T09:56:46
Spectrometer Frequency	300.13
Spectral Width	5995.2
Lowest Frequency	-1209.7
Nucleus	1H
Acquired Size	32768
Spectral Size	65536

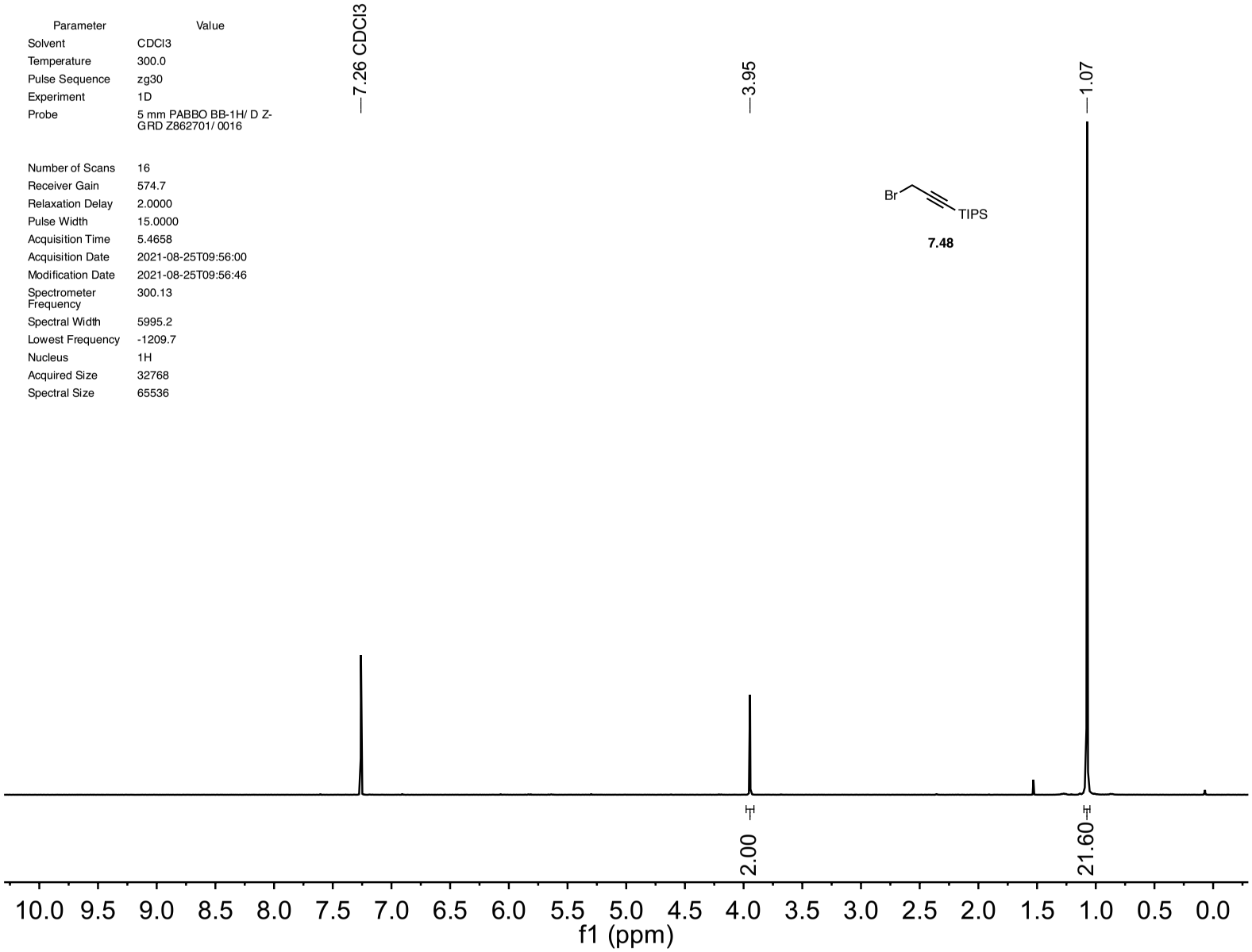

Parameter	Value
Solvent	CDCl3
Temperature	298.0
Pulse Sequence	zg30
Experiment	1D
Probe	Z119248_0002 (DCH 500S2 C/ H-D-05 Z LT)
Number of Scans	8
Receiver Gain	12.1
Relaxation Delay	2.0000
Pulse Width	10.0000
Acquisition Time	3.2768
Acquisition Date	2021-08-11T11:04:24
Modification Date	2021-08-11T11:04:25
Spectrometer Frequency	500.13
Spectral Width	10000.0
Lowest Frequency	-2011.3
Nucleus	1H
Acquired Size	32768
Spectral Size	65536

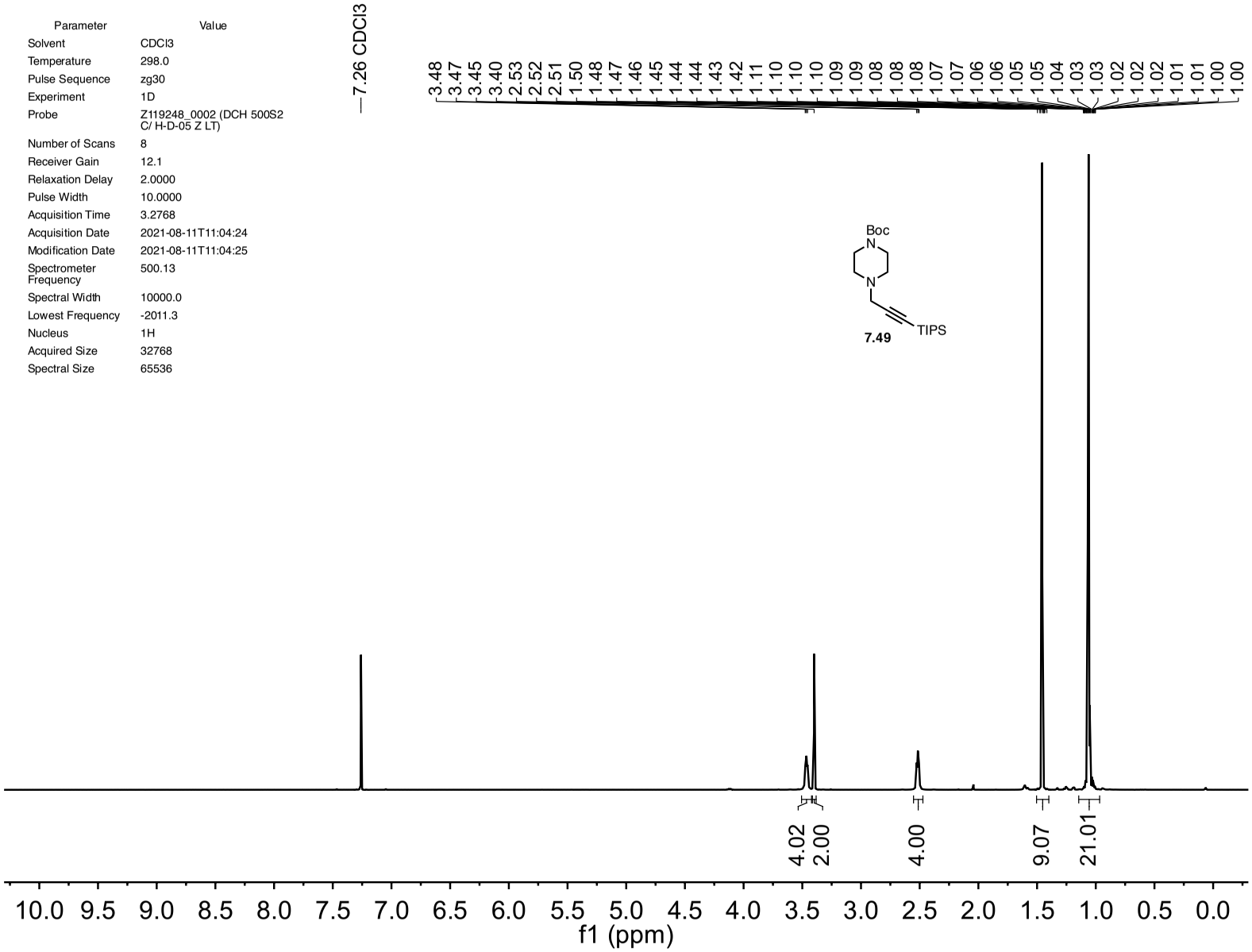

Parameter	Value
Solvent	CDCl3
Temperature	297.8
Pulse Sequence	zgpg30
Experiment	1D
Probe	5 mm PABBO BB/ 19F-1H/ D Z-GRD Z108618/ 0656
Number of Scans	500
Receiver Gain	189.8
Relaxation Delay	2.0000
Pulse Width	10.0000
Acquisition Time	1.2976
Acquisition Date	2021-08-11T11:35:00
Modification Date	2021-08-11T11:36:00
Spectrometer Frequency	100.62
Spectral Width	25252.5
Lowest Frequency	-1042.4
Nucleus	13C
Acquired Size	32768
Spectral Size	65536

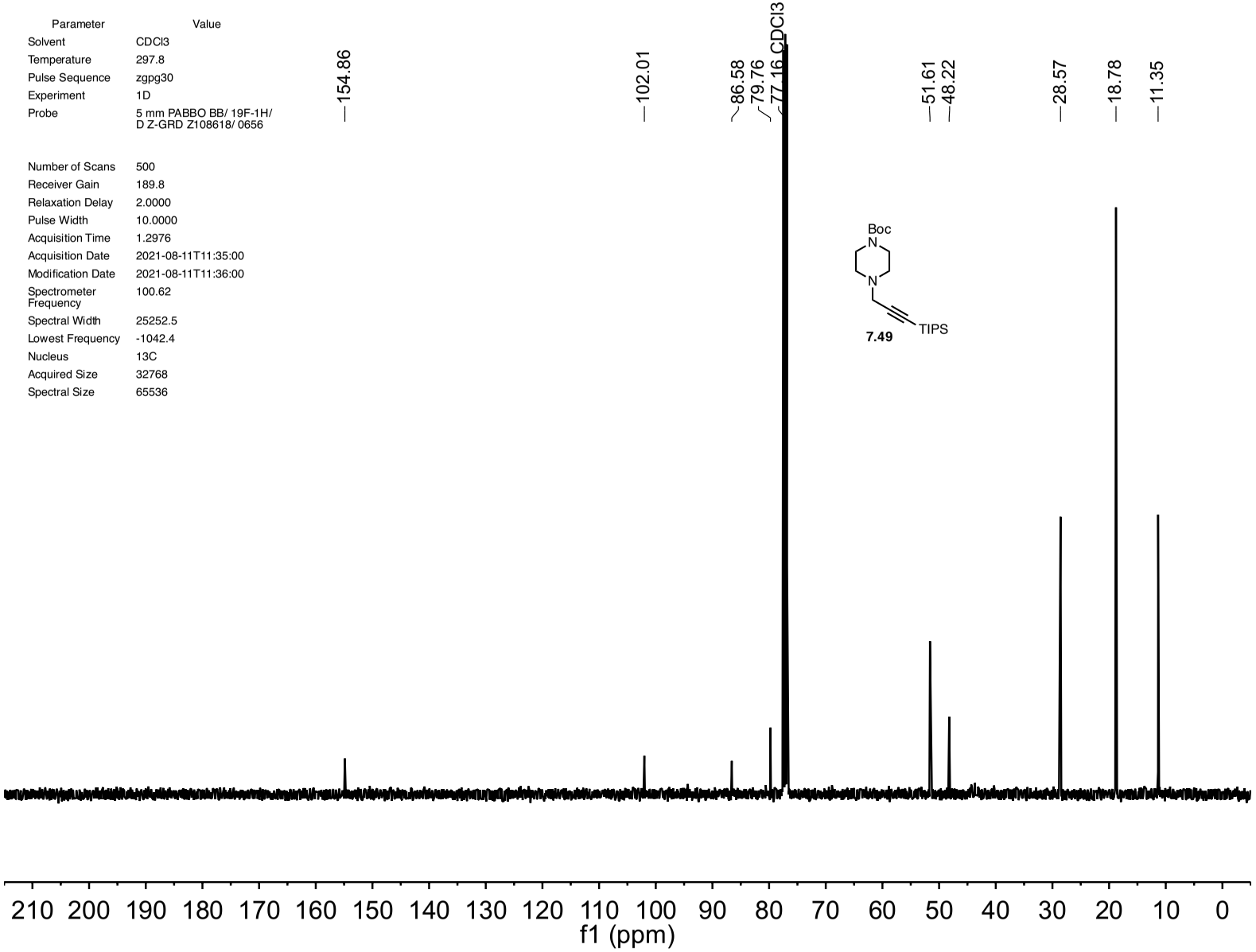

Parameter	Value
Solvent	CDCl3
Temperature	297.0
Pulse Sequence	zg30
Experiment	1D
Probe	5 mm PABBO BB/ 19F-1H/ D Z-GRD Z108618/ 0656
Number of Scans	32
Receiver Gain	155.8
Relaxation Delay	2.0000
Pulse Width	15.0000
Acquisition Time	3.2998
Acquisition Date	2021-11-07T15:21:00
Modification Date	2021-11-07T15:21:14
Spectrometer Frequency	400.13
Spectral Width	8012.8
Lowest Frequency	-1623.2
Nucleus	1H
Acquired Size	26441
Spectral Size	65536

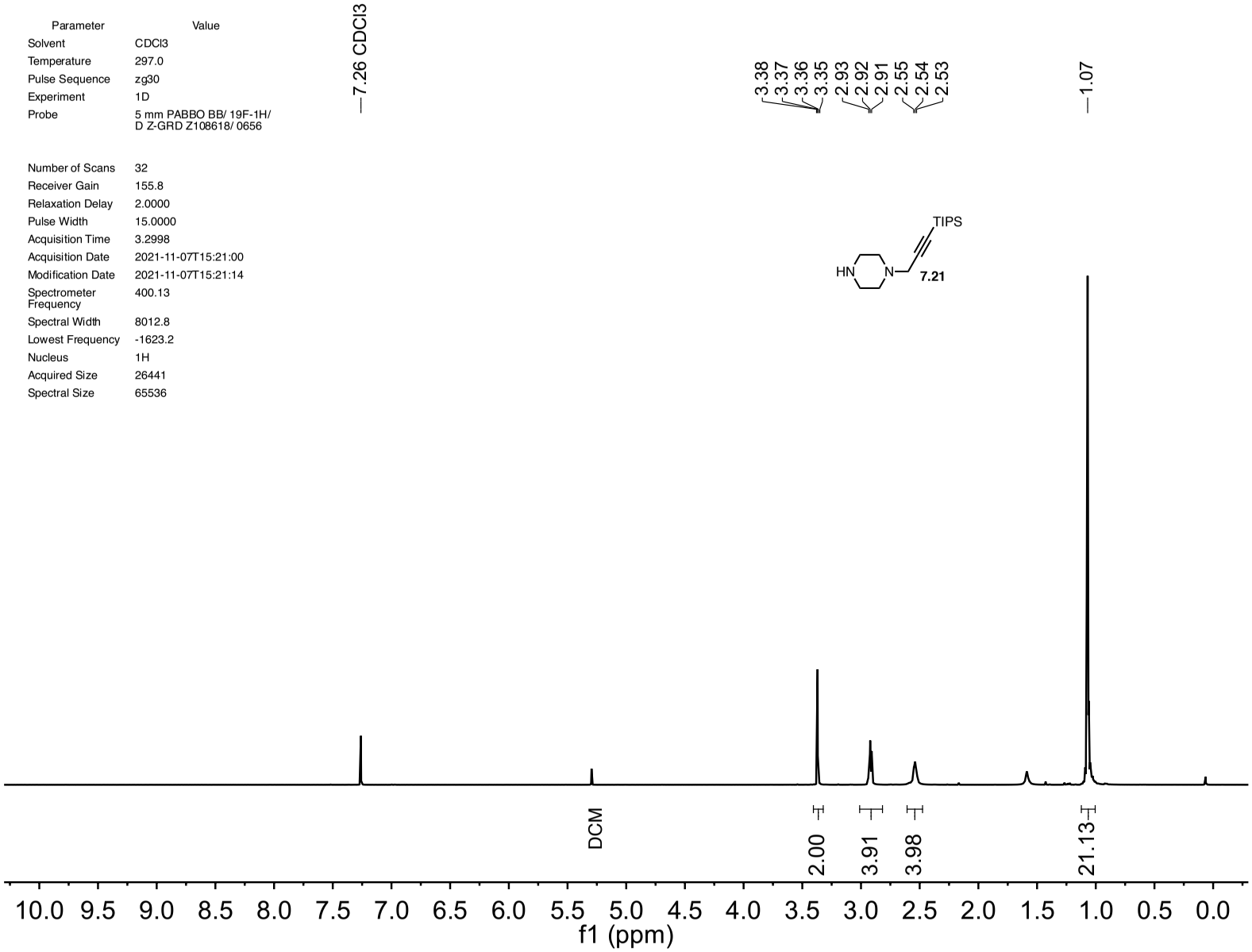

Parameter	Value
Solvent	CDCl3
Temperature	297.4
Pulse Sequence	zgpg30
Experiment	1D
Probe	5 mm PABBO BB/ 19F-1H/ D Z-GRD Z108618/ 0656
Number of Scans	550
Receiver Gain	189.8
Relaxation Delay	2.0000
Pulse Width	10.0000
Acquisition Time	1.2976
Acquisition Date	2021-11-08T19:54:00
Modification Date	2021-11-08T19:54:55
Spectrometer Frequency	100.62
Spectral Width	25252.5
Lowest Frequency	-1042.9
Nucleus	13C
Acquired Size	32768
Spectral Size	65536

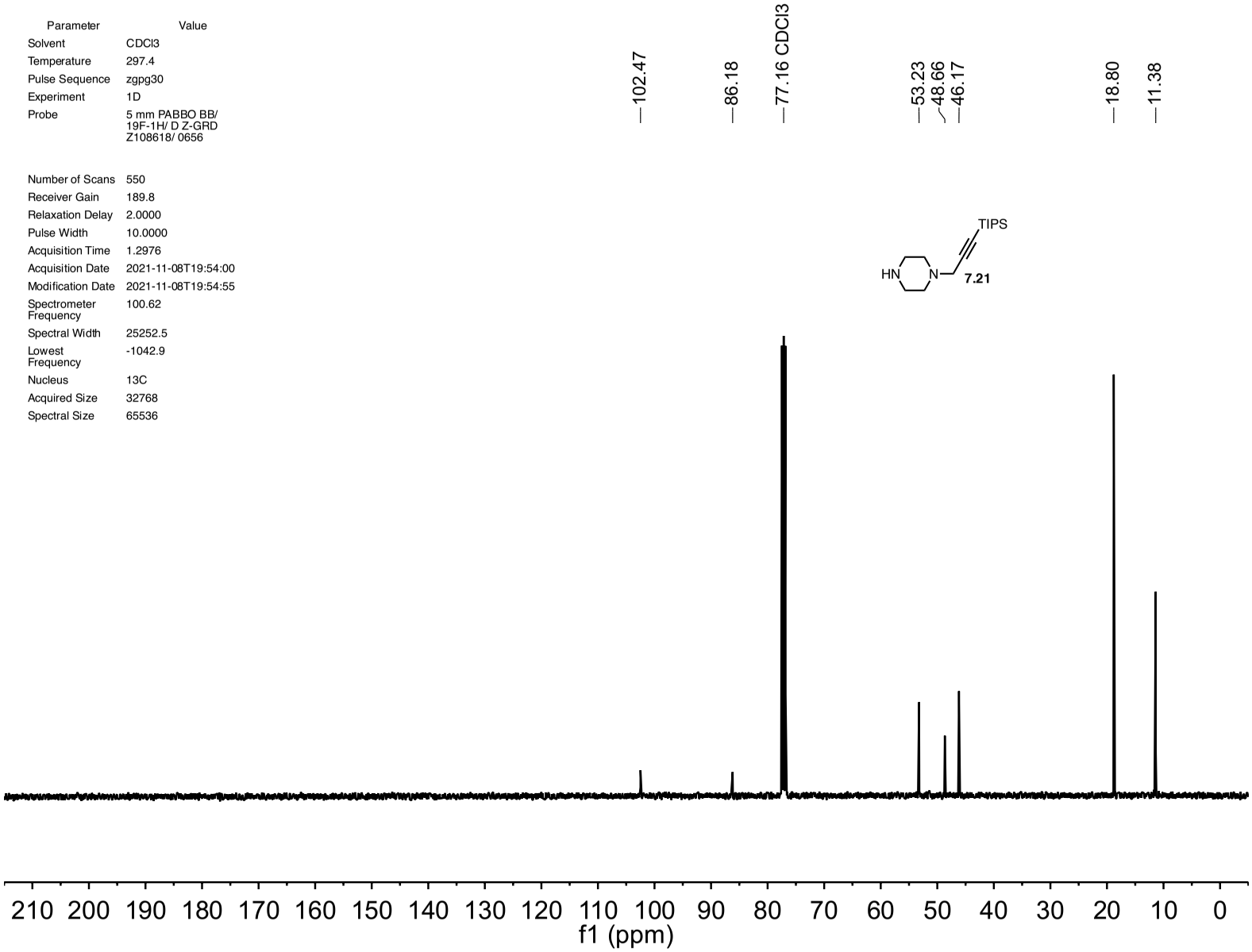

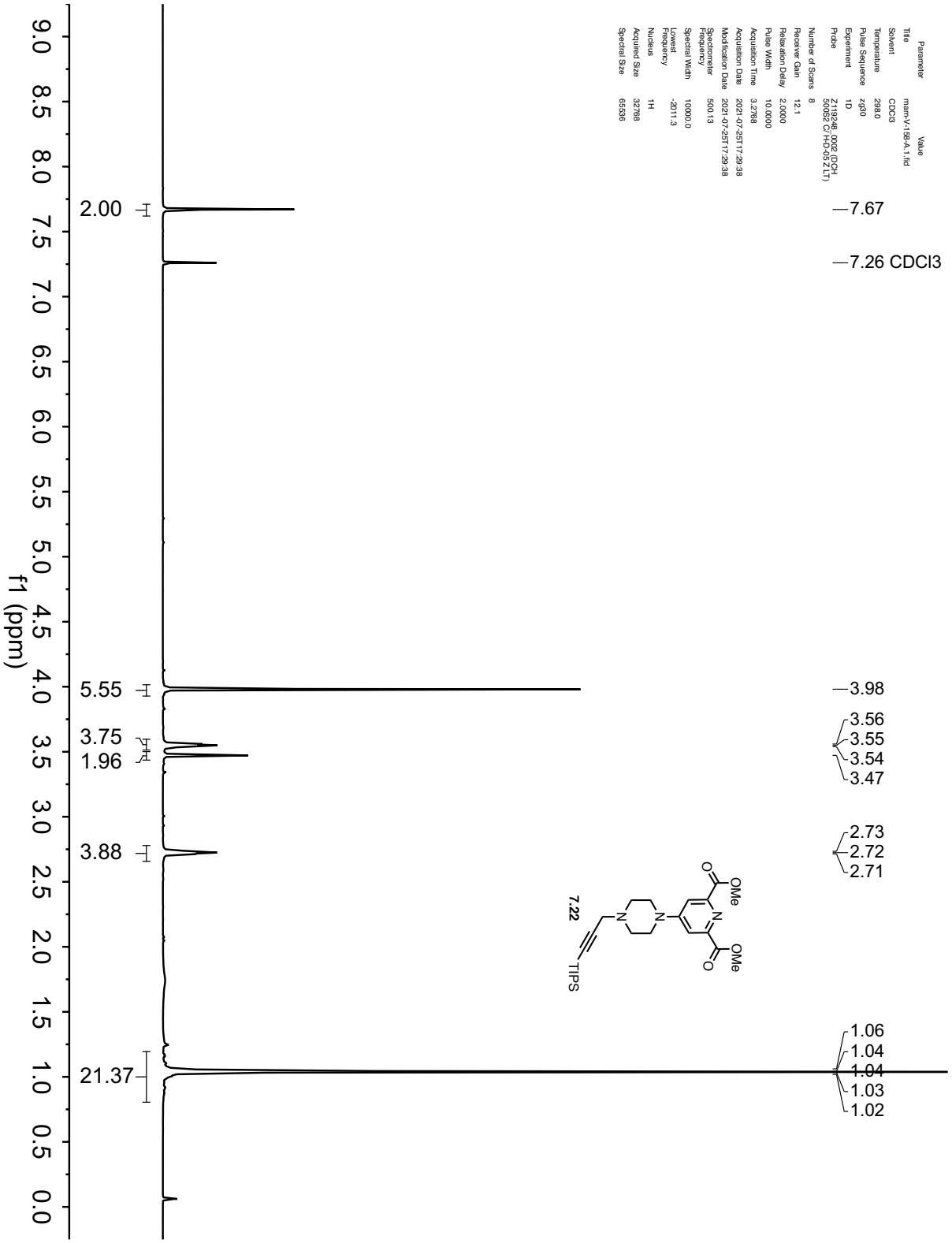
Parameter Value
Title main-V-158-A.1.fid
Solvent CDCl3
Temperature 298.0
Pulse Sequence zg30
Experiment 1D
Probe Z119248_0002 (DCH 5005S2 C/ H-D-05 Z LT)
Number of Scans 8
Receiver Gain 12.1
Relaxation Delay 2.0000
Pulse Width 10.0000
Acquisition Time 3.2768
Acquisition Date 2021-07-25T17:29:38
Modification Date 2021-07-25T17:29:38
Spectrometer Frequency 500.13
Spectral Width 10000.0
Lowest Frequency -2011.3
Nucleus 1H
Acquired Size 32768
Spectral Size 65536
7.67
7.26 CDCl3
3.98
3.56
3.55
3.54
3.47
2.73
2.72
2.71
1.06
1.04
1.04
1.03
1.02
2.00
5.55
3.75
1.96
3.88
21.37
f1 (ppm)
9.0 8.5 8.0 7.5 7.0 6.5 6.0 5.5 5.0 4.5 4.0 3.5 3.0 2.5 2.0 1.5 1.0 0.5 0.0
7:22
OMe
OMe
TIPS

Parameter	Value
Title	mam-V-158-A
Solvent	CDCl3
Temperature	299.6
Pulse Sequence	zgpg30
Experiment	1D
Probe	5 mm PABBO BB/ 19F-1H/ D Z-GRD Z108618/ 0656
Number of Scans	550
Receiver Gain	189.8
Relaxation Delay	2.0000
Pulse Width	10.0000
Acquisition Time	1.2976
Acquisition Date	2021-07-26T14:25:00
Modification Date	2021-07-26T14:25:34
Spectrometer Frequency	100.62
Spectral Width	25252.5
Lowest Frequency	-1043.0
Nucleus	13C
Acquired Size	32768
Spectral Size	65536

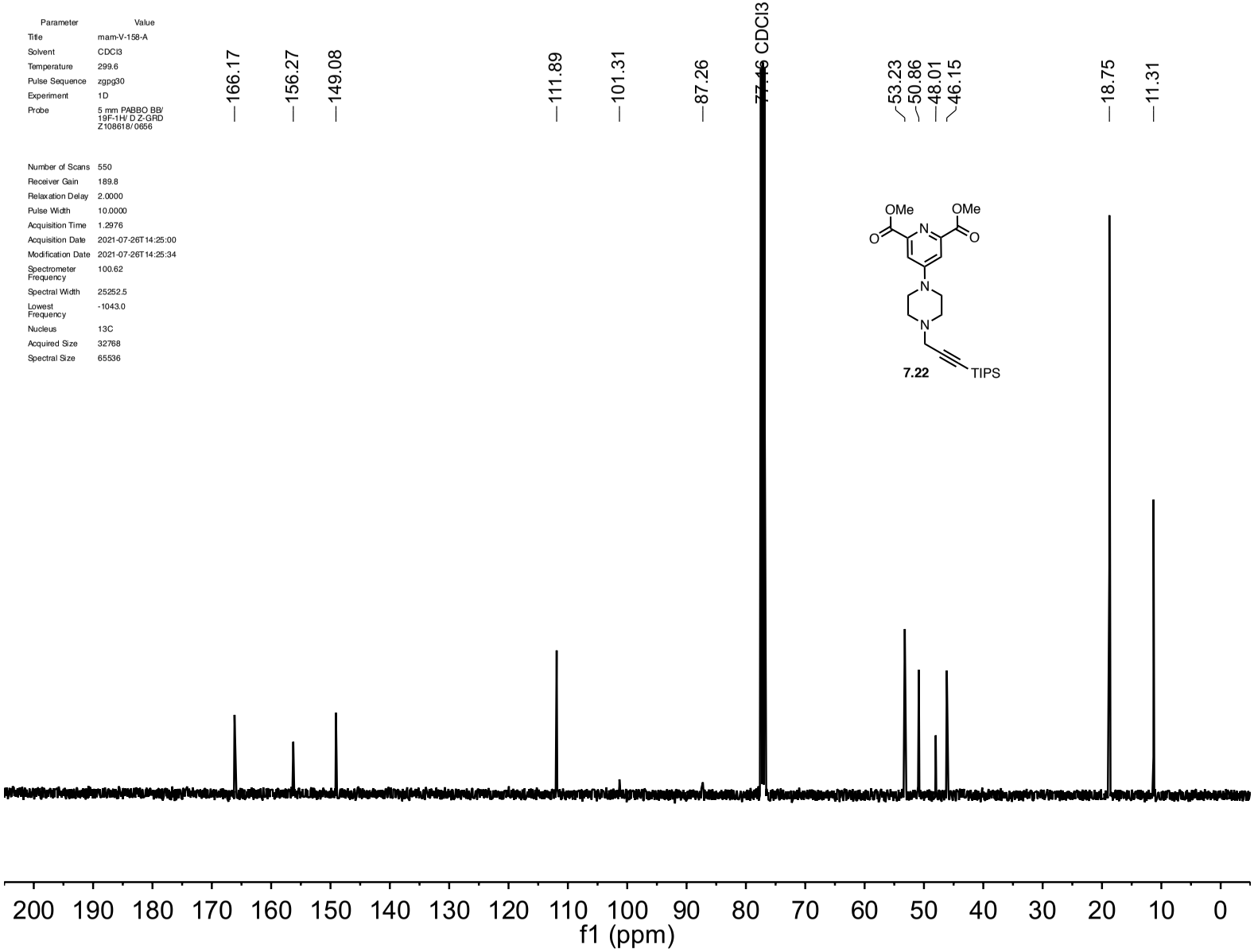

Parameter	Value
Solvent	CDCl3
Temperature	297.4
Pulse Sequence	zg30
Experiment	1D
Probe	5 mm PABBO BB/ 19F-1H/ D Z-GRD Z108618/ 0656
Number of Scans	16
Receiver Gain	155.8
Relaxation Delay	2.0000
Pulse Width	15.0000
Acquisition Time	3.2998
Acquisition Date	2021-09-23T21:03:00
Modification Date	2021-09-23T21:03:32
Spectrometer Frequency	400.13
Spectral Width	8012.8
Lowest Frequency	-1623.2
Nucleus	1H
Acquired Size	26441
Spectral Size	65536

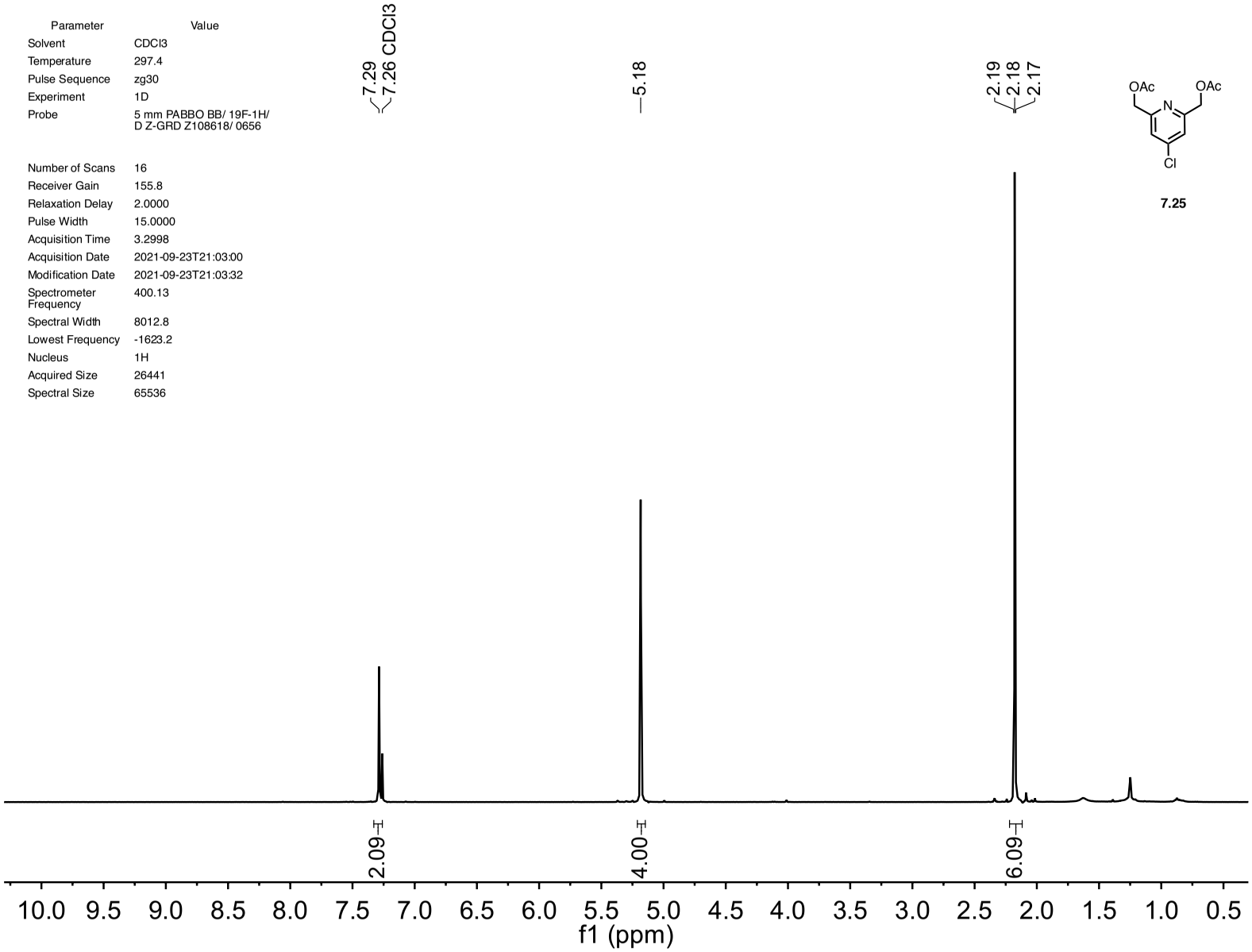

Parameter	Value
Solvent	CDCl3
Temperature	298.3
Pulse Sequence	zgpg30
Experiment	1D
Probe	5 mm PABBO BB/ 19F-1H/ D Z-GRD Z108618/ 0656
Number of Scans	500
Receiver Gain	189.8
Relaxation Delay	2.0000
Pulse Width	10.0000
Acquisition Time	1.2976
Acquisition Date	2021-09-23T21:32:00
Modification Date	2021-09-23T21:32:45
Spectrometer Frequency	100.62
Spectral Width	25252.5
Lowest	-1043.1

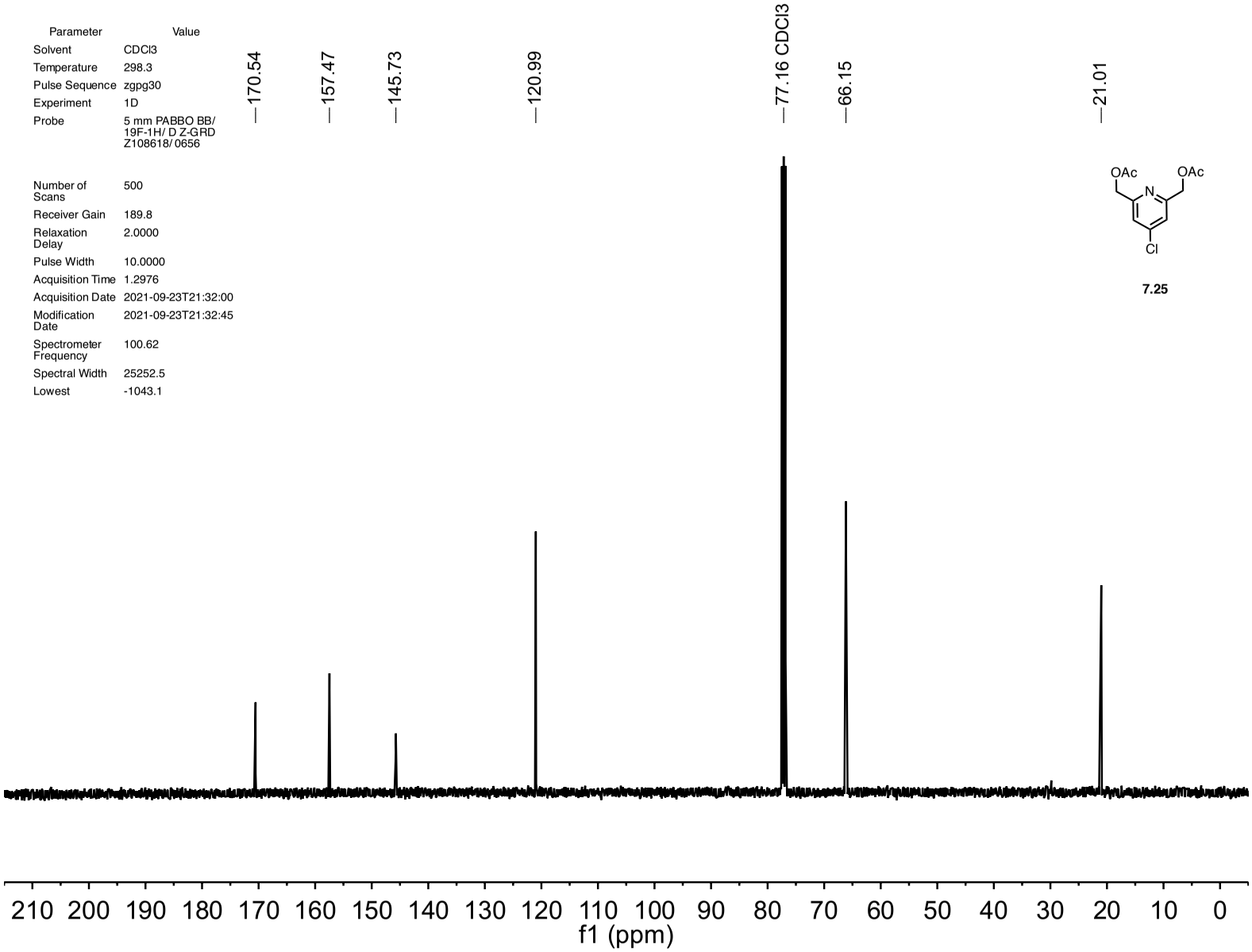

Parameter	Value
Solvent	CDCl3
Temperature	296.9
Pulse Sequence	zg30
Experiment	1D
Probe	5 mm PABBO BB/ 19F-1H/ D Z-GRD Z108618/ 0656
Number of Scans	32
Receiver Gain	189.8
Relaxation Delay	2.0000
Pulse Width	15.0000
Acquisition Time	3.2998
Acquisition Date	2021-10-07T10:51:00
Modification Date	2021-10-07T10:51:10
Spectrometer Frequency	400.13
Spectral Width	8012.8
Lowest Frequency	-1623.2
Nucleus	1H
Acquired Size	26441
Spectral Size	65536

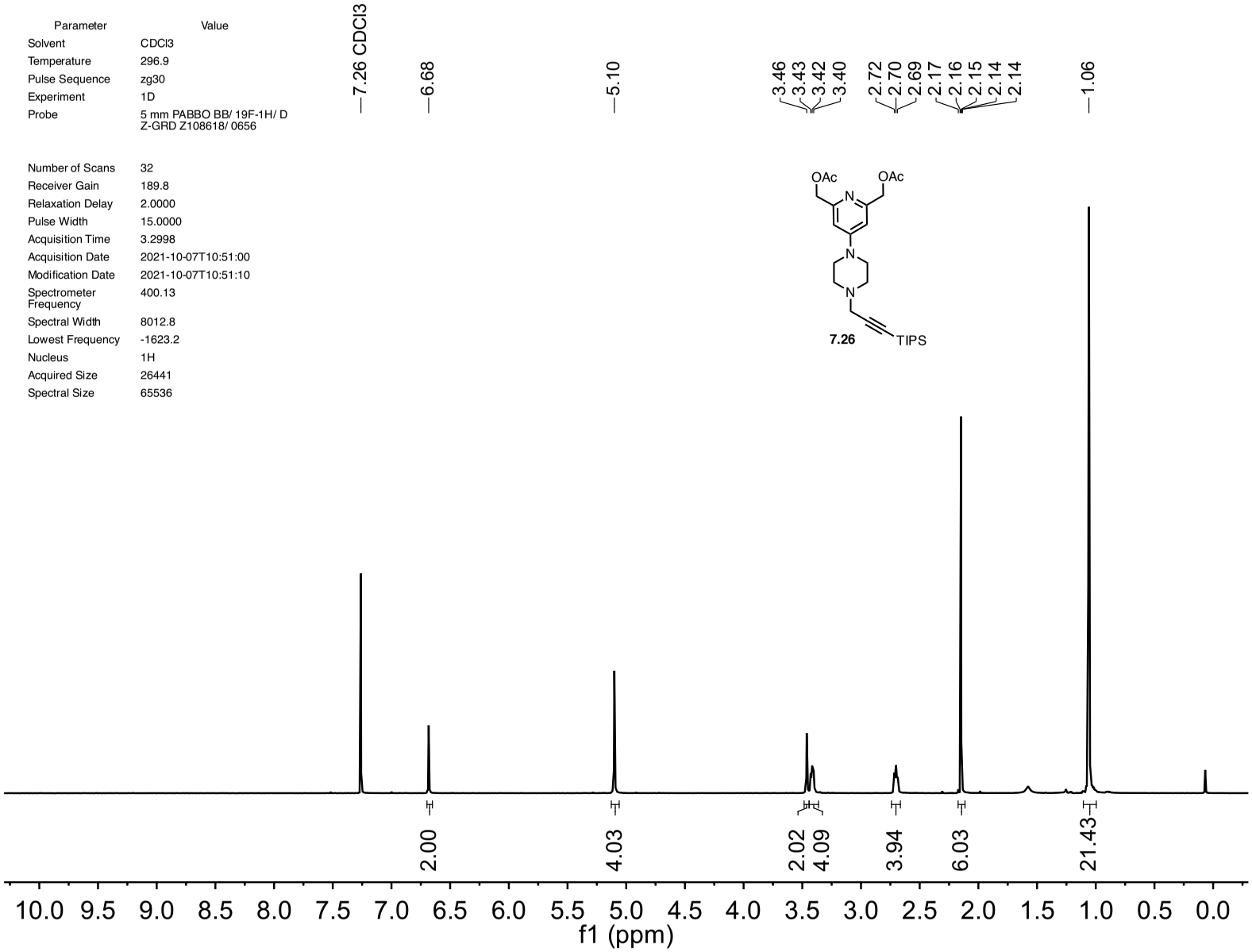

Parameter	Value
Solvent	CDCl3
Temperature	298.0
Pulse Sequence	zgpg30
Experiment	1D
Probe	5 mm PABBO BB/ 19F-1H/ D Z-GRD Z108618/ 0656

Number of Scans	500
Receiver Gain	189.8
Relaxation Delay	2.0000
Pulse Width	10.0000
Acquisition Time	1.2976
Acquisition Date	2021-10-02T20:08:00
Modification Date	2021-10-02T20:08:18
Spectrometer Frequency	100.62
Spectral Width	25252.5
Lowest Frequency	-1044.4
Nucleus	13C
Acquired Size	32768
Spectral Size	65536

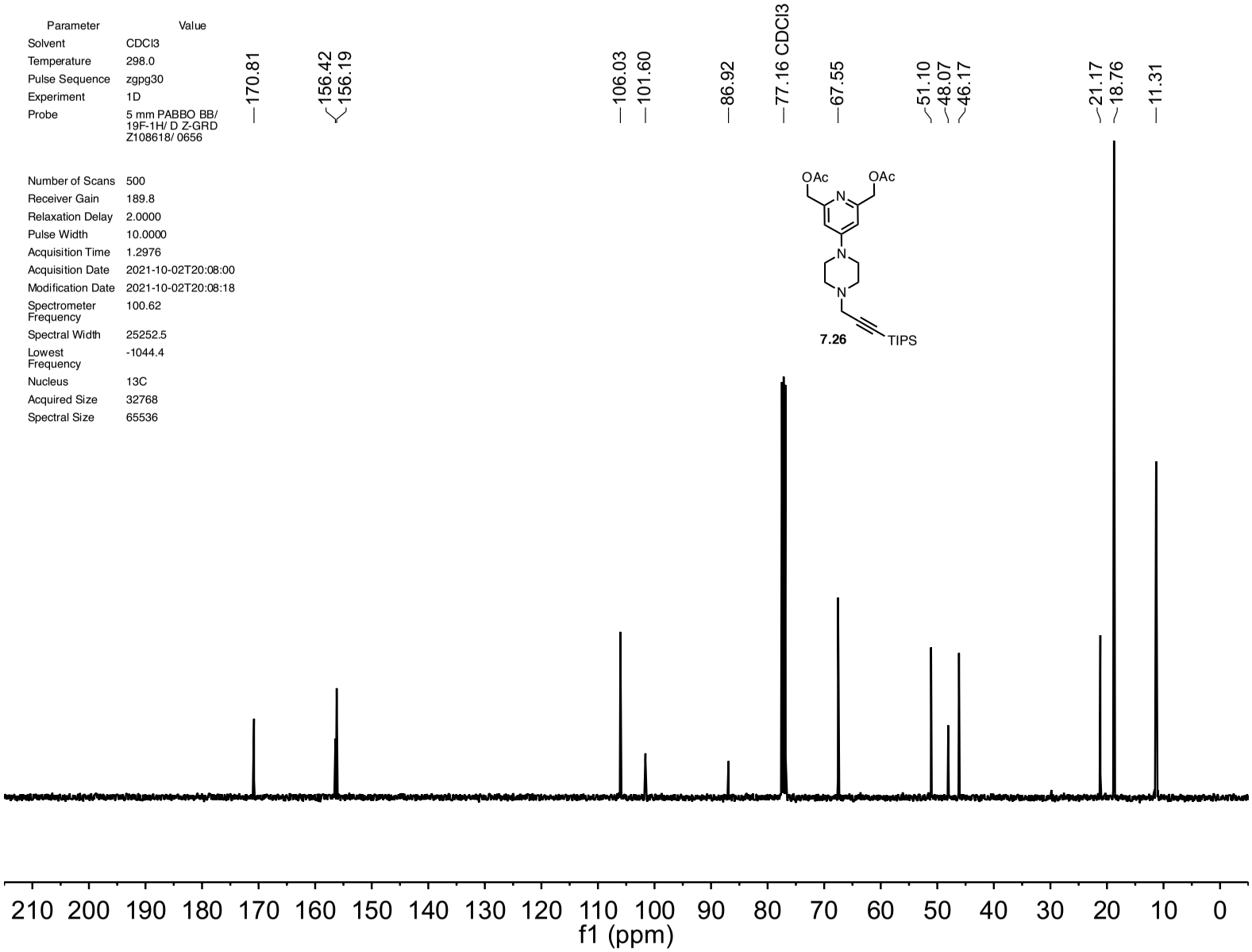

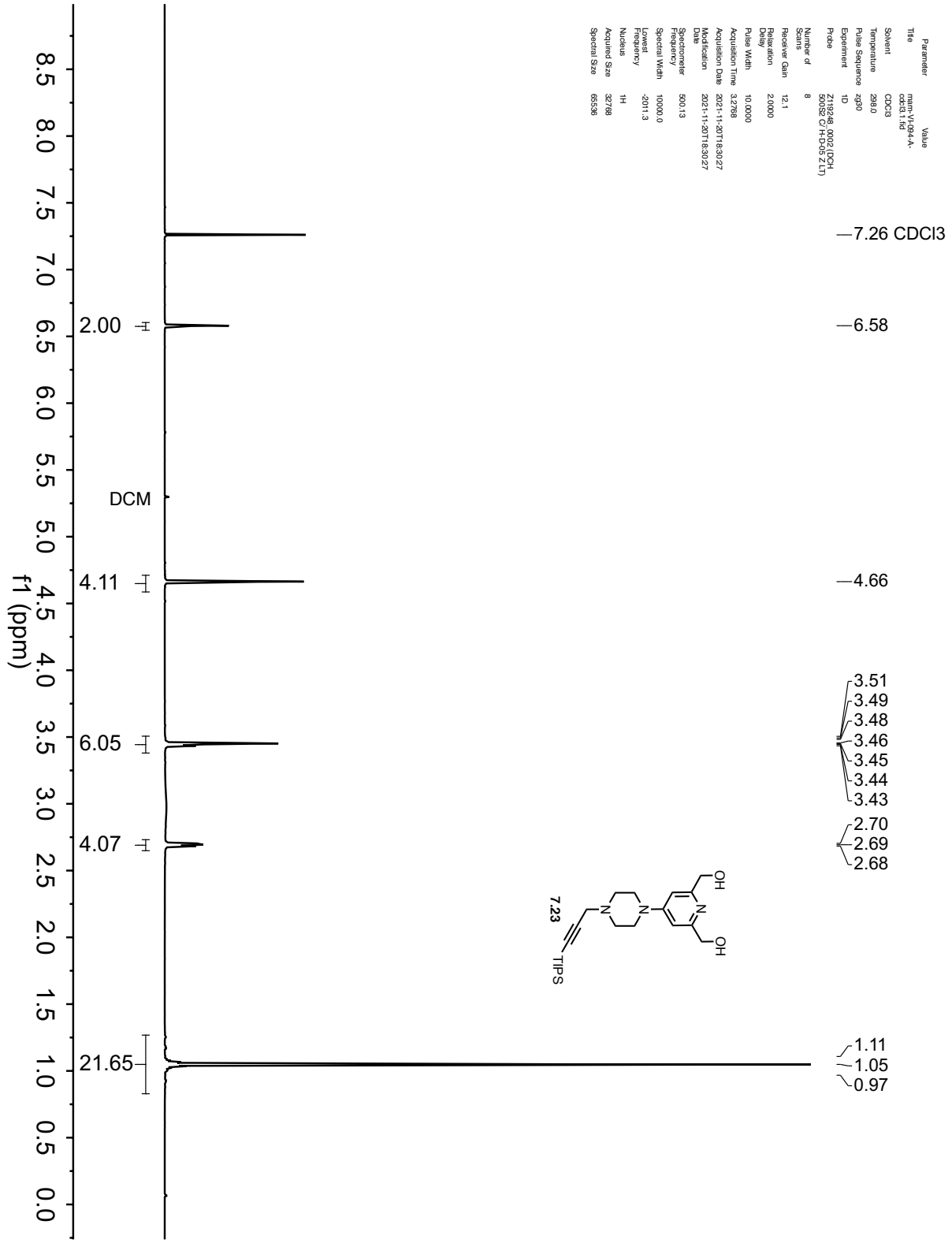
Parameter Value
Title mpm-VI-094-A-cdcl3-1.fid
Solvent CDCl3
Temperature 298.0
Pulse Sequence zg30
Experiment 1D
Probe Z119248_0002 (DCH 500S2 C/ H-D-05 Z Lt)
Number of Scans 8
Receiver Gain 12.1
Relaxation Delay 2.0000
Pulse Width 10.0000
Acquisition Time 3.2768
Acquisition Date 2021-11-20T18:30:27
Modification Date 2021-11-20T18:30:27
Spectrometer Frequency 500.13
Spectral Width 10000.0
Lowest Frequency -2011.3
Nucleus 1H
Acquired Size 32768
Spectral Size 65536
7.26 CDCl3
6.58
4.66
3.51
3.49
3.48
3.46
3.45
3.44
3.43
2.70
2.69
2.68
1.11
1.05
0.97
2.00
DCM
4.11
6.05
4.07
21.65
f1 (ppm)
7.23
TIPS
OH
OH
N
N
N

Parameter	Value
Title	mam-VI-094-A-cdcl3.13.fid
Solvent	CDCl3
Temperature	298.0
Pulse Sequence	zgpg30
Experiment	1D
Probe	Z119248_0002 (DCH 500S2 C/ H-D-05 Z LT)
Number of Scans	200
Receiver Gain	204.5
Relaxation Delay	2.0000
Pulse Width	10.5000
Acquisition Time	1.0486
Acquisition Date	2021-11-20T18:51:23
Modification Date	2021-11-20T18:51:24
Spectrometer Frequency	125.77
Spectral Width	31250.0
Lowest Frequency	-1144.9
Nucleus	13C
Acquired Size	32768
Spectral Size	65536

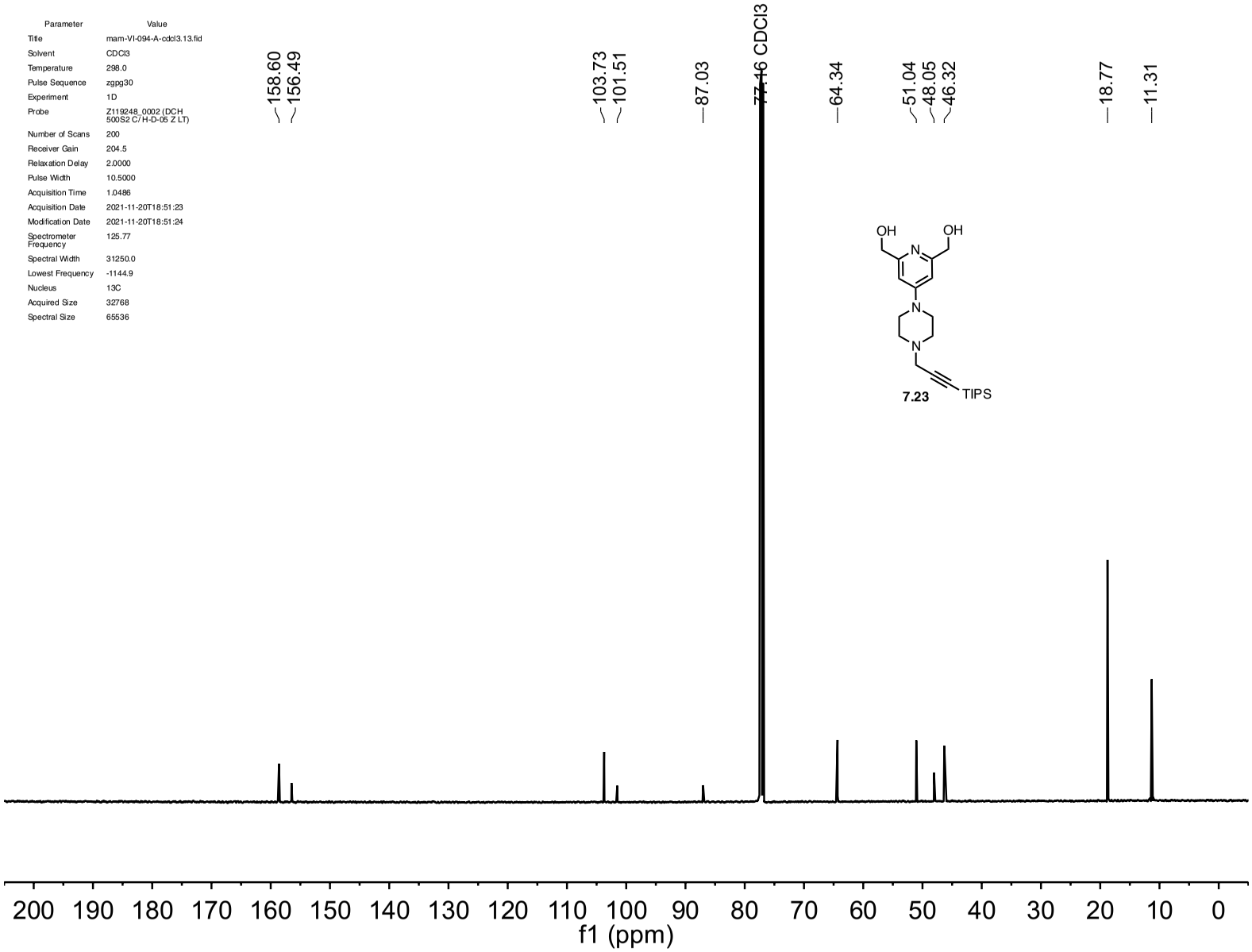

Parameter	Value
Title	mam-VI-081-B
Solvent	CDCl3
Temperature	296.8
Pulse Sequence	zg30
Experiment	1D
Probe	5 mm PABBO BB/ 19F-1H/ D Z-GRD Z108618/ 0656

Number of Scans	8
Receiver Gain	53.4
Relaxation Delay	2.0000
Pulse Width	15.0000
Acquisition Time	3.2998
Acquisition Date	2021-11-23T22:03:00
Modification Date	2021-11-23T22:03:08
Spectrometer Frequency	400.13
Spectral Width	8012.8
Lowest Frequency	-1623.2
Nucleus	1H
Acquired Size	26441
Spectral Size	65536

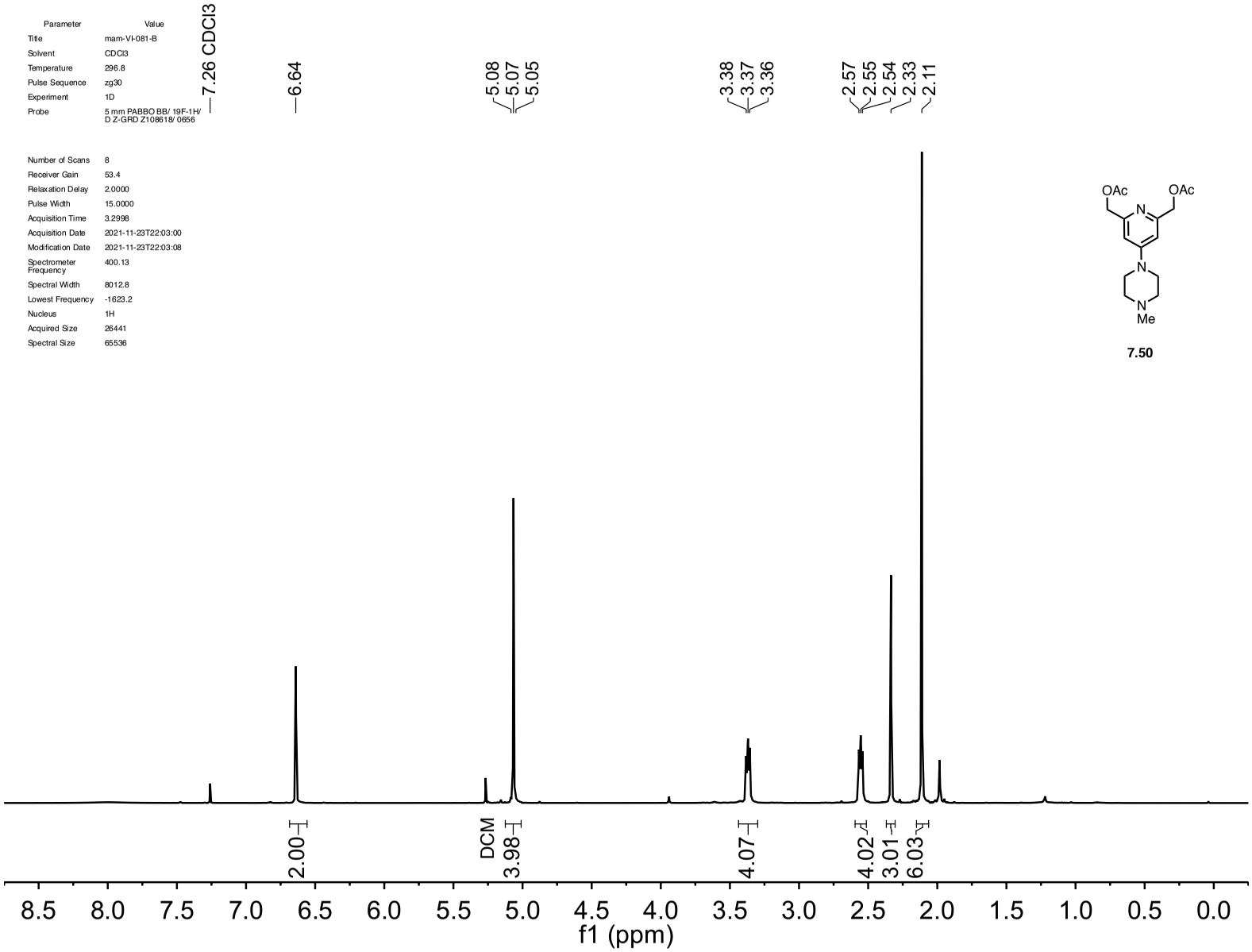

7.50

Parameter	Value
Title	mam-VI-081-B
Solvent	CDCl3
Temperature	298.0
Pulse Sequence	zgpg30
Experiment	1D
Probe	5 mm PABBO BB/ 19F-1H/ D Z-GRD Z108618/ 0656
Number of Scans	550
Receiver Gain	189.8
Relaxation Delay	2.0000
Pulse Width	10.0000
Acquisition Time	1.2976
Acquisition Date	2021-11-24T11:38:00
Modification Date	2021-11-24T11:38:38
Spectrometer Frequency	100.62
Spectral Width	25252.5
Lowest Frequency	-1048.8
Nucleus	13C
Acquired Size	32768
Spectral Size	65536

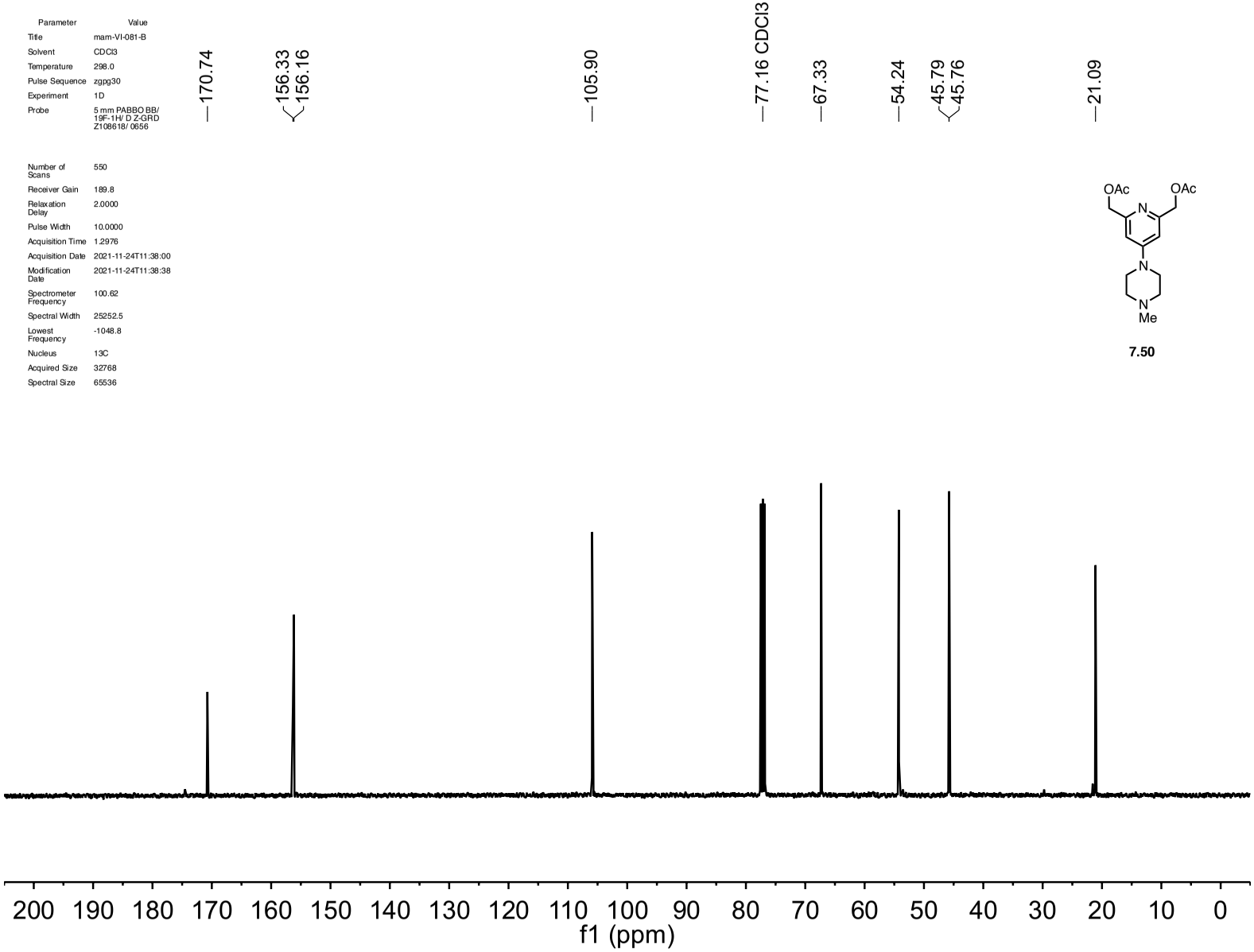

7.50

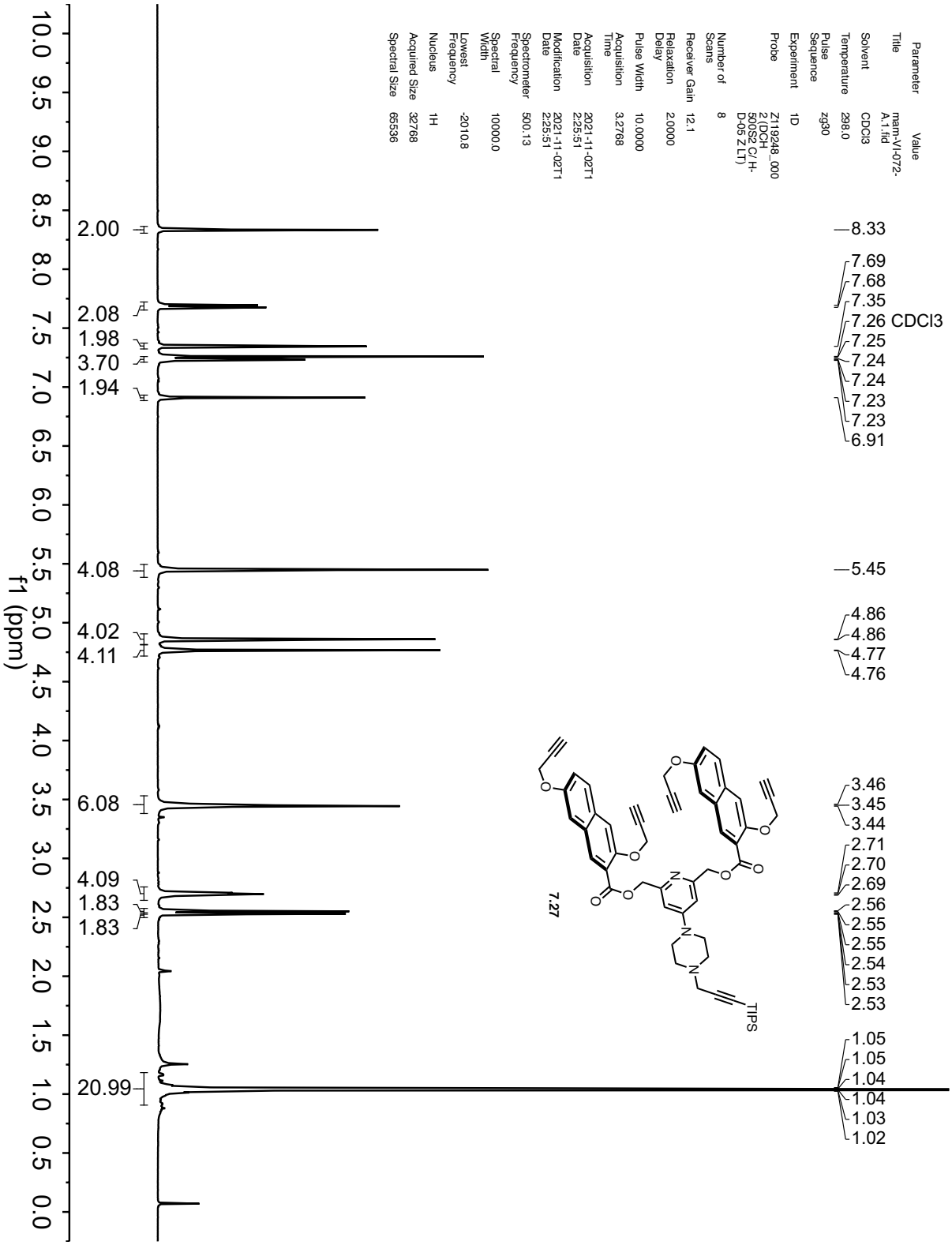
Parameter Value
Title mam-VI-072-A.1.fid
Solvent CDCl3
Temperature 298.0
Pulse Sequence zg30
Experiment 1D
Probe Z119248_0002 (DCH 500S2 C/H-D-05 Z LT)
Number of Scans 8
Receiver Gain 12.1
Relaxation Delay 2.0000
Pulse Width 10.0000
Acquisition Time 3.2768
Acquisition Date 2021-11-02T12:25:51
Modification Date 2021-11-02T12:25:51
Spectrometer Frequency 500.13
Spectral Width 10000.0
Lowest Frequency -2010.8
Nucleus 1H
Acquired Size 32768
Spectral Size 65536
f1 (ppm)
10.0 9.5 9.0 8.5 8.0 7.5 7.0 6.5 6.0 5.5 5.0 4.5 4.0 3.5 3.0 2.5 2.0 1.5 1.0 0.5 0.0
2.00
2.08
1.98
3.70
1.94
4.08
4.02
4.11
6.08
4.09
1.83
1.83
20.99
8.33
7.69
7.68
7.35
7.26 CDCl3
7.25
7.24
7.24
7.23
7.23
6.91
5.45
4.86
4.86
4.77
4.76
3.46
3.45
3.44
2.71
2.70
2.69
2.56
2.55
2.55
2.54
2.53
2.53
1.05
1.05
1.04
1.04
1.03
1.02
7.27
TIPS

Parameter	Value
Title	mam-VI-072-A
Solvent	CDCl3
Temperature	297.8
Pulse Sequence	zgpg30
Experiment	1D
Probe	5 mm PABBO BB/ 19F-1H/ D Z-GRD Z108618/ 0656
Number of Scans	525
Receiver Gain	189.8
Relaxation Delay	2.0000
Pulse Width	10.0000
Acquisition Time	1.2976
Acquisition Date	2021-11-02T14:37:00
Modification Date	2021-11-02T14:37:11
Spectrometer Frequency	100.62
Spectral Width	25252.5
Lowest Frequency	-1043.3
Nucleus	13C
Acquired Size	32768
Spectral Size	65536

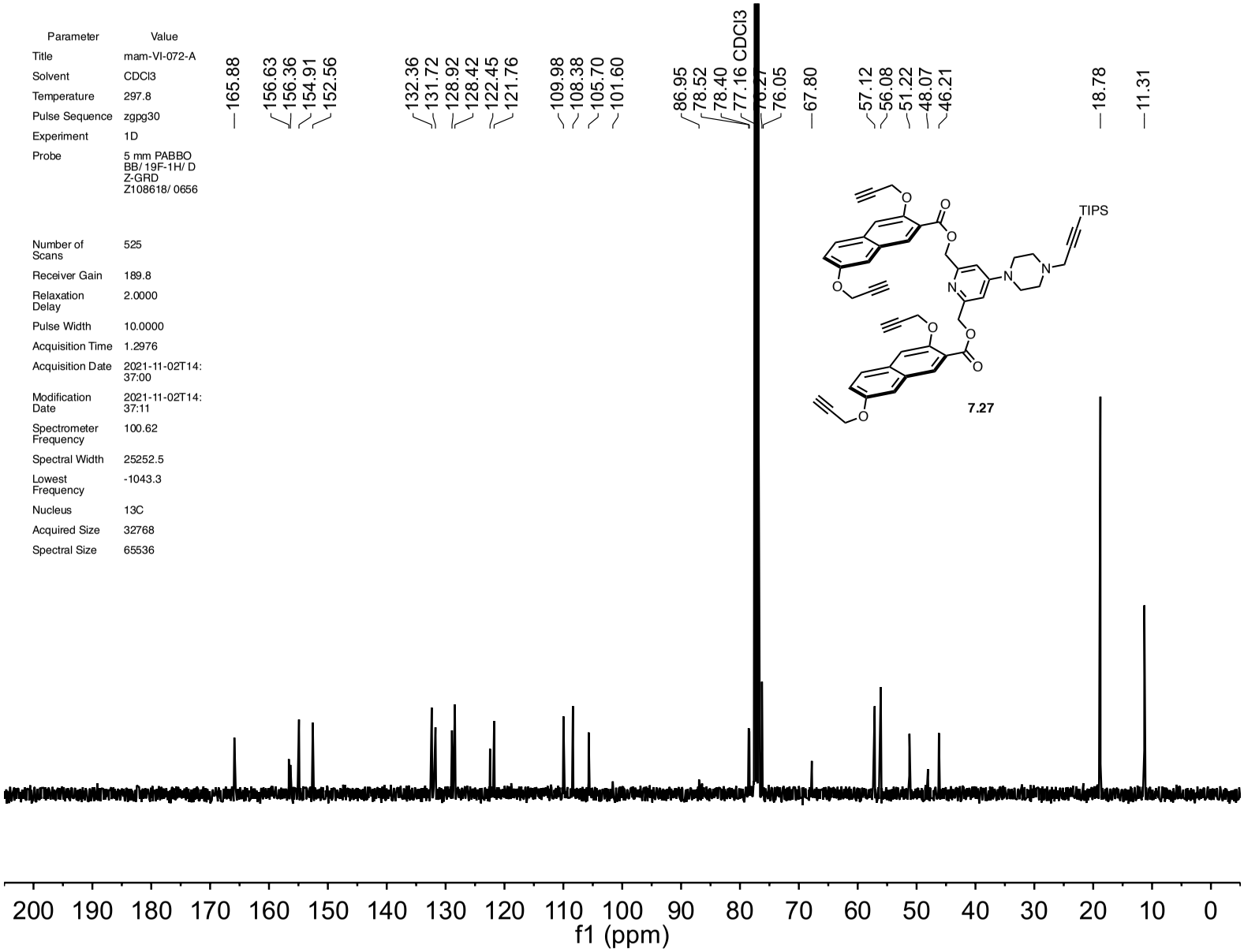

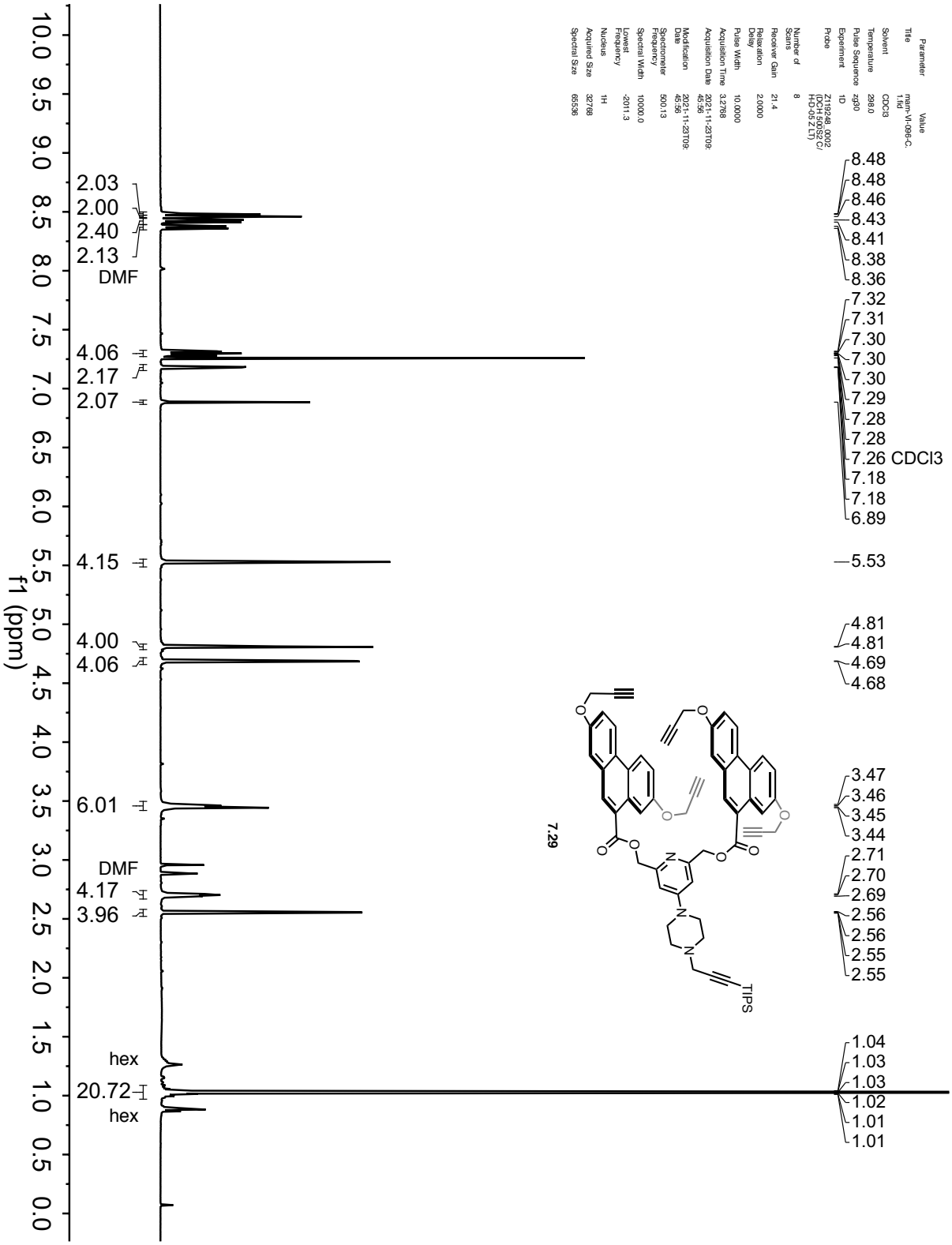
Parameter Value
Title mmm-VI-086-C.
1.fid
Solvent CDCl3
Temperature 298.0
Pulse Sequence zg30
Experiment 1D
Probe Z119248_0002 (BBO H-BB-D-05 Z-L1) (HD-US Z-L1)
Number of Scans 8
Receiver Gain 21.4
Relaxation Delay 2.0000
Pulse Width 10.0000
Acquisition Time 3.2768
Acquisition Date 2022-11-23T09:46:36
Modification Date 2022-11-23T09:46:36
Spectrometer Frequency 500.13
Spectral Width 10000.0
Lowest Frequency -2011.3
Nucleus 1H
Acquired Size 32768
Spectral Size 65536
f1 (ppm)
2.03
2.00
2.40
2.13
DMF
4.06
2.17
2.07
4.15
4.00
4.06
6.01
DMF
4.17
3.96
hex
20.72
hex
8.48
8.48
8.46
8.43
8.41
8.38
8.36
7.32
7.31
7.30
7.30
7.30
7.29
7.28
7.28
7.26 CDCl3
7.18
7.18
6.89
5.53
4.81
4.81
4.69
4.68
3.47
3.46
3.45
3.44
2.71
2.70
2.69
2.56
2.56
2.55
2.55
1.04
1.03
1.03
1.02
1.01
1.01
7.29
TIPS

Parameter	Value
Title	mam-VI-096-C.13.fid
Solvent	CDCl3
Temperature	298.0
Pulse Sequence	zgpg30
Experiment	1D
Probe	Z119248_0002 (DCH 500S2 C/ H-D-05 Z LT)
Number of Scans	2147
Receiver Gain	204.5
Relaxation Delay	2.0000
Pulse Width	10.5000
Acquisition Time	1.0486
Acquisition Date	2021-11-23T11:55:13
Modification Date	2021-11-23T11:55:15
Spectrometer Frequency	125.77
Spectral Width	31250.0
Lowest Frequency	-1145.2
Nucleus	13C
Acquired Size	32768
Spectral Size	65536

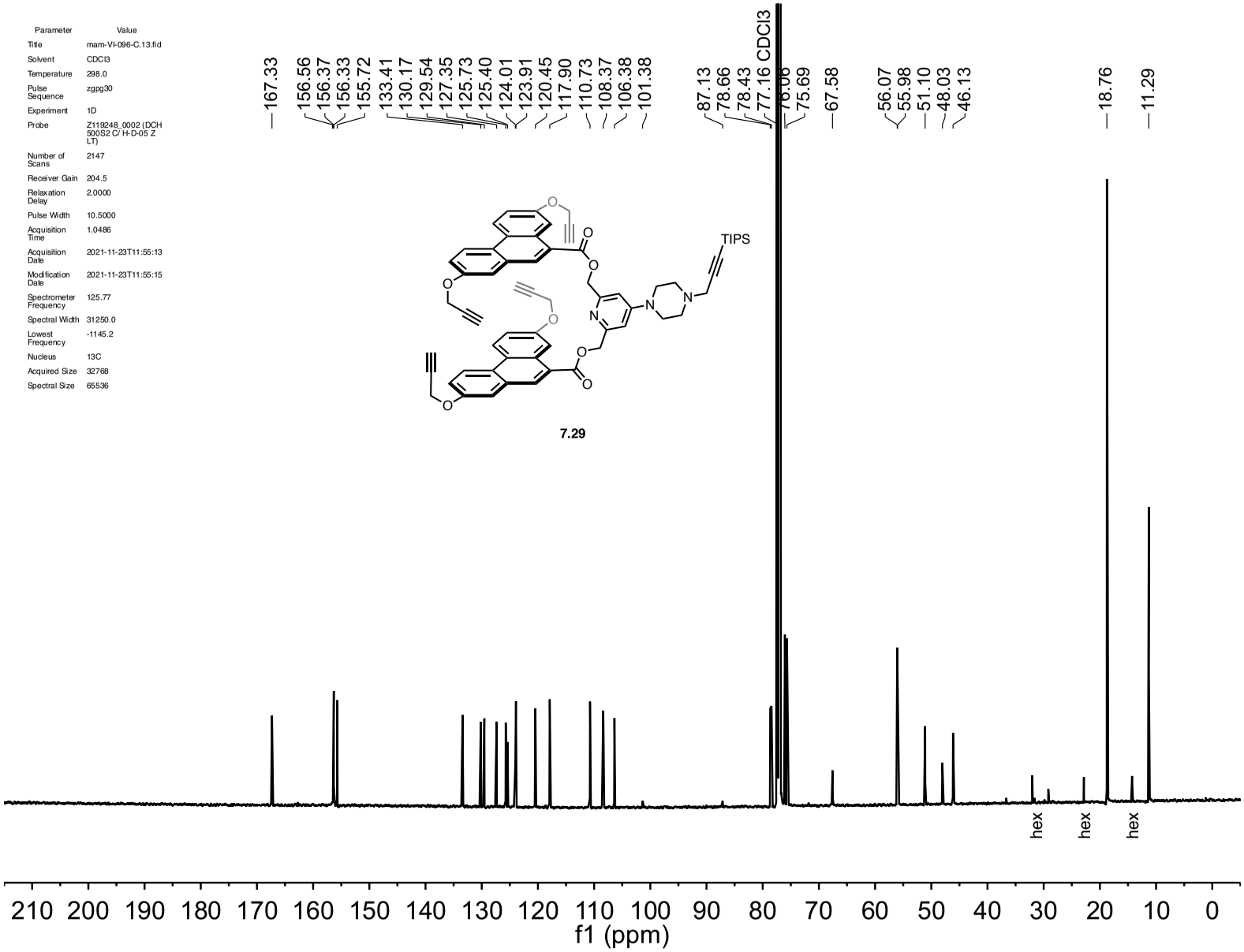

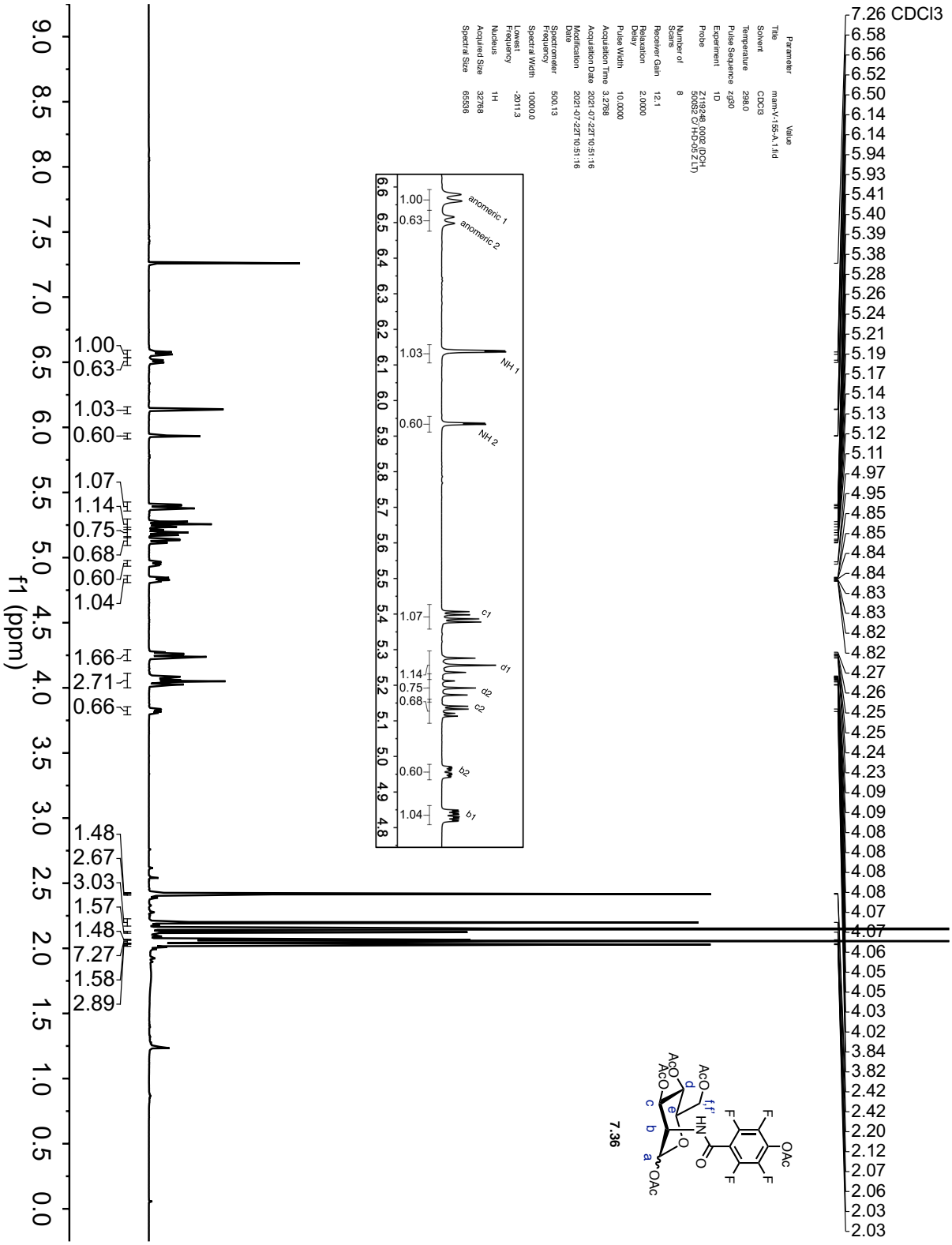
7.26 CDCl3
6.58
6.56
6.52
6.50
6.14
6.14
5.94
5.93
5.41
5.40
5.39
5.38
5.28
5.26
5.24
5.21
5.19
5.17
5.14
5.13
5.12
5.11
4.97
4.95
4.85
4.85
4.84
4.84
4.83
4.83
4.82
4.82
4.27
4.26
4.25
4.25
4.24
4.23
4.09
4.09
4.08
4.08
4.08
4.08
4.07
4.07
4.06
4.05
4.05
4.03
4.02
3.84
3.82
2.42
2.42
2.20
2.12
2.07
2.06
2.03
2.03
Parameter Value
Title mam-V-155-A.1.fid
Solvent CDCl3
Temperature 298.0
Pulse Sequence zg30
Experiment 1D
Probe Z119248_0002 (DCH, 50652 C/ H-D-08 Z LT)
Number of Scans 8
Receiver Gain 12.1
Relaxation Delay 2.0000
Pulse Width 10.000
Acquisition Time 3.2768
Acquisition Date 2021-07-22T10:51:16
Modification Date 2021-07-22T10:51:16
Spectrometer Frequency 500.13
Spectral Width 10000.0
Lowest Frequency -2011.3
Nucleus 1H
Acquired Size 32768
Spectral Size 65536
anomeric 1
anomeric 2
NH 1
NH 2
c1
d1
d2
c2
b2
b1
1.00
0.63
1.03
0.60
1.07
1.14
0.75
0.68
0.60
1.04
1.66
2.71
0.66
1.48
2.67
3.03
1.57
1.48
7.27
1.58
2.89
f1 (ppm)
7.36
AcO
AcO
AcO
OAc
OAc
HN
O
O
F
F
F
F
F
OAc
a
b
c
d
e
f,f'

Parameter	Value
Title	mam-V-155-A
Solvent	CDCl3
Temperature	297.7
Pulse Sequence	cosygpmfphpp
Experiment	COSY
Probe	5 mm PABBO BB/ 19F-1H/ D Z-GRD Z108618/ 0656
Number of Scans	4
Receiver Gain	60.3
Relaxation Delay	2.0000
Pulse Width	15.0000
Acquisition Time	0.3256
Acquisition Date	2021-07-22T20:37:00
Modification Date	2021-07-22T21:18:12
Spectrometer Frequency	(400.13, 400.13)
Spectral Width	(3144.7, 3144.7)
Lowest Frequency	(12.9, 12.9)
Nucleus	(1H, 1H)
Acquired Size	(1024, 256)
Spectral Size	(1024, 1024)

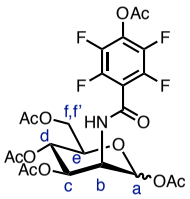

7.36

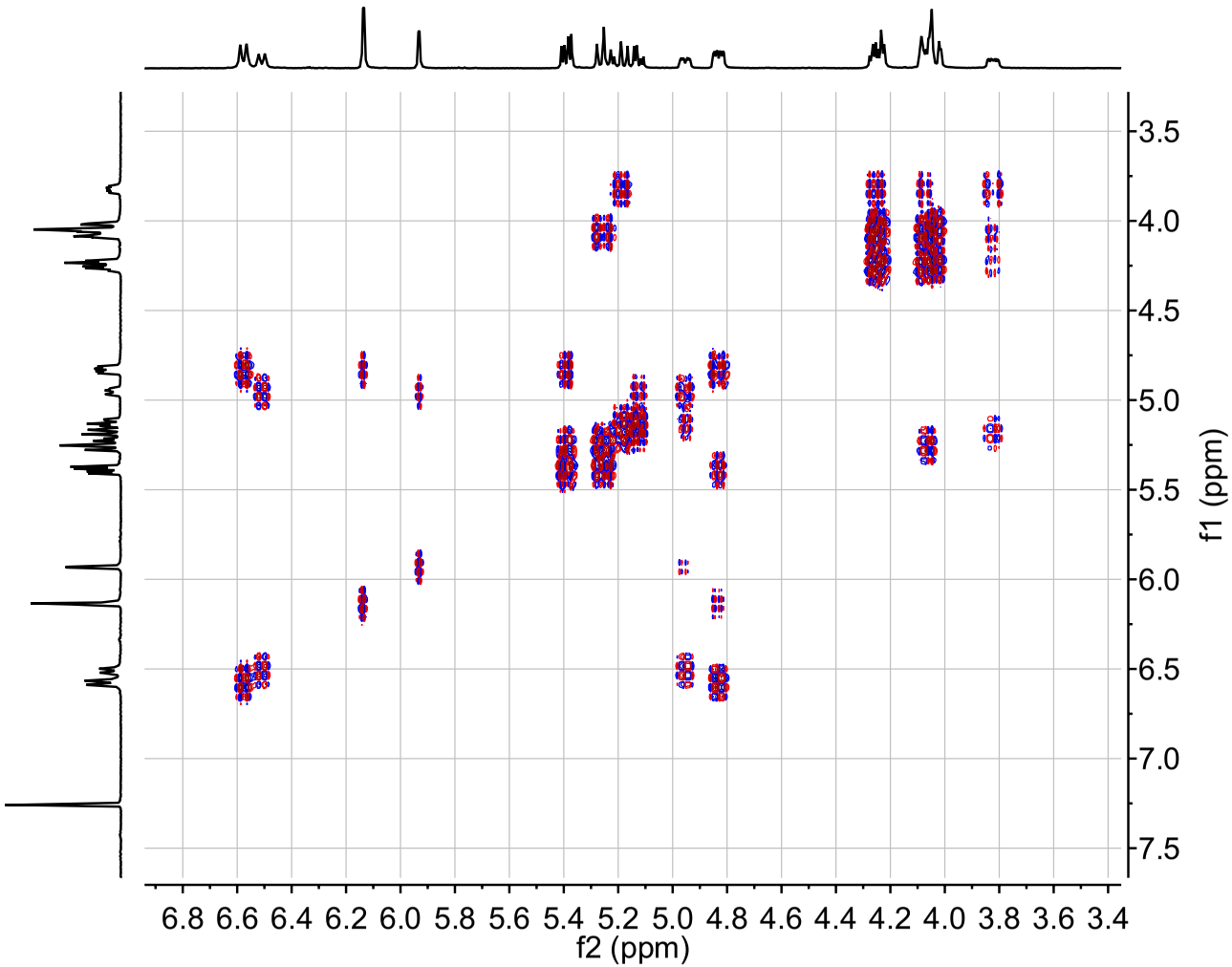

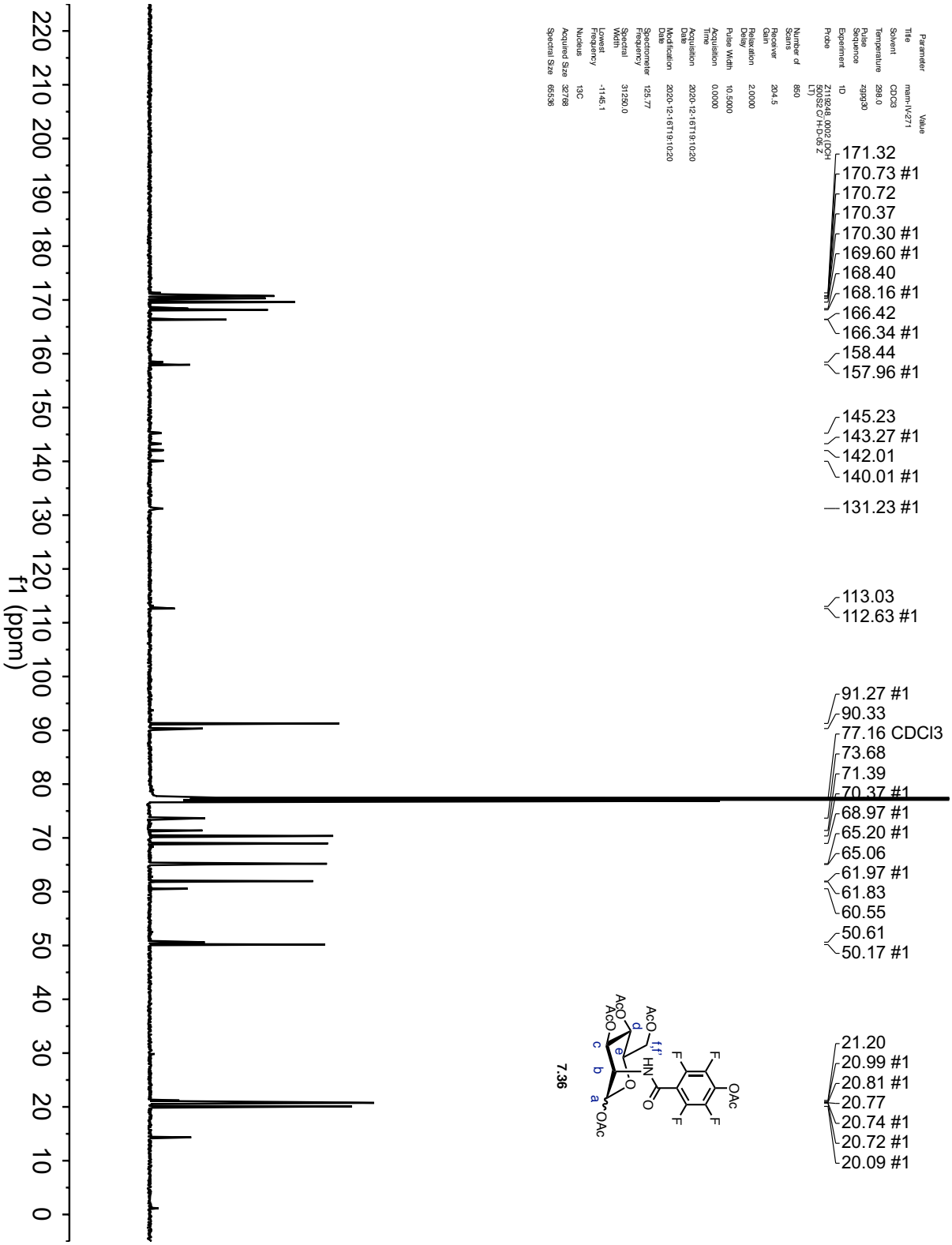
Parameter Value
Title mam-IV-271
Solvent CDCl3
Temperature 298.0
Pulse Sequence zgpg30
Experiment 1D
Probe Z119248_0002 (DCH 500S2 C/ H-D-05 Z L1)
Number of Scans 850
Receiver Gain 204.5
Relaxation Delay 2.0000
Pulse Width 10.5000
Acquisition Time 0.0000
Acquisition Date 2020-12-16T19:10:20
Modification Date 2020-12-16T19:10:20
Spectrometer Frequency 125.77
Spectral Width 31250.0
Lowest Frequency -1145.1
Nucleus 13C
Acquired Size 32768
Spectral Size 65536
171.32
170.73 #1
170.72
170.37
170.30 #1
169.60 #1
168.40
168.16 #1
166.42
166.34 #1
158.44
157.96 #1
145.23
143.27 #1
142.01
140.01 #1
131.23 #1
113.03
112.63 #1
91.27 #1
90.33
77.16 CDCl3
73.68
71.39
70.37 #1
68.97 #1
65.20 #1
65.06
61.97 #1
61.83
60.55
50.61
50.17 #1
21.20
20.99 #1
20.81 #1
20.77
20.74 #1
20.72 #1
20.09 #1
7.36
f1 (ppm)

Parameter	Value
Title	mam-IV-271
Solvent	CDCl3
Temperature	296.1
Pulse Sequence	zgfhigqn.2
Experiment	1D
Probe	5 mm PABBO BB/ 19F-1H/ D Z-GRD Z108618/ 0656
Number of Scans	8
Receiver Gain	189.8
Relaxation Delay	1.0000
Pulse Width	14.5000
Acquisition Time	1.7476
Acquisition Date	2020-12-15T20:01:00
Modification Date	2020-12-15T20:01:59
Spectrometer Frequency	376.46
Spectral Width	75000.0
Lowest Frequency	-75149.8
Nucleus	19F
Acquired Size	131072
Spectral Size	262144

-140.73 -140.74 -140.75 -140.75 -140.77 -140.81 -140.82 -140.83 -140.84 -140.84 -140.90 -140.91 -140.91 -140.92 -140.94 -140.97 -140.99 -141.00 -141.01 -150.69 -150.70 -150.71 -150.71 -150.73 -150.77 -150.79 -150.79 -150.80 -150.81 -150.86 -150.87 -150.88 -150.90 -150.93 -150.95 -150.96 -150.96 -150.97

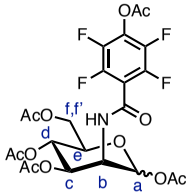

7.36

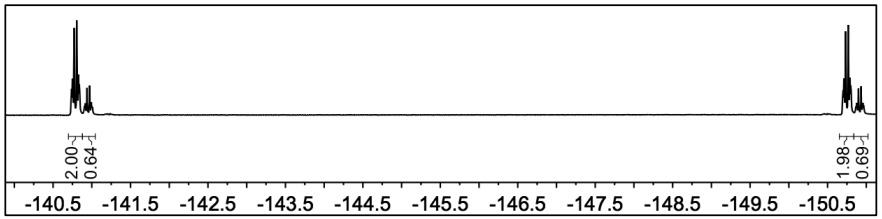

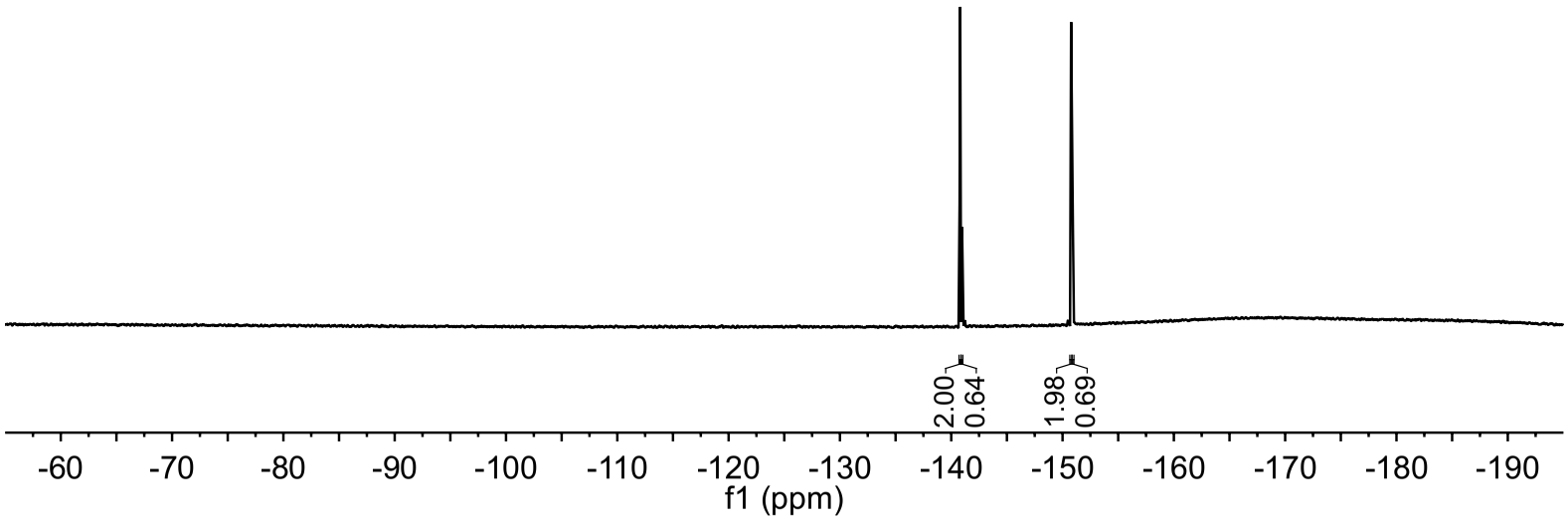

Parameter	Value
Title	mam-V-98-A.1.fid
Solvent	CDCl3
Temperature	298.0
Pulse Sequence	zg30
Experiment	1D
Probe	Z119248_0002 (DCH 500S2 C/ H-D-05 Z LT)
Number of Scans	8
Receiver Gain	12.1
Relaxation Delay	2.0000
Pulse Width	10.0000
Acquisition Time	3.2768
Acquisition Date	2021-06-02T13:58:53
Modification Date	2021-06-02T13:58:53
Spectrometer Frequency	500.13
Spectral Width	10000.0
Lowest Frequency	-2011.3
Nucleus	1H
Acquired Size	32768
Spectral Size	65536

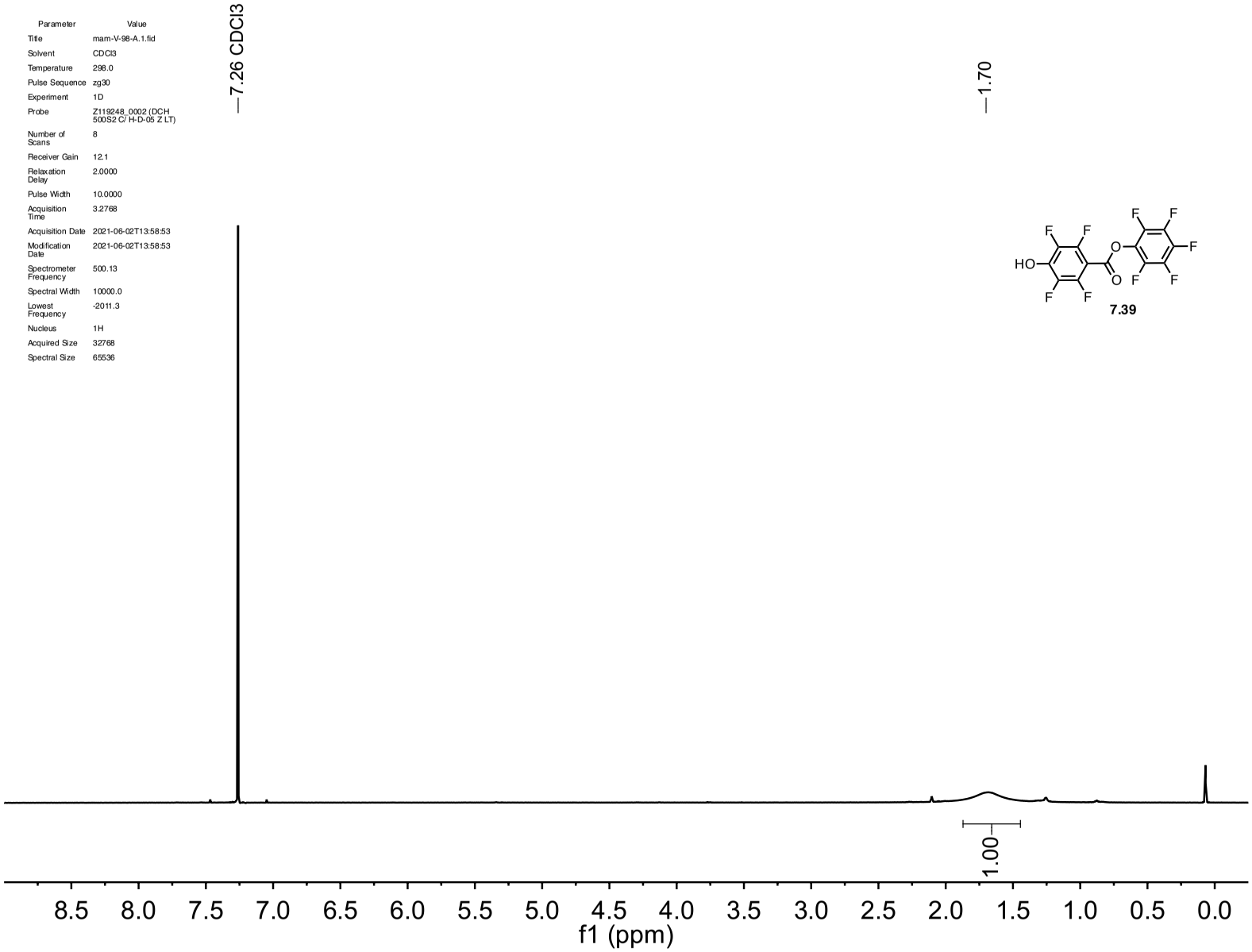

Parameter	Value
Title	mam-V-098-A
Solvent	CDCl3
Temperature	296.7
Pulse Sequence	zgfhigqn.2
Experiment	1D
Probe	5 mm PABBO BB/ 19F-1H/ D Z-GRD Z108618/ 0656

Number of Scans	16
Receiver Gain	189.8
Relaxation Delay	1.0000
Pulse Width	14.5000
Acquisition Time	1.1534
Acquisition Date	2021-06-02T14:26:00
Modification Date	2021-06-02T14:27:00
Spectrometer Frequency	376.46
Spectral Width	113636.4
Lowest Frequency	-94468.0
Nucleus	19F
Acquired Size	131072
Spectral Size	262144

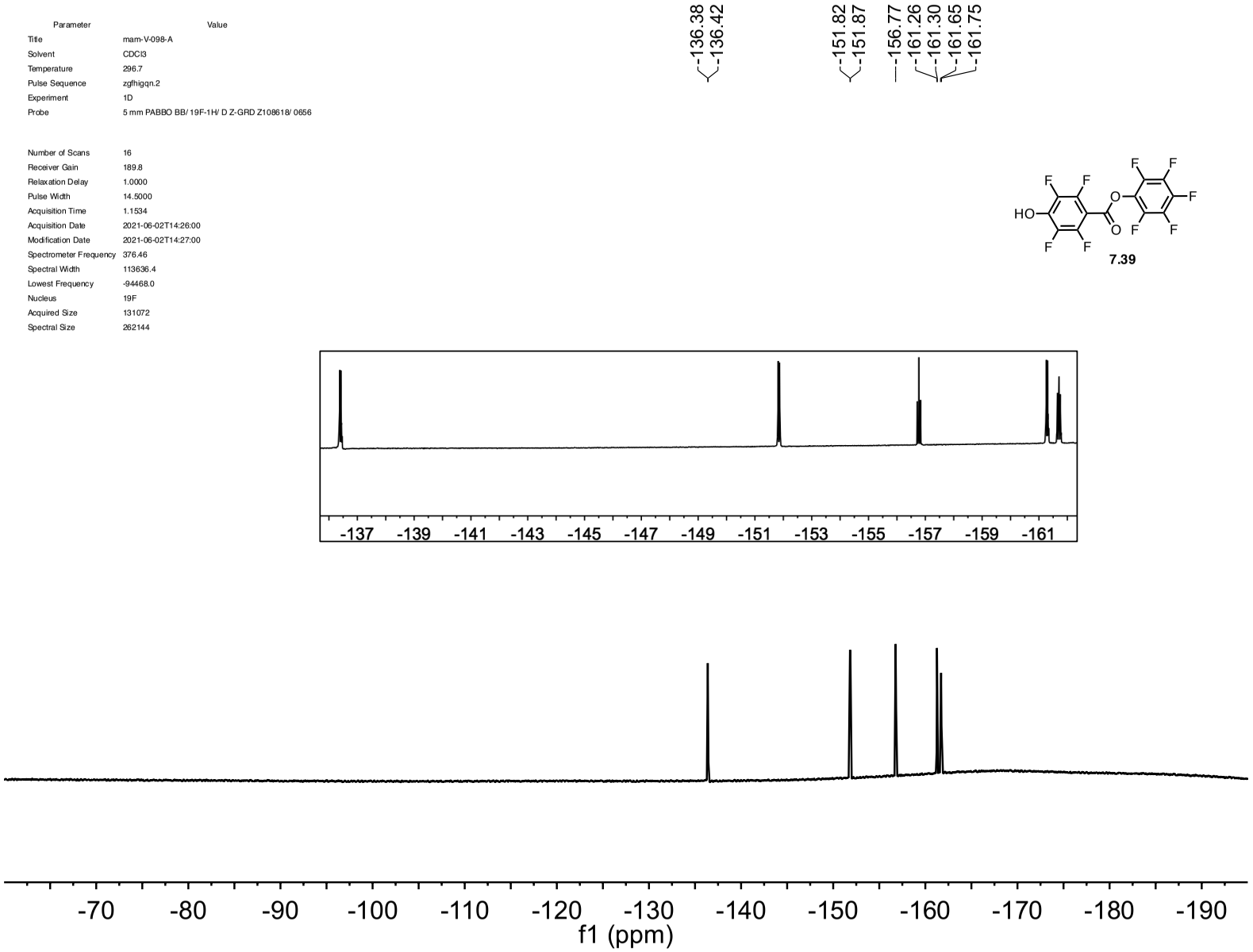

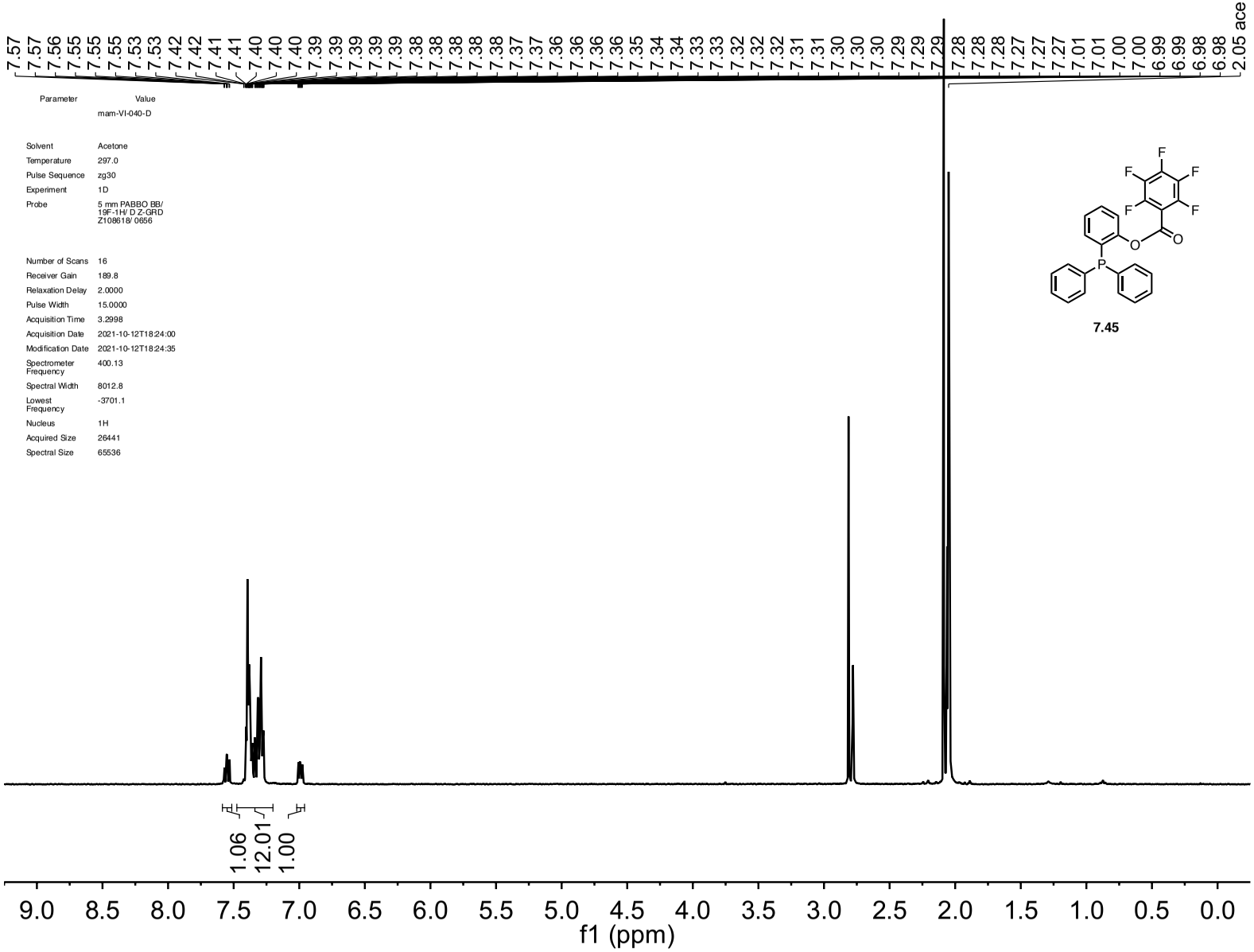
7.57 7.57 7.56 7.55 7.55 7.55 7.53 7.53 7.42 7.42 7.41 7.41 7.40 7.40 7.40 7.39 7.39 7.39 7.39 7.39 7.38 7.38 7.38 7.38 7.37 7.37 7.36 7.36 7.36 7.36 7.35 7.34 7.34 7.33 7.33 7.32 7.32 7.32 7.31 7.31 7.30 7.30 7.30 7.29 7.29 7.29 7.28 7.28 7.28 7.27 7.27 7.27 7.01 7.01 7.00 7.00 6.99 6.99 6.98 6.98 2.05 ace
Parameter Value
mam-VI-040-D
Solvent Acetone
Temperature 297.0
Pulse Sequence zg30
Experiment 1D
Probe 5 mm PABBO BB/ 19F-1H/ D Z-GRD Z108618/ 0656
Number of Scans 16
Receiver Gain 189.8
Relaxation Delay 2.0000
Pulse Width 15.0000
Acquisition Time 3.2998
Acquisition Date 2021-10-12T18:24:00
Modification Date 2021-10-12T18:24:35
Spectrometer Frequency 400.13
Spectral Width 8012.8
Lowest Frequency -3701.1
Nucleus 1H
Acquired Size 26441
Spectral Size 65536
F
F
F
F
F
O
O
P
7.45
1.06
12.01
1.00
9.0 8.5 8.0 7.5 7.0 6.5 6.0 5.5 5.0 4.5 4.0 3.5 3.0 2.5 2.0 1.5 1.0 0.5 0.0
f1 (ppm)

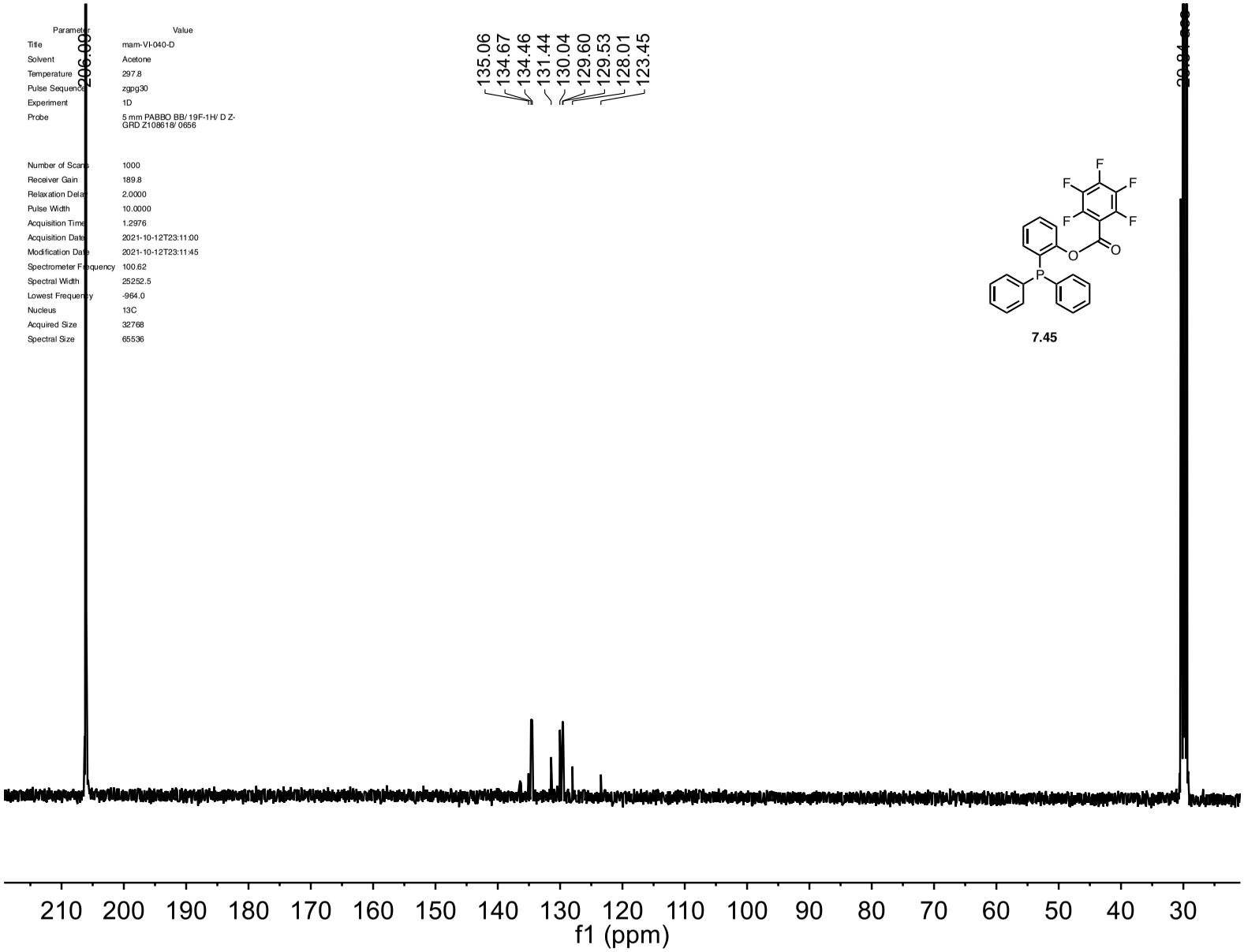

Parameter	Value
Title	mam-VI-040-D
Solvent	Acetone
Temperature	297.8
Pulse Sequence	zgpg30
Experiment	1D
Probe	5 mm PABBO BB/ 19F-1H/ D Z-GRD Z108618/ 0656
Number of Scans	1000
Receiver Gain	189.8
Relaxation Delay	2.0000
Pulse Width	10.0000
Acquisition Time	1.2976
Acquisition Date	2021-10-12T23:11:00
Modification Date	2021-10-12T23:11:45
Spectrometer Frequency	100.62
Spectral Width	25252.5
Lowest Frequency	-964.0
Nucleus	13C
Acquired Size	32768
Spectral Size	65536

Parameter	Value
Title	mam-VI-040-D
Solvent	Acetone
Temperature	297.1
Pulse Sequence	zgfhigqn.2
Experiment	1D
Probe	5 mm PABBO BB/ 19F-1H/ D Z-GRD Z108618/ 0656

Number of Scans	16
Receiver Gain	189.8
Relaxation Delay	1.0000
Pulse Width	14.5000
Acquisition Time	1.7476
Acquisition Date	2021-10-12T18:28:00
Modification Date	2021-10-12T18:28:47
Spectrometer Frequency	376.46
Spectral Width	75000.0
Lowest Frequency	-75149.8
Nucleus	19F
Acquired Size	131072
Spectral Size	262144

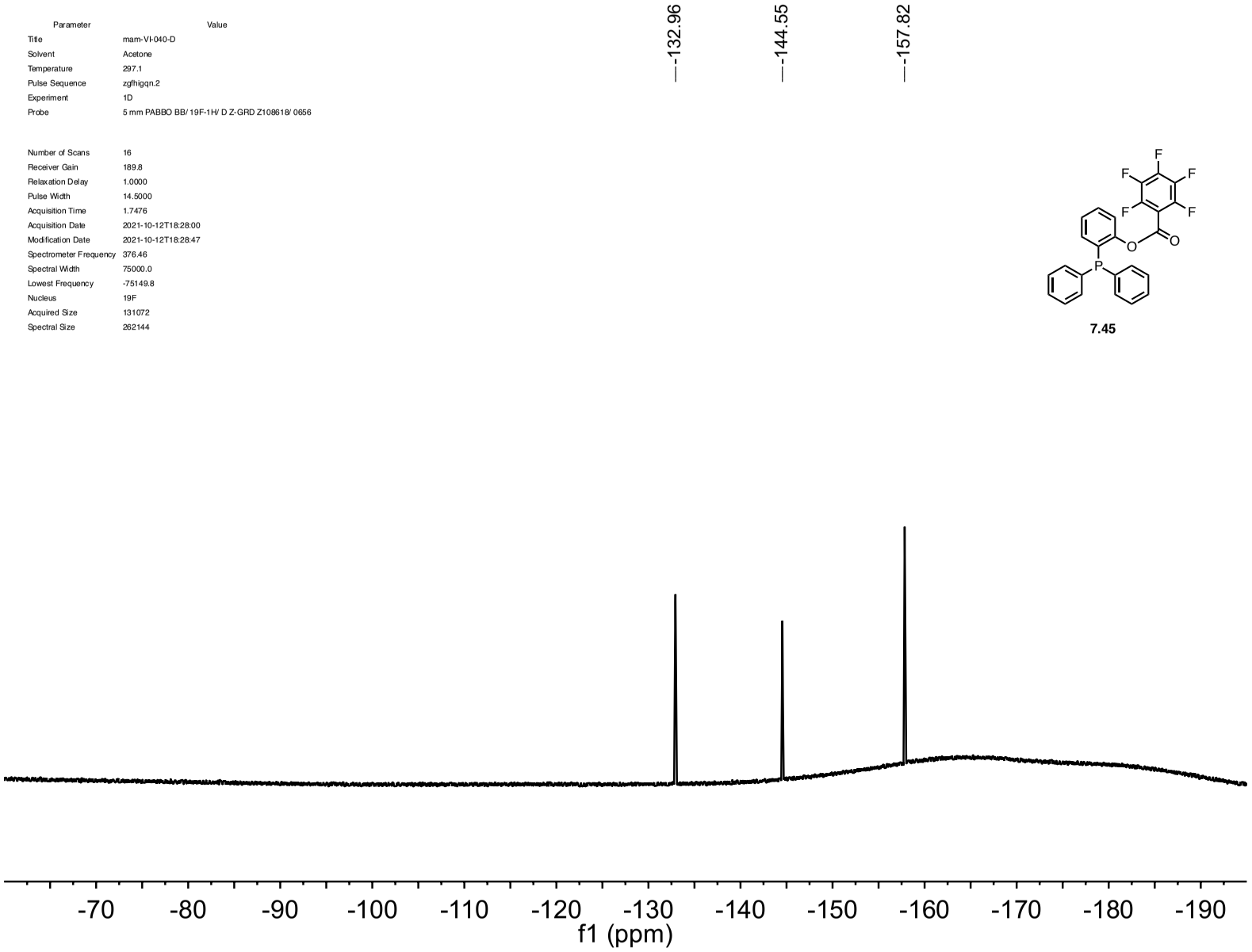

7.45

Parameter	Value
Title	mam-VI-040-D
Solvent	Acetone
Temperature	297.1
Pulse Sequence	zgpg30
Experiment	1D
Probe	5 mm PABBO BB/ 19F-1H/ D Z-GRD Z108618/ 0656
Number of Scans	8
Receiver Gain	189.8
Relaxation Delay	2.0000
Pulse Width	14.0000
Acquisition Time	0.9961
Acquisition Date	2021-10-12T18:26:00
Modification Date	2021-10-12T18:26:31
Spectrometer Frequency	161.98
Spectral Width	131578.9
Lowest Frequency	-65789.5
Nucleus	31P
Acquired Size	131072
Spectral Size	262144

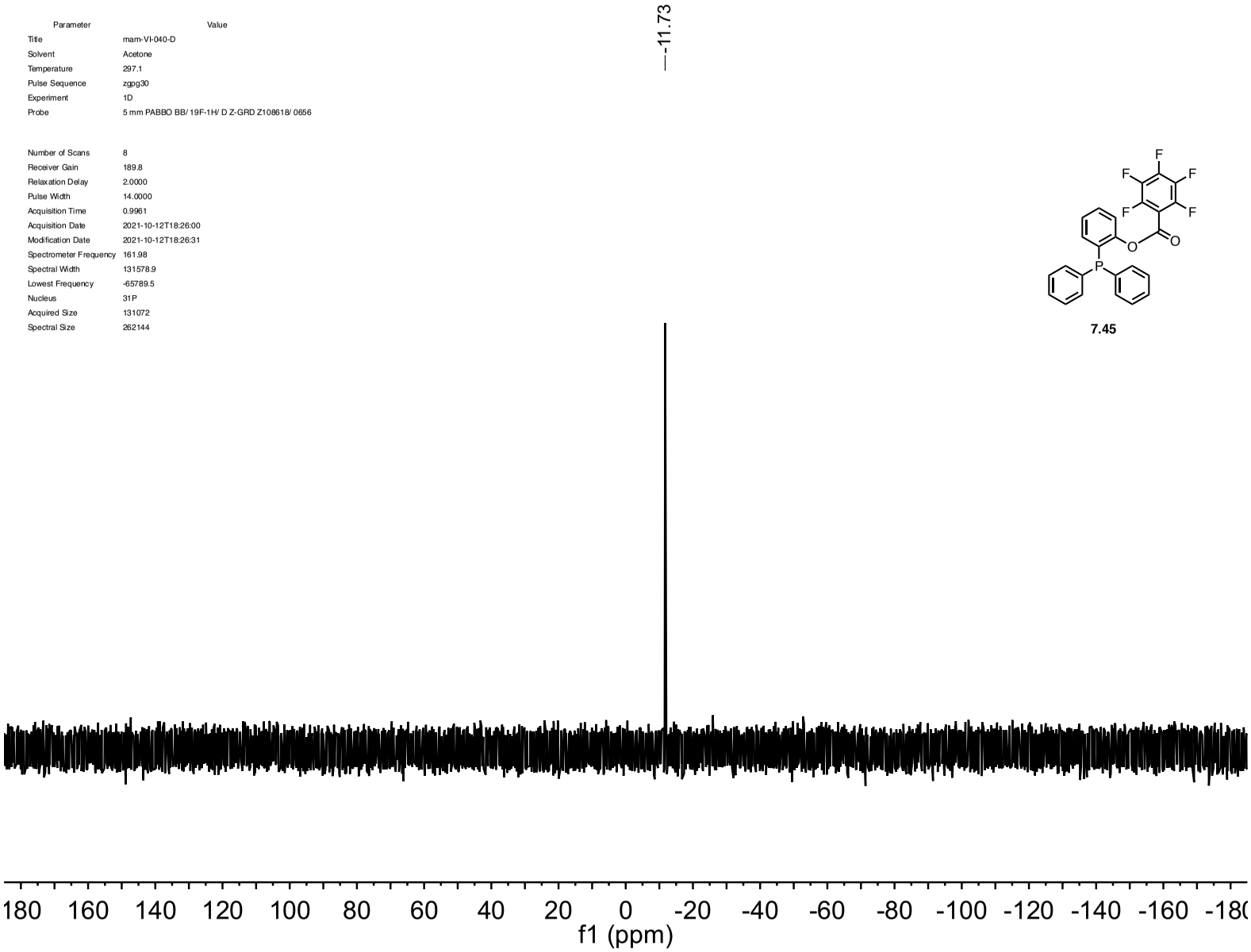

7.45

7.7 References

(1) Kataki-Anastasakou, A.; Hernandez, S.; Sletten, E. M. Cell-Surface Labeling via Bioorthogonal Host-Guest Chemistry. *ACS Chem. Biol.* **2021**, *16*, 2124–2129.

(2) Wesener, D. A.; Dugan, A.; Kiessling, L. L. Recognition of Microbial Glycans by Soluble Human Lectins. *Curr. Opin. Struct. Biol.* **2017**, *44*, 168–178.

(3) Crocker, P. R.; Paulson, J. C.; Varki, A. Siglecs and Their Roles in the Immune System. *Nat. Rev. Immunol.* **2007**, *7*, 255–266.

(4) Lee, R. T.; Lee, Y. C. Affinity Enhancement by Multivalent Lectin–Carbohydrate Interaction. *Glycoconj. J.* **2000**, *17*, 543–551.

(5) Kiessling, L. L.; Gestwicki, J. E.; Strong, L. E. Synthetic Multivalent Ligands in the Exploration of Cell-Surface Interactions. *Curr. Opin. Chem. Biol.* **2000**, *4*, 696–703.

(6) Rao, J.; Lahiri, J.; Isaacs, L.; Weis, R. M.; Whitesides, G. M. A Trivalent System from Vancomycin·d-Ala-d-Ala with Higher Affinity Than Avidin·Biotin. *Science* **1998**, *280*, 708–711.

(7) Lee, G. Y.; Hu, E.; Rheingold, A. L.; Houk, K. N.; Sletten, E. M. Arene-Perfluoroarene Interactions in Solution. *J. Org. Chem.* **2021**, *86*, 8425–8436.

(8) Sundhoro, M.; Jeon, S.; Park, J.; Ramström, O.; Yan, M. Perfluoroaryl Azide Staudinger Reaction: A Fast and Bioorthogonal Reaction. *Angew. Chemie* **2017**, *129*, 12285–12289.

(9) Chefalo, P.; Pan, Y.; Nagy, N.; Guo, Z.; Harding, C. V. Efficient Metabolic Engineering of GM3 on Tumor Cells by N-Phenylacetyl-D-Mannosamine. *Biochemistry* **2006**, *45*, 3733–3739.

(10) Han, S.; Collins, B. E.; Bengtson, P.; Paulson, J. C. Homomultimeric Complexes of CD22 in B Cells Revealed by Protein-Glycan Cross-Linking. *Nat. Chem. Biol.* **2005**, *1*, 93–97.

(11) Luchansky, S. J.; Goon, S.; Bertozzi, C. R. Expanding the Diversity of Unnatural Cell-Surface Sialic Acids. *ChemBioChem* **2004**, *5*, 371–374.

(12) Sandbhor, M. S.; Soya, N.; Albohy, A.; Zheng, R. B.; Cartmell, J.; Bundle, D. R.; Klassen, J. S.; Cairo, C. W. Substrate Recognition of the Membrane-Associated Sialidase NEU3 Requires a Hydrophobic Aglycone. *Biochemistry* **2011**, *50*, 6753–6762.

(13) Lin, B.; Wu, X.; Zhao, H.; Tian, Y.; Han, J.; Liu, J.; Han, S. Redirecting Immunity via Covalently Incorporated Immunogenic Sialic Acid on the Tumor Cell Surface. *Chem. Sci.* **2016**, *7*, 3737–3741.

(14) Brotzel, F.; Ying, C. C.; Mayr, H. Nucleophilicities of Primary and Secondary Amines in Water. *J. Org. Chem.* **2007**, *72*, 3679–3688.

(15) Keppler, O. T.; Hinderlich, S.; Langner, J.; Schwartz-Albiez, R.; Reutter, W.; Pawlita, M. UDP-GlcNAc 2-Epimerase: A Regulator of Cell Surface Sialylation. *Science* **1999**, *284*, 1372–1376.

(16) Jacobs, C. L.; Goon, S.; Yarema, K. J.; Hinderlich, S.; Hang, H. C.; Chai, D. H.; Bertozzi, C. R. Substrate Specificity of the Sialic Acid Biosynthetic Pathway. *Biochemistry* **2001**, *40*, 12864–12874.

(17) Du, J.; Meledeo, M. A.; Wang, Z.; Khanna, H. S.; Paruchuri, V. D. P.; Yarema, K. J. Metabolic Glycoengineering: Sialic Acid and Beyond. *Glycobiology* **2009**, *19*, 1382–1401.

(18) Patterson, D. M.; Nazarova, L. A.; Xie, B.; Kamber, D. N.; Prescher, J. A. Functionalized Cyclopropenes as Bioorthogonal Chemical Reporters. *J. Am. Chem. Soc.* **2012**, *134*, 18638–18643.

(19) Ahad, A. M.; Jensen, S. M.; Jewett, J. C. A Traceless Staudinger Reagent to Deliver

Diazirines. *Org. Lett.* **2013**, *15*, 5060–5063.

(20) Patterson, D. M.; Jones, K. A.; Prescher, J. A. Improved Cyclopropene Reporters for Probing Protein Glycosylation. *Mol. Biosyst.* **2014**, *10*, 1693–1697.

(21) Thordarson, P. Determining Association Constants from Titration Experiments in Supramolecular Chemistry. *Chem. Soc. Rev.* **2011**, *40*, 1305–1323.

(22) Brynn Hibbert, D.; Thordarson, P. The Death of the Job Plot, Transparency, Open Science and Online Tools, Uncertainty Estimation Methods and Other Developments in Supramolecular Chemistry Data Analysis. *Chem. Commun.* **2016**, *52*, 12792–12805.

(23) Wang, F.; Zhang, J.; Ding, X.; Dong, S.; Liu, M.; Zheng, B.; Li, S.; Wu, L.; Yu, Y.; Gibson, H. W.; Huang, F.; Wang, F.; Zhang, J.; Dong, S.; Liu, M.; Zheng, B.; Li, S.; Wu, L.; Huang, F.; Ding, X.; Yu, Y.; Gibson, H. W. Metal Coordination Mediated Reversible Conversion between Linear and Cross-Linked Supramolecular Polymers. *Angew. Chemie Int. Ed.* **2010**, *49*, 1090–1094.

(24) Hamilton, A. D.; Little, D. Nucleotide Base Recognition: Synthesis of Artificial Receptors Containing Two Distinct Binding Regions for the Complexation of Bis-Thymine Derivatives. *J. Chem. Soc. Chem. Commun.* **1990**, 297–300.

(25) Ossola, A.; Macerata, E.; Mossini, E.; Giola, M.; Gullo, M. C.; Arduini, A.; Casnati, A.; Mariani, M. 2,6-Bis(1-Alkyl-1H-1,2,3-Triazol-4-Yl)-Pyridines: Selective Lipophilic Chelating Ligands for Minor Actinides. *J. Radioanal. Nucl. Chem.* **2018**, *318*, 2013–2022.

(26) Pokhodylo, N. T.; Tupychak, M. A.; Shyyka, O. Y.; Obushak, M. D. Some Aspects of the Azide-Alkyne 1,3-Dipolar Cycloaddition Reaction. *Russ. J. Org. Chem.* **2019**, *55*, 1310–1321.

(27) Rodríguez, J. F.; Burton, K. I.; Franzoni, I.; Petrone, D. A.; Scheipers, I.; Lautens, M.

Palladium-Catalyzed Hydride Addition/C-H Bond Activation Cascade: Cycloisomerization of 1,6-Diynes. *Org. Lett.* **2018**, *20*, 6915–6919.